Broadband Microstrip Antennas

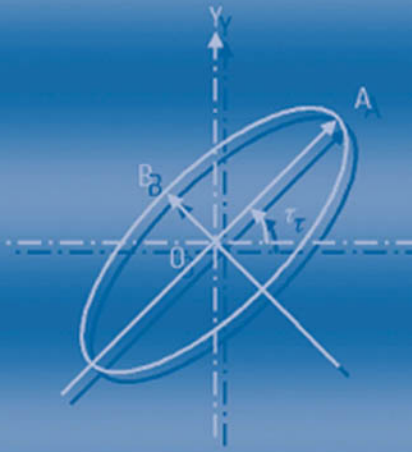

Girish Kumar | K.P. Ray

Broadband Microstrip Antennas

For a listing of recent titles in the *Artech House Antennas and Propagation Library,* turn to the back of this book.

Broadband Microstrip Antennas

Girish Kumar
K. P. Ray

Artech House
Boston • London
www.artechhouse.com

Library of Congress Cataloging-in-Publication Data
Kumar, Girish.
Broadband microstrip antennas / Girish Kumar and K.P. Ray.
p. cm. — (Artech House antennas and propagation library)
Includes bibliographical references and index.
ISBN 1-58053-244-6 (alk. paper)
1. Microstrip antennas. I. Ray, K. P. II. Title.
TK7871.67.M5 K85 2003
621.382'4—dc21 2002033256

British Library Cataloguing in Publication Data
Kumar, Girish
Broadband microstrip antennas. — (Artech House antennas and propagation library)
1. Microstrip antennas 2. Broadband communication systems I. Title
II. Ray, K. P.
621.3'824

ISBN 1-58053-244-6

Cover design by Gary Ragaglia

685 Canton Street
Norwood, MA 02062

International Standard Book Number: 1-58053-244-6
Library of Congress Catalog Card Number: 2002033256

10 9 8 7 6 5 4 3 2 1

To our family members

Contents

Foreword

Although printed microstrip radiators were first proposed as early as 1953, the first actual microstrip antenna appeared in 1974, more than 20 years after the original suggestion was made. *Microstrip Antennas,* published by Artech House in 1980, was the first book on microstrip antennas. Ever since then, I have kept track of the books published on this and related topics. There are 11 of them on my shelf here at the University of Colorado at Boulder, and there are also a number of other books with chapters on microstrip antennas and similar items. However, going through the detailed synopsis, examining the table of contents, and reviewing the manuscripts for various chapters for *Broadband Microstrip Antennas* that were sent to me, I find that this book deserves a rightful place among the library of books on printed antennas. There are two other microstrip antenna books that carry the word "broadband" in their titles. The first, *Broadband Patch Antennas,* by Jean-François Zurcher and Fred Gardiol (both close friends of mine), was published by Artech House in 1995. This book, the first to address broadband designs, emphasizes the *strip-slot-foam-inverted patch* (SSFIP) approach to expanding the operating frequency range of microstrip antennas. In this approach the radiation and feed functions are designed on separate layers and are thus optimized separately. The other book to address broadband designs for microstrip patches is more recent. Kin-Lu Wong's *Compact and Broadband Microstrip Antennas* (John Wiley, 2002) arrived at my desk this spring. Three chapters in this book (Chapters 7, 8, and 9) address broadband antennas. These chapters do not emphasize a single approach but present the various available broadbanding techniques.

Broadband Microstrip Antennas by Professor Girish Kumar and Dr. K. P. Ray is wholly dedicated to broadband microstrip antenna designs only. After the first introductory chapter, there are seven chapters on various designs for microstrip patches, and another chapter dealing with tunable and dual-frequency microstrip antennas. Thus, *Broadband Microstrip Antennas* should find a place on the desk of every antenna researcher and designer interested in increased bandwidth from microstrip patches.

Personally, this book embodies a milestone in the professional career of one of my graduate students and a very close friend, Girish Kumar. Girish wrote his doctoral thesis, ''Broadband Microstrip Antennas Using Coupled Resonators,'' at the Indian Institute of Technology (IITK) India from 1979 to 1982, and I have observed his illustrious career develop steadily since then. My congratulations to Girish for another worthwhile contribution to our microstrip antenna community!

Artech House has demonstrated its leading role in the timely publication of books on emerging RF and microwave technologies to help designers in the industry and researchers in academia. Since 1980, when Artech House published the first book on microstrip antennas, seven out of eleven published books on microstrip antennas have been published by Artech House. Undoubtedly, I express the sentiments of the microstrip antenna community by taking this opportunity to thank Artech House for books on printed antenna technology.

K. C. Gupta
October 2002
University of Colorado at Boulder
Boulder, Colorado

Preface

Microstrip antennas (MSAs) have several advantages, including that they are lightweight and small-volume and that they can be made conformal to the host surface. In addition, MSAs are manufactured using printed-circuit technology, so that mass production can be achieved at a low cost.

MSAs, which are used for defense and commercial applications, are replacing many conventional antennas. However, the types of applications of MSAs are restricted by the antennas' inherently narrow *bandwidth* (BW). Accordingly, increasing the BW of the MSA has been a primary goal of research in the field. This is reflected in the large number of papers on the subject published in journals and conference proceedings. In fact, several broadband MSA configurations have been reported in the last few decades. As a result, there is a need for a book that comprehensively covers various MSA configurations.

Organization of the Book

This book aims to detail various broadband MSA configurations, collecting in one volume the information that is currently scattered around in various journals, conference proceedings, and books. This book explains concepts of several broadband techniques, providing suitable examples without getting into mathematical detail. Many theoretical simulations and parametric studies have been especially carried out to provide physical insight into antennas. In addition, several tips and approximate expressions are included for quick

calculations. An attempt has been made to make the text self-contained and to cover different aspects of MSAs in order to be useful for students, teachers, practicing engineers, and researchers. In accordance with this goal, the language of the book is kept as simple as possible without losing technical objectivity, so that readers can quickly grasp the ideas contained within. A summary is given at the end of each chapter to highlight the important points given in the chapter.

The book generally uses three dielectric constant values of the substrate to give examples. One is a low-cost glass-epoxy substrate, whose dielectric constant ϵ_r ranges from 3.8 to 4.7. This substrate is very useful for prototype and preliminary testing to prove the new designs and could be used in a suspended microstrip configuration to obtain broad BW. Another frequently used substrate is glass-reinforced Teflon, whose ϵ_r varies between 2.1 and 2.6. In addition, a third value of ϵ_r equal to 1 has been used to yield maximum BW.

The book is divided into nine chapters covering different aspects of MSAs. The main focus is on BW-enhancement techniques, but other important configurations such as compact, tunable, dual-band, circularly polarized MSAs—including ultra-broadband planar monopole antennas—are also discussed in detail.

Chapter 1 introduces the MSA configuration and discusses its advantages, disadvantages, and applications. In addition, Chapter 1 briefly describes various theoretical methods for the analysis of MSAs and presents definitions of the BW, expressions, and graphs for the quick evaluation of BW. This is followed by a review of various broadband, tunable, dual-band, compact, and circularly polarized MSAs.

Chapter 2 discusses the analysis and design of regularly shaped patches such as rectangular, circular, semicircular, triangular, and annular-ring patches. Chapter 2 also describes the effects of various parameters, compares several patches, and covers suspended and broadband configurations.

Many techniques are available to increase the BW of the MSAs; these are discussed in Chapters 3–5. Chapter 3 discusses the multiresonator technique in a planar configuration, elaborating on the mechanism of gap, direct, and hybrid coupling for broad BWs in rectangular, circular, semicircular, and triangular microstrip patches.

Chapter 4 describes multilayer broadband configurations, presenting electromagnetic and aperture coupling mechanisms and discussing a microstrip and coaxial feed for electromagnetically coupled configurations. In addition, Chapter 4 covers nonresonant and resonant aperture-coupled MSAs.

Next, Chapter 5 presents stacked multiresonators for broad BWs with increased gain and discusses multiresonator-stacked rectangular and circular MSAs. The log-periodic MSA array in a multilayer configuration is also described.

The drive for smaller electronic systems pushes not only integrated-circuit technology but also antenna technology. There is increasing emphasis on the compact MSA, and it is expected that requirement for the compact broadband MSA will increase in the future. Thus, Chapter 6 presents compact configurations using shorting posts, resistive loading, and slots. These compact MSA elements are used in both planar and multilayer configurations to obtain broad BW. Patch antennas with a U-slot loaded yield a 30–40% BW with good radiation characteristics.

Tunable and dual-band MSAs are very useful where broadband response is difficult to achieve over the required frequency range. Also, a dual-band response can be used for transmit and receive purposes. These configurations are discussed in Chapter 7, which covers the frequency tunability of MSAs using stub loading, shorting posts, varactor diodes, air gaps, and ferrite substrates. In addition, Chapter 7 describes dual-frequency MSAs using higher order modes, stub loading, shorting posts, lumped elements, and slots. Multiresonators in planar and stacked configurations also yield a dual-band response.

Chapter 8 defines *circular polarization* (CP), dual- and single-feed CP, compact CP, and broadband CP MSAs and arrays. Dual-feed CP MSAs are used in planar and stacked multiresonator configurations to increase the BW of the antenna. Single-feed MSAs are used in sequential-rotation arrays to realize broad BW.

The MSA in its conventional form does not give multi-octave BW, because of its resonant nature. Modified MSA configurations are required to obtain octave BW. Chapter 9 details planar monopole antennas, which are variations of MSAs, and clearly describes the analogy between planar monopole antennas and MSAs. Chapter 9 also presents theoretical explanations for achieving multi-octave BW and gives simple design equations to predict the lower frequency corresponding to a *voltage standing-wave ratio* (VSWR) = 2. In addition, several planar monopole antennas—namely, rectangular, square, triangular, hexagonal, circular, and elliptical monopole antennas—are discussed.

The book also contains three appendixes: Appendix A discusses various characteristics of the dielectric substrate, which is a backbone of the MSA and decides the performance of the antenna. The MSA is an extension of microstrip line. Appendix B presents important expressions for the rectangular

patch. These expressions are also applicable to the microstrip transmission line. Appendix C covers the *multiport network model* (MNM) for analyzing rectangular MSA. The MNM is a very flexible, simple, and accurate model. It also gives physical insight into the working of the antenna.

Acknowledgments

We authors are indebted to Professor K. C. Gupta of the University of Colorado at Boulder, for all his guidance and help in writing this book. It is he who introduced the fascinating subject of MSAs to us and inspired us to write this book. His kind encouragement and motivation during the preparation of the manuscript are highly appreciated. We are particularly thankful to reviewers who carefully went through the manuscript and gave valuable suggestions. Thanks are also due to Zeland Software, Inc., in Freemont, California, whose IE3D software has been extensively used to verify many experimental and theoretical results and to generate several examples for the book.

Our sincere thanks go to all the research scholars, graduate students, and research engineers working in the microwave laboratory at the Indian Institute of Technology (IIT) in Bombay, India, for their help at various stages of the book. We would also like to thank Mr. R. Patwardhan for his excellent drawing of most of the figures in this book. We also offer sincere thanks to the personnel at Artech House for their help and patience throughout the preparation of the manuscript. In addition, we would like to acknowledge the financial support provided by the Curriculum Development Program (CDP), of IIT, Bombay, India.

Last but not the least, we express our appreciation and gratitude to our families for their encouragement, understanding, and patience during the writing of this book.

Girish Kumar and K. P. Ray
India
October 2002

1

An Introduction to Microstrip Antennas

1.1 Introduction

Deschamps first proposed the concept of the MSA in 1953 [1]. However, practical antennas were developed by Munson [2, 3] and Howell [4] in the 1970s. The numerous advantages of MSA, such as its low weight, small volume, and ease of fabrication using printed-circuit technology, led to the design of several configurations for various applications [5–9]. With increasing requirements for personal and mobile communications, the demand for smaller and low-profile antennas has brought the MSA to the forefront.

An MSA in its simplest form consists of a radiating patch on one side of a dielectric substrate and a ground plane on the other side. The top and side views of a *rectangular MSA* (RMSA) are shown in Figure 1.1. However, other shapes, such as the square, circular, triangular, semicircular, sectoral, and annular ring shapes shown in Figure 1.2, are also used.

Radiation from the MSA can occur from the fringing fields between the periphery of the patch and the ground plane. The length L of the rectangular patch for the fundamental TM_{10} mode excitation is slightly smaller than $\lambda/2$, where λ is the wavelength in the dielectric medium, which in terms of free-space wavelength λ_o is given as $\lambda_o/\sqrt{\epsilon_e}$, where ϵ_e is the effective dielectric constant of a microstrip line of width W. The value of ϵ_e is slightly less than the dielectric constant ϵ_r of the substrate because the fringing fields from the patch to the ground plane are not confined in the

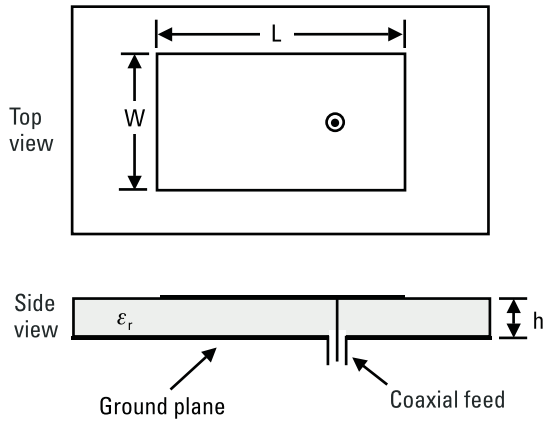

Figure 1.1 MSA configuration.

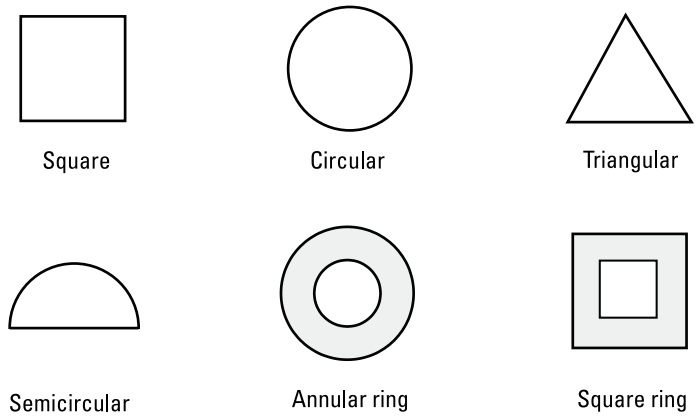

Figure 1.2 Different shapes of microstrip patches.

dielectric only, but are also spread in the air. To enhance the fringing fields from the patch, which account for the radiation, the width W of the patch is increased. The fringing fields are also enhanced by decreasing the ϵ_r or by increasing the substrate thickness h. Therefore, unlike the *microwave integrated circuit* (MIC) applications, MSA uses microstrip patches with larger width and substrates with lower ϵ_r and thicker h. The details of various substrates used for MSA are given in Appendix A. For MSA applications in the microwave frequency band, generally h is taken greater than or equal to 1/16th of an inch (0.159 cm). A typical comparison of MSA with MIC in the microwave frequency range is given in Table 1.1.

Table 1.1
A Comparison of MIC and MSA

	MIC	MSA
h	$\leq$ 0.159 cm	$\geq$ 0.159 cm
ϵ_r	$\geq$ 9.8	$\leq$ 9.8
W	Small	Large
Radiation	Minimized	Maximized

1.2 Characteristics of MSAs

The MSA has proved to be an excellent radiator for many applications because of its several advantages, but it also has some disadvantages. The advantages and disadvantages of the MSA are given in Sections 1.2.1 and 1.2.2.

1.2.1 Advantages

MSAs have several advantages compared to the conventional microwave antennas. The main advantages of MSAs are listed as follows:

- They are lightweight and have a small volume and a low-profile planar configuration.
- They can be made conformal to the host surface.
- Their ease of mass production using printed-circuit technology leads to a low fabrication cost.
- They are easier to integrate with other MICs on the same substrate.
- They allow both linear polarization and CP.
- They can be made compact for use in personal mobile communication.
- They allow for dual- and triple-frequency operations.

1.2.2 Disadvantages

MSAs suffer from some disadvantages as compared to conventional microwave antennas. They are the following:

- Narrow BW;
- Lower gain;
- Low power-handling capability.

MSAs have narrow BW, typically 1–5%, which is the major limiting factor for the widespread application of these antennas. Increasing the BW of MSAs has been the major thrust of research in this field, and broad BW up to 70% has been achieved [9, 10]. Various broadband MSA configurations are summarized in this chapter, and they are detailed in the following chapters.

1.2.3 Applications of MSAs

The advantages of MSAs make them suitable for numerous applications [6–11]. The telemetry and communications antennas on missiles need to be thin and conformal and are often MSAs. Radar altimeters use small arrays of microstrip radiators. Other aircraft-related applications include antennas for telephone and satellite communications. Microstrip arrays have been used for satellite imaging systems. Patch antennas have been used on communication links between ships or buoys and satellites. Smart weapon systems use MSAs because of their thin profile. Pagers, the *global system for mobile communication* (GSM), and the *global positioning system* (GPS) are major users of MSAs. Some of the applications of MSAs are listed in Table 1.2.

1.3 Feeding Techniques

The MSA can be excited directly either by a coaxial probe or by a microstrip line. It can also be excited indirectly using electromagnetic coupling or aperture coupling and a coplanar waveguide feed, in which case there is no

Table 1.2
Typical Applications of MSAs

System	Application
Aircraft and ship antennas	Communication and navigation, altimeters, blind landing systems
Missiles	Radar, proximity fuses, and telemetry
Satellite communications	Domestic direct broadcast TV, vehicle-based antennas, communication
Mobile radio	Pagers and hand telephones, man pack systems, mobile vehicle
Remote sensing	Large lightweight apertures
Biomedical	Applicators in microwave hyperthermia
Others	Intruder alarms, personal communication, and so forth

direct metallic contact between the feed line and the patch [9–12]. Feeding technique influences the input impedance and characteristics of the antenna, and is an important design parameter.

The coaxial or probe feed arrangement is shown in Figure 1.1. The center conductor of the coaxial connector is soldered to the patch. The main advantage of this feed is that it can be placed at any desired location inside the patch to match with its input impedance. The disadvantages are that the hole has to be drilled in the substrate and that the connector protrudes outside the bottom ground plane, so that it is not completely planar. Also, this feeding arrangement makes the configuration asymmetrical.

A patch excited by microstrip line feed is shown in Figure 1.3(a). This feed arrangement has the advantage that it can be etched on the same substrate, so the total structure remains planar. The drawback is the radiation from the feed line, which leads to an increase in the cross-polar level. Also, in the millimeter-wave range, the size of the feed line is comparable to the patch size, leading to increased undesired radiation.

For thick substrates, which are generally employed to achieve broad BW, both the above methods of direct feeding the MSA have problems. In the case of a coaxial feed, increased probe length makes the input impedance more inductive, leading to the matching problem. For the microstrip feed, an increase in the substrate thickness increases its width, which in turn increases the undesired feed radiation. The indirect feed, discussed below, solves these problems. An electromagnetically coupled RMSA is shown in Figure 1.3(b). The electromagnetic coupling is also known as proximity coupling [9, 12, 13]. The feed line is placed between the patch and the ground plane, which is separated by two dielectric media. The advantages of this feed configuration include the elimination of spurious feed-network radiation; the choice between two different dielectric media, one for the patch and the other for the feed line to optimize the individual performances; and an increase in the BW due to the increase in the overall substrate thickness of the MSA. The disadvantages are that the two layers need to be aligned properly and that the overall thickness of the antenna increases.

Another method for indirectly exciting a patch employs aperture coupling [14]. In the aperture-coupled MSA configuration, the field is coupled from the microstrip line feed to the radiating patch through an electrically small aperture or slot cut in the ground plane, as shown in Figure 1.3(c). The coupling aperture is usually centered under the patch, leading to lower cross-polarization due to symmetry of the configuration. The shape, size, and location of the aperture decide the amount of coupling from the feed line to the patch [15–17]. The slot aperture can be either resonant or

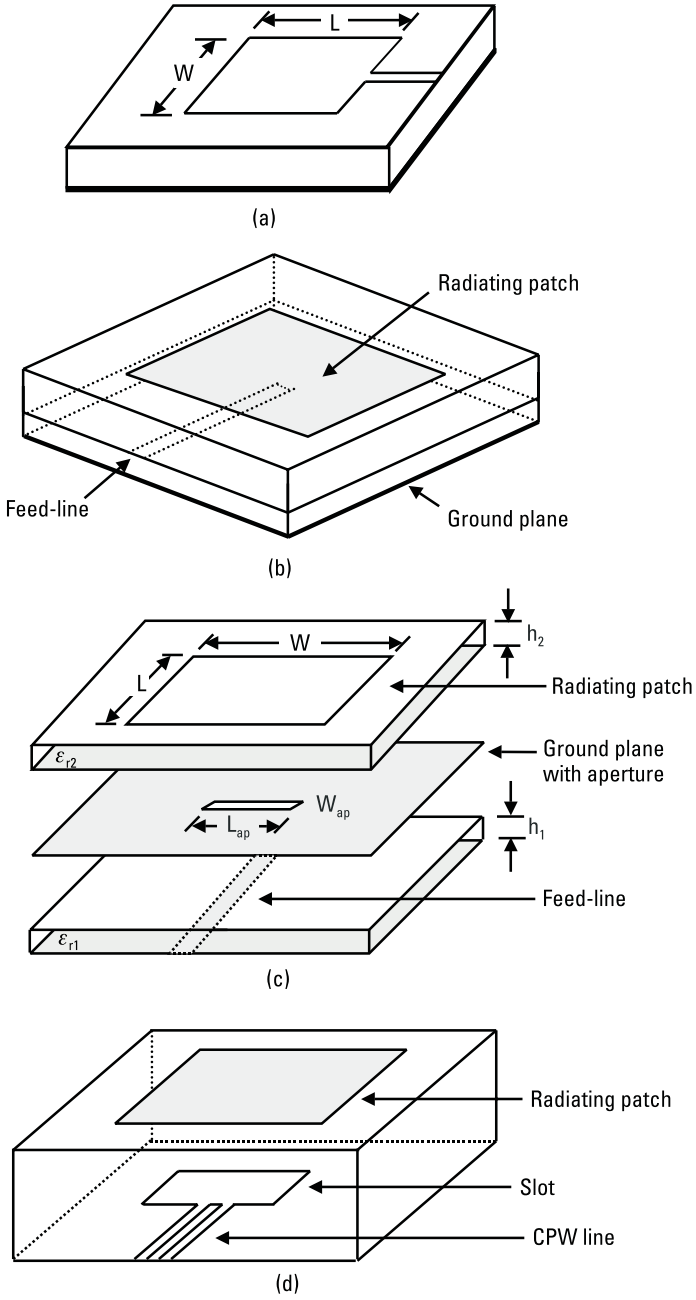

Figure 1.3 Rectangular MSA fed by (a) microstrip line, (b) electromagnetic coupling, (c) aperture coupling, and (d) coplanar waveguide (CPW).

nonresonant [10, 11]. The resonant slot provides another resonance in addition to the patch resonance thereby increasing the BW at the expense of an increase in back radiation. As a result, a nonresonant aperture is normally used. The performance is relatively insensitive to small errors in the alignment of the different layers. Similar to the electromagnetic coupling method, the substrate parameters of the two layers can be chosen separately for optimum antenna performance. This feeding method gives increased BW as described in Chapter 4.

The coplanar waveguide feed, shown in Figure 1.3(d), has also been used to excite the MSA [18]. In this method, the coplanar waveguide is etched on the ground plane of the MSA. The line is excited by a coaxial feed and is terminated by a slot, whose length is chosen to be between 0.25 and 0.29 of the slot wavelength. The main disadvantage of this method is the high radiation from the rather longer slot, leading to the poor front-to-back ratio. The front-to-back ratio is improved by reducing the slot dimension and modifying its shape in the form of a loop [19].

1.4 Methods of Analysis

The MSA generally has a two-dimensional radiating patch on a thin dielectric substrate and therefore may be categorized as a two-dimensional planar component for analysis purposes. The analysis methods for MSAs can be broadly divided into two groups.

In the first group, the methods are based on equivalent magnetic current distribution around the patch edges (similar to slot antennas). There are three popular analytical techniques:

- The transmission line model;
- The cavity model;
- The MNM.

In the second group, the methods are based on the electric current distribution on the patch conductor and the ground plane (similar to dipole antennas, used in conjunction with full-wave simulation/numerical analysis methods). Some of the numerical methods for analyzing MSAs are listed as follows:

- The *method of moments* (MoM);
- The *finite-element method* (FEM);
- The *spectral domain technique* (SDT);
- The *finite-difference time domain* (FDTD) method.

This section briefly describes these methods.

1.4.1 Transmission Line Model

The transmission line model is very simple and helpful in understanding the basic performance of a MSA. The microstrip radiator element is viewed as a transmission line resonator with no transverse field variations (the field only varies along the length), and the radiation occurs mainly from the fringing fields at the open circuited ends. The patch is represented by two slots that are spaced by the length of the resonator. This model was originally developed for rectangular patches but has been extended for generalized patch shapes. Many variations of this method have been used to analyze the MSA [9, 20–22].

Although the transmission line model is easy to use, all types of configurations can not be analyzed using this model since it does not take care of variation of field in the orthogonal direction to the direction of propagation.

1.4.2 Cavity Model

In the cavity model, the region between the patch and the ground plane is treated as a cavity that is surrounded by magnetic walls around the periphery and by electric walls from the top and bottom sides. Since thin substrates are used, the field inside the cavity is uniform along the thickness of the substrate [23–25]. The fields underneath the patch for regular shapes such as rectangular, circular, triangular, and sectoral shapes can be expressed as a summation of the various resonant modes of the two-dimensional resonator.

The fringing fields around the periphery are taken care of by extending the patch boundary outward so that the effective dimensions are larger than the physical dimensions of the patch. The effect of the radiation from the antenna and the conductor loss are accounted for by adding these losses to the loss tangent of the dielectric substrate. The far field and radiated power are computed from the equivalent magnetic current around the periphery.

An alternate way of incorporating the radiation effect in the cavity model is by introducing an impedance boundary condition at the walls of the cavity. The fringing fields and the radiated power are not included inside

the cavity but are localized at the edges of the cavity. However, the solution for the far field, with admittance walls is difficult to evaluate [9].

1.4.3 MNM

The MNM for analyzing the MSA is an extension of the cavity model [9, 26, 27]. In this method, the electromagnetic fields underneath the patch and outside the patch are modeled separately. The patch is analyzed as a two-dimensional planar network, with a multiple number of ports located around the periphery. The multiport impedance matrix of the patch is obtained from its two-dimensional Green's function. The fringing fields along the periphery and the radiated fields are incorporated by adding an equivalent edge admittance network. The segmentation method is then used to find the overall impedance matrix. The radiated fields are obtained from the voltage distribution around the periphery. Appendix C details this method.

The above three analytical methods offer both simplicity and physical insight. In the latter two methods, the radiation from the MSA is calculated from the equivalent magnetic current distribution around the periphery of the radiating patch, which is obtained from the corresponding voltage distribution. Thus, the MSA analysis problem reduces to that of finding the edge voltage distribution for a given excitation and for a specified mode. These methods are accurate for regular patch geometries, but—except for MNM with contour integration techniques—they are not suited for arbitrary shaped patch configurations. For complex geometries, the numerical techniques described below are employed [9].

1.4.4 MoM

In the MoM, the surface currents are used to model the microstrip patch, and volume polarization currents in the dielectric slab are used to model the fields in the dielectric slab. An integral equation is formulated for the unknown currents on the microstrip patches and the feed lines and their images in the ground plane [28]. The integral equations are transformed into algebraic equations that can be easily solved using a computer. This method takes into account the fringing fields outside the physical boundary of the two-dimensional patch, thus providing a more exact solution. This book makes extensive use of a commercially available software IE3D [29] based on MoM to analyze various MSA configurations.

1.4.5 FEM

The FEM, unlike the MoM, is suitable for volumetric configurations. In this method, the region of interest is divided into any number of finite surfaces or volume elements depending upon the planar or volumetric structures to be analyzed [30]. These discretized units, generally referred to as finite elements, can be any well-defined geometrical shapes such as triangular elements for planar configurations and tetrahedral and prismatic elements for three-dimensional configurations, which are suitable even for curved geometry. It involves the integration of certain basis functions over the entire conducting patch, which is divided into a number of subsections. The problem of solving wave equations with inhomogeneous boundary conditions is tackled by decomposing it into two boundary value problems, one with Laplace's equation with an inhomogeneous boundary and the other corresponding to an inhomogeneous wave equation with a homogeneous boundary condition [10].

1.4.6 SDT

In the SDT, a two-dimensional Fourier transform along the two orthogonal directions of the patch in the plane of substrate is employed. Boundary conditions are applied in Fourier transform plane. The current distribution on the conducting patch is expanded in terms of chosen basis functions, and the resulting matrix equation is solved to evaluate the electric current distribution on the conducting patch and the equivalent magnetic current distribution on the surrounding substrate surface. The various parameters of the antennas are then evaluated [31].

1.4.7 FDTD Method

The FDTD method is well-suited for MSAs, as it can conveniently model numerous structural inhomogenities encountered in these configurations [10]. It can also predict the response of the MSA over the wide BW with a single simulation. In this technique, spatial as well as time grid for the electric and magnetic fields are generated over which the solution is required. The spatial discretizations along three Cartesian coordinates are taken to be same. The E cell edges are aligned with the boundary of the configuration and H-fields are assumed to be located at the center of each E cell. Each cell contains information about material characteristics. The cells containing the sources are excited with a suitable excitation function, which propagates along the structure. The discretized time variations of the fields are deter-

mined at desired locations. Using a line integral of the electric field, the voltage across the two locations can be obtained. The current is computed by a loop integral of the magnetic field surrounding the conductor, where the Fourier transform yields a frequency response.

The above numerical techniques, which are based on the electric current distribution on the patch conductor and the ground plane, give results for any arbitrarily shaped antenna with good accuracy, but they are time-consuming. These methods can be used to plot current distributions on patches but otherwise provide little of the physical insight required for antenna design.

1.5 Review of Various Broadband Techniques for MSAs

As mentioned earlier, the most serious limitation of the MSA is its narrow BW. The BW could be defined in terms of its VSWR or input impedance variation with frequency or in terms of radiation parameters. For the circularly polarized antenna, BW is defined in terms of the *axial ratio* (AR) [9]. Therefore, before describing the various methods for increasing the BW, the various definitions of the BW are described.

1.5.1 Definition of BW

The VSWR or impedance BW of the MSA is defined as the frequency range over which it is matched with that of the feed line within specified limits. The BW of the MSA is inversely proportional to its quality factor Q and is given by [32]

$$\mathrm{BW} = \frac{\mathrm{VSWR} - 1}{Q\sqrt{\mathrm{VSWR}}} \tag{1.1}$$

where VSWR is defined in terms of the input reflection coefficient Γ as:

$$\mathrm{VSWR} = \frac{1 + |\Gamma|}{1 - |\Gamma|} \tag{1.2}$$

The Γ is a measure of reflected signal at the feed-point of the antenna. It is defined in terms of input impedance Z_{in} of the antenna and the characteristic impedance Z_0 of the feed line as given below:

$$\Gamma = \frac{Z_{\text{in}} - Z_0}{Z_{\text{in}} + Z_0} \tag{1.3}$$

The BW is usually specified as frequency range over which VSWR is less than 2 (which corresponds to a return loss of 9.5 dB or 11% reflected power). Sometimes for stringent applications, the VSWR requirement is specified to be less than 1.5 (which corresponds to a return loss of 14 dB or 4% reflected power). Conversion of BW from one VSWR level to another can be accomplished by

$$\frac{\text{BW}_1}{\text{BW}_2} = \frac{(\text{VSWR}_1 - 1)}{\sqrt{\text{VSWR}_1}} \frac{\sqrt{\text{VSWR}_2}}{(\text{VSWR}_2 - 1)} \tag{1.4}$$

where BW_1 and BW_2 correspond to VSWR_1 and VSWR_2, respectively.

The variation of percentage BW for VSWR ≤ 2 and efficiency η of a square MSA with normalized substrate thickness h/λ_0 for two different values of ϵ_r (2.2 and 10) are given in Figure 1.4(a). Also, the variation of percentage BW with frequency for three commonly used values of h and $\epsilon_r = 2.32$ is given in Figure 1.4(b). The BW of a single-patch antenna increases with an increase in the substrate thickness and a decrease in the ϵ_r of the substrate [9, 33, 34]. The BW is approximately 15% for $\epsilon_r = 2.2$ and $h = 0.1\lambda_0$. The ϵ_r can be chosen close to 1 to obtain a broader BW. The larger thickness of the substrate gives rise to an increase in probe reactance

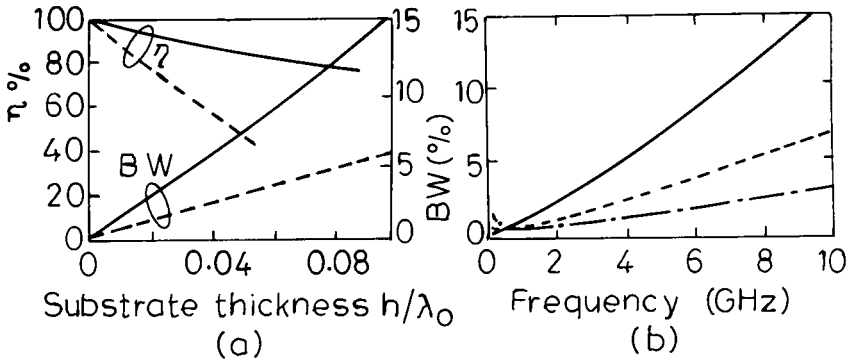

Figure 1.4 (a) Variation of percentage BW and efficiency of a square MSA versus h/λ_0. (——) $\epsilon_r = 2.2$, (- - -) $\epsilon_r = 10$ and (b) variation of percentage BW with frequency for three values of h and $\epsilon_r = 2.32$: (——) 0.318, (- - -) 0.159, (– – –) 0.079 cm.

for the coaxial feed and the excitation of surface waves, which reduces the efficiency η of the antenna as can be seen from Figure 1.4(a). The efficiency of the MSA is defined in Appendix C. The BW enhancement of the single regularly shaped MSA is discussed in Chapter 2.

The expressions for approximately calculating the percentage BW of the RMSA in terms of patch dimensions and substrate parameters is given by

$$\%\text{BW} = \frac{Ah}{\lambda_0\sqrt{\epsilon_r}}\sqrt{\frac{W}{L}} \tag{1.5}$$

where

$$A = 180 \text{ for } \frac{h}{\lambda_0\sqrt{\epsilon_r}} \leq 0.045$$

$$A = 200 \text{ for } 0.045 \leq \frac{h}{\lambda_0\sqrt{\epsilon_r}} \leq 0.075$$

$$A = 220 \text{ for } \frac{h}{\lambda_0\sqrt{\epsilon_r}} \geq 0.075$$

where W and L are the width and length of the RMSA. With an increase in W, BW increases. However, W should be taken less than λ to avoid excitation of higher order modes. For other regularly shaped patches, values of equivalent W can be obtained by equating the area with that of the RMSA as described in Chapter 2 [35, 36].

Another simplified relation for quick calculation of BW (in megahertz) for VSWR = 2 of the MSA operating at frequency f in gigahertz, with h expressed in centimeters, is given by [37]

$$\text{BW} \cong 50hf^2 \tag{1.6}$$

The BW can also be defined in terms of the antenna's radiation parameters. It is defined as the frequency range over which radiation parameters such as the gain, *half-power beamwidth* (HPBW), and sidelobe levels are within the specified minimum and maximum limits. This definition is more complete as it also takes care of the input impedance mismatch, which also contributes to change in the gain.

The expression for approximately calculating the directivity D of the RMSA is given by

$$D \cong 0.2W + 6.6 + 10 \log\left(1.6/\sqrt{\epsilon_r}\right) \text{ dB} \tag{1.7}$$

For other geometries, the values of equivalent W can be obtained by equating its area with that of the RMSA as described in Chapter 2 [35, 36].

The above definitions for BW are mainly for a linearly polarized MSA. For a circularly polarized MSA, the BW is generally limited by its AR. This BW is the frequency range over which AR is less than a maximum limit (e.g., 3 or 6 dB).

There are various techniques for increasing the BW of the MSAs. The main techniques used to increase the BW are presented briefly in the following sections.

1.5.2 Modified Shape Patches

The regular MSA configurations, such as rectangular and circular patches have been modified to rectangular ring [38] and circular ring [39], respectively, to enhance the BW. The larger BW is because of a reduction in the quality factor Q of the patch resonator, which is due to less energy stored beneath the patch and higher radiation. When a U-shaped slot is cut inside the rectangular patch, it gives a BW of approximately 40% for VSWR ≤ 2 [40]. Similar results are obtained when a U-slot is cut inside a circular or a triangular MSA [41, 42]. These configurations are discussed in detail in Chapter 6.

1.5.3 Planar Multiresonator Configurations

The planar stagger–tuned coupled multiple resonators yield wide BW in the same way as in the case of multistage tuned circuits. Several configurations are available yielding BW of 5–25% [43–49]. Various parasitic patches like narrow strips, shorted quarter-wavelength rectangular patches, and rectangular resonator patches have been gap-coupled to the central-fed rectangular patch. Three combinations of gap-coupled rectangular patches are shown in Figure 1.5. To reduce the criticality of the gap coupling, direct coupling as depicted in Figure 1.6 has been used to obtain broad BW. Both gap and direct (hybrid) coupling have been used with *circular MSAs* (CMSAs) and *equilateral triangular MSAs* (ETMSAs) to yield broad BW.

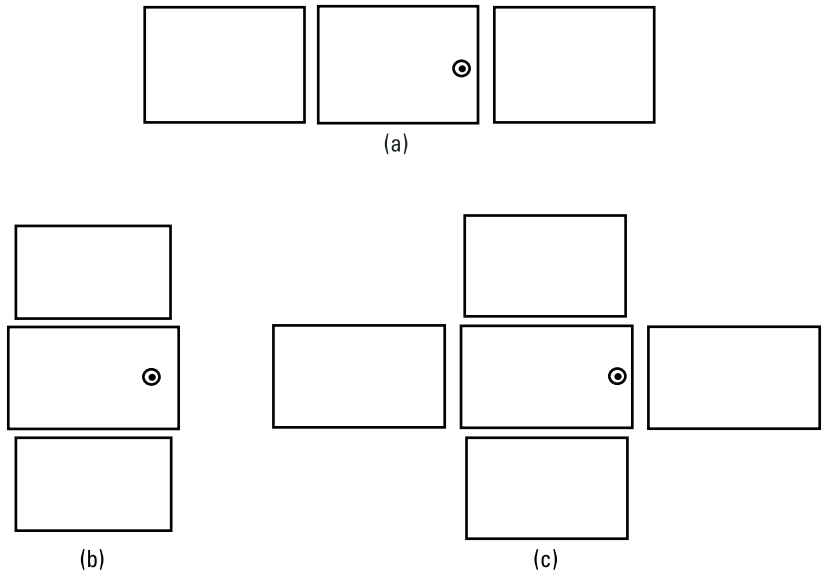

Figure 1.5 Various gap-coupled multiresonator RMSA configurations: (a) three RMSAs gap-coupled along radiating edges, (b) three RMSAs gap-coupled along nonradiating edges, and (c) five gap-coupled RMSAs.

These planar multiresonator configurations yield broad BW but have the following disadvantages:

- The large size, which makes them unsuitable as an array element;
- The variation in the radiation pattern over the impedance BW.

A modification of the multiresonator patches—to avoid the abovementioned problems—entails using five or six narrow strips that are gap-coupled along the width [49]. This yielded wide BW with a relatively small variation in pattern over the BW. Various broadband planar multiresonator configurations are covered in Chapter 3.

1.5.4 Multilayer Configurations

In the multilayer configuration, two or more patches on different layers of the dielectric substrate are stacked on each other. Based on the coupling mechanism, these configurations are categorized as electromagnetically coupled or aperture-coupled MSAs.

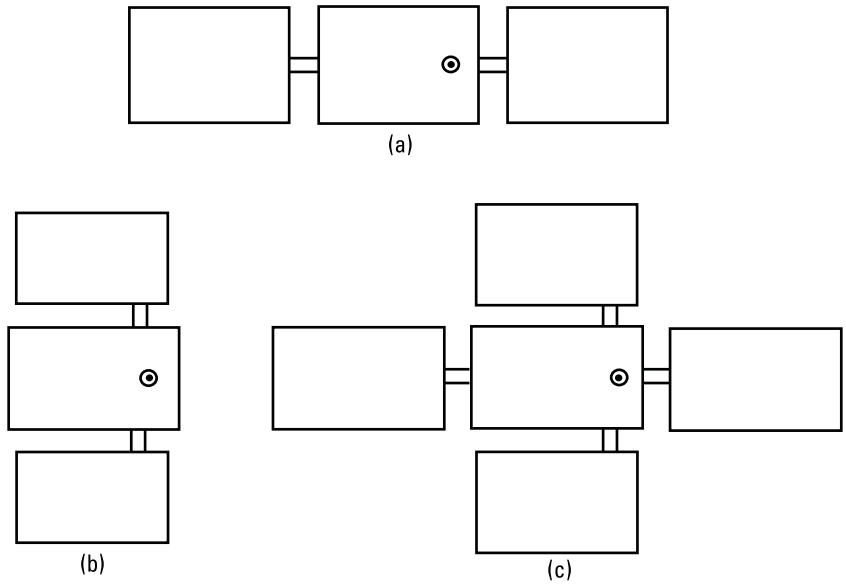

Figure 1.6 Various direct-coupled multiresonators: (a) three RMSAs direct-coupled along radiating edges, (b) three RMSAs direct-coupled along nonradiating edges, and (c) five direct-coupled RMSAs.

1.5.4.1 Electromagnetically Coupled MSAs

In the electromagnetically coupled MSA, one or more patches at the different dielectric layers are electromagnetically coupled to the feed line located at the bottom dielectric layer as shown in Figure 1.3(b). Alternatively, one of the patches is fed by a coaxial probe and the other patch is electromagnetically coupled. Either the bottom or top patch is fed with a coaxial probe as shown in Figure 1.7. The patches can be fabricated on different substrates, and accordingly the patch dimensions are to be optimized so that the resonance frequencies of the patches are close to each other to yield broad BW. These

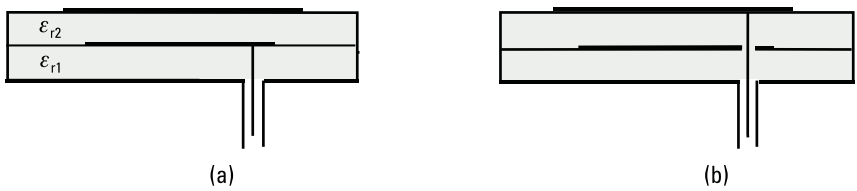

Figure 1.7 An electromagnetically coupled MSA, in which (a) the bottom patch is fed and (b) the top patch is fed.

two layers may be separated by either air-gap or foam yielding BW of 15–30% [50–56].

1.5.4.2 Aperture-Coupled MSAs

In the aperture-coupled MSA, the field is coupled from the microstrip feed line placed on the other side of the ground plane to the radiating patch through an electrically small aperture/slot in the ground plane, as shown in Figure 1.3(c). Two different dielectric substrates could be chosen, one for the patch and the other for the feed line to optimize the individual performances. The coupling to the patch from the feed line can be maximized by choosing the optimum shape of the aperture [14–16]. Two patches of rectangular or circular shapes, which are stacked on each other in different dielectric layers yield around 30% BW [57–60]. A BW of nearly 70% has been obtained by stacking patches with resonant apertures [61].

The multilayer broadband MSAs, unlike single-layer multiresonator configurations, show a very small degradation in radiation pattern over the complete VSWR BW. The drawback of these structures is the increased height, which is not desirable for conformal applications and increased back radiation for aperture-coupled MSAs. Multilayered configurations using both electromagnetic as well as aperture coupling are described in Chapter 4.

1.5.5 Stacked Multiresonator MSAs

The planar and stacked multiresonator techniques are combined to further increase the BW and gain. A probe-fed single rectangular or circular patch located on the bottom layer has been used to excite multiple rectangular or circular patches on the top layer, respectively [62, 63]. Besides increasing the BW, these configurations also provide an increase in gain as described in Chapter 5.

1.5.6 Impedance-Matching Networks for Broadband MSAs

The impedance-matching networks are used to increase the BW of the MSA. Some examples that provide about 10% BW are the rectangular MSA with a coplanar microstrip impedance-matching network and an electromagnetically coupled MSA with single-stub matching as shown in Figure 1.8 [12, 64–66].

1.5.7 Log-Periodic MSA Configurations

The concept of log-periodic antenna has been applied to MSA to obtain a multi-octave BW. In this configuration, the patch dimensions are increased

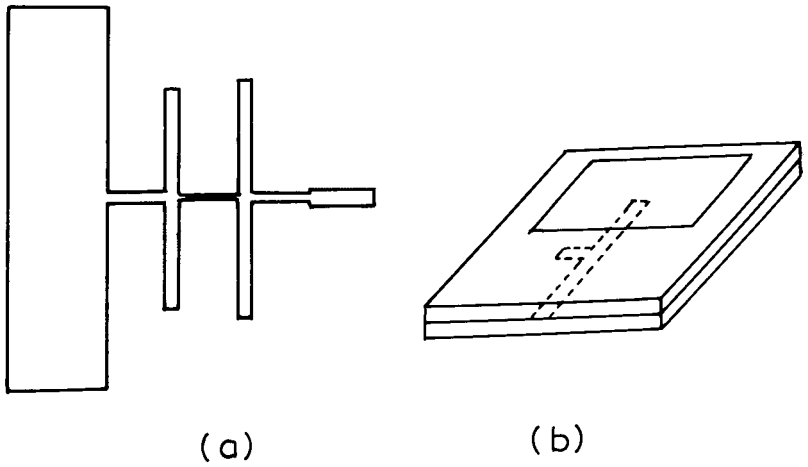

Figure 1.8 (a) Rectangular MSA with a coplanar microstrip impedance-matching network and (b) single-stub matched electromagnetically coupled MSA.

logarithmically and the subsequent patches are fed at 180° out of phase with respect to the previous patch [67–70]. The main disadvantage of this configuration is that the radiation pattern varies significantly over the impedance BW as described in Chapter 5.

1.5.8 Ferrite Substrate-Based Broadband MSAs

The multiresonant behavior of a patch on a ferrite substrate yields a broad BW of about three octaves by changing the magnetic field. Also, the dimensions of the patch are reduced because of the high dielectric constant of the ferrite substrate. However, the efficiency of these antennas is poor because of lossy substrate and requires external magnetic fields, which makes it bulky [71–73].

The methods for increasing the BW of MSA are continuously getting upgraded. The search for an ideal broadband MSA is still continuing. Perhaps a combination of various approaches would lead to an optimum broadband configuration.

1.6 Broadband Compact MSAs

The size of a half-wavelength ($\lambda/2$) RMSA is too large in the *ultra-high frequency* (UHF) band. There is a need for a compact MSA for personal

mobile communication and other applications. A shorted $\lambda/4$ RMSA has the same resonance frequency as that of a $\lambda/2$ RMSA, with half the area [74]. The resonance frequency reduces further as the width of the shorting plate decreases [74, 75]. Similarly, compact MSA in circular and triangular configurations is realized by placing shorting posts at the zero potential lines [76, 77]. A single shorting post yields a maximum reduction in the resonance frequency of the rectangular, circular, and triangular MSAs [78–80]. The compact antennas have also been realized by cutting slots in regularly shaped antennas. The requirements of these compact broadband MSAs will increase in the future due to the ever-growing miniaturization of communication systems. The BW of the compact MSA has been increased in both planar as well as multilayer configurations [81–83]. Compact and broadband compact MSAs are described in detail in Chapter 6.

1.7 Tunable and Dual-Band MSAs

Tunable MSAs are of interest in many systems as they can be tuned over a large frequency range. These tunable antennas provide an alternative to large-BW antennas, especially when a large BW is required for encompassing several narrowband channels. The tunable MSA is realized by changing the length of the small stub attached to the regularly shaped MSA [84, 85], or by changing the number of shorting posts used to make a compact configuration [74, 76, 77]. Tunability is also achieved by integrating active devices such as varactor or PIN diodes along with the MSA [86].

When an antenna must operate at two frequencies that are far apart, a dual-frequency antenna can be used to avoid the use of two separate antennas. When two or more resonance frequencies of a MSA are close to each other, a broad BW is obtained. When these are separated, dual-band operation is obtained. In general, all the methods described earlier for increasing the BW of MSAs can be utilized to obtain dual-band characteristics. In the single-layer MSA, dual-band operation is achieved by using either slot or shorting pins or varactor or optically tuned diodes or by selecting the proper length of a stub [9, 85–89]. In multilayer configurations, either electromagnetic or aperture coupling could be used for dual-frequency operation [90–92]. The separation between the two frequencies is obtained by adjusting the air gap between the two layers or by changing the dimensions of the patches. These configurations are described in Chapter 7.

1.8 Broadband Circularly Polarized MSAs

CP is particularly useful for a number of radar, communication, and navigation systems because the rotational orientations of the transmitter and the receiver antennas are unimportant in relation to the received signal strength. With linearly polarized signals, on the other hand, there will be only very weak reception if the transmitter and receiver antennas are nearly orthogonal. Also, the circularly polarized wave reverses its sense of polarization from right-hand to left-hand CP and vice versa after reflection from regular objects. The system will then tend to discriminate the reception of such reflected signals from other signals arising from direct paths on reflections from irregular shapes.

CP is generated when two orthogonal modes are excited in a phase quadrature with equal magnitude. A rectangular or circular MSA generates CP when fed at two orthogonal points with equal amplitude and 90° phase difference. CP can also be generated by using a single-feed MSA. Single-feed MSA configurations include diagonal fed nearly square, corner chopped square, and square with diagonal slot. Similar variations are possible for circular and triangular MSAs. Broadband CP is obtained by using dual-feed multiple planar or stacked patches, or single-feed MSA in a sequential rotation array configuration. The details of these CP configurations are presented in Chapter 8 [9, 10, 32, 93–98].

1.9 Broadband Planar Monopole Antennas

MSA in its regular shape cannot yield multi-octave BW because of its resonant nature. Some modification of the MSA configuration is required to obtain an octave BW. If a rectangular patch without the substrate and ground plane is fed at the edge by a coaxial feed with a perpendicular ground plane, then the patch will have an effective dielectric constant equal to 1 with large h. Both of these factors yield broad BW. This modified configuration can be thought of as a planar rectangular monopole antenna [99]. Other configurations such as triangular, hexagonal, circular, and elliptical monopoles also yield broad BW. An elliptical monopole with an ellipticity of 1.1 yields BW of 1:11 for VSWR $\leq$ 2 [100–102]. These configurations are discussed in detail in Chapter 9.

1.10 Summary

MSAs have several advantages over conventional microwave antennas, such as their light weight, small volume, and planar configuration. Various methods for analyzing MSAs are briefly described. These antennas are used in UHF to millimeter-wave frequency bands. The main limitation in the ever-increasing applications of these antennas is their narrow BW. Fortunately, the BW can be increased by using a thick substrate with a low dielectric constant. Other methods for increasing the BW of MSAs include planar gap-coupled and directly coupled multiresonators, stacked electromagnetically coupled or aperture-coupled patches, impedance-matching techniques, log-periodic configurations, and ferrite substrates. A U-slot loaded MSA is one of the most promising broadband antennas.

There is increasing demand for compact antennas. Various compact MSA configurations using shorting posts and slots have been described. The BW of the compact MSA increases with multiple resonator techniques. Various methods to realize tunable, dual-frequency, and circularly polarized MSAs are also covered. Variations of MSAs leading to planar monopole antennas are discussed for multi-octave BWs.

References

[1] Deschamps, G. A., "Microstrip Microwave Antennas," *Proc. 3rd USAF Symposium on Antennas,* 1953.

[2] Munson, R. E., "Single Slot Cavity Antennas Assembly," U.S. Patent No. 3713162, January 23, 1973.

[3] Munson, R. E., "Conformal Microstrip Antennas and Microstrip Phased Arrays," *IEEE Trans. Antennas Propagation,* Vol. AP-22, 1974, pp. 74–78.

[4] Howell, J. Q., "Microstrip Antennas," *IEEE Trans. Antennas Propagation,* Vol. AP-23, January 1975, pp. 90–93.

[5] Bahl, I. J., and P. Bhartia, *Microstrip Antennas,* Dedham, MA: Artech House, 1980.

[6] Carver, K. R., and J. W. Mink, "Microstrip Antenna Technology," *IEEE Trans. Antennas Propagation,* Vol. AP-29, January 1981, pp. 2–24.

[7] Mailloux, R. J., et al., "Microstrip Array Technology," *IEEE Trans. Antennas Propagation,* Vol. AP-29, January 1981, pp. 25–37.

[8] James, J. R., et al., "Some Recent Development in Microstrip Antenna Design," *IEEE Trans. Antennas Propagation,* Vol. AP-29, January 1981, pp. 124–128.

[9] James, J. R., and P. S. Hall, *Handbook of Microstrip Antennas,* Vol. 1, London: Peter Peregrinus Ltd., 1989.

[10] Lee, H. F., and W. Chen, *Advances in Microstrip and Printed Antennas,* New York: John Wiley & Sons, 1997.

[11] Sainati, R. A., *CAD of Microstrip Antennas for Wireless Applications,* Norwood, MA: Artech House, 1996.

[12] Pozar, D. M., and B. Kaufman, "Increasing the Bandwidth of a Microstrip Antenna by Proximity Coupling," *Electronics Letters,* Vol. 23, No. 8, 1987, pp. 368–369.

[13] Roy, J. S., et al., "Some Experimental Investigations on Electromagnetically Coupled Microstrip Antennas on Two Layer Substrate," *Microwave Optical Tech. Letters,* Vol. 4, No. 9, 1991, pp. 236–238.

[14] Pozar, D. M., "Microstrip Antenna Aperture-Coupled to a Microstrip Line," *Electronics Letters,* Vol. 21, No. 2, 1985, pp. 49–50.

[15] Pozar, M., and S. D. Targonski, "Improved Coupling for Aperture-Coupled Microstrip Antennas," *Electronics Letters,* Vol. 27, No. 13, 1991, pp. 1129–1131.

[16] Rathi, V., G. Kumar, and K. P. Ray, "Improved Coupling for Aperture-Coupled Microstrip Antennas," *IEEE Trans. Antennas Propagation,* Vol. AP-44, No. 8, 1996, pp. 1196–1198.

[17] MacKinchan, J. C., et al., "A Wide Bandwidth Microstrip Sub-Array for Array Antenna Application Using Aperture Coupling," *IEEE AP-S Int. Symp. Digest,* 1989, pp. 878–881.

[18] Menzel, W., and W. Grabherr, "Microstrip Patch Antenna with Coplanar Feed Line," *IEEE Microwave and Guided Wave Letters,* Vol. 1, No. 11, 1991, pp. 340–342.

[19] Smith, R. L., and J. T. Williams, "Coplanar Waveguide Feed for Microstrip Patch Antenna," *Electronics Letters,* Vol. 28, No. 25, 1992, pp. 2272–2274.

[20] Bhatacharya, A. K., and R. Garg, "Generalized Transmission Line Model for Microstrip Patches," *IEE Proc. Microwaves, Antennas Propagation,* Pt. H, Vol. 132, No. 2, 1985, pp. 93–98.

[21] Dubost, G., and G. Beauquet, "Linear Transmission Line Model Analysis of a Circular Patch Antenna," *Electronics Letters,* Vol. 22, October 1986, pp. 1174–1176.

[22] Babu, S., I. Singh, and G. Kumar, "Improved Linear Transmission Line Model for Rectangular, Circular and Triangular Microstrip Antennas," *IEEE AP-S Int. Symp. Digest,* July 1997, pp. 614–617.

[23] Lo, Y. T., D. Solomon, and W. F. Richards, "Theory and Experiment on Microstrip Antennas," *IEEE Trans. Antennas Propagation,* Vol. AP-27, March 1979, pp. 137–145.

[24] Richards, W. F., Y. T. Lo, and D. D. Harrison, "An Improved Theory for Microstrip Antennas and Applications," *IEEE Trans. Antennas Propagation,* Vol. AP-29, January 1981, pp. 38–46.

[25] Lo, T., and S. W. Lee, *Antenna Handbook,* New York: Van Nostrand Reinhold, 1988.

[26] Okoshi, T., and T. Miyoshi, "The Planar Circuit—An Approach to Microwave Integrated Circuitry," *IEEE Trans. Microwave Theory Tech.,* Vol. 20, April 1972, pp. 245–252.

[27] Gupta, K. C., and P. C. Sharma, "Segmentation and Desegmentation Techniques for the Analysis of Two Dimensional Microstrip Antennas," *IEEE AP-S Int. Symp. Digest,* 1981, pp. 19–22.

[28] Newman, E. H., and P. Tulyathan, "Analysis of Microstrip Antennas Using Method of Moments," *IEEE Trans. Antennas Propagation,* Vol. AP-29, January 1981, pp. 47–53.

[29] IE3D 7.0, Zeland Software Inc., Fremont, CA.

[30] Silvester, P., "Finite Element Analysis of Planar Microwave Network," *IEEE Trans. Microwave Theory Tech.,* Vol. MTT-21, 1973, pp. 104–108.

[31] Itoh, T., and W. Menzel, "A Full-Wave Analysis Method for Open Microstrip Structure," *IEEE Trans. Antennas Propagation,* Vol. AP-29, January 1981, pp. 63–68.

[32] Pozar, D. M., and D. H. Schaubert, *Microstrip Antennas: The Analysis and Design of Microstrip Antennas and Arrays,* New York: IEEE Press, 1995.

[33] Derneryd, A. G. and A. G. Lind, "Extended Analysis of Rectangular Microstrip Resonator Antennas," *IEEE Trans. Antennas Propagation,* Vol. AP–27, November 1979, pp. 846–849.

[34] James, J. R., P. S. Hall, and C. Wood, *Microstrip Antenna Theory and Design,* London: Peter Peregrinus, 1981.

[35] Ray, K. P., "Broadband, Dual-Frequency and Compact Microstrip Antennas," Ph.D. thesis, Indian Institute of Technology, Bombay, India, 1999.

[36] Ray, K. P., and G. Kumar, "Determination of the Resonant Frequency of Microstrip Antennas," *Microwave Optical Tech. Letters,* Vol. 23, No. 2, 1999, pp. 114–117.

[37] Johnson, R. C., *Antenna Engineering Handbook,* 3rd ed., New York: McGraw-Hill, 1993.

[38] Palanisamy, V., and R. Garg, "Rectangular Ring and H-Shaped Microstrip Antennas Alternative to Rectangular Patch Antennas," *Electronics Letters,* Vol. 21, No. 19, 1985, pp. 874–876.

[39] Chew, W. C., "A Broadband Annular Ring Microstrip Antennas," *IEEE Trans. Antennas Propagation,* Vol. AP-30, September 1982, pp. 918–922.

[40] Huynh, T., and K. F. Lee, "Single-Layer Single-Patch Wideband Microstrip Antenna," *Electronics Letters,* Vol. 31, No. 16, 1995, pp. 1310–1312.

[41] Luk, K. M., K. F. Lee, and W. L. Tam, "Circular U-Slot Patch with Dielectric Superstrate," *Electronics Letters,* Vol. 33, No. 12, 1997, pp. 1001–1002.

[42] Wong, K. L., and Hsu W. H., "Broadband Triangular Microstrip Antenna with U-Shaped Slot," *Electronics Letters,* Vol. 33, No. 25, 1997, pp. 2085–2087.

[43] Wood, C., "Improved Bandwidth of Microstrip Antennas Using Parasitic Elements," *Proc. IEE,* Pt. H, Vol. 127, 1980, pp. 231–234.

[44] Kumar, G., and K. C. Gupta, "Broadband Microstrip Antennas Using Additional Resonators Gap-Coupled to the Radiating Edges," *IEEE Trans. Antennas Propagation,* Vol. AP-32, December 1984, pp. 1375–1379.

[45] Kumar, G., and K. C. Gupta, "Nonradiating Edges and Four Edges Gap-Coupled Multiple Resonator, Broadband Microstrip Antennas," *IEEE Trans. Antennas Propagation,* Vol. AP-33, February 1985, pp. 173–178.

[46] Kumar, G., and K. C. Gupta, "Directly Coupled Multiple Resonator Wideband Microstrip Antennas," *IEEE Trans. Antennas Propagation,* Vol. AP-33, June 1985, pp. 588–593.

[47] Ray, K. P., and G. Kumar, "Multifrequency and Broadband Hybrid-Coupled Circular Microstrip Antennas," *Electronics Letters,* Vol. 33, No. 6, 1997, pp. 437–438.

[48] Bhatnagar, P. S., et al., "Hybrid Edge Gap and Directly Coupled Triangular Microstrip Antenna," *Electronics Letters,* Vol. 22, No. 16, 1986, pp. 853–855.

[49] Anandan, K., and K. G. Nair, "Compact Broadband Microstrip Antennas," *Electronics Letters,* Vol. 22, No. 20, 1986, pp. 1064–1065.

[50] Hall, P. S., C. Wood, and C. Garrett, "Wide Bandwidth Microstrip Antennas for Circuit Integration," *Electronics Letters,* Vol. 15, July 1979, pp. 458–460.

[51] Sabban, A., "A New Broadband Stacked Two-Layer Microstrip Antenna," *IEEE AP-S Int. Symp. Digest,* June 1983, pp. 63–66.

[52] Chen, A. H., A. Tulintseff, and R. M. Sorbello, "Broadband Two-Layer Microstrip Antenna," *IEEE AP-S Int. Symp. Digest,* Vol. 2, June 1984, pp. 251–254.

[53] Bhatnagar, P. S., et al., "Experimental Study of Stacked Triangular Microstrip Antenna," *Electronics Letters,* Vol. 22, No. 16, 1986, pp. 864–865.

[54] Araki, K., et al., "Numerical Analysis of Circular Disc Microstrip Antennas with Parasitic Elements," *IEEE Trans. Antennas Propagation,* Vol. AP-34, December 1986, pp. 1390–1394.

[55] Lee, R. Q., K. F. Lee, and J. Bobinchak, "Characteristics of a Two-Layer Electromagnetically Coupled Rectangular Patch Antenna," *Electronics Letters,* Vol. 23, No. 20, 1987, pp. 1070–1072.

[56] Roy, J. S., "A Broadband Microstrip Antenna," *Microwave Optical Tech. Letters,* Vol. 19, No. 4, 1998, pp. 307–308.

[57] Croq, F., A. Papiernik, and P. Brachart, "Wideband Aperture-Coupled Microstrip Subarray," *IEEE AP-S Int. Symp. Digest,* May 1990, pp. 1128–1131.

[58] Baumer, C., "Analysis of Slot Coupled Circular Microstrip Patch Antennas," *Electronics Letters,* Vol. 28, No. 15, 1992, pp. 1454–1455.

[59] El Yazidi, M., "Analysis of Aperture-Coupled Circular Microstrip Antenna," *Electronics Letters,* Vol. 29, No. 11, 1993, pp. 1021–1022.

[60] Luk, K. M., K. F. Tong, and T. M. Au, "Offset Dual Patch Microstrip Antenna," *Electronics Letters,* Vol. 29, No. 18, 1993, pp. 1635–1636.

[61] Targonski, S. D., R. B. Waterhouse, and D. M. Pozar, "Design of Wideband Aperture Stacked Patch Microstrip Antenna," *IEEE Trans. Antennas Propagation,* Vol. AP-46, No. 9, 1998, pp. 1245–1251.

[62] Legay, H., and L. Shafai, "A New Stacked Microstrip Antenna with Large Bandwidth and High Gain," *IEEE AP-S Int. Symp. Digest,* 1993, pp. 948–951.

[63] Balakrishnan, B., and G. Kumar, "Wideband and High Gain Electromagnetically Coupled Circular Microstrip Antennas," *IEEE AP-S Int. Symp. Digest,* June 1998, pp. 1112–1115.

[64] Pues, H. G., and A. R. Van De Capelle, "An Impedance Matching Technique for Increasing the Bandwidth of Microstrip Antennas," *IEEE Trans. Antennas Propagation,* Vol. AP-37, No. 11, 1989, pp. 1345–1354.

[65] Pues, H. G., and A. R. Van De Capelle, "Wideband Impedance Matching Microstrip Resonator Antennas," *Proc. IEE 2nd Int. Conf. Antennas Propagation,* Pt. 1, 1981, pp. 402–405.

[66] Fong, K. S., H. F. Pues, and M. J. Withers, "Wideband Multilayer Coaxial-Fed Microstrip Antenna Element," *Electronics Letters,* Vol. 21, May 1985, pp. 497–498.

[67] Hall, P. S., "Multi-Octave Bandwidth Log-Periodic Microstrip Antenna Array," *IEE Proc. Microwaves, Antennas Propagation,* Pt. H, Vol. 133, No. 2, April 1986, pp. 127–138.

[68] Kakkar, R., and G. Kumar, "Stagger Tuned Microstrip Log-Periodic Antennas," *IEEE AP-S Int. Symp. Digest,* July 1996, pp.1262–1265.

[69] Popovic, B. D., et al., "Broadband Quasi-Microstrip Antenna," *IEEE Trans. Antennas Propagation,* Vol. AP-43, No. 10, 1995, pp. 1148–1152.

[70] Gitin, M. M., et al., "Broadband Characterization of Millimeter-Wave Log-Periodic Antennas by Photoconductive Sampling," *IEEE Trans. Antennas Propagation,* Vol. AP-42, No. 3, 1994, pp. 335–339.

[71] Mishra, R. K., S. S. Patnaik, and N. Das, "Tuning of Microstrip Antenna on Ferrite Substrate," *IEEE Trans. Antennas Propagation,* Vol. AP-41, No. 2, 1993, pp. 230–233.

[72] Pozar, D. M., and V. Sanchez, "Magnetic Tuning of a Microstrip Antenna on a Ferrite Substrate," *Electronics Letters,* Vol. 24, June 1988, pp. 729–731.

[73] Das, N., S. K. Chowdhury, and J. S. Chatterjee, "Circular Microstrip Antenna on Ferrimagnetic Substrate," *IEEE Trans. Antennas Propagation,* Vol. AP-31, January 1983, pp. 188–190.

[74] Hirasawa, K., and M. Haneishi, *Analysis, Design, and Measurement of Small and Low-Profile Antennas,* Norwood, MA: Artech House, 1992.

[75] Sanad, M., "Effect of the Shorting Posts on Short Circuit Microstrip Antennas," *IEEE AP-S Int. Symp. Digest,* 1994, pp. 794–797.

[76] Satpathy, S., K. P. Ray, and G. Kumar, "Compact Shorted Variations of Circular Microstrip Antennas," *Electronics Letters,* Vol. 34, No. 2, 1998, pp. 137–138.

[77] Satpathy, S., G. Kumar, and K. P. Ray, "Compact Shorted Variations of Triangular Microstrip Antennas," *Electronics Letters,* Vol. 34, No. 8, 1998, pp. 709–711.

[78] Waterhouse, R., "Small Microstrip Patch Antenna," *Electronics Letters,* Vol. 31, No. 8, 1995, pp. 604–605.

[79] Wong, K.-L., and S. C. Pan, "Compact Triangular Microstrip Antenna," *Electronics Letters,* Vol. 33, No. 6, 1997, pp. 433–434.

[80] Satpathy, S., K. P. Ray, and G. Kumar, "Compact Microstrip Antennas Using a Single Post," *Proc. NSAML,* New Delhi, India, March 1998, pp. 69–72.

[81] Ray, K. P., and G. Kumar, "Wideband Gap-Coupled Compact Sectoral Microstrip Antennas," *Proc. ISAP–2000,* August 2000.

[82] Ray, K. P., and G. Kumar, "Compact Gap-Coupled Shorted 90° Sectoral Microstrip Antennas for Broadband and Dual Band Operations," *Microwave Optical Tech. Letters,* Vol. 26, No. 3, 2000, pp. 143–145.

[83] Waterhouse R. B., "Broadband Stacked Shorted Patch," *Electronics Letters,* Vol. 35, No. 2, 1999, pp. 98–99.

[84] Plessis, M. Du., and J. H. Cloete, "Tuning Stub for Microstrip Patch Antenna," *IEEE AP-S Int. Symp. Digest,* June 1993, pp. 964–967.

[85] Ray, K. P., and G. Kumar, "Tunable and Dual-Band Circular Microstrip Antenna with Stubs," *IEEE Trans. Antennas Propagation,* Vol. 48, July 2000, pp. 1036–1039.

[86] Bhartia, P., and I. J. Bahl, "A Frequency Agile Microstrip Antenna," *IEEE AP-S Int. Symp. Digest,* May 1982, pp. 304–307.

[87] Maci, S., and G. B. Gentili, "Dual-Frequency Patch Antennas," *IEEE AP Magazine,* Vol. 39, No. 6, 1997, pp. 13–19.

[88] Schaubert, H., et al., "Microstrip Antennas with Frequency Agility and Polarization Diversity," *IEEE Trans. Antennas Propagation,* Vol. AP-29, January 1981, pp.118–123.

[89] Richards, W. F., S. E. Davidson, and S. A. Long, "Dual Band Reactively Loaded Microstrip Antenna," *IEEE Trans. Antennas Propagation,* Vol. AP-33, May 1985, pp. 556–561.

[90] Long, S. A., and M. D. Walton, "A Dual-Frequency Stacked Circular-Disc Antenna," *IEEE Trans. Antennas Propagation,* Vol. AP-27, March 1979, pp. 270–273.

[91] Syankal, M., and H. R. Hassani, "Characteristics of Stacked Rectangular and Triangular Patch Antennas for Dual Band Application," *Proc. IEE 8th International Conference on Antennas and Propagation,* Edinburgh, Scotland, March 1993.

[92] Yazdi, M. L., M. Himdi, and J. P. Daniel, "Aperture-Coupled Microstrip Antenna for Dual Frequency Operation," *Electronics Letters,* Vol. 29, No. 17, 1993, pp. 1506–1508.

[93] Sharma, P. C., and K. C. Gupta, "Analysis and Optimized Design of Single Feed Circularly Polarized Microstrip Antennas," *IEEE Trans. Antennas Propagation,* Vol. 31, No. 6, 1983, pp. 949–955.

[94] Targonski, S. D., and D. M. Pozar, "Design of Wideband Circularly Polarized Aperture-Coupled Microstrip Antennas," *IEEE Trans. Antennas Propagation,* Vol. 41, No. 2, 1993, pp. 214–220.

[95] Pozar, D. M., and S. M. Duffy, "A Dual-Band Circularly Polarized Aperture-Coupled Stacked Microstrip Antenna for Global Positioning Satellite," *IEEE Trans. Antennas Propagation,* Vol. 45, No. 11, 1997, pp. 1618–1625.

[96] Bhattacharya, A. K., and L. Shafai, "A Wider Band Microstrip Antenna for Circular Polarization," *IEEE Trans. Antennas Propagation,* Vol. 36, No. 2, 1988, pp. 157–163.

[97] Kraft, U. R., "An Experimental Study on 2 × 2 Sequential Rotation Arrays with Circularly Polarized Microstrip Radiators," *IEEE Trans. Antennas Propagation,* Vol. AP-45, No. 10, 1997, pp. 1459–1466.

[98] Iwasaki, H., T. Nakajima, and Y. Suzuki, "Gain Improvement of Circularly Polarized Array Antenna Using Linearly Polarized Elements," *IEEE Trans. Antennas Propagation,* Vol. 43, No. 6, 1995, pp. 604–608.

[99] Ray, K. P., et al., "Broadband Planar Rectangular Monopole Antennas," *Microwave Optical Tech. Letters,* Vol. 28, No. 1, 2001, pp. 55–59.

[100] Honda, S., et al., "A Disc Monopole Antenna with 1:8 Impedance BW and Omnidirectional Radiation Pattern," *Proc. ISAP,* Sapporo, Japan, 1992, pp. 1145–1148.

[101] Hammoud, M., P. Poey, and F. Colombel, "Matching the Input Impedance of a Broadband Disc Monopole," *Electronics Letters,* Vol. 29, February 1993, pp. 406–407.

[102] Agarwall, N. P., G. Kumar, and K. P. Ray, "Wideband Planar Monopole Antennas," *IEEE Trans. Antennas Propagation,* Vol. 46, No. 2, 1998, pp. 294–295.

2

Regularly Shaped Broadband MSAs

2.1 Introduction

An MSA in its simple form consists of a radiating patch on one side of a thin dielectric substrate backed by a ground plane. The radiating patch could be of any arbitrary shape, but it is generally taken as a regular shape for the ease of analysis and understanding of the antenna characteristics [1–6]. This chapter considers various regularly shaped MSAs, such as rectangular, circular, semicircular, equilateral triangular, 30°–60°–90° triangular, and annular ring patches. In addition, their characteristics, such as input impedance, BW, radiation pattern, and gain for various substrates, are described.

The BW of the MSA is directly proportional to the substrate thickness h and inversely proportional to the square root of its dielectric constant ϵ_r as described in Chapter 1. As a result, a thicker substrate with a low dielectric constant is generally used to obtain broad BW. One of the commonly used substrates for MSA is fiberglass-reinforced synthetic substrate, whose ϵ_r is typically between 2.1 to 2.6. This substrate has low dielectric loss (tan δ in the range of 0.0006 to 0.002) resulting in better efficiency, η. For low-cost applications or for initial design and testing, inexpensive glass-epoxy substrate (ϵ_r in the range of 3.8 to 4.7) is used. Sometimes, air or foam substrate (ϵ_r = 1–1.1) is used to enhance the BW. Alternatively, suspended microstrip configuration can be used; this increases the total thickness and decreases the effective dielectric constant of the patch.

2.2 RMSAs

One of the simplest and widely used MSA configurations is the RMSA. Figure 2.1 shows the top and side views of a coaxial-fed RMSA along with the coordinate system. A rectangular patch is defined by its length L and width W. For a simple microstrip line, the width is much smaller than the wavelength. However, for the RMSA, the width is comparable to the wavelength to enhance the radiation from the edges. Since the substrate thickness is much smaller than the wavelength, the RMSA is considered to be a two-dimensional planar configuration for analysis.

For the fundamental TM_{10} mode, the length L should be slightly less than $\lambda/2$, where λ is the wavelength in the dielectric medium. Here, λ is equal to $\lambda_0/\sqrt{\epsilon_e}$, where λ_0 is the free-space wavelength and ϵ_e is the effective dielectric constant of the patch. The value of ϵ_e is slightly less than ϵ_r, because the fringing fields around the periphery of the patch are not confined in the dielectric substrate but are also spread in the air as shown in Figure 2.2(a). The expression for calculating the value of ϵ_e is given in Appendix B, which also accounts for the dispersion effect. However, for quick analysis or design, the following approximate formula for ϵ_e could be used [1]:

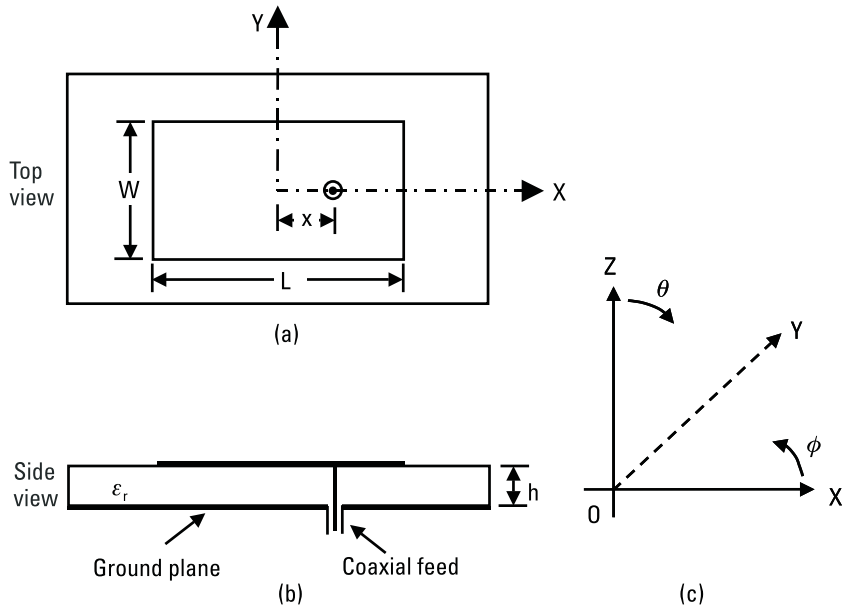

Figure 2.1 (a) Top and (b) side views of a rectangular MSA and (c) coordinate system.

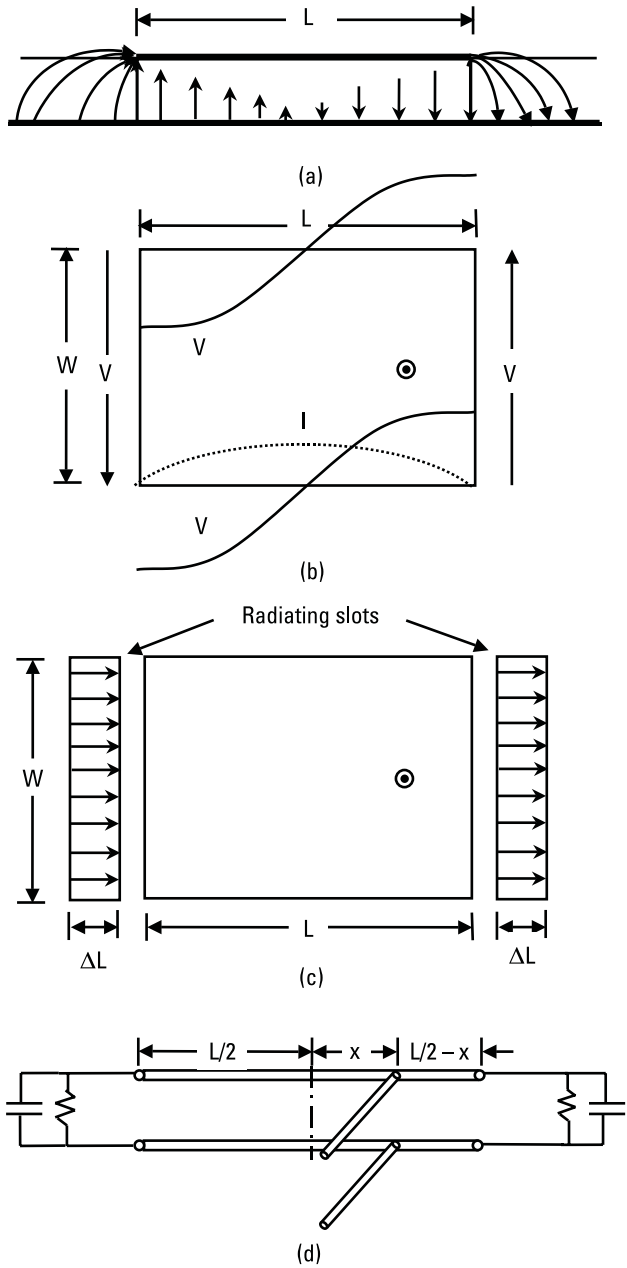

Figure 2.2 Fundamental TM_{10} mode of RMSA: (a) E-field distribution, (b) (——) voltage and (· · ·) current variation, (c) two radiating slots, and (d) equivalent transmission line model.

$$\epsilon_e = \frac{(\epsilon_r + 1)}{2} + \frac{(\epsilon_r - 1)}{2}\left[1 + \frac{10h}{W}\right]^{-1/2} \tag{2.1}$$

The fundamental TM_{10} mode implies that the field varies one $\lambda/2$ cycle along the length, and there is no variation along the width of the patch. The variation of voltage V around the periphery and the current I along the length is shown in Figure 2.2(b). Along the width of the patch, the voltage is maximum and current is minimum due to the open end. It may be observed from Figure 2.2(a) that the vertical components of the *electric field* (E-field) at the two edges along the width are in opposite directions and hence cancel one another in the broadside direction, whereas the horizontal components are in same direction and hence combine in the broadside direction. Therefore, the edges along the width are termed as radiating edges. The fields due to the sinusoidal distribution along the length cancel in the broadside direction, and hence the edges along the length are known as nonradiating edges. The fringing fields along the width can be modeled as radiating slots as shown in Figure 2.2(c).

An RMSA operating at TM_{10} mode can be visualized as a transmission line, because the field is uniform along the width and varies sinusoidally along the length. The fringing fields along the edges and radiation from the slots are modeled by their equivalent capacitance and radiation resistance, respectively as shown in Figure 2.2(d).

To account for the fringing fields, instead of adding the capacitor at the edges, the dimensions around the periphery of the patch can be extended outwards. This can be explained in terms of the two parallel rectangular plates of dimensions L and W, which are separated by a dielectric substrate of thickness h. If the fringing fields along the periphery are ignored, then the capacitance of the two parallel plates will be

$$C = \epsilon_o \epsilon_r \frac{WL}{h} \tag{2.2}$$

However, due to the fringing capacitance (because of the fringing fields), the effective capacitance C_e of the two parallel plates increases. One of the ways to account for the fringing capacitance is to extend the dimensions of the plate outward, and the value of C_e can be calculated from:

$$C_e = \epsilon_o \epsilon_r \frac{W_e L_e}{h} \tag{2.3}$$

where, L_e and W_e are the effective dimensions and are equal to:

$$L_e = L + 2\Delta L \tag{2.4}$$

$$W_e = W + 2\Delta W \tag{2.5}$$

The ΔL and ΔW are the extensions along the L and W, respectively. The expressions for calculating their values are given in Appendix B, which also accounts for the dispersion effect. Using these closed-form expressions, the variations of $\Delta L/h$ and ϵ_e with W/h for various values of ϵ_r are given in Figure 2.3. For a given value of ϵ_r, the values of $\Delta L/h$ and ϵ_e increase with an increase in W/h. These plots do not account for the dispersion effect at the higher frequencies. As the frequency increases, the electrical thickness of the substrate (i.e., h/λ_0) increases. The variations of $\Delta L/h$ and ϵ_e with $f.h$ (or h/λ_0) for three values of ϵ_r (2.3, 4.3, and 9.8) and a thickness of W/h (0.1, 1, and 10), obtained from expressions given in Appendix B, are plotted in Figure 2.4. The frequency is in gigahertz, and h is in millimeters. As the frequency increases, the fields are more confined to the substrate, hence $\Delta L/h$ decreases and ϵ_e increases.

For RMSA, generally $W >> h$, so for quick analysis or design, the extension in length may be approximately calculated by the following simple formula:

$$\Delta L = \frac{h}{\sqrt{\epsilon_e}} \tag{2.6}$$

Since the effective length of the patch is equal to $\lambda/2$, it can be calculated for a given resonance frequency f_0 as:

$$L_e = L + 2\Delta L = \frac{\lambda_0}{2\sqrt{\epsilon_e}} = \frac{c}{2f_0\sqrt{\epsilon_e}} \tag{2.7}$$

where c = velocity of light in free space = 3×10^{10} cm/sec. This expression simplifies to

$$L_e = \frac{15}{f_0\sqrt{\epsilon_e}} \tag{2.8}$$

where L_e is in cm and f_0 is in gigahertz. For a given length L, f_0 is calculated from

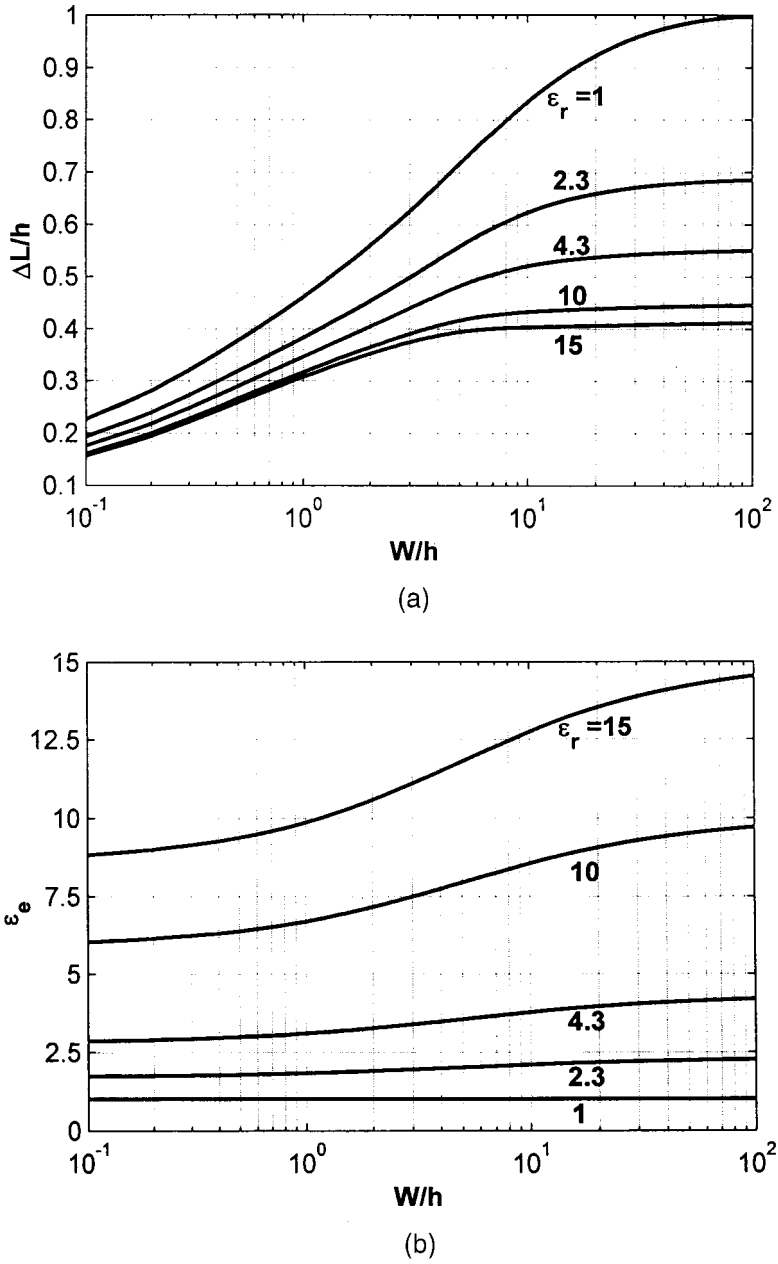

Figure 2.3 Variations of (a) $\Delta L/h$ and (b) ϵ_e for various values of ϵ_r and W/h.

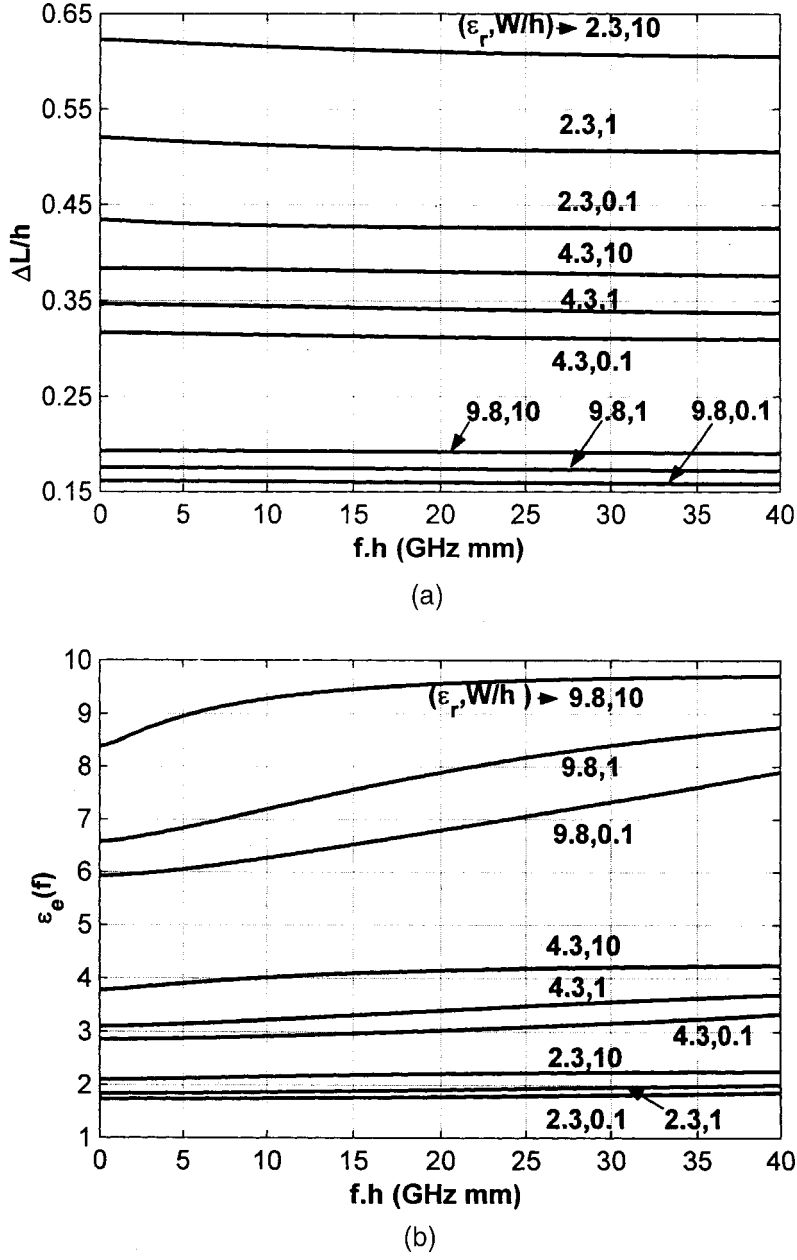

Figure 2.4 Variation of (a) $\Delta L/h$ and (b) $\epsilon_e(f)$ with $f.h$ for various values of ϵ_r and W/h.

$$f_0 = \frac{c}{2L_e\sqrt{\epsilon_e}} = \frac{15}{L_e\sqrt{\epsilon_e}} \tag{2.9}$$

In general, the resonance frequency of the RMSA excited at any TM_{mn} mode is obtained using the following expression [4]:

$$f_0 = \frac{c}{2\sqrt{\epsilon_e}}\left[\left(\frac{m}{L}\right)^2 + \left(\frac{n}{W}\right)^2\right]^{1/2} \tag{2.10}$$

where m and n are the modes along the L and W, respectively.

To calculate ϵ_e, the value of W should be known. For an RMSA to be an efficient radiator, W should be taken equal to a half wavelength corresponding to the average of the two dielectric mediums (i.e., substrate and air) [1].

$$W = \frac{c}{2f_0\sqrt{\dfrac{(\epsilon_r + 1)}{2}}} \tag{2.11}$$

The width W of the patch can be taken smaller or larger than the value obtained using (2.11). If W is smaller, then the BW and gain will decrease. If W is larger, then the BW increases due to the increase in the radiated fields. The directivity also increases due to the increase in the aperture area as given in (1.7). However, if W is too large, then the higher order modes could get excited. For example, the RMSA shown in Figure 2.1 is fed with a coaxial feed, and the feed is placed in the middle of the width to avoid the excitation of the orthogonal TM_{01} mode (i.e., where W may become $\lambda/2$). However, it will excite the TM_{02} mode, when W is equal to λ. In this case, the resonance frequency corresponding to the TM_{02} mode will be close to that of the TM_{10} mode, thereby causing interference leading to radiation pattern impurity.

The radiation pattern of the RMSA for the TM_{10} mode could be calculated by combining the radiation pattern of the two slots of length W_e and width ΔL on the infinite ground plane, which are spaced at a distance $L + \Delta L$. The normalized patterns in the E-plane (E_θ in $\phi = 0°$ plane) and the H-plane (E_ϕ in $\phi = 90°$ plane) are given by

$$E_\theta = \frac{\sin\left(\dfrac{k_0 \Delta L \sin\ \theta}{2}\right)}{\dfrac{k_0 \Delta L \sin\ \theta}{2}} \cos\left(\frac{k_0 (L + \Delta L)}{2} \sin\ \theta\right) \tag{2.12}$$

$$E_\phi = \frac{\sin\left(\dfrac{k_0 W_e}{2} \sin\ \theta\right)}{\dfrac{k_0 W_e}{2} \sin\ \theta} \cos\ \theta \tag{2.13}$$

where θ is the angle measured from the broadside as shown in Figure 2.1. For thin substrates, the normalized expression for E_θ reduces to

$$E_\theta = \cos\left(\frac{k_0 (L + \Delta L)}{2} \sin\ \theta\right) \tag{2.14}$$

The radiated power is obtained by integrating the radiated fields, from where the radiation resistance can be obtained as described in Appendix C. Another way of finding the total radiation resistance is by first calculating the radiation resistance R_r of the slot, which is approximately given by

$$\begin{aligned} R_r &= 120 \frac{\lambda_0}{W_e} && \text{for } W_e > 2\lambda_0 \\ R_r &= \frac{1}{\left[\dfrac{W_e}{120\lambda_0} - \dfrac{1}{60\pi^2}\right]} && \text{for } 0.35\lambda_0 < W_e \leq 2\lambda_0 \\ R_r &= 90\left(\frac{\lambda_0}{W_e}\right)^2 && \text{for } W_e \leq 0.35\lambda_0 \end{aligned} \tag{2.15}$$

Instead of using the above expressions, the following single-line formula could be used with better accuracy [4]

$$R_r = \frac{w_e^2}{6(60 + w_e^2)} \tag{2.16}$$

where $w_e = k_0 W_e$ and k_0 = free-space wave propagation constant = $2\pi/\lambda_0$.

For the fundamental TM_{10} mode, since the voltage is maximum and the current is minimum at the edges, the input impedance of the RMSA varies from a zero value at its center to the maximum value at the radiating edges. To obtain impedance matching with the coaxial probe (generally a 50-Ω feed line), the feed point should be placed at the location where the input impedance of the antenna matches the characteristic impedance of the feed.

For the coaxial feed at a distance x from the center, the input impedance of the RMSA at resonance can be approximately calculated as:

$$R_{\text{in}} = R_e \sin^2\left(\frac{\pi x}{L}\right) \qquad \text{for } 0 \le x \le L/2 \tag{2.17}$$

where

$$R_e = \frac{1}{2(G_r + G_m)} \tag{2.18}$$

where $G_r = 1/R_r$ is the slot conductance and G_m is the mutual conductance, which accounts for the mutual coupling between the two slots and is given by

$$G_m = G_r F_g \tag{2.19}$$

$$F_g = J_0(l) + \frac{p^2}{24 - p^2} J_2(l) \tag{2.20}$$

where $l = k(L + \Delta L)$, $p = k\Delta L$, $J_0(l)$ and $J_2(l)$ are zero- and second-order Bessel functions, respectively.

This formulation for input resistance neglects the conductor loss corresponding to the radiating patch and the ground plane and the dielectric loss due to the substrate. Hence, it always predicts the higher value of the input resistance. A detailed analysis procedure based on MNM is given in Appendix C, which accounts for all these losses.

Instead of coaxial feed, a microstrip line feed could also be used to excite the antenna. The RMSA can be fed by a microstrip line along its nonradiating edge at a distance x from the center, which is same as that of the coaxial feed (because the impedance remains uniform along the width) as shown in Figure 2.5(a). However, if the value of W is comparable to L,

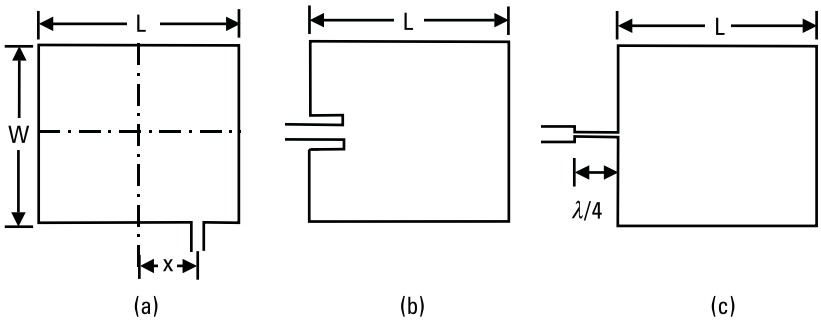

Figure 2.5 RMSA with microstrip line feed along its (a) nonradiating edge, (b) radiating edge with inset feed, and (c) radiating edge with quarter-wave transformer.

then the orthogonal TM_{01} mode may get excited. If the microstrip feed is placed along its radiating edge, then either an inset microstrip feed—as shown in Figure 2.5(b)—or a quarter-wave transformer could be used to transform the large input impedance at the edge to that of the 50Ω, as shown in Figure 2.5(c). The characteristic impedance Z_0 of the quarter-wave transformer is given by $\sqrt{50R_e}$, where R_e is the edge input resistance at the resonance.

The width of the quarter-wave microstrip line is calculated from its Z_0 using the expressions given in Appendix B. The variation of Z_0 of the microstrip line with W/h for various values of ϵ_r is given in Figure 2.6(a). With an increase in W/h or ϵ_r, Z_0 decreases. The variation of Z_0 with $f.h$ for various values of W/h and $\epsilon_r = 10$ is plotted in Figure 2.6(b). As the frequency increases, the fields are more confined to the substrate, which decreases W_e and hence Z_0 increases.

2.2.1 Parametric Study of RMSAs

A coaxial-fed RMSA of $L = 3$ cm and $W = 4$ cm is considered to study the effects of various parameters on its performance. The probe diameter is taken as 0.12 cm for the 50-Ω coaxial probe feed using an SMA connector. The substrate parameters are $\epsilon_r = 2.55$, $h = 0.159$ cm, and $\tan\delta = 0.001$. The antenna has been analyzed using commercially available IE3D software based on MoM [7]. The theoretical results obtained using this software are in good agreement with the reported measured and theoretical results [1–6]. The size of the ground plane is considered to be infinite unless finite ground plane size is specified.

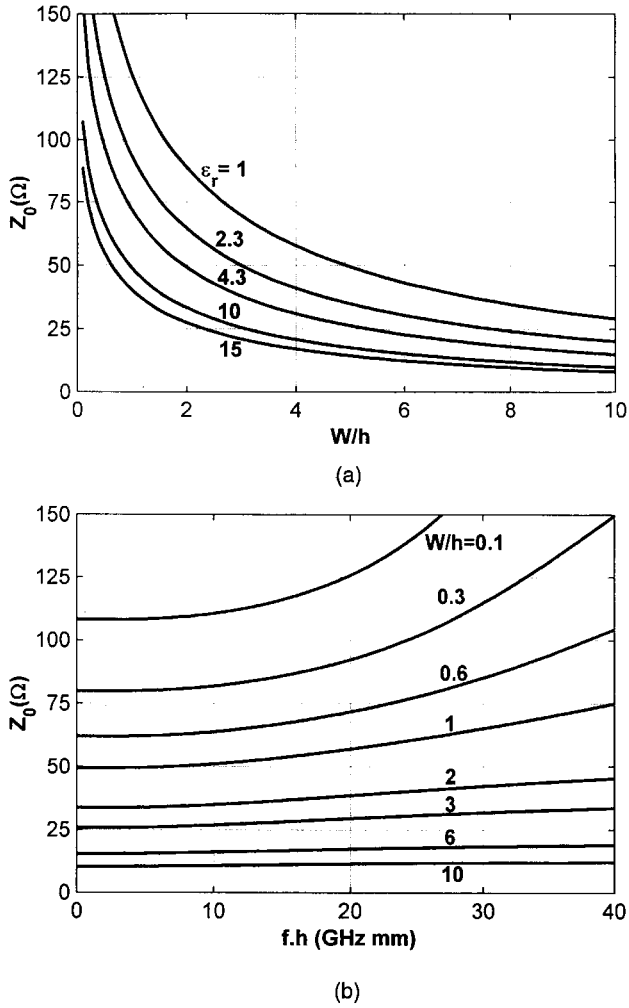

Figure 2.6 Variation of Z_0 with (a) W/h for various values of ϵ_r, and (b) $f.h$ for various values of W/h and $\epsilon_r = 10$.

2.2.1.1 Effect of Feed-Point Location

For three different feed-point locations from the center of the patch (i.e., $x = 0.55$, 0.6, and 0.65 cm), the variations of the input impedance Z_{in} and VSWR with frequency are shown in Figure 2.7(a, b). With an increase in frequency, the input impedance moves in the clockwise direction in the Smith chart. As x increases from 0.55 cm to 0.65 cm (i.e., the feed point is shifted toward the edge), the input impedance loci shifts in the right

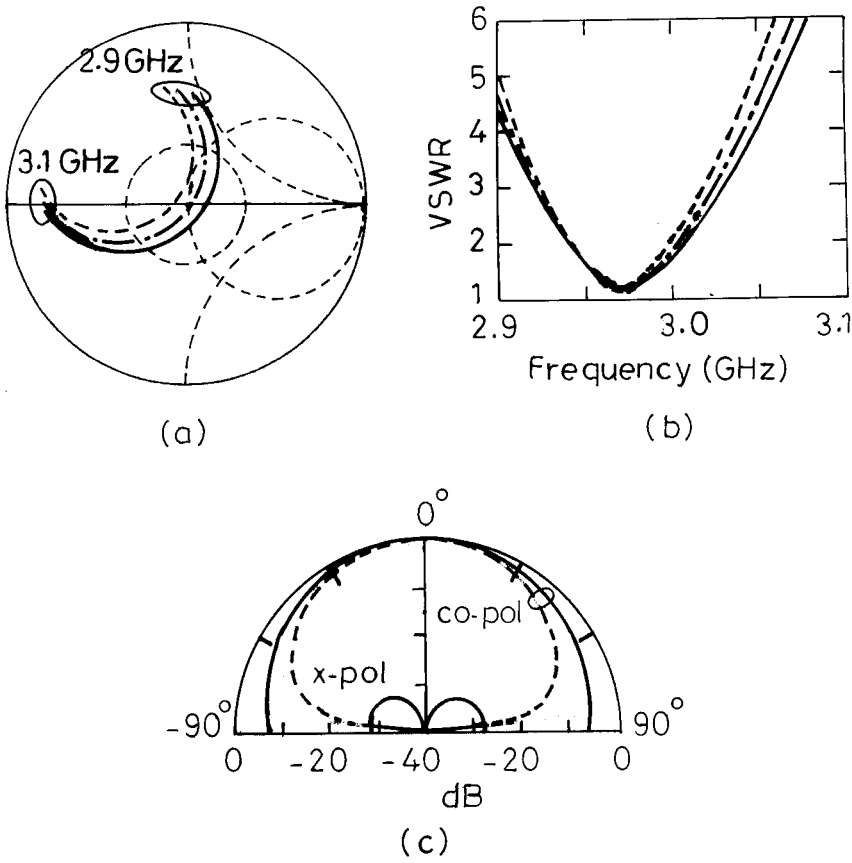

Figure 2.7 (a) Input impedance and (b) VSWR plots of the RMSA for three different values of x, (- - -) 0.55, (– – –) 0.60, and (——) 0.65 cm, and (c) its radiation pattern at 2.975 GHz for x = 0.65 cm; (——) E-plane copolar and cross-polar and (- - -) H-plane copolar.

direction on the Smith chart implying that the impedance is increasing. Looking at only the VSWR plots, the impedance variation with change in the feed point is not apparent but is obvious from the impedance plots. The resonance frequency of the RMSA obtained using IE3D is 2.974 GHz. The resonance frequency calculated using (2.9), (2.1), (2.4), and (2.6) is 3.003 GHz, which is within 1% of the above value, thereby validating the simplified expressions.

A perfect match with a 50-Ω feed line is obtained for x = 0.59 cm, which gives a BW of 60 MHz for VSWR ≤ 2; however, it is not the maximum BW. A larger BW of 64 MHz for x = 0.65 cm is obtained for which Z_{in}

at the resonance is 62Ω. The reason will be obvious if one sees the impedance variation on the Smith chart. For x = 0.65 cm, the input impedance plot crosses the VSWR = 2 circle at the points, which are closer to diameter of the circle, implying larger frequency range within the circle, and hence larger BW. However, the maximum BW of 65 MHz is obtained for x = 0.67 cm, for which R_{in} = 66Ω. In this case, the impedance plot crosses the VSWR = 2 circle exactly along the diameter.

The radiation pattern in the E-plane (E_θ in the ϕ = 0° and 90° planes) and H-plane (E_ϕ in the ϕ = 90° plane) of the RMSA at 2.975 GHz for x = 0.65 cm is shown in Figure 2.7(c). The copolar components in the E and H planes are E_θ in ϕ = 0° and E_ϕ in ϕ = 90° planes, respectively. The radiation is in the broadside direction, and HPBW in the E and H planes are 105° and 76°, respectively. The directivity D and efficiency η are 7.4 dB and 87%, respectively, which gives a gain $G(= \eta D)$ of the antenna as 6.8 dB. The cross-polar components in the E and H planes are E_θ in ϕ = 90° and E_ϕ in ϕ = 0° planes, respectively. Since E_ϕ in the ϕ = 0° plane is less than 40 dB, it is not shown in the figure. The magnitude of E_θ in the ϕ = 90° plane is less than 40 dB in the broadside direction, and its maximum level is below 27 dB as compared to the maximum copolar level.

2.2.1.2 Effect of W

The width W of the RMSA has significant effect on the input impedance, BW, and gain of the antenna. For four different values of W (2, 3, 4, and 5 cm), the input impedance and VSWR plots for x = 0.65 cm are given in Figure 2.8.

With an increase in W from 2 cm to 5 cm, the following effects are observed:

- The resonance frequency decreases from 3.034 GHz to 2.962 GHz due to the increase in ΔL and ϵ_e.
- The input impedance at resonance decreases from 180Ω to 36Ω, because the radiation from the radiating edge increases, which decreases the radiation resistance as can be seen from (2.16).
- The BW of the antenna increases; however, it is not very evident from these plots, because the feed point is not optimum for the different widths. Accordingly, a better comparison will be obtained when the feed point is optimized for the individual widths.
- The aperture area of the antenna increases resulting in an increase in the directivity, efficiency, and, hence, gain. The HPBW in the

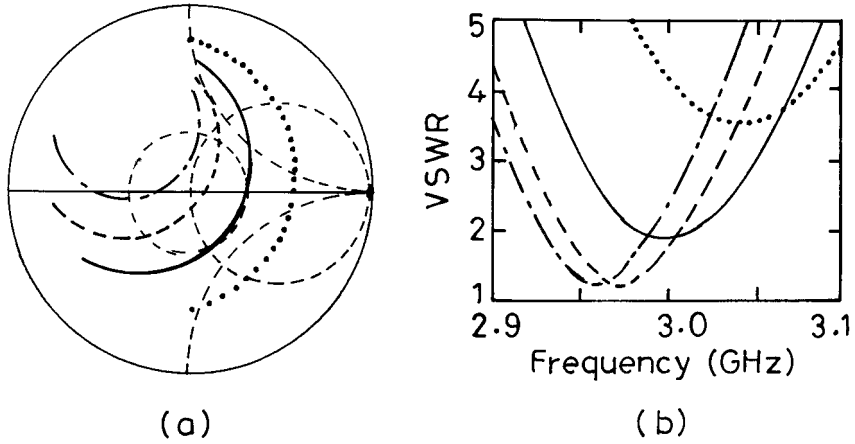

Figure 2.8 (a) Input impedance and (b) VSWR plots of the RMSA for four different W: (· · ·) 2, (——) 3, (- - -) 4, (– – –), 5 cm.

H-plane decreases, whereas it remains almost the same in the E-plane, because the increase in the width is in the H-plane.

With an increase in W, the input impedance decreases, so the feed point is shifted toward the edge to obtain input resistance R_{in} in the range of 50Ω to 65Ω; the results are summarized in Table 2.1. As W increases from 2 cm to 5 cm, the value of x is increased from 0.35 cm to 0.75 cm, and the BW increases from 42 MHz to 73 MHz. The HPBW in the E-plane remains around 105°, but in the H-plane, it decreases from 86° to 70°. The gain of the RMSA increases from 6.2 dB to 7.0 dB.

Table 2.1
Effect of W on the Performance of RMSA
(L = 3 cm, ϵ_r = 2.55, h = 0.159 cm, and tan δ = 0.001)

W (cm)	x (cm)	f_0 (GHz)	R_{in} (Ω)	BW (MHz)	Gain (dB)	HPBW (E- and H-planes)
2	0.35	3.034	57	42	6.2	(105, 86)°
3	0.50	2.993	61	54	6.5	(105, 81)°
4	0.65	2.973	62	64	6.8	(105, 76)°
5	0.75	2.962	53	73	7.0	(105, 70)°

2.2.1.3 Effect of h

The input impedance and VSWR plots for two different values of h (0.159 cm and 0.318 cm) are shown in Figure 2.9 for L = 3 cm, W = 4 cm, ϵ_r = 2.55, and x = 0.7 cm. With an increase in h from 0.159 cm to 0.318 cm, the following effects are observed:

- With the increase in h, the fringing fields from the edges increase, which increases the extension in length ΔL and hence the effective length, thereby decreasing the resonance frequency. On the other hand with the increase in h, the W/h ratio reduces, which decreases ϵ_e and hence increases the resonance frequency. However, the effect of the increase in ΔL is dominant over the decrease in ϵ_e. Therefore, the net effect is to decrease the resonance frequency.
- The input impedance plot moves clockwise (i.e., an inductive shift occurs) due to the increase in the probe inductance of the coaxial feed.
- The BW of the antenna increases from 64 MHz to 124 MHz. However, for the thicker substrate, this BW is not the maximum. It increases further to 135 MHz, when the feed point is optimized to x = 0.85 cm.

The directivity of the antenna increases marginally because the effective aperture area is increased marginally due to increase in ΔL. However, η

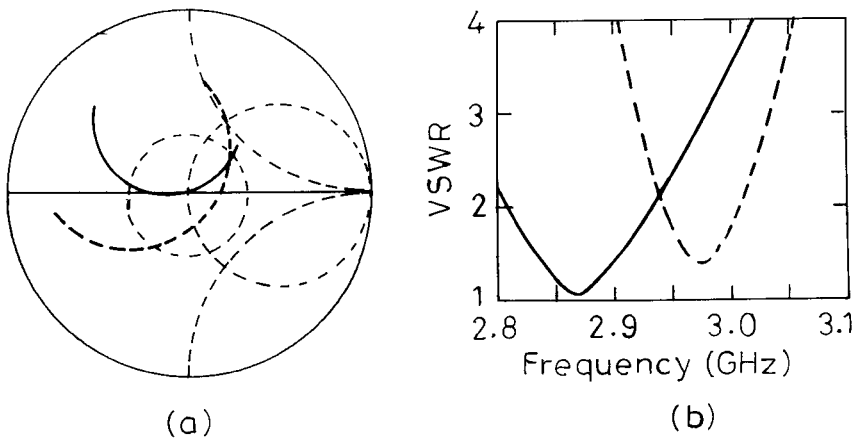

Figure 2.9 (a) Input impedance and (b) VSWR plots of the RMSA for two different values of h: (- - -) 0.159 and (——) 0.318 cm.

decreases from 87% to 81%, due to an increase in the cross-polar level from 28 dB to 22 dB and surface-wave propagation. Generally, η increases with an increase in the substrate thickness initially due to the increase in the radiated power, but thereafter, it starts decreasing because of the higher cross-polar level and excitation of the surface wave [8].

The surface waves get excited and travel along the dielectric substrate (i.e., between the ground plane and the dielectric-to-air interface due to total internal reflection). When these waves reach the edges of the substrate, they are reflected, scattered, and diffracted causing a reduction in gain and an increase in end-fire radiation and cross-polar levels. This also increases the cross coupling between the array elements. The excitation of surface waves is a function of ϵ_r and h. The power loss in the surface waves increases with an increase in the normalized thickness h/λ_0 of the substrate. The loss due to surface waves can be neglected when h satisfies the following criterion [9]:

$$\frac{h}{\lambda_0} \leq \frac{0.3}{2\pi\sqrt{\epsilon_r}} \tag{2.21}$$

The value of h = 0.318 cm is very close to the above criterion. When h is further increased to 0.5 cm, the BW increases to 256 MHz for x = 1.4 cm, but the surface waves increase considerably, thereby reducing η to 67%. Also, the cross-polar level increases to 17 dB because of the increase in the probe length. The probe acts as a top-loaded monopole antenna, whose radiation increases with the increase in its length. Since the monopole has only the E_θ component, it gets added vectorially to E_θ in the ϕ = 0° plane of RMSA, but it appears as cross-polar component in the ϕ = 90° plane.

2.2.1.4 Effect of ϵ_r

For RMSA with L = 3 cm, W = 4 cm, and h = 0.159 cm, when ϵ_r is decreased to 1, the resonance frequency increases to 4.541 GHz. The BW of the antenna is 167 MHz for the feed at x = 0.7 cm. This increase in BW is due to a decrease in ϵ_r and an increase in h/λ_0, because the resonance frequency has increased.

A better comparison of effect of ϵ_r is obtained when the antenna is designed to operate in the same frequency range for different values of ϵ_r. Therefore, with change in the dielectric constant from ϵ_{r1} to ϵ_{r2}, the L and W dimensions of the RMSA are scaled with a factor of $\sqrt{\epsilon_{e1}}/\sqrt{\epsilon_{e2}}$. For operation around 3 GHz, the dimensions of the patch for four different

values of ϵ_r (1, 2.55, 4.3, and 9.8) are shown in Table 2.2. The location of the feed point is optimized so that R_{in} is in the range of 50–65Ω for broader BW. With a decrease in ϵ_r from 9.8 to 1, the size of the patch increases and the BW increases from 30 MHz to 74 MHz due to increase in the fringing fields. Also, the gain of the antenna increases from 4.4 dB to 10.0 dB due to an increase in the aperture area.

2.2.1.5 Effect of Probe Diameter

An RMSA can be fed with different types of connectors, such as SMA, TNC, and N type connectors, depending upon the application. The diameters of these connectors are different, and as the probe diameter d increases, the probe inductance decreases for the same substrate thickness. Generally, the probe is modeled as an inductor, because the impedance of the probe is predominantly inductive. However, a more accurate value of the impedance of the coaxial probe is obtained by adding the reactance X_C of the capacitance between the patch and the ground plane and the probe inductance X_L, given by [10]:

$$X_C = -\frac{1}{\omega C} = -\frac{h}{\omega \epsilon_o \epsilon_r L_e W_e} \tag{2.22}$$

$$X_L = \frac{120\pi h}{\lambda_0}\left[\ln\left(\frac{2\lambda_0}{\pi d}\right) - 0.577\right] \tag{2.23}$$

For L = 3 cm, W = 4 cm, ϵ_r = 2.55, h = 0.159 cm, and x = 0.7 cm, the input impedance and VSWR plots for two connectors (SMA with d = 0.12 cm and N-type with d = 0.4 cm) are shown in Figure 2.10. With an increase in the probe diameter, the probe inductance decreases and hence

Table 2.2
Effect of ϵ_r on the Performance of RMSA
(h = 0.159 cm and tan δ = 0.001)

ϵ_r	L (cm)	W (cm)	x (cm)	f_0 (GHz)	R_{in} (Ω)	BW (MHz)	Gain (dB)
1	4.65	6.2	1.00	2.997	54	74	10.0
2.55	3.0	4.0	0.65	2.974	62	64	6.8
4.3	2.3	3.1	0.40	2.986	52	49	5.6
9.8	1.51	2.0	0.20	3.002	51	30	4.4

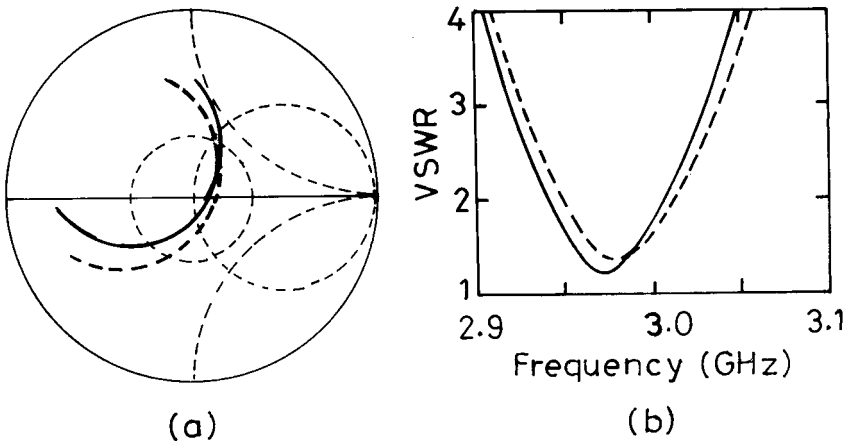

Figure 2.10 (a) Input impedance and (b) VSWR plots of the RMSA for two different connectors: (——) SMA and (- - -) N-type.

the impedance plot moves in the anticlockwise direction, and resonance frequency increases slightly.

2.2.1.6 Effect of Finite Ground Plane

The above results have been obtained using infinite ground plane. The transmission line, cavity model, and MNM only consider infinite ground plane. However, in practice, the size of the ground plane is finite. The finite ground plane effect can be taken into account by numerical techniques. However, it should be noted that the simulation time is least when the ground plane is infinite because then only the patch is analyzed with its perfect image. For the finite ground plane, on the other hand, both the patch and the ground plane are divided into number of segments and hence the simulation time increases. Also, as the size of the ground plane increases, the simulation time increases. The RMSA has been analyzed for various ground plane sizes using IE3D. It is observed that when the size of the ground plane is greater than the patch dimensions by approximately six times the substrate thickness all around the periphery, the results are similar to that of the infinite ground plane. For L = 3 cm, W = 4 cm, x = 0.7 cm, ϵ_r = 2.55, h = 0.159 cm, and tan δ = 0.001, input impedance and VSWR plots for infinite and finite ground planes (length = 5 cm and width = 6 cm) are shown in Figure 2.11(a, b). For this finite ground plane, the resonance frequency of the RMSA is almost the same but the input impedance is slightly higher than that of the infinite ground plane.

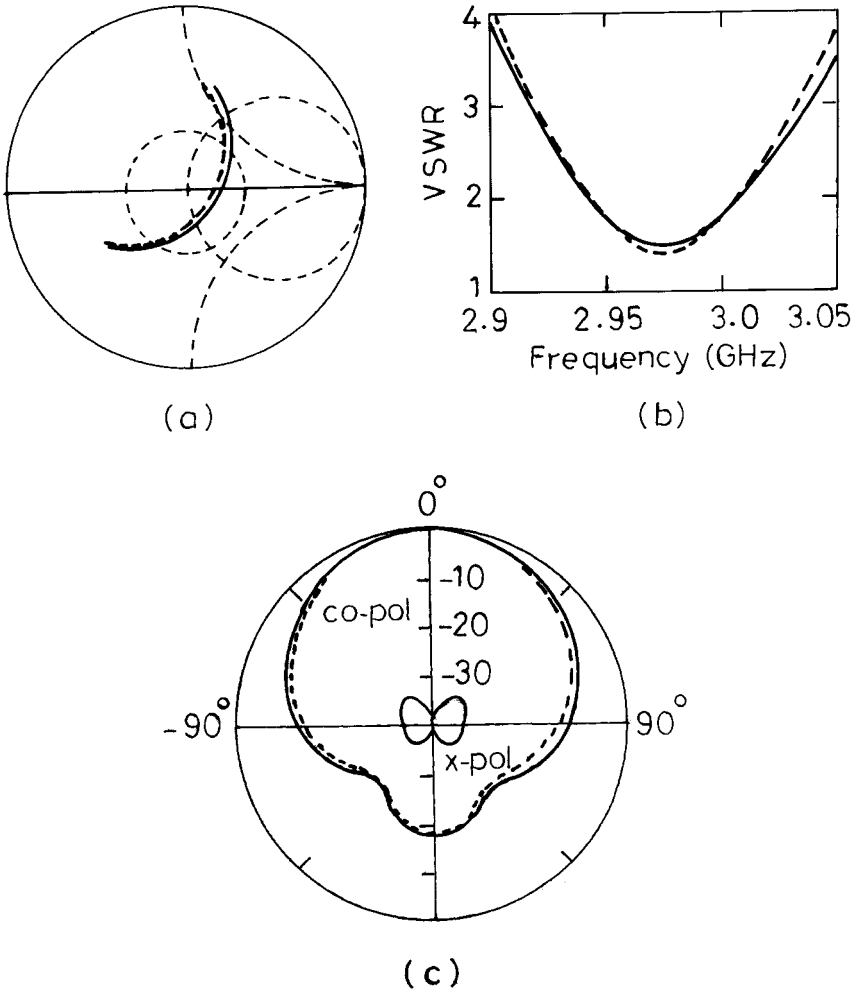

Figure 2.11 (a) Input impedance and (b) VSWR plots of the RMSA for (——) finite and (- - -) infinite ground planes, and (c) its radiation pattern on the finite ground plane: (——) E-plane copolar and cross-polar and (- - -) H-plane copolar.

The radiation pattern of the RMSA with finite ground plane is shown in Figure 2.11(c). For the finite ground plane, the back lobes are present, whereas for the infinite ground plane, there are no back lobes in the radiation pattern as shown in Figure 2.7(c).

2.2.1.7 Effect of Loss Tangent

Substrates having a low dielectric loss are expensive. For initial testing or for designing new MSA configurations, sometimes low-cost substrates are

used, but generally these have larger tan δ value. Hence, it is important to know the effect of tan δ on the performance of the antenna. For L = 3 cm, W = 4 cm, ϵ_r = 2.55, h = 0.159 cm, x = 0.7 cm, and three different values of tan δ (0.001, 0.01, and 0.02), the input impedance and VSWR plots are shown in Figure 2.12. With an increase in tan δ from 0.001 to 0.02, the loss in the dielectric material increases and hence Z_{in} decreases, so the impedance plot shifts toward the left side. The increase in loss tangent also decreases the impedance variation and increases the loss in the patch leading to an increase in BW and a decrease in efficiency.

A glass epoxy substrate, which is generally used as printed circuit board for analog and digital circuits, could be used for low-cost applications or for preliminary testing of new configurations of MSA. The ϵ_r of the substrate varies typically from 3.8 to 4.7 and tan δ varies from 0.01 to 0.03 in the microwave frequency band. For L = 3 cm, W = 4 cm, ϵ_r = 4.3, and h = 0.159 cm, the feed point is optimized for three values of tan δ (0.01, 0.02, and 0.03); the results are summarized in Table 2.3. When tan δ increases, the dielectric loss increases, which reduces the input impedance, so the feed point is shifted slightly toward the edge for impedance matching. As tan δ increases from 0.01 to 0.03, the resonance frequency remains at 2.321 GHz, but BW increases from 46 MHz to 75 MHz. The directivity D remains around 6.5 dB, but η decreases from 55% to 33%, thereby decreasing the gain from 3.9 dB to 1.7 dB.

2.2.1.8 Effect of Cover

MSAs are sometimes covered with a dielectric layer to protect them from the environment, or painted with dielectric material, or placed inside a

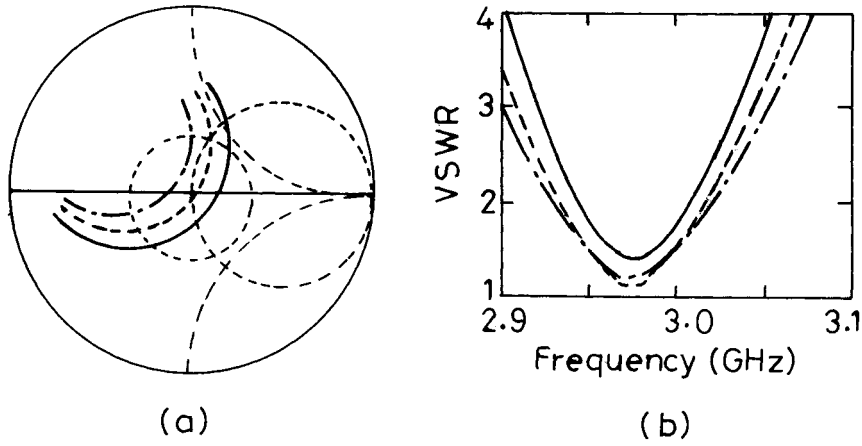

Figure 2.12 (a) Input impedance and (b) VSWR plots of the RMSA for different values of tan δ: (——) 0.001, (- - -) 0.01, and (– – –) 0.02.

Table 2.3
Effect of tan δ on the Performance of RMSA
(L = 3 cm, W = 4 cm, ϵ_r = 4.3, and h = 0.159 cm)

tan δ	x (cm)	R_{in} (Ω)	BW (MHz)	η (%)
0.01	0.7	60	46	55
0.02	0.8	54	61	40
0.03	0.9	53	75	33

radome with some air gap. The dielectric layer influences the characteristics of the antenna and, in general, reduces the resonance frequency due to increase in the ϵ_e [11].

The RMSA with L = 3 cm, W = 4 cm, ϵ_r = 2.55, h = 0.159 cm, and x = 0.7 cm is covered with a substrate with dielectric constant ϵ_{r1} and thickness h_1 as shown in Figure 2.13(a). For several values of h_1 with

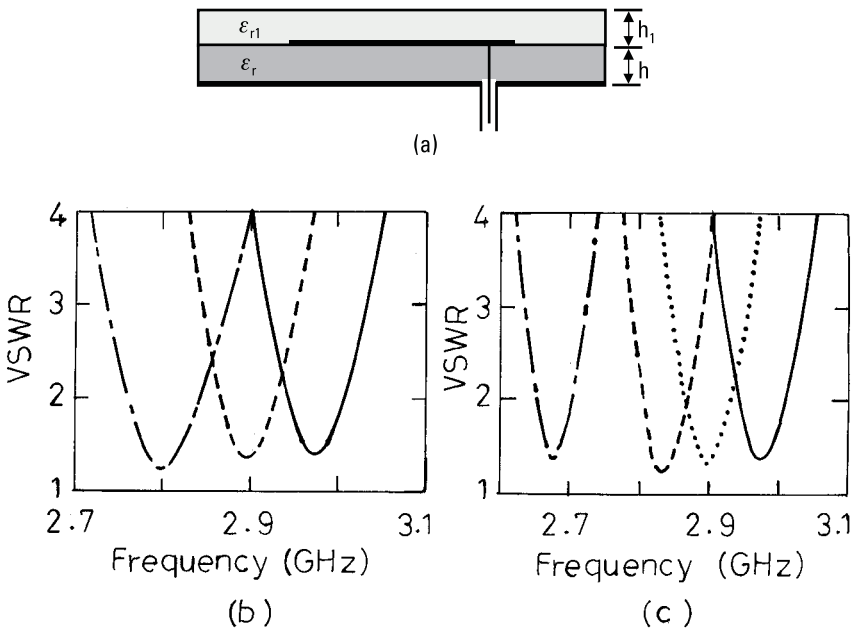

Figure 2.13 (a) RMSA with a dielectric cover and its VSWR plots for (b) ϵ_{r1} = 2.55 and different h_1: (——) 0, (i.e., no cover), (- - -) 0.1, and (— — —) 1 cm; (c) h_1 = 0.1 cm and different ϵ_{r1}: (——) no cover, (· · ·) 2.55, (- - -) 4.3, and (— — —) 10.

ϵ_{r1} = 2.55, the results are summarized in Table 2.4, and for three values of h_1 (0, 0.1, and 1.0 cm), the VSWR plots are given in Figure 2.13(b). As h_1 increases from 0 to 1.0 cm, the resonance frequency decreases from 2.975 to 2.801 GHz, because fringing fields are now more confined within the dielectric medium, thereby increasing the value of ϵ_e. The gain of the antenna remains around 6.7 dB for h_1 = 0.0 to 1.0 cm. For h_1 = 1.0 cm, the BW is 80 MHz, which increases to 101 MHz, when the feed point is shifted to x = 0.9 cm.

For three different values of ϵ_{r1} (2.55, 4.3, and 10) with h_1 = 0.1 cm, VSWR plots are shown in Figure 2.13(c). For comparison, a VSWR plot of RMSA without cover is also shown in Figure 2.13(c). The results are summarized in Table 2.5. With an increase in ϵ_{r1}, the resonance frequency decreases due to an increase in the effective dielectric constant of the patch. The decrease in the resonance frequency implies that h/λ_0 is decreased, and hence BW decreases. However, the gain remains around 6.7 dB.

When the MSA is covered with a dielectric radome, generally an air gap is present between the patch and the dielectric cover. The radome could

Table 2.4
Effect of h_1 on the Performance of RMSA
(L = 3 cm, W = 4 cm, ϵ_r = 2.55, h = 0.159 cm, x = 0.7 cm, and ϵ_{r1} = 2.55)

h_1 (cm)	R_{in} (Ω)	f_0 (GHz)	BW (MHz)
0	73	2.975	63
0.05	72	2.921	61
0.10	71	2.900	62
0.50	58	2.827	69
1.00	38	2.801	80

Table 2.5
Effect of ϵ_{r1} on the Performance of RMSA
(L = 3 cm, W = 4 cm, ϵ_r = 2.55, h = 0.159 cm, x = 0.7 cm, and h_1 = 0.1 cm)

ϵ_{r1}	f_0 (GHz)	BW (MHz)
2.55	2.900	62
4.30	2.835	59
10.0	2.678	51

be of any shape, but generally a flat radome is preferred for MSAs. A flat radome of dielectric constant ϵ_{r1} and thickness h_1 with an air gap Δ is shown in Figure 2.14(a). For three different values of Δ (0.1, 0.3, and 1.0 cm) with $\epsilon_r = \epsilon_{r1} = 2.55$ and $h = h_1 = 0.159$ cm, VSWR plots are shown in Figure 2.14(b). As Δ increases from 0.1 to 1.0 cm, the resonance frequency increases from 2.944 to 2.975 GHz. The gain increases slightly due to the increase in the resonance frequency. For $\Delta = 1.0$ cm, the resonance frequency is same as that of the RMSA without a radome.

2.2.2 Higher Order Modes of RMSA

As described earlier, the radiation pattern of the RMSA is in the broadside direction for the fundamental TM_{10} mode. An RMSA operating at its second-order mode yields a conical pattern, whereas it has broadside radiation pattern at its third-order mode [4, 12].

An RMSA with $L = 3$ cm, $W = 4$ cm, $\epsilon_{r1} = 2.55$, $h = 0.159$ cm, and $x = 0.7$ cm is considered, which has been studied earlier for the fundamental

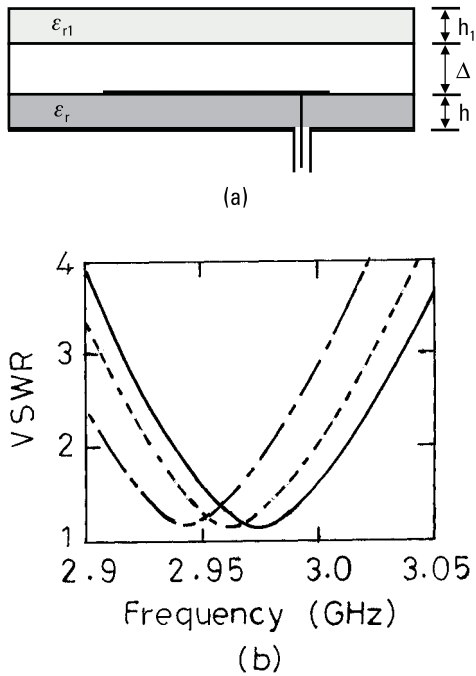

Figure 2.14 (a) RMSA with a flat radome with an air gap, and (b) its VSWR plots for different Δ: (– – –) 0.1, (- - -) 0.3, and (——) 1.0 cm.

mode. It operates at TM_{02} mode, when W is equal to λ at f_0 = 4.567 GHz. In this case, the voltage is uniform along the length and varies two half-wavelengths along the width. The input impedance and VSWR plots are shown in Figure 2.15(a, b). It may be observed that the input impedance is too high. If the feed point is moved along the x-axis, then the impedance does not change, because the field is uniform along the length for TM_{02} mode. If the feed point is moved along the y-axis, then the input impedance varies, because the field has λ variation along the W. For the feed at x = 0 and y = 0.5 cm, the input impedance and VSWR plots are also shown in Figure 2.15(a, b). A BW of 96 MHz (2.1%) is obtained. The radiation

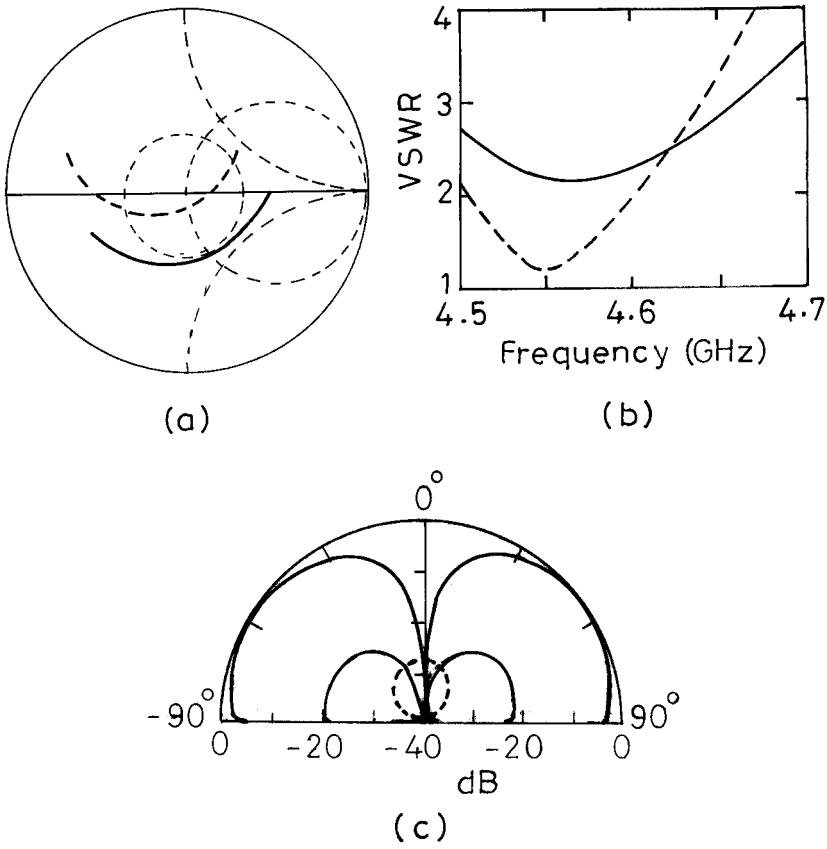

Figure 2.15 (a) Input impedance and (b) VSWR plots of RMSA excited at TM_{02} mode for two feed-point locations: (——) x = 0.7 cm, y = 0 and (- - -) x = 0, y = 0.5 cm. (c) Radiation pattern for TM_{02} mode at 4.56 GHz: (——) E-plane copolar and cross-polar, (- - -) H-plane copolar.

pattern at 4.56 GHz is shown in Figure 2.15(c). Only E_θ is present in the $\phi = 90°$ plane, and the radiation pattern is conical with the maximum along $\theta = 55°$. The gain of the antenna is 8.0 dB. The other components in the $\phi = 0°$ and 90° planes are below 20 dB.

If a square patch is considered with $L = W = 3$ cm, then either TM_{02} mode or TM_{20} mode could be excited by placing the feed along the x- or y-axis, respectively. The resonance frequency for the second order mode is around 6 GHz, which is twice the frequency of the fundamental TM_{10} mode. If the feed is placed at $x = 0.75$ cm, $y = 0$, then only the TM_{02} mode is excited because it lies along the null axis of the TM_{20} mode. Only E_θ is present in the $\phi = 90°$ plane, and all the other components are very small. If the feed is placed at $x = 0$, $y = 0.75$ cm, then the TM_{20} mode is excited and only E_θ is present in the $\phi = 0°$ plane. For both cases, the response is the same except for the rotation of the ϕ plane. The VSWR plot is shown in Figure 2.16. A BW of 231 MHz is obtained at 6.0 GHz. The D and η are 8.4 dB and 64%, respectively, resulting in a gain of 6.5 dB.

When the feed is placed at the center ($x = 0$, $y = 0$), then both the modes are equally excited but the input impedance is very high. By shifting the feed-point along the diagonal to $x = 0.4$ cm, $y = 0.4$ cm, better matching is obtained. The BW is 255 MHz at 6.0 GHz as shown in Figure 2.16. As before, E_θ is conical but now it is present in all the ϕ directions. Therefore, D decreases to 5.1 dB, and η is 56%. The pattern is similar to that of a vertical monopole antenna on an infinite ground plane. Thus, a vertical

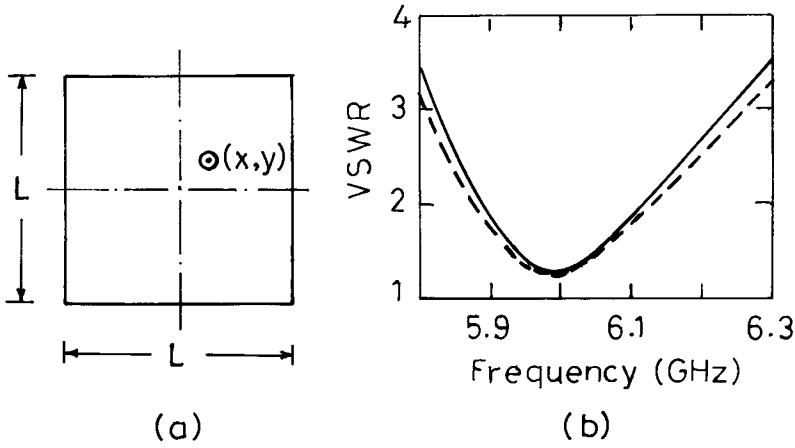

Figure 2.16 (a) Square MSA excited at the second-order mode and its (b) VSWR plots for the feed at (——) $x = 0.75$ cm, $y = 0$ and (- - -) $x = 0.4$ cm, $y = 0.4$ cm.

monopole antenna can be replaced by a horizontal MSA with the same radiation characteristics.

A square MSA with $L = 9$ cm is considered for the TM_{30} mode. The length of the patch has been increased by three times as compared to that of the RMSA for the fundamental mode, so that its resonance frequency remains around 3 GHz. To excite TM_{30} mode, the feed is placed at $x = 1.5$ cm, $y = 0$ as shown in Figure 2.17(a). The voltage distribution along the length indicates three $\lambda/2$ cycle variations. The voltage is uniform along the width. The resonance frequency is 3.07 GHz, and the BW is 31 MHz. The radiation pattern at 3.07 GHz is shown in Figure 2.17(b). The radiation pattern is in the broadside direction, as in the case of the fundamental mode. In the E-plane, the pattern has a narrow main lobe with two sidelobes. In the H-plane, the pattern is in the broadside with no sidelobes. The D and η are 10.3 dB and 67%, respectively. The D of the third-order mode is much larger than that of the fundamental mode, due to the larger aperture area.

2.2.3 Orthogonal Feeds for Dual Polarization

In polarization diversity applications, it is necessary to transmit in one polarization and receive in the orthogonal polarization. A square or rectangular MSA with two orthogonal feed points gives two orthogonal polarizations. An orthogonal dual-fed square MSA yields dual polarization at the same frequency, whereas a rectangular MSA yields dual polarization at two separate

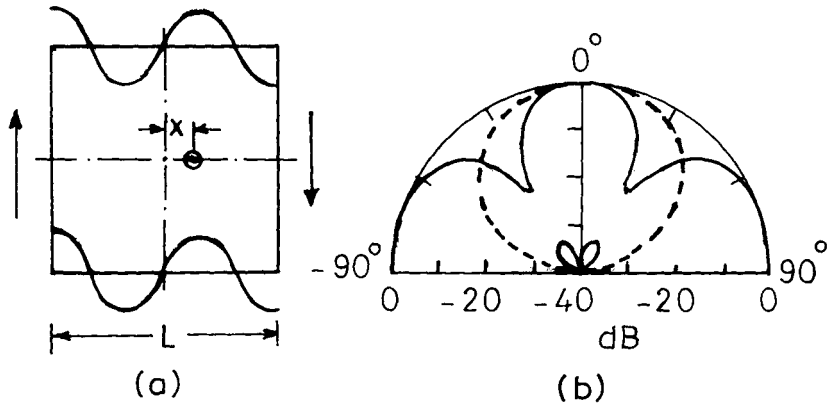

Figure 2.17 (a) RMSA excited at the TM_{30} mode and (b) its radiation pattern at 3.07 GHz: (——) E-plane copolar and cross-polar, (- - -) H-plane copolar.

frequencies corresponding to length L and width W being equal to $\lambda/2$. A dual-fed RMSA has been analyzed using the cavity model and MNM [13–15].

A square patch with L = 4.6 cm and two feeds at x = 1.0 cm and y = 1.0 cm is shown in Figure 2.18(a). The substrate parameters are ϵ_r = 4.3, h = 0.16 cm, and tan δ = 0.02. The theoretical and measured input impedance loci at one of the feeds for the fundamental mode are shown in Figure 2.18(b). The theoretical results are obtained using MNM. The theoretical and measured resonance frequencies are 1.552 GHz and 1.547 GHz, respectively. The variations of theoretical and measured isolation between the two

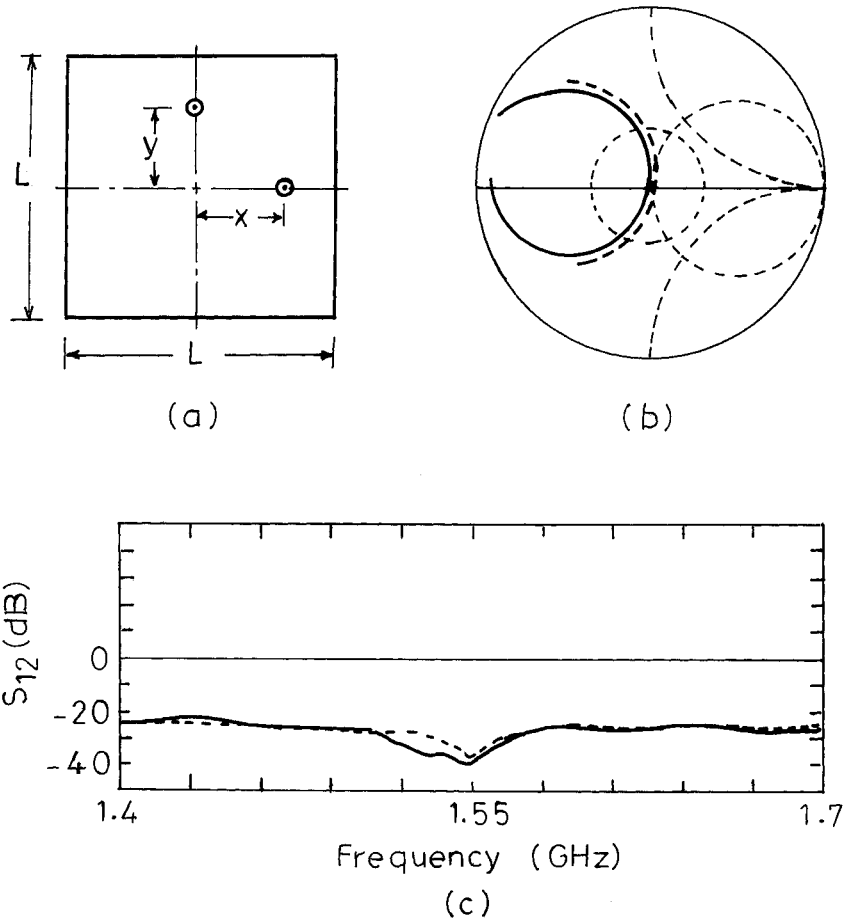

Figure 2.18 (a) Square MSA with two orthogonal feeds and its (b) input impedance loci at one of the ports and (c) isolation between the two orthogonal modes: (- - -) theoretical and (——) measured.

ports (S_{12}) with frequency are shown in Figure 2.18(c), and its values are 35 dB and 40 dB at the center frequency, respectively.

An RMSA with L = 10.1 cm and W = 7.9 cm with two orthogonal feeds is shown in Figure 2.19(a). The substrate parameters are ϵ_r = 4.3, h = 0.16 cm, and tan δ = 0.02. It yields dual-frequency operation with orthogonal polarization. The two frequencies correspond to the TM_{10} and TM_{01} modes of the RMSA. For the feed point at x = 3.8 cm, the TM_{10} mode is excited, and the theoretical and the measured input impedance loci

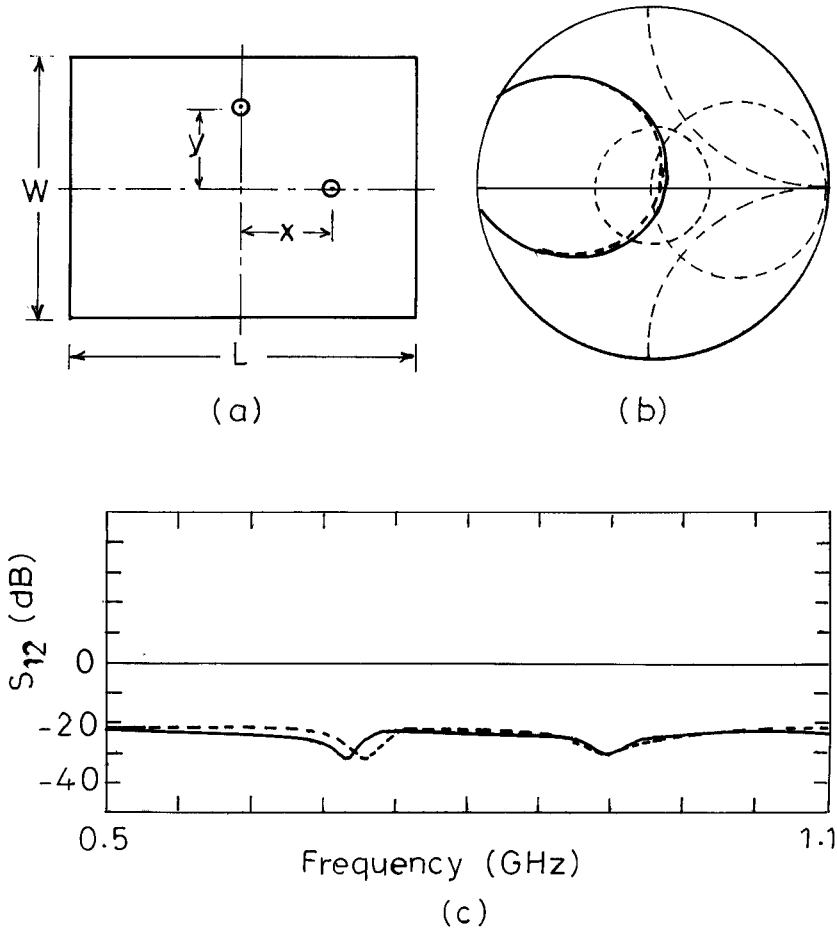

Figure 2.19 (a) An RMSA with two orthogonal feeds, and its (b) input impedance loci, and (c) isolation between the two orthogonal modes: (- - -) theoretical and (——) measured.

are shown in Figure 2.19(b). The antenna has been analyzed using MNM [14, 15]. The theoretical and measured resonance frequencies are 915 MHz and 913 MHz, respectively. For the feed at y = 2.9 cm, the TM_{01} mode is excited. The theoretical and measured resonance frequencies are 715 MHz and 712 MHz, respectively. The theoretical and measured values of S_{12} are shown in Figure 2.19(c). The isolation between the two orthogonal modes at the two resonance frequencies is nearly 30 dB. An isolation of 30 dB is adequate for most of the practical applications; therefore an MSA with dual feeds could eliminate the use of a duplexer or circulator in a wireless communication system.

2.2.4 Circularly Polarized RMSA

An RMSA shown in Figure 2.1(a) yields linear polarization. CP can be obtained by feeding the RMSA at two orthogonal points with equal amplitude and 90° phase difference. Alternatively, a single-feed modified RMSA also yields CP. Some of the examples are nearly square-patch-fed along the diagonal, corner-chopped square MSA, and square MSA with a slot in the center [16]. Chapter 8 details these configurations.

2.2.5 Broadband Suspended RMSA

The BW of the MSA increases with an increase in h and a decrease in ϵ_r. The effect of the increase in h and the decrease in ϵ_r can also be realized using the suspended-microstrip configuration as shown in Figure 2.20(a). The patch is fabricated on one side of the dielectric substrate, and it is suspended in air with an air gap of Δ. The suspended configuration consisting of two dielectric layers can be replaced by a single layer of equivalent dielectric constant ϵ_{eq} of thickness $h + \Delta$ as shown in Figure 2.20(b). The value of ϵ_{eq} is approximately calculated by equating the total capacitance of the two configurations:

$$C_{eq} = \frac{\epsilon_o \epsilon_{eq} WL}{h + \Delta} = \frac{\dfrac{\epsilon_o \epsilon_r WL}{h} \dfrac{\epsilon_o WL}{\Delta}}{\dfrac{\epsilon_o \epsilon_r WL}{h} + \dfrac{\epsilon_o WL}{\Delta}} \tag{2.24}$$

The expression on the right-hand side corresponds to the equivalent series capacitance due to the dielectric layer and air spacing between the patch and the ground plane. This expression simplifies to

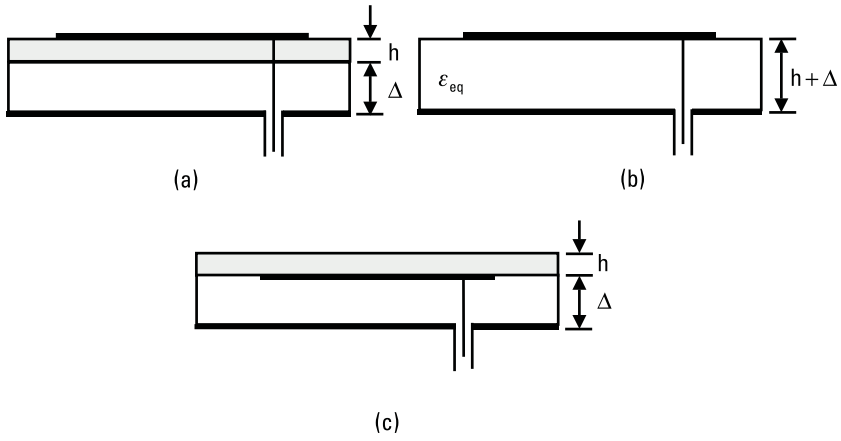

Figure 2.20 (a) Suspended MSA, (b) equivalent configuration, and (c) inverted suspended MSA.

$$\epsilon_{eq} = \frac{\epsilon_r(h + \Delta)}{\epsilon_r \Delta + h} \tag{2.25}$$

The above expression neglects the fringing fields. This value of ϵ_{eq} should be used in place of ϵ_r to calculate the resonance frequency of the suspended RMSA using (2.1) and (2.9).

The value of ϵ_{eq} is tabulated for two values of ϵ_r (2.55 and 4.3) with h = 0.159 cm for different values of Δ in Table 2.6. The ϵ_{eq} decreases significantly even for a small air gap of 0.01 cm for ϵ_r = 4.3. For large air gap of 1 cm, ϵ_{eq} for two values of ϵ_r approaches unity. Instead of air spacing, foam can be used whose ϵ_r is typically in the range of 1.05 to 1.1. One of

Table 2.6
Variation of ϵ_{eq} with Δ for Two Values of ϵ_r

Δ (cm)	ϵ_{eq} for ϵ_r = 2.55	4.3
0.01	2.3358	3.5975
0.02	2.1736	3.1416
0.05	1.8602	2.4029
0.10	1.5953	1.8908
0.20	1.3684	1.5149
0.50	1.1719	1.2272
1.00	1.0910	1.1177

the advantages of using a suspended configuration is that a low-cost glass epoxy substrate can be used without degrading the overall performance of the antenna.

Instead of using a suspended configuration, an inverted suspended configuration as shown in Figure 2.20(c) could be used. In this case, the top dielectric substrate acts as a protective layer that can be painted, so a separate radome is not necessary. This configuration can be considered as an MSA on air substrate with a dielectric cover.

To further compare suspended and inverted configurations, an example of broadband MSA around 900 MHz is considered, which is used for mobile and cellular communication. The BW required is around 70 MHz. A square MSA of L = 14 cm with air spacing of h = 2 cm from the ground plane that is fed with a 50-Ω coaxial line through an N-type connector (diameter = 0.4 cm) meets this requirement. However, this would require a metallic patch, which is to be suspended in the air either using foam substrate or by using dielectric screws at the edges. Instead a low-cost glass epoxy substrate (ϵ_r = 4.3) with a large dielectric loss (tan δ = 0.02) or a low-loss expensive dielectric substrate (ϵ_r = 2.3 and tan δ = 0.001) could be used in either suspended or inverted suspended configurations. The thickness of these substrates is taken as h = 0.159 cm, which increases the total height to 2.159 cm. The results for all these cases are summarized in Table 2.7. In the suspended or inverted configuration, as ϵ_r increases from 2.3 to 4.3, the frequency decreases by about 30 MHz (approximately 3%), and BW and gain decrease slightly. The performance of the lossy substrate is only marginally poor. Instead of suspended configuration if inverted configuration is used, the frequency increases slightly for both the substrates, because the total height of the patch from the ground plane is reduced from 2.159 cm

Table 2.7
Comparison of Suspended Configurations of Square MSA
(L = 14 cm, Δ = 2 cm, h = 0.159 cm, x = 6.5 cm)

Configuration	Frequency Range for VSWR $\leq$ 2 (MHz)	BW (MHz)	Gain (dB)
Suspended with ϵ_r = 1	935 to 1,019	84	9.5
Suspended with ϵ_r = 2.3	889 to 970	81	9.3
Suspended with ϵ_r = 4.3	858 to 934	76	9.2
Inverted with ϵ_r = 2.3	909 to 988	79	9.5
Inverted with ϵ_r = 4.3	880 to 955	75	9.4

to 2.0 cm, which reduces the extension in length due to fringing fields. The BW decreases and gain increases slightly.

2.2.6 Broadband Thick RMSA with Various Probes

The BW of the MSA increases with an increase in h but the probe inductance also increases as given by (2.23) [17]. Due to an increase in the inductance, the input impedance locus shifts upward in the clockwise direction. As a result, it may not even cross the real axis in the Smith chart. The probe inductance may decrease if its diameter is increased, but it is limited by the type of connectors to be used. Various techniques are used to compensate for probe inductance as described below:

2.2.6.1 Rectangular Patch Suspended in Air

A rectangular patch of L = 3 cm and W = 4 cm is suspended in air. For the probe at x = 1.4 cm using the SMA connector, the input impedance and VSWR plots for three values of h (2, 3, and 4 cm) are shown in Figure 2.21. As h increases, the impedance loci shifts upward in the clockwise direction, due to an increase in the probe inductance, and the resonance frequency decreases due to increase in the effective dimensions of the patch. For a larger h, the input impedance is always inductive. Therefore, for a thicker substrate to obtain broad BW, this large inductance must be compensated for as described in the following sections.

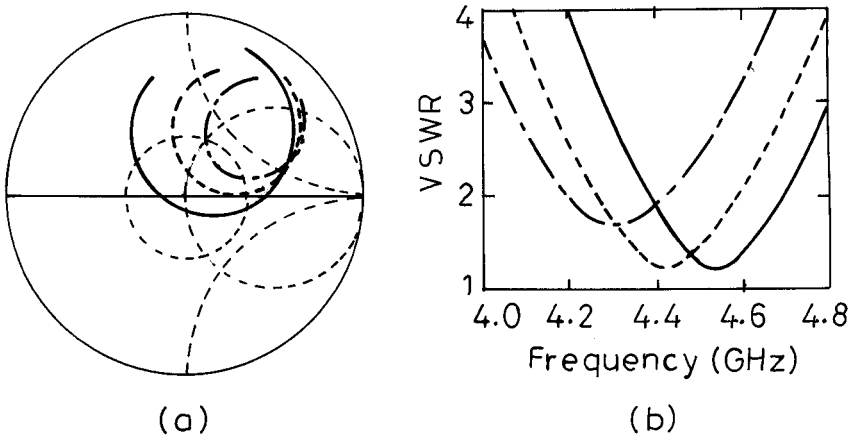

Figure 2.21 (a) Input impedance and (b) VSWR plots of a rectangular patch suspended in air for three values of h (——) 2, (- - -) 3, and (- · -) 4 cm.

2.2.6.2 RMSA with Probe Compensation

The probe compensation could be achieved by reducing the inductance. The probe inductance could be reduced by reducing the probe height or by increasing the probe diameter or by adding series capacitance. The series capacitance is realized either by physically adding a lumped capacitor or in several other ways as shown in Figure 2.22 [18]. In Figure 2.22(a), the series capacitor is realized by etching a small hole in the patch around the probe [19]. In Figure 2.22(b), the probe is extended beyond the patch, and a small conducting strip is soldered at its tip; alternatively, the probe can be just below the patch with the metallic strip as shown in Figure 2.22(c) [20]. Chapter 4 provides the details of using a metallic strip underneath the radiating patch.

An RMSA with an L-shaped wire probe is shown in Figure 2.22(d). The L-shaped probe excites the RMSA of $L = 2.5$ cm and $W = 3.0$ cm. The patch is supported by a foam layer of thickness $h = 0.66$ cm. The L-shaped wire probe of diameter 0.1 cm is connected to the inner conductor of a 50-Ω SMA connector. The length of the horizontal arm is 1.05 cm and its spacing from the patch is 0.11 cm. The horizontal portion of the L-shaped probe forms an open circuit stub of length less than $\lambda/4$ with the patch (so

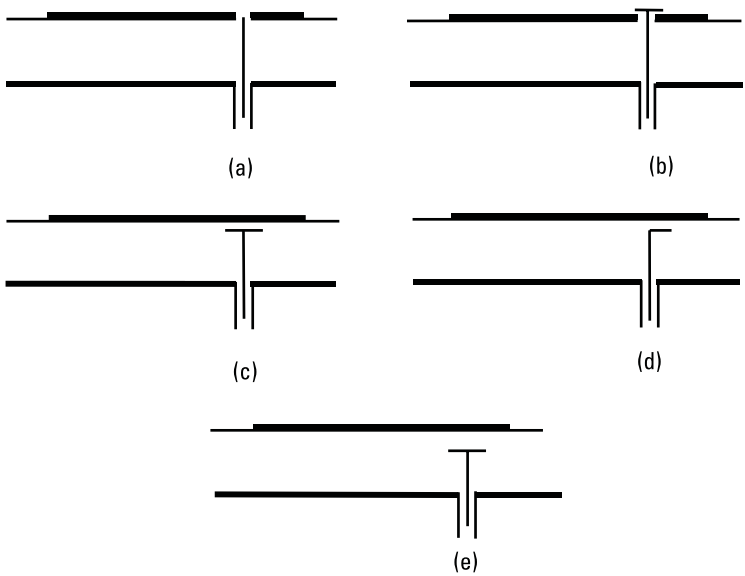

Figure 2.22 RMSA with different types of probe compensation: (a) small hole around the probe, (b) copper strip at the tip of probe, (c) metallic strip connected to the probe under the patch, (d) L-shaped probe, and (e) T-shaped probe.

that the impedance is capacitive). Together with the inductance of the vertical portion of the L-shaped probe, the stub acts as a series-resonant element with a resonance frequency close to that of the fundamental mode of the patch. The BW from 3.76 GHz to 5.44 GHz (36%) is obtained. The average gain over the BW is 7.5 dB [21]. Instead of an L-shaped probe, a T-shaped wire probe is used as shown in Figure 2.22(e), in which the horizontal arm is extended on both the sides of the vertical arm. This gives symmetrical excitation with slightly improved BW of 40% [22].

2.2.6.3 Three-Dimensional Feed

Another way of reducing the large feed probe inductance is to feed through the thick vertical metal plate, which is connected to the patch. This feed arrangement is also known as three-dimensional (3-D) transition [23, 24]. The fed RMSA is suspended over the ground plane and supported by a nonconductive pin at the center as shown in Figure 2.23(a). The 3-D transition connecting the patch to a perpendicular connector, could be either uniformly inclined or vertically tapered. The tapering of the width of the 3-D transition allows for the matching of the antenna impedance with a coaxial feed. By using 3-D transition, an efficient radiating patch can be designed at a large height from the ground plane (up to a quarter-wavelength at a higher frequency), leading to broad BW.

The top, front, and side views of the suspended three-dimensional MSA, along with the dimensional details in centimeters, are shown in Figure 2.23(b–d), respectively. The theoretical (obtained using IE3D) and measured VSWR plots of this antenna are shown in Figure 2.23(e). The measured frequency range for VSWR ≤ 2 is from 2.2 GHz to 4.3 GHz (90%). The radiation pattern is in the broadside direction at lower frequencies, but it becomes conical at higher frequency because of excitation of higher order modes.

In the above configuration, a notch has been cut in the patch and a slant feed has been used. Comparable response is achieved without a notch in the rectangular patch and by using vertically straight transition instead of inclined feed, making the configuration simpler to fabricate.

2.2.7 Frequency and Impedance Scaling of RMSA

Whether one designs an RMSA using simple design equations or using any sophisticated software (commercially available or developed in-house), the experimental results do not always perfectly match with the theoretical results. There could be several reasons:

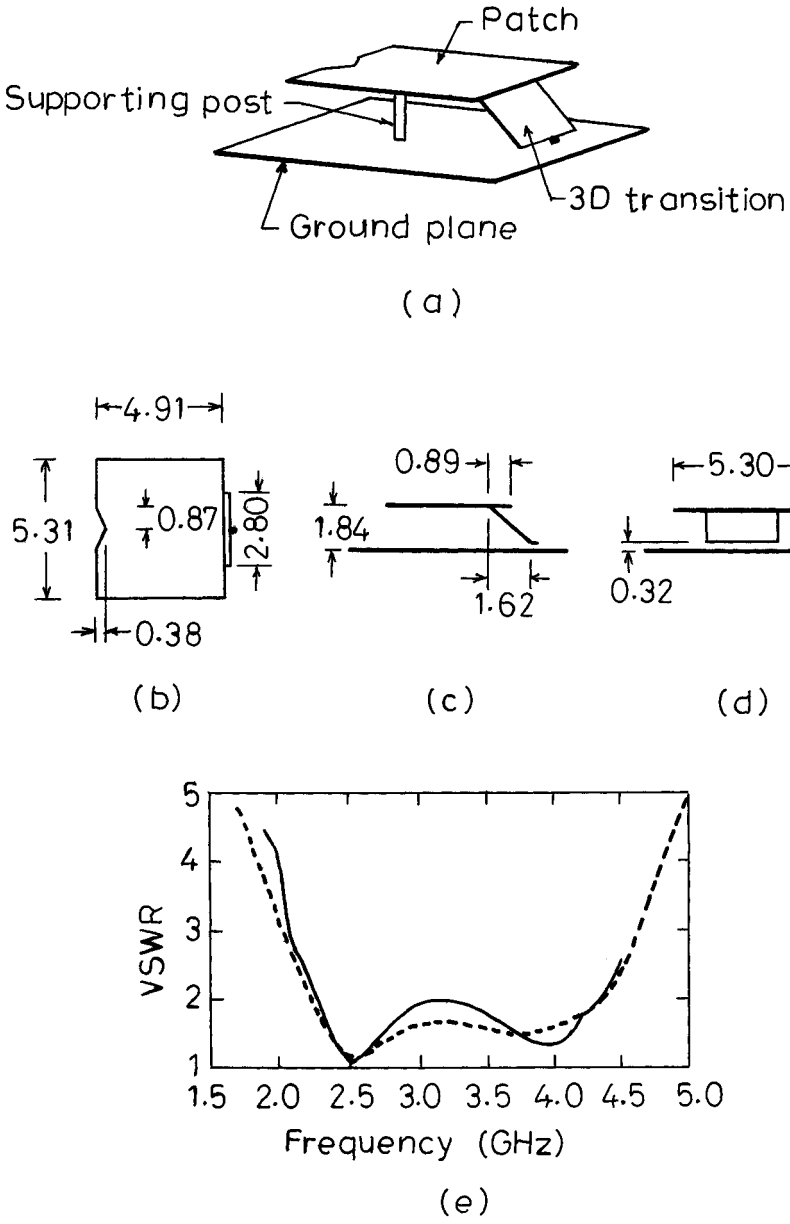

Figure 2.23 (a) Suspended patch fed by a 3-D transition; its (b) top, (c) side, and (d) front views; and (e) its VSWR plots (——) theoretical, (- - -) measured.

- Theoretical modeling is not 100% accurate.
- There could be a fabrication error in the dimensions and the probe position.
- There could be tolerance in the ϵ_r and h of the substrate.

These would result in frequency deviation and mismatch in the input impedance. The deviation in the frequency can be taken care of by either using the frequency-tuning methods described in Chapter 7 or by fabricating another RMSA. For fabricating another RMSA, its required length can be calculated by simply using the frequency scaling concept

$$L_{\text{required}} = L_{\text{measured}} * f_{\text{measured}} / f_{\text{required}} \tag{2.26}$$

Similarly, width can be scaled. If the measured input impedance Z_{in} is not matched, then the probe position x is to be changed. The new position x_{new} for the required input impedance Z_{required} can be obtained as:

$$Z_e = Z_{\text{in}} / \sin^2(\beta x) \tag{2.27}$$

$$\begin{aligned} Z_{\text{required}} &= Z_e \sin^2(\beta x_{\text{new}}) \\ &= Z_{\text{in}} \sin^2(\beta x_{\text{new}}) / \sin^2(\beta x) \end{aligned} \tag{2.28}$$

which simplifies to

$$x_{\text{new}} = (1/\beta) \cdot \sin^{-1} \sqrt{(Z_{\text{required}} / Z_{\text{in}}) \cdot \sin^2(\beta x)} \tag{2.29}$$

where $\beta = 2\pi/\lambda$.

By fabricating another antenna with dimensions obtained using (2.26) and (2.29), the measured values should match with the desired resonance frequency and input impedance values.

2.3 CMSAs

A CMSA, shown in Figure 2.24, is another widely used configuration. In the case of the RMSA, the field variation underneath the patch is defined in terms of sine or cosine functions. On the other hand, the fields for a CMSA are defined in terms of the Bessel function.

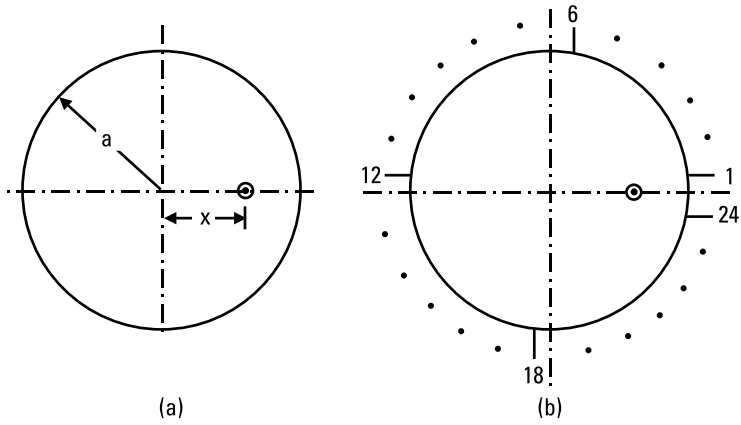

Figure 2.24 (a) Circular MSA and (b) its multiport network model.

2.3.1 Resonance Frequency

The resonance frequency of a CMSA is obtained using the formula [4, 25]:

$$f_0 = \frac{K_{nm}\, c}{2\pi a_e \sqrt{\epsilon_e}} \tag{2.30}$$

where K_{nm} is the mth root of the derivative of the Bessel function of order n [1, 4].

For the fundamental TM_{11} mode, the value of K_{nm} is 1.84118. The a_e and ϵ_e are the effective radius and the effective dielectric constant of the CMSA, respectively. The fringing fields along the circumference of the CMSA are taken into account by replacing the patch radius a by the effective radius a_e [4, 25–31]

$$a_e = a\left[1 + \frac{2h}{\pi a \epsilon_r}\left\{\ln\left(\frac{a}{2h}\right) + 1.41\epsilon_r + 1.77 + \frac{h}{a}(0.268\epsilon_r + 1.65)\right\}\right]^{1/2} \tag{2.31}$$

The value of ϵ_e is obtained using

$$\epsilon_e = C(a, h, \epsilon_o \epsilon_r)/C(a, h, \epsilon_o) \tag{2.32}$$

where $C(a, h, \epsilon_o \epsilon_r)$ and $C(a, h, \epsilon_o)$ are the total capacitances of the dominant TM_{11} mode of CMSA with and without a dielectric substrate, respectively. These can be calculated as

$$C(a, h, \epsilon_o \epsilon_r) = \frac{0.8525 \epsilon_o \epsilon_r \pi a^2}{h} + 0.5 C_f \tag{2.33}$$

In (2.33), the first term is the main capacitance of the disc and the second term is the fringing capacitance, C_f, which is given by [27, 28],

$$C_f = 2a\epsilon_o \left[\ln\left(\frac{a}{2h}\right) + 1.41\epsilon_r + 1.77 + \frac{h}{a}(0.268\epsilon_r + 1.65) \right] \tag{2.34}$$

$C(a, h, \epsilon_o)$ is calculated by putting $\epsilon_r = 1$ in (2.33) and (2.34). For thin substrates, ϵ_r should be used instead of ϵ_e in (2.30), and for thick substrates ($h > 0.05\lambda_0$), ϵ_e should be used.

Alternatively, a_e and ϵ_e could also be computed by equating the area of the CMSA with that of the RMSA for which accurate closed-form expressions accounting for the dispersion effect are available [4, 25]. The length L of the RMSA is taken as diameter $2a$ of the CMSA, which is important from the field variation point of view. The width W of the RMSA is then calculated by equating its area with that of the CMSA, which comes out to be $W = \pi a/2$. For these values of L and W, effective L_e and W_e are calculated using equations given in Appendixes B and C. From the effective dimensions of the RMSA, a_e is obtained as

$$a_e = \sqrt{\frac{L_e W_e}{\pi}} \tag{2.35}$$

The measured resonance frequency of CMSA for various values of a, h, and ϵ_r are shown in Table 2.8 and are compared with the theoretical resonance frequency obtained using (2.31) and (2.35). The agreement of the two methods with measured results is good for thick as well as thin substrates. Therefore, either of these formulations can be used to determine a_e and ϵ_e.

2.3.2 Input Impedance and Voltage Distribution

A CMSA of $a = 3$ cm with a feed point at $x = 0.9$ cm on the substrate having $\epsilon_r = 2.33$, $h = 0.159$ cm, and $\tan\delta = 0.002$ is considered. It is analyzed using MNM by dividing its periphery into 24 ports as shown in Figure 2.24(b). This number of ports is required to obtain convergence of

Table 2.8
Resonance Frequency f_0 of CMSA for Various Values of a, h and ϵ_r

a (cm)	h (cm)	ϵ_r	h/λ	Measured f_0 (GHz)	Theoretical f_0 (GHz) Using (2.31)	(2.35)
3.493	0.1588	2.50	0.013	1.570	1.556	1.567
1.270	0.0794	2.59	0.018	4.070	4.175	4.203
3.493	0.3175	2.50	0.025	1.510	1.522	1.531
13.894	1.2700	2.70	0.026	0.378	0.370	0.372
4.950	0.2350	4.55	0.014	0.825	0.827	0.827
3.975	0.2350	4.55	0.017	1.030	1.027	1.028
2.990	0.2350	4.55	0.023	1.360	1.358	1.358
2.000	0.2350	4.55	0.034	2.003	2.009	2.002
1.040	0.2235	4.55	0.063	3.750	3.744	3.707
0.770	0.2350	4.55	0.083	4.945	4.938	4.881

results [32]. For the fundamental TM_{11} mode, the input impedance is zero at the center and maximum at the periphery along the feed line. The measured and theoretical input impedance loci are given in Figure 2.25(a). The measured and theoretical resonance frequencies are 1.867 GHz and 1.865 GHz, with corresponding BW of 26.5 MHz and 25 MHz, respectively. The voltage distribution along the periphery of the CMSA for unit input current at f_0 = 1.865 GHz at the 24 peripheral ports is given in Figure 2.25(b). The

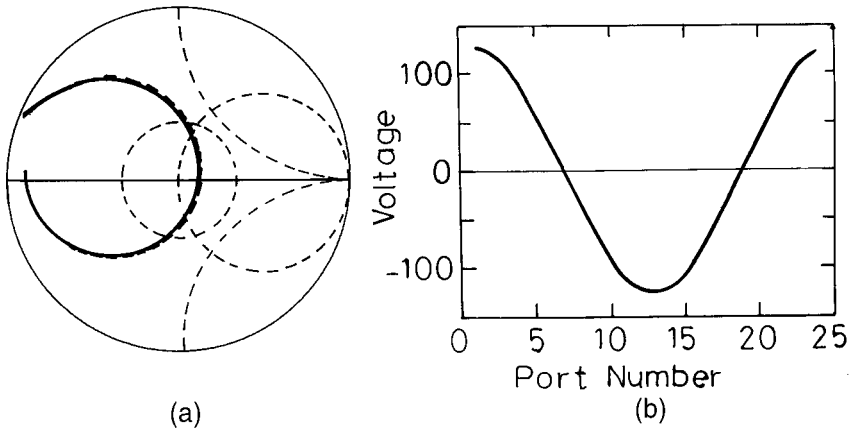

Figure 2.25 (a) Input impedance loci of the CMSA, (- - -) theoretical and (——) measured, and (b) voltage distribution along the periphery of the CMSA.

voltage has one $\lambda/2$ cycle variation along one half of the circumference as well as along the diameter, indicating the excitation of the TM_{11} mode.

2.3.3 Radiation Pattern

From the voltage distribution along these peripheral ports, the radiation pattern is computed [1, 32]. The theoretical and measured radiation patterns in the E and H planes are given in Figure 2.26. The radiation is in the broadside direction, and the theoretical gain is 6.4 dB. The measured cross-polar levels are below 20 dB. The deviation between the theoretical and the experimental patterns is due to the finite ground plane of the circular patch.

The normalized radiation pattern of the CMSA may also be calculated using the following equations [1]:

$$E_\theta = [J_{n+1}(k_0 a \sin\theta) - J_{n-1}(k_0 a \sin\theta)] \cos n\phi \tag{2.36}$$

$$E_\phi = [J_{n+1}(k_0 a \sin\theta) + J_{n-1}(k_0 a \sin\theta)] \cos\theta \sin n\phi \tag{2.37}$$

where J_{n+1} and J_{n-1} are the Bessel functions of order $n + 1$ and $n - 1$, respectively.

2.3.4 Effect of Loss Tangent

For a CMSA of $a = 3$ cm, $\epsilon_r = 2.33$, and $h = 0.159$ cm, the variations of the input impedance along the radius for tan δ from 0.0001 to 0.05 are shown in Figure 2.27(a). As tan δ increases from 0.0001 to 0.05, the input

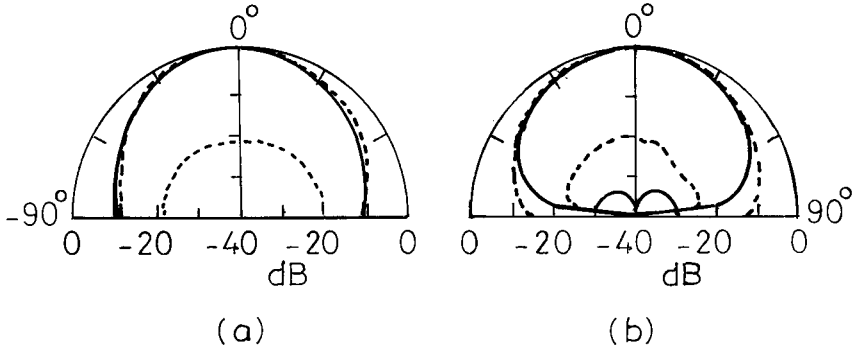

Figure 2.26 Radiation pattern of the CMSA in the (a) E-plane and (b) H-plane: (——) theoretical and (- - -) measured.

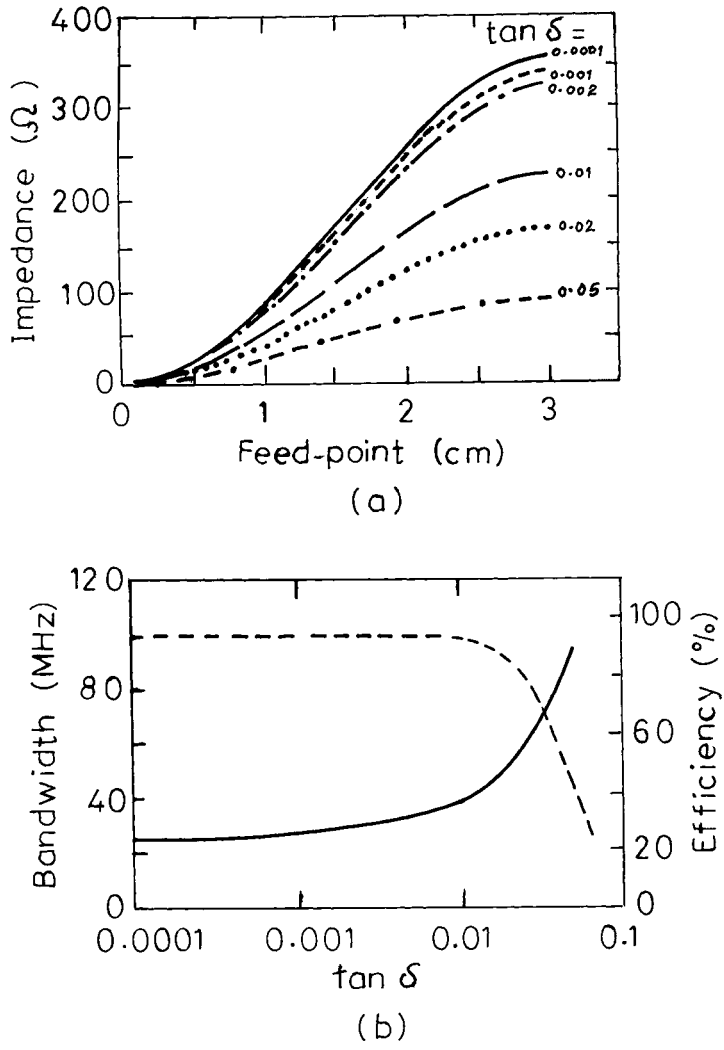

Figure 2.27 (a) Variation of input impedance with feed point, and (b) variation of (——) BW and (- - -) η of the CMSA with tan δ.

impedance at the periphery decreases from 357Ω to 93Ω. Hence, to match with 50Ω, the feed point x has to be moved away from the center if a substrate with a larger tan δ is to be used. The BW and η as a function of tan δ at f_0 = 1.865 GHz are shown in Figure 2.27(b) for the individually optimized feed point. As tan δ increases from 0.0001 to 0.05, the BW increases from 24.5 MHz (1.3%) to 96 MHz (5.1%). This increase in BW

is due to an increase in the dielectric losses in the substrate. The η of the antenna decreases from 99.9% to 27.8%, so gain reduces. Thus, the MSA on a lossy substrate gives wider BW with reduced η and hence lower gain.

2.3.5 Broadband CMSAs

To increase the BW of the CMSA of a = 3 cm, ϵ_r is reduced to 1 and h is increased to 0.5 cm. For x = 1.5 cm, the BW is 185 MHz at 2.663 GHz. Thus, with an increase in h from 0.159 to 0.5 cm and a decrease in ϵ_r from 2.33 to 1, the resonance frequency increases from 1.867 GHz to 2.663 GHz, the percentage BW increases from 1.3% to 6.9%, and gain increases from 6.4 dB to 9.7 dB at the corresponding center frequency. These results are similar to that for the RMSA.

2.3.6 Analysis of Higher Order Modes

For the fundamental TM_{11} mode of the CMSA, the maximum radiation is in the broadside direction. When the CMSA is excited at the TM_{21} mode, a conical pattern is obtained. The resonance frequency for the higher order modes is proportional to K_{nm}. The K_{nm} values and the measured and calculated frequencies for various modes of CMSA are shown in Table 2.9 [25, 32]. The calculated frequencies, obtained by equating the effective area of CMSA with that of the effective RMSA as described in Section 2.3.1, are in good agreement with the experimental values.

The voltage distribution along the circumference of the CMSA at f_0 = 3.107 GHz for the TM_{21} mode is given in Figure 2.28. The voltage has two $\lambda/2$ cycle variations along one-half of the circumference, and one cycle variation along the diameter, which is in accordance with excitation of the TM_{21} mode. The input impedance is zero at the center and has a

Table 2.9
Resonance Frequencies for Various Modes of a CMSA
(a = 3 cm, ϵ_r = 2.33, h = 0.159 cm, tan δ = 0.002, and x = 0.9 cm)

Mode	K_{nm}	Measured Frequency (GHz)	Calculated Frequency (GHz)
TM_{11}	1.84118	1.867	1.877
TM_{21}	3.05424	3.112	3.107
TM_{02}	3.83171	3.880	3.892
TM_{12}	5.33140	5.397	5.397

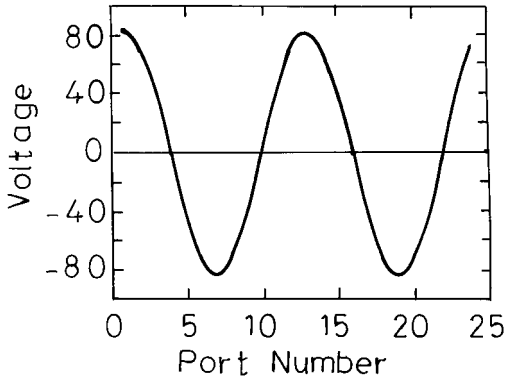

Figure 2.28 Voltage distribution along the periphery of the CMSA for the TM_{21} mode.

maximum value of 158Ω at the periphery, which is much less than that of the fundamental mode. For the feed at x = 1.7 cm, the theoretical and measured input impedance loci are shown in Figure 2.29. The measured BW is 71 MHz. The theoretical and measured radiation pattern in the E- and H-planes are shown in Figure 2.30. There is a null in the broadside direction, and the pattern is conical with beam maxima along $\theta = 40°$.

The main advantage of the CMSA over the RMSA is as follows. The resonance frequency of the CMSA is given in terms of K_{nm}. As a result, the ratios between the fundamental and the higher order modes' frequencies include such values as 1: 1.6588: 2.0812: 2.28179. The harmonics generated by any oscillator or transmitter are multiples of the fundamental frequency,

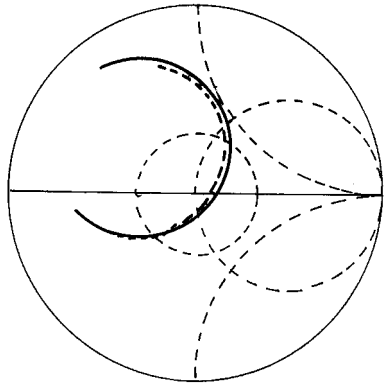

Figure 2.29 Input impedance loci of the CMSA for the TM_{21} mode: (- - -) theoretical and (——) measured.

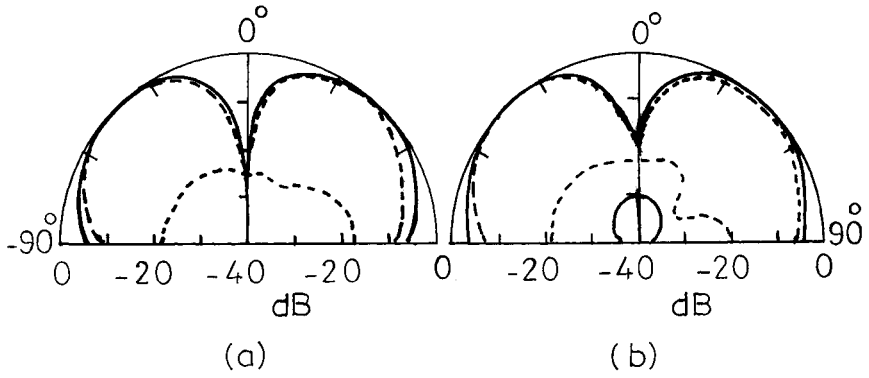

Figure 2.30 Radiation pattern of the CMSA for the TM_{21} mode in the (a) E-plane and (b) H-plane: (——) theoretical and (- - -) measured.

which will not excite the higher order modes of CMSA; hence, it will reject them. An RMSA, on the other hand, radiates or receives all the undesired harmonics as these coincide with its higher order modes.

2.3.7 Circularly Polarized CMSAs

CP can be obtained by feeding the CMSA at two orthogonal points with equal amplitude and 90° phase difference. Alternatively, a single-feed modified CMSA also yields CP. Some of examples include elliptical patch with an ellipticity ratio equal to 1.01 to 1.10, diametrically opposite peripheral slots, and a CMSA with a slot in the center [4, 16]. Chapter 8 details these configurations.

2.3.8 Dual-Orthogonal Feed CMSAs

A CMSA with two feeds at the orthogonal locations is shown in Figure 2.31(a). It yields dual polarization at the same resonance frequency, which is similar to that of the square MSA. For a = 3 cm, ϵ_r = 4.3, h = 0.159 cm, tan δ = 0.02, and feeds at $x = y$ = 1.1 cm, the measured input impedance plot at one of the feeds and isolation S_{12} between the two feeds are shown in Figure 2.31(b, c). The measured BW is 29 MHz at f_0 = 1.325 GHz. The isolation between the two feeds at the resonance frequency is 38 dB [14].

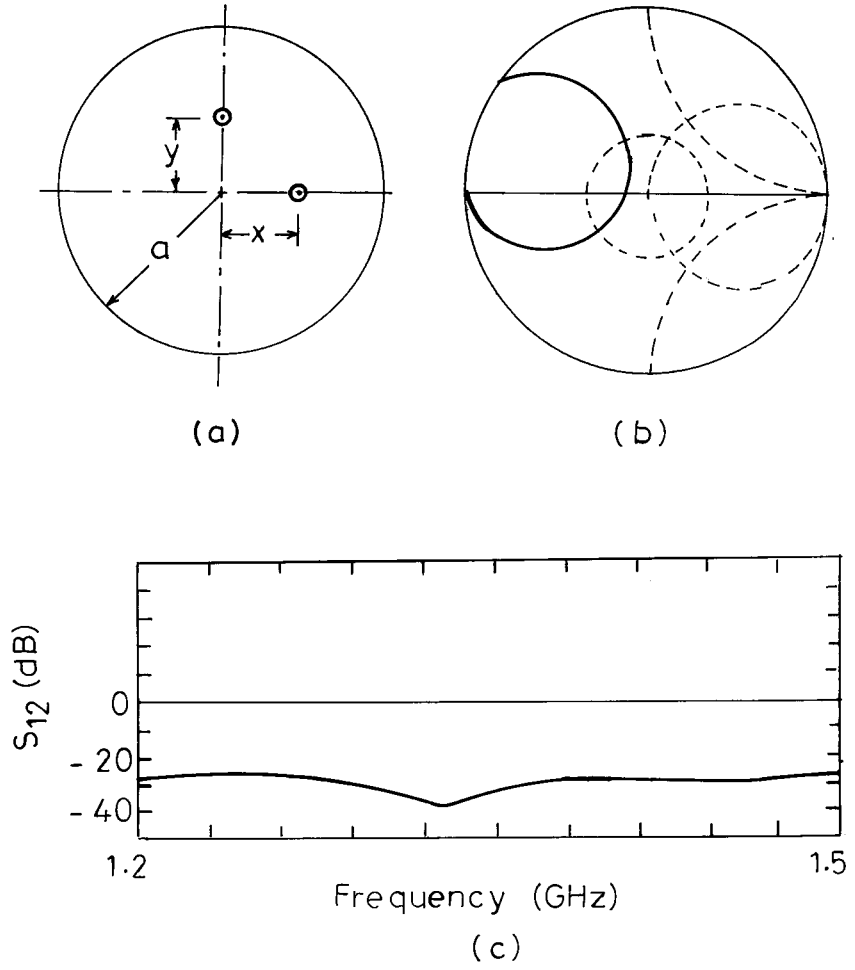

Figure 2.31 (a) Dual-orthogonal feed CMSA and its measured (b) input impedance plot and (c) isolation between the two feeds.

2.4 Semicircular MSAs

A *semicircular CMSA* (SCMSA) with half the area of a CMSA has the same resonance frequency as that of a CMSA [25, 33]. The resonance frequency of the SCMSA is calculated using the same expression as that of a CMSA given by (2.30). However, the expressions given for the effective dielectric constant and effective radius of the CMSA cannot be directly used for SCMSA, as its area is different and the straight edge also contributes to the

fringing fields and radiation [27, 28]. The effective dielectric constant and extension in the periphery of the SCMSA are obtained by equating its area with that of an equivalent RMSA as shown in Figure 2.32. The length L of the RMSA is taken equal to the diameter $2a$ of the SCMSA, and the width W of the RMSA is calculated to be equal to $W = \pi a/4$. For this W of the equivalent RMSA, the effective dielectric constant ϵ_e and the edge extensions for all the four sides of the RMSA are calculated [4, 25]. Finally, the effective radius a_e of the SCMSA is determined by equating its area to that of the expanded RMSA.

2.4.1 Input Impedance and Voltage Distribution

An SCMSA of radius $a = 3.0$ cm, $\epsilon_r = 2.33$, $h = 0.159$ cm, and $\tan\delta = 0.002$ is analyzed using MNM. In all, 40 ports are required along the periphery

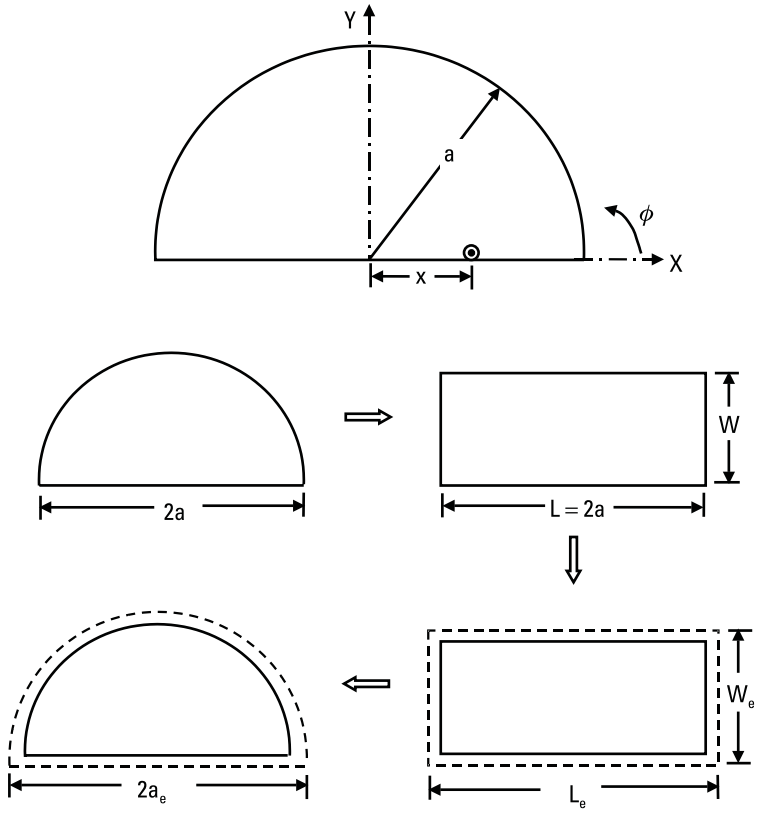

Figure 2.32 Semicircular MSA and its equivalence to RMSA.

of the SCMSA as shown in Figure 2.33(a) for a convergence of results. The port number starts from the center, goes around the curved edge, and ends at the center. The voltage distribution along the periphery at the resonance frequency f_0 = 1.864 GHz at the 40 peripheral ports is given in Figure 2.33(b). The magnitude of the voltage is maximum at the two end points of the diameter. For the TM_{11} mode, there is a half-wavelength voltage variation along the circumference as well as along the diameter [33].

The variation of theoretical input impedance along the radius of the SCMSA for the fundamental TM_{11} mode at f_0 = 1.864 GHz is shown in Figure 2.34(a). The input impedance at the periphery is 612Ω, which is almost double when compared to that of the CMSA for the same value of tan δ = 0.002. This is because the area of the SCMSA is half of that of the CMSA. From the impedance variation along the radius, the feed point for matching with a 50-Ω coaxial feed is at x = 0.6 cm, which is closer to the center as compared to x = 0.9 cm for CMSA. The theoretical and measured input impedance loci are shown in Figure 2.34(b). The theoretical and measured resonance frequencies are 1.864 GHz and 1.859 GHz, respectively, which are close to those of the CMSA with the same radius.

2.4.2 Radiation Pattern

The theoretical and measured radiation patterns in the E- and H-planes are shown in Figure 2.35. The small discrepancy in the two patterns and the increase in the measured cross-polar levels are due to the finite size of the

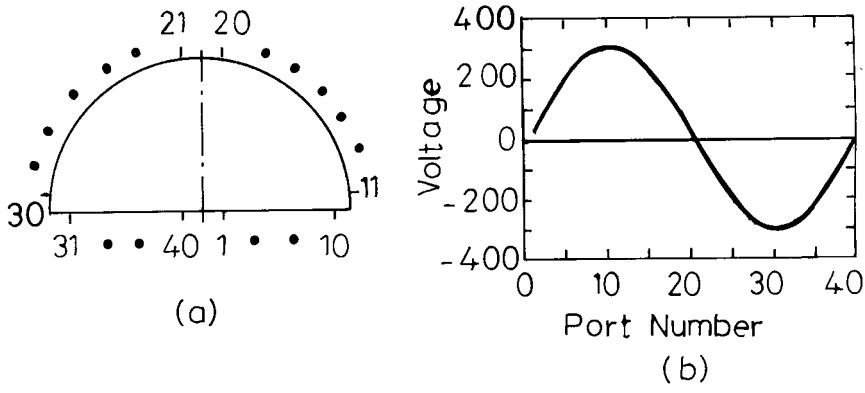

Figure 2.33 (a) SCMSA with 40 peripheral ports and (b) voltage distribution along the peripheral ports.

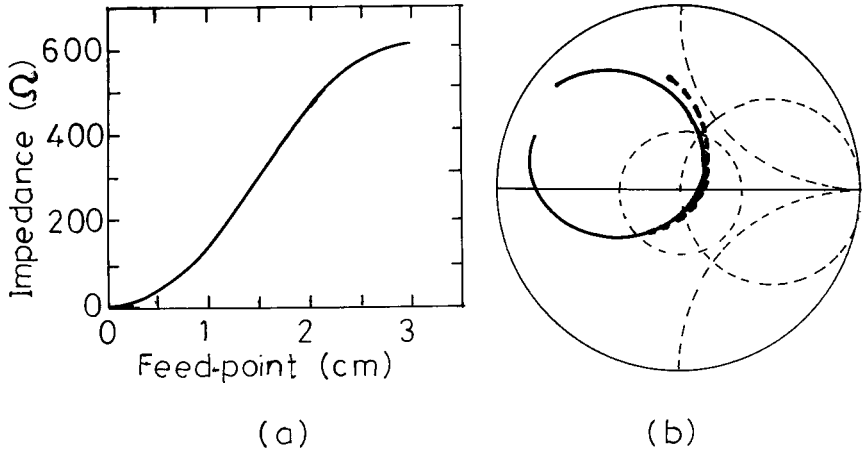

Figure 2.34 (a) Variation of input impedance along the radius of the SCMSA and (b) input impedance plots for feed at x = 0.6 cm: (- - -) theoretical and (——) measured.

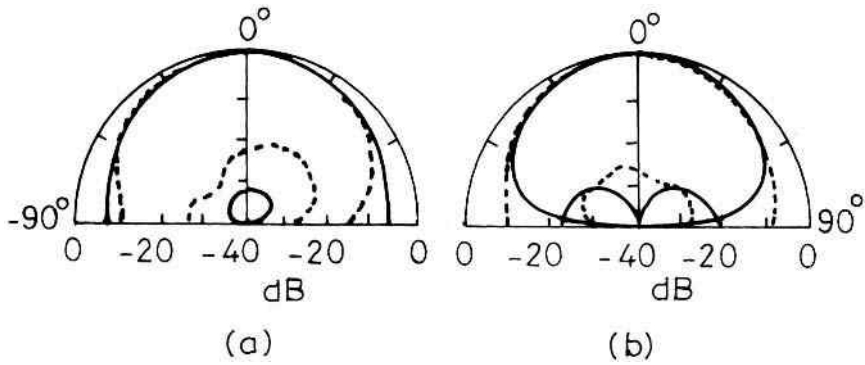

Figure 2.35 Radiation patterns of the SCMSA in the (a) E-plane and (b) H-plane: (——) theoretical and (- - -) measured.

ground plane (10 cm × 10 cm). The radiation pattern is similar to the TM_{11} mode of the CMSA.

2.4.3 Broadband SCMSAs

The BW of a SCMSA is increased by using a thick air substrate with a low dielectric constant. An SCMSA of a = 3 cm with ϵ_r = 1 and h = 0.5 cm and a feed at x = 1.0 cm yields a BW of 120 MHz (4.6%) at 2.634 GHz.

The gain of the antenna is 9.1 dB. In comparison with the CMSA of radius a = 3 cm, the resonance frequency of the SCMSA is nearly same, but its BW is 120 MHz, which is smaller than the 185-MHz BW of the CMSA. This is because of the larger impedance variation due to its half the area as compared to CMSA. The gain of SCMSA is slightly smaller than that of the CMSA, even though it has half the area. This is because the straight edge of the SCMSA also radiates.

2.4.4 Analysis of Higher Order Modes of the SCMSAs

The resonance frequency of the higher order modes of the SCMSA is obtained by substituting various K_{nm} values into (2.30). The a_e and ϵ_e for different frequencies are calculated again using their equivalence with the RMSA. The theoretical and measured resonance frequencies for various modes of the SCMSA are shown in Table 2.10.

For the TM_{21} mode of the SCMSA, the voltage distribution along its periphery at 3.077 GHz is given in Figure 2.36(a). There is a two-half-wavelength variation along the circumference (ports 11 to 30) and a one-half-wavelength variation along the diameter (ports 31 to 40 and 1 to 10). The input impedance at the periphery is 238Ω, which is much smaller than 612Ω corresponding to the fundamental mode. For the feed at x = 1.3 cm, the theoretical and measured input impedance loci are shown in Figure 2.36(b). The theoretical and measured BWs are 60 MHz and 58 MHz, respectively.

The theoretical and measured radiation patterns in the E- and H-planes are shown in Figure 2.37. The maximum radiation is in the broadside direction, but polarization is changed from the ϕ = 0° to 90° plane. This change in polarization can be visualized from the voltage variation around the periphery for the TM_{21} mode of the SCMSA. In the E-plane, the

Table 2.10
Resonance Frequencies for Various Modes of a SCMSA
(a = 3 cm, ϵ_r = 2.33, h = 0.159 cm, tan δ = 0.002, and x = 0.6 cm)

Mode	Measured f_0 (GHz)	Calculated f_0 (GHz)
TM_{11}	1.859	1.863
TM_{21}	3.026	3.077
TM_{02}	3.925	3.860
TM_{12}	5.367	5.355

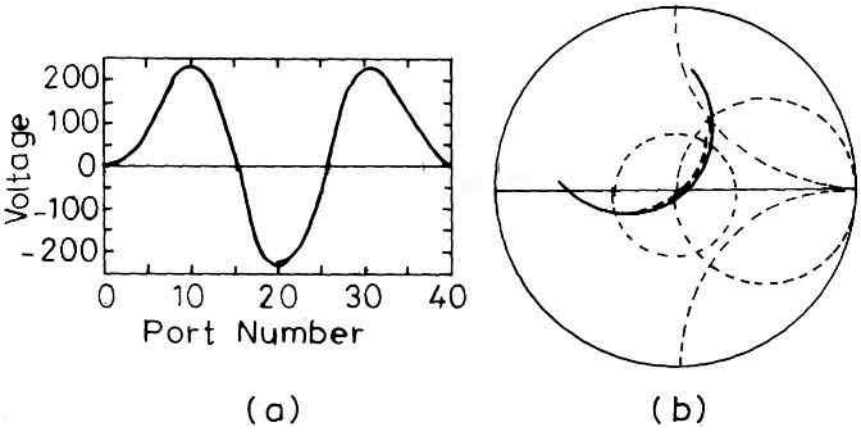

Figure 2.36 (a) Voltage distribution along the periphery of the SCMSA for the TM_{21} mode and (b) input impedance loci of the SCMSA for the TM_{21} mode: (- - -) theoretical and (——) measured.

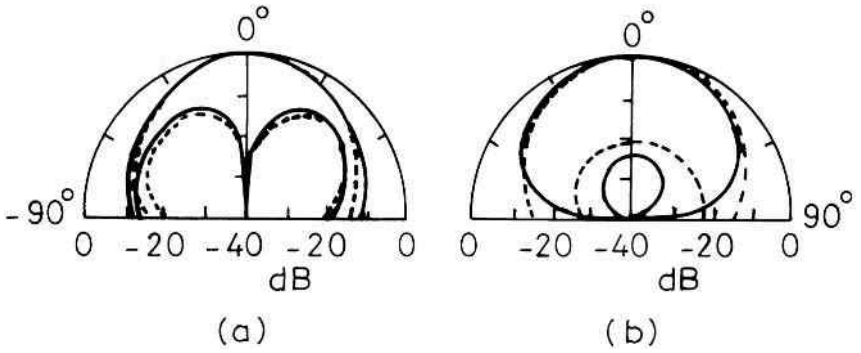

Figure 2.37 Radiation pattern of the SCMSA for the TM_{21} mode in the (a) E-plane and (b) H-plane: (——) theoretical and (- - -) measured.

maximum cross-polar level is 10 dB along $\theta = 40°$ but in the H-plane, it remains below 20 dB. This pattern is significantly different than the conical pattern of CMSA for the TM_{21} mode [33].

2.5 ETMSAs

An ETMSA is shown in Figure 2.38(a). The resonance frequency of the ETMSA is given by [25]:

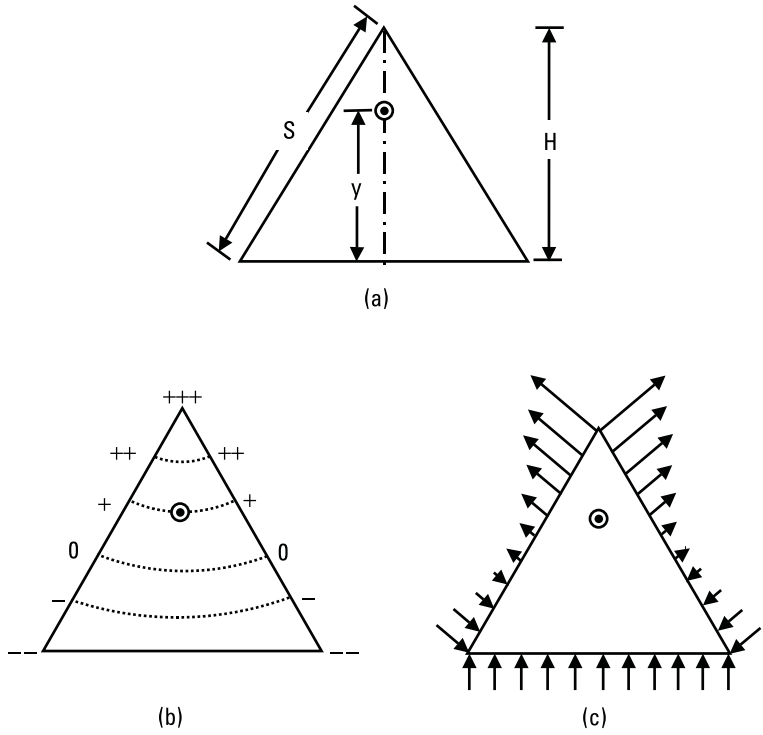

Figure 2.38 (a) ETMSA and its (b) voltage distribution along the periphery, and (c) vector representation.

$$f_{mnl} = f_{mn} = \frac{2c(m^2 + mn + n^2)^{1/2}}{3S_e\sqrt{\epsilon_e}} \tag{2.38}$$

where S_e is the effective side length, and $m + n + l = 0$. Instead of using m, n, and l, only m, n has been used for simplicity, it is implied that $l = -(m + n)$.

The precise closed-form expressions for S_e and ϵ_e are not readily available, and they are required to calculate the resonance frequency accurately. These values have been obtained using various methods [34–37]. In one of the methods, the area of the ETMSA is equated with a CMSA to calculate radius of the CMSA, from which effective radius is obtained, and then the S_e of the ETMSA is calculated by equating back the area of the enlarged CMSA [35–37]. Another method calculates these parameters by equating the area of the ETMSA with an RMSA as described in previous sections

[25]. Alternatively, the following approximate formula can be used for quick estimate of S_e:

$$S_e = S + \frac{4h}{\sqrt{\epsilon_e}} \tag{2.39}$$

where ϵ_e is obtained from (2.1) by replacing W with $S/2$.

For the ETMSA with the side length S = 10 cm and the substrate parameters ϵ_r = 2.32, h = 0.159 cm, and tan δ = 0.001, the calculated resonance frequencies for various modes of ETMSA using different methods and measured values are shown in Table 2.11. The calculated resonance frequencies for various modes of ETMSA using (2.39) are within 1% of the measured values.

For the fundamental TM_{10} mode of the ETMSA, the magnitude of voltage variation along the periphery is shown as + and −, and the vector representation of the field variation is shown in Figure 2.38(b, c). More numbers of + or −, or a larger arrow size are used to show that the magnitude is large.

The measured and theoretical input resistance variations for various feed-point locations along the height are shown in Figure 2.39(a). The input impedance is very large at the vertex of the ETMSA along the feed axis. The impedance matching with 50Ω could be obtained by feeding the antenna at either above or below the null position, which is at the center of the ETMSA. For y = 3.8 cm, the BW of the antenna is 8 MHz (0.6%).

The simulated radiation pattern at 1.283 GHz is shown in Figure 2.39(b). The E-plane is along the feed axis. The radiation is in the broadside direction but the cross-polar levels are higher as compared to that of the

Table 2.11
Resonance Frequency of an ETMSA for Various Modes
(S = 10 cm, ϵ_r = 2.32, h = 0.159 cm and tan δ = 0.001)

Mode	Measured Frequency (GHz)	Calculated Frequency in Gigahertz Using [35, 36]	[25]	(2.39)
TM_{10}	1.280	1.273	1.291	1.283
TM_{11}	2.242	2.205	2.235	2.223
TM_{20}	2.550	2.546	2.577	2.566
TM_{21}	3.400	3.369	3.405	3.395
TM_{30}	3.824	3.820	3.855	3.849

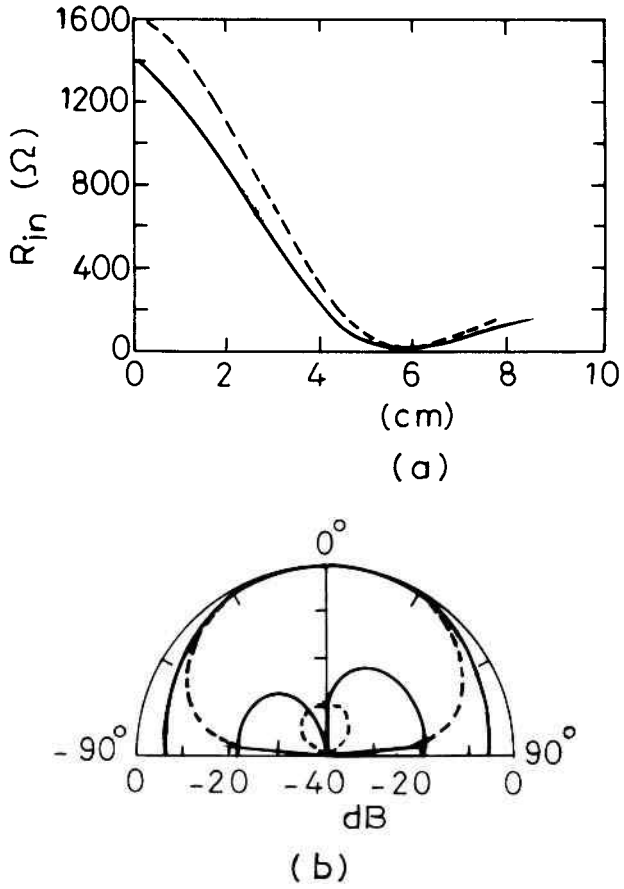

Figure 2.39 (a) Input impedance variation along the height of the ETMSA for the fundamental TM_{10} mode: (——) theoretical and (- - -) measured, and (b) theoretical radiation pattern: (——) E-plane and (- - -) H-plane.

RMSA and CMSA, because the fields are not symmetrical in the two orthogonal planes of the ETMSA. The gain of the antenna is 5.9 dB.

For the lower four modes (i.e., TM_{10}, TM_{11}, TM_{20}, and TM_{21} modes) the input impedance loci of ETMSA for the feed at y = 4 cm is shown in Figure 2.40. The resonance frequencies corresponding to these modes are given in Table 2.11. For the TM_{11} mode, the radiation pattern is conical, whereas for the TM_{20} and TM_{21} modes, the radiation is in the broadside direction, which is similar to that of the fundamental TM_{10} mode. One of the interesting features of the ETMSA is that by feeding it at y = 4 cm, all the three modes with a broadside radiation pattern get excited with VSWR $\leq$ 2.

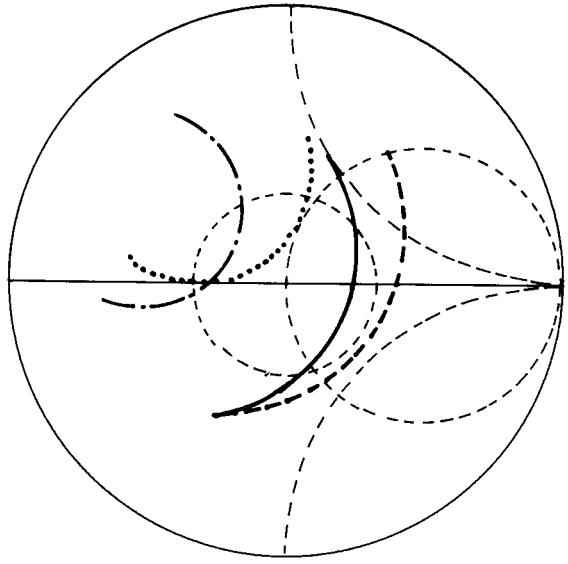

Figure 2.40 Input impedance loci for the lower four modes of the ETMSA: (——) TM_{10}, (- - -) TM_{11}, (· · ·) TM_{20}, and (– – –) TM_{21} modes.

2.6 30°-60°-90° Triangular MSAs

A 30°-60°-90° *triangular MSA* (TMSA) is shown in Figure 2.41. Since its area is half of that of an ETMSA, it is referred to as a *half-ETMSA* (HETMSA). The resonance frequency of the two configurations is same, when their height is same and is given by (2.38) [38]. For s = 10 cm, the impedance matching is obtained for y = 3.5 cm. The resonance frequency is 1.283 GHz, BW is 6 MHz, and gain is 5.3 dB. In comparison with the ETMSA, the area of the HETMSA is half, the BW decreases from 8 MHz to 6 MHz, gain

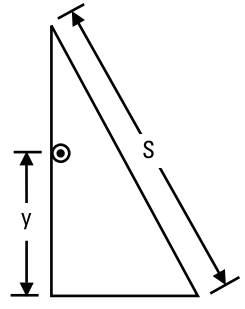

Figure 2.41 A 30°-60°-90° triangular MSA.

decreases from 5.9 dB to 5.3 dB, and cross-polar levels in the broadside direction increase from 18 dB to 10 dB.

2.7 Annular Ring MSAs

An *annular ring MSA* (ARMSA) is shown in Figure 2.42. The outer and inner radii are a and b, respectively. The ARMSA can be considered as a removal of a smaller inner concentric circle from the outer circle. The resonance frequency of the ARMSA is always smaller than that of the CMSA because of its larger resonant length. The resonance frequency of the ARMSA is given by [4]:

$$f_{nm} = \frac{X_{nm}\, c}{2\pi b\sqrt{\epsilon_e}} \tag{2.40}$$

where c is the velocity of light and X_{nm} represents the roots of the equation

$$J_n'(CX_{nm})\, Y_n'(X_{nm}) - J_n'(X_{nm})\, Y_n'(CX_{nm}) = 0 \tag{2.41}$$

$J_n(x)$ and $Y_n(x)$ are the Bessel functions of the first and second kind, and $C = a/b$. The values of X_{nm} for various modes of ARMSA with $C = 2$ are given in Table 2.12.

2.8 Comparison of Various Configurations for Broad BW

Table 2.13 gives a comparison of various regularly shaped probe-fed MSA configurations, such as rectangular, circular, semicircular, equilateral triangu-

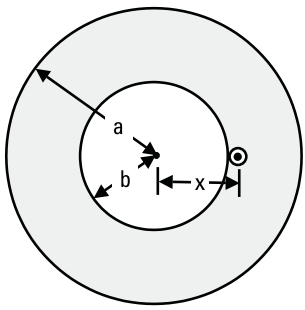

Figure 2.42 An ARMSA.

Table 2.12
Values of X_{nm} for Various Modes of ARMSA with $a/b = 2$

nm	1	2	3	4	5
0	—	3.1966	6.3123	9.4445	12.5812
1	0.6773	3.2825	6.3532	9.4713	12.6012
2	1.3406	3.5313	6.4747	9.5516	12.6612
3	1.9789	3.9201	6.6738	9.6842	12.7607
4	2.5876	4.4182	6.9461	9.8677	12.8989
5	3.1694	4.9929	7.2868	10.1000	13.0750

Table 2.13
Comparison of Various Regularly Shaped Broadband MSAs
($\epsilon_r = 1$, $h = 0.5$ cm, and $d = 0.12$ cm)

Configuration	Dimension (cm)	*x* or *y* (cm)	f_0 (GHz)	BW (MHz)	Gain (dB)	Area (cm^2)
RMSA	$L = 5.2$ $W = 6.0$	1.8	2.602	171	9.8	31.20
CMSA	$a = 3.0$	1.5	2.663	185	9.7	28.27
SCMSA	$a = 3.0$	1.0	2.634	120	9.1	14.14
ETMSA	$S = 6.5$	2.9	2.676	132	9.2	17.42
HETMSA	$S = 6.5$	2.6	2.595	81	8.9	8.71
ARMSA	$a = 2.8$ $b = 1.0$	1.1	2.655	132	9.6	21.48

lar, 30°-60°-90° triangular, and annular ring. The substrate with $\epsilon_r = 1$ and $h = 0.5$ cm is taken to realize broad BW for all theses configurations. The patch dimensions are chosen in such a way that the resonance frequency of all these antennas operating in their fundamental mode is around 2.6 GHz. The RMSA and CMSA have the largest BW, but RMSA has larger gain and area. The ARMSA has a smaller area and BW than the CMSA, but the gain is comparable. An SCMSA has half the area of the CMSA and has a smaller BW, but its gain is only slightly less. An ETMSA has a smaller BW and gain but its area is also smaller. The most compact antenna among all these configurations is the HETMSA, but it has the least BW. However, gain is only slightly less than the other configurations. As a result, if BW and gain are the main requirements, RMSA or CMSA should be used. However, if compact size is required, then SCMSA or HETMSA should be used.

2.9 Summary

This chapter discusses the regularly shaped MSA configurations: rectangular, circular, semicircular, equilateral triangular, 30°-60°-90° triangular, and annular ring. Design and analysis of the RMSA, including simplified formulas, are given. The effects of varying several parameters—such as the feed-point location; probe diameter; width of the patch; ϵ_r, h, and tan δ of the substrate; and finite ground plane size—on the resonance frequency, input impedance, BW, and gain are described in detail. The BW of the RMSA increases with an increase in the width and substrate thickness and a decrease in ϵ_r. The suspended as well as inverted RMSA configurations also yield wide BW. For thicker substrate, the probe compensation technique is also discussed. The dual-feed RMSA, SMSA, and CMSA are described for dual-polarized applications. The radiation pattern is in the broadside direction for the TM_{10} and TM_{30} modes.

For other regularly shaped geometries, the expressions for resonance frequency are given. Since the effects of various parameters on the performance of the antennas are similar, these are described very briefly to avoid repetition. Finally, a comparison of the characteristics of all these configurations on a thick substrate with $\epsilon_r = 1$ has been carried out, and the suitability of using various shapes for different applications is discussed.

References

[1] Bahl, I. J., and P. Bhartia, *Microstrip Antennas,* Dedham, MA: Artech House, 1980.

[2] Carver, K. R., and J. W. Mink, "Microstrip Antenna Technology," *IEEE Trans. Antennas Propagation,* Vol. AP-29, January 1981, pp. 2–24.

[3] James, J. R., et al., "Some Recent Developments in Microstrip Antenna Design," *IEEE Trans. Antennas Propagation,* Vol. AP-29, January 1981, pp. 124–128.

[4] James, J. R., and P. S. Hall, *Handbook of Microstrip Antennas,* Vol. 1, London: Peter Peregrinus Ltd., 1989.

[5] Sainati, R. A., *CAD of Microstrip Antennas for Wireless Applications,* Norwood, MA: Artech House, 1996.

[6] Lee, H. F., and W. Chen, *Advances in Microstrip and Printed Antennas,* New York: John Wiley & Sons, 1997.

[7] IE3D 7.0, Zeland Software Inc., Fremont, CA, 2000.

[8] Zurcher, J. F., and F. E. Gardiol, *Broadband Patch Antennas,* Norwood, MA: Artech House, 1995.

[9] Garg, R., et al., *Microstrip Antenna Design Handbook,* Norwood, MA: Artech House, 2001.

[10] Alarjani, B. M., and J. S. Dahele, "Feed Reactance of Rectangular Microstrip Patch Antenna with Probe Feed," *Electronics Letters,* Vol. 36, 2000, pp. 388–390.

[11] Bahl, I. J., P. Bhartia, and S. S. Stuchly, "Design of Microstrip Antennas Covered with a Dielectric Layer," *IEEE Trans. Antennas Propagation,* Vol. 30, 1982, pp. 314–318.

[12] Srinivasan, V., K. T. V. Reddy, and G. Kumar, "Multiport Network Model Analysis of Second- and Third-Order Modes of Rectangular Microstrip Antennas," *Microwave Optical Tech. Letters,* Vol. 26, No. 1, 2000, pp. 8–10.

[13] Richards, W. F., Y. T. Lo, and D. D. Harrison, "An Improved Theory for Microstrip Antennas and Applications," *IEEE Trans. Antennas Propagation,* Vol. AP-29, January 1981, pp. 38–46.

[14] Srinivasan, V., K. P. Ray, and G. Kumar, "Dual Feed Microstrip Antennas for Orthogonal Polarization," *NSAML,* New Delhi, India, March 2000, pp. 43–46.

[15] Srinivasan, V., "Multiport Network Model for Variations in Rectangular Microstrip Antennas," Ph.D. thesis, Indian Institute of Technology, Bombay, India, 2000.

[16] Sharma, P. C., and K. C. Gupta, "Analysis and Optimized Design of Single Feed Circularly Polarized Microstrip Antennas," *IEEE Trans. Antennas Propagation,* Vol. AP-31, 1983, pp. 949–955.

[17] Chang, E., S. A. Long, and W. F. Richards, "An Experimental Investigations of Electrically Thick Rectangular Microstrip Antennas," *IEEE Trans. Antennas Propagation,* Vol. AP-34, No. 6, 1986, pp. 767–772.

[18] Griffins, J. M., and J. R. Forrest, "Broadband Circular Disc Microstrip Antennas," *Electronics Letters,* Vol. 18, No. 6, 1982, pp. 267–269.

[19] Hall, P. S., "Probe Compensation in Thick Microstrip Patches," *Electronics Letters,* Vol. 23, May 1987, pp. 606–607.

[20] Fong, K. S., H. F. Pues, and M. J. Withers, "Wideband Multilayer Coaxial Fed Microstrip Antenna Elements," *Electronics Letters,* Vol. 21, No. 11, 1985, pp. 497–499.

[21] Luk, K. M., et al., "Broadband Microstrip Patch Antenna," *Electronics Letters,* Vol. 34, 1998, pp. 1442–1443.

[22] Mak, C. L., K. F. Lee, and K. M. Luk, "A Novel Broadband Patch Antenna with a T-Shaped Probe," *IEE Proc. Microwaves, Antennas Propagation,* Pt. H, Vol. 147, 2000, pp. 73–76.

[23] Herscovici, N., "New Considerations in the Design of Microstrip Antennas," *IEEE Trans. Antenna Propagation,* Vol. AP-46, No. 6, 1998, pp. 807–812.

[24] Herscovici, N., "A Wideband Single-Layer Patch Antenna," *IEEE Trans. Antenna Propagation,* Vol. AP-46, No. 4, 1998, pp. 471–474.

[25] Ray, K. P. and G. Kumar, "Determination of the Resonant Frequency of Microstrip Antennas," *Microwave Optical Tech. Letters,* Vol. 23, No. 2, 1999, pp. 114–117.

[26] Benalla, A., and K. C. Gupta, "Analysis of Two-Port Circular Microstrip Patch Antennas Using Multiport Network Model," *Proc. ISAP,* 1989, pp. 9–12.

[27] Abboud, F., J. P. Damiano, and A. Papiernik, "New Determination of Resonant Frequency of Circular Disc Microstrip Antenna: Application to Thick Substrate," *Electronics Letters,* Vol. 24, No. 17, 1988, pp. 1104–1106.

[28] Kumprasert, N., and W. Kiranon, "Simple and Accurate Formula for the Resonant Frequency of the Circular Microstrip Disk Antenna," *IEEE Trans. Antenna Propagation,* Vol. AP-43, No. 11, 1995, pp. 1331–1333.

[29] Howell, J. Q., "Microstrip Antenna," *IEEE Trans. Antennas Propagation,* Vol. AP-23, January 1975, pp. 90–93.

[30] Wolff, I., and N. Knoppik, "Rectangular and Circular Microstrip Disk Capacitors and Resonators," *IEEE Trans. Microwave Theory Tech.,* Vol. MTT-22, 1974, pp. 857–864.

[31] Derneryd, A. G., "Microstrip Disc Antenna Covers Multiple Frequency," *Microwave Journal,* 1978, pp. 77–79.

[32] Ray, K. P., "Broadband, Dual-Frequency and Compact Microstrip Antennas," Ph. D. thesis, Indian Institute of Technology, Bombay, India, 1999.

[33] Ray, K. P., and G. Kumar, "Multiport Network Model for Fundamental and Higher Order Modes of Semicircular Microstrip Antennas," *Microwave Optical Tech. Letters,* Vol. 28. No. 4, 2001, pp. 237–241.

[34] Dahele, J. S., and K. F. Lee, "On the Resonant Frequencies of the Triangular Patch Antenna," *IEEE Trans. Antennas Propagation,* Vol. AP-35, January 1987, pp. 100–101.

[35] Garg, R., and S. A. Long, "An Improved Formula for the Resonant Frequencies of the Triangular Microstrip Patch Antenna," *IEEE Trans. Antennas Propagation,* Vol. AP-36, 1988, p. 570.

[36] Singh, R., A. De, and R. S. Yadava, "Comments on an Improved Formula for the Resonant Frequency of the Triangular Microstrip Patch Antenna," *IEEE Trans. Antennas Propagation,* Vol. AP-39, 1991, pp. 1443–1444.

[37] Kumprasert, N., and W. Kiranon, "Simple and Accurate Formula for the Resonant Frequency of the Equilateral Triangular Microstrip Patch Antennas," *IEEE Trans. Antennas Propagation,* Vol. AP-42, No. 8, 1994, pp. 1178–1178.

[38] Satpathy, S., G. Kumar, and K. P. Ray, "Compact Shorted Variations of Triangular Microstrip Antennas," *Electronics Letters,* Vol. 34, No. 8, 1998, pp. 709–711.

3

Planar Multiresonator Broadband MSAs

3.1 Introduction

The BW of the MSA increases with an increase in the substrate thickness h or with a decrease in the dielectric constant ϵ_r. However, there is a practical limit on increasing the h, and if increased beyond $0.1\lambda_0$, surface-wave propagation takes place, resulting in degradation in antenna performance. Also, with an increase in h, the probe inductance increases and probe-compensation techniques have to be employed to obtain impedance matching as described in Chapter 2.

Practical MSAs with about 10% BW for VSWR ≤ 2 have been realized using a thick substrate with a low ϵ_r; however the BW obtained is not enough for many broadband applications, such as L-band radar (1.4–1.7 GHz = 19% BW), satellite TV in C-band (3.7–4.2 GHz = 12.5% BW), EMI/EMC, and spread spectrum applications. Therefore, broadband configurations are required for increasing the BW.

This chapter describes the planar multiple-resonator technique using microstrip patches for broadband operation. Only a single patch is fed, and the other patches are parasitically coupled. The coupling between the multiple resonators has been realized by using either a small gap between the patches or directly connecting the patches through a thin microstrip line. Sometimes, hybrid (gap and direct) coupling is used, in which the multiple resonators are placed close to each other with a gap smaller than $2h$, and shorting

strips are connected between the patches. Rectangular, circular, semicircular, equilateral, or isosceles triangular shaped patches have been used in the coupled configurations yielding a BW of 5 to 20% for VSWR ≤ 2 [1–5].

3.2 Mechanism of Parasitic Coupling for Broad BW

A patch placed close to the fed patch gets excited through the coupling between the two patches. Such a patch is known as a parasitic patch. If the resonance frequencies f_1 and f_2 of these two patches are close to each other, then broad BW is obtained as shown in Figure 3.1. The overall input VSWR will be the superposition of the responses of the two resonators resulting in a wide BW. If the BW is narrow for the individual patch, then the difference between f_1 and f_2 should be small as shown in Figure 3.1(a). If the BW of the individual patch is large, then the difference in the two frequencies should be large to yield an overall wide BW as shown in Figure 3.1(b). This can also be explained in terms of input impedance plot on the Smith chart. A loop is observed on the Smith chart due to the coupling between the two patches as described in the following sections.

3.3 Gap-Coupled RMSAs

An RMSA excited at the fundamental TM_{10} mode has one $\lambda/2$ cycle variation in the field along its length and has uniform field along its width. The edges along the width and length of the RMSA are known as radiating and nonradiating edges, respectively, as described in Chapter 2. Section 3.3.1 describes the effect of placing parasitic patches along the radiating, nonradiating, or all the four edges of the RMSA [6–8].

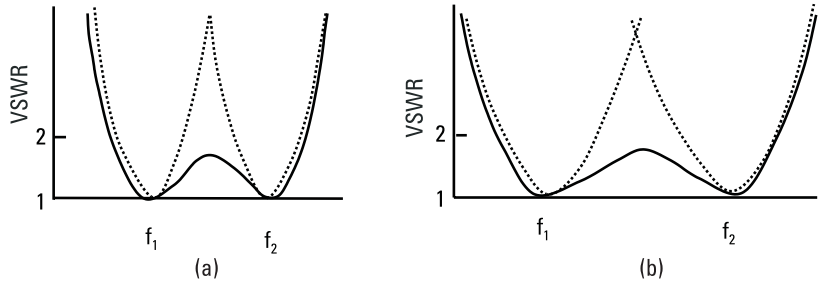

Figure 3.1 VSWR plots of two coupled resonators having (a) narrow and (b) wide BW: (· · ·) individual resonators and (——) overall response.

3.3.1 Radiating-Edge Gap-Coupled RMSAs

Either one or two parasitic rectangular patches can be placed along one or both of the radiating edges of the fed rectangular patch with a small gap between them. Initially, the effect of one parasitic patch on the performance of the antenna is discussed.

3.3.1.1 One Parasitic Patch

An RMSA with one parasitic rectangular patch placed along one of its radiating edges is shown in Figure 3.2(a). The dimensions of the fed patch are taken as L = 3 cm and W = 4 cm, and the feed point is located at x = 0.7 cm. The substrate parameters are ϵ_r = 2.55, h = 0.159 cm, and tan δ = 0.001. When a parasitic patch of length L_1 = 2.9 cm and width W = 4 cm is placed next to the fed patch with a gap s = 0.1 cm, it gets excited due to coupling with fringing fields along the width of the fed rectangular patch. The antenna has been analyzed using IE3D software based

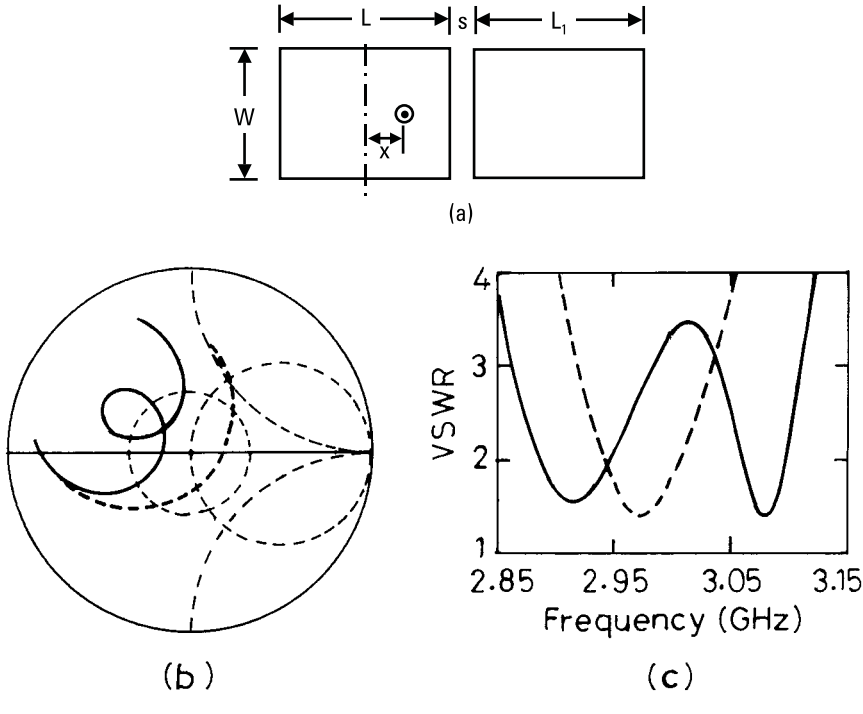

Figure 3.2 (a) Two radiating edges of gap-coupled RMSA and (b) input impedance and (c) VSWR plots of a single RMSA (- - -) and RMSA with one parasitic patch (——).

on MoM [9]. The input impedance and VSWR plots of a single RMSA and RMSA with one parasitic patch are shown in Figure 3.2(b, c). A loop is observed in the impedance plot of the RMSA with a parasitic patch, which is due to the coupling between the two patches. The position of the loop is shifted to the left side of the Smith chart due to the increase in the radiation from the two patches, which decreases the overall radiation resistance of the antenna and hence decreases the input impedance.

To increase the input impedance at resonance, the feed point is shifted to x = 1.1 cm (i.e., toward the nearer edge), where the impedance is higher. For the feed point at x = 0.7 and 1.1 cm, the input impedance and VSWR plots are shown in Figure 3.3. As expected, with an increase in x the input impedance plot shifts toward the right side of the Smith chart (i.e., toward the higher impedance value), and now the loop is within the VSWR = 2 circle. For x = 1.1 cm, the BW for VSWR $\leq$ 2 is 207 MHz (~7%). This BW is more than three times the BW of a single RMSA.

The length of the parasitic patch determines the position of the loop on the Smith chart. For three different lengths of the parasitic patch (L_1 = 2.8, 2.9, and 3.0 cm), the input impedance and VSWR plots are shown in Figure 3.4. As L_1 increases, the resonance frequency of the parasitic patch decreases, and the loop is formed at the lower frequency of the fed patch on the impedance plot. Therefore, as L_1 increases, the position of the loop moves in the anti-clockwise direction on the Smith chart.

The size of the loop depends upon the gap between the two patches. The input impedance and VSWR plots for three different values of gap

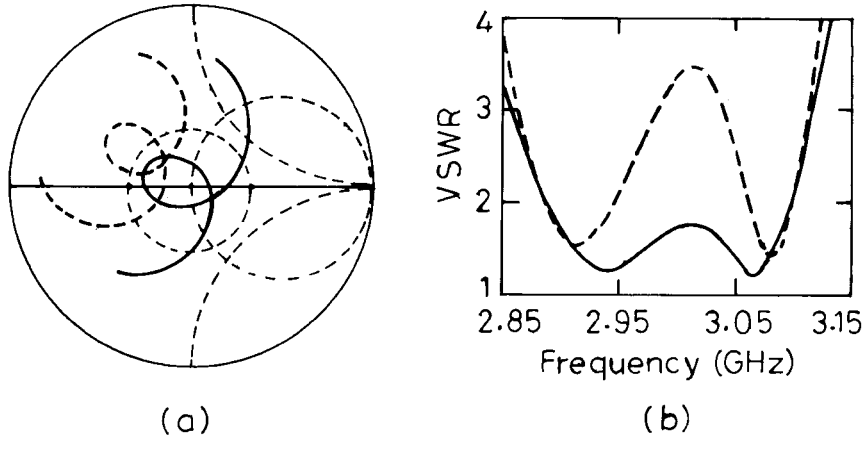

Figure 3.3 (a) Input impedance and (b) VSWR plots of two gap-coupled RMSAs for two feed-point locations x: (- - -) 0.7 and (——) 1.1 cm.

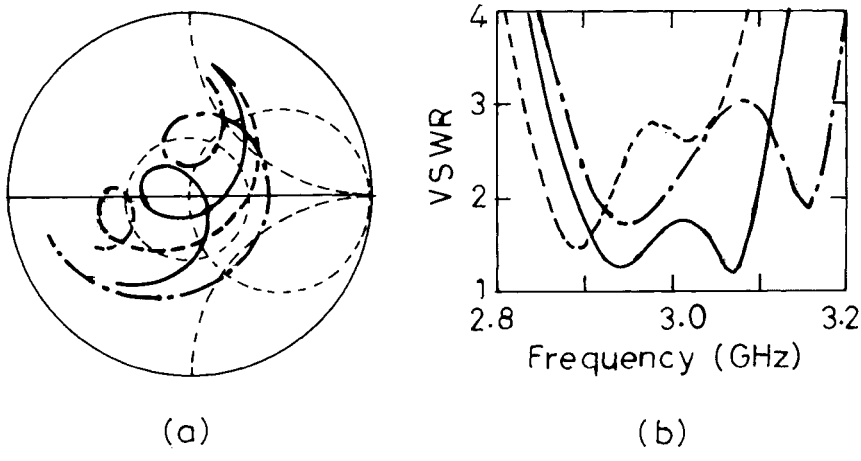

Figure 3.4 (a) Input impedance and (b) VSWR plots of two gap-coupled RMSAs for three values of L_1: (- - -) 2.8, (——) 2.9, and (– – –) 3.0 cm.

(s = 0.05, 0.1, and 0.15 cm) are shown in Figure 3.5. As the gap increases, the coupling between the two patches decreases and hence the loop size decreases. Maximum BW is obtained when the loop in the impedance plot is completely inside the VSWR = 2 circle and its size is as large as possible. For s = 0.1 cm, broader BW of 207 MHz is obtained because of larger loop size as compared to 161 MHz for s = 0.15 cm.

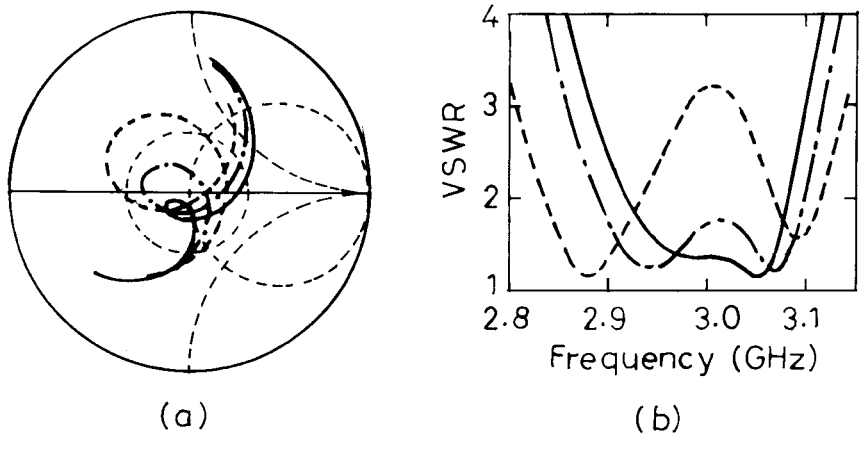

Figure 3.5 (a) Input impedance and (b) VSWR plots of two gap-coupled RMSA for three values of s: (- - -) 0.05, (– – –) 0.1, and (——) 0.15 cm.

For s = 0.05 cm, the coupling between the two patches is strong, resulting in a large loop that is not contained within VSWR = 2 circle. However, this configuration is useful for dual-band operation at 2.884 and 3.093 GHz with the corresponding BWs of 97 and 47 MHz, respectively. Chapter 7 describes the dual-band MSA configurations in detail.

For the two gap-coupled RMSA with s = 0.1 cm, the radiation patterns in the E- and H-planes at the three frequencies (2.9, 3.0, and 3.1 GHz, which are near the lower band edge, center, and upper band edge frequencies, respectively) are shown in Figure 3.6. In the H-plane, there is not much change in the radiation pattern at the three frequencies. However, in the E-plane, as the frequency increases, the beam maxima shifts away from the broadside. At the higher frequency, the parasitic patch is resonant; hence its radiation is more dominant. Since the parasitic patch sees a phase delay as compared to that of the fed patch, the beam maxima shifts away from the broadside to θ = 45° as the frequency increases from 2.9 GHz to 3.1 GHz. The cross-polar levels in the E-plane remain below 25 dB and in the H-plane, they are below 40 dB at all the three frequencies.

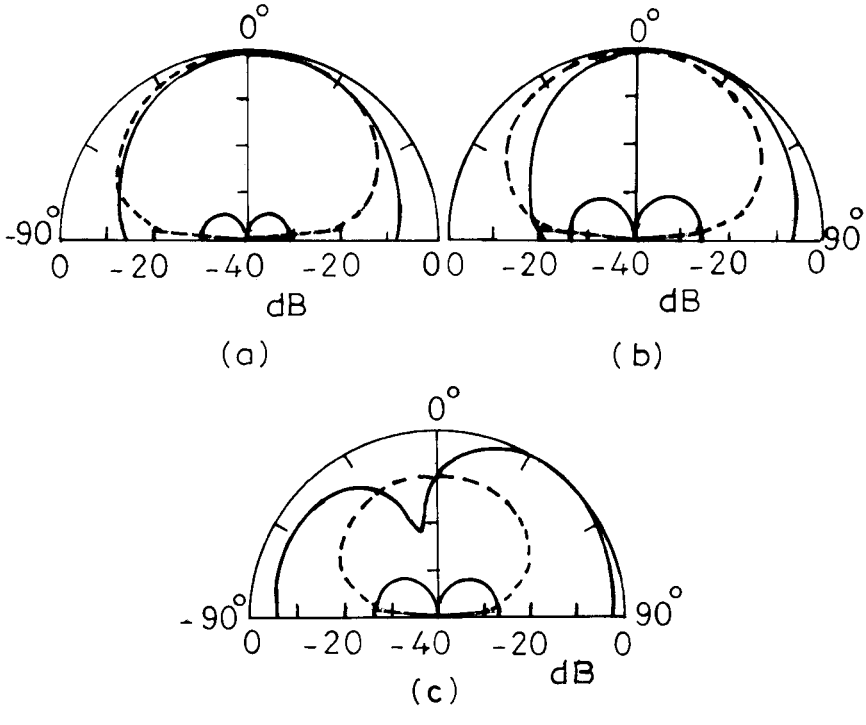

Figure 3.6 Radiation pattern of two gap-coupled RMSA at frequencies (a) 2.9 GHz, (b) 3.0 GHz, and (c) 3.1 GHz: (——) E-plane and (- - -) H-plane.

3.3.1.2 Two Equal Parasitic Patches

When a parasitic patch is placed along one of the radiating edges of the RMSA, the BW of the antenna increases. However, as the frequency increases within the BW, the beam maxima shifts away from the broadside and the pattern is not symmetrical with respect to the broadside direction, which is not acceptable for many applications.

To obtain the symmetrical pattern with the broadside, identical parasitic patches are gap-coupled to both the radiating edges of the fed patch as shown in Figure 3.7(a). In this arrangement, both the parasitic patches will experience the same phase delay. Since the two parasitic patches are on the opposite sides of the fed patch, one patch will shift the beam maxima in the $+\theta$ direction, while the other patch will shift it in the $-\theta$ direction. The overall pattern of three patches will be the superposition of the individual pattern, and hence it will remain symmetrical with the broadside direction.

For the two gap-coupled RMSA, the loop is within VSWR = 2 circle with L_1 = 2.9 cm and s = 0.1 cm, so another identical parasitic patch is placed on the other side of the fed RMSA with s = 0.1 cm to improve the

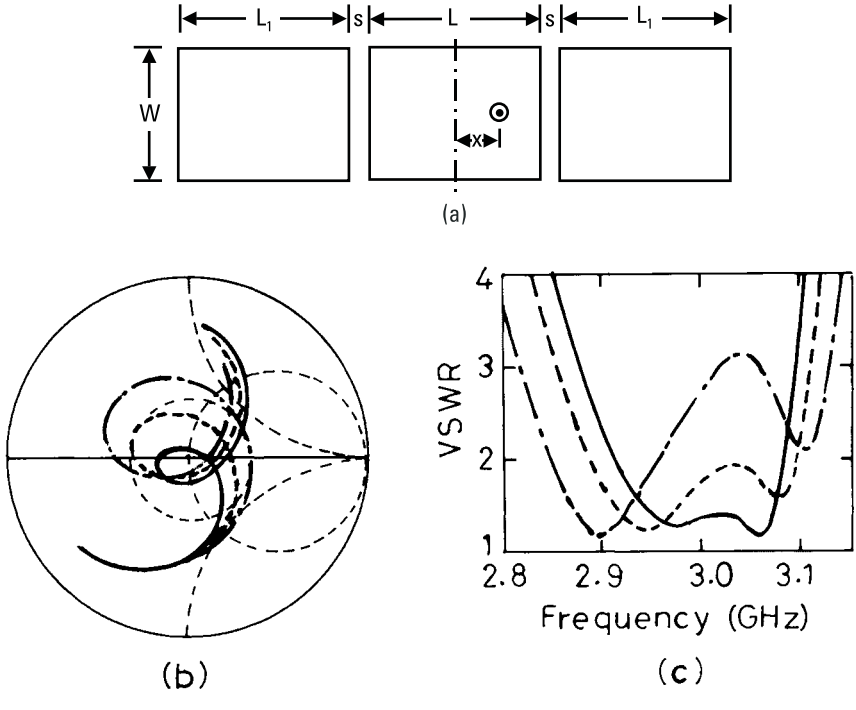

Figure 3.7 (a) Three gap-coupled RMSA and its (b) input impedance and (c) VSWR plots for three values of s: (– – –) 0.1, (- - -) 0.15, and (——) 0.2 cm.

radiation pattern characteristics as described above. The input impedance and VSWR plots for the three-radiating-edge gap-coupled RMSA is shown in Figure 3.7(b, c). The loop size is large compared to the two gap-coupled RMSA, because two coupled patches are resonant at the same frequency and hence the coupling is greater. The loop size is reduced by increasing the gap between the fed and the parasitic patches. The input impedance and VSWR plots for two different values of s (0.15 cm and 0.2 cm) are also shown in Figure 3.7. The loop in the impedance plot for s = 0.15 and 0.2 cm is completely inside the VSWR = 2 circle, yielding BWs of 209 MHz and 171 MHz, respectively. The BW for s = 0.15 cm is larger than that for s = 0.20 cm because of the larger loop size.

The radiation patterns in the E- and H-planes near the two-band edge frequencies (2.89 GHz and 3.09 GHz) for s = 0.15 cm are shown in Figure 3.8. The variation of the pattern in the H-plane over the entire BW is very small. The HPBW in the H-plane remains nearly the same as that of the single RMSA, because there are no parasitic patches in this plane. In the E-plane, the beam maxima is in the broadside direction. However, as the frequency increases, the sidelobes begin to appear due to the large overall length of the antenna in this plane. Also, at the higher frequency, the parasitic patches are resonant, which means that they experience phase delay with respect to the central patch. Hence, the beam will try to shift in the $+\theta$ and $-\theta$ directions. The net result is that sidelobes are formed in the E-plane pattern along these directions. The HPBW in the E-plane is smaller than that of the two gap-coupled configurations due to increase in the aperture area. The gain of the three gap-coupled RMSA is 9.4 dB at 3 GHz, which is 2.7 dB more than the single RMSA. Thus, by adding two parasitic patches,

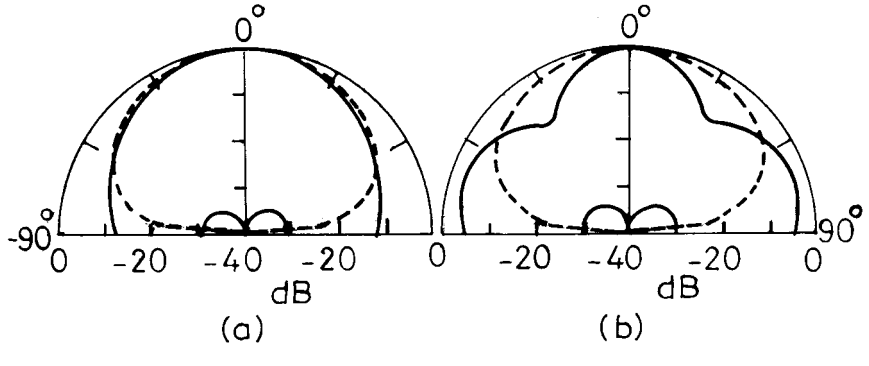

Figure 3.8 Radiation pattern of three gap-coupled RMSA at frequencies (a) 2.89 and (b) 3.09 GHz: (——) E-plane and (- - -) H-plane.

the gain of the antenna increases from 6.7 dB to 9.4 dB, and the BW increases from 65 MHz to 209 MHz at the expense of increase in the size of the antenna.

The BW of the three gap-coupled RMSA can be increased by increasing h, as in the case of single RMSA. However, as shown in Figure 3.1, if the BW of an individual patch is large, then the difference between the two patch dimensions should also be large to obtain broader BW. So, when h is increased from 0.159 cm to 0.318 cm, and if the parasitic patch of length L_1 = 2.9 cm is placed along both the radiating edges of the RMSA, then the BW will not be optimum. Also, the coupling between the fed and parasitic patches depends upon the s/h ratio and not on the s value alone, so the gap has been increased from 0.15 cm to 0.3 cm for three gap-coupled RMSA. For the feed at x = 1.4 cm, the input impedance plot is shown in Figure 3.9. As expected, in this case, the BW is not optimum and the loop is not inside the VSWR = 2 circle, instead it is formed in the lower frequency region. To bring the loop within the VSWR = 2 circle, the length L_1 of the parasitic patch is decreased, so the loop will be formed in the higher frequency region and therefore moves in the clockwise direction. For L_1 = 2.75 cm, the input impedance and VSWR plots are also shown in Figure 3.9. The loop is completely inside the VSWR = 2 circle, yielding a BW of 335 MHz (11.3%). The gain of the antenna at 3 GHz is 9.2 dB. The gain is slightly decreased as compared to that of the antenna with h = 0.159 cm due to an increase in the surface waves.

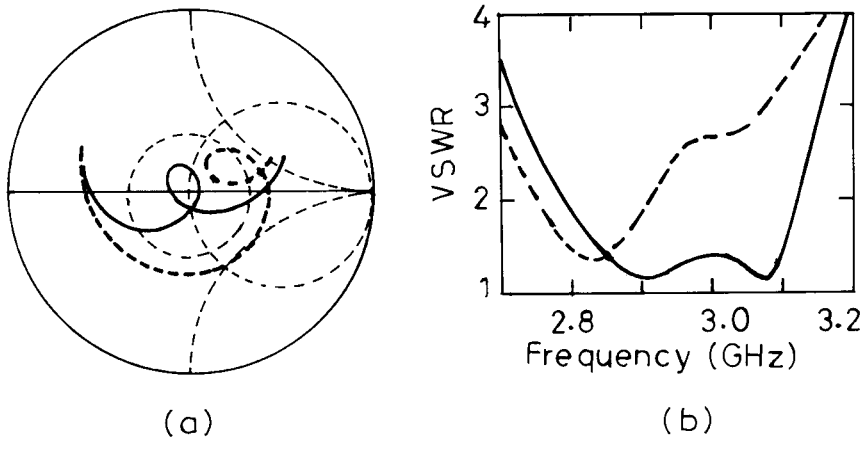

Figure 3.9 (a) Input impedance and (b) VSWR plots of three gap-coupled RMSA with h = 0.318 cm for two values of L_1: (- - -) 2.9 cm and (——) 2.75 cm.

The BW of the three gap-coupled RMSA increases further when a thicker substrate with a lower dielectric constant is used. For $\epsilon_r = 1$ and $h = 0.5$ cm, the length L of the fed patch is increased to 5 cm, so that its resonance frequency is around 3 GHz. The width W has been reduced to 3 cm to increase the input impedance of the antenna for proper impedance matching with a 50-Ω coaxial feed. For $L_1 = 4$ cm, $s = 0.4$ cm and $x = 2.2$ cm, the input impedance and VSWR plots are shown in Figure 3.10. The parasitic patch length L_1 is much smaller than L, because for a broadband patch, the difference between the fed and parasitic patch frequencies should be large. A BW of 461 MHz (15.3%) is obtained, whereas for a single RMSA on the same substrate with $L = 5$ cm, $W = 3$ cm, and feed at $x = 0.9$ cm, the BW is 130 MHz (2.4%).

The radiation pattern of the antenna in the E and H-planes near the two band-edge frequencies (2.775 GHz and 3.225 GHz) is shown in Figure 3.11. The radiation pattern in the H-plane remains in the broadside direction at all the frequencies. Whereas in the E-plane, the radiation pattern is in the broadside direction at the lower frequency but at the higher frequency, two sidelobes are formed. These two sidelobes are due to the excitation of the parasitic patches, which experience large phase delay with respect to the fed patch at a higher frequency. At 3 GHz, the gain of the antenna is 11.2 dB.

3.3.1.3 Two Unequal Parasitic Patches

The BW of the three gap-coupled RMSA can also be increased further by choosing the parasitic patches of different lengths L_1 and L_2 as shown in

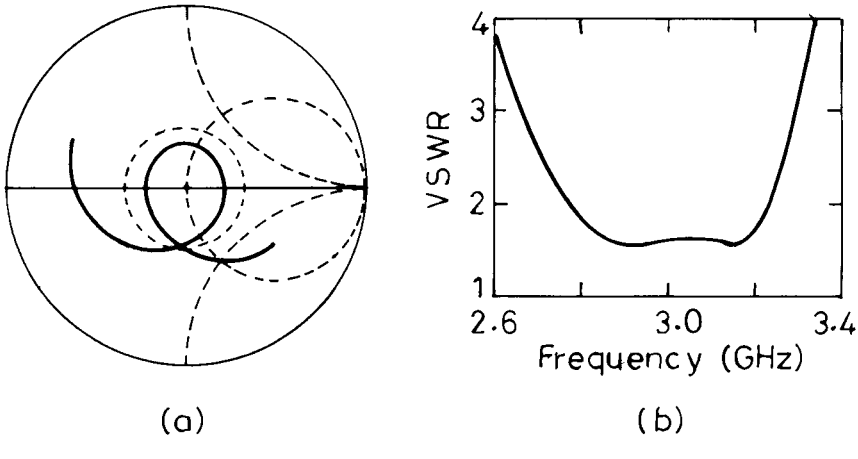

Figure 3.10 (a) Input impedance and (b) VSWR plots of a three gap-coupled RMSA with $\epsilon_r = 1$ and $h = 0.5$ cm.

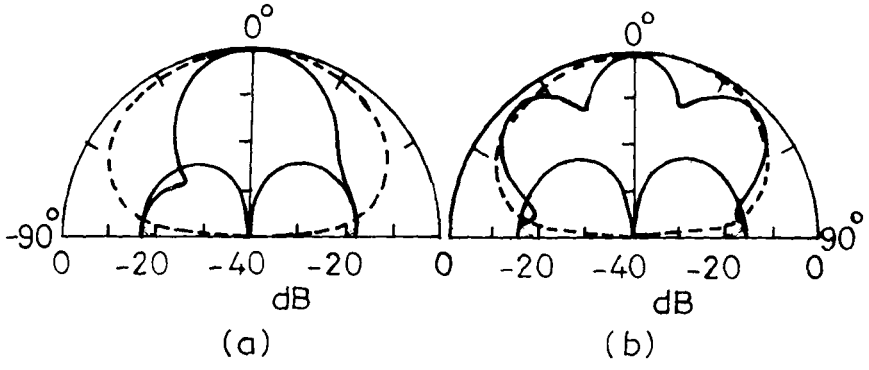

Figure 3.11 Radiation pattern of a three gap-coupled RMSA with $\epsilon_r = 1$ and $h = 0.5$ cm at two frequencies. (a) 2.775 GHz and (b) 3.225 GHz: (——) E-plane and (- - -) H-plane.

Figure 3.12(a). The length L_1 is taken slightly greater than the length L_2, so that the two parasitic patches will be resonant at different frequencies. If these frequencies are close to each other, broad BW is obtained. The input impedance and VSWR plots for $L = 3.0$ cm, $W = 4.0$ cm, $L_1 = 3.0$ cm, $s = 0.1$ cm, $x = 1.4$ cm with $\epsilon_r = 2.55$, $h = 0.159$ cm, $\tan \delta = 0.001$, and two values of L_2 (2.8 cm and 2.85 cm) are shown in Figure 3.12(b, c). Two loops are formed in the impedance plots, which are due to the different resonance frequencies of the two parasitic patches. Both the loops are inside the VSWR = 2 circle. A larger BW of 328 MHz is obtained for $L_2 = 2.8$ cm as compared to the BW of 289 MHz for $L_2 = 2.85$ cm. For $L_2 = 2.85$ cm, the separation between the two loops is less as compared to that for $L_2 = 2.8$ cm because of the smaller difference in length with respect to $L_1 = 3$ cm. Similar separation in the higher frequency range may also be noted from VSWR plot. If the difference between the lengths of the two parasitic patches is further reduced, then the second loop is formed within the first loop. If both parasitic lengths are reduced from $L_1 = 3$ cm and $L_2 = 2.85$ cm to $L_1 = 2.95$ cm and $L_2 = 2.8$ cm (i.e., the difference between the two parasitic patches is same), then the shape of the loops in the impedance plot remains the same, except that their position is shifted clockwise due to the decrease in both the parasitic lengths.

For the three gap-coupled RMSA with $L_1 = 3$ cm and $L_2 = 2.8$ cm, the radiation pattern at three frequencies (near the center and the two band-edge frequencies) is shown in Figure 3.13. In the H-plane, the radiation pattern remains nearly the same over the entire BW. However, in the E-plane, the radiation pattern varies with frequency. At 2.85 GHz, the central patch

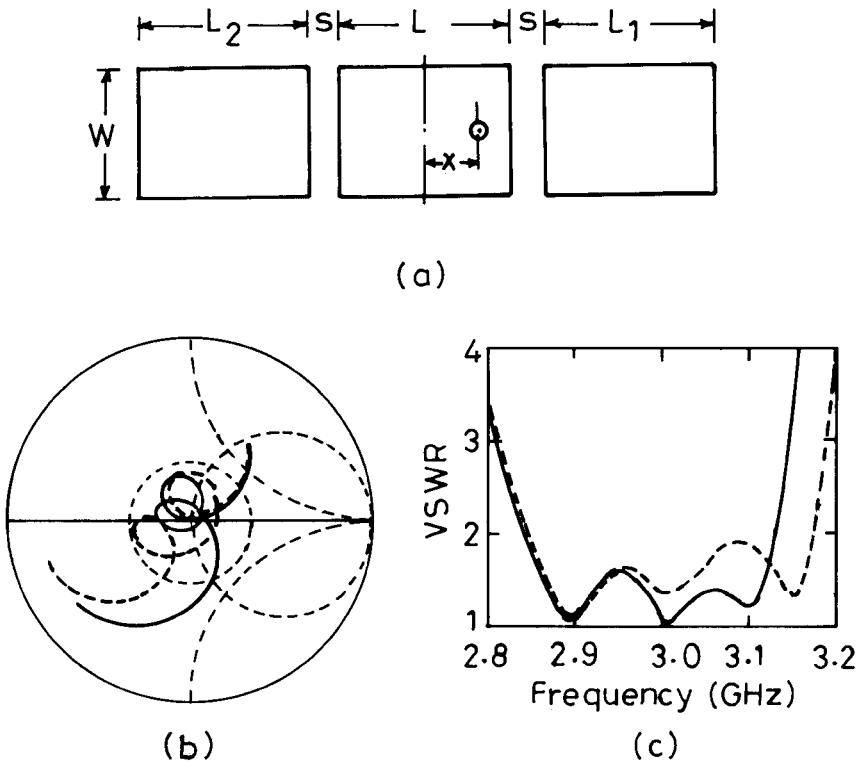

Figure 3.12 (a) A three gap-coupled RMSA with unequal parasitic patches, and its (b) input impedance and (c) VSWR plots for two values of L_2: (- - -) 2.8 cm and (——) 2.85 cm.

is resonant, so the maximum radiation is in the broadside direction. At 3.01 GHz, the radiation from the parasitic patch of length L_1 is dominant, so the beam shifts to +30° from the broadside. At 3.17 GHz, the parasitic patch of length L_2 is resonant, so the beam shifts along the −55° direction. The shift in the pattern is more in the $-\theta$ direction because it experiences larger phase delay from the feed point as it is resonant at a higher frequency. However, along the broadside direction, the beam remains within 5 dB of its maximum value at all the frequencies within the BW. So, the broad impedance BW is useful only if this amount of pattern variation is acceptable.

Similarly, broad impedance BW from 2.597 GHz to 3.194 GHz is obtained for $\epsilon_r = 1$ with $h = 0.5$ cm, $L = 5$ cm, $L_1 = 4.5$ cm, $L_2 = 4$ cm, $W = 3$ cm, $s = 0.3$ cm, and $x = 2.2$ cm. This impedance BW of 597 MHz is larger than the impedance BW of 502 MHz for two parasitic patches of

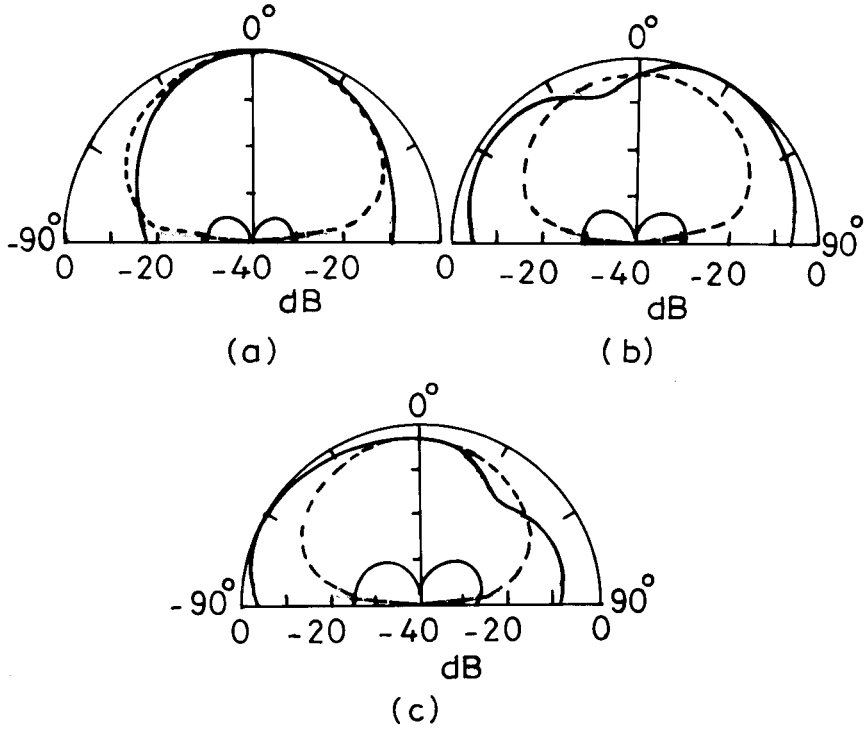

Figure 3.13 Radiation pattern of a three gap-coupled RMSA with L_1 = 3.0 cm and L_2 = 2.8 cm at three frequencies (a) 2.85 GHz, (b) 3.01 GHz, and (c) 3.17 GHz: (——) E_θ in the ϕ = 0° and 90° planes and (- - -) E_ϕ in the ϕ = 90° plane.

equal length ($L_1 = L_2 = 4$ cm). However, the beam maxima varies from the broadside to the $+\theta$ and $-\theta$ directions with an increase in the frequency within the BW.

The theoretical and experimental input impedance and VSWR plots for a three gap-coupled RMSA with unequal parasitic patches are shown in Figure 3.14 [7]. The dimensions of the antenna are L = 2.7 cm, L_1 = 2.615 cm, L_2 = 2.51 cm, W = 3.9 cm, s = 0.165 cm, and x = 1.23 cm, and the substrate parameters are ϵ_r = 2.55, h = 0.159 cm, and tan δ = 0.001. The two loops in the impedance plot are inside the VSWR = 2 circle. The theoretical and measured BWs are 294 MHz and 331 MHz, respectively. The theoretical and measured radiation patterns at three frequencies in the E-plane are given in Figure 3.15(a, b). As discussed earlier, the E-plane pattern varies over the BW. However, along the broadside direction, it remains within approximately 2 dB in the entire frequency range. In the

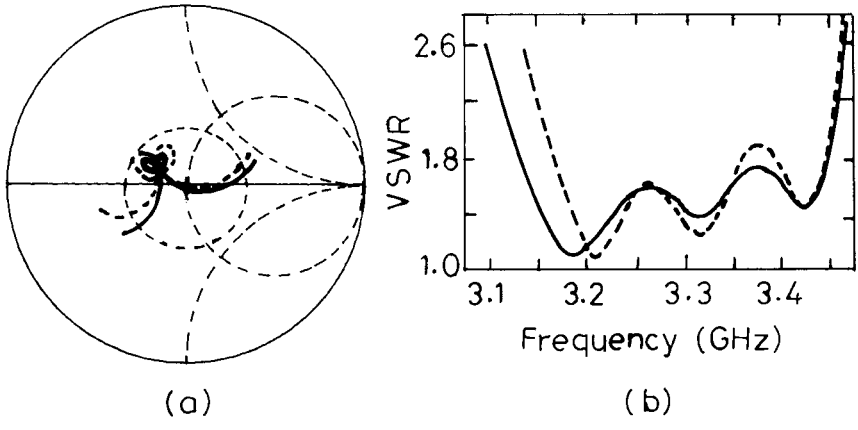

Figure 3.14 (a) Input impedance and (b) VSWR plots of a three-radiating-edge gap-coupled RMSA with unequal parasitic patches: (——) theoretical and (- - -) experimental.

H-plane, there is not much variation in the pattern within the BW. Hence, the theoretical measured pattern is given only at 3.2 GHz in Figure 3.15(c).

In the above cases, if the difference in patch lengths is large, and the gap between the fed and parasitic patches is small, then dual- and triple-band operations can be obtained as described in Chapter 7.

3.3.2 Nonradiating-Edge Gap-Coupled RMSAs

Instead of placing two parasitic rectangular patches along the radiating edges of the centrally fed RMSA, these could be placed along its nonradiating edges as shown in Figure 3.16(a) [9]. The gaps between the fed and the parasitic patches should be smaller as compared to those in the radiating edge-coupled RMSA. Because the field varies sinusoidally along the non-radiating edge, the coupling will be smaller as compared to the coupling along the radiating edge, where the field is uniform.

Initially, the parasitic patches are identical. For L = 3 cm, W = 4 cm, s = 0.05 cm, length of the parasitic patches $L_1 = L_2$ = 2.9 cm, and feed at x = 1.1 cm, with substrate parameters ϵ_r = 2.55, h = 0.159 cm, and tan δ = 0.001, the input impedance and VSWR plots are shown in Figure 3.16(b, c). These dimensions are similar to that of the three-radiating-edge gap-coupled RMSA except for the smaller value of air gaps. There is a single loop in the impedance plot, and the BW is 159 MHz (5.3%). The effect of various parameters on the performance of the antenna is similar to that of the

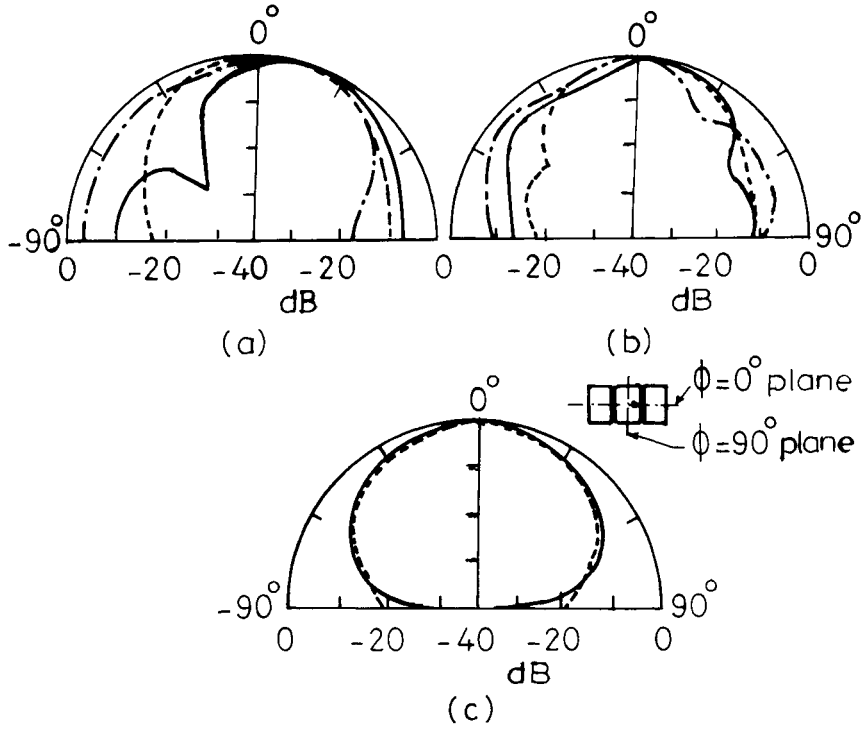

Figure 3.15 Radiation pattern of a three gap-coupled RMSA with unequal parasitic patches: (a) theoretical and (b) experimental pattern in E-plane at three frequencies—(- - -) 3.19 GHz, (——) 3.29 GHz, and (– – –) 3.39 GHz; (c) H-plane pattern at 3.2 GHz: (——) theoretical and (- - -) experimental.

radiating-edges gap-coupled RMSA. When the substrate thickness h is increased from 0.159 cm to 0.318 cm, the various parameters, such as, L_1, L_2, s, and x have to be optimized to obtain broad BW. For $L_1 = L_2 = 2.7$ cm, $s = 0.05$ cm, and $x = 1.4$ cm, the input impedance and VSWR plots are also shown in Figure 3.16(b, c). The BW is 319 MHz (10.5%).

The radiation patterns near the two band-edge frequencies (2.88 GHz and 3.19 GHz) for the thicker substrate are shown in Figure 3.17. In the E-plane, the radiation pattern is similar to that of a single RMSA. As the frequency increases within the BW, the HPBW decreases and the sidelobe level increases. In the H-plane, at the lower frequency, the pattern is maximum in the broadside direction. As the frequency increases, three lobes are formed in the pattern due to the phase delay experienced by the resonant parasitic patches. The gain of the antenna is 8.1 dB at 3 GHz.

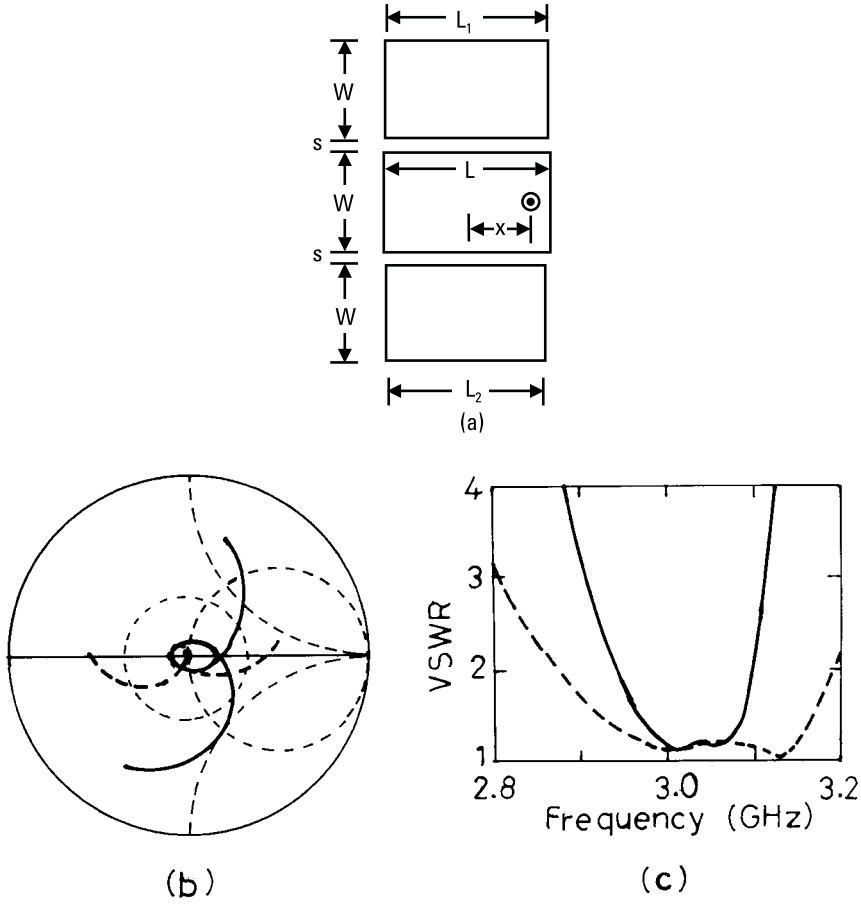

Figure 3.16 (a) Nonradiating-edges gap-coupled RMSA with two parasitic patches and its (b) input impedance and (c) VSWR plots for two values of h: (——) 0.159 cm and (- - -) 0.318 cm.

Since the width of each patch is larger than the length, the overall width of the gap-coupled antenna becomes too large. The width of the each patch is therefore reduced from 4 to 3 cm for a thicker substrate. For L = 3 cm, W = 3 cm, $L_1 = L_2$ = 2.7 cm, s = 0.05 cm, and x = 1.4 cm, the input impedance and VSWR plots are shown in Figure 3.18. The BW is 390 MHz (12.7%), which is comparable to that of the antenna with W = 4 cm. However, the gain of the antenna is reduced from 8.1 dB to 7.5 dB because of the decrease in the aperture area.

The BW of the antenna increases when the two parasitic patches are of unequal lengths. For L = 3 cm, W = 3 cm, L_1 = 2.8 cm, L_2 = 2.6 cm,

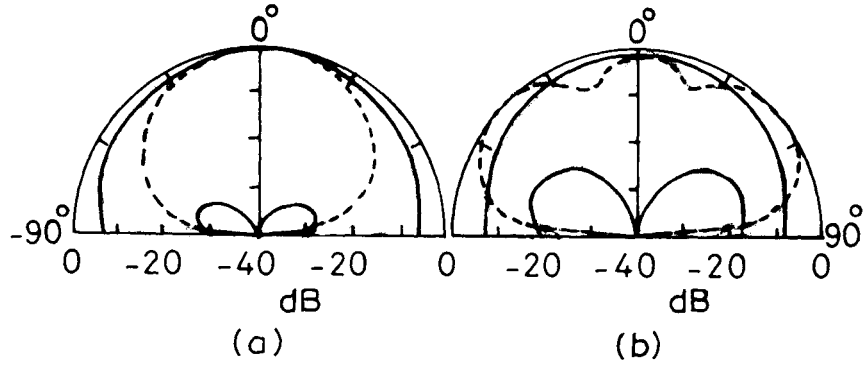

Figure 3.17 Radiation pattern of nonradiating-edge gap-coupled RMSA for h = 0.318 cm at frequencies (a) 2.88 GHz and (b) 3.19 GHz: (——) E_θ in the ϕ = 0° and 90° planes and (- - -) E_ϕ in the ϕ = 90° plane.

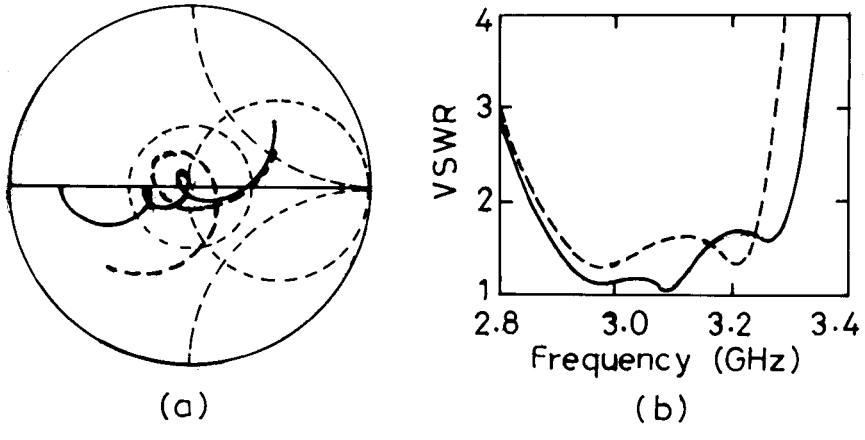

Figure 3.18 (a) Input impedance and (b) VSWR plots of nonradiating-edge gap-coupled RMSA with W = 3 cm for equal and unequal parasitic lengths: (- - -) L_1 = L_2 = 2.7 cm and (——) L_1 = 2.8 cm and L_2 = 2.6 cm.

s = 0.05 cm, and x = 1.0 cm, the input impedance and VSWR plots are shown in Figure 3.18. The two loops present in the impedance plot are due to the different resonance frequencies of the two parasitic patches. The BW of the antenna is 447 MHz (14.5%), which is more than that of the antenna with equal parasitic patches.

For unequal parasitic elements, the radiation patterns at three frequencies (2.86, 3.08, and 3.29 GHz) are shown in Figure 3.19. In the E-plane, there is a small variation in the pattern over the BW, but in the H-plane,

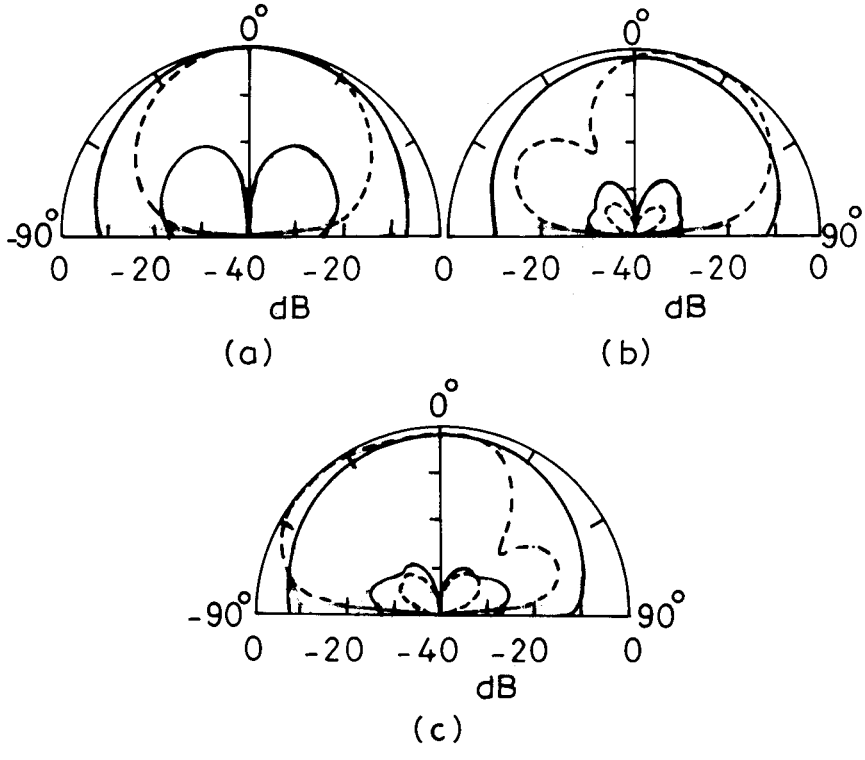

Figure 3.19 Radiation pattern of nonradiating-edge gap-coupled RMSA with L_1 = 2.8 cm and L_2 = 2.6 cm at frequencies (a) 2.86, (b) 3.08, and (c) 3.29 GHz: (——) E_θ in the ϕ = 0° and 90° planes and (- - -) E_ϕ in the ϕ = 90° plane.

radiation pattern varies significantly. At the lower frequency, the radiation from the central patch is dominant, so the beam is maximum along the broadside. At the center frequency, the top patch is resonant; hence the pattern maxima is shifted along the $+\theta$ direction. At the higher frequency, the bottom patch is resonant, so the pattern is shifted along the $-\theta$ direction. As a result, the broad BW is obtained at the expense of degradation in the radiation pattern.

3.3.3 Four-Edge Gap-Coupled RMSAs

When the parasitic patches are placed along all the four edges of the RMSA [8], as shown in Figure 3.20, both BW and gain increase. The patches along the radiating and the nonradiating edges are separately taken equal. However, the patches along the two orthogonal edges are taken to be unequal lengths,

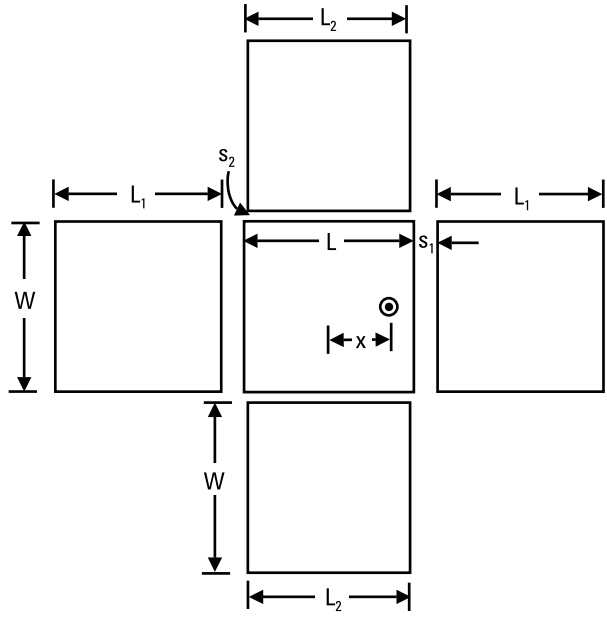

Figure 3.20 Four-edge gap-coupled RMSA.

so that their resonance frequency is different but close to each other to yield broad BW. The gap along the nonradiating edges is taken smaller than that of the radiating edges, because field varies sinusoidally along the nonradiating edges.

For L = 3 cm, W = 3 cm, L_1 = 2.9 cm, s_1 = 0.15 cm, L_2 = 2.85 cm, s_2 = 0.05 cm, ϵ_r = 2.55, h = 0.159 cm, tan δ = 0.001, and feed at x = 1.2 cm, the input impedance and VSWR plots are shown in Figure 3.21(a, b). The BW for VSWR ≤ 2 is 263 MHz (8.6%). The gain at 3.05 GHz is 9.9 dB.

For a thicker substrate (h = 0.318 cm) with parameters L = 3 cm, W = 3 cm, L_1 = 2.75 cm, s_1 = 0.25 cm, L_2 = 2.55 cm, s_2 = 0.05 cm, and feed at x = 1.4 cm, the input impedance and VSWR plots are shown in Figure 3.21(c, d). The BW is 569 MHz (18.2%). The radiation pattern of the antenna at three frequencies (2.84, 3.12, and 3.40 GHz) is shown in Figure 3.22. The variation in the radiation pattern may be noted over the BW. The gain of the antenna is 9.2 dB at 3 GHz.

3.3.4 Design Guidelines for Gap-Coupled RMSAs

It has been observed that the two gap-coupled RMSA and the three-unequal gap-coupled RMSA with unequal parasitic elements yield wide BW. How-

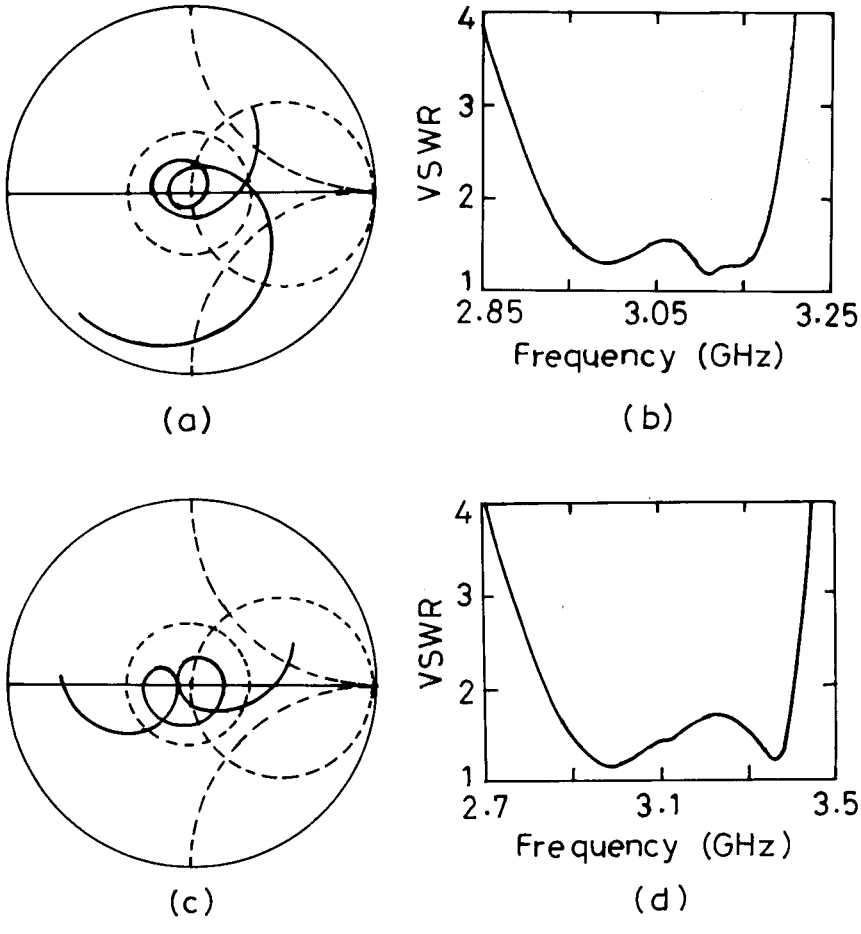

Figure 3.21 Response of a four-edge gap-coupled RMSA: (a) Input impedance and (b) VSWR plots for h = 0.159 cm and (c) input impedance and (d) VSWR plots for h = 0.318 cm.

ever, the maxima of radiation patterns shifts away from the broadside within the BW, which is not acceptable for many applications. The three gap-coupled RMSA configuration with identical parasitic elements has typically three times the BW of a single element with a broadside radiation pattern throughout the BW.

Since the three gap-coupled RMSA has a stable radiation pattern over the BW, let us take an example of its design for the required BW from f_L to f_H. The fed patch should be designed at $f_1 = f_L + \Delta f$ with a BW of $2\Delta f$, where $\Delta f = (f_H - f_L)/6$. The substrate parameters and patch dimensions

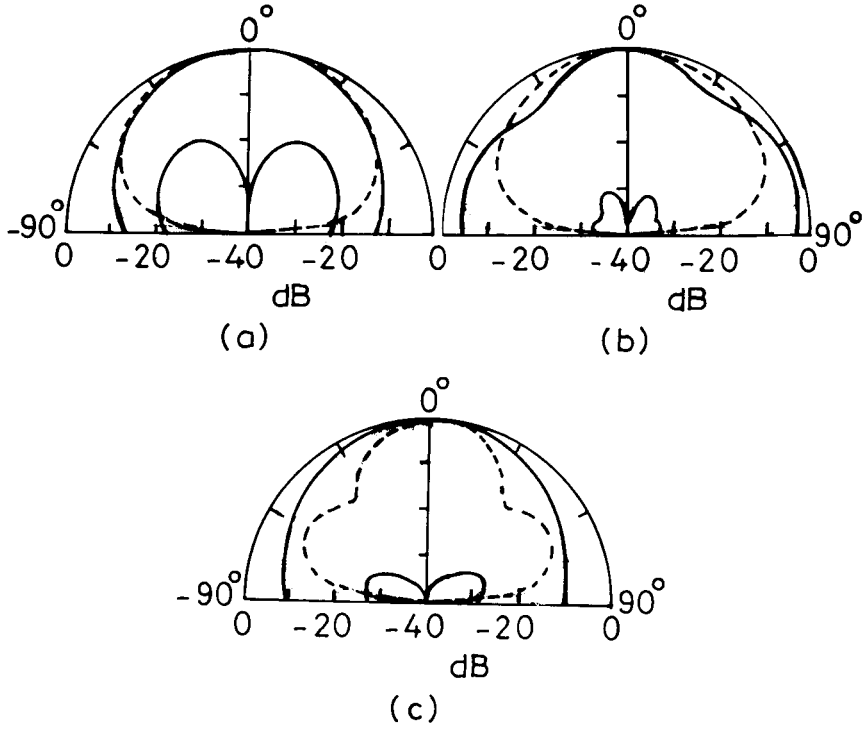

Figure 3.22 Radiation pattern of four-edge gap-coupled RMSA at frequencies (a) 2.84, (b) 3.12, and (c) 3.40 GHz: (——) E_θ in the ϕ = 0° and 90° planes and (- - -) E_ϕ in the ϕ = 90° plane.

should be chosen accordingly to yield this resonance frequency and BW. The length of the two identical parasitic patches should be chosen such that their resonance frequency $f_2 = f_H - \Delta f$.

The gap between the fed and parasitic patches depends primarily on ϵ_r and h of the substrate. If the spacing is too small, then the coupling between the patches is more likely to lead to a bigger loop size in the impedance loci, which comes out of the VSWR = 2 circle. On the other hand, a larger gap reduces the loop size thereby reducing the BW. The spacing increases with h and reduces with ϵ_r. A good starting point for the value of the gap is around $0.8h$ for the radiating-edge gap-coupled RMSA and around $0.3h$ for the nonradiating-edge gap-coupled RMSA. The location of the feed point x for the coupled configuration is always shifted more toward the edge as compared to that of a single patch. For ϵ_r = 1 with large h, matching is obtained generally near the edge of the fed RMSA.

The above guidelines can be used for the initial design of three gap-coupled RMSA. The optimization of the BW can be carried out by looking at the location and size of the loop on the Smith chart after studying the effect of various parameters on the impedance plot of the antenna. The above concept can be extended to a five gap-coupled RMSA and other gap-coupled CMSA and TMSA configurations described in the following sections.

3.3.5 Other Gap-Coupled Multiresonator RMSAs

One of the drawbacks of placing $\lambda/2$-resonant patches along the radiating or the nonradiating or all the four edges of the centrally fed rectangular patch is, that the size of the antenna becomes large and hence unsuitable to be used as an array element. However, linear arrays of radiating or nonradiating-edge gap-coupled RMSAs could always be used to increase the gain. To reduce the size of these gap-coupled antennas, several configurations are possible, with an overall size of less than λ_0. In Figure 3.23(a), two thin parasitic patches (narrow strips) are placed along the nonradiating edge of the RMSA fabricated on a Teflon fiberglass substrate with h = 0.32 cm [2, 10]. The dimensions shown in Figure 3.23 are in centimeters. The gaps between the patches are kept close to two-and-a-half to three times the

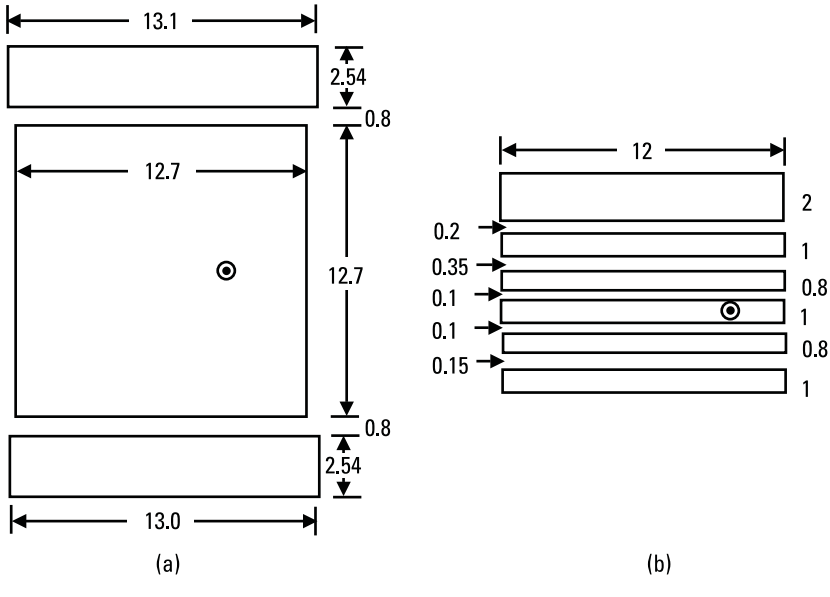

Figure 3.23 Two different broadband nonradiating-edge gap-coupled RMSAs: (a) rectangular patch with two narrow strips and (b) six gap-coupled narrow strips.

substrate thickness. The dimensions of the narrow strips and the gap between the fed patch and the strips are optimized so that the resonance frequencies of the strips and the patch are close to each other to yield broad BW. The experimental BW of this configuration is more than twice the BW of a single patch.

Instead of placing two narrow parasitic strips along the nonradiating edge of the RMSA, the patch itself is divided into a number of narrow strips (printed dipoles) [11, 12]. Six narrow strips of equal lengths but different widths are gap-coupled to each other as shown in Figure 3.23(b). The dimensions shown in Figure 3.23(b) are optimized for the antenna to operate around 875 MHz. The substrate parameters are $\epsilon_r = 2.2$ and $h = 0.08$ cm. The measured BW is equal to 10 times of that of a single patch of the same overall area. Since the size of the patch is compact, the measured radiation pattern is stable over this large BW.

Instead of splitting the patch into different widths, it can be divided into two parts along the length, with the edges of the two parts at the extreme ends shorted with the ground plane. Each part acts as a shorted $\lambda/4$ RMSA, which is gap-coupled to the other part as shown in Figure 3.24(a). This concept can be extended to radiating, nonradiating, and four-edge gap-coupled RMSAs, in which the parasitic patches are replaced by shorted $\lambda/4$ rectangular patches. A fed RMSA with two parasitic shorted $\lambda/4$ rectangular patches along its radiating edges is shown in Figure 3.24(b). Its BW is more than two times of that of the single RMSA [13].

3.4 Directly Coupled RMSAs

The gap along the nonradiating-edge for some of the gap-coupled configurations becomes critical and sometimes unrealizable for controlling the coupling to obtain the desired response. In these cases, multiple resonators can be connected with thin microstrip lines to increase the coupling in a process known as direct coupling [14].

3.4.1 Radiating-Edge Directly Coupled RMSAs

Three directly coupled rectangular patches are shown in Figure 3.25(a). Only the central patch is fed, and the adjoining two rectangular patches along its radiating edges are connected by thin microstrip lines. The strips are generally located at the midpoint of the widths of the patches so that the antenna is symmetrical with the feed-point axis. The lengths of these connecting strips

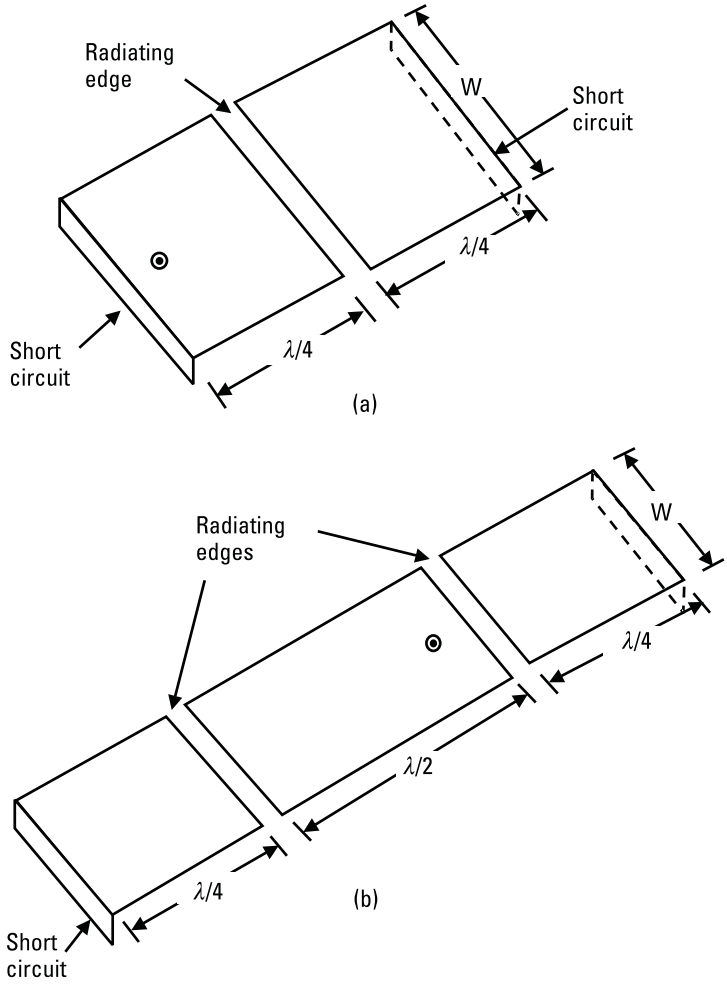

Figure 3.24 (a) Two gap-coupled shorted rectangular patches and (b) an RMSA with two gap-coupled shorted rectangular patches.

are greater than twice the substrate thickness to minimize coupling through the gaps between the patches. When the length is less than this, hybrid (gap and direct) coupling occurs as now the coupling between the patches is through the gap as well as due to the connecting strip.

For the radiating-edge directly-coupled RMSA with L = 3 cm, L_1 = 2.85 cm, L_2 = 2.55 cm, W = 2 cm, s = 1.1 cm, w = 0.03 cm, feed at x = 0.9 cm, ϵ_r = 2.55, h = 0.318 cm, and tan δ = 0.001, the measured BW is 548 MHz (17.1% at 3.2 GHz) [14]. This BW is approximately five times

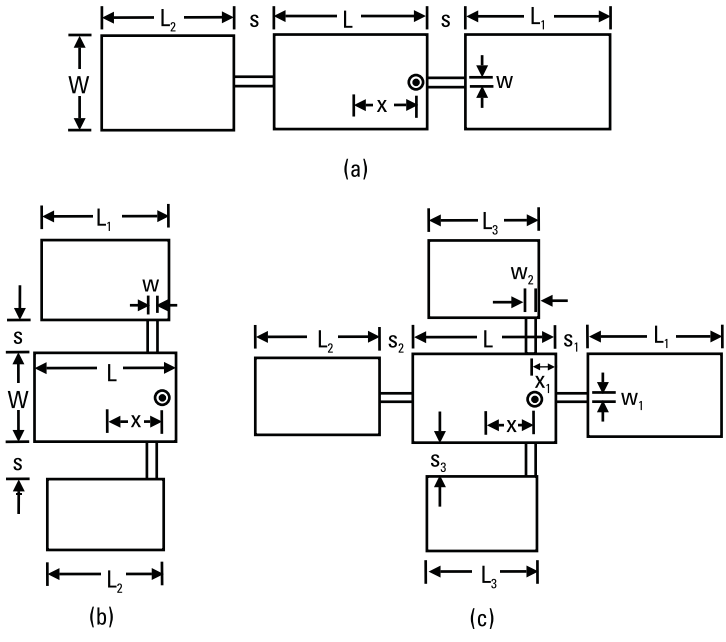

Figure 3.25 Directly coupled RMSA along (a) radiating, (b) nonradiating, and (c) four edges.

the BW of that of the single RMSA. Since the two coupled patches along the radiating edges have different dimensions, it results in a shift in the beam maximum direction within the BW in the E-plane. In the H-plane, however, the beam maxima remains in the broadside direction [14].

3.4.2 Nonradiating-Edge Directly Coupled RMSAs

The nonradiating-edge directly coupled RMSA is shown in Figure 3.25(b). The location of the connecting strip has a significant effect on the coupling between the patches, because the field varies sinusoidally along the length of the patch. Large coupling is obtained when connecting strips are shifted near the edges of the patches. Also, coupling between the fed patch and the coupled patch increases with increase in the width of the strip.

For L = 3 cm, W = 2 cm, L_1 = 2.71 cm, L_2 = 2.45 cm, s = 0.7 cm, w = 0.27 cm, location of the strip from the edge x_1 = 0.6 cm, and feed at x = 0.95 cm, the measured BW of 605 MHz (18.3% at 3.31 GHz) is obtained [14]. In this case, coupled patches of different dimensions are in

the H-plane, so there is variation in the beam maxima in the H-plane over the BW. In the E-plane, the beam maxima remains in the broadside direction.

3.4.3 Four-Edge Directly Coupled RMSAs

The four-edge directly coupled RMSA is shown in Figure 3.25(c). The patches coupled to the radiating edges have different lengths, whereas patches coupled along the nonradiating edge have the same length. The optimized dimensions are L = 3 cm, W = 2 cm, L_1 = 2.85 cm, L_2 = 2.635 cm, L_3 = 2.35 cm, s_1 = 1.31 cm, s_2 = 1.06 cm, s_3 = 0.71 cm, w_1 = 0.025 cm, w_2 = 0.044 cm, x_1 = 0.71 cm, and feed at x = 1.02 cm [14]. The measured BW is 810 MHz, which is 24% at 3.38 GHz and seven times of that of the single RMSA. In the H-plane, the radiation pattern has beam maxima in the broadside direction, whereas in the E-plane the beam maxima shifts from the broadside in a $+\theta$ to $-\theta$ direction within the BW.

3.4.4 Multiresonator Impedance-Matching Network

The BW of the MSA can also be increased by using the impedance-matching technique [15, 16]. A coplanar multiresonator configuration is shown in Figure 3.26(a). It consists of an RMSA with coplanar microstrip impedance-

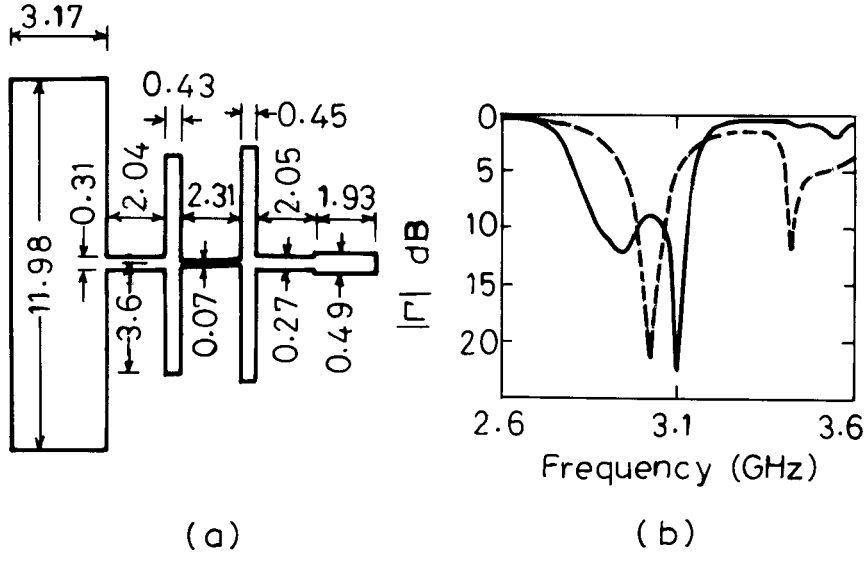

Figure 3.26 (a) RMSA with matching stubs and (b) reflection coefficient Γ plots of (- - -) RMSA only and (——) RMSA with matching stub.

matching network. The structure is designed as a three-element modified Chebychev network, where the first element is the antenna itself. The other two resonators are parallel stubs, at a half-wavelength each at resonant frequency. For ϵ_r = 2.2 and h = 0.08 cm, the length of the rectangular patch is 3.17 cm and the width is 11.98 cm at f_0 = 3.027 GHz. The large width is taken so that the input impedance is 50Ω at the radiating edge.

The dimensions of the matching network for a 50-Ω microstrip feed line are shown in the figure. The measured return loss Γ plots of the antenna with and without matching network are shown in Figure 3.26(b). The RMSA without the matching network has a fundamental frequency of 3.025 GHz, and the higher order mode is at 3.424 GHz due to its large width. The RMSA with the impedance-matching network yielded a BW of 275 MHz (9.1%) for the return loss of 8.8 dB (VSWR = 2.14). The radiation pattern is stable throughout the entire BW but has a higher cross-polar level.

The planar multiresonator technique discussed above uses only the rectangular patch as an element to enhance the BW. This technique is extended to circular, semicircular, and triangular patches [17–21] in the following sections.

3.5 Gap- and Hybrid-Coupled CMSAs

A CMSA excited at its fundamental TM_{11} mode shows one $\lambda/2$ cycle variation of the field along its half of the circumference. The field is maximum at the diametrically opposite points along the feed-axis. When the parasitic patches are placed along the feed-axis, the coupling is maximum, whereas when the patches are placed perpendicular to the feed-axis, the coupling will be negligible because of the null of the electric field. The parasitic circular patches placed along the feed axis could be either gap-coupled or directly coupled or hybrid-coupled to yield a broad BW.

3.5.1 Gap-Coupled CMSAs

Several gap-coupled CMSA configurations are described for broadband operation; they have been analyzed using IE3D. A CMSA of radius a = 2.2 cm with ϵ_r = 2.33, h = 0.159 cm, tan δ = 0.001, and a feed point at x = 0.65 cm from the center of the patch has a BW of 42 MHz (1.7%) for VSWR ≤ 2. The gain of the antenna at f_0 = 2.522 GHz is 6.8 dB.

To improve the BW and gain of the single CMSA with a symmetric broadside pattern, two identical parasitic circular patches are placed on either

side of the fed patch along the feed-axis as shown in Figure 3.27(a). For a = 2.2 cm, a_1 = 2.175 cm, s = 0.05 cm, and x = 1.0 cm, the input impedance and VSWR plots are shown in Figure 3.27(b, c). The loop is within a VSWR = 2 circle yielding a BW of 90 MHz (3.5%). The coupling between the parasitic and fed circular patches is weak due to the curved surfaces. The gap between the parasitic and fed circular patch is taken much smaller than that of radiating-edge gap-coupled RMSA configurations to improve the coupling. The radiation pattern of the antenna at 2.49 GHz and 2.57 GHz (near the band-edge frequencies) are shown in Figure 3.27(d, e). At a lower frequency, the radiation is maximum in the broadside direction. However, at a higher frequency, the maxima shifts away from the broadside because radiation from the parasitic patches is dominant. The gain of the antenna at 2.53 GHz is 9.5 dB.

The BW and gain are further improved by using a five gap-coupled CMSA. If the two additional parasitic patches are placed orthogonal to the feed-axis of the fed patch [i.e., along the $+Y$ and $-Y$ axis of Figure 3.27(a)] there will be no coupling to these additional parasitic patches due to the null voltage of the fed patch along this axis. As a result, two different configurations of the five gap-coupled CMSA can be used as shown in Figure 3.28. To obtain symmetrical pattern, identical parasitic patches are selected. In Figure 3.28(a), four parasitic patches are placed at an angle of $\pm 45°$ to the fed patch axis. The parasitic patches are only coupled with the fed patch. For a = 2.2 cm, a_1 = 2.15 cm, s = 0.05 cm, and x = 1.0 cm, the input impedance and VSWR plots are shown in Figure 3.29(a, b). The loop is within the VSWR = 2 circle, and the BW is 145 MHz (5.7%). The radiation patterns at two frequencies (2.47 GHz and 2.62 GHz) are shown in Figure 3.29(c, d). The variation of the pattern is small over the BW. The gain of the antenna at 2.54 GHz is 10.3 dB, which is 3.5 dB more than the single CMSA.

In Figure 3.28(b), the coupling to the parasitic patches is not only through the fed patch but also through the adjacent parasitic patches. For a = 2.2 cm, a_1 = 2.15 cm, x = 1.0 cm, s = 0.05 cm, and s_1 = 0.10 cm, the BW is 134 MHz (5.3%) and the gain of the antenna at f_0 = 2.53 GHz is 10.4 dB.

To increase the BW further, gap-coupled CMSAs with ϵ_r = 1 and h = 0.4 cm are considered in the above frequency range. For a single patch of radius a = 3.1 cm with a feed at x = 1.3 cm, the BW is 135 MHz at 2.59 GHz. For the three gap-coupled CMSA with a = 3.1 cm, a_1 = 2.7 cm, s = 0.1 cm, and x = 2.2 cm, the BW is 440 MHz (16.2%).

For the five gap-coupled CMSA with a single-coupling configuration shown in Figure 3.28(a), with a = 3.1 cm, a_1 = 2.7 cm, s = 0.1 cm and

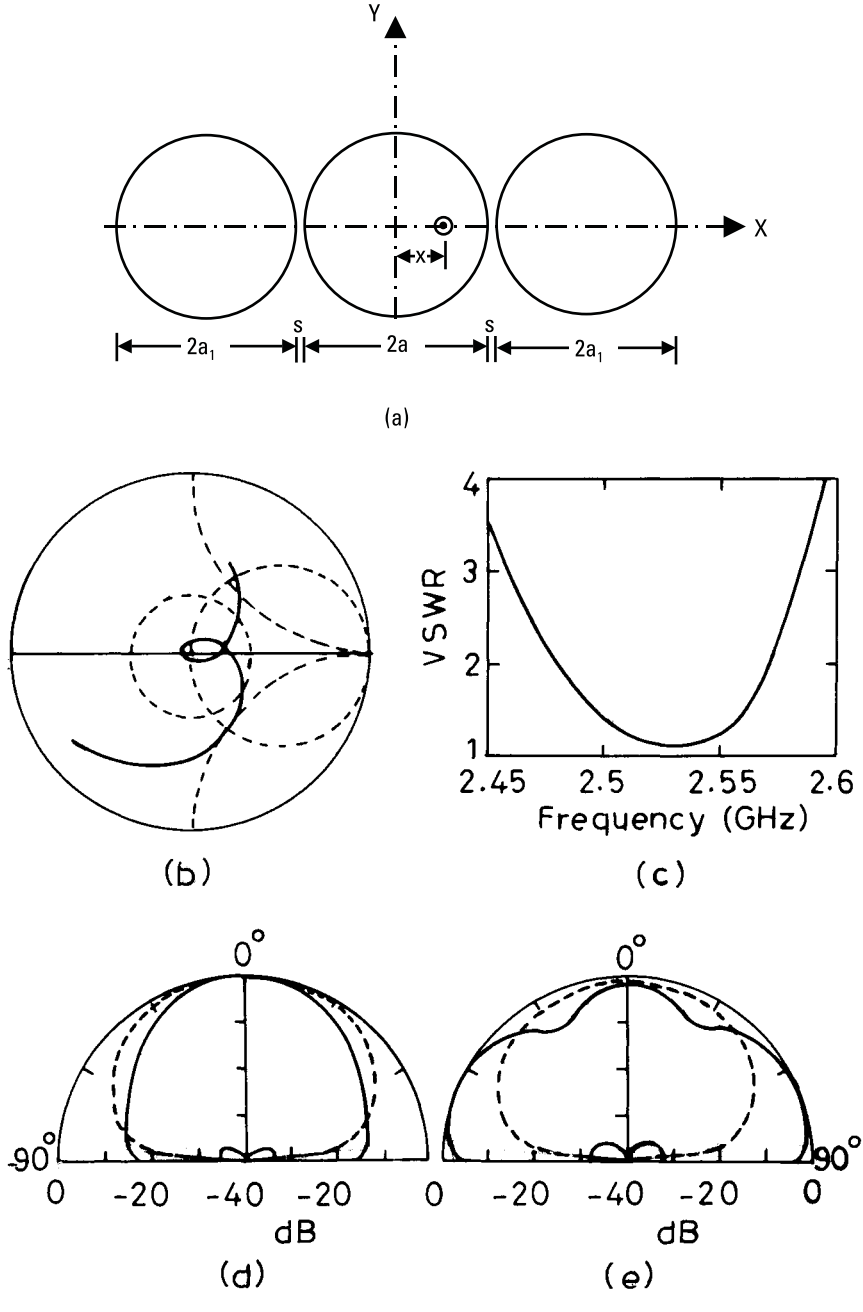

Figure 3.27 (a) Three gap-coupled CMSA and its (b) input impedance and (c) VSWR plots, with a radiation pattern at (d) 2.49 GHz and (e) 2.57 GHz. (——) E-plane and (- - -) H-plane.

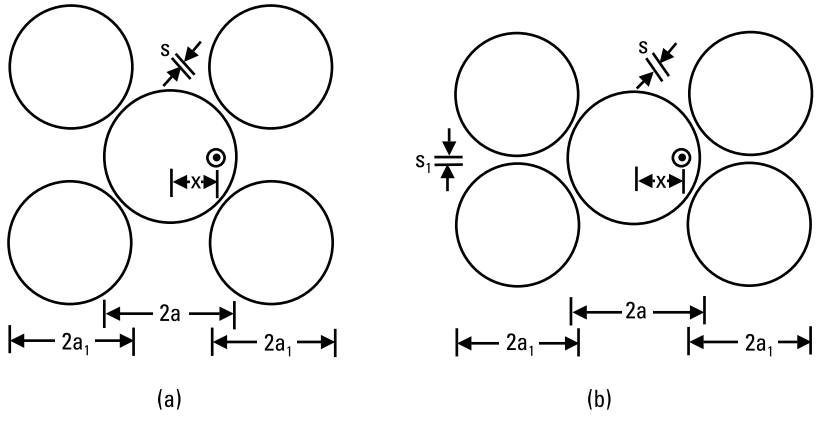

Figure 3.28 Five gap-coupled CMSA: (a) single coupling and (b) dual coupling.

x = 2.2 cm, the BW is 453 MHz (16.7%). For the dual-coupling configuration shown in Figure 3.28(b) with a = 3.1 cm, a_1 = 2.65 cm, s = 0.2 cm, s_1 = 0.3 cm, and x = 2.7 cm, the BW is 500 MHz (18.0%).

The BW and gain comparison of these gap-coupled CMSA configurations are given in Table 3.1. The five gap-coupled CMSA shown in Figure 3.28(b) yielded a maximum BW of 500 MHz with a gain of 12.7 dB. These configurations have a wider BW and simpler feed as compared to the similarly sized CMSA array.

3.5.2 Hybrid-Coupled CMSAs

When the radii of the two circular parasitic patches are taken differently to improve BW, then the coupling between the fed patch and the parasitic patches decreases. Hence, to improve the coupling, either the gap is to be reduced or hybrid coupling can be used [17]. A coaxially fed circular patch of diameter $2a$ = 3.1 cm with two parasitic patches of diameters $2a_1$ = 3.2 cm and $2a_2$ = 3 cm with spacing s = 0.1 cm is shown in Figure 3.30(a). The substrate parameters are ϵ_r = 4.3, h = 0.159 cm, and tan δ = 0.01. For x = 1.2 cm, the measured input impedance and VSWR plots of only gap-coupled CMSA (without a shorting strip) are shown in Figure 3.30(b, c). Two loops are tending to form, but because of small coupling between the curved surfaces of the circular patches, they are not pronounced. The ratio of the two frequencies of the parasitic CMSAs in the two loop positions is equal to the ratio of their respective radii.

To increase the coupling, shorting strips are used as shown in Figure 3.30(a). A shorting strip of width w = 0.1 cm is placed between the fed and

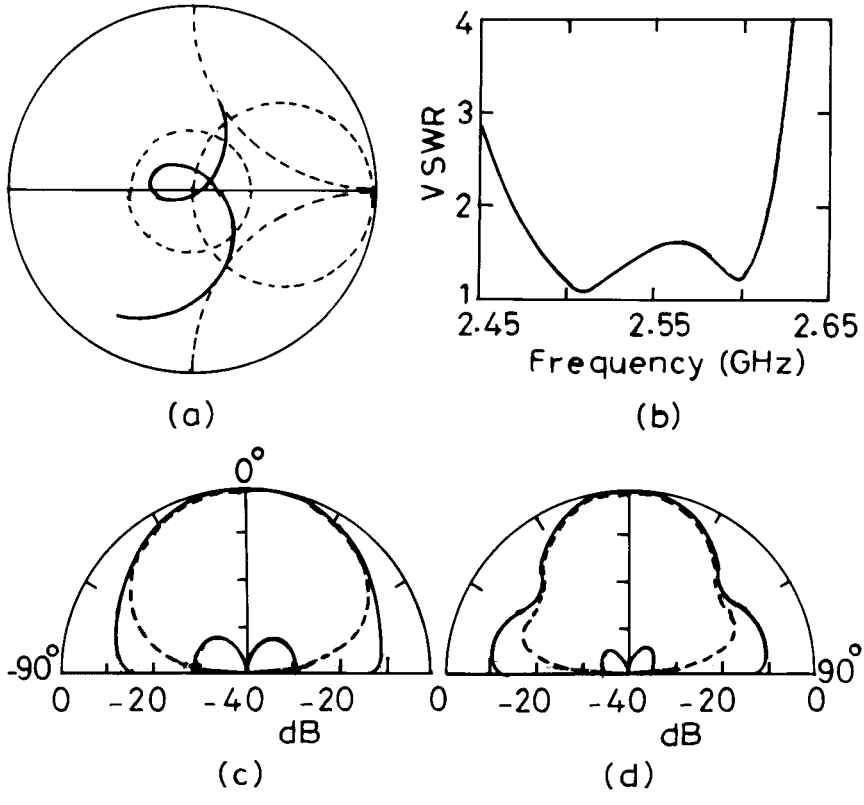

Figure 3.29 (a) Input impedance and (b) VSWR of a five gap-coupled CMSA. Radiation pattern at (c) 2.47 and (d) 2.61 GHz. (——) E_θ in the $\phi = 0°$ and 90° planes and (- - -) E_ϕ in the $\phi = 90°$ plane.

Table 3.1
Comparison of Gap-Coupled CMSA with $\epsilon_r = 1$ and $h = 0.4$ cm

Configuration	f_0 (GHz)	BW (MHz)	Gain (dB)
Single CMSA	2.59	135	9.7
Three gap-coupled CMSA	2.71	440	11.8
Five gap-coupled CMSA with single coupling	2.71	453	11.8
Five gap-coupled CMSA with dual coupling	2.77	500	12.7

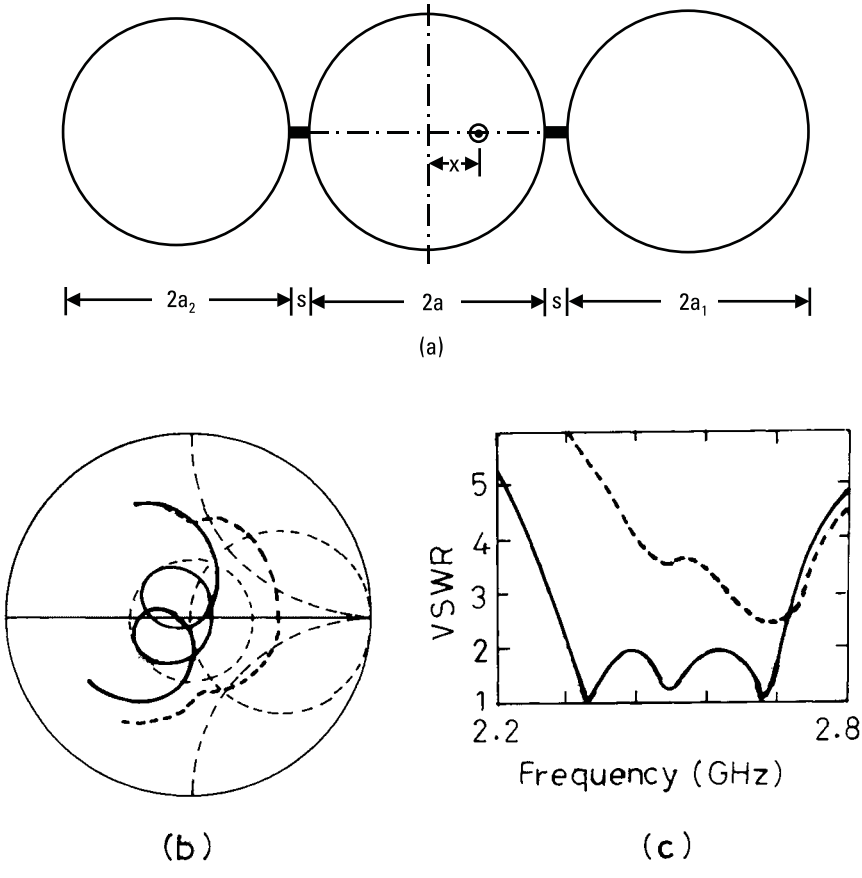

Figure 3.30 (a) Three hybrid-coupled CMSA and its measured (b) input impedance and (c) VSWR plots for (- - -) gap and (——) hybrid-coupling.

the parasitic patches on both the sides. The measured input impedance and VSWR plots are shown in Figure 3.30(b, c). Two distinct loops are formed within the VSWR = 2 circle. The BW is 370 MHz (14.8%), which is 7.4 times of that of the single CMSA.

The measured radiation patterns in the E- and H-planes at the center and the two band-edge frequencies are shown in Figure 3.31. The radiation pattern in the H-plane is in the broadside direction at all the three frequencies. In the E-plane, the radiation is maximum in the broadside at the central frequency, but it shifts away from the broadside at the two band-edge frequencies. At a lower frequency, the radiation from the larger patch is dominant, whereas at a higher frequency radiation from the smaller patch

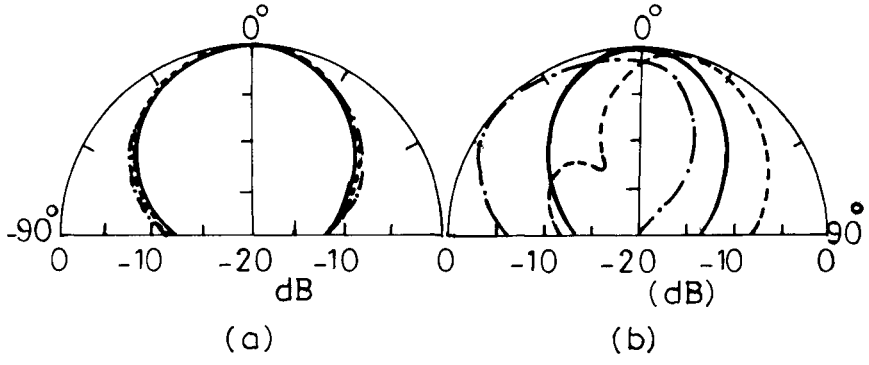

Figure 3.31 Radiation pattern of three hybrid-coupled CMSA: (a) H-plane and (b) E-plane at (- - -) 2.320 GHz, (——) 2.450 GHz, and (– – –) 2.680 GHz.

is dominant. However, the E-field pattern along the broadside is within 2 dB at all the three frequencies.

3.6 Gap-Coupled SCMSAs

A two gap-coupled SCMSA configuration is shown in Figure 3.32(a). This configuration can be obtained by splitting a circular patch into two equal halves with a small gap *s* in between the two patches. One patch is fed with 50-Ω coaxial line, and the other patch is gap-coupled. The dimensions of

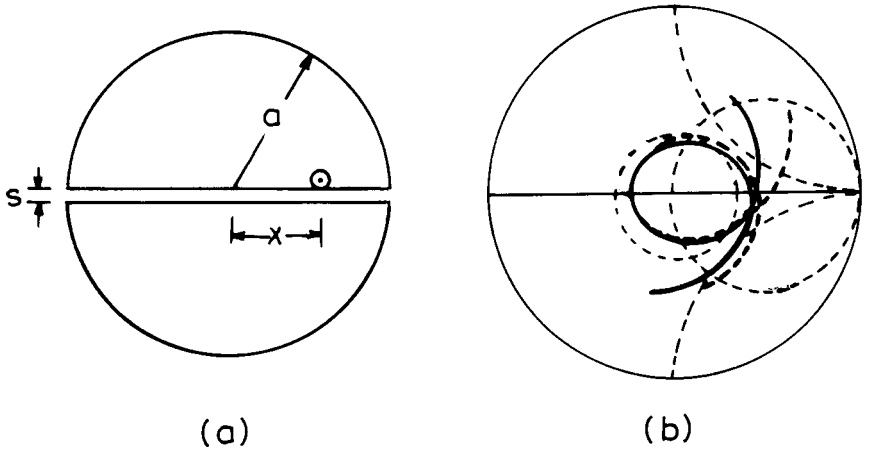

Figure 3.32 (a) Two gap-coupled SCMSA and (b) its input impedance plot: (- - -) theoretical and (——) measured.

the antenna are radius a = 1.45 cm, s = 0.125 cm, and x = 0.5 cm with substrate parameters ϵ_r = 4.3, h = 0.159 cm, and tan δ = 0.02. The theoretical and measured input impedance loci are shown in Figure 3.32(b). The theoretical results are obtained using MNM. The measured BW is 143 MHz at f_0 = 2.720 GHz, which is more than twice the BW of CMSA with the same radius and fabricated on the same substrate [18, 19]. There is not much variation in the radiation pattern over the BW, and it is similar to that of CMSA.

3.7 Gap- and Hybrid-Coupled TMSAs

In this section, various gap- and hybrid-coupled TMSAs are described for broad BW.

3.7.1 Two Gap-Coupled 30°-60°-90° TMSAs

A two gap-coupled 30°-60°-90° TMSA configuration is shown in Figure 3.33(a). This configuration is obtained by splitting an ETMSA into two equal halves with a small gap between the two patches. Only one patch is fed, while the other patch is parasitically coupled. The hypotenuse length S of the 30°-60°-90° TMSA is 3.2 cm; the gap s between the two patches is 0.12 cm; and the feed is at y = 0.3 cm. The substrate parameters are ϵ_r = 4.3, h = 0.159 cm, and tan δ = 0.02. The gap-coupled antenna is

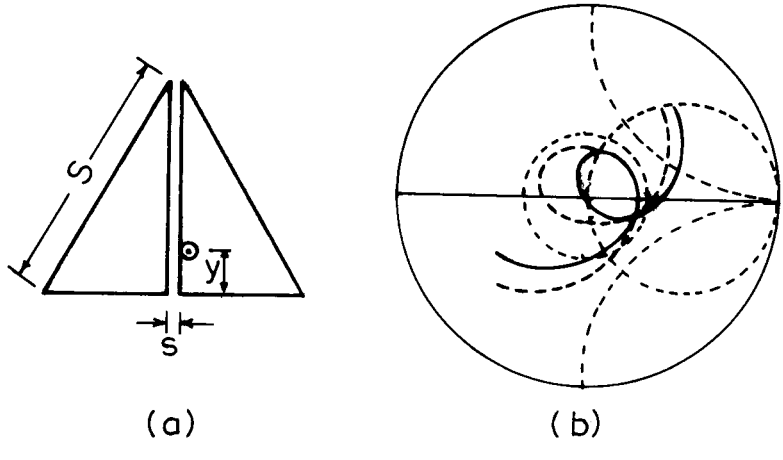

Figure 3.33 (a) Two gap-coupled 30°-60°-90° TMSA and (b) its input impedance plot: (- - -) theoretical and (——) measured.

analyzed using MNM [18]. The theoretical and measured input impedance plots are shown in Figure 3.33(b). The measured BW is 170 MHz, whereas the BW of the corresponding ETMSA of side length 3.2 cm is 70 MHz at 2.89 GHz. The BW of gap-coupled antenna is more than twice of that of the ETMSA with a similar size and radiation pattern.

3.7.2 Three Gap-Coupled ETMSAs

Three gap-coupled ETMSAs are shown in Figure 3.34(a). This configuration is more compact as compared to the gap-coupled RMSA or CMSA. The substrate parameters are $\epsilon_r = 2.33$, $h = 0.159$ cm, and $\tan\delta = 0.001$. The fed patch side length is taken as $S = 5.8$ cm; parasitic patches are chosen to be identical for symmetrical pattern; and its side length S_1 is optimized to

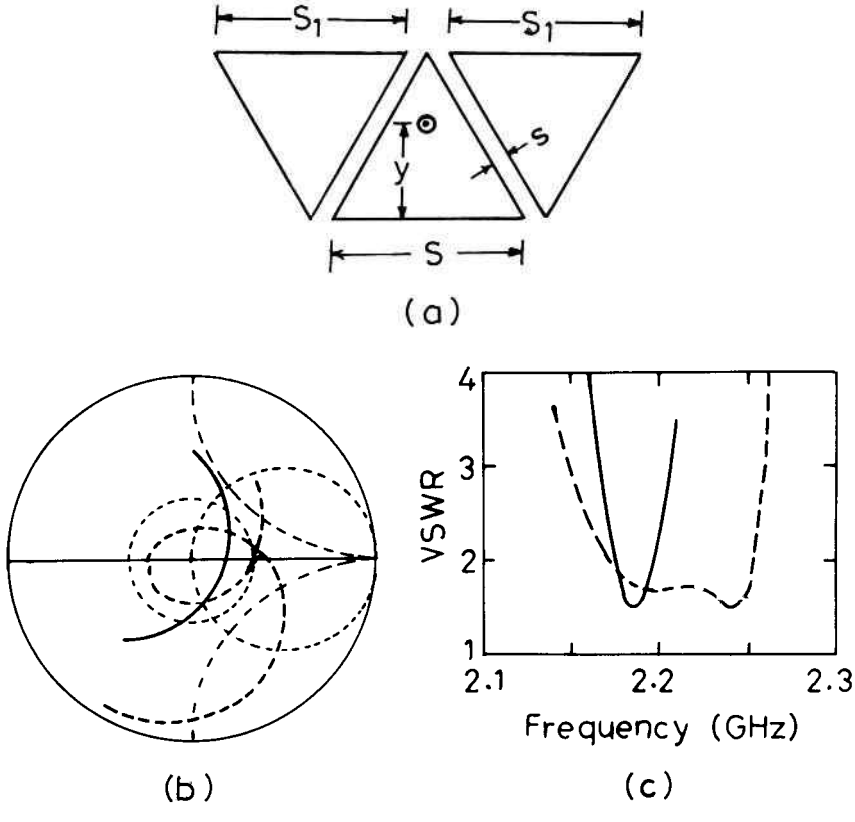

Figure 3.34 (a) Three gap-coupled ETMSA; (b) input impedance and (c) VSWR plots of (——) single ETMSA and (- - -) three gap-coupled ETMSA.

be 5.65 cm for broad BW. For the feed point at y = 2.73 cm and gap s = 0.2 cm, the input impedance and VSWR plots obtained using IE3D are shown in Figure 3.34(b, c). The loop is within the VSWR = 2 circle, and a BW of 83 MHz (3.7%) is obtained. For comparison, the input impedance and VSWR plots for a single ETMSA of side length S = 5.8 cm and feed at y = 2.3 cm are also shown in Figure 3.34. The BW of single ETMSA is 21 MHz (1%). The percentage BW of the three gap-coupled ETMSA is 3.7 times of that of the single ETMSA.

There is a very small variation in the radiation pattern over the BW of the gap-coupled ETMSA; hence, it is shown only at a frequency of 2.24 GHz in Figure 3.35. The gain is 7.6 dB and the maximum cross-polar level is 14 dB. In comparison, the gain of the single ETMSA is 6.4 dB and the cross-polar level is below 19 dB.

The BW of the gap-coupled ETMSA can be increased by using thick substrate with low dielectric constant. For a single ETMSA with S = 8.4 cm, y = 3.4 cm, ϵ_r = 1, h = 0.4 cm, the input impedance and VSWR plots are shown in Figure 3.36. A BW of 58 MHz is obtained. For a three gap-coupled ETMSA configuration with S = 8.4 cm, S_1 = 7.8 cm, s = 0.2 cm, and y = 4.1 cm, the input impedance and VSWR plots are also shown in Figure 3.36. The BW increases to 204 MHz, which is 3.5 times of that of the single patch.

The radiation patterns at 2.1 GHz and 2.3 GHz (near the band-edge frequencies) are shown in Figure 3.37. With an increase in frequency from 2.1 to 2.3 GHz, the radiation pattern varies and the cross-polar level increases significantly to the extent that the radiation becomes maximum along θ = 30° at 2.3 GHz. At a higher frequency, the parasitic patches are resonant, and therefore experience a large phase delay with respect to the fed patch; hence, the beam maxima shifts away from broadside.

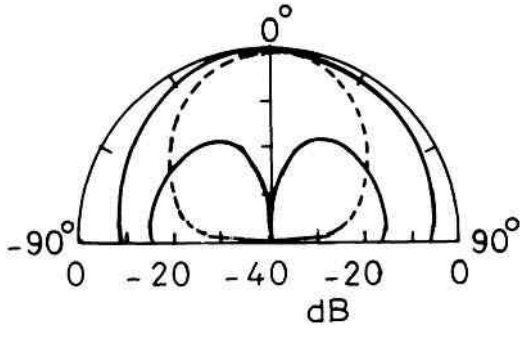

Figure 3.35 Radiation pattern of three gap-coupled ETMSA at 2.240 GHz: (——) H-plane and (- - -) E-plane.

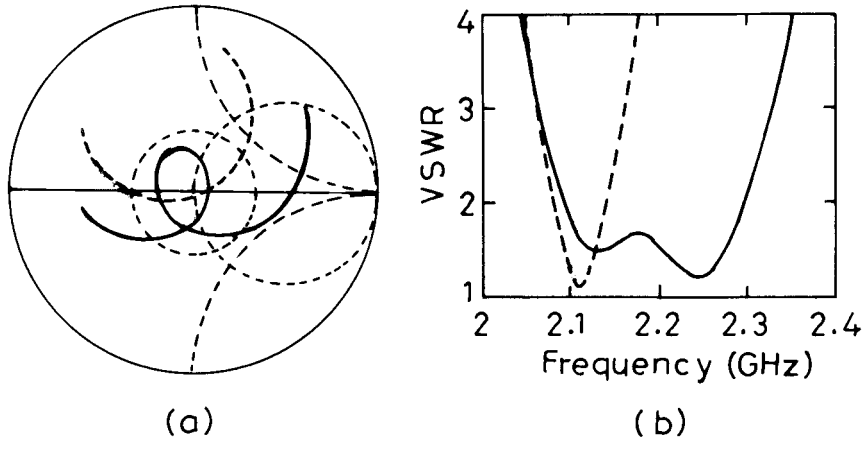

Figure 3.36 (a) Input impedance and (b) VSWR plots of (- - -) single ETMSA and (——) three gap-coupled ETMSA.

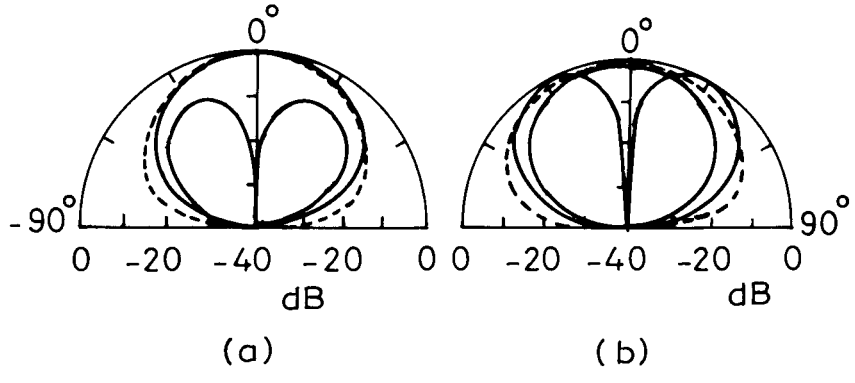

Figure 3.37 Radiation pattern of three gap-coupled ETMSA with ϵ_r = 1 and h = 0.4 cm at (a) 2.1 GHz and (b) 2.3 GHz: (——) H-plane and (- - -) E-plane.

To reduce the pattern variation over the BW, an *isosceles TMSA* (ITMSA) with the same height and a reduced base length can be used instead of an ETMSA. This reduces the center to center distances between the fed and the parasitic patches, and hence parasitic patches experience a smaller phase delay.

3.7.3 Three Gap-Coupled ITMSAs

A three gap-coupled ITMSA configuration is shown in Figure 3.38(a). The center-fed ITMSA has a height H = 7.27 cm and base b = 6.0 cm, and the

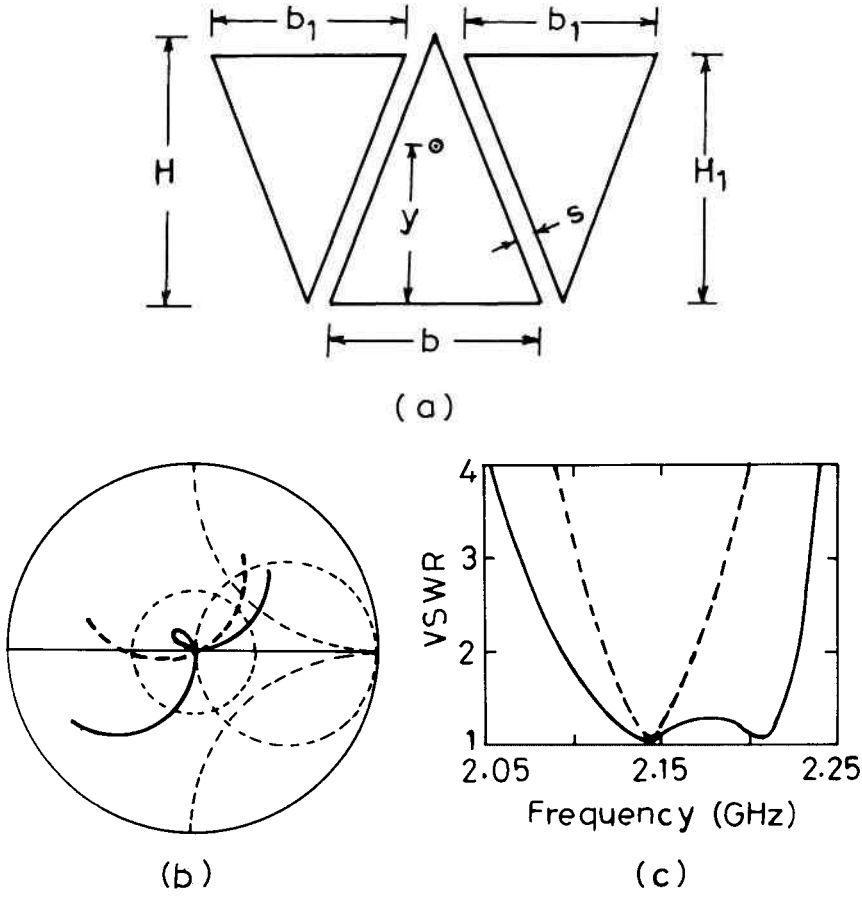

Figure 3.38 (a) Three gap-coupled ITMSA, (b) input impedance, and (c) VSWR plots of (- - -) single ITMSA and (——) three gap-coupled ITMSA.

optimized parasitic patch dimensions are H_1 = 6.9 cm and b_1 = 5.7 cm for s = 0.1 cm. For the feed at y = 3.8 cm, the input impedance and VSWR plots are given in Figure 3.38(b, c). A BW of 135 MHz is obtained. For comparison, the input impedance and VSWR plots for the single ITMSA with H = 7.27 cm, b = 6.0 cm, and y = 3.37 cm are also shown in Figure 3.38. The BW is 51 MHz.

The variation of the radiation pattern of three gap-coupled ITMSA is small over the entire BW; hence it is shown only at 2.16 GHz in Figure 3.39. The gain of the antenna is 10 dB while the cross-polar levels are below 17 dB. In comparison, the gain of a single ITMSA is 9.1 dB at 2.145 GHz,

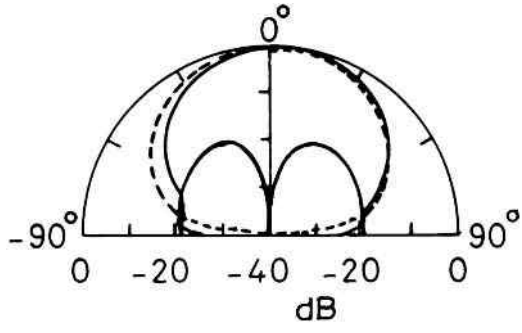

Figure 3.39 Radiation pattern of three gap-coupled ITMSA at 2.16 GHz: (——) E-plane and (- - -) H-plane.

and the cross-polar levels are below 19 dB. In comparison with the three gap-coupled ETMSA, the BW of the three gap-coupled ITMSA is much smaller, but its size is also smaller and it is suitable as an array element. Also, the radiation pattern is stable over the BW.

The BW of the gap-coupled antenna can be further increased if the parasitic triangular patches are selected to be slightly unequal so that their resonance frequencies are slightly different. However, this reduces the coupling between the fed and the parasitic patches. The coupling could be increased either by reducing the gap between the patches or by employing hybrid coupling, in which shorting strips are used between the patches [20].

3.7.4 Four Hybrid-Coupled ETMSAs

Instead of the three-coupled ETMSAs, four hybrid-coupled ETMSAs can also be used [21]. Only the central patch is fed and the coupling to the parasitic patches is controlled by both gap and the shorting strips as shown in Figure 3.40. The patch along the radiating edge of the central fed ETMSA is gap-coupled, whereas the patches along the nonradiating edge are coupled through the shorting strips. The dimensions of the optimized antenna are shown in centimeters, and substrate parameters are $\epsilon_r = 2.55$ and $h = 0.16$ cm. The measured BW is 11.3% at 3.19 GHz, which is 5.4 times the BW of a single ETMSA. The radiation pattern remains in the broadside direction in both the planes in the complete BW, but HPBW varies from 55° to 72° in the E-plane and 40° to 70° in the H-plane. The main drawback of this antenna is its increased size, which makes it unsuitable as an array element.

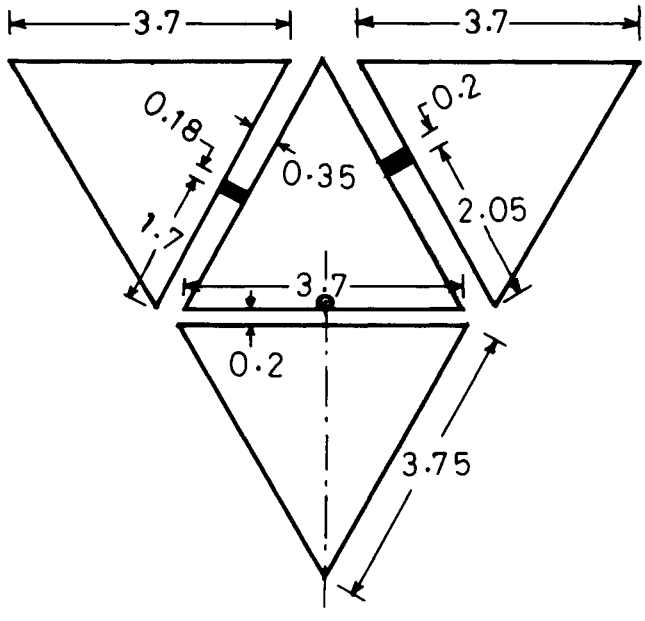

Figure 3.40 Four hybrid-coupled ETMSA.

3.8 Summary

This chapter describes the multiresonator technique in planar configuration to yield broadband response. The BW of the coupled MSA increases when the resonance frequencies of the fed patch and the parasitically coupled patches are close to each other. Various regularly shaped MSAs, such as the RMSA, CMSA, SCMSA, ETMSA, ITMSA, and 30°-60°-90° TMSA, are coupled to their corresponding parasitic elements either by gap, direct, or hybrid coupling. Initially, a two radiating-edge gap-coupled RMSA configuration is described, and the effects of the feed-point location, gap between the patch, and the parasitic patch length on the input impedance plot are explained. Then three rectangular patches that are gap-coupled along their radiating or nonradiating edge are discussed for equal and unequal lengths of the parasitic elements. The concept is extended to a four-edge gap-coupled RMSA, which yields broad BW with higher gain.

Instead of using parasitic rectangular patches, narrow strips could be placed along the nonradiating edge to increase the BW of RMSA. Alternatively, the width of the patch has been divided into number of narrow strips (printed dipoles) with a gap between the strips to obtain broad BW. A $\lambda/2$ open circuit RMSA is divided into a two gap-coupled $\lambda/4$ short circuited

RMSA. Similarly, various equal and unequal coupled multiresonator configurations using CMSA and TMSA yielding wide BW are discussed. Both theoretical and experimental results are included to explain the broadband mechanism. If the dimensions of the parasitic patches are different, then the beam maxima of the radiated fields shifts away from the broadside direction in the two opposite directions at the two band-edge frequencies within the VSWR BW. This problem is reduced when the parasitic patches are identical with some decrease in the BW.

When the number of coupled resonators increases, the BW and gain increase but the size of the configuration also increases making it unsuitable as an array element. Compact broadband configurations such as gap-coupled RMSAs with narrow strips, two-coupled SCMSAs, 30°-60°-90° TMSAs, and three gap-coupled ITMSAs could be used in the broadband array.

The major advantage of these coplanar broadband configurations is that the BW is increased without increasing the thickness of the MSA. As a result, their planar characteristics are retained, which makes them conformal to different host surfaces. In this respect, five-coupled RMSAs, five-coupled CMSAs, and four-coupled ETMSAs with identical parasitic elements are the promising broadband configurations, as they give large BW and gain with a stable radiation pattern in the entire BW.

References

[1] Bahl, I. J., and P. Bhartia, *Microstrip Antennas,* Dedham, MA: Artech House, 1980.

[2] James, J. R., and P. S. Hall, *Handbook of Microstrip Antennas,* Vol. 1, London: Peter Peregrinus, Ltd., 1989.

[3] Gupta, K. C., and A. Benalla, *Microstrip Antenna Design,* Norwood, MA: Artech House, 1988.

[4] Pozar, D. M., and D. H. Schaubert, *Microstrip Antennas: The Analysis and Design of Microstrip Antennas and Arrays,* New York: IEEE Press, 1995.

[5] Lee, H. F., and W. Chen, *Advances in Microstrip and Printed Antennas,* New York: John Wiley & Sons, 1997.

[6] Kumar, G., "Broadband Microstrip Antennas Using Coupled Resonators," Ph.D. thesis, Indian Institute of Technology, Kanpur, India, 1982.

[7] Kumar, G., and K. C. Gupta, "Broadband Microstrip Antennas Using Additional Resonators Gap-Coupled to the Radiating Edges," *IEEE Trans. Antennas Propagation,* Vol. AP-32, December 1984, pp. 1375–1379.

[8] Kumar, G., and K. C. Gupta, "Nonradiating Edges and Four Edges Gap-Coupled with Multiple Resonator, Broad Band Microstrip Antennas," *IEEE Trans. Antennas Propagation,* Vol. AP-33, February 1985, pp. 173–178.

[9] IE3D 7.0, Zeland Software, Inc., Fremont, CA, 2000.

[10] Schaubert, D. H., and F. G. Farrar, "Some Conformal, Printed Circuit Antenna Design," *Proc. Workshop Print. Circuit Antenna Tech.,* New Mexico State University, Las Cruces, NM, October 1979, pp. 5.1–5.21.

[11] Anandan, C. K., and K. G. Nair, "Compact Broadband Microstrip Antennas," *Electronics Letters,* Vol. 22, No. 20, 1986, pp. 1064–1065.

[12] Anandan, C. K., P. K. Mohanan, and K. G. Nair, "Broadband Gap-Coupled Microstrip Antenna," *IEEE Trans. Antennas Propagation,* Vol. AP-38, 1990, pp. 1581–1586.

[13] Wood, C., "Improved Bandwidth of Microstrip Antennas Using Parasitic Elements," *Proc. IEE,* Pt. H, Vol. 127, 1980, pp. 231–234.

[14] Kumar, G., and K. C. Gupta, "Directly Coupled Multiple Resonator Wideband Microstrip Antennas," *IEEE Trans. Antennas Propagation,* Vol. AP-33, June 1985, pp. 588–593.

[15] Pozar, D. M., and B. Kaufman, "Increasing the Bandwidth of a Microstrip Antenna by Proximity Coupling," *Electronics Letters,* Vol. 23, No. 8, 1987, pp. 368–369.

[16] Pues, H. G., and A. R. Van De Capelle, "An Impedance Matching Technique for Increasing the Bandwidth of Microstrip Antennas," *IEEE Trans. Antennas Propagation,* Vol. AP-37, No. 11, 1989, pp. 1345–1354.

[17] Ray, K. P., and G. Kumar, "Multifrequency and Broadband Hybrid-Coupled Circular Microstrip Antennas," *Electronics Letters,* Vol. 33, No. 6, 1997, pp. 437–438.

[18] Nile, M. B., A. A. Rasheed, and G. Kumar, "Broadband Gap-Coupled Semicircular and Triangular Microstrip Antennas," *IEEE AP-S Int. Symp. Digest,* July 1994, pp. 1202–1205.

[19] Ray K. P., and G. Kumar, "Hybrid-Coupled Microstrip Antennas," *IETE Technical Review,* Vol. 16, No. 1, 1999, pp. 81–84.

[20] Ray, K. P., "Broadband, Dual-Frequency and Compact Microstrip Antennas," Ph.D. thesis, Indian Institute of Technology, Bombay, India, 1999.

[21] Bhatnagar, P. S., et al., "Hybrid Edge Gap and Directly Coupled Triangular Microstrip Antenna," *Electronics Letters,* Vol. 22, No. 16, 1986, pp. 853–855.

4

Multilayer Broadband MSAs

4.1 Introduction

In Chapter 3, the BW of the MSA was increased by using several planar-coupled resonators. There are two main disadvantages of these broadband configurations. First, the overall planar size of the antenna increases, which makes it an unsuitable array element (although the three coupled resonator configurations could be used as elements in a linear array). Second, the radiation pattern varies over the BW in many cases.

This chapter again uses multiple resonators to increase the BW, but instead of using the planar-coupled technique, two or more patches on different layers of the dielectric substrates are stacked on each other. This method increases the overall height of the antenna but the size in the planar direction remains the same as that of the single-patch antenna. Thus, these multilayer configurations are suitable as array elements. Based on the coupling mechanism, these configurations are categorized as *electromagnetically coupled MSAs* (ECMSAs) or *aperture-coupled MSAs* (ACMSAs). These multilayer MSA configurations yield BW of nearly 70% for VSWR ≤ 2, and the variation of the radiation pattern over the impedance BW is small [1–6]. The ECMSA and ACMSA configurations are discussed separately in the following sections.

4.2 Electromagnetically Coupled MSAs

Two configurations of an ECMSA are shown in Figure 4.1. The bottom patch is fed with a coaxial line, and the top parasitic patch is excited due

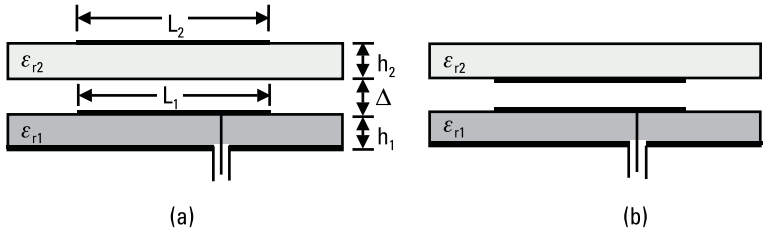

Figure 4.1 Electromagnetically coupled MSA: (a) normal and (b) inverted configurations.

to electromagnetic coupling with the bottom patch. The patches can be fabricated on different substrates, and an air gap or foam material can be introduced between these layers to increase the BW. In the normal configuration, as shown in Figure 4.1(a), the parasitic patch is on the upper side of the substrate. In the inverted configuration shown in Figure 4.1(b), the top patch is on the bottom side of the upper substrate. In this case, the top dielectric layer also acts as a protective layer from the environment. The antenna dimensions are optimized so that the resonance frequencies of the two patches are close to each other to yield broad BW. This concept is applicable to any arbitrary shaped patch. The ECMSAs with two to three layers of microstrip patches (rectangular, circular, and triangular) provide an impedance BW of 10–30% for VSWR ≤ 2 [1–7]. The increase in the BW is obtained due to an increase in the overall height of the antenna, a decrease in the effective dielectric constant ϵ_e (if an air or foam substrate is inserted in between the two patches), and the multiresonator effect.

Instead of feeding the bottom patch, the top patch can be fed by coaxial probe, which passes through the bottom patch as shown in Figure 4.2. The bottom patch is not directly connected with the probe; instead a small hole is made around the feed. It gets excited through the electromagnetic coupling arising from the probe and the upper patch. This configuration does not offer any advantage as compared to the configurations given in Figure 4.1, so it is not discussed in detail.

4.2.1 Microstrip Line Feed ECMSAs

Besides the two-layer-stacked ECMSA configurations discussed above, electromagnetic coupling is also used to excite the patch on the top layer through

Figure 4.2 Electromagnetically coupled MSA with feed connected to top patch.

the microstrip line feed in the bottom layer as shown in Figure 4.3. This configuration has the advantage that the microstrip feed line could be fabricated on a thin high dielectric constant substrate, so that radiation from the feed is negligible and the top patch can be fabricated on a thick substrate with a low dielectric constant (or suspended configuration) for a large BW. Also, there is no direct connection between the feed and the patch. A small misalignment between the patch and the feed, unlike in the case of coaxial feed where it is very critical, does not change the characteristics of the antenna as described below.

An exploded 3-D view of square and circular patches that are electromagnetically fed with a microstrip line are shown in Figure 4.3. The length of the square patch is L and the radius of the circular patch is a. The microstrip line is fabricated on a dielectric substrate with a dielectric constant ϵ_{r1} and thickness h_1, and the radiating patch is fabricated on a substrate with a dielectric constant ϵ_{r2} and thickness h_2. Generally, ϵ_{r1} is chosen to be greater than or equal to ϵ_{r2}, and h_1 is taken smaller than or equal to h_2, so that the radiation from the microstrip line is small. Even for $h_1 = h_2$, the top patch sees the ground plane at a height of $H = h_1 + h_2$, so the radiation from the patch will be more than that from the microstrip line. The theoretical results obtained using the MoM for various patch dimensions and substrate parameters are summarized below [8].

For $\epsilon_{r1} = \epsilon_{r2}$ and $h_1 = h_2$, the variations of percentage BW for VSWR ≤ 2 and efficiency η with a normalized total substrate thickness (H/λ, where $H = (h_1 + h_2)$ and $\lambda = \lambda_0/\sqrt{\epsilon_{r1}}$) for three values of ϵ_{r1} (1.1, 2.55, and 10.5) are given in Figure 4.4. These curves are valid for both square and circular ECMSA, because both percentage BW and η of the antenna depend on the substrate parameters. As ϵ_r or H/λ increases, percentage BW increases but η decreases. A BW of 20% is obtained for $\epsilon_{r1} = \epsilon_{r2} = 1.1$ and $H/\lambda = 0.13$.

For different combinations of ϵ_{r1} and ϵ_{r2}, the percentage BW and η plots versus H/λ for $h_1 = h_2$ are given in Figure 4.5. As H/λ increases to

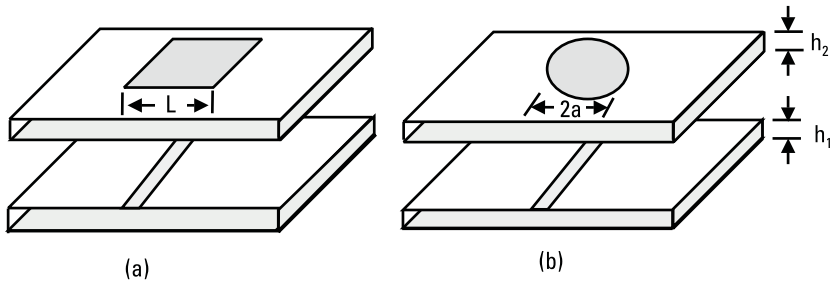

Figure 4.3 ECMSA with microstrip line feed: (a) rectangular and (b) circular patch.

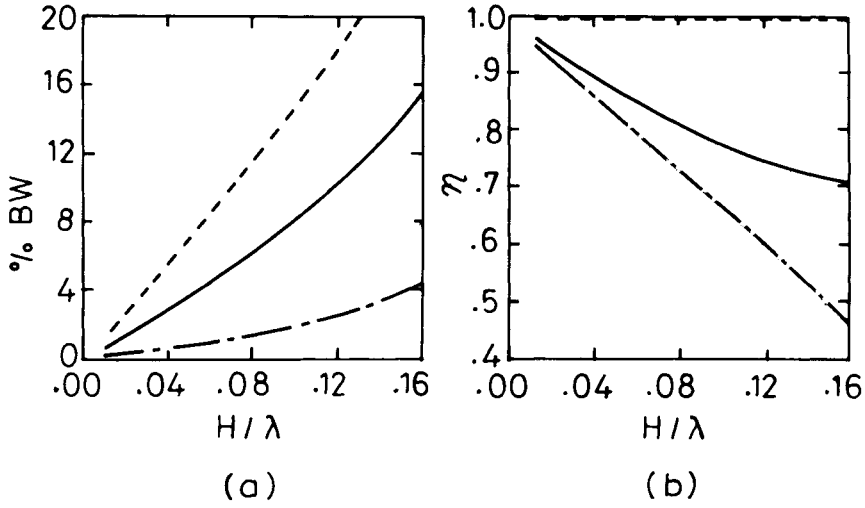

Figure 4.4 Variation of (a) percentage BW and (b) η with H/λ of an ECMSA with a microstrip line feed for different values of $\epsilon_{r1} = \epsilon_{r2}$. (- - -) 1.1, (——) 2.55, and (– – –) 10.5.

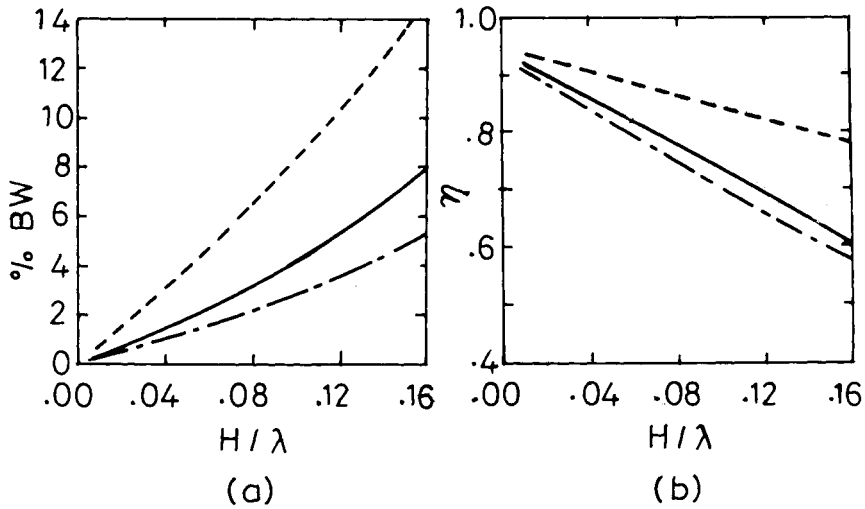

Figure 4.5 Variation of (a) percentage BW and (b) η with H/λ of an ECMSA with a microstrip line feed for different combinations of ϵ_{r1} and ϵ_{r2}: (- - -) ϵ_{r1} = 2.55 and ϵ_{r2} = 1.1, (——) ϵ_{r1} = 6.0 and ϵ_{r2} = 2.55, and (– – –) ϵ_{r1} = 10.5 and ϵ_{r2} = 2.55.

0.16 for ϵ_{r1} = 2.55 and ϵ_{r2} = 1.1, the percentage BW increases to more than 14% but η decreases to 78%. These plots are useful to select the substrate parameters for desired values of frequency, percentage BW, and η. After selecting the substrate parameters, the dimensions of the square and circular patches can be obtained using Figures 4.6 and 4.7 for $\epsilon_{r1} = \epsilon_{r2}$ and for different combinations of ϵ_{r1} and ϵ_{r2}, respectively. These curves are for $h_1 = h_2$. For example, an RMSA is to be designed at the center frequency f_0 = 3.6 GHz, and the substrates have the following parameters: $\epsilon_{r1} = \epsilon_{r2}$ = 2.55 and $h_1 = h_2$ = 0.159 cm. As a result, H/λ is equal to 0.06, for which the percentage BW is equal to 4.5% as obtained from Figure 4.4. The value of $H/(L/2)$ is 0.27 from Figure 4.6, which gives L = 2.36 cm. Alternatively, these curves could be used to calculate the resonance frequency for given patch dimensions.

If the substrates with these dielectric constant values (ϵ_{r1} and ϵ_{r2}) are not available, one can always extrapolate these plots or the frequency scaling concept described in Section 2.2.7 could be used to calculate the patch dimensions. Let the available substrate have $\epsilon_{r1} = \epsilon_{r2} = \epsilon_r$ = 2.22 and $h_1 = h_2 = h$ = 0.159 cm. By using the frequency scaling method, the modified L for the above case will be $2.36\sqrt{2.55}/\sqrt{2.22} \cong 2.5$ cm. The top view of the square patch fed with microstrip line in the bottom layer is shown in Figure 4.8(a). For three different values of microstrip feed length from the central

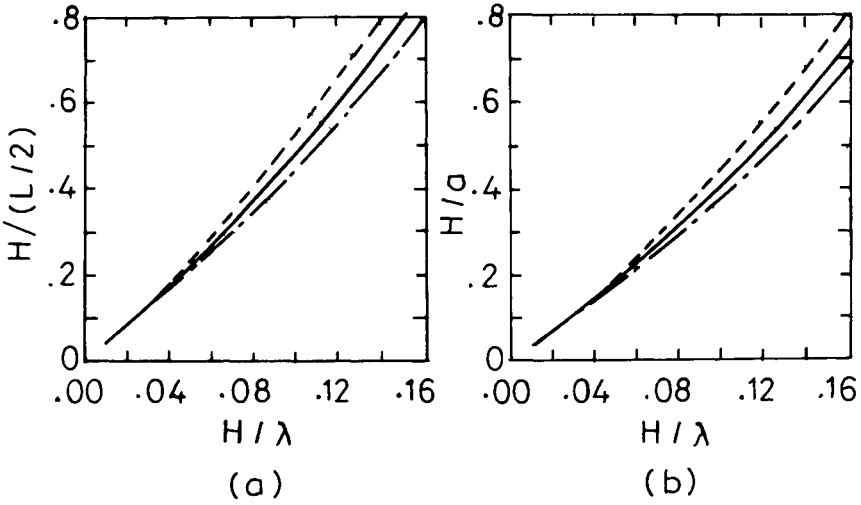

Figure 4.6 Variation of patch size with H/λ of ECMSA with microstrip line feed. (a) Square and (b) circular patches for different values of $\epsilon_{r1} = \epsilon_{r2}$: (- - -) 1.1, (——) 2.55, and (– – –) 10.5.

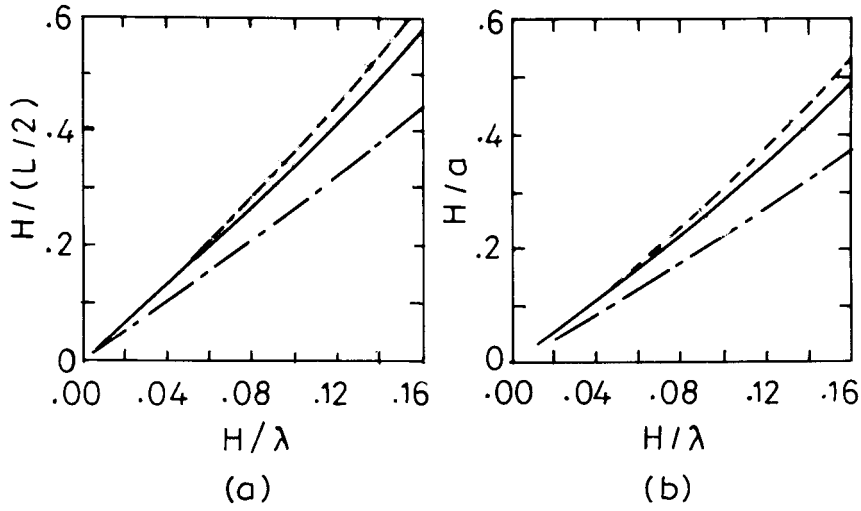

Figure 4.7 Variation of patch size with H/λ of ECMSA with microstrip line feed. (a) Square and (b) circular patch for different combinations of ϵ_{r1} and ϵ_{r2}, (- - -) ϵ_{r1} = 2.55, ϵ_{r2} = 1.1, (——) ϵ_{r1} = 6.0, ϵ_{r2} = 2.55, and (– – –) ϵ_{r1} = 10.5, ϵ_{r2} = 2.55.

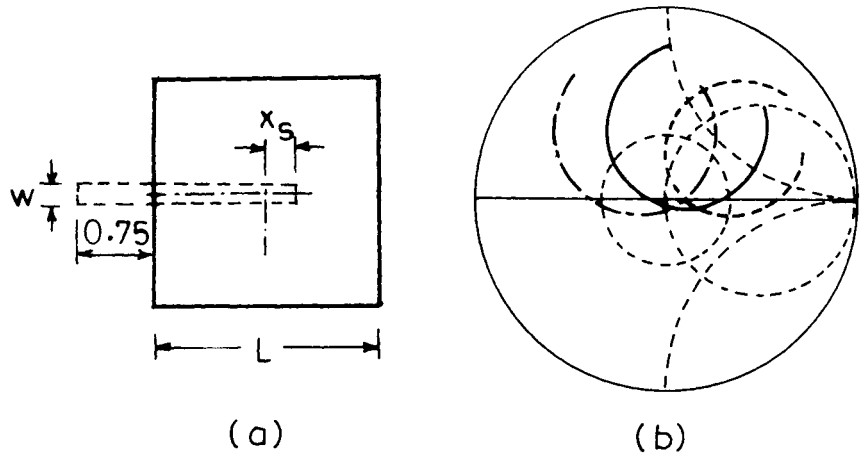

Figure 4.8 (a) Top view of the square microstrip patch fed with microstrip line and (b) input impedance plots for three values of x_s: (- - -) –0.4 cm, (——) 0.0 cm, and (– – –) 0.4 cm.

point (x_s = −0.4 cm, 0, and 0.4 cm, where x_s = 0 implies that the open end of the feed is aligned with the center of the patch), the input impedance plots obtained using IE3D [9] are plotted in Figure 4.8(b). The feed length outside the patch is kept constant at 0.75 cm and the width of the feed line is taken as w = 0.4 cm, which makes its characteristic impedance Z_0 approximately equal to 50Ω. With an increase in x_s from −0.4 cm to 0.4 cm, the input impedance plot moves in the clockwise direction. The BW for x_s = 0 is 180 MHz at 3.64 GHz (4.9%). This percentage BW is slightly more than that obtained from Figure 4.4 for $\epsilon_{r1} = \epsilon_{r2}$ = 2.55, which is due to the decrease in the value of ϵ_r to 2.22.

Another example of the microstrip line-fed ECMSA is shown in Figure 4.9(a). The dimensions shown in the figure are in centimeters, and the substrate parameters are ϵ_r = 2.2 and h = 0.158 cm. When the tuning stub is not connected, the input impedance is approximately 40Ω at the resonance as shown in Figure 4.9(b). The impedance matching is obtained by connecting a tuning stub, whose length and position are shown in Figure 4.9(a). This concept is similar to that of the single-stub impedance-matching technique. The measured input impedance plot with a tuning stub is also shown in Figure 4.9(b). The BW for VSWR ≤ 2 is from 3.375 GHz to 3.855 GHz, which is 13% [10]. These results agree with the simulated results obtained using IE3D.

The disadvantage of the microstrip line-fed ECMSA is that the BW realized is not large even though the total antenna thickness is increased. If the microstrip feed line is replaced by a resonant patch in the bottom layer

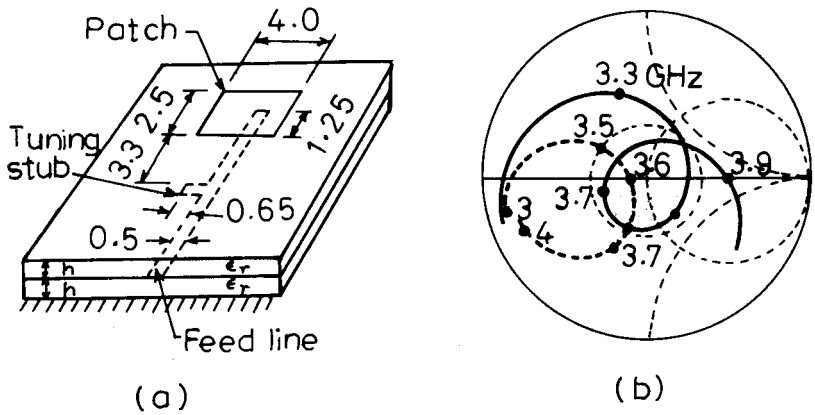

Figure 4.9 (a) Rectangular ECMSA with tuning stub and (b) measured input impedance plots for (——) with and (- - -) without tuning stub.

and the dimensions of the bottom and top patches are optimized, a much wider BW can be obtained. The bottom patch could be fed either by microstrip line or coaxial probe.

4.2.2 Parametric Study of Coaxial-Fed Square ECMSAs

The top and side views of a coaxial-fed square ECMSA are shown in Figure 4.10. The lengths of the bottom and top square patches are L_1 and L_2, respectively. The various parameters that govern the resonance frequencies of the two patches are its lengths, substrate parameters (two substrates could have different parameters), and the air gap Δ between the two patches. When the resonance frequencies of the two patches are close to each other, a broad BW is obtained. The effects of various parameters on the performance of the antenna are discussed in the following sections.

4.2.2.1 Effect of Varying the Length of the Top Square Patch

The lower square patch length L_1 is taken as 2.5 cm, which is same as that of the previous case and a substrate with parameters ϵ_r = 2.22, h = 0.159 cm, and tan δ = 0.001 is used for both the layers. The top square patch length L_2 is varied from 0.5 cm to 2.6 cm. For the feed point at x = 0.85 cm and air gap Δ = 0, the theoretical input impedance and VSWR plots, obtained using IE3D, for four values of L_2 are shown in Figure 4.11. As L_2 is increased from 0.5 cm to 2 cm, there is no change in the impedance

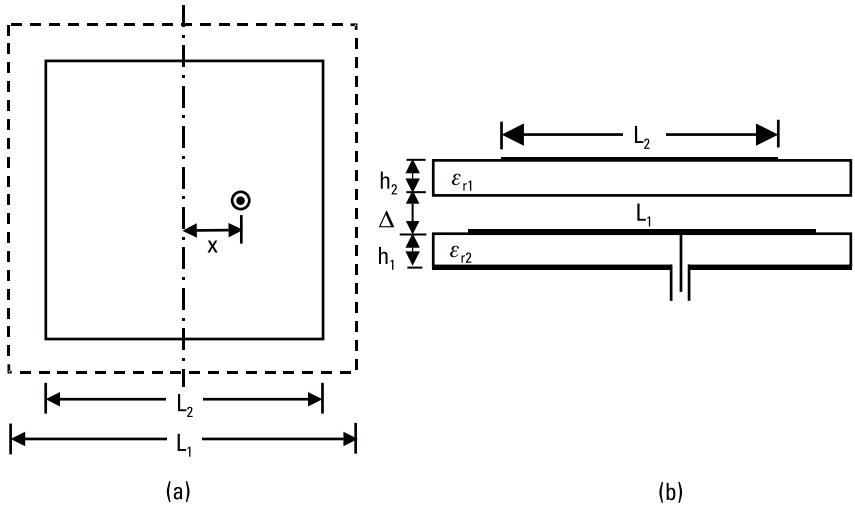

Figure 4.10 (a) Top and (b) side views of a coaxial-fed square ECMSA.

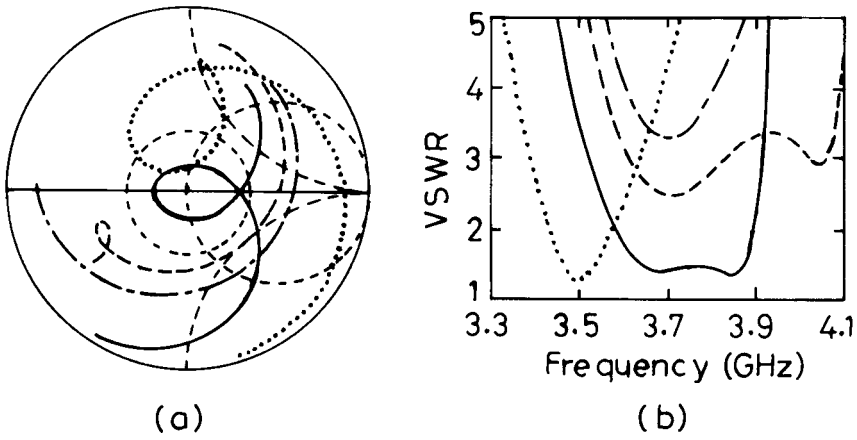

Figure 4.11 (a) Input impedance and (b) VSWR plots of a coaxial-fed stacked-square ECMSA for four values of L_2: (– – –) 2.0 cm, (- - -) 2.3 cm, (——) 2.45 cm, and (· · ·) 2.6 cm.

plot in the frequency range from 3.3 GHz to 4.1 GHz. This is because the resonance frequency of the top patch is much larger than that of the fed patch. As L_2 increases to 2.3 cm, a loop is formed in the impedance plot in the above frequency range, because the resonance frequencies of the two patches are comparable to each other. In this case, the bottom patch experiences the superstrate effect, so its effective dielectric constant increases toward ϵ_r, which reduces its resonance frequency as described in Section 2.2.1.8. The fringing fields for the top patch are more than the bottom patch because of its increased substrate thickness ($H = 2h$) from the ground plane, thereby making the effective dimension of the top patch nearly same as that of the bottom patch. However, the effective dielectric constant of the top patch is smaller than that of the bottom patch because of the fringing field in the free space. Therefore, the resonance frequency of the top patch is larger than that of the bottom patch and hence the loop in the impedance plot is formed in the higher frequency region.

When L_2 is further increased from 2.3 cm to 2.6 cm, the resonance frequency of the top patch decreases, so the position of the loop moves in the lower frequency region of the impedance plot (i.e., in the anticlockwise direction). Also, the size of the loop increases because the coupling between the two patches increases owing to the larger overlap area. For L_2 = 2.45 cm, the loop is within the VSWR = 2 circle. The BW of the antenna is 315 MHz (8.4%), which is much larger than the BW of 180 MHz obtained for microstrip line-fed ECMSA described in Section 4.2.1 with the same printed area and height.

The radiation pattern of the antenna at 3.75 GHz is shown in Figure 4.12. It is observed that the variation of the pattern over the entire BW is very small. The radiation pattern is in the broadside direction with cross-polar levels less than 25 dB. The gain of the antenna at 3.75 GHz is 6.8 dB. For comparison, a single-square MSA of length L = 2.5 cm having ϵ_r = 2.22 and h = 0.318 cm (which is equivalent to the thickness of the ECMSA) with a coaxial feed at x = 0.6 cm yielded BW of 205 MHz and gain of 6.7 dB at 3.7 GHz. Thus, two stacked-square MSAs yield 50% more BW with slightly more gain as compared to a single-square MSA with the same volume.

4.2.2.2 Effect of Varying Length of the Bottom Square Patch

After observing the effect of L_2 on the performance of the antenna, the effect of L_1 is discussed. The upper square patch length L_2 is fixed at 2.5 cm and the substrate parameters are chosen the same as above with Δ = 0 and x = 0.85 cm. For three values of L_1 (2.50, 2.55, and 2.60 cm), the input impedance and VSWR plots are shown in Figure 4.13. As L_1 increases from 2.5 cm to 2.6 cm, the resonance frequency of the bottom patch becomes smaller than that of the top patch, and hence the loop due to the parasitic patch is formed in the higher frequency region of the fed patch (i.e., the loop in the impedance plot shifts in the clockwise direction on the Smith chart). This effect is similar to that of the previous case, where the loop position moves clockwise, when the top patch frequency increases with respect to the fed patch. For L_1 equal to 2.55 cm and 2.6 cm, the loop remains within the VSWR = 2 circle yielding a BW of 308 MHz and 311 MHz, respectively. It may be observed that the difference in the two patch

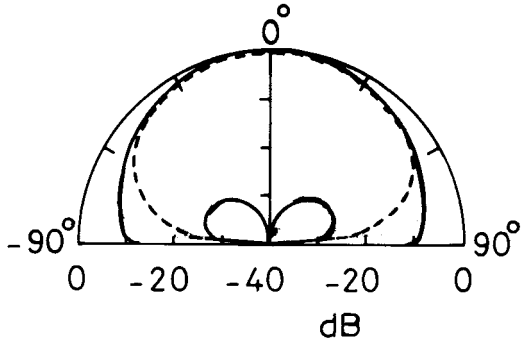

Figure 4.12 Radiation pattern of coaxial-fed square ECMSA at 3.75 GHz: (——) E_θ in the φ = 0° and 90° planes and (- - -) E_φ in the φ = 90° plane.

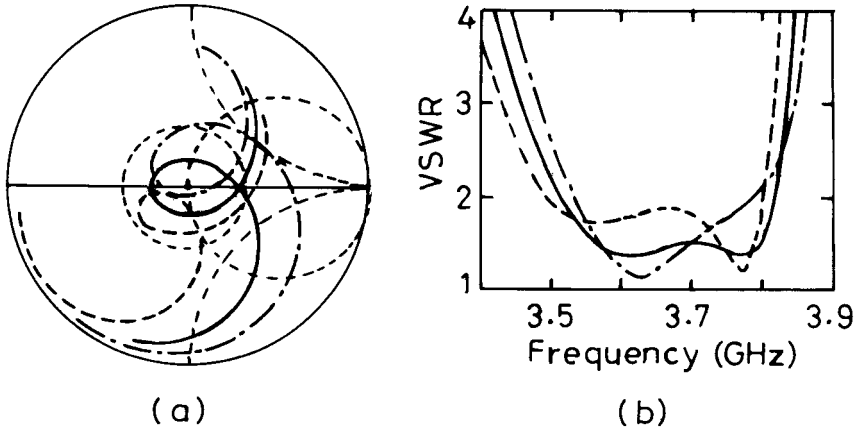

Figure 4.13 (a) Input impedance and (b) VSWR plots of coaxial-fed square ECMSA for three values of L_1: (– – –) 2.5 cm, (——) 2.55 cm, and (- - -) 2.6 cm.

dimensions is more important than their actual values for the loop to be within the VSWR = 2 circle to yield a broad BW.

4.2.2.3 Effect of Misalignment of the Top Square Patch

During the fabrication of the stacked MSA, it is possible that there may be some offset in the alignment of the two patches in the horizontal plane. For a 0.1-cm misalignment of the top patch with respect to the bottom patch along the width and length (*ox* and *oy*, respectively), the theoretical input impedance and VSWR plots for L_1 = 2.5 cm, L_2 = 2.45 cm, and x = 0.85 cm are shown in Figure 4.14. If the misalignment is along the width of the patch (i.e., *oy* = 0.1 cm), there is no appreciable change in the performance of the antenna. However, when the offset is along the length (i.e., *ox* = ±0.1 cm), the size of the loop increases, because the top patch is moved toward the higher impedance of the bottom patch, which increases the coupling. Since the loop size is increased and it is within the VSWR = 2 circle, the BW of the antenna increases. If the offset is along the diagonal, then the effect is the same as that of offset along the length, because small offset along the width has no effect on the performance of the antenna [11].

The fabrication alignment error could also be in the vertical direction, so a very small air gap Δ could be formed between the two patches. This air gap may not be avoidable due to minor deformation in the substrates and because of solder placed at the feed point of the bottom patch. For three values of Δ, the input impedance and VSWR plots are shown for L_1 = 2.5 cm and L_2 = 2.45 cm in Figure 4.15. As the air gap increases from

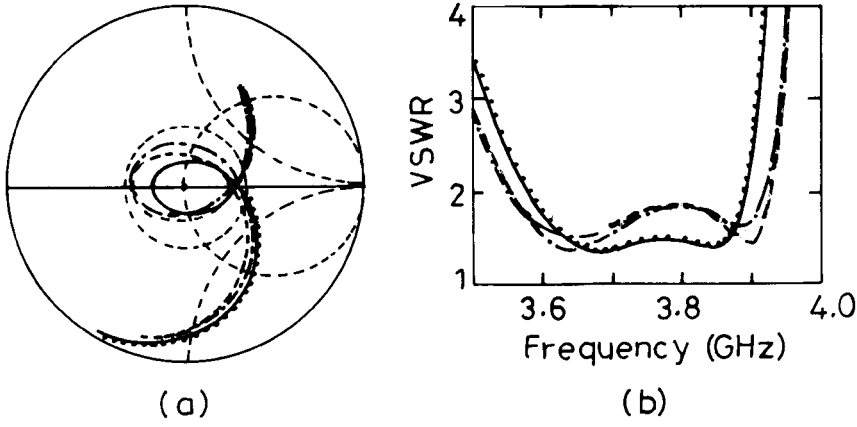

Figure 4.14 (a) Input impedance and (b) VSWR plots of the coaxial-fed square ECMSA for different offset values: (——) no offset, (· · ·) *oy* = 0.1 cm, (– – –) *ox* = 0.1 cm, and (- - -) *ox* = –0.1 cm.

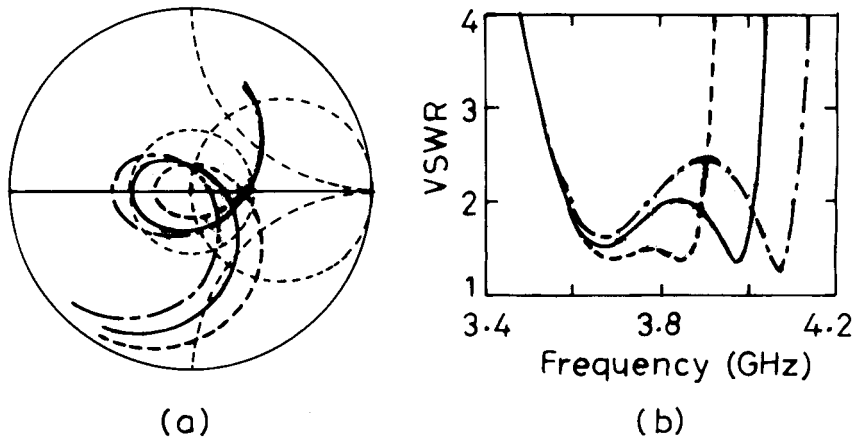

Figure 4.15 (a) Input impedance and (b) VSWR plots of the coaxial-fed square ECMSA for three values of Δ: (- - -) 0.0 cm, (——) 0.01 cm, and (– – –) 0.02 cm.

0 to 0.02 cm, the effective dielectric constant of the top patch decreases, and the total height increases slightly, which increases the fringing field and hence the loop size. For $\Delta = 0.02$ cm, the loop goes outside the VSWR = 2 circle.

A further increase in the air gap reduces the mutual coupling between the two patches. Then, the loop size starts decreasing, and it can be brought back inside the VSWR = 2 circle. Therefore, at times, it is desirable to

intentionally have a finite air gap between the two patches and then optimize the performance of the antenna for broad BW as described next.

4.2.2.4 Effect of Varying the Air Gap Between Two Stacked Patches

The air gap between the fed patch and the parasitic patch plays an important role in getting wide BW. With increase in the air gap Δ, the total height of the antenna increases, and the effective dielectric constant experienced by the top patch reduces. Both of these factors increase the BW. For $L_1 = L_2 =$ 2.5 cm and substrate parameters the same as above, the input impedance and VSWR plots for three values of Δ (0.1, 0.3, and 0.4 cm) with $x = 1.1$ cm are shown in Figure 4.16. With an increase in Δ from 0.1 cm to 0.4 cm, the size of the loop decreases, because the coupling decreases due to the increase in the spacing between the two patches. For $\Delta = 0.3$ cm and 0.4 cm, the loop is inside the VSWR = 2 circle yielding BW of 816 MHz and 760 MHz (20.6% and 19.4%). This antenna covers the frequency band of 3.7 GHz to 4.2 GHz of the C-band satellite communication. The pattern is in the broadside direction with very little variation over the entire BW. The gain of the antenna is 8.3 dB at 3.95 GHz. Thus, BW and gain increase at the expense of increase in the total height of the antenna.

In the above frequency range of 3.7 GHz to 4.2 GHz, generally a horn antenna (circular waveguide with peripheral chokes, for which the total diameter including the peripheral choke is more than 16 cm and the length is more than 8.5 cm) is used as a feed for an 8-foot reflector antenna. The horn antenna can be easily replaced by the above-stacked MSA, which has

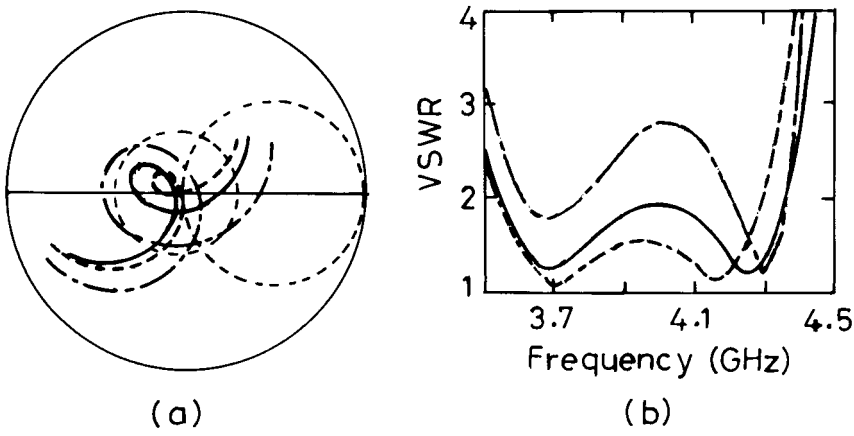

Figure 4.16 (a) Input impedance and (b) VSWR plots of square ECMSA for three values of Δ: (– – –) 0.1 cm, (——) 0.3 cm, and (- - -) 0.4 cm.

much smaller dimensions and hence less blockage as compared to that of the bulky horn antenna.

Instead of using the normal mode configuration, the inverted mode configuration shown in Figure 4.1(b) can also be used. The advantage of this configuration is that the top substrate acts as a protective layer that can be painted and sealed at the top without degrading the performance of the antenna. For $L_1 = L_2 = 2.5$ cm, $x = 1.19$ cm, and $\Delta = 0.6$ cm, the BW is 795 MHz, which is similar to that obtained in the normal mode configuration.

Until now, the effect of Δ has been discussed for increasing the BW, but the gain has not been optimized. By increasing Δ further, the gain of the antenna can be increased [12, 13]. For $L_1 = L_2 = 2.5$ cm and substrate parameters the same as above, the center frequency f_0, BW, and gain near the center frequency are given for various values of Δ (0.5 cm to 6.0 cm) in Table 4.1. For all these cases, the feed-point location x is optimized; its value is also given in Table 4.1. For lower than this value of Δ, the BW and gain are discussed earlier. When Δ is increased from 0.5 to 2.0 cm ($0.066\lambda_0$ to $0.26\lambda_0$), the BW of the antenna decreases from 684 MHz to 58 MHz and the gain of the antenna decrease from 8.0 to 5.3 dB. Hence these values of Δ are not useful. When Δ is increased from 2.0 cm to 3.0 cm ($0.26\lambda_0$ to $0.4\lambda_0$), the BW of the antenna decreases further from 58 MHz to 39 MHz, but the gain of the antenna increases from 5.3 dB to 7.2 dB. However, when Δ is increased further from 3.0 cm to 4.5 cm ($0.4\lambda_0$ to $0.6\lambda_0$), the BW of the antenna increases from 39 MHz to 85 MHz, and

Table 4.1
Effect of Air Gap Δ Between the Two Patches on the BW and Gain of Square ECMSA

Δ (cm)	x (cm)	f_0 (GHz)	BW (MHz)	Gain (dB)
0.5	1.10	3.885	684	8.0
1.0	0.60	3.930	167	7.8
1.5	0.40	3.878	85	6.3
2.0	0.35	3.844	58	5.3
2.5	0.30	3.821	45	5.5
3.0	0.30	3.802	39	7.2
3.5	0.30	3.785	41	9.2
4.0	0.35	3.772	54	10.6
4.5	0.40	3.765	85	10.6
5.0	0.50	3.787	134	9.3
5.5	0.50	3.804	132	7.4
6.0	0.50	3.810	108	5.9

the gain of the antenna increases from 7.2 dB to 10.6 dB. When Δ is increased to 5.0 cm ($0.66\lambda_0$), the BW increases to 134 MHz, but the gain decreases to 9.3 dB. A further increase in Δ to 6.0 cm ($0.8\lambda_0$) decreases both the BW and gain of the antenna. Therefore, depending upon the wide BW or high gain requirement, the air gap Δ between the two patches can be chosen accordingly.

4.2.2.5 Effect of the Air Gap Between the Fed Patch and the Ground Plane

The air gap can also be introduced between the fed patch and the ground plane as shown in Figure 4.17. As a result, both the fed and the parasitic patches are in suspended configuration. For a small gap Δ_1 between the fed patch and the ground plane, the effective dielectric constant seen by the fed patch is reduced significantly, and its value can be obtained using (2.25). Thus, the fed patch dimensions are to be increased to operate in the above frequency range. For $\epsilon_{r1} = \epsilon_{r2} = 2.22$, $h_1 = h_2 = 0.159$ cm, $\Delta_1 = 0.1$ cm, $L_1 = 2.9$ cm, $L_2 = 2.5$ cm, $\Delta_2 = 0.25$ cm, and $x = 1.1$ cm, the input impedance and VSWR plots are shown in Figure 4.18. A BW of 743 MHz (18.8%) is obtained and the gain of the antenna is 8.3 dB at 3.95 GHz.

4.2.3 Coaxial-Fed Stacked CMSAs

A CMSA, rather than an RMSA or a square MSA, could also be stacked to obtain a broad BW. A low-cost stacked CMSA is also designed for operation in the 3.7–4.2 GHz range [14]. A two-layered stacked CMSA is shown in Figure 4.19(a). The antenna is fabricated in inverted configuration, so that the substrate provides protective dielectric cover for the antenna. Both the patches are fabricated on a glass-epoxy substrate having $\epsilon_r = 4.3$, $h = 0.159$ cm, and tan $\delta = 0.02$. The radius of the bottom patch a_1 is calculated to be 1.03 cm near the center frequency using (2.30). The radius of the top

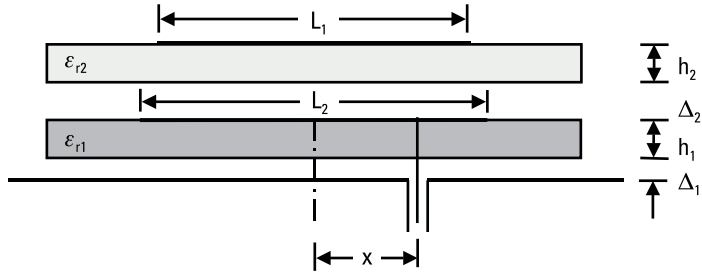

Figure 4.17 Suspended stacked-square ECMSA.

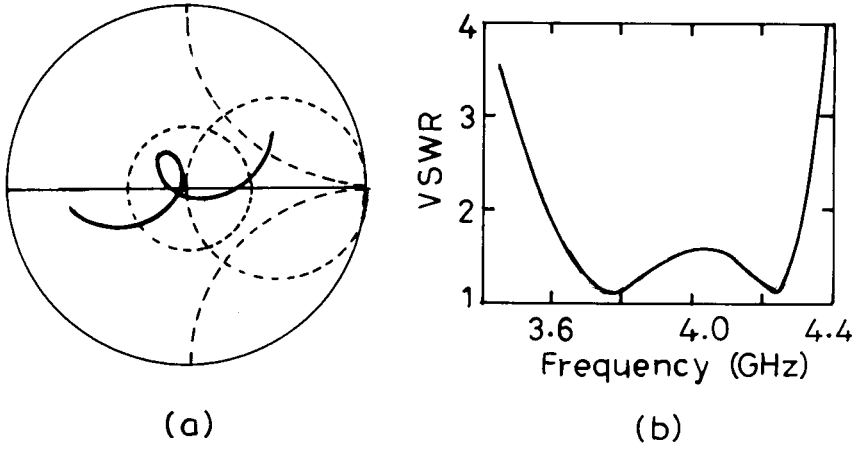

Figure 4.18 (a) Input impedance and (b) VSWR plots of suspended stacked-square ECMSA.

patch a_2 is optimized so that its resonance frequency is close to that of the bottom patch and is found to be equal to 1.18 cm for Δ = 0.6 cm. The air gap is maintained by a four-Teflon spacer of thickness 0.6 cm. The bottom patch is fed at x = 0.82 cm. To obtain the symmetric radiation pattern and reduce the back radiation from the MSA to excite an 8-foot parabolic dish antenna, a peripheral choke is incorporated as shown in Figure 4.19(a). It is realized by wrapping thin copper foil around the substrate at a radius equal to 3 cm ($0.4\lambda_0$), making it a cavity-backed configuration. The measured input impedance and VSWR plots are shown in Figure 4.19(b, c). The VSWR is less than 1.5 in the frequency range from 3.62 GHz to 4.30 GHz (17.2%). For VSWR $\leq$ 2, the BW is from 3.55 GHz to 4.36 GHz (20.5%). The measured HPBWs in the E- and H-planes at 3.95 GHz are 67° and 60°, respectively. The cross-polar and backlobe levels are 20 dB below the copolar levels in both the planes.

The BW of the cavity-backed stacked CMSA increases further by adding an air gap Δ_1 between the lower substrate and the ground plane as shown in Figure 4.20(a). Due to air gap Δ_1, the effective dielectric constant seen by the bottom patch reduces and the total thickness of the bottom patch from the ground plane increases. Both of these factors result in increase in the BW. For a_1 = 1.55 cm, a_2 = 1.05 cm, Δ_1 = 0.25 cm, Δ_2 = 0.6 cm, and x = 1.38 cm, the measured input impedance and VSWR plots are shown in Figure 4.20(b, c) [14]. The measured BW for VSWR $\leq$ 2 is 1.22 GHz (30%). Instead of a two-layered ECMSA, multilayered configurations can be optimized for broad BW or higher gain [15].

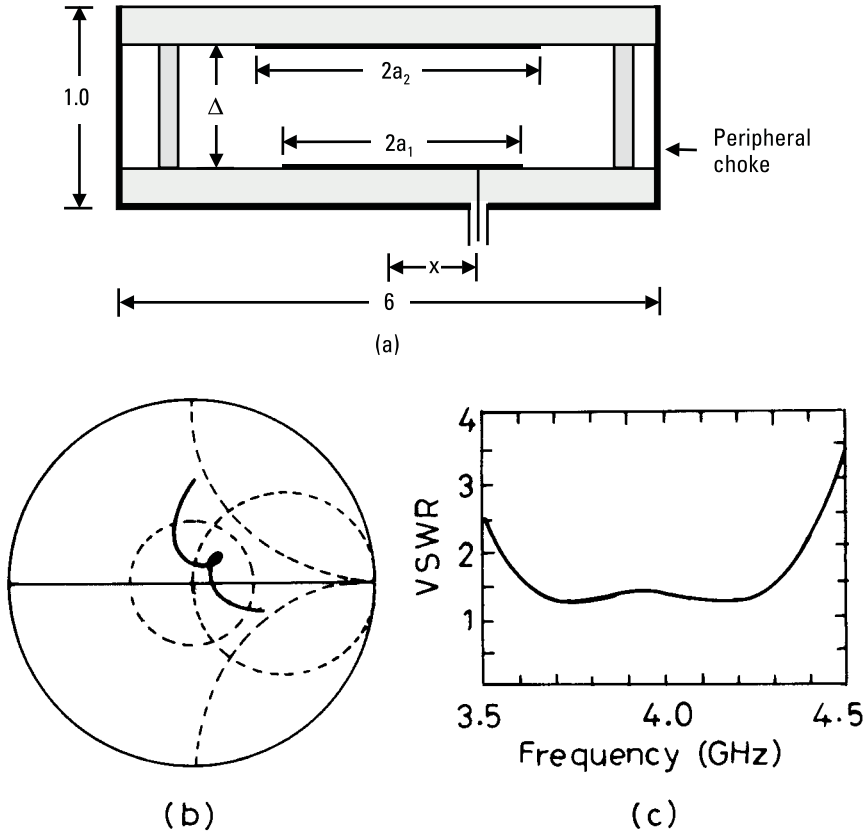

Figure 4.19 (a) Stacked CMSA with peripheral choke, and its measured (b) input impedance and (c) VSWR plots.

4.2.4 Coaxial-Fed Stacked ETMSAs

Instead of square and circular patches, equilateral triangular patches could also be stacked as shown in Figure 4.21(a) to obtain wide BW [16, 17]. Only the bottom triangular patch of side length S_1 = 3.7 cm is fed at x = 1.35 cm. The top triangular patch of side length S_2 is stacked with an air gap Δ. The two substrates are chosen to be the same with parameters $\epsilon_{r1} = \epsilon_{r2} = 2.55$ and $h_1 = h_2 = 0.16$ cm. The variation of BW as a function of air gap for various values of S_2/S_1 is given in Figure 4.21(b). For various values of S_2/S_1, maximum BW is obtained when Δ is in the range of 0.4 cm to 0.6 cm. With a further increase in Δ, the BW decreases due to a decrease in the coupling between the two patches, which decreases the loop size as observed in the case of stacked RMSA. For Δ = 0.5 cm and

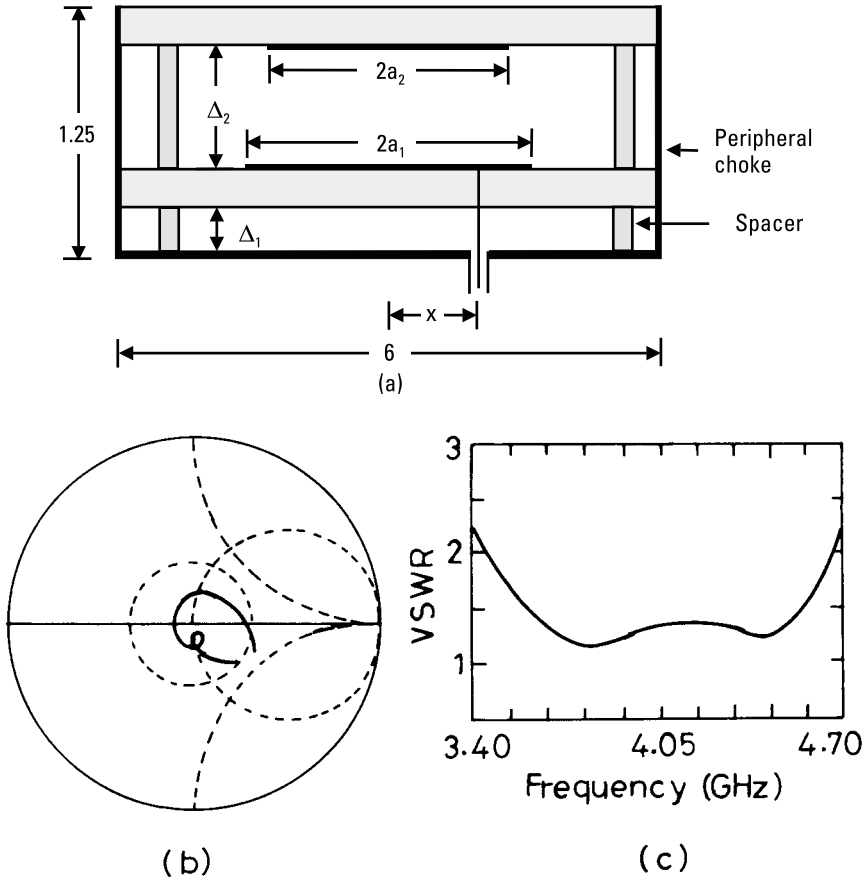

Figure 4.20 (a) Stacked suspended CMSAs with peripheral choke and its measured (b) input impedance and (c) VSWR plots.

S_2/S_1 = 1, the BW is nearly 600 MHz at the center frequency around 3.4 GHz. For this case, the measured HPBW in the E-plane varies from 55° to 65°, and in the H-plane it varies from 75° to 85° over the entire BW. The cross-polar levels are less than 17 dB as compared to copolar levels.

4.2.5 Design Example Using Stacked-Square MSA on Air Substrate

An MSA is required to operate in the 900-MHz band with 100-MHz BW. To start with, a single-square MSA of length L = 14.5 cm is designed for ϵ_r = 1 and h = 2 cm (which could be realized by using copper or aluminum sheet suspended in air), as shown in Figure 4.22(a). The probe diameter is

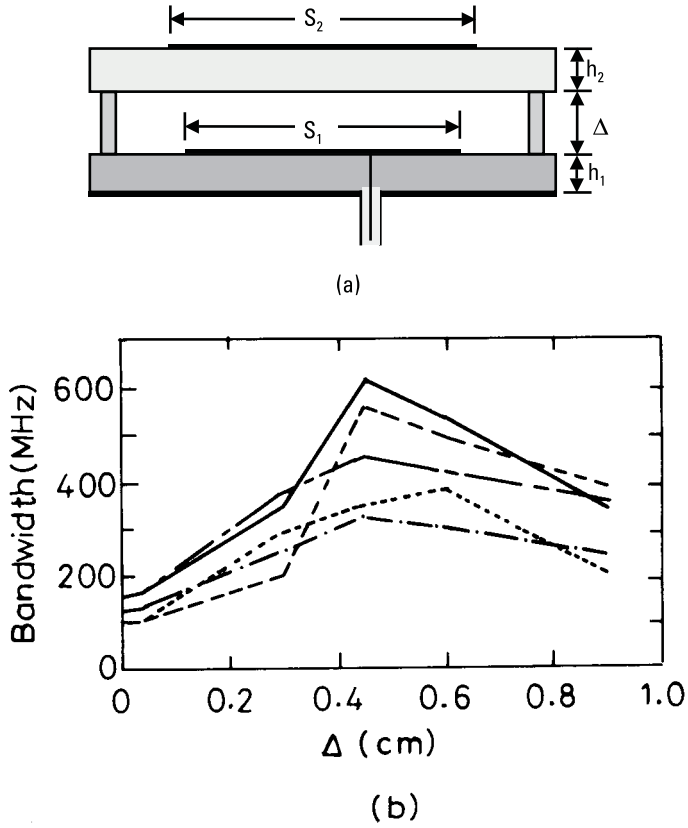

Figure 4.21 (a) Two-stacked TMSA with an air gap between the two patches, and its (b) BW variation with air gap Δ for various values of S_2/S_1: (——) 1.00, (— · —) 1.06, (- - -) 0.98, (· · ·) 1.04, and (– · –) 1.02.

taken as 0.2 cm, which corresponds to the TNC/BNC connector. The feed point is taken near the radiating edge. The BW for VSWR $\leq$ 2 is 68 MHz at the center frequency f_0 = 930 MHz, which does not meet the BW requirement. If the thickness of the antenna is increased further to increase the BW, it increases the inductance of the feed probe, which makes impedance matching difficult and reduces the efficiency of the antenna. To reduce the inductance of the feed probe, its length is reduced and the tip of the probe is loaded with a small square patch, which then indirectly excites the top patch through capacitive coupling. In Figure 4.22(b), the loaded small square patch is kept close to the top patch, whereas in Figure 4.22(c) this patch is kept midway between the patch and the ground plane. The overall thickness of the antenna is kept the same as 2 cm for purposes of comparison. These

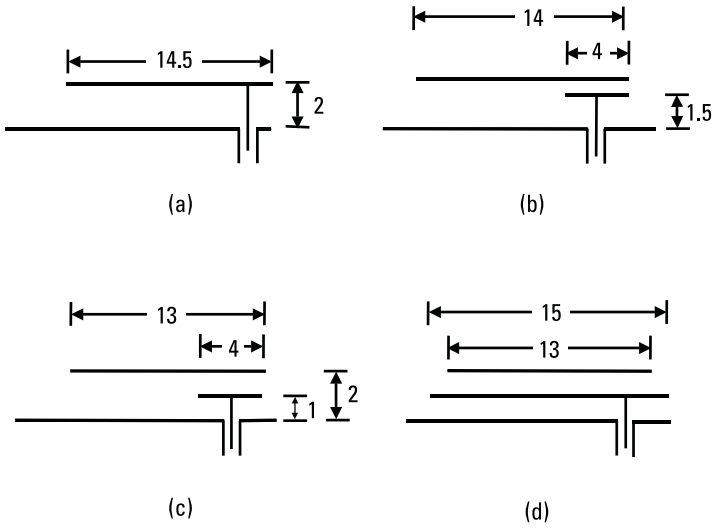

Figure 4.22 Square MSA for the 900-MHz band fed with (a) coaxial probe, (b) and (c) modified probe, and (d) resonant patch.

two configurations, whose dimensions are shown in Figure 4.22(b, c), yielded BW of 88 MHz and 82 MHz, respectively. Both the configurations yield a wider BW than the probe-fed patch but do not cover the required BW.

Instead of feeding the top patch through capacitive coupling from the small fed patch, a resonant patch of length 15 cm is used at h = 1 cm, and the top patch length is optimized to be 13 cm, as shown in Figure 4.22(d). The BW is 129 MHz at f_0 = 959 MHz, which meets the requirement; it is also larger than all the other cases. The performance of these four configurations is summarized in Table 4.2. The gain of all the four cases is comparable. Therefore, the resonant-stacked MSA is a better choice for obtaining larger BW than the coaxial-fed or modified probe-fed MSA.

Table 4.2
Various RMSA Configurations for 900-MHz Band

Configurations Shown in Figure 4.22	f_0 (MHz)	BW (MHz)	Gain (dB)
(a)	930	68	9.6
(b)	908	88	9.5
(c)	932	82	9.3
(d)	959	129	9.6

4.3 ACMSAs

Similar to electromagnetic coupling, aperture coupling is another indirect method of feeding the resonant patch. It was first proposed in 1985 for enhancement of the BW of the MSA [18]. By optimizing the various parameters including the aperture dimensions, a BW of nearly 70% has been achieved. An ACMSA consists of two substrates separated by a ground plane. The exploded and top views of a rectangular ACMSA are shown in Figure 4.23. The top substrate contains the radiating element, and the bottom substrate contains the microstrip feed line. A small aperture is cut in the ground plane to allow coupling from the open-circuited microstrip feed line to the radiating patch. In Figure 4.23, a rectangular aperture of length L_{ap} and width W_{ap} is shown with an offset of x_{os} and y_{os}, but it is generally placed in the center of the patch for maximum coupling and symmetric radiation pattern. The coupling aperture could be small, known as a nonreso-

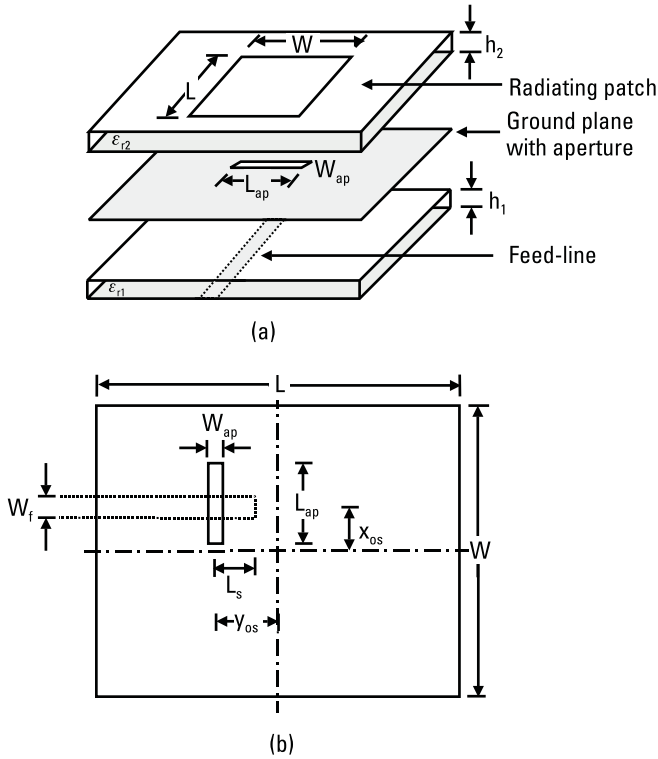

Figure 4.23 ACMSA: (a) exploded and (b) top views.

nant aperture, or comparable to a half-wavelength, known as a resonant aperture.

The ACMSA has several advantages:

- The top patch could be fabricated on a thick low dielectric substrate to enhance the BW, and the feed network on the other side of the ground plane could be on a thin high dielectric substrate to reduce radiation losses.
- Radiation from the feed network does not interfere with the main radiation pattern, since the ground plane separates the two substrates.
- The excess reactance of the antenna can be compensated for by varying the length L_s of the open-circuited microstrip stub.
- The input impedance is easily controlled by the size, shape, and position of the aperture.

The ACMSA also has certain disadvantages. The total thickness of the antenna is large as compared to a probe-fed MSA. Also, the back radiation occurs more through the coupling aperture in the ground plane, which can be reduced by using a small aperture.

Several techniques have been used to analyze the ACMSA. These techniques include the transmission line model [19, 20], the cavity model [21–23], the integral equation method [24–29]. All these techniques predict the performance of the antenna reasonably well. Section 4.3.1 details a parametric study of the basic ACMSA configuration based on the results obtained using the integral equation technique [3, 24].

4.3.1 Parametric Study of ACMSAs

The performance of an ACMSA depends on various parameters, including patch dimensions; aperture shape, dimensions, and location; dielectric constant and thickness of the two layers; and dimensions of the microstrip feed line. The resonant length of the patch decides the resonance frequency of the antenna. Therefore, the radiating rectangular patch dimensions are fixed at L = 4 cm and W = 3 cm and the top substrate parameters are ϵ_r = 2.54 and h = 0.16 cm. The effects of varying the length of the feed line, size and location of rectangular aperture, and substrate parameters on the input impedance loci of the ACMSA are discussed below by varying one parameter at a time [24].

4.3.1.1 Effect of the Length of the Feed Line

For the feed-line substrate the same as that of the patch substrate, the feed-line width W_f is 0.442 cm for the characteristic impedance $Z_0 = 50\Omega$. The aperture length and width are taken as $L_{ap} = 1.12$ cm and $W_{ap} = 0.155$ cm, respectively. The patch is centered over the aperture (i.e., $x_{os} = 0$ and $y_{os} = 0$). For various values of the stub length L_S, the measured and theoretical input impedance loci in the frequency range of 2,150 MHz to 2,275 MHz are shown in Figure 4.24. When L_S is increased from 0.4 cm to 2.0 cm, the impedance loci moves in the clockwise direction. If the input impedance at a single frequency is plotted for various stub lengths, the locus approximately follows a constant resistance contour (i.e., the stub provides only the reactance to the input impedance loci). The impedance Z_S provided by the open-ended stub with characteristic impedance Z_0 and length L_S is given by

$$Z_S = -jZ_0/\tan(\beta L_S) \tag{4.1}$$

Thus, the length of the stub can be varied to achieve a reactance compensation for matching purposes in the antenna design.

4.3.1.2 Effect of the Aperture Dimensions

The patch on the top layer gets excited from the microstrip feed line through the aperture in the ground plane. The length and the width of the aperture determine the amount of coupling to the patch. For fixed aperture width $W_{ap} = 0.11$ cm, $L_S = 2.0$ cm, and the other dimensions of the antenna the same as those in the previous case, the effect of varying the aperture length

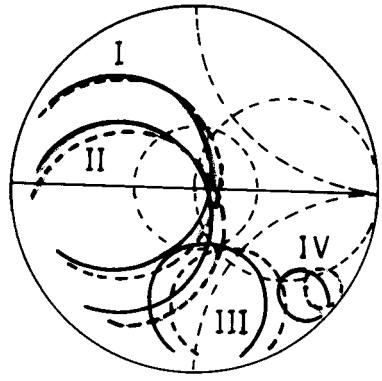

Figure 4.24 Input impedance loci of ACMSA for different values of stub length L_S: (I) 2.0 cm, (II) 1.6 cm, (III) 0.8 cm, and (IV) 0.4 cm; (- - -) theoretical and (——) measured.

from 0.9 cm to 1.4 cm on the input impedance loci is indicated in Figure 4.25. As the aperture length is increased, coupling increases, which results in an increase in the resonant input impedance. This leads to an increase in the radius of the impedance plot and hence it moves right on the Smith chart (i.e., toward the higher impedance value). For a small slot length, the patch is undercoupled and the resonant resistance is small. Therefore, the length of the aperture can be varied to achieve the desired resistive part of the input impedance.

As mentioned earlier, the resonance frequency of the ACMSA depends mainly on the resonant dimension of the patch, but it is affected by the length of the aperture. The variation of the resonance frequency and the real part of the input impedance with the length of the rectangular aperture is shown in Figure 4.26. With an increase in the length of the aperture from 0.9 cm to 1.4 cm, the resonance frequency decreases from 2,263 MHz to 2,170 MHz (about 4%) and the resistive part of the input impedance increases from 20 to 136Ω. The perfect match of 50Ω is achieved for L_{ap} = 1.09 cm at 2,233 MHz.

With an increase in the width of the aperture, the coupling increases. The effect of an increase in the width of the aperture is similar to that of an increase in the aperture length.

4.3.1.3 Effect of Aperture Location

Small variations in the patch position over the aperture (i.e., misalignment of the patch in the y or x directions over the slot) does not affect the input impedance much, but the change becomes significant for larger patch offsets.

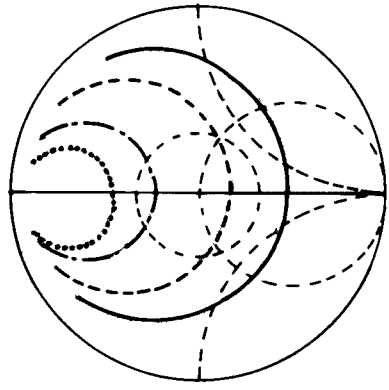

Figure 4.25 Theoretical input impedance loci for four values of aperture length L_{ap}: (——) 1.4, (- - -) 1.2, (– · –) 1.0, and (· · ·) 0.9 cm.

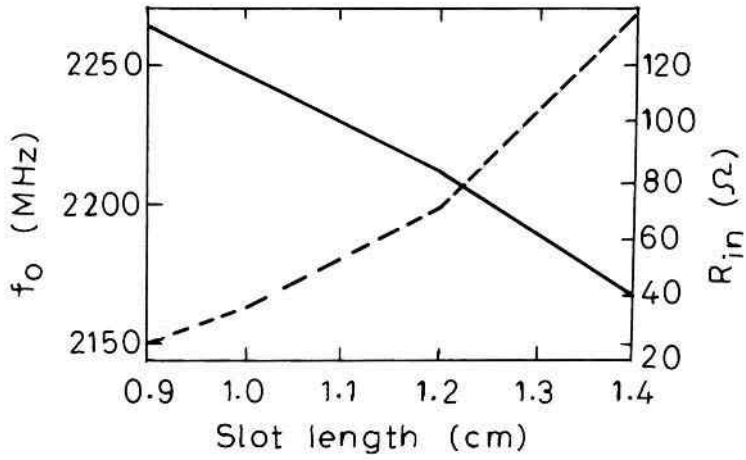

Figure 4.26 Variation of (——) resonance frequency and (- - -) input resistance of ACMSA with slot length L_{ap}.

The ACMSA with an offset y_{os} along the resonant length of the patch is shown in Figure 4.27(a). For three values of y_{os} (0.5, 1.0, and 1.5 cm) with L_s = 2.0 cm, L_{ap} = 1.12 cm, and W_{ap} = 0.155 cm, the theoretical and measured input impedance loci are shown in Figure 4.27(b). With an increase in the offset, the coupling decreases, and the input impedance loci shifts

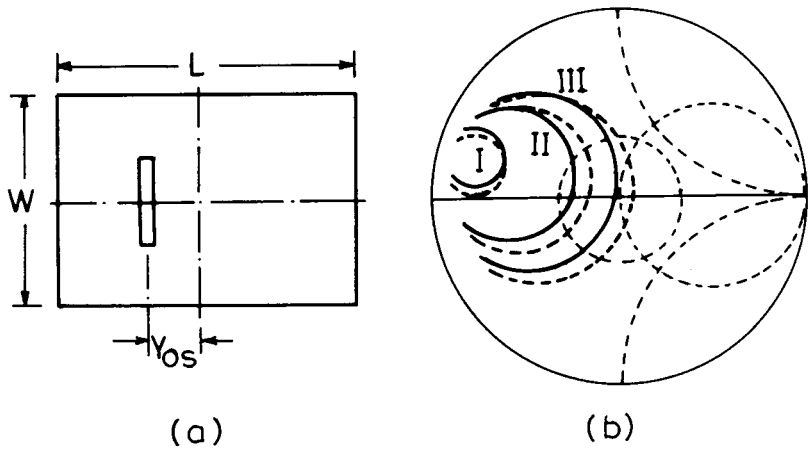

Figure 4.27 (a) ACMSA with an offset along the length of the patch and its (b) input impedance loci for three values of y_{os} [1.5 cm (I), 1.0 cm (II), and 0.5 cm (III)]: (——) measured and (- - -) theoretical.

toward the lower impedance value and its size reduces. This is expected because the current variation along the length of the resonant patch is sinusoidal with maximum current at the center and zero current at the edges of the patch. The flatness of the sinusoidal current at the center does not affect the input impedance when the offset is small, but with an increase in offset, input impedance decreases.

The ACMSA with an offset x_{os} along the width of the patch is shown in Figure 4.28(a). The measured impedance loci for various values of x_{os} are shown in Figure 4.28(b). For small offset, the coupling does not change much, because the field is uniform along the width of the patch. As the offset increases, the coupling increases slightly until the edge of the aperture is aligned with the edge of the patch resulting in an increase in the real part of the input impedance. With a further increase in the offset (i.e., as the slot comes out of the patch), coupling decreases and hence the input impedance plot shifts toward the left side of the impedance plot (i.e., toward the lower impedance region). In general, an aperture aligned centrally below the patch leads to an optimum ACMSA configuration, because it forms symmetric excitation, resulting in very good cross-polarization characteristics as compared to the conventional MSA, where the feed is not symmetrical.

4.3.1.3 Effect of Substrate Parameters

The substrate parameters of the radiating patch and microstrip feed line have a significant effect on the input impedance of the ACMSA. With an

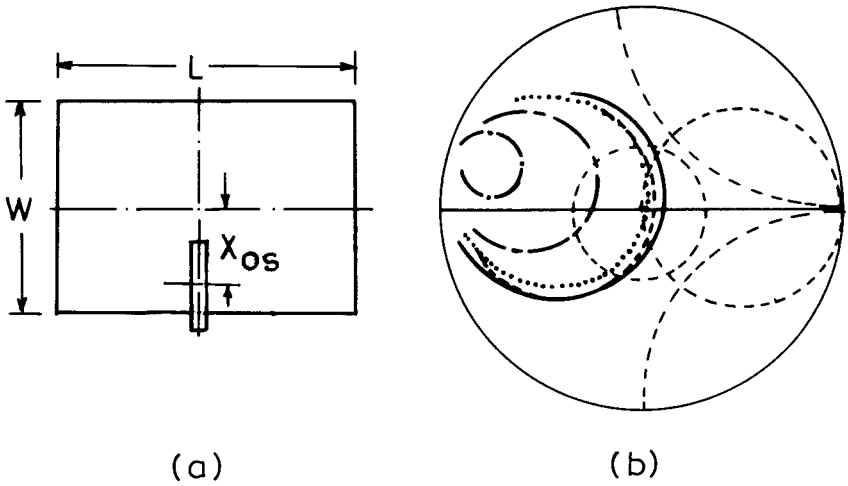

Figure 4.28 (a) ACMSA with an offset along the width of the patch and its (b) measured input impedance loci for various values of x_{os}: (- - -) 0.5 cm, (——) 1.0 cm, (· · ·) 1.25 cm, (— · —) 1.5 cm, and (– · –) 1.75 cm.

increase in the dielectric constant ϵ_{r1}, the field is less spread out and the electrical length of the aperture increases, which increases coupling. The increase in coupling results in an increase in the resonant input resistance. As the thickness of the substrates increases, the coupling decreases, and hence the input impedance loci shifts toward the left side of the Smith chart. This reduction in coupling can be compensated for by increasing the length or width of the aperture [24].

In addition to the length, width, and location of the aperture, the shape of the aperture is an important parameter in designing the ACMSA. Various shapes of coupling apertures are discussed in Section 4.3.2 [18, 20, 24, 30–33].

4.3.2 Effect of the Shape of the Coupling Aperture

The coupling aperture in an ACMSA is generally smaller than the size of the resonant patch, so that most of the radiated power is due to the patch, with the backlobe radiation from the slot typically 15–20 dB below the forward main beam. Since the patch is normally centered over the aperture, magnetic polarization of the slot is the dominant mechanism for coupling, which depends on the shape and size of the coupling aperture. Hence, it is desirable to use a shape that has maximum coupling for a given size. This allows the antenna to be impedance-matched with a smaller aperture. Smaller aperture areas result in lower back radiation levels, leading to less spurious radiation in the back region and improved efficiency.

The original ACMSA used a circular aperture, which was proposed in 1985 [18]. Since then, various shapes have been used to obtain large coupling with smaller aperture area, as shown in Figure 4.29. Compared to the circular aperture, a thin rectangular aperture shown in Figure 4.29(a) gives much stronger coupling. The coupling can be increased by using longer or wider rectangular apertures shown in Figure 4.29(b, c). The coupling increases if instead of using rectangular aperture, an ''H''-shaped aperture, shown in Figure 4.29(d), is used. A dog bone-shaped aperture could be used, which has rounded edges as compared to that of the ''H''-shaped aperture. The coupling obtained in these two cases is comparable. For a simple rectangular slot, the transverse electric field must vanish at the end of the aperture. By adding a slot at the end of the rectangular aperture (i.e., the ''H''-shaped aperture), the field becomes nearly uniform along the aperture and hence the coupling increases. Other nonlinear shaped apertures ''U'' and ''L'' could also be used [20, 33], but the ''H''- or dog bone-shaped aperture yields better coupling. A bowtie or butterfly shaped aperture, shown in Figure 4.29(e), also gives more coupling and higher resonant impedance as compared

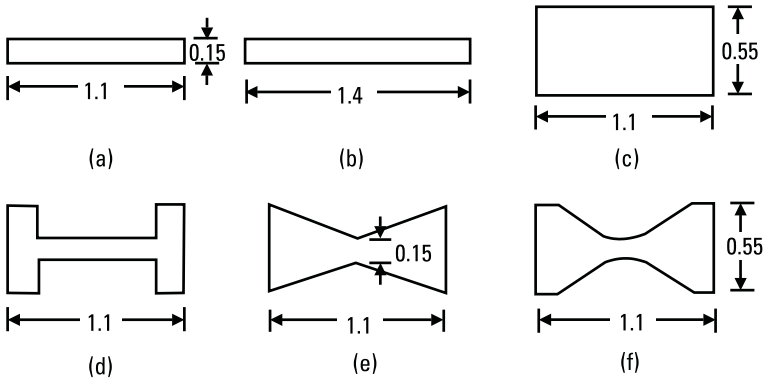

Figure 4.29 Various aperture shapes with dimensions used in ACMSA: (a) rectangular, (b) longer rectangular, (c) wider rectangular, (d) "H"-shape, (e) bowtie, and (f) hourglass.

to the rectangular aperture. An hourglass shaped aperture, shown in Figure 4.29(f), uses the features of both the dog bone- and the bowtie-shaped apertures without any sharp edges and hence gives maximum coupling.

The effect of coupling due to various aperture shapes on the performance of a rectangular ACMSA is discussed below. A rectangular patch of L = 4 cm and W = 3 cm is chosen for the top layer. The top and bottom substrates are the same with parameters ϵ_r = 4.3 and h = 0.16 cm. The width and the length of the microstrip feed line are taken as W_f = 0.3 cm and L_S = 2 cm, respectively. These dimensions are kept the same for all the experiments except for the coupling aperture, whose shapes and dimensions are shown in Figure 4.29 [33].

The measured input impedance loci for different apertures shown in Figure 4.29 are shown in Figure 4.30 in the frequency range of 1.6–2 GHz. For the rectangular aperture of length L_{ap} = 1.1 cm and width w_{ap} = 0.15 cm, the coupling is very small, as indicated by the small resistive component and small loop size. When the length of the aperture is increased from 1.1 cm to 1.4 cm, a bigger loop is obtained, implying that the coupling increases with an increase in aperture length. Similarly, when the width of the aperture is increased from 0.15 cm to 0.55 cm with L_{ap} = 1.1 cm, the coupling increases. The "H"- and bowtie-shaped apertures yield more coupling than the rectangular aperture of same length. In fact, the coupling is even more than the larger rectangular aperture of length L_{ap} = 1.4 cm. The "H"-shaped aperture, which is a simplified version of the dog-bone aperture, has higher resonant impedance implying larger coupling than the bowtie-shaped aper-

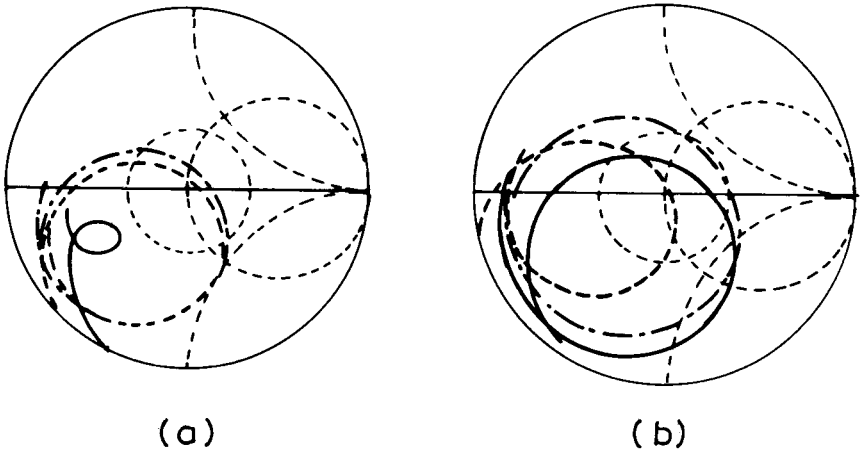

Figure 4.30 Measured input impedance loci of a rectangular ACMSA for various aperture shapes shown in Figure 4.29: (a) (——) rectangular, (- - -) longer rectangular, and (– · –) bowtie, and (b) (- - -) wider rectangular, (——) H-shaped, and (– · –) hourglass.

ture. The loop size for the hourglass-shaped aperture is maximum, and it has the highest resonant impedance as compared to all the other aperture shapes. The reason for the maximum coupling shown by hourglass-shaped aperture is that the advantages of both "H" and bowtie shapes have been combined, and the sharp discontinuities have been removed, which makes the field distribution inside the aperture more uniform [33].

In general, the shape of the aperture should be chosen in such a way that it gives maximum coupling with the smallest size of the aperture so that the BW of the antenna can be increased by increasing h_2 or by reducing ϵ_{r2} with minimum back radiation.

To increase the BW of the ACMSA, multiple patches are stacked on each other, with resonance frequencies close to each other to realize broad BW. The air gap or foam substrate is also used between the patches to further enhance the BW as described in Section 4.3.3.

4.3.3 Stacked ACMSAs

The experimental results using the stacked RMSA and CMSA are described. The air gap has been used between the patch and the ground plane and between the two patches, which increases the total thickness of the ACMSA and hence its BW. A nonresonant hourglass-shaped aperture is used for all the experiments because it gives maximum coupling.

4.3.3.1 Dual-Stacked Rectangular ACMSAs

The exploded and side views of a dual-stacked rectangular ACMSA are shown in Figure 4.31(a, b) [34]. The rectangular patch dimensions are L = 4 cm and W = 5 cm. Glass epoxy substrates (ϵ_r = 4.3, h = 0.16 cm, and tan δ = 0.02) are used for the feed line and the radiating patches. The feed line width is taken as 0.3 cm for $Z_0 \cong 50\Omega$ and L_s is taken as 2 cm. The air gap spacings Δ_1 and Δ_2 are provided by using dielectric spacers at the edges. Both the patches are centered over the coupling aperture for maximum coupling. The dimensions of the hourglass-shaped aperture are 2×0.8 cm as shown in Figure 4.31(c). For Δ_1 = 0.06 cm and Δ_2 = 0.28 cm, the measured input impedance and VSWR plots are shown in Figure 4.32(a, b). The measured BW for VSWR $\leq$ 2 is 501 MHz (24.9%).

4.3.3.2 Triple-Stacked Rectangular ACMSAs

In a triple-stacked ACMSA configuration, another parasitic patch is added symmetrically on top of the second patch. For three layers of rectangular

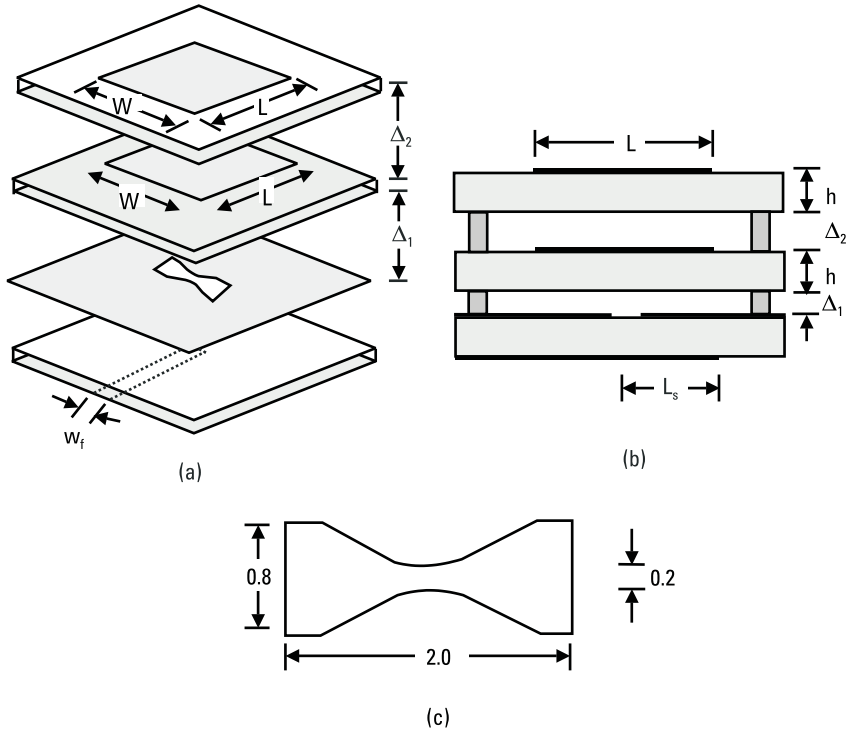

Figure 4.31 Dual-stacked rectangular ACMSA: (a) exploded view, (b) side view, and (c) dimensions of the hourglass-shaped aperture.

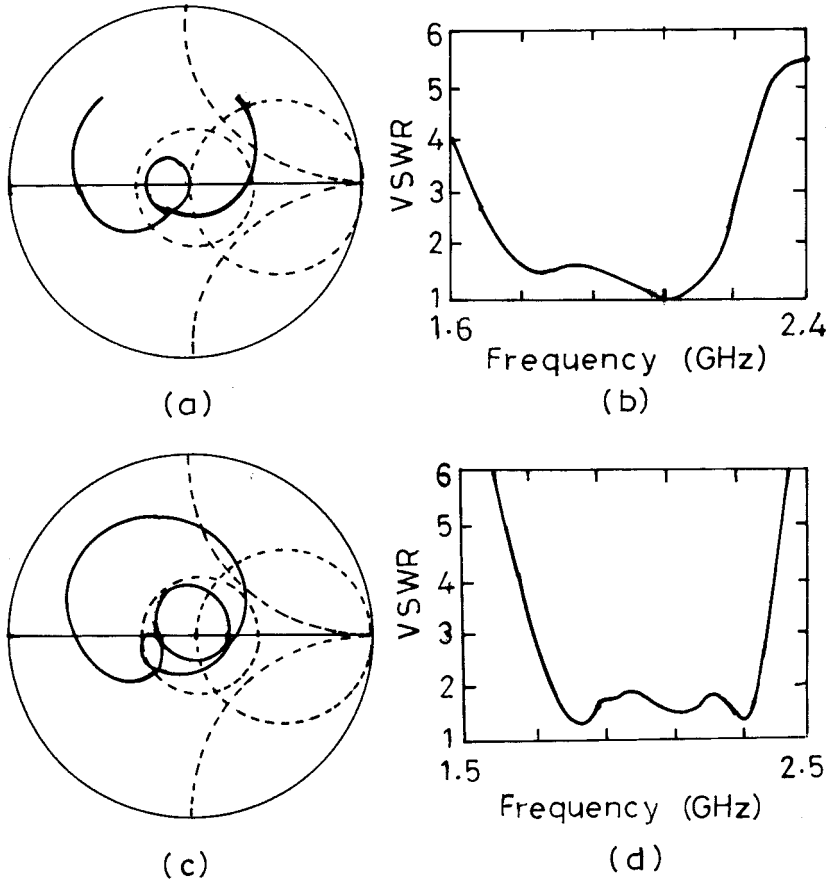

Figure 4.32 Measured input impedance and VSWR plots of stacked rectangular ACMSA with L = 4 cm and W = 5 cm. (a) and (b) two and (c) and (d) three stacked patches.

patches of L = 4 cm and W = 5 cm with Δ_1 = 0.09 cm, Δ_2 = 0.62 cm, and Δ_3 = 0.3 cm (where Δ_3 is the air gap between the top two patches), the measured input impedance and VSWR plots are shown in Figure 4.32(c, d). Another loop is observed in the Smith chart, which is due to the additional parasitic element. The measured BW is 602 MHz (29.5%). Instead of using the top patch in the normal mode, it could be inverted, so that the top dielectric substrate acts as a protective cover for the antenna. For this case with Δ_3 = 0.4 cm, the measured BW is 596 MHz (29.4%) at 2.025 GHz.

The measured radiation pattern of the triple-stacked rectangular ACMSA at 2.3 GHz is in the broadside direction. The HPBWs in the

E- and H-planes are 78° and 74°, respectively, which are smaller than those of the single patch antenna [34]. This indicates a higher gain for the stacked ACMSA. The cross-polar level is 17 dB below the copolar level and the front-to-back (F/B) ratio is around 8–10 dB. The back radiation is due to the aperture in the ground plane and the finite size of the ground plane.

4.3.3.3 Stacked Circular ACMSAs

Similar to the stacked RMSA configurations, dual- and triple-stacked ACMSA, with circular patches are also used for wideband operation. For a dual-stacked circular ACMSA with patch radius a = 2.5 cm, Δ_1 = 0.09 cm, and Δ_2 = 1.02 cm, the measured BW is 515 MHz, which is 24.9% at 2.065 GHz. For a triple-stacked circular ACMSA with Δ_1 = 0.09 cm, Δ_2 = 0.62 cm, and Δ_3 = 0.2 cm, the measured BW is 579 MHz, which is 28.4% at 2.042 GHz [34].

4.3.4 Resonant Slot ACMSAs

In the previous section, the size of the aperture is small in comparison to the resonant length of the radiating patch, and hence it is nonresonant at the operating frequency of the antenna. However, a larger BW is obtained by using the resonant rectangular aperture, instead of the small slot, at the expense of an increase in the F/B ratio. A larger BW is obtained because both the patch and the aperture are resonant, giving rise to a double-tuned resonance effect. The resonant aperture increases the coupling to the radiating patch, thereby increasing the size of the loop in the impedance plot. The coupling has to be reduced so that the loop is within the desired VSWR circle on the Smith chart. The dimension of the aperture cannot be decreased to reduce the coupling as it is resonant and is governed by the frequency of operation. The coupling is reduced with an increase in the thickness of the patch substrate and a decrease in the dielectric constant, which results in an increase in the BW. Therefore, for the resonant ACMSA configuration, a thick substrate with a low dielectric constant is used. In this case, a BW of up to 20% for a single patch and nearly 70% for multiple stacked patches is achieved as described below [35–41].

4.3.4.1 Strip-Slot Foam-Inverted Patch Antenna

A *strip slot foam inverted patch* (SSFIP) antenna [36, 37] is shown in Figure 4.33. The name SSFIP comes from the fact that at the bottom layer, there is a microstrip line; above that, a slot is cut in the ground plane, followed by foam substrate and then an inverted microstrip patch. The square radiating

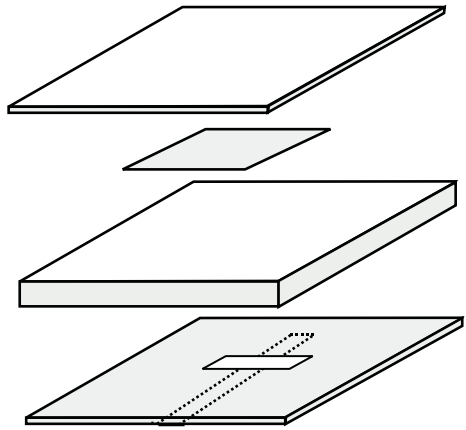

Figure 4.33 Exploded view of SSFIP antenna.

patch of length L = 1.07 cm is deposited on the underside of a thin substrate (ϵ_r = 4.32 and h = 0.01 cm), which also serves as a protecting cover. Between the patch and the ground plane, a low dielectric constant foam substrate (ϵ_r = 1.07 and h = 0.2 cm) is used to increase the BW. The patch is excited through a coupling slot (L_{ap} = 1.2 cm, w_{ap} = 0.04 cm) by a microstrip line printed on a substrate having ϵ_r = 2.33 and h = 0.051 cm underneath the ground plane. For a single patch, the measured BW is 13.2% and the measured gain variation is over 8.2–8.8 dB in the frequency range of 9.15–10.4 GHz.

4.3.4.2 Aperture-Stacked Patch Antenna

A larger BW of 50–70% is obtained if the stacked patches are fed with a resonant aperture. For the case of two stacked patches with a resonant slot, two loops are formed, representing the interaction between three resonators (two patches and one resonant slot). This configuration is also known as an aperture-stacked patch. All the parametric studies discussed for the ACMSA with a small aperture also apply to the ACMSA having resonant aperture. The SDT is used to analyze the antennas, and the optimized dimensions are shown in Figure 4.34 [41].

The dimensions of the antenna are critical in the sense that the coupling between three resonators—namely, the aperture and lower and upper patches—has to be optimum to yield a broad BW. When the aperture size is changed, there is pronounced effect on the lower frequency loop, which represents the interaction between the aperture and the lower patch, while there is a minor effect on the higher frequency loop (which is formed due

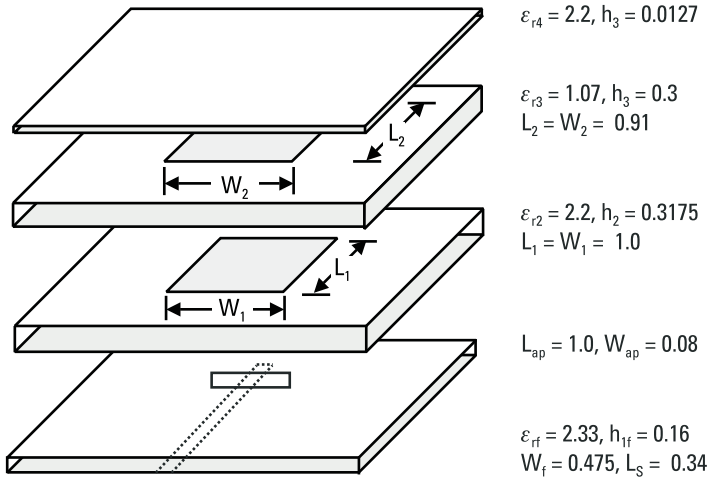

Figure 4.34 Optimized dimensions of a multilayered aperture-stacked square patch antenna.

to the mutual coupling effect between the two patches). The increase in the aperture length increases the coupling to the lower patch and hence the loop size increases. The size of the lower patch is a very important factor as it comes in between the aperture and the top patch influencing the formation of both the loops in the impedance locus. It is observed that the relative dimensions of the two patches are important as opposed to their absolute dimensions for the location of loops in the impedance plot. The size of the aperture and dimensions of both the patches are to be optimized together so that both the loops are inside the VSWR = 2 circle yielding a broad BW. With an increase in the thickness of the lower substrate, the coupling to the lower patch decreases; this reduces the size of the lower frequency loop. Similarly, the coupling to the upper patch reduces if the upper-layer thickness is increased. All these above mentioned parameters have to be optimized simultaneously for a substantial increase in the BW. For the optimized dimensions of the antenna in centimeters as shown in Figure 4.34, the theoretical input impedance plot is shown in Figure 4.35. Two loops representing the interaction between the three resonators are formed; they are within the VSWR = 2 circle, yielding a large-impedance BW. A BW of approximately 5 GHz has been obtained at the center frequency of 9 GHz, which is around 55%.

The dimensions of the antenna are further optimized to increase the BW. Foam is added between the patch and the ground plane, thereby

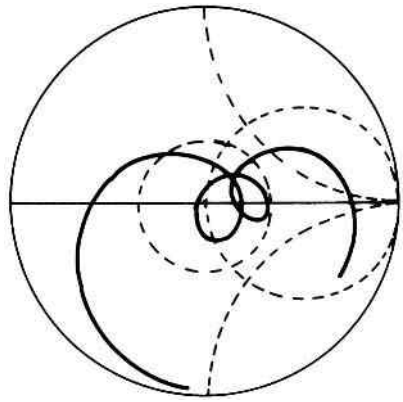

Figure 4.35 Theoretical input impedance plot of aperture-stacked square patch antenna.

increasing its total height and reducing its effective dielectric constant. The width of both the patches is increased to boost the BW. Since the size of the aperture is governed by the desired frequency of operation, the coupling cannot be controlled by changing the dimensions of the aperture. An alternate way to control the coupling is to use the dual-offset feed. The impedance of each feed line is 100Ω at the slot and is obtained through a power divider. The thickness of the feed substrate is reduced to increase the coupling. The optimized dimensions in centimeters are shown in Figure 4.36.

The theoretical and measured return loss (Γ) and gain plots are given in Figure 4.37. The theoretical BW for VSWR ≤ 2 is 5.05–10.1 GHz (67%), and the measured BW is 5.07–10.38 GHz (69%). The gain of around 7 dB is achieved in the complete VSWR BW. The theoretical F/B of 8–14 dB is achieved over most of the band, which drops to 6 dB at the higher band edge.

These multilayer broadband MSA configurations exhibit very small variation in the radiation pattern over the entire VSWR BW. The drawback of these structures is the increased thickness, which is not desirable for conformable applications, and increased back radiation in the case of ACMSA.

4.4 Summary

This chapter describes multilayer MSA configurations to increase the BW of the antenna. Based on the coupling mechanism, these antennas are classified as ECMSA or ACMSA. These configurations have many advantages, including

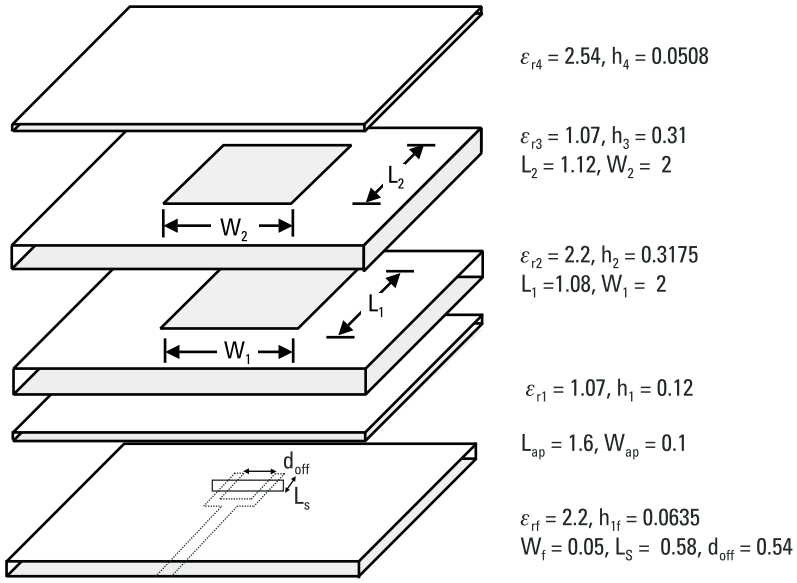

Figure 4.36 Optimized dimensions of a multilayered aperture-stacked square patch antenna for broad BW.

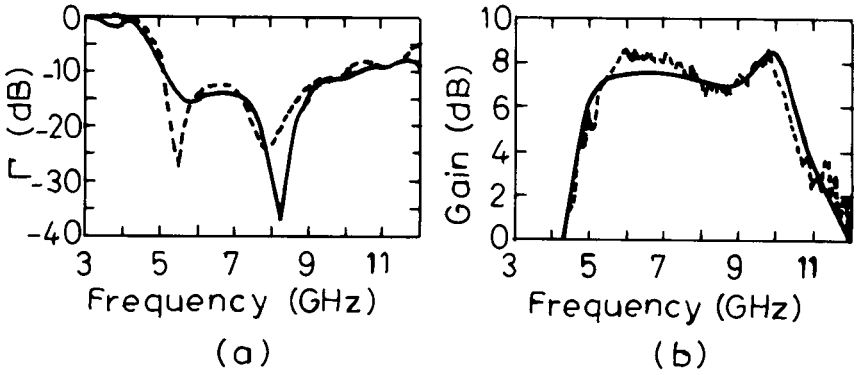

Figure 4.37 (a) VSWR and (b) gain plots of the aperture-stacked patch antenna: (——) theoretical and (- - -) measured.

wide BW, reduction in spurious feed network radiation, freedom in antenna design, and a symmetric radiation pattern with low cross-polarization. The basic characteristics and the effects of various parameters on the overall antenna performance are discussed.

In the ECMSA, the patch in the upper layer is excited through electromagnetic coupling from either the microstrip line or coaxial-fed patch in

the bottom layer. For the coaxial-fed rectangular ECMSA, the effects of various parameters, such as the dielectric constant, thickness of the substrate, patch dimensions, and the air gap between the two patches on the performance of the antenna, are described. These parameters have been optimized to obtain either broadband or high gain antenna. The ECMSA configurations with circular and triangular patches are also discussed.

In the ACMSA, the radiating patch is excited through an electrically small aperture/slot cut in the ground plane by the microstrip feed line placed on the other side of the ground plane. Two different dielectric substrates may be chosen, one for the patch and the other for the feed line to optimize the individual performances. The effect of variation in patch dimensions, the parameters of both of the substrates, and the size and shape of the aperture on the input impedance of the ACMSA is discussed. Using an optimum hourglass-shaped aperture, which yields maximum coupling, multiple stacked RMSAs and CMSAs with variable air gap separations are described for increasing the BW. A BW of up to 30% has been obtained around 2 GHz.

The ACMSA configuration with a resonant aperture yields wide BW by proper optimization of the coupling between the patch and the resonant slot. By stacking another patch on the single element, known as an aperture-stacked antenna, a maximum BW of nearly 69% has been obtained.

References

[1] James, J. R., and P. S. Hall, *Handbook of Microstrip Antennas,* Vol. 1, London: Peter Peregrinus, Ltd., 1989.

[2] Gupta, K. C, and A. Bennella, *Microstrip Antennas Theory and Design,* Norwood, MA: Artech House, 1988.

[3] Pozar, D. M., and D. H. Schaubert, *Microstrip Antennas: The Analysis and Design of Microstrip Antennas and Arrays,* New York: IEEE Press, 1995.

[4] Sainati, R. A., *CAD of Microstrip Antennas for Wireless Applications,* Norwood, MA: Artech House, 1996.

[5] Lee, H. F., and W. Chen, *Advances in Microstrip and Printed Antennas,* New York: John Wiley & Sons, Inc., 1997.

[6] Damiano, J. P., J. Bennegueouche, and A. Papiernik, "Study of Multilayer Antennas with Radiating Elements of Various Geometry," *Proc. IEE, Microwaves, Antennas Propagation,* Pt. H, Vol. 137, No. 3, 1990, pp. 163–170.

[7] Sabban, A., "A New Broadband Stacked Two Layer Microstrip Antenna," *IEEE AP-S Int. Symp. Digest,* June 1983, pp. 63–66.

[8] Splitt, G., and M. Davidovitz, "Guidelines for the Design of Electromagnetically Coupled Microstrip Patch Antennas on Two-Layered Substrate," *IEEE Trans. Antennas Propagation,* Vol. AP-38, No. 7, 1990, pp. 1136–1140.

[9] IE3D 7.0, Zeland Software, Inc., Fremont, CA.

[10] Pozar, D. M, and B. Kaufman, "Increasing the Bandwidth of a Microstrip Antenna by Proximity Coupling," *Electronics Letters,* Vol. 23, No. 8, 1987, pp. 368–369.

[11] Daniel, A. E., G. Kumar, and K. P. Ray, "Reliability of Electromagnetically Coupled Microstrip Antennas," *Proc. ICQRC,* Mumbai, India, December 2001, pp. 6.2.1–6.2.4.

[12] Lee, R. Q., K. F. Lee, and J. Bobinchak, "Characteristics of a Two Layer Electromagnetically Coupled Rectangular Patch Antenna," *Electronics Letters,* Vol. 23, No. 20, September 1987, pp. 1070–1072.

[13] Lee, R. Q., and K. F. Lee, "Experimental Study of the Two-Layer Electromagnetically Coupled Rectangular Patch Antenna," *IEEE Trans. Antennas Propagation,* Vol. AP-38, August 1990, pp. 1298–1302.

[14] Singh, A. K., and G. Kumar, "EMCP Microstrip Antennas as Feed for Satellite Receiver," *IEEE AP-S Int. Symp. Digest,* June 1996, pp. 1274–1277.

[15] Revankar, U. K., and A. Kumar, "Experimental Investigation of Three Layer Electromagnetically Coupled Circular Microstrip Antenna," *Electronics Letters,* Vol. 27, No. 13, 1991, pp. 1187–1189.

[16] Bhatnagar, P. S., et al., "Experimental Study of Stacked Triangular Microstrip Antenna," *Electronics Letters,* Vol. 22, No. 16, 1986, pp. 864–865.

[17] Daniel, J. P., et al., "Research on Planar Antennas and Arrays: Structures Rayonnantes," *IEEE Antennas Propagation Magazine,* Vol. AP-35, No. 1, 1993, pp.14–38.

[18] Pozar, D. M., "Microstrip Antenna Aperture Coupled to a Microstrip Line," *Electronics Letters,* Vol. 21, No. 2, 1985, pp. 49–50.

[19] Himdi, M., J. P. Daniel, and C. Terret, "Transmission Line Analysis of Aperture-Coupled Microstrip Antennas," *Electronics Letters,* Vol. 25, 1989, pp. 1229–1230.

[20] El Yazidi, M., M. Himdi, and J. P. Daniel, "Transmission Line Analysis of Nonlinear Slot-Coupled Microstrip Antennas," *Electronics Letters,* Vol. 28, 1992, pp. 1406–1408.

[21] Himdi, M., J. P. Daniel, and C. Terret, "Analysis of an Aperture-Coupled Microstrip Antenna Using Cavity Method," *Electronics Letters,* Vol. 25, No. 6, 1989, pp. 391–392.

[22] Saed, M. A., "Efficient Method for Analysis and Design of Aperture-Coupled Rectangular Microstrip Antenna," *IEEE Trans. Antennas Propagation,* Vol. AP-41, 1993, pp. 986–988.

[23] El Yazidi, M., M. Himdi, and J. P. Daniel, "Aperture-Coupled Microstrip Antenna for Dual Frequency Operation" *Electronics Letters,* Vol. 29, 1993, pp. 1506–1508.

[24] Sullivan, P. L., and D. H. Schaubert, "Analysis of an Aperture-Coupled Microstrip Antenna," *IEEE Trans. Antennas Propagation,* Vol. AP-34, No. 8, 1986, pp. 977–984.

[25] Pozar, D. M., "A Reciprocity Method of Analysis for Printed Slot and Slot-Coupled Microstrip Antennas," *IEEE Trans. Antennas Propagation,* Vol. AP-34, 1986, pp. 1439–1445.

[26] Pozar, D. M., and S. M. Voda, "A Rigorous Analysis of a Microstripline Fed Patch Antenna," *IEEE Trans. Antennas Propagation,* Vol. AP-35, 1987, pp. 1343–1350.

[27] Targonski, S. D., and D. M. Pozar, "Design of Wideband Circularly Polarized Aperture Coupled Microstrip Antennas," *IEEE Trans. Antennas Propagation,* Vol. AP-41, 1993, pp. 214–220.

[28] Ittipibbon, A., et al., "A Modal Expansion Method of Analysis and Measurement on Aperture-Coupled Microstrip Antenna," *IEEE Trans. Antennas Propagation,* Vol. AP-39, 1991, pp. 1567–1574.

[29] Bhattacharya, A. K., Y. M. M. Antar, and A. Ittipiboon, "Spectral Domain Analysis of Aperture-Coupled Microstrip Antennas," *Proc. IEE Antennas Propagation Microwaves,* Pt. H, Vol. 139, 1992, pp. 459–464.

[30] Pozar, D. M., and S. D. Targonski, "Improved Coupling for Aperture Coupled Microstrip Antennas," *Electronics Letters,* Vol. 27, No. 13, June 1991, pp. 1129–1131.

[31] Yang, X. H., and L. Shafai, "Wideband Techniques for the Aperture Coupled Microstrip Antennas," *IEEE AP-S Int. Symp. Digest,* 1993, pp. 952–955.

[32] Hall, R. C., and J. R. Sanford, "Performance Enhancement for Aperture Coupled Microstrip Antenna," *IEEE AP-S Int. Symp. Digest,* Vol. 2, 1992, 1040–1043.

[33] Rathi, V., G. Kumar, and K. P. Ray, "Improved Coupling for Aperture Coupled Microstrip Antennas," *IEEE Trans. Antennas Propagation,* Vol. AP-44, No. 8, 1996, pp. 1196–1198.

[34] Kumar, G., and R. K. Kotapati, "Aperture Coupled Microstrip Antennas," *IETE Technical Review,* Vol. 16, No. 1, 1999, pp. 85–88.

[35] Gronau, G., and I. Wolff, "Aperture Coupling of a Rectangular Microstrip Resonator," *Electronics Letters,* Vol. 22, No. 10, 1986, pp. 554–556.

[36] Zurcher, J. F., "The SSFIP: A Global Concept for High Performance Broadband Planar Antennas," *Electronics Letters,* Vol. 24, No. 23, 1988, pp. 1433–1435.

[37] Zurcher, J. F., and F. E. Gardiol, *Broadband Patch Antennas,* Norwood, MA: Artech House, 1995.

[38] Croq, F., and A. Papiernik, "Large Bandwidth Aperture Coupled Microstrip Antenna," *Electronics Letters,* Vol. 26, No. 16, 1990, pp. 1293–1294.

[39] Luk, K. M., K. F. Tong, and T. M. Au, "Offset Dual-Patch Microstrip Antenna," *Electronics Letters,* Vol. 29, No. 18, 1993, pp. 1635–1636.

[40] Targonski, S. D., R. B. Waterhouse, and D. M. Pozar, "Wideband Aperture Coupled Stacked Patch Antenna Using Thick Substrates," *Electronics Letters,* Vol. 32, No. 21, 1996, pp. 1941–1942.

[41] Targonski, S. D., R. B. Waterhouse, and D. M. Pozar, "Design of Wideband Aperture Stacked Patch Microstrip Antenna," *IEEE Trans. Antennas Propagation,* Vol. AP-46, No. 9, 1998, pp. 1245–1251.

5

Stacked Multiresonator MSAs

5.1 Introduction

Chapters 2–4 described several MSA configurations for broadband operation. The BW of the MSA increases with an increase in substrate thickness and a decrease in the dielectric constant as described in Chapter 2. Also, the BW of the antenna increases when multiresonators are coupled in planar or stacked configurations as described in Chapters 3 and 4, respectively.

This chapter combines the above techniques (i.e., planar multiple resonators are stacked on each other using a thick substrate with a low dielectric constant to realize broadband antennas with a higher gain than the antennas described in the earlier chapters). This chapter describes several configurations, in which multiple patches are taken in the bottom layer and a single patch is taken in the top layer. Alternatively, a single patch is placed in the bottom layer, and multiple patches are taken in the top layer. This is followed by multiple patches in both the bottom and the top layers. A single patch with four stacked patches yields broad BW with a high gain [1, 2].

The bottom patch can be excited either by a microstrip line or a coaxial feed or through electromagnetic or aperture coupling. The method of excitation influences the bottom patch characteristics and does not significantly affect the performance of the stacked patches. Therefore, this chapter discusses only the coaxial-fed patches, but the concept can be extended to other types of feeding techniques.

5.2 Stacked Multiresonator Rectangular Patches on Thick Substrates

The stacking of a multiresonator RMSA is considered in the S-band (2–4 GHz) on a thick substrate with a low dielectric constant to realize broad BW. Initially, a single RMSA, three and five gap-coupled RMSAs, and single-stacked RMSA configurations are described briefly. (They are covered in detail in Chapters 2–4.) This is followed by stacked multiresonator RMSA configurations. For all these cases, the patches in the bottom layer have $\epsilon_r = 1$ and $h = 0.5$ cm.

A coaxial-fed RMSA is shown in Figure 5.1. For $L = 5$ cm, $W = 3$ cm, and $x = 0.9$ cm, the BW for VSWR ≤ 2 is 129 MHz (4.8%) at the center frequency of 2.672 GHz.

A three gap-coupled RMSA configuration is shown in Figure 5.2, in which two rectangular parasitic patches are placed along the radiating edges of central coaxial-fed RMSA. For $L = 5$ cm, $W = 3$ cm, $L_1 = 4$ cm, $s = 0.4$ cm, and $x = 2.4$ cm, the BW is 463 MHz (15.4%) as described in Section 3.3.1.

To increase the BW further, two additional parasitic patches are placed along either side of the nonradiating edges of the centrally fed patch. A five gap-coupled RMSA configuration is shown in Figure 5.3(a). The parasitic

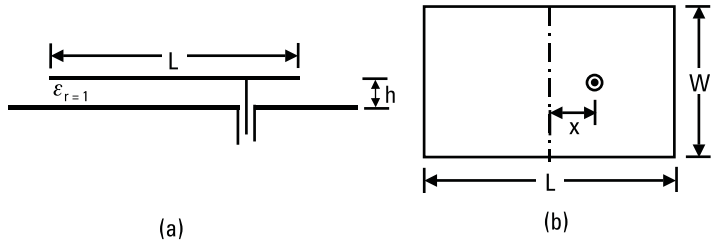

Figure 5.1 RMSA: (a) side and (b) top views.

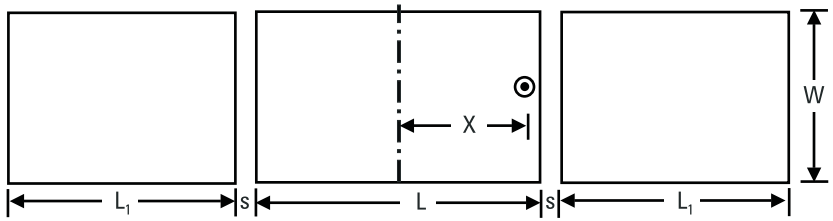

Figure 5.2 Three gap-coupled RMSA with $\epsilon_r = 1$ and $h = 0.5$ cm.

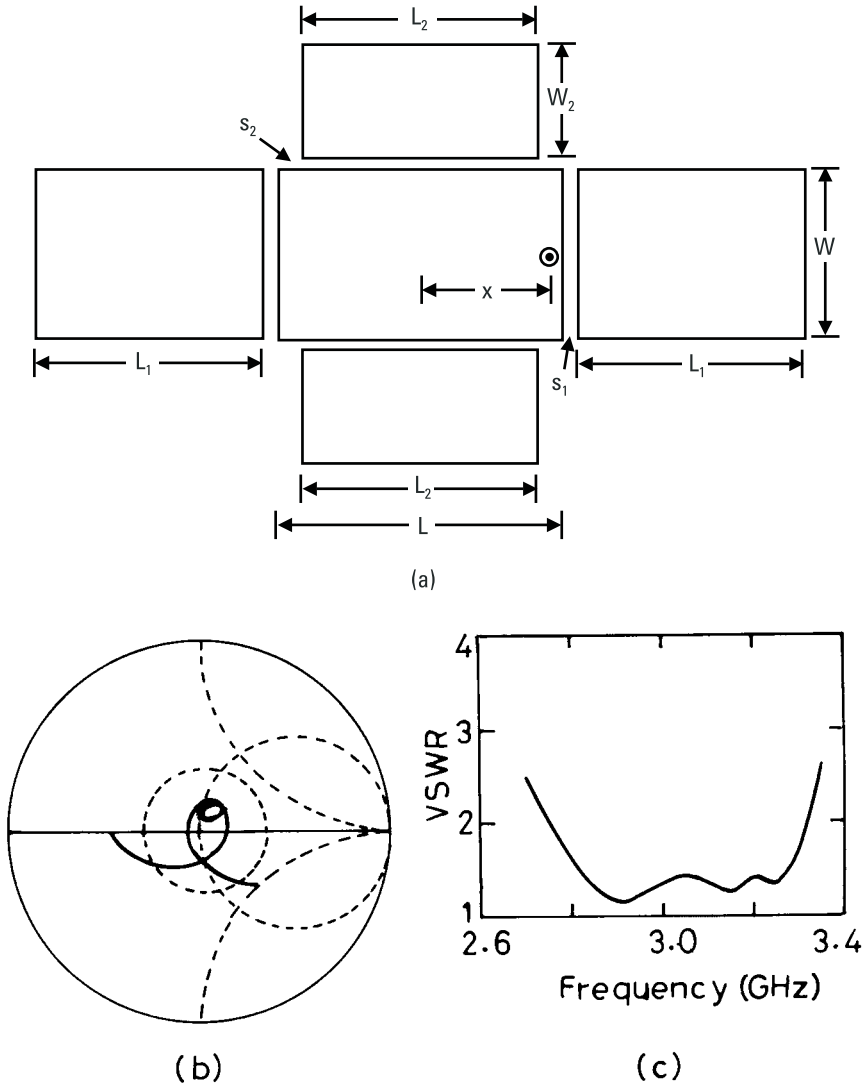

Figure 5.3 (a) Five gap-coupled RMSA and its (b) input impedance and (c) VSWR plots.

patches of length L_2 and width W_2 along the nonradiating edges are chosen to be identical for symmetrical radiation pattern. The gap s_2 between the fed and the parasitic patches along the nonradiating edges is taken smaller than s_1, because the fields vary sinusoidally along the length of the patch. The width W_2 of these parasitic patches is reduced to 2 cm, so that the orthogonal mode does not get excited. Because of the large BW of these

configurations, the width of the patch along the nonradiating edges could become a resonant length at the higher frequency leading to the orthogonal polarization. This problem is not there for the patches placed along the radiating edges, because the central patch is fed along the middle of the width, ensuring that the fundamental mode corresponding to the width of the patch will not get excited.

For L_1 = 3.9 cm, L_2 = 4.2 cm, s_1 = 0.4 cm, s_2 = 0.05 cm, and x = 2.4 cm, the theoretical input impedance and VSWR plots, obtained using IE3D software [3], are shown in Figure 5.3(b, c). Two loops are formed in the impedance plot due to the parasitic elements along the radiating and the nonradiating edges. Both the loops are within the VSWR = 2 circle leading to the broad BW of 574 MHz (18.9%), which is more than the BW of the three gap-coupled RMSA. The radiation pattern of the antenna in the E- and H-planes at three frequencies (2.75, 3.05, and 3.32 GHz) is shown in Figure 5.4. In the H-plane, the pattern remains in the broadside direction at all the frequencies. In the E-plane, on the other hand, the

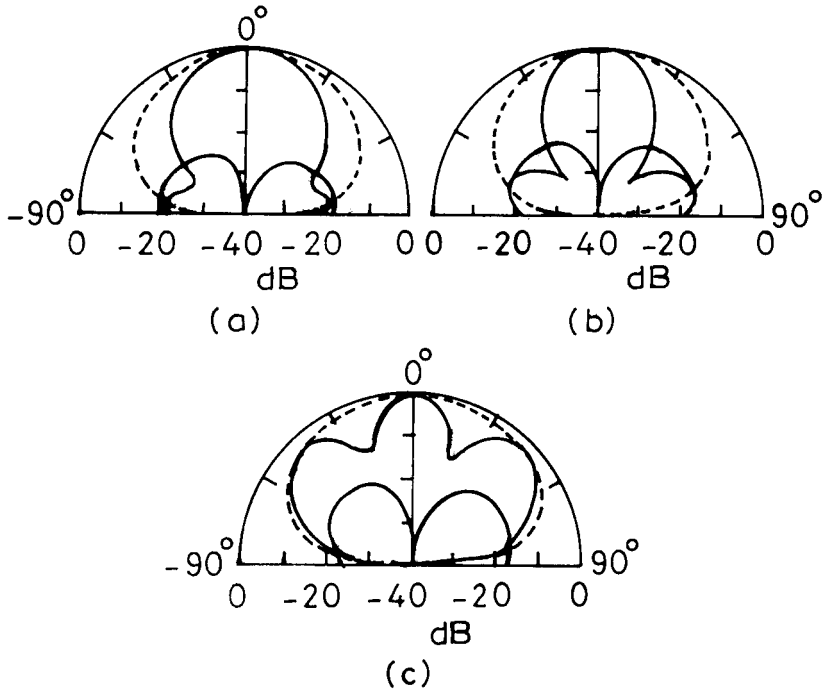

Figure 5.4 Radiation pattern of five gap-coupled RMSA on an air substrate at frequencies (a) 2.75, (b) 3.05, and (c) 3.32 GHz: (——) E-plane and (- - -) H-plane.

radiation pattern is in the broadside direction at the lower two frequencies, but three lobes are formed at the higher frequency. The two sidelobes are within 1 dB of the main lobe. This antenna can be used as a multiple-beam antenna at this frequency. These two sidelobes are due to the excitation of the parasitic patches along the radiating edges, which experience a large phase delay with respect to the fed patch at higher frequency. The variation of gain with frequency is shown in Figure 5.5. At the center frequency of 3.05 GHz, the gain is 12.1 dB. However, at the higher frequency, the gain decreases due to three lobes and has a dip at 3.15 GHz. A flatter gain is obtained when all the parasitic patches have equal length. For $L_1 = L_2 = 3.9$ cm, $s_1 = 0.4$ cm, $s_2 = 0.1$ cm and $x = 2.4$ cm, a single loop is observed in the input impedance plot instead of two loops when $L_1 \neq L_2$. The BW reduces slightly to 548 MHz. The variation of gain with frequency is shown in Figure 5.5. The gain is more than 10 dB in the entire VSWR ≤ 2 BW.

Instead of using multiple resonators in the planar configuration, one patch is stacked on the other patch to increase the BW as described in Chapter 4. Only the bottom patch is fed and the top patch is electromagnetically coupled as shown in Figure 5.6(a). The patch on the bottom layer is shown in dotted lines and the patch on the top layer is shown in solid lines. For the parasitic patch length $L_1 = 4.3$ cm, air gap between the fed patch and the parasitic patch $h_1 = 0.4$ cm, $L = 5$ cm, $W = 3$ cm, $h = 0.5$ cm, and $x = 1.4$ cm, the theoretical input impedance and VSWR plots are shown in

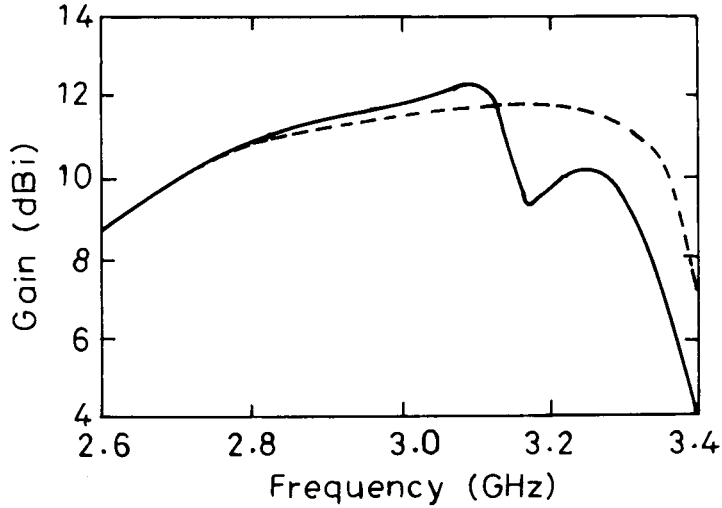

Figure 5.5 Gain variation with frequency of five gap-coupled RMSA: (——) $L_1 = 3.9$ cm, $L_2 = 4.2$ cm and (- - -) $L_1 = L_2 = 3.9$ cm.

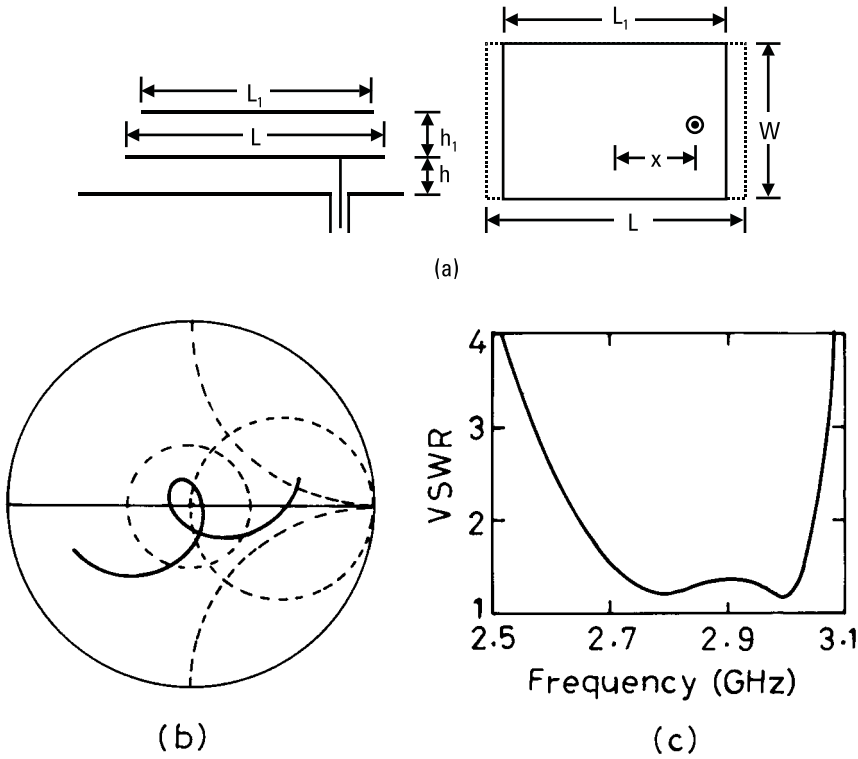

Figure 5.6 (a) Single-stacked RMSA and its (b) input impedance and (c) VSWR plots.

Figure 5.6(b, c). A loop is formed in the impedance plot, which is within the VSWR = 2 circle. The BW of the antenna is 405 MHz (14.2%). The radiation is in the broadside direction, and the variation in the pattern is very small over the entire BW. At 2.85 GHz, the gain is 9.1 dB. The BW of the stacked RMSA is nearly 3.1 times of that of the single RMSA with comparable gain, at the expense of an increase in the antenna thickness from 0.5 cm to 0.9 cm.

In the planar configuration, the total length of the antenna increases but the height of the antenna remains the same as that of the single RMSA. In the stacked configuration, on the other hand, the total length of the antenna remains the same as that of the single patch, while its thickness increases. By combining these two techniques (i.e., by stacking multiple resonators on each other), the overall BW or gain of the antenna increases due to the increase in both the length and thickness of the antenna. Several of these configurations are described in the following sections. For comparing

the performance of all these configurations, the dimensions of the fed RMSA are kept the same as above (i.e., L = 5 cm, W = 3 cm, ϵ_r = 1, h = 0.5 cm, and probe diameter = 0.12 cm) until and unless specified otherwise.

5.2.1 Three Rectangular Patches at the Bottom and One Patch on the Top

Three gap-coupled rectangular patches are placed on the bottom layer, and one rectangular patch is stacked on the centrally fed patch (3B1T RMSA) as shown in Figure 5.7(a) [4]. The various parameters that are to be optimized are the parasitic patch dimensions, the gap between the elements, and the feed-point location. To start with, the optimized dimensions obtained separately for the three gap-coupled planar RMSA and two stacked rectangular patches are taken. For L_1 = 4 cm, s = 0.4 cm, x = 2.4 cm, L_2 = 4.3 cm,

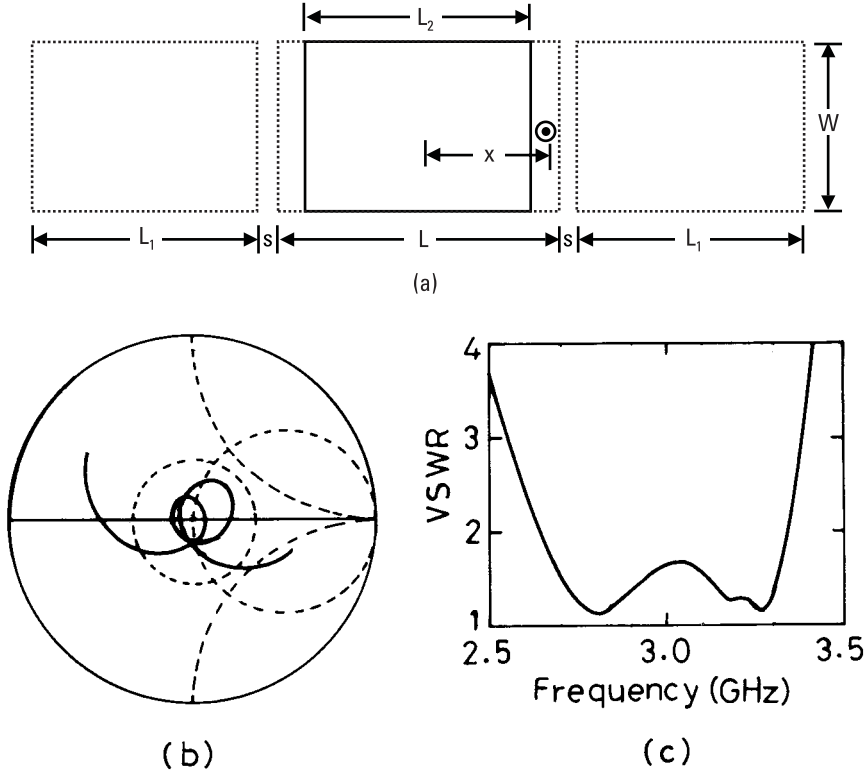

Figure 5.7 (a) Three gap-coupled rectangular patches on the bottom layer with one patch on the top layer and its (b) input impedance and (c) VSWR plots.

and h_1 = 0.4 cm, there are two loops in the impedance plot, which are due to the parasitic patches in the planar and stacked configurations. However, the loops are not inside the VSWR = 2 circle because of the loading effect. Nevertheless, it provides a good starting point. The dimensions of the antenna are optimized to bring both the loops inside the VSWR = 2 circle. For L_1 = 3.9 cm, L_2 = 4.1 cm, h_1 = 0.4 cm, and s = 0.3 cm, the input impedance and VSWR plots are shown in Figure 5.7(b, c). The two loops are inside the VSWR = 2 circle. The loop in the lower frequency region is due to L_2 and the second loop is due to L_1. The BW of the antenna is 704 MHz (23.5%). This BW is much higher than the BW of the single-stacked patch or three gap-coupled planar RMSA.

The variation of gain with frequency is shown in Figure 5.8. The gain is more than 10 dB in the lower frequency range, but it decreases sharply at the higher frequency due to the splitting of the main beam into three lobes.

The radiation characteristics of the antenna are improved when the resonance frequency of the top and the bottom parasitic patches is nearly the same. This will only give a single loop instead of two loops in the impedance plot, which will decrease the overall BW of the antenna. However, the radiation from all the parasitic patches will be around the same frequency, which will enhance the gain within the BW. For L_1 = L_2 = 3.95 cm, s = 0.3 cm and h_1 = 0.4 cm, the input impedance and VSWR plots are

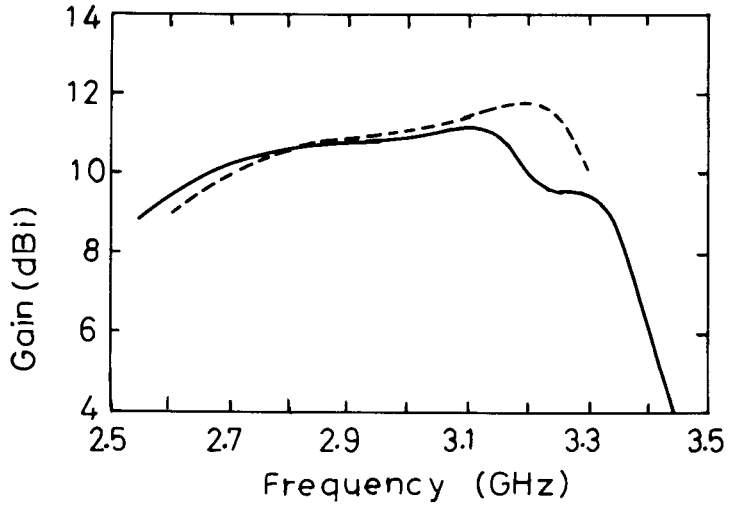

Figure 5.8 Variation of gain with frequency for 3B1T RMSA for two cases: (——) L_1 = 3.9 cm, L_2 = 4.1 cm and (- - -) L_1 = L_2 = 3.95 cm.

shown in Figure 5.9. There is only one loop in the impedance plot, and the BW is decreased to 585 MHz. The variation of gain with frequency for this case is also shown in Figure 5.8. The gain of the antenna does not fall off at the higher frequency within the impedance BW as in the previous case when $L_1 \neq L_2$.

5.2.2 One Rectangular Patch at the Bottom and Three Patches on the Top

Instead of placing three patches on the bottom layer and one on the top layer, the configuration with one rectangular patch on the bottom layer with three gap-coupled patches on the top layer (1B3T RMSA) is shown in Figure 5.10(a) [4]. Only the bottom patch is fed, and the three parasitic gap-coupled patches on the top layer are aligned symmetrically with respect to the radiating edges of the bottom patch for symmetrical radiation pattern. The dimensions of the three top parasitic patches are chosen to be equal, so that their resonance frequencies are the same to yield a relatively flatter gain curve in the upper frequency range within the VSWR BW, as observed in the previous case. For L_1 = 3.6 cm, s = 0.25 cm, and h_1 = 0.4 cm, the input impedance and VSWR plots are shown in Figure 5.10(b, c). Only one loop appears in the impedance plot as the parasitic patches are identical. The BW is 782 MHz (26.1%). In general, the BW of the 1B3T RMSA is greater than that of the 3B1T RMSA, because in this case, all the three parasitic patches are at the higher height from the ground plane. The variation of gain with

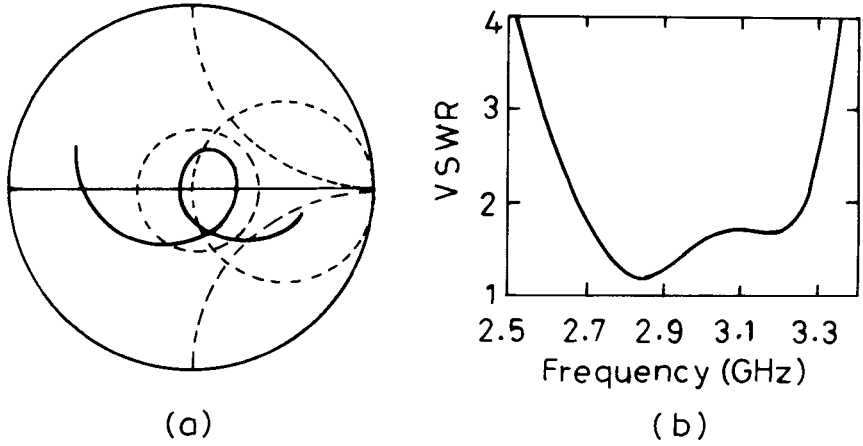

Figure 5.9 (a) Input impedance and (b) VSWR plots of 3B1T RMSA with $L_1 = L_2$ = 3.95 cm.

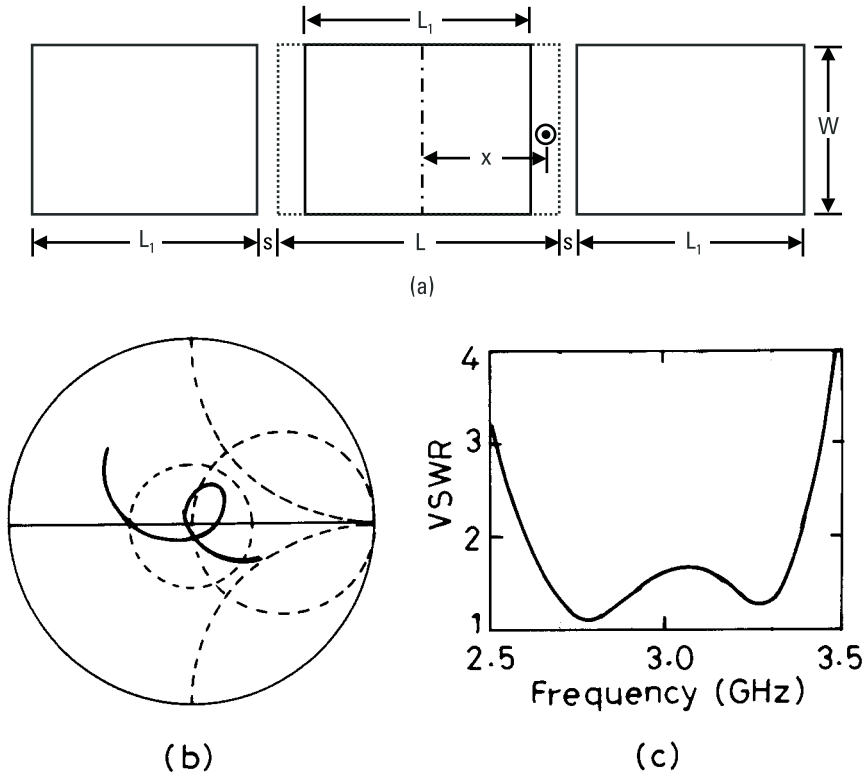

Figure 5.10 (a) One patch on bottom layer and three gap-coupled rectangular patches on the top layer, its (b) input impedance and (c) VSWR plots, and (d) variation of gain with frequency for (——) 1B3T and (- - -) 3B3T RMSAs.

frequency is shown in Figure 5.10(d). The gain remains more than 10 dB over the entire BW. Thus, 1B3T configuration has better performance than that of the 3B1T RMSA.

5.2.3 Three Rectangular Patches at the Bottom and Three Patches on the Top

After studying the BW and gain of 3B1T and 1B3T RMSA configurations, the next natural choice would be to look at the configuration where three patches are placed at the bottom layer and three patches are symmetrically stacked on the top layer as shown in Figure 5.11 [4]. Only the central bottom rectangular patch is fed; all the other rectangular patches are parasitically coupled. All the top patches are centered over the bottom rectangular

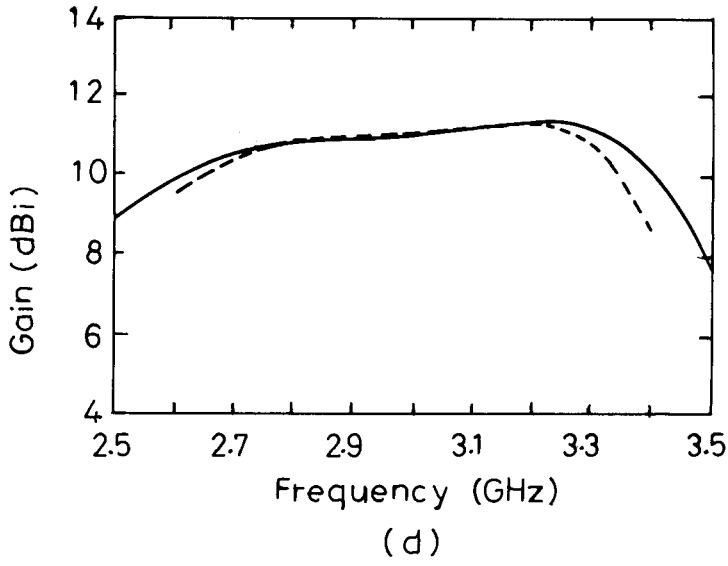

Figure 5.10 (Continued.)

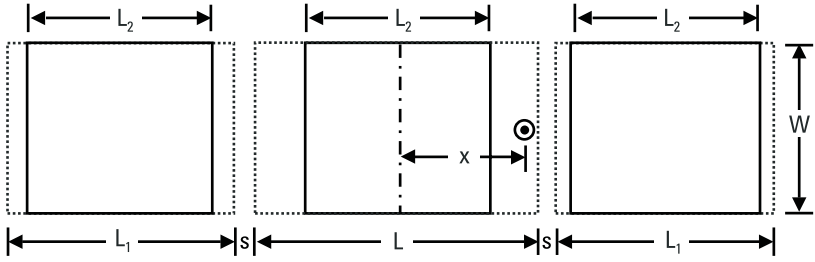

Figure 5.11 Three gap-coupled rectangular patches on the bottom as well as on the top layers.

patches. For L_1 = 3.8 cm, s = 0.3 cm, x = 2.4 cm, L_2 = 3.4 cm, and h_1 = 0.4 cm, the BW is 734 MHz (24.4%). The variation of gain with frequency is shown in Figure 5.10(d). Both the BW and gain are comparable to that of the 1B3T configuration, and there is no significant improvement in performance using the 3B3T configuration, because the additional elements are not properly coupled.

5.2.4 One Rectangular Patch at the Bottom and Five Patches on the Top

It has been observed that a five gap-coupled RMSA yields better BW and gain than that of the three gap-coupled RMSA. Also, a 1B3T configuration

gives better performance than that of the 3B1T configuration. Therefore, the results for only one fed patch at the bottom layer and five rectangular patches at the top layer (1B5T RMSA), shown in Figure 5.12(a) are given. The length L_1 of all the parasitic patches is taken as equal to 3.6 cm and the width W_1 of the parasitic patches along the nonradiating edge is taken

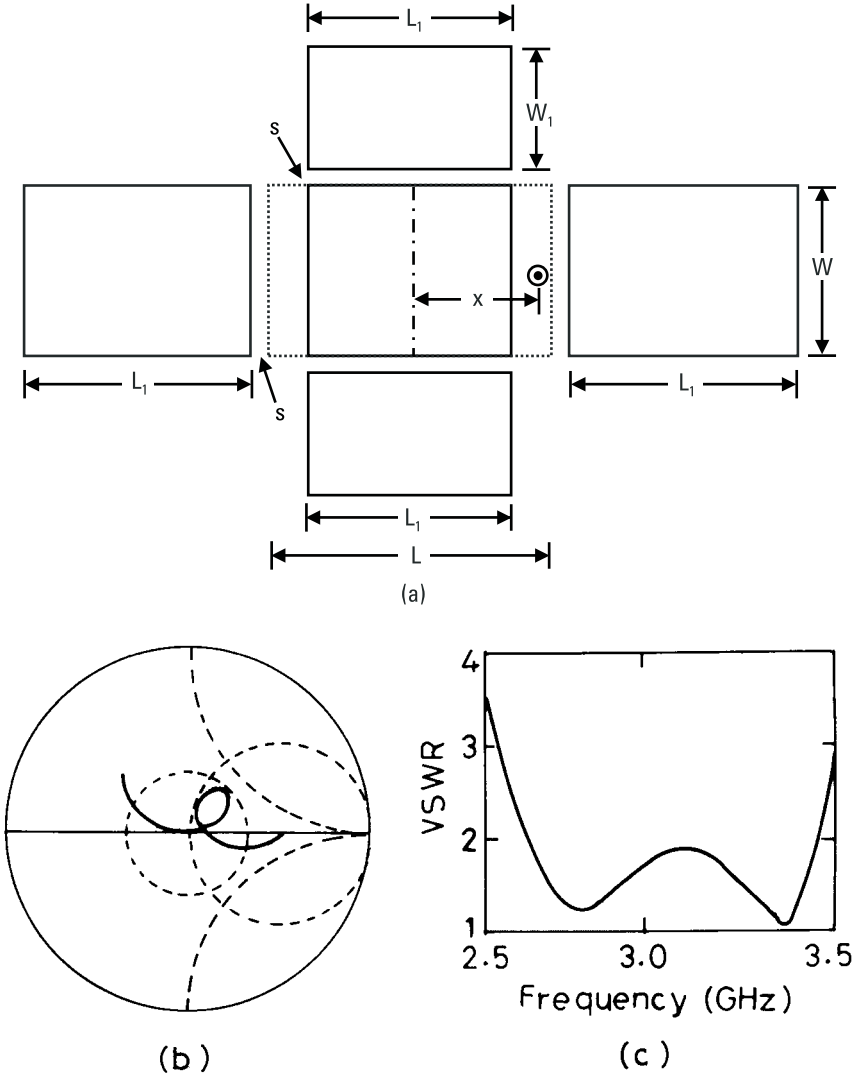

Figure 5.12 (a) One rectangular patch on the bottom layer and five gap-coupled patches on the top layer and its (b) input impedance and (c) VSWR plots.

to be equal to 2 cm. For s = 0.1 cm, h_1 = 0.4 cm, and x = 2.4 cm, the input impedance and VSWR plots are shown in Figure 5.12(b, c). There is only one loop in the impedance plot, because the length of all the parasitic patches is same. The BW of the antenna is 920 MHz (30.7%). The 1B5T RMSA has a much wider BW with a flatter gain response as compared to that of the five gap-coupled RMSA at the expense of an increase in the overall height of the antenna.

The BW and gain comparison of all the above configurations are given in Table 5.1. The gain is given at a single frequency, which is close to the center frequency. The stacked multiresonator RMSA configurations have a better performance than that of the planar multiresonator or single-stacked RMSA. For example, the BWs of three gap-coupled and 1B1T RMSA configurations are 463 MHz and 405 MHz, respectively, whereas a much larger BW of 782 MHz is obtained for 1B3T RMSA, which is a combination of these two configurations. Also, the gain of 1B3T RMSA is much flatter over the entire VSWR BW as compared to the other two configurations. Out of all these configurations, 1B5T RMSA yields a maximum BW of 920 MHz with a flatter gain response.

5.2.5 One Rectangular Patch at the Bottom and Two Patches on the Top

In all the three and five gap-coupled stacked configurations (1B3T, 3B1T, 3B3T, and 1B5T), the overall length of the antenna is very large, and in some cases, the radiation pattern varies over the BW, which makes them unsuitable for many applications. These can be taken care of by using two identical patches on the top layer with one fed patch on the bottom layer.

Table 5.1
Comparison of Various Planar and Stacked RMSA Configurations

Configurations	BW (MHz)	Approx. f_0 (GHz)	Gain (dB)
Single-patch	129	2.66	9.1
Three gap-coupled	463	3.00	11.3
Five gap-coupled	574	3.05	12.1
One bottom/one top	405	2.85	9.1
Three bottom/one top	704	3.00	11.1
One bottom/three top	782	3.00	10.9
Three bottom/three top	734	3.00	11.3
One bottom/five top	920	3.00	11.7

Two coupled patches on the bottom layer with one patch stacked on the top layer is not considered, because the radiation pattern shifts away from the broadside direction as the frequency increases within the VSWR BW for the two gap-coupled RMSA as described in Section 3.3. As a result, the stacking of rectangular patches on the two gap-coupled patches in the bottom layer will not yield optimum results.

A single-fed RMSA on the bottom layer with two patches symmetrically placed on the top layer is shown in Figure 5.13(a). The two patches on the top layer are chosen to be identical for a symmetrical radiation pattern. For the given bottom patch dimensions, the broad BW of the antenna is obtained for a different height h_1 of the top layer by optimizing the length L_1 of the parasitic patch and the center-to-center spacing (2 *ox*) between them. For

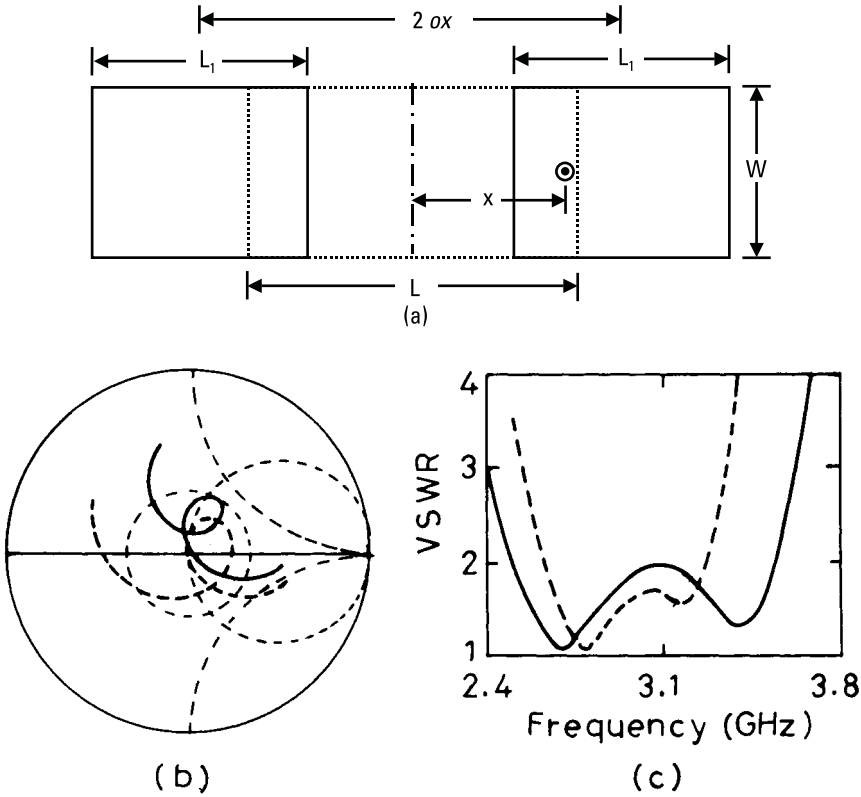

Figure 5.13 (a) One rectangular patch on the bottom layer and two patches on the top layer and the (b) input impedance and (c) VSWR plots for two values of h_2: (- - -) 0.4 cm and (——) 0.9 cm.

L = 5.0 cm, W = 3.0 cm, h = 0.5, cm, x = 2.4 cm, and various values of h_1, the optimized dimensions of L_1 and *ox*, along with BW and a gain at 3.0 GHz are given in Table 5.2. With an increase in h_1, the effective length of the top patch increases due to an increase in the fringing fields; hence the length L_1 of the top patch is reduced so that the loop in the impedance plot is within VSWR = 2 circle. Also, with an increase in h_1, the coupling between the bottom and the top patch decreases. The coupling is increased by changing the value of *ox* (center-to-center horizontal spacing between the lower and upper patches in the x-direction), and maximum coupling is obtained when *ox* is approximately equal to $L/2$. This is because the edges of the fed patches act as magnetic currents, giving maximum coupling to the top patches when its edges coincide with the maximum magnetic field region (i.e., the center) of the top patches.

As h_1 increases from 0.4 cm to 1.1 cm, the length L_1 is to be decreased from 3.8 cm to 3.2 cm, so that the loop is within the VSWR = 2 circle and the value of *ox* is decreased from 4.7 cm to 2.5 cm to increase the coupling. The center frequency of the antenna remains at around 3.0 GHz. For two values of h_1 (0.4 cm and 0.9 cm), the input impedance and VSWR plots are shown in Figure 5.13(b, c). As h_1 is increased from 0.4 cm to 0.9 cm, the BW of the antenna increases from 650 MHz to 1,043 MHz, because the total height of the antenna increases. When h_1 is increased further, the BW decreases slightly because the loop size decreases due to the decrease in the coupling, which cannot be increased, as the offset ox has been optimized for maximum coupling.

The radiation pattern in the E- and H-planes of the 1B2T RMSA for h_1 = 0.9 cm at 2.5 GHz and 3.5 GHz (near the two band-edge frequencies)

Table 5.2
Variation of BW and Gain of 1B2T RMSA with h_1
(L = 5 cm, W = 3 cm, x = 2.4 cm, and h = 0.5 cm)

h_1 (cm)	L_1 (cm)	*ox* (cm)	BW (MHz)	Gain (dB)
0.4	3.8	4.7	650	11.3
0.5	3.7	4.5	789	11.3
0.6	3.6	4.4	819	11.2
0.7	3.6	4.3	847	11.1
0.8	3.4	4.0	958	10.9
0.9	3.4	3.7	1,043	10.8
1.0	3.4	3.4	1,011	10.7
1.1	3.2	2.5	997	10.0

are shown in Figure 5.14. The radiation is in the broadside direction at both the frequencies, but two sidelobes appear at the higher frequency due to the phase delay experienced by the top parasitic patches. However, the gain remains above 10 dB in the entire BW.

In the above 1B2T configuration, the bottom and top metallic patches are suspended in air. Instead, these patches are fabricated on a low-cost glass-epoxy substrate (ϵ_r = 4.3, h = 0.159 cm, and tan δ = 0.02), and then used in a suspended microstrip configuration as shown in Figure 5.15(a). For L = 5.8 cm, W = 3.6 cm, d = 0.2 cm, x = 2.8 cm, Δ = 0.4 cm, L_1 = 3.8

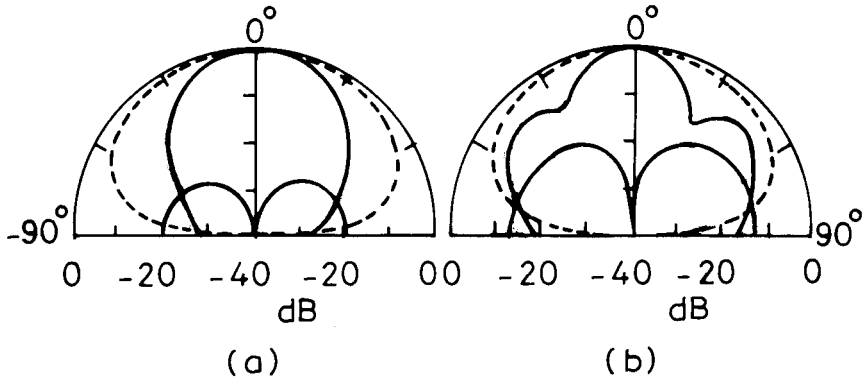

Figure 5.14 Radiation pattern of 1B2T RMSA with h_1 = 0.9 cm at frequencies (a) 2.5 and (b) 3.5 GHz: (——) E-plane and (- - -) H-plane.

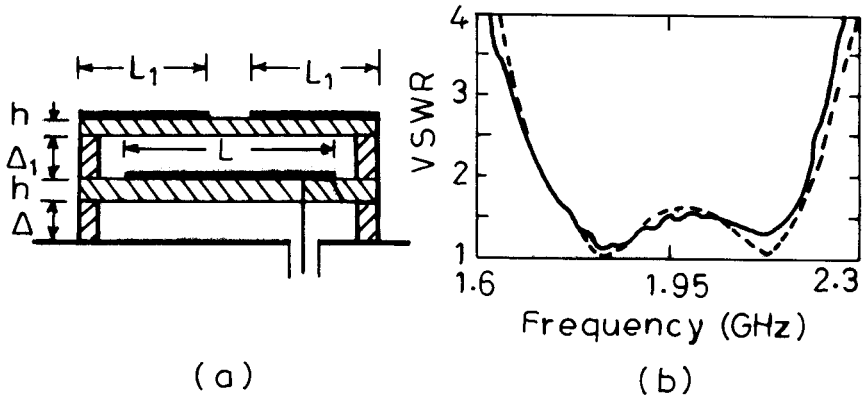

Figure 5.15 (a) One rectangular patch on the bottom layer and two patches on the top layer fabricated on a glass-epoxy substrate with an air gap between them and (b) its VSWR plot: (——) measured and (- - -) theoretical.

cm, W_1 = 3.6 cm, 2 *ox* = 5.0 cm and Δ_1 = 1.1 cm, the theoretical and measured VSWR plots are shown in Figure 5.15(b). The measured and theoretical BWs are 673 MHz and 697 MHz, respectively. The theoretical gain of the antenna remains flat at approximately 9 dB with a less than 1-dB drop at the extreme band-edge frequencies.

5.2.6 One Rectangular Patch at the Bottom and Four Patches on the Top

Instead of two rectangular patches on the top layer, four patches on the top layer are considered as shown in Figure 5.16. Two patches of the top layer of the 1B2T RMSA are displaced from the feed axis along the width of the fed patch, and another two patches are placed symmetrically with respect to the feed axis. All the top four patches are chosen to be identical for a symmetrical radiation pattern. Also, the width W_1 of the top patches is reduced as compared to the bottom patch. Because the top patches are getting fed along the diagonal from the bottom patch, and if W_1 is comparable to L_1 then the orthogonal mode of the top patch will also get excited. As in the case of two top patches, this configuration can be optimized for a broad BW for different height h_1. However, the number of parameters that are to be optimized is increased; these are length L_1 and width W_1 of the top patches and offsets along the *x*- and *y*-axes (*ox* and *oy*). The effects of L_1 and the offset along the *x*-axis on the performance of the antenna are the same as in the case of the 1B2T RMSA. The coupling decreases with an increase in the offset along the *y*-axis, which reduces the size of the loop in the impedance plot. With a decrease in W_1, the radiation resistance of

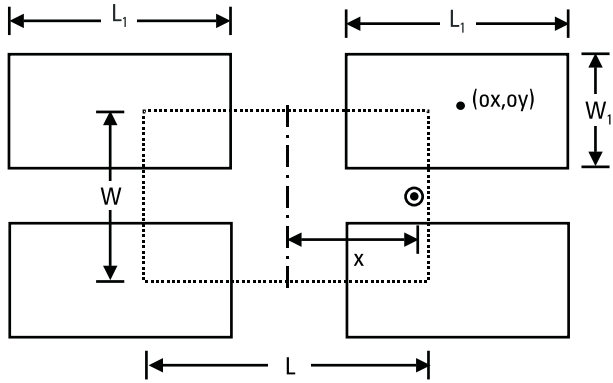

Figure 5.16 One rectangular patch on the bottom layer and four patches on the top layer.

the top patch increases, and hence the input impedance plot shifts to the right side on the Smith chart.

The BW and gain of the antenna for various values of h_1 (0.4 cm to 0.8 cm) are shown in Table 5.3. The optimized values of L_1 and offsets *ox* and *oy* are also given in Table 5.3. With an increase in the value of h_1 from 0.4 cm to 0.8 cm, the length L_1 is decreased from 3.9 cm to 3.6 cm to bring the loop inside the VSWR = 2 circle. As h_1 increases, the BW of the antenna increases from 816 MHz to 1,070 MHz, but the gain near the center frequency decreases from 12.7 dB to 11.5 dB, due to a decrease in the values of offsets *ox* and *oy*, which reduces the overall size of the antenna. The radiation pattern in the E- and H-planes of 1B4T RMSA for h_1 = 0.7 cm at 2.5 GHz and 3.4 GHz is shown in Figure 5.17. The radiation is in the broadside direction in both the planes. With an increase in frequency, the HPBW decreases and the cross-polar level increases in the E-plane.

Table 5.3
Variation of BW and Gain of the 1B4T RMSA with h_1
(L = 5 cm, W = 3 cm, W_1 = 2 cm, x = 2.4 cm, and h = 0.5 cm)

h_1 (cm)	L_1 (cm)	*ox*, *oy* (cm)	f_0 (GHz)	BW (MHz)	Gain (dB)
0.4	3.9	3.8, 2.3	2.938	816	12.7
0.5	3.9	3.7, 2.2	2.915	868	12.2
0.6	3.8	3.6, 2.1	2.930	910	12.3
0.7	3.7	3.5, 2.0	2.955	933	12.0
0.8	3.6	3.2, 1.7	2.958	1,070	11.5

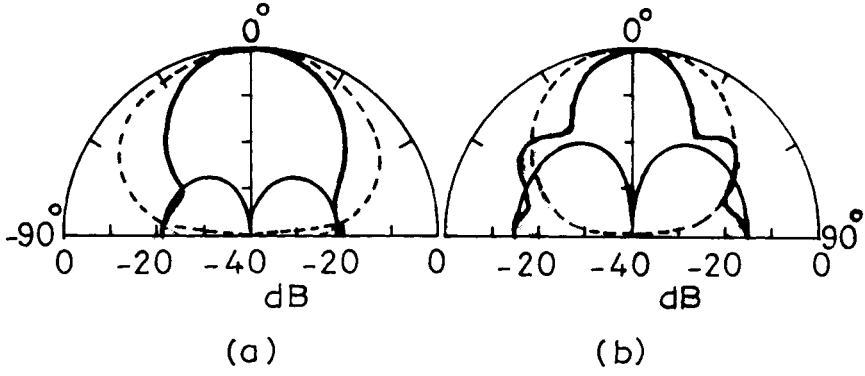

Figure 5.17 Radiation pattern of the 1B4T RMSA with h_1 = 0.7 cm at frequencies (a) 2.5 GHz and (b) 3.4 GHz: (——) E-plane and (- - -) H-plane.

5.3 Effect of Probe Diameter on Multiresonator Stacked RMSAs

It is observed that for h_1 = 0.7 cm for the 1B4T RMSA, the loop is formed in the inductive region in the Smith chart. For all the above cases, h = 0.5 cm and the diameter of the center conductor of the coaxial probe (SMA connector) is taken as 0.12 cm, which adds a large inductance to the input impedance. By increasing the diameter of the probe, the loop in the impedance plot can be shifted down. Therefore, instead of using an SMA connector, a BNC/TNC (probe diameter = 0.2 cm) or an N-type connector (probe diameter = 0.4 cm) could be used. With an increase in the probe diameter, its inductance decreases, and hence the loop in the impedance plot shifts down toward the center. This provides an opportunity to increase the loop size for a larger BW. As a result, the coupling is increased by reducing *ox* and *oy*, which increases the loop size. For three different values of probe diameter (0.12, 0.2, and 0.4 cm), the coupling is optimized such that the loop remains within the VSWR = 2 circle, and the broad BW obtained is shown in Table 5.4. With an increase in the probe diameter from 0.12 cm to 0.4 cm, the BW increases from 933 MHz to 1,341 MHz without affecting the radiation pattern and gain of the antenna.

Similarly, the BW can be increased for some of the other stacked RMSA configurations discussed earlier when the loop size is small and is in the inductive region. In these cases, the coupling has to be increased to increase the size of the loop to obtain wider BW.

5.4 One Rectangular Patch at the Bottom and Four Patches on the Top on a Thin Dielectric Substrate

In the above cases, the bottom and top metallic patches are suspended in air to optimize the BW and gain of the antennas. The BW of the antenna

Table 5.4
Effect of Diameter of the Feed Probe on the BW of 1B4T RMSA

Probe Diameter (cm)	*ox*, *oy* (cm)	BW (MHz)
0.12	3.5, 2.0	933
0.2	3.3, 1.8	1,119
0.4	2.5, 1.2	1,341

can also be increased by using a thin dielectric substrate for the patch on the bottom layer, and the patches on the top layer are used in a suspended microstrip configuration as shown in Figure 5.18(a). The substrate parameters are $\epsilon_r = 2.55$, $h = 0.159$ cm, and $\tan \delta = 0.001$. The top patches are chosen to be identical with their width smaller than the length to avoid the excitation of higher order modes. For bottom patch dimensions $L = 2.2$ cm and $W = 1.6$ cm with the feed point at $x = 1.04$ cm, the top patch length L_1 and the offsets *ox* and *oy* are optimized for different values of air gap Δ between the two patches by keeping the top patch width $W_1 = 1.0$ cm. The variation of BW and gain with Δ are given in Table 5.5. The input impedance and VSWR plots for two values of Δ (0 and 0.3 cm) are shown in Figure 5.18(b, c). For $\Delta = 0$, the BW of the antenna is 788 MHz (20.0%), which is on the same order as in [1, 2]. As Δ increases, the coupling decreases, which is increased by reducing the offsets *ox* and *oy*. With an increase in Δ from 0 to 0.3 cm, the BW of the antenna increases to 1,188 MHz due to the increase in the overall height of the antenna and a decrease in the effective dielectric constant of the top patches. However, for $\Delta = 0.3$ cm, the gain decreases slightly due to a decrease in the offsets along the *ox* and *oy* axes, which reduces the overall size of the radiating aperture.

The low-cost version of the 1B4T configuration can be realized by fabricating the patches on a low-cost glass-epoxy substrate ($\epsilon_r = 4.3$, $h = 0.159$ cm and $\tan \delta = 0.02$), and then using them in a suspended microstrip configuration as shown for 1B2T in Figure 5.15(a).

For $L = 5.8$ cm, $W = 3.6$ cm, $d = 0.2$ cm, $x = 2.8$ cm, $\Delta = 0.4$ cm, $L_1 = 3.7$ cm, $W_1 = 2.5$ cm, *ox* = 2.15 cm, *oy* = 1.55 cm and $\Delta_1 = 1.1$ cm, the theoretical and measured VSWR plots are shown in Figure 5.19. The measured and theoretical BWs are 684 MHz and 657 MHz, respectively. The theoretical gain of the antenna remains flat at approximately 9 dB with a less than 1-dB drop at the extreme band-edge frequencies.

5.5 Stacked Multiresonator CMSAs

Instead of rectangular patches in the multiresonator stacked configurations, circular patches may also be used to obtain a wide BW with higher gain. All the parasitic patches are chosen to be identical to yield a symmetrical radiation pattern with a flatter gain as described earlier for rectangular patches. The dimensions of the fed CMSA (diameter = $2a = 6.2$ cm) and its substrate parameters ($\epsilon_r = 1$ and $h = 0.4$ cm) are kept constant for all the configurations for comparison purposes. For a single CMSA with the coaxial feed at

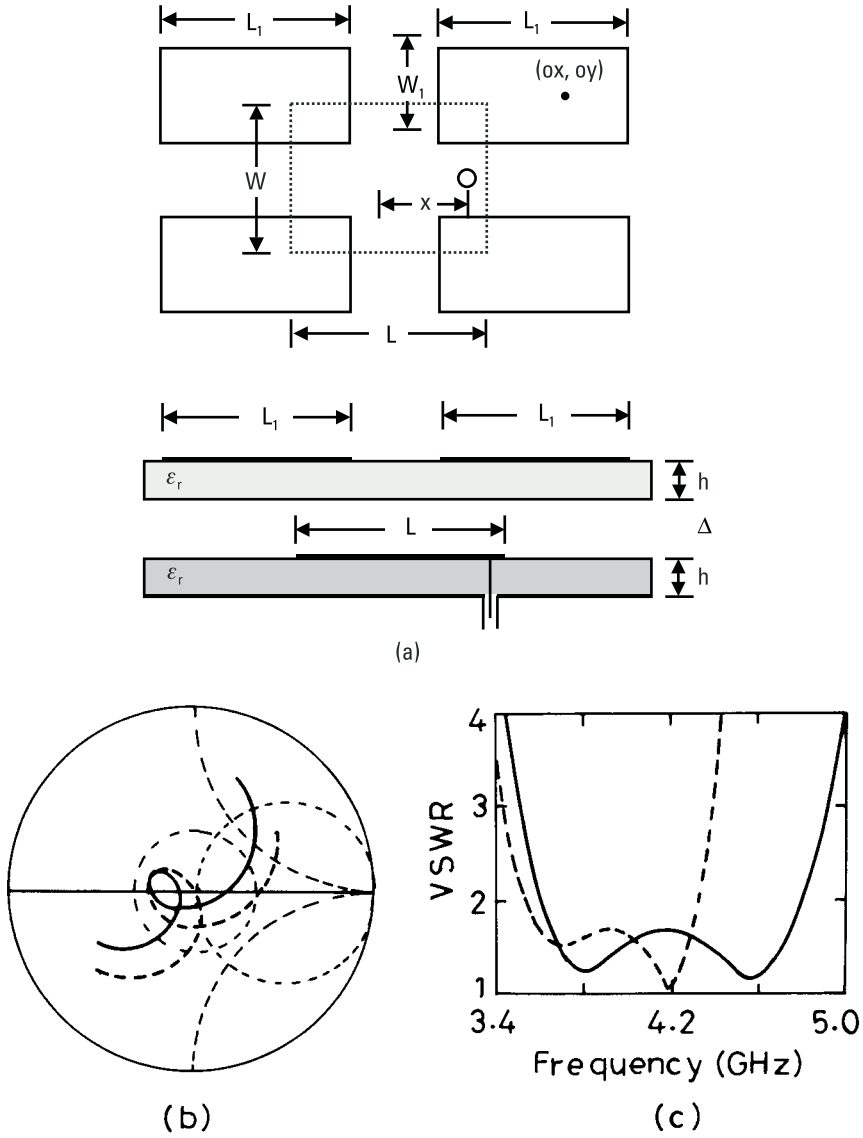

Figure 5.18 (a) One rectangular patch on the bottom layer and four patches on the top layer on a thin dielectric substrate with air gap Δ between them and its (b) input impedance and (c) VSWR plots for two values of Δ: (- - -) 0 and (——) 0.3 cm.

Table 5.5
Variation of BW and Gain with Δ for 1B4T RMSA on a Thin Substrate
(L = 2.2 cm, W = 1.6 cm, W_1 = 1.0 cm, x = 1.04 cm, ϵ_r = 2.55, and h = 0.159 cm)

Δ (cm)	L_1 (cm)	*ox*, *oy* (cm)	f_0 (GHz)	BW (MHz)	Gain (dB)
0.0	2.0	1.6, 1.2	3.935	788	9.4
0.1	2.2	1.2, 1.2	4.078	858	9.4
0.2	2.1	1.0, 1.0	4.205	1,025	9.5
0.3	2.0	0.6, 0.6	4.208	1,188	9.1

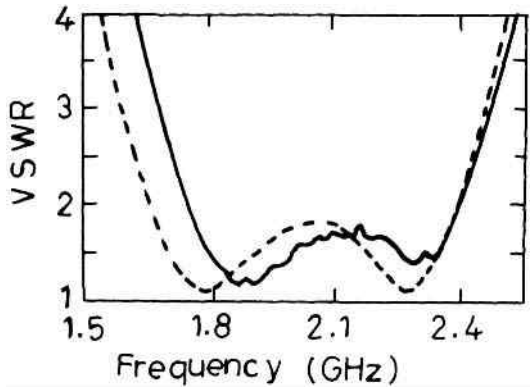

Figure 5.19 VSWR plots of one rectangular patch on the bottom layer and four patches on the top layer in a suspended microstrip configuration: (——) measured and (- - -) theoretical.

x = 1.4 cm, as shown in Figure 5.20(a), a BW of 136 MHz is obtained at f_0 = 2.601 GHz. To increase the BW, three and five gap-coupled CMSA configurations are used as shown in Figure 5.20(b, c). In Figure 5.20(b), two parasitic patches are placed along the feed axis, whereas in Figure 5.20(c), four parasitic patches are placed at ±45° from the feed axis in the four quadrants. In all these configurations, the gap between the fed and the parasitic circular patches is smaller than that of the corresponding RMSA configurations, because the coupling between the patches is less due to its curved surfaces. The diameters of all the parasitic patches are equal to 5.4 cm, and the gap between the fed and the parasitic patches is 0.1 cm. For three and five gap-coupled CMSAs, the theoretical BWs are 441 MHz (16.3%) and 454 MHz (16.8%).

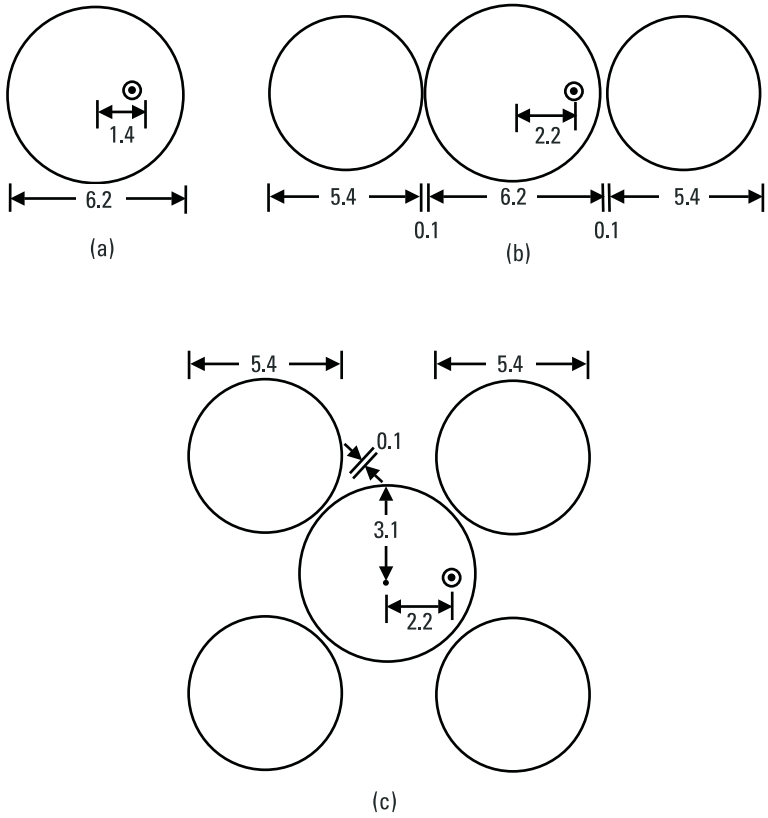

Figure 5.20 (a) Single, (b) three gap-coupled, and (c) five gap-coupled CMSAs.

Various configurations with a single coaxial-fed circular patch on the bottom layer with one, three, and five circular patches on the top layer are shown in Figure 5.21. The bottom patches are represented by dotted lines, and the top patches are represented by solid lines. All the dimensions shown in Figure 5.21 are in centimeters. A single-stacked CMSA (1B1T CMSA) with a top patch radius = 2.4 cm and spacing between the two patches h_1 = 0.4 cm yields a BW of 366 MHz (13.1%).

For three circular patches on the top (1B3T CMSA) as shown in Figure 5.21(b), the VSWR and gain plots are shown in Figure 5.22. For comparison, the VSWR and gain plots of their planar counterparts (i.e., three gap-coupled CMSA) are also shown in Figure 5.22. Similarly, the VSWR and gain plots of the 1B5T and five gap-coupled CMSA are shown in Figure 5.23. The BWs of the 1B3T and 1B5T CMSA configurations are 634 MHz (23.1%)

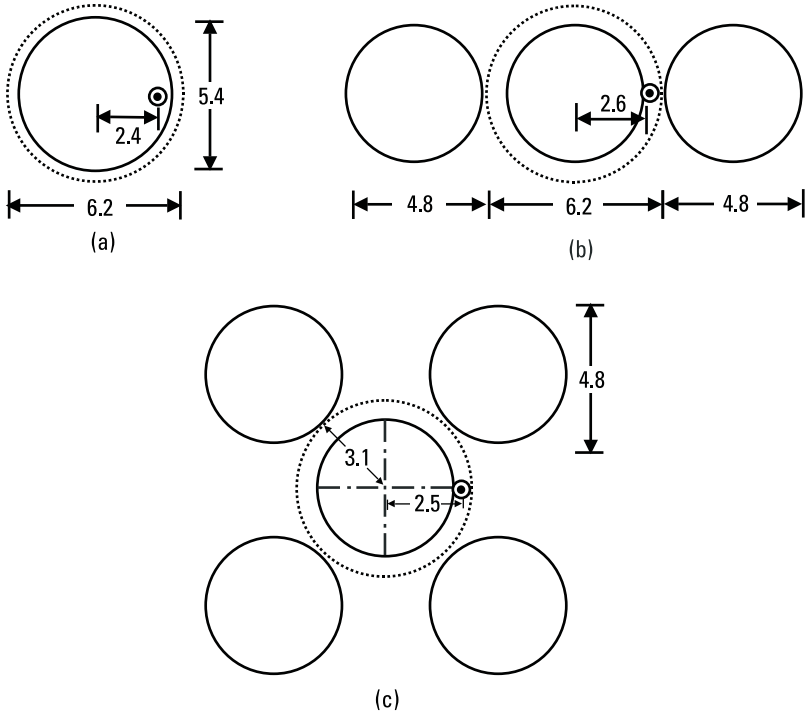

Figure 5.21 One circular patch on the bottom layer and (a) one, (b) three, and (c) five parasitic circular patches on the top layer.

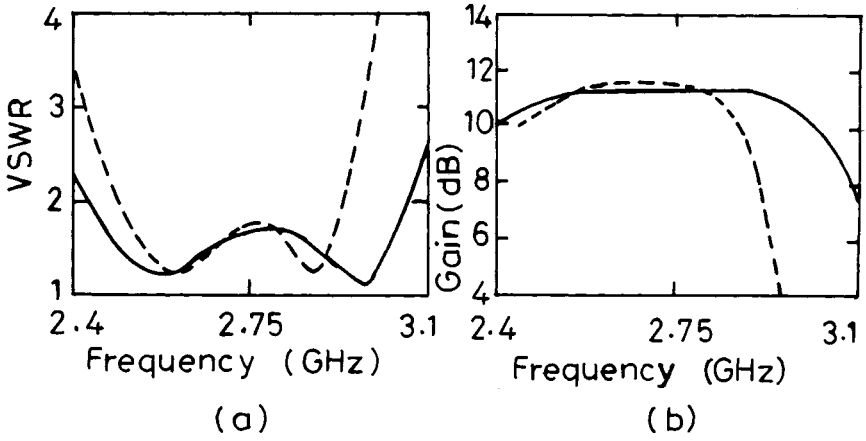

Figure 5.22 (a) VSWR and (b) gain plots of (——) 1B3T and (- - -) three gap-coupled CMSA.

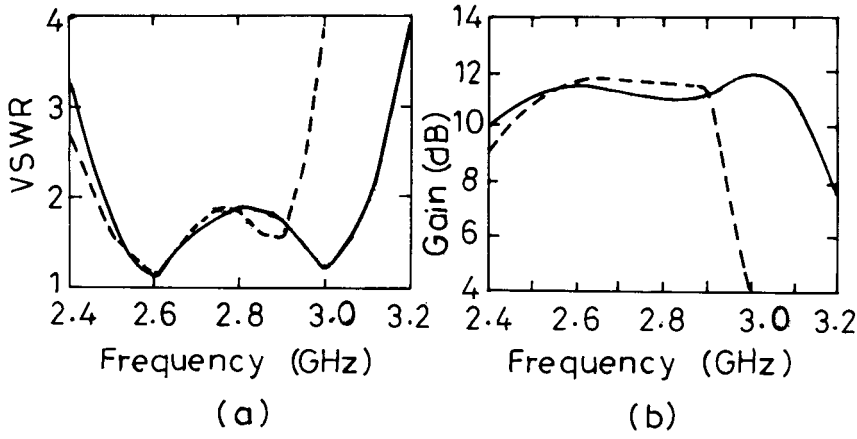

Figure 5.23 (a) VSWR and (b) gain plots of (——) 1B5T and (- - -) five gap-coupled CMSA.

and 657 MHz (23.6%). The gain of 1B5T is slightly larger than the gain of 1B3T because of the larger aperture area. It can be noted from these comparisons that the stacked multiresonator configurations give a much larger BW as compared to their planar counterparts with comparable gain within their respective BWs.

The 1B2T and 1B4T CMSA configurations with dimensions in centimeters are shown in Figure 5.24. The probe diameter d is taken as 0.4 cm, as it gives a smaller inductance as compared to $d = 0.12$ cm. The dimensions of the 1B2T and 1B4T CMSA configuration are optimized with $h_1 = 1.2$ and 1.0 cm, respectively, for broad BW. The comparisons of VSWR and gain variation with frequency are given in Figure 5.25. The 1B2T and 1B4T CMSA configurations yield a very large BW of 1,010 MHz and 1,209 MHz, respectively. The gain of 1B2T remains more than 10 dB over the BW, whereas for 1B4T, the gain is around 11 dB in the lower frequency range due to a larger aperture area. However, it decreases sharply in the higher frequency range because of the splitting of the main lobe into multiple beams.

For all these stacked CMSA configurations, the BW and gain are compared in Table 5.6. The 1B4T CMSA has a maximum BW of 1,209 MHz, and 1B5T CMSA has a maximum gain of 11.8 dB around the center frequency.

A low-cost realization of 1B4T CMSA is shown in Figure 5.26(a). Both the bottom and top layer patches are fabricated on a glass-epoxy substrate ($\epsilon_r = 4.3$, $h = 0.159$ cm, and $\tan \delta = 0.02$). The top patches are

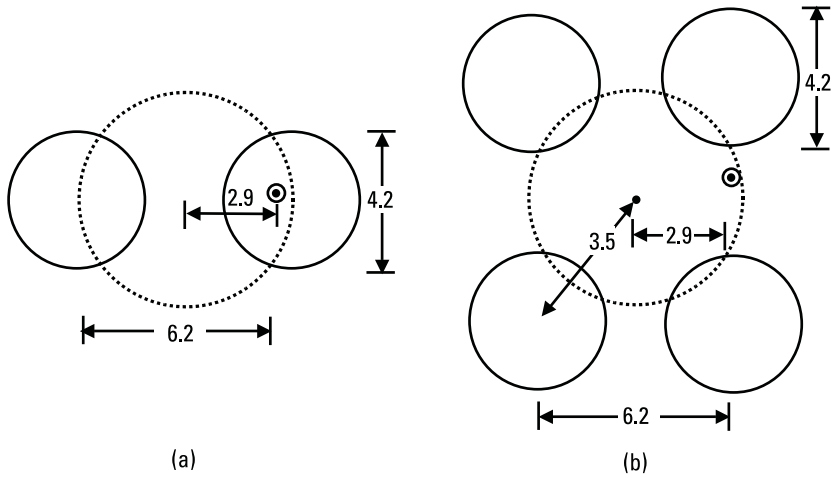

Figure 5.24 One circular patch on the bottom layer and (a) two and (b) four parasitic circular patches on the top layer.

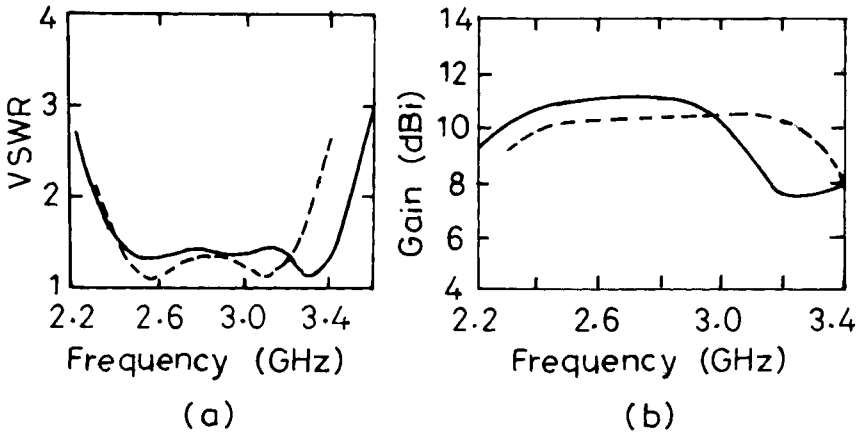

Figure 5.25 (a) VSWR and (b) gain plots of (- - -) 1B2T and (——) 1B4T CMSA configurations.

used in a suspended configuration, with an air gap of 0.6 cm between the two dielectric layers [5]. The dimensions of the patches are shown in Figure 5.26. The theoretical and measured input impedance and VSWR plots are shown in Figure 5.26(b, c). The measured BW for VSWR ≤ 2 is 280 MHz (15.2%). The theoretical results are in agreement with the measured results. The size of the loop is small, and it is formed in the lower impedance region

Table 5.6
Comparison of Various CMSA Configurations
(a = 3.1 cm, ϵ_r = 1 and h = 0.4 cm)

Configurations	BW (MHz)	Gain Around the Center Frequency	
		f_0 (GHz)	Gain (dB)
Single patch	136	2.60	9.7
Three gap-coupled	441	2.70	11.8
Five gap-coupled	454	2.70	11.8
One bottom/one top	366	2.80	9.9
One bottom/three top	634	2.80	11.6
One bottom/five top	657	2.80	11.4
One bottom/two top	1,010	2.80	10.5
One bottom/four top	1,209	2.90	11.1

because of the lossy substrate. If the air gap is reduced, then the loop size will increase and will go outside the VSWR = 2 circle.

Similarly, a 1B5T CMSA fabricated on a glass-epoxy substrate with an air gap of 0.35 cm between the two dielectric layers is shown in Figure 5.27(a). The measured input impedance and VSWR plots shown in Figure 5.27(b, c) are in agreement with the theoretical results obtained using IE3D. The loop size is bigger than the previous case, because of the smaller air gap between the two layers. The measured BW for VSWR $\leq$ 2 is 367 MHz (17.1%).

A log-periodic MSA array could be realized in a multilayered configuration and can therefore be categorized as multilayered multiresonator configuration as described below.

5.6 Log-Periodic MSA Arrays

The principle of the log-periodic antenna has been applied to the MSA array to obtain multi-octave BW [6, 7]. It requires scaling of all the dimensions of the array in a log-periodic manner. This is illustrated for electromagnetically coupled MSA array in Figure 5.28(a). The multiple rectangular patches are placed on the top layer, where they are fed by a tapered microstrip line on the bottom layer. The substrate thickness h, patch length L, patch width W, width of the microstrip line w, and spacing d between the mth and $(m + 1)$th elements are related to the scale factor $1/\tau$ by

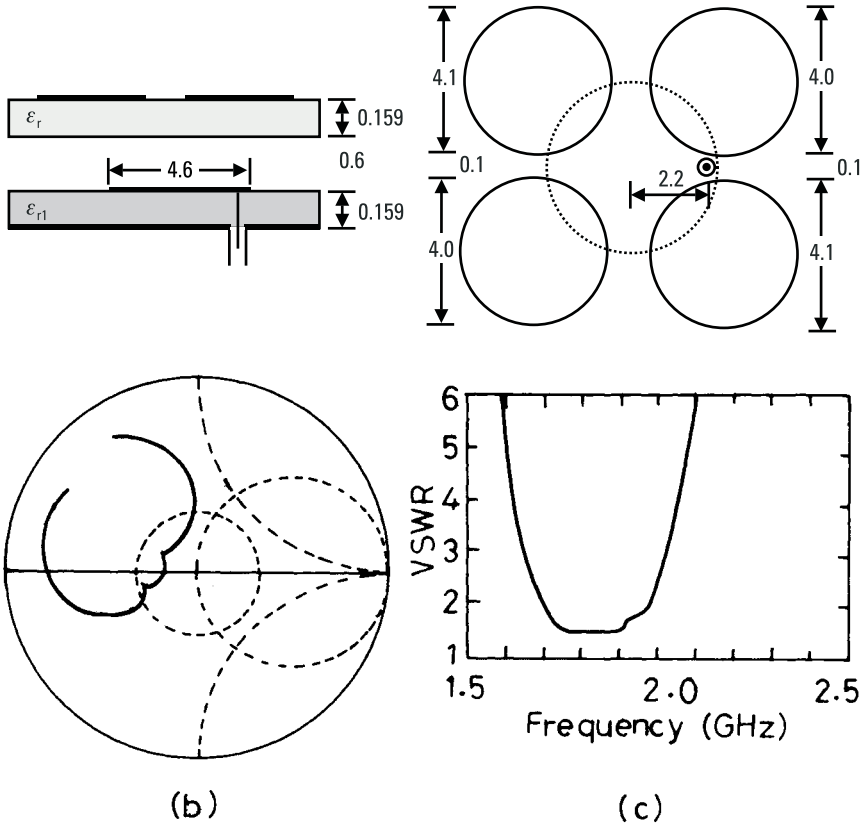

Figure 5.26 (a) One circular patch on the bottom layer and four parasitic circular patches on the top layer in a suspended configuration and its measured (b) input impedance and (c) VSWR plots.

$$\frac{1}{\tau} = \frac{h_{m+1}}{h_m} = \frac{L_{m+1}}{L_m} = \frac{W_{m+1}}{W_m} = \frac{w_{m+1}}{w_m} = \frac{d_{m+1}}{d_m} \tag{5.1}$$

To realize this log-periodic MSA array, scaled values of L and W of the rectangular patches and the tapered microstrip line can easily be fabricated. However, thickness in both the substrates is to be tapered in a logarithmic fashion, which is difficult from a fabrication point of view. To make the fabrication more practical, a uniform substrate thickness is chosen with a uniform width w of microstrip feed as shown in Figure 5.28(b). Although this simplified configuration does not strictly follow the log-periodic principle, it still yields a large BW.

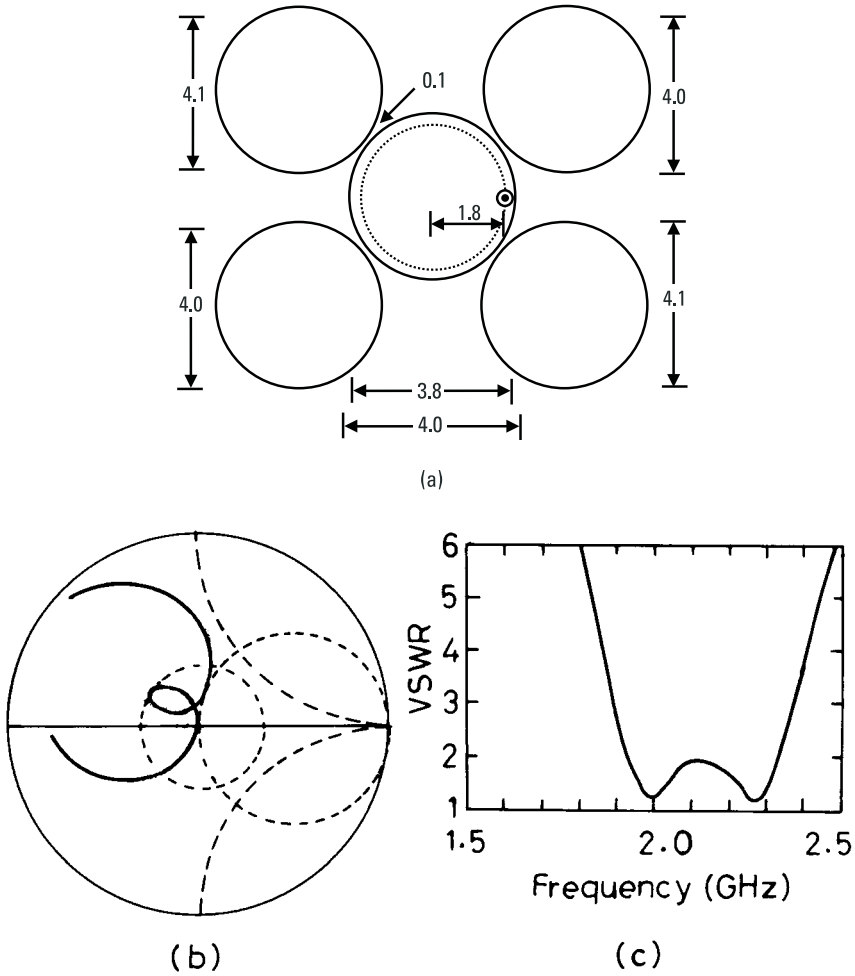

Figure 5.27 (a) One circular patch on the bottom layer and five parasitic circular patches on the top layer in suspended configuration, and its measured (b) input impedance and (c) VSWR plots.

A series feed array with varying dimensions of square patches is shown in Figure 5.29(a). All the square patches are fed with a $\lambda/4$-long microstrip line to obtain impedance matching. Here, λ corresponds to the frequency where individual patches are resonant. The ends of these quarter-wave transformers are connected to the main feed line [8, 9]. The main feed line has characteristic impedance of $Z_0 \cong 50\Omega$ and its width w_m is 0.3 cm. It is terminated in a matched load at the open end to absorb nonradiated power.

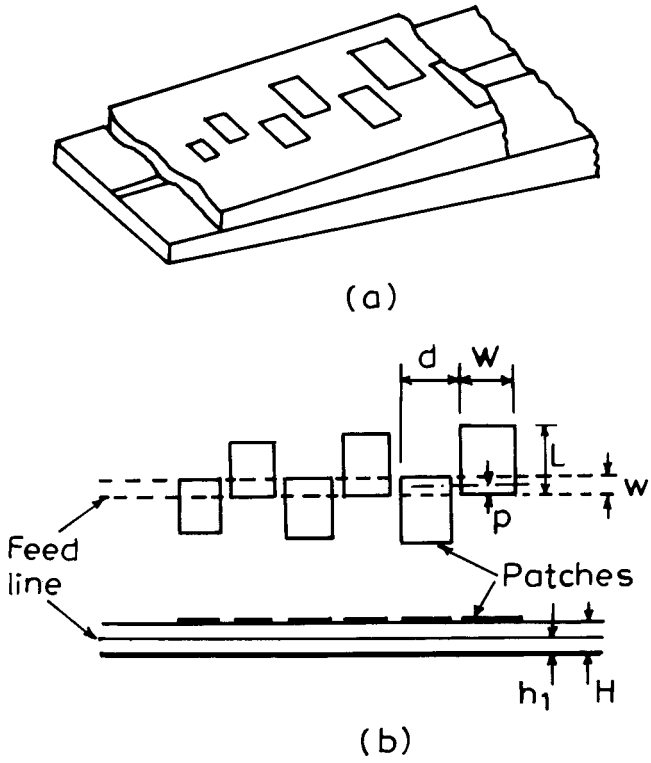

Figure 5.28 (a) Electromagnetically coupled log-periodic MSA array and (b) its simplified configuration.

The array is fabricated in the suspended microstrip configuration on a glass-epoxy substrate (ϵ_r = 4.3, h = 0.159 cm, and tan δ = 0.002) with an air gap Δ = 0.159 cm from the ground plane. The presence of the air gap increases the total height and reduces the effective dielectric constant. This results in an increased BW of the individual patch.

The elements are numbered from the input side, and the dimensions of the log-periodic MSA array are listed in Table 5.7. The input impedance of the square resonators is calculated using the improved transmission line model, which is then transformed to 50Ω by using a quarter-wave transformer. The distance between the two adjacent branch lines is taken as a half-wavelength at the corresponding resonance frequency of the patches. This is similar to the criss-cross feed in a log-periodic dipole array [10], so that a phase difference of 180° is added to each element. The measured VSWR is better than 2.3 from 1.3 GHz to 4.0 GHz as shown in Figure

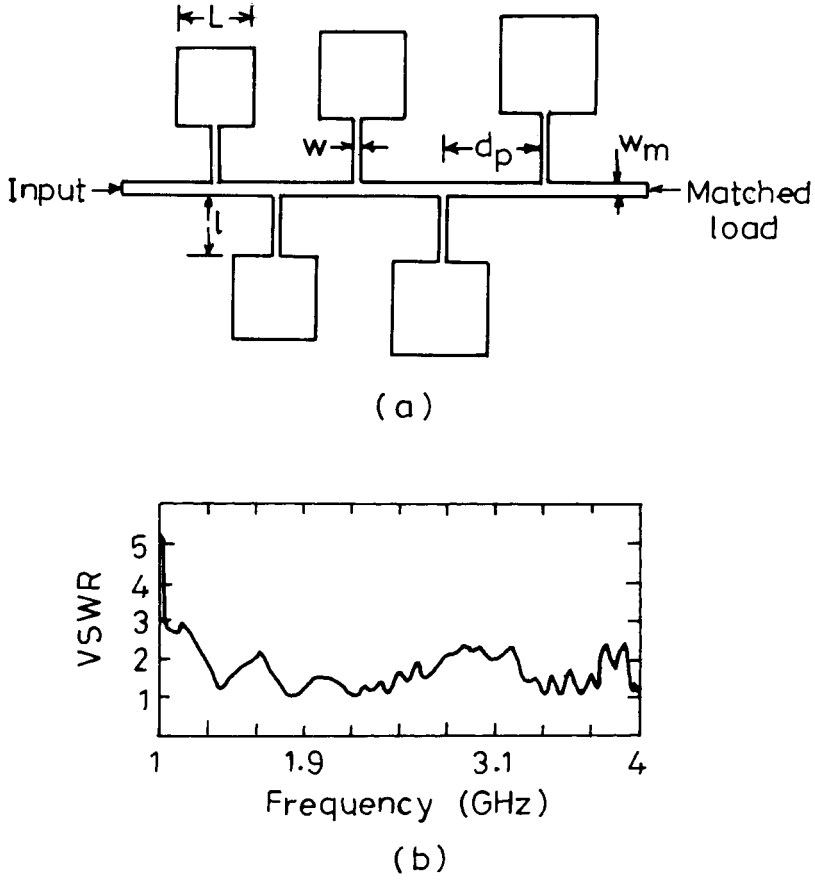

Figure 5.29 (a) A series feed log-periodic MSA array configuration and its (b) measured VSWR plot.

Table 5.7
Dimension of the Log-Periodic MSA Array

Number	f_0 (GHz)	L (cm)	l (cm)	w (cm)	d_p (cm)
1	2.68	3.94	2.20	0.32	4.39
2	2.82	3.72	2.09	0.32	4.18
3	2.97	3.54	1.98	0.40	3.97
4	3.13	3.36	1.88	0.43	3.76
5	3.29	3.19	1.79	0.44	3.58

5.29(b). The radiation pattern for this array is in the broadside direction at 2.5 GHz, whereas the conventional log-periodic dipole array gives an end-fire radiation pattern. The disadvantage of this configuration is that the pattern deviates from the broadside as the frequency changes due to the scanning effect of the array.

5.7 Summary

Planar multiresonators and stacked MSA techniques are combined to yield a wide BW with a higher gain. Several two-layered configurations are discussed, in which only a single patch on the bottom layer is fed by a coaxial probe; all the other patches in the same layer are gap-coupled, and on the top layer they are electromagnetically coupled to the fed patch. Initially, the results of a single rectangular patch, three and five gap-coupled rectangular patches, and stacked patches on the air substrate are described. This is followed by a discussion of three gap-coupled rectangular patches on the bottom layer and a single patch on the top layer. Alternatively, a single patch is considered in the bottom layer and three identical patches are used on the top layer. The latter configuration yields a broader BW, since all the parasitic patches are at a larger height from the ground plane. The three patches in the bottom layer with three patches in the top layer do not yield any significant improvement in performance. One bottom patch with five parasitic patches on the top layer yielded a broad BW of 920 MHz (30.1%), with a higher gain. Also, one bottom patch with two or four rectangular patches in the top layer yielded a wide BW of more than 1 GHz with a larger gain. These antennas have also been used in a suspended microstrip configuration for a large BW and gain.

The above configurations have also been investigated by replacing rectangular patches with circular patches; these investigations have yielded similar results. The stacked multiresonator rectangular or CMSAs yield a BW of 25% to 30% with a small variation in the radiation pattern over the entire BW at the expense of an increase in height and overall dimensions.

The concept of a log-periodic antenna array using MSA elements is discussed for a broad BW. A stagger-tuned log-periodic MSA array is described in which all the rectangular patch dimensions are scaled logarithmically. A large BW of 1.3 GHz to 4 GHz has been obtained for VSWR $\leq$ 2.3, but the radiation pattern varies over the BW.

References

[1] Legay, H., and L. Shafai, "A New Stacked Microstrip Antenna with Large Bandwidth and High Gain," *IEEE AP-S Int. Symp. Digest,* June 1993, pp. 948–951.

[2] Legay, H., and L. Shafai, "New Stacked Microstrip Antenna with Large Bandwidth and High Gain," *IEE Proc. Microwaves, Antennas Propagation,* Pt. H, Vol. 141, No. 3, June 1994, pp. 199–204.

[3] IE3D 7.0, Zeland Software, Inc., Fremont, CA, 2000.

[4] Kumar, G., and K. P. Ray, "Stacked Gap-Coupled Multiresonator Rectangular Microstrip Antennas," *IEEE AP-S Int. Symp. Digest,* Boston, MA, July 2001, pp. 514–517.

[5] Balakrishnan, B., and G. Kumar, "Wideband and High Gain Broadband Electromagnetically Coupled Microstrip Antennas," *IEEE AP-S Int. Symp. Digest,* June 1998, pp. 1112–1115.

[6] Hall, P. S., "Multi-Octave Bandwidth Log-Periodic Microstrip Antenna Array," *IEE Proc. Microwaves, Antennas Propagation,* Pt. H, Vol. 133, No. 2, 1986, pp. 127–136.

[7] Pozar, D. M., and D. H. Schaubert, *Microstrip Antennas: The Analysis and Design of Microstrip Antennas and Arrays,* New York: IEEE Press, 1995.

[8] Pues, H., et al., "Wideband Quasi Log-Periodic Microstrip Antennas," *IEE Proc. Microwaves, Antennas Propagation,* Pt. H, Vol. 128, June 1981, pp. 159–163.

[9] Kakkar, R., and G. Kumar, "Stagger Tuned Microstrip Log-Periodic Antenna," *IEEE AP-S Int. Symp. Digest,* June 1996, pp. 1262–1265.

[10] Isbell, D. E., "Log-Periodic Dipole Array," *IRE Trans.,* Vol. AP-8, May 1960, pp. 260–267.

6

Compact Broadband MSAs

6.1 Introduction

Personal mobile communication and other miniaturized communication systems need a small-sized MSA. The size of the regularly shaped MSA operating in the UHF band is quite large because its resonant length is inversely proportional to frequency. To design a smaller antenna at these frequencies, conventional MSA configurations, such as rectangular and circular configurations, need to be modified. Also, to design a broadband antenna array, the element should have large BW. The planar multiresonator broadband antennas described in Chapter 3 generally have a large size that makes them unsuitable to be used as elements in an array. Compact broadband elements need to be designed for this purpose.

Compact MSAs can be designed with substrate having a higher dielectric constant ϵ_r. In this case, the size of the regularly shaped MSAs will be much smaller than that of the low dielectric constant substrate at a given resonance frequency, but the BW is small. For a RMSA of length L = 1.51 cm, width W = 2 cm, and feed point at x = 0.2 cm, on a substrate having ϵ_r = 9.8 and thickness h = 0.159 cm, the BW for VSWR $\leq$ 2 is 30 MHz at the center frequency f_0 = 3.002 GHz. In comparison, the BW of a RMSA of L = 3 cm, W = 4 cm, and x = 0.65 cm with ϵ_r = 2.55 and h = 0.159 cm, is 64 MHz at 2.974 GHz as described in Chapter 2. Thus, by increasing ϵ_r from 2.55 to 9.8, the area decreases by a factor of about four, but the BW decreases from 64 MHz to 30 MHz, and the gain decreases from 6.8 dB to 4.4 dB.

This chapter describes various compact MSA configurations that are obtained by modifying regular shapes, such as rectangular, circular, and triangular patches, by using shorting posts or by cutting slots in the metallic patch. The broadband techniques discussed in Chapters 3 and 4 have been used with these compact configurations to realize broadband compact MSAs.

6.2 Compact Shorted RMSAs

An RMSA operating in the fundamental TM_{10} mode has a resonant length of $\lambda/2$; the voltage distribution along its length is shown in Figure 6.1(a). The zero potential field is along the line OO, which is in the middle of the resonant length. By shorting the patch along the line OO to the ground

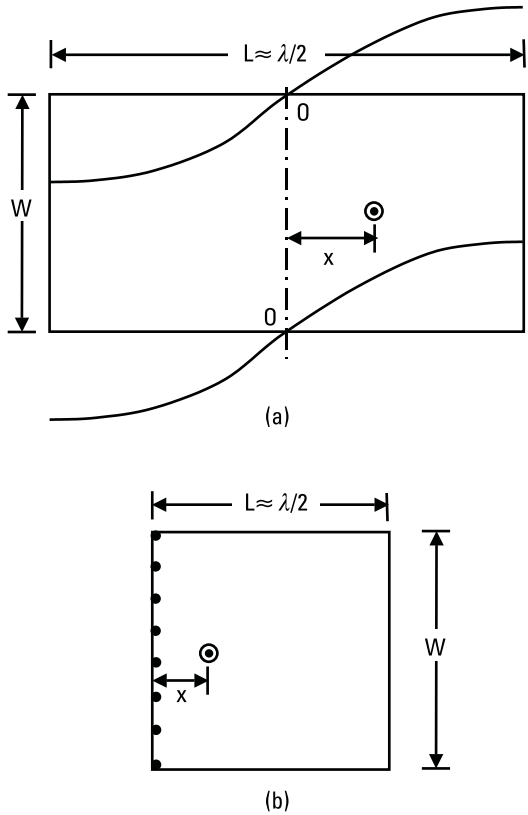

Figure 6.1 (a) Field distribution of the fundamental TM_{10} mode of RMSA and (b) shorted $\lambda/4$ RMSA.

plane, and by using only half of the patch, a compact shorted RMSA is realized with $\lambda/4$ length as shown in Figure 6.1(b) [1]. This antenna has nearly the same resonance frequency as that of a $\lambda/2$ RMSA, but the size is reduced by one-half (here the resonant length is $\lambda/4$). The shorting can be realized either by using a shorting plate or by placing number of shorting posts.

Consider an example of $\lambda/2$ RMSA of length L = 6.6 cm, W = 3.3 cm, and x = 0.6 cm with substrate parameters ϵ_r = 2.33, h = 0.159 cm, and tan δ = 0.001. It has a resonance frequency of 1.472 GHz, and its BW is 10 MHz. Its size is reduced by half when a shorted RMSA with $L = W$ = 3.3 cm is taken. The width of the RMSA is fully shorted by using closely spaced shorting posts, and the feed point is located at x = 0.4 cm from the shorted edge. The MNM [2], described in Appendix C, has been used to analyze the shorted RMSA. The field variation is rapid in the case of the shorted configuration, so more numbers of ports should be taken along the periphery for the analysis as compared to that for RMSA. The unshorted ports are loaded with its radiation resistance, and the shorted ports are loaded with zero resistance.

The theoretical and measured input impedance and VSWR plots of the shorted RMSA are shown in Figure 6.2. The theoretical and measured resonance frequencies are 1.442 GHz and 1.447 GHz, respectively, and the measured and theoretical BWs are 9 MHz. These results are in good agreement with the results obtained using IE3D, which is based on the MoM [3]. The resonance frequency of the shorted RMSA is slightly smaller

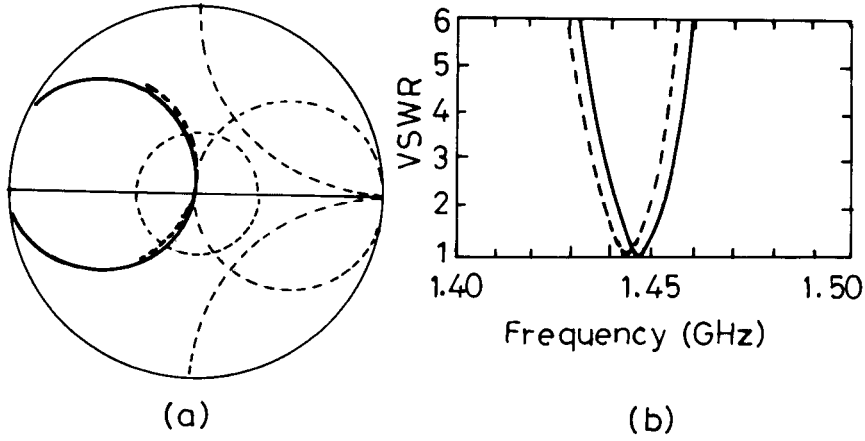

Figure 6.2 (a) Input impedance and (b) VSWR plots of shorted RMSA: (- - -) theoretical and (——) experimental.

than the corresponding $\lambda/2$ RMSA due to the inductance of the shorting posts; the BW is also slightly smaller. The measured radiation pattern of the shorted RMSA at the resonance frequency is shown in Figure 6.3. The radiation is in the broadside direction, but the cross-polar levels are higher than those of the $\lambda/2$ RMSA. Also, the gain of the $\lambda/2$ RMSA is higher than the shorted $\lambda/4$ RMSA due to its larger size.

For comparison, RMSAs with different lengths and different substrate parameters are analyzed using IE3D, and the results are summarized in Table 6.1. The width of the patch and the thickness of the substrate are kept constant. For L = 6.6 cm, the resonance frequency and the BW of the unshorted RMSA are approximately the same as that of shorted RMSA, but the directivity and efficiency are much higher due to the larger size.

For cases 2 and 3, it may be noted that for the same size, the unshorted RMSA on the substrate with a higher ϵ_r (= 9.3) yields a lesser BW than the fully shorted RMSA on a lower ϵ_r (= 2.33), but the directivity and η are

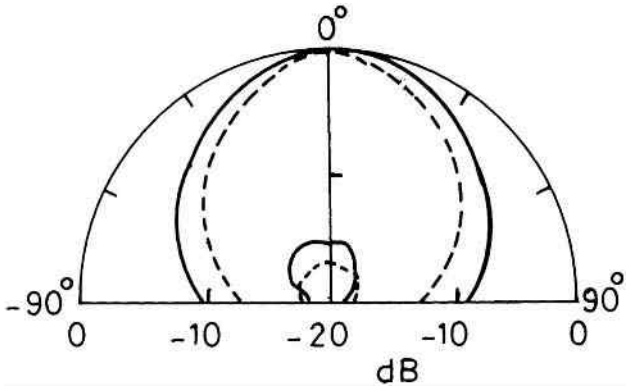

Figure 6.3 Measured radiation pattern of a shorted RMSA: (- - -) E-plane and (——) H-plane.

Table 6.1
Comparison of Shorted and Unshorted RMSA
(W = 3.3 cm, h = 0.159 cm, and tan δ = 0.001)

Cases	Configuration	L (cm)	ϵ_r	x (cm)	f_0 (GHz)	BW (MHz)	D (dB)	η (%)
1	Unshorted	6.6	2.33	0.6	1.472	10	7.1	74
2	Unshorted	3.3	9.3	0.4	1.472	7	5.6	68
3	Fully shorted	3.3	2.33	0.5	1.455	9	4.4	34

higher and the cross-polar levels are much smaller. Accordingly, to design a compact MSA, one can choose either an unshorted MSA with a higher ϵ_r or a fully shorted RMSA on a lower ϵ_r depending upon whether a higher gain or wider BW is required.

6.2.1 Partially Shorted RMSAs

A partially shorted RMSA is shown in Figure 6.4(a). The resonance frequency of the RMSA reduces when shorting width w_s is reduced [1]. The reduction of w_s results in larger resonant length (from A to B), which approximately corresponds to $\lambda/4$, and hence resonance frequency decreases. The antenna is analyzed using MNM after dividing its extended periphery into number of segments as shown in Figure 6.4(b). The theoretical and experimental resonance frequency f_0 and input impedance Z_{in} for various shorting ratios (w_s/W) with feed at x = 0.4 cm are given in Table 6.2. The voltage distribution along the peripheral ports (1 to 60) for two values of shorting ratio (0.1 and 0.6) at their corresponding resonance frequencies is shown in Figure 6.5.

As shorting ratio decreases from 1 to 0.1, the measured resonance frequency reduces from 1.447 GHz to 0.881 GHz implying nearly 40% reduction. The maximum error between the theoretical and experimental resonance frequencies is 1.24%. With decrease in shorting ratio from 1 to 0.1, the real part of the measured Z_{in} increases from 50.7Ω to 528Ω. In order to obtain impedance matching with the 50-Ω coaxial line, the feed-point has to be shifted closer to the shorting post as w_s decreases.

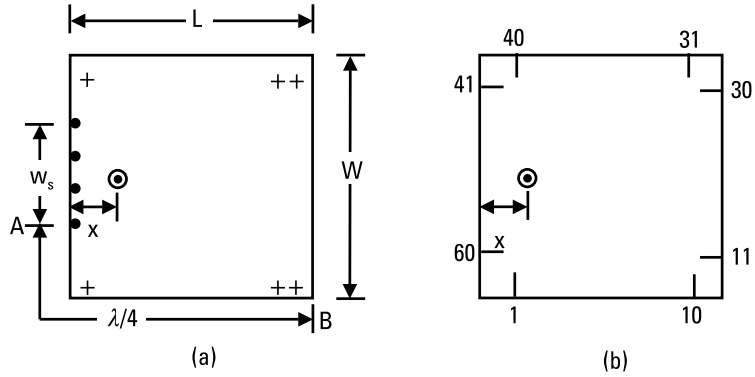

Figure 6.4 (a) Partially shorted RMSA and (b) its multiport network model.

Table 6.2
Variation of Resonance Frequency with Shorting Ratio for Partially Shorted RMSA ($L = W = 3.3$ cm, $\epsilon_r = 2.33$, $h = 0.159$ cm, $\tan\delta = 0.001$, and $x = 0.4$ cm)

Shorting Ratio w_s/W	Experimental Results f_0 (GHz)	Z_{in} (Ω)	Theoretical Results f_0 (GHz)	Z_{in} (Ω)	Error in f_0 (%)
0.1	0.881	$528 + j2.8$	0.893	$535 - j5$	+1.24
0.2	1.028	$300 - j0.5$	1.025	$282 - j3$	–0.27
0.3	1.126	$212 + j1.3$	1.123	$179 - j1$	–0.25
0.4	1.206	$142 - j3.7$	1.203	$126 - j4$	–0.23
0.5	1.294	$95.5 - j0.7$	1.296	$81.2 - j2$	+0.12
0.6	1.345	$73.1 - j0.2$	1.348	$66.8 + j3$	+0.20
0.7	1.393	$59 + j0.3$	1.389	$59.6 + j2$	–0.25
0.8	1.420	$53.4 - j1.1$	1.419	$52.5 - j3$	–0.06
0.9	1.440	$51.9 - j1.7$	1.436	$50.9 - j.1$	–0.25
1.0	1.447	$50.7 - j0.0$	1.442	$50.1 + j0$	–0.31

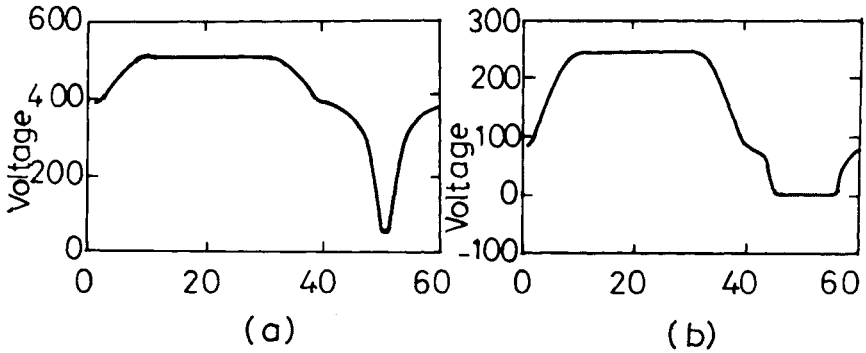

Figure 6.5 Voltage distribution of partially shorted RMSA for two values of shorting ratios w_s/W (a) 0.1 and (b) 0.6.

The resonance frequency f_0 of the partially shorted RMSA can be approximately calculated by equating the length from A to B to $\lambda/4$, and it is given by

$$f_0 = \frac{3}{4[L_e + (W_e - w_s)/2]\sqrt{\epsilon_e}} \text{ GHz} \tag{6.1}$$

where L_e and W_e are the effective length and width of the shorted RMSA in centimeters, and ϵ_e is the effective dielectric constant, whose values can be obtained from expressions given in Chapter 2 and Appendixes B and C.

The resonance frequency of the shorted RMSA decreases with a decrease in the shorting ratio, and it has the lowest value for a single shorting post [4–6]. As a result, for a given frequency, the RMSA with a single shorting post will have the smallest size. Therefore, the effect of varying the dimensions of the RMSA with a single short on its resonance frequency is discussed to realize a compact antenna.

6.2.2 Effect of Dimensions of RMSAs with a Single Shorting Post

A compact RMSA with a single shorting post in the middle of the edge along the width is shown in Figure 6.6(a). For the fixed length L, the resonance frequency varies with the change in the width W as can be noted from (6.1). For an RMSA with L = 3.3 cm, the theoretical resonance frequency and BW obtained using MNM for different values of W are shown in Table 6.3. The diameter of the shorting post is taken as 0.06 cm. As W increases from 0.5 cm to 4.0 cm, the feed-point location x has to be decreased from 0.40 cm to 0.08 cm to obtain impedance matching. The resonance frequency decreases from 2.178 GHz to 0.790 GHz with a corresponding decrease in BW from 2.1% to 0.5%. Accordingly, with an increase in W, the resonance frequency decreases considerably; hence, the overall BW decreases due to a decrease in the electrical thickness h/λ_0 of the substrate. These results are different than those for the conventional RMSA, in which with an increase in W, the resonance frequency decreases slightly due to increase in ϵ_e and the BW of the antenna increases.

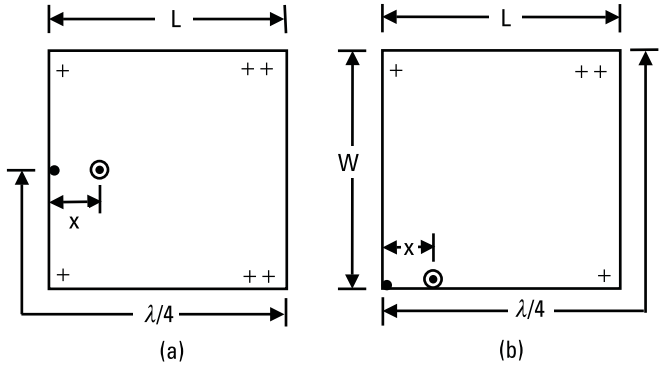

Figure 6.6 An RMSA with a single shorting post at the (a) middle of the edge along the width and (b) corner.

Table 6.3
Theoretical Resonance Frequency of a Single Shorted RMSA for Various Values of W (L = 3.3 cm, ϵ_r = 2.33, h = 0.159 cm, and tan δ = 0.001)

Width W (cm)	x (cm)	f_0 (GHz)	Z_{in} (Ω)	VSWR	BW (%)
0.5	0.40	2.178	$57.2 - j1.0$	1.14	2.1
1.0	0.20	1.688	$62.9 - j1.4$	1.29	1.2
1.5	0.13	1.392	$60.9 - j0.7$	1.22	0.9
2.0	0.10	1.196	$53.8 - j1.0$	1.08	0.8
2.5	0.10	1.054	$66.8 + j2.6$	1.34	0.7
3.0	0.08	0.946	$55.5 + j1.6$	1.21	0.6
3.5	0.08	0.860	$62.5 - j0.5$	1.25	0.6
4.0	0.08	0.790	$67.1 + j4.1$	1.35	0.5

The resonance frequency of the RMSA with a single shorting post in the middle of the edge along the width can be approximately calculated by modifying (6.1) as [6]:

$$f_0 = \frac{3}{4(L_e + W_e/2)\sqrt{\epsilon_e}} \text{ GHz} \tag{6.2}$$

This formula neglects the effect of the shorting post diameter. The resonance frequency decreases slightly with a decrease in the shorting post diameter, which is due to an increase in the inductance of the shorting post.

Since the resonance frequency of the RMSA with a single short is governed by the length $L_e + W_e/2$, L and W are varied such that $L + W/2$ = 8 cm, to observe the effect on the BW of the antenna. The theoretical results obtained using the MNM are summarized in Table 6.4. The resonance frequency remains constant for a larger W, but increases marginally for a smaller W, which is due to the decrease in ϵ_e. For a larger W, Z_{in} reduces due to the increase in the radiation from the width of the patch; therefore, the feed point x is moved away from the shorting post for matching. The BW increases slightly from 1.15% to 1.26% as W increases from 3 cm to 8 cm, but the area of the patch increases from 19.5 cm^2 to 32 cm^2 [6]. Thus, depending upon the space availability, a compact RMSA can be designed using (6.2).

6.2.3 Effect of the Position of the Single Shorting Post

When the single shorted RMSA shown in Figure 6.6(a) is fabricated on a higher dielectric constant substrate, its resonance frequency reduces further.

Table 6.4
Theoretical Resonance Frequency of a RMSA with Single Short for $L + W/2 = 8$ cm ($\epsilon_r = 2.33$, $h = 0.159$ cm, and $\tan \delta = 0.001$)

W (cm)	L (cm)	x (cm)	f_0 (MHz)	Z_{in} (Ω)	BW (%)	Area (cm^2)
3.0	6.5	0.16	434	$56.7 + j0.2$	1.15	19.5
4.0	6.0	0.16	427	$51.2 - j2.4$	1.21	24.0
5.0	5.5	0.16	423	$48.4 + j0.6$	1.23	27.5
6.0	5.0	0.23	423	$57.8 + j0.8$	1.23	30.0
7.0	4.5	0.26	423	$51.9 - j0.9$	1.24	31.5
8.0	4.0	0.33	423	$54.9 + j0.8$	1.26	32.0

A single shorted RMSA with $L = W = 4.6$ cm is fabricated on a glass-epoxy substrate with $\epsilon_r = 4.3$, $h = 0.159$ cm, and $\tan \delta = 0.02$. For the shorting post diameter = 0.06 cm and $x = 0.6$ cm, the measured resonance frequency f_0 is 471 MHz. In comparison, a $\lambda/2$ RMSA with $L = W = 4.6$ cm has the resonance frequency $f_0 = 1.549$ GHz.

The resonance frequency reduces further when the shorting post is placed at one corner of the RMSA as shown in Figure 6.6(b). In this case, voltage distribution varies from zero at the short location to a maximum value at the diagonally opposite corner. Hence, the resonance frequency can be approximately calculated by equating $L_e + W_e = \lambda/4$. For $x = 0.5$ cm, the measured resonance frequency is 377 MHz, which is much smaller than the 471 MHz obtained in the previous case.

Thus, a single short at the corner of the RMSA results in a most compact configuration. The resonance frequency of the conventional RMSA reduces from 1.549 GHz to 377 MHz, when a single short is placed at one of its corners, resulting in area reduction factor of 16.8.

6.3 Compact Shorted CMSA and Its Variations

Similar to the compact shorted RMSA, the size of a CMSA is reduced by shorting along its zero potential lines [7]. For the fundamental TM_{11} mode, the field is zero along the diameter perpendicular to the feed-axis, as shown in Figure 6.7(a). Therefore, by shorting along the zero field line OO to the ground plane, and by using only one-half of the patch, a compact shorted SCMSA is realized as shown in Figure 6.7(b). A SCMSA with an open boundary, as shown in Figure 6.7(c), has a similar field distribution and

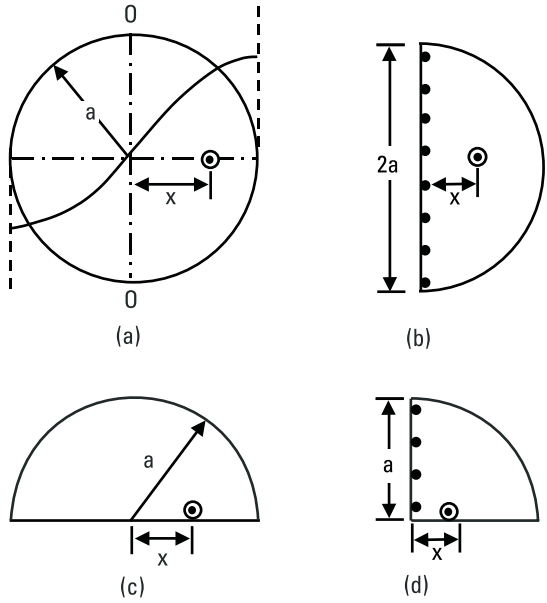

Figure 6.7 Variations of CMSA: (a) conventional CMSA with its voltage distribution along the feed-axis for the fundamental TM_{11} mode, (b) shorted SCMSA, (c) SCMSA, and (d) shorted 90°-sectoral MSA.

approximately the same resonance frequency as that of a CMSA with half the area [8]. The area is reduced to one-fourth of that of a circle by shorting along the zero field lines of a SCMSA, resulting in a shorted 90°-sectoral MSA as shown in Figure 6.7(d). The resonance frequencies of the shorted semicircular and 90°-sectoral MSAs are further reduced by decreasing the shorting width as in the case of shorted RMSA.

6.3.1 CMSAs and SCMSAs

For comparison with shorted variations of CMSA, the results for CMSAs and SCMSAs are described first. For a CMSA of radius a = 3 cm, feed-point at x = 0.9 cm with ϵ_r = 2.33, h = 0.159 cm, and tan δ = 0.002, the theoretical (obtained using the MNM) and measured resonance frequencies are 1.868 GHz and 1.866 GHz, respectively. For a SCMSA of radius a = 3 cm and x = 0.7 cm, the theoretical and measured resonance frequencies are 1.863 GHz and 1.859 GHz, respectively, which are close to that of the CMSA.

6.3.2 Shorted SCMSAs and 90°-Sectoral MSAs

A shorted SCMSA with closely spaced shorting posts along the diameter with a feed at $x = 0.65$ cm is shown in Figure 6.7(b). The measured resonance frequency is 1.788 GHz, which is slightly lower than that of the CMSA due to the inductance of the shorting posts. For a shorted 90°-sectoral MSA, shown in Figure 6.7(d), the feed is taken at $x = 0.3$ cm, which is closer to the shorting post, because the impedance variation is large due to the compact size of the antenna. The measured resonance frequency is 1.761 GHz.

The measured VSWR plots for these four configurations are shown in Figure 6.8. The comparisons of resonance frequency, BW, and area are given in Table 6.5. The shorted configurations have a slightly smaller BW as compared to the conventional CMSA. The fully shorted 90°-sectoral MSA has an area equal to one-fourth of that of the CMSA with approximately the same resonance frequency with smaller BW.

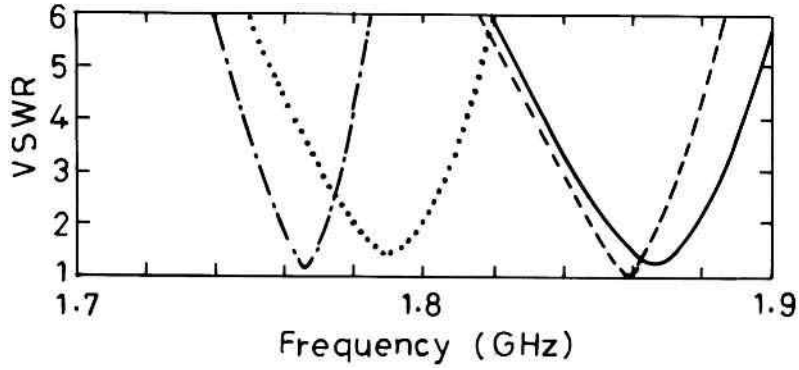

Figure 6.8 Measured VSWR plots of variations of CMSA: (——) CMSA, (- - -) SCMSA, (· · ·) shorted SCMSA, and (– · –) shorted 90°-sectoral MSA.

Table 6.5
Comparison of Different Variations of CMSA
($a = 3$ cm, $\epsilon_r = 2.33$, $h = 0.159$ cm, and $\tan\delta = 0.002$)

Variations of CMSA	x (cm)	f_0 (GHz)	BW (MHz)	BW (%)	Area (cm^2)
CMSA	0.9	1.866	25	1.3	28.27
SCMSA	0.7	1.863	18	0.9	14.13
Shorted SCMSA	0.65	1.788	22	1.2	14.13
Shorted 90°-sectoral MSA	0.3	1.761	14	0.8	7.06

The measured radiation patterns of the CMSA, SCMSA, and shorted 90°-sectoral MSA are compared in Figure 6.9. The shorted 90°-sectoral MSA has a wider HPBW and higher cross-polar levels than the other configurations. The gain of the compact antenna reduces due to reduction in the size [7].

6.3.3 Partially Shorted SCMSAs and 90°-Sectoral MSAs

The resonance frequency of both the shorted SCMSA and 90°-sectoral MSA decreases with a reduction in the shorting width. As the shorting ratio (shorting width to straight edge length) decreases from 1.0 to 0.1, the resonance frequency of the shorted SCMSA and 90°-sectoral MSA reduces by 46% and 40%, respectively, with a corresponding decrease in the BW. The area of the 90°-sectoral MSA with a shorting ratio of 0.1 is 11.6% of that of a CMSA operating at the same resonance frequency.

6.3.4 Compact CMSA with a Single Shorting Post

The resonance frequency of a CMSA reduces considerably when a single shorting post is placed at the periphery as shown in Figure 6.10 [9]. The radius of the patch is a = 2.65 cm and the feed point is at x = 0.55 cm from the shorting post. The substrate parameters are ϵ_r = 4.3, h = 0.159 cm, and tan δ = 0.02. The diameters of the probe feed and the shorting post are 0.12 cm and 0.06 cm, respectively. The measured resonance frequency is 458 MHz, which is 0.29 times the resonance frequency (1.572 GHz) of the corresponding unshorted CMSA. However, the BW of the shorted CMSA

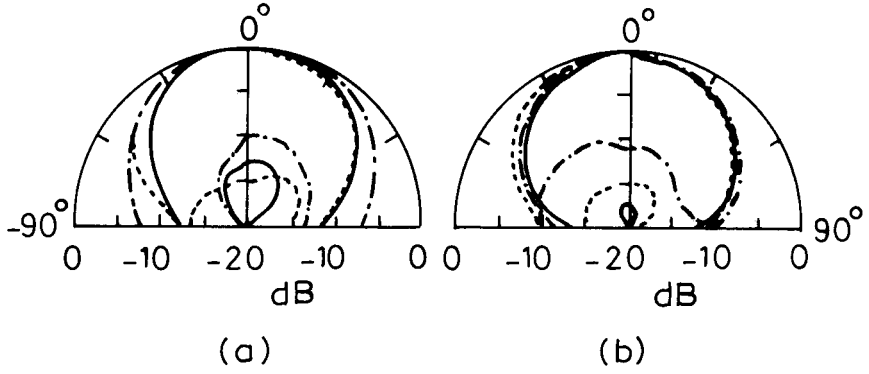

Figure 6.9 Radiation pattern in the (a) E-plane and (b) H-plane: (——) CMSA, (- - -) SCMSA, and (– · –) shorted 90°-sectoral MSA.

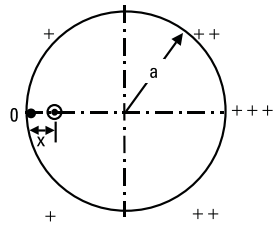

Figure 6.10 CMSA with a single shorting post.

is 6 MHz (1.3%), which is much smaller as compared to the BW of 33 MHz (2%) of the corresponding unshorted CMSA.

The voltage distribution along the periphery of the CMSA with a single short is also shown in Figure 6.10. More numbers of the "+" sign indicates a larger magnitude of voltage. The lowest resonance frequency of the single shorted CMSA is approximately calculated by modifying (2.30) for calculating the resonance frequency of the fundamental TM_{11} mode of CMSA as

$$f_0 = \frac{8.791}{a_{e1}\sqrt{\epsilon_e}} \text{ GHz} \tag{6.3}$$

where

$$a_{e1} = \pi a_e \text{ in cm} \tag{6.4}$$

and a_e is the effective radius of the CMSA.

The resonance frequency of the CMSA decreases approximately by a factor of π when a single shorting post is placed at the periphery. In practice, the decrease in the frequency is more than this factor due to the inductance of the shorting post, whose value depends upon its diameter.

6.4 Compact Shorted TMSAs and Sectoral MSAs

The concept of shorting post is also extended to the TMSA [10]. An ETMSA is shown in Figure 6.11(a). The zero potential line is shown by the dotted line. By shorting along this line and splitting the ETMSA into two parts, a shorted 60°-sectoral antenna and its complement are realized as shown in Figure 6.11(b, c). Both the antennas have nearly the same resonance frequency as that of the ETMSA but with reduced area. Similarly, a 30°-60°-90°

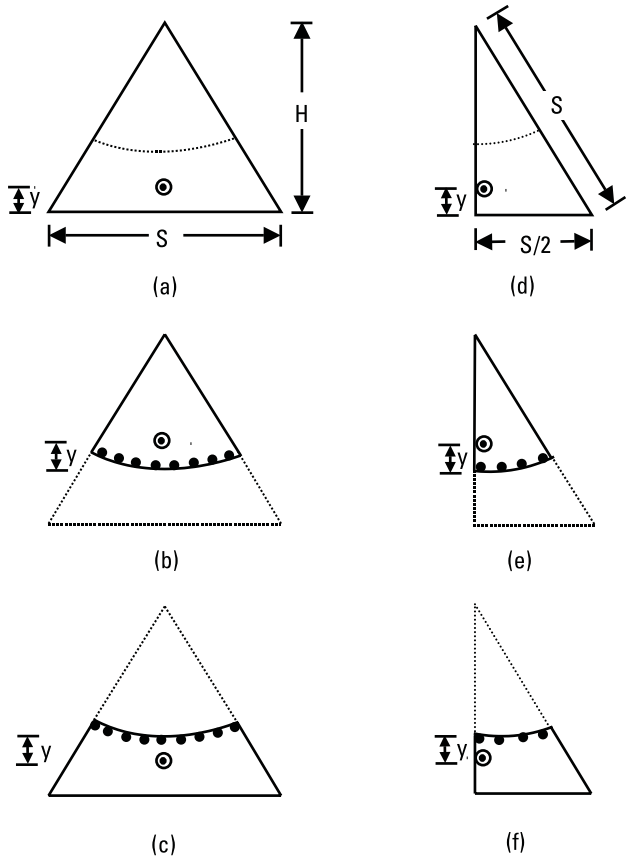

Figure 6.11 TMSA and its variations. (a) Equilateral TMSA, (b) shorted 60°-sectoral MSA, (c) complement of the shorted 60°-sectoral MSA, (d) 30°-60°-90° TMSA, (e) shorted 30°-sectoral MSA, and (f) complement of the shorted 30°-sectoral MSA.

TMSA (half of ETMSA), which has the same resonance frequency as that of the ETMSA, could be shorted along the zero potential line as shown in Figure 6.11(d). By splitting the patch into two parts, a compact shorted 30°-sectoral MSA and its complement are realized as shown in Figure 6.11(e, f).

6.4.1 ETMSA and Its Variations

An ETMSA of side length S = 4.33 cm and feed point at y = 0.6 cm from the base is shown in Figure 6.11(a). The substrate parameters are ϵ_r = 2.33,

h = 0.159 cm, and tan δ = 0.002. The measured VSWR plot is shown in Figure 6.12. The resonance frequency is 2.810 GHz with a BW of 47 MHz.

The ETMSA has zero potential at 2.5 cm from the vertex. Hence, a shorted 60°-sectoral MSA of radius a = 2.5 cm with feed at y = 0.3 cm is fabricated as shown in Figure 6.11(b). The measured VSWR plot for the fully shorted curved surface is shown in Figure 6.12. The resonance frequency is 2.734 GHz with a BW of 37 MHz. The resonance frequency is smaller than that of the corresponding ETMSA due to the finite inductance of the shorting posts. When the shorting length is reduced, the resonance frequency decreases further. For a single shorting post in the center of the curved edge, the field distribution is forced to become zero only at a point, thereby increasing the resonant dimension of the antenna, which in turn reduces the resonance frequency by 24%.

The shorted complement of 60°-sectoral MSA is shown in Figure 6.11(c). The VSWR plot for y = 0.2 cm is shown in Figure 6.12. The resonance frequency is 2.709 GHz with a BW of 43 MHz. As the shorting ratio decreases from 1.0 to 0.17, the resonance frequency decreases from 2.709 GHz to 2.001 GHz. Thus, frequency is further reduced by 22% for the same patch dimensions [10].

The measured radiation patterns in the E- and H-planes of an ETMSA, fully shorted 60°-sectoral, and its complement MSA are shown in Figure 6.13. For these antennas, the radiation is in the broadside direction. The HPBW in the E- and H-planes are 97° and 95° for shorted 60°-sectoral MSA and 105° and 75° for its complement antenna as compared to that of 72° and 78° for ETMSA, respectively. The gain of the shorted antennas

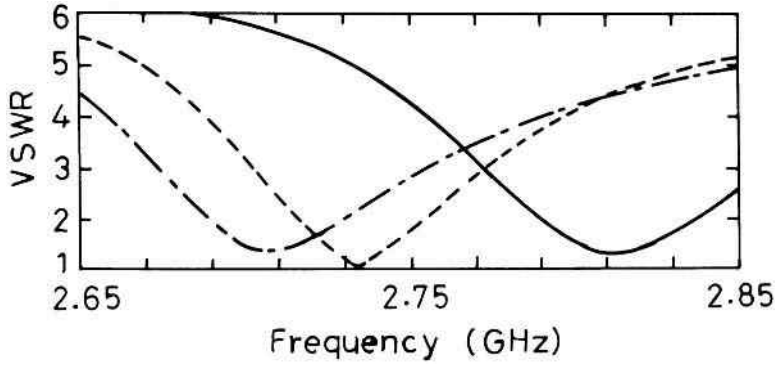

Figure 6.12 VSWR plots of (——) ETMSA, (- - -) shorted 60°-sectoral MSA, and (– · –) complement of shorted 60°-sectoral MSA.

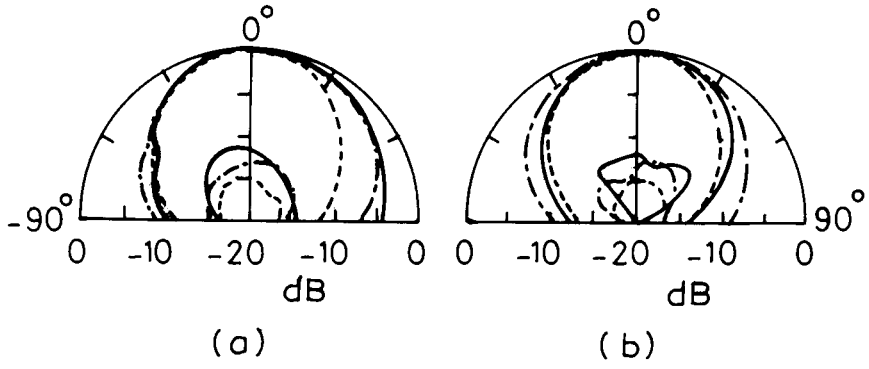

Figure 6.13 Radiation pattern in the (a) E- and (b) H-planes: (- - -) ETMSA, (– · –) shorted 60°-sectoral MSA, and (——) complement of shorted 60°-sectoral MSA.

is smaller than that of the ETMSA because of reduced area. The cross-polar components are below 10 dB for all these antennas.

6.4.2 30°-60°-90° TMSA and Its Variations

A 30°-60°-90° TMSA of side length S = 4.33 cm has exactly half the area of the corresponding ETMSA with nearly the same resonance frequency. The measured VSWR plot for y = 0.9 cm is shown in Figure 6.14. The resonance frequency is 2.809 GHz with a BW of 38 MHz.

Similar to the shorted 60°-sectoral MSA, a shorted 30°-sectoral MSA of radius a = 2.5 cm and a feed point at y = 0.2 cm is shown in Figure 6.11(e). The measured VSWR plot is shown in Figure 6.14. The resonance frequency is 2.713 GHz with a BW of 36 MHz. As the shorting ratio decreases from 1.0 to 0.25, the resonance frequency decreases from 2.713 GHz to 2.340 GHz.

The complement of the 30°-sectoral MSA with a feed point at y = 0.15 cm is shown in Figure 6.11(f). The VSWR plot is shown in Figure 6.14. The measured resonance frequency is 2.708 GHz with a BW of 28 MHz. As the shorting ratio decreases from 1.0 to 0.25, the resonance frequency decreases from 2.708 GHz to 2.299 GHz.

The measured radiation patterns for all these three antennas are in the broadside direction. The HPBW in the E- and H-planes are 70° and 105° for 30°-60°-90° TMSA, 104° and 90° for shorted 30°-sectoral MSA, and 105° and 80° for its complement antenna, respectively.

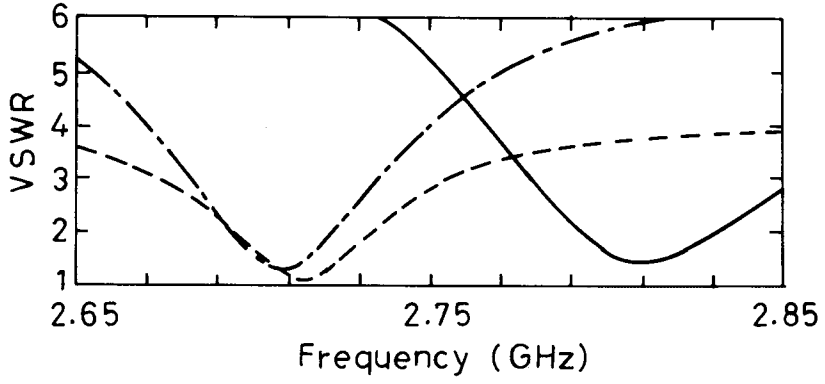

Figure 6.14 VSWR plots of (——) 30°-60°-90° TMSA and (- - -) shorted 30°-sectoral MSA and (– · –) the complement of shorted 30°-sectoral MSA.

6.4.3 Comparison of Variations of TMSAs

The performances of all the fully shorted variations of TMSA are compared in Table 6.6. All these antennas have approximately the same resonance frequency with a comparable BW except for a complement of 30°-sectoral MSA, which has the smallest BW. The shorted 30°-sectoral MSA has an area reduction of almost five times with a slight reduction in BW in comparison with the corresponding unshorted ETMSA. A further reduction in resonance frequency is achieved by reducing the shorting length.

6.4.4 Compact ETMSA with a Single Short

An ETMSA with a single shorting post at the vertex is shown in Figure 6.15 [11]. The shorted patch with a side length S = 6.4 cm and a feed point

Table 6.6
Comparison of Variations in TMSA
(ϵ_r = 2.33, h = 0.159 cm, and tan δ = 0.002)

MSA Configuration	y (cm)	f_0 (GHz)	Z_{in} (Ω)	BW (MHz)	Area (cm^2)
ETMSA	0.6	2.810	62.3 – j0.2	43	8.12
30°-60°-90° TMSA	0.9	2.809	66.4 – j3.2	38	4.06
Shorted 60°-sectoral	0.3	2.734	51.4 – j0.3	37	3.27
Shorted 30°-sectoral	0.2	2.713	53.3 – j1.1	36	1.64
Complement of 60°-sectoral	0.2	2.709	56.7 – j1.7	43	4.85
Complement of 30°-sectoral	0.15	2.708	64.5 – j2.2	28	2.43

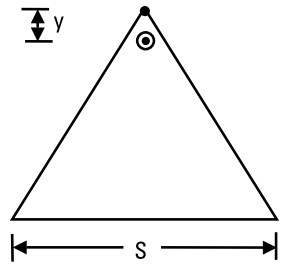

Figure 6.15 ETMSA with a single short.

at y = 0.6 cm from the vertex is fabricated on a glass-epoxy substrate. The measured resonance frequency is 372 MHz, which is approximately one-fourth of the resonance frequency of 1.486 GHz for the unshorted ETMSA.

6.5 Chip-Resistor-Loaded Square MSAs

An MSA with a single shorting post is compact, but it has narrow BW. If the shorting post is replaced with a chip resistor, the BW is increased [12, 13]. The resonance frequency is tuned by varying the location of the chip resistor.

A chip-resistor-loaded square MSA of length L = 3.4 cm with ϵ_r = 2.33, h = 0.159 cm, and tan δ = 0.002 is shown in Figure 6.16. The chip resistor is located at r = 0.2 cm. The antenna has been analyzed using MNM. The chip resistor is considered as an additional port and is loaded by its impedance value. The performance of the antenna for different values of

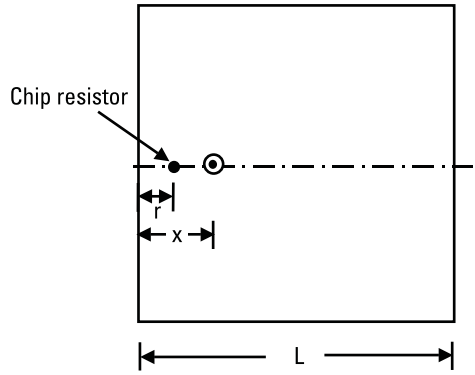

Figure 6.16 Single chip-resistor-loaded square MSA.

chip resistor is summarized in Table 6.7. As the value of the chip resistor increases from 0 to 2Ω, the feed point has to be moved away from the resistor for impedance matching and the impedance BW for VSWR ≤ 2 increases from 9 MHz to 145 MHz. There is little variation in the resonance frequency, but the efficiency of the RMSA decreases from 19% to 12%. The decrease in efficiency is due to the increase in ohmic loss in the resistor. As a result, the broader BW is achieved at the cost of a reduction in the efficiency. The radiation pattern remains in the broadside direction for all the cases [13].

6.6 Slot-Loaded MSAs

The shorting post–loaded MSA is a compact antenna but it suffers from the disadvantages of poor gain and degradation in the radiation pattern. An alternate way to reduce the resonance frequency of the MSA is to increase the path length of the surface current by cutting slots in the radiating patch.

6.6.1 C-Shaped MSA

A C-shaped MSA, shown in Figure 6.17(a), can be derived from an RMSA, by cutting a slot along one of its nonradiating edges [14]. This configuration can be analyzed using the MNM by segmenting it into three RMSAs as shown in Figure 6.17(b). The length and width of the slot are l and w, respectively. The feed point is symmetrically located at a distance x from the center. The voltage distribution along the periphery of the C-shaped MSA near the resonance frequency and the corresponding fringing fields are shown in Figure 6.17(c, d). A greater number of + or −, or a larger size of

Table 6.7
Performance of Chip-Resistor-Loaded Square MSA for Different Resistance Values (L = 3.4 cm, ϵ_r = 2.33, h = 0.159 cm, and tan δ = 0.002)

Resistance (Ω)	x (cm)	f_0 (MHz)	BW (MHz)	η (%)
0	0.29	989	9	19
0.5	0.55	988	40	17
1.0	0.85	986	76	15
1.5	1.20	986	102	13
2.0	1.70	986	145	12

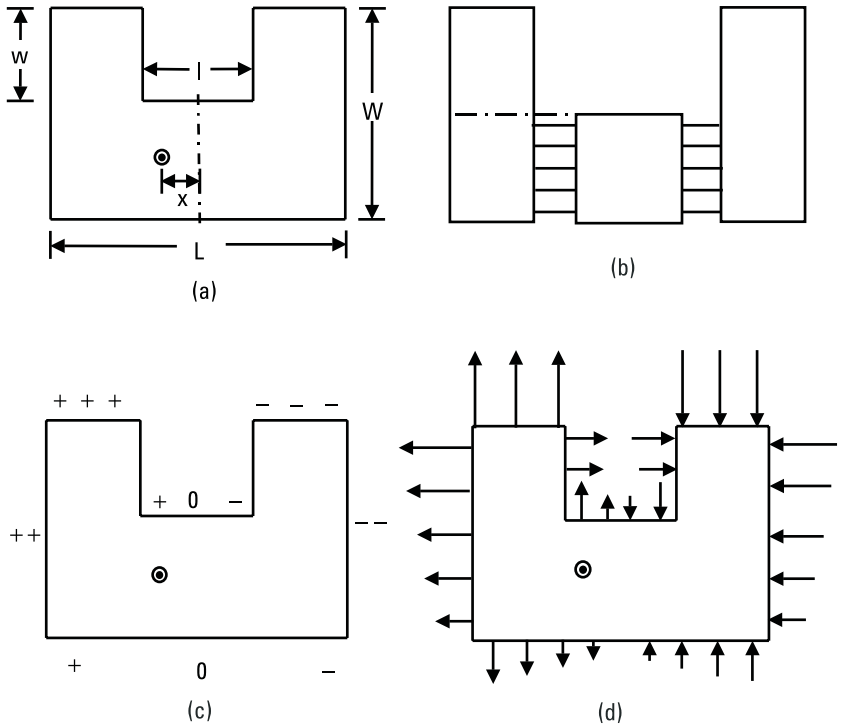

Figure 6.17 (a) C-shaped MSA, (b) its MNM model, (c) electric field distribution, and (d) fringing fields.

arrows implies a larger magnitude of voltage. With an increase in the width and length of the slot, the surface current path increases from one open end to the other open end. This increased resonant length results in the reduction of the resonance frequency.

For $L = 6$ cm and $W = 4$ cm, the effect of varying the slot dimensions on the performance of C-shaped MSA is described. The theoretical results obtained using IE3D are summarized in Table 6.8. The substrate parameters are also given in Table 6.8. Without a slot, C-shaped MSA becomes RMSA, and its resonance frequency is 1.606 GHz with a BW of 12 MHz. As the slot dimensions ($w \times l$) are increased from (1 cm × 1 cm) to (3 cm × 1 cm), the resonance frequency f_0 decreases from 1.448 GHz to 0.900 GHz, and the impedance variation increases, so the feed point has to be shifted toward the center for proper impedance matching. Also, the BW decreases from 8 MHz to 2 MHz. The decrease in BW is due to a decrease in the h/λ_0 of the antenna. When the slot length is increased from 1 cm to 4 cm,

Table 6.8
Effect of Slot Dimensions on the Performance of C-Shaped MSA
(L = 6 cm, W = 4 cm, ϵ_r = 2.33, h = 0.159 cm, and tan δ = 0.002)

$w \times l$ (cm, cm)	x (cm)	f_0 (GHz)	BW (MHz)	D (dB)	η (%)
0×0	0.70	1.606	12	7.2	79
1×1	0.55	1.448	8	7.1	70
2×2	0.40	1.142	3	6.9	42
3×1	0.30	0.900	2	6.8	16
3×4	0.30	0.904	2	6.8	15

while keeping w = 3 cm, the resonance frequency increases slightly because ϵ_e of the C-shaped MSA decreases.

The approximate resonance frequency of the antenna can be calculated by equating $(L_e + 2w) = \lambda/2$. However, for smaller slot dimensions, a better approximation could be obtained by taking the average of this length and the length of the RMSA without a slot, which gives $(L_e + w) = \lambda/2$. Here, L_e is the effective length of the patch and $\lambda = \lambda_o/\sqrt{\epsilon_e}$. The value of ϵ_e is to be calculated for the effective width along the length of the C-shaped MSA.

The radiation pattern of the C-shaped MSA is in the broadside direction. With an increase in the slot dimensions, the cross-polar level increases but remains below 15 dB. Also, directivity D and efficiency η of the antenna decrease due to the cancellation of the radiation between the outer and inner edges of the C-shaped MSA as shown in Figure 6.17(d).

Instead of the rectangular slot, other shapes of slots, such as triangular and curvilinear, could be used. However, the shape of the aperture has a small effect on the resonance frequency and the input impedance of the antenna [15].

6.6.2 H-Shaped MSA

An H-shaped MSA, shown in Figure 6.18(a), is obtained by cutting equal slots along both the nonradiating edges of the RMSA [16]. The outer dimensions ($L \times W$) of the H-shaped MSA are taken as 6 cm × 4 cm, which are the same as that of the C-shaped MSA. The feed point is positioned at the middle of the width, so that the orthogonal mode does not get excited. The antenna is analyzed using IE3D for various slot dimensions, and the results are summarized in Table 6.9. As the slot width w is increased, the

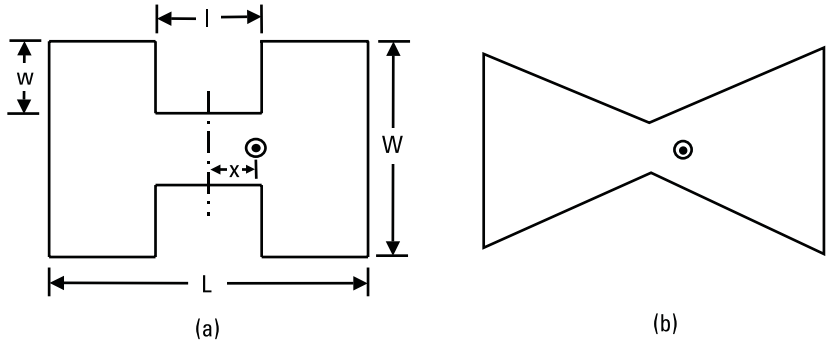

Figure 6.18 (a) H-shaped MSA and (b) bowtie MSA.

Table 6.9
Effect of the Slot Dimensions on the Performance of an H-Shaped MSA
(L = 6 cm, W = 4 cm, ϵ_r = 2.33, h = 0.159 cm, and tan δ = 0.002)

$w \times l$ (cm, cm)	x (cm)	f_0 (GHz)	BW (MHz)	D (dB)	η (%)
0 × 0	0.70	1.606	12	7.2	79
0.5 × 1	0.60	1.495	9	7.1	73
1 × 1	0.40	1.309	5	7.0	59
1.5 × 1	0.25	1.061	2	6.9	32
1.5 × 2	0.25	0.981	2	6.9	25
1.5 × 4	0.30	1.001	2	6.9	25

feed point x is shifted toward the center for impedance matching. With an increase in w from 0.5 cm to 1.5 cm (keeping l = 1 cm), the resonance frequency decreases from 1.495 GHz to 1.061 GHz, but BW decreases drastically from 9 MHz to 2 MHz and η decreases from 73% to 32%. When the length of the slot l is increased from 1 cm to 4 cm (keeping w = 1.5 cm), the resonance frequency decreases slightly from 1.061 GHz to 0.981 GHz and then increases slightly to 1.001 GHz. The approximate resonance frequency can be calculated by equating $(L_e + 2w) = \lambda/2$. However, for smaller slot dimensions, a better approximation is obtained by taking the average of this length and the length of the RMSA without a slot, which gives $(L_e + w) = \lambda/2$.

A bowtie MSA configuration is a variation of the H-shaped MSA [17]. In this case, two triangular shaped slots are cut along the nonradiating edges

of the RMSA as shown in Figure 6.18(b). The effects of varying the triangular slot dimensions are similar to that of the H-shaped MSA.

6.6.3 Rectangular Ring MSA

A *rectangular ring MSA* (RRMSA) is formed when a rectangular slot is cut in the center of the RMSA as shown in Figure 6.19(a) [16]. With an increase in the slot dimensions, the RMSA becomes RRMSA and then a printed loop antenna, and the resonance frequency decreases [18]. The results obtained using IE3D for various values of slot dimensions w and l are summarized in Table 6.10. For L = 6 cm and W = 4 cm, as ($w \times l$) are

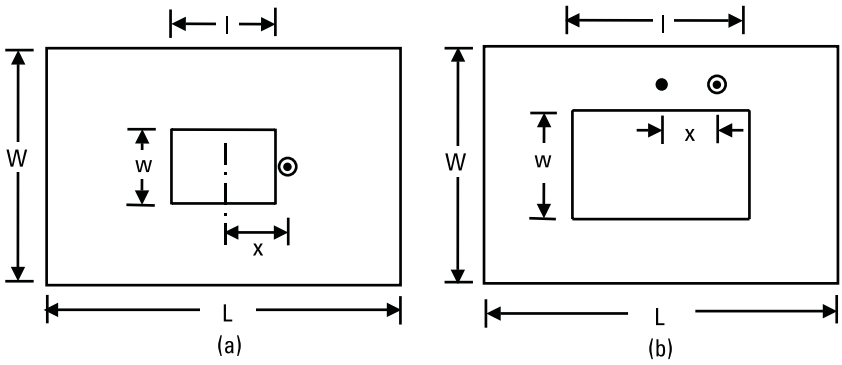

Figure 6.19 (a) RRMSA and (b) RRMSA with short.

Table 6.10
Effect of the Slot Dimensions on the Performance of the RRMSA
(L = 6 cm, W = 4 cm, ϵ_r = 2.33, h = 0.159 cm, and tan δ = 0.002)

$w \times l$ (cm, cm)	x (cm)	f_0 (GHz)	Z_{in} (Ω)	BW (MHz)	η (%)
0×0	0.70	1.606	62	12	79
0.5×0.5	0.32	1.595	56	10	78
1×0.5	0.32	1.560	56	11	77
1×1	0.57	1.537	125	—	75
RRMSA with a shorting post					
1×1	0.55	1.541	51	10	76
2×2	0.40	1.324	54	5	60
2×3	0.4	1.314	50	5	59
2×4	0.45	1.348	57	5	61

increased from (0, 0) to (1 cm, 1 cm), the resonance frequency decreases from 1.606 GHz to 1.537 GHz, because the path length of the surface current increases due to an increase in the slot dimensions. The approximate resonance frequency of the RRMSA can be calculated by equating $(L + w) = \lambda/2$. When the slot dimensions are small, a better approximation is obtained by equating $(L_e + w/2) = \lambda/2$.

For the larger slot dimensions, the input impedance is very large and it is difficult to match with the 50-Ω coaxial line. Therefore, a shorting post is placed in the center of one of the sides, and then impedance matching is obtained by placing the feed near the shorting post as shown in Figure 6.19(b). This shorting does not alter the overall field distribution around the periphery, and hence the resonance frequency remains almost the same. The optimized feed point and the BW for different slot dimensions for the RRMSA with a short are also given in Table 6.10.

The radiation pattern of the RRMSA is similar to that of an RMSA. With an increase in the slot dimensions, the directivity of the antenna remains around 7.1 dB, but the efficiency decreases, resulting in a decrease in the gain of the antenna.

The comparison of RMSA and the other configurations, which are obtained by cutting a slot in the RMSA, is shown in Table 6.11. The outer dimensions are kept constant in all the cases and the total slot area is kept approximately the same. The C-shaped MSA is the most compact configuration but it has the worst efficiency, and the RRMSA gives the least reduction in frequency but has the higher efficiency and hence larger gain.

6.7 Slot- and Short-Loaded MSAs

It has been observed in Sections 6.2–6.4 that by using shorting posts, the resonance frequency reduces. Also, by cutting a slot in the patch, the frequency

Table 6.11
Comparison of Various MSA Configurations with and Without Slot
(L = 6 cm, W = 4 cm, ϵ_r = 2.33, h = 0.159 cm, and tan δ = 0.002)

Type of MSA	Slot Dimensions $w \times l$ (cm)	f_0 (GHz)	BW (MHz)	D (dB)	η (%)
Rectangular	0 × 0	1.606	12	7.2	79
C-shaped	3 × 1	0.900	2	6.8	16
H-shaped	1.5 × 1	1.061	2	6.9	32
Rectangular Ring	1.8 × 1.7	1.378	6	7.1	64

of the MSA is reduced as described in Section 6.6. The resonance frequency reduces significantly if both of these techniques are combined. However, the BW and gain of these antennas reduce due to a decrease in the effective aperture area.

6.7.1 Shorted C-Shaped MSA

As discussed earlier, the C-shaped antenna is a compact configuration as compared to the RMSA. A C-shaped MSA with one of its narrow edges partially shorted is shown in Figure 6.20. The resonance frequency of the C-shaped MSA is reduced by approximately half, when this edge is fully shorted (i.e., $w_s = (L - l)/2$. The dimensions of the shorted patch are $L = 6$ cm, $W = 4$ cm, and $l = w = 2$ cm. Shorting posts of diameter 0.1 cm have been used. The antenna is fabricated on a substrate with $\epsilon_r = 4.3$, $h = 0.159$ cm, and $\tan \delta = 0.02$. The MNM is used to analyze the antenna. The theoretical and measured resonance frequencies are 438 MHz and 411 MHz, respectively.

The resonance frequency of the antenna is further reduced by partially shorting the edge. The theoretical and measured resonance frequencies for various shorting widths w_s are given in Table 6.12. As the shorting width w_s decreases from 2 cm to a single short, the measured resonance frequency decreases from 411 MHz to 367 MHz [19, 20]. The area of a C-shaped MSA with a single short is 1/16.7 of that of the RMSA operating at the same resonance frequency.

6.7.2 Shorted H-Shaped MSA

A shorted H-shaped MSA shown in Figure 6.21(a) is also a compact configuration [21]. One of the radiating edges of the antenna is shorted by 10

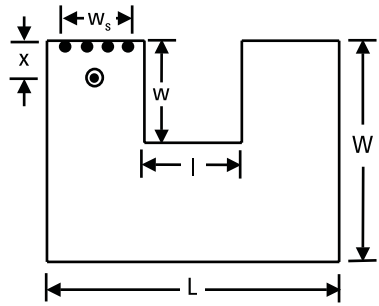

Figure 6.20 Partially shorted C-shaped MSA.

Table 6.12
Resonance Frequency f_0 for Partially Shorted C-Shaped MSA for Various Values of w_s

w_s (cm)	Theoretical f_0 (MHz)	Measured f_0 (MHz)
Single short	368	367
0.6	401	394
1.2	418	409
1.6	428	410
2.0	438	411

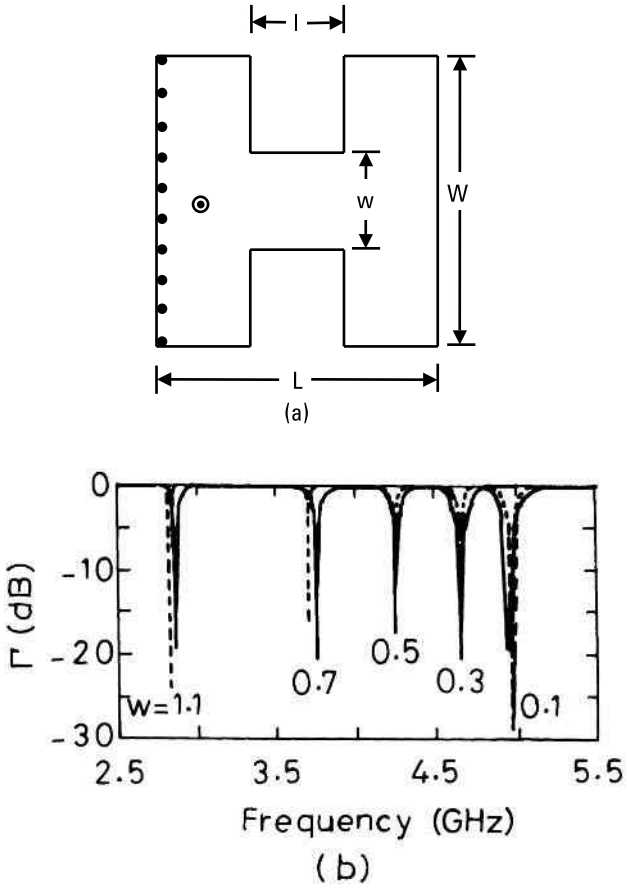

Figure 6.21 (a) Shorted H-shaped MSA and (b) its reflection coefficient Γ for various values of w: (- - -) theoretical and (——) measured.

shorting posts of diameter 0.1 cm. The antenna is fabricated on substrate with ϵ_r = 2.2 and h = 0.0508 cm. The outer dimensions of the antenna are L = 0.955 cm and W = 1.1 cm. For slot length l = 0.455 cm and different values of slot depth w, the theoretical and measured reflection coefficients Γ are shown in Figure 6.21(b). As w increases from 0.1 cm to 1.1 cm, the resonance frequency decreases from approximately 5.0 GHz to 2.86 GHz (i.e., by more than 40%). For all the cases, the radiation pattern is in the broadside direction with a cross-polar level better than 17 dB.

6.8 Planar Broadband Compact MSAs

The compact MSAs described in earlier sections have a smaller BW and gain compared to the regularly shaped MSA due to their smaller size. The BW of these compact MSAs can be increased by using a thicker substrate or by using the planar multiresonator technique [22] or by stacking them in the multilayer configuration as described in Chapters 3 and 4, respectively. In the planar multiresonator technique, the compact coaxially fed element is gap- or hybrid-coupled to the compact parasitic elements. These hybrid-coupled configurations also give dual-frequency operation, which is discussed in Chapter 7.

6.8.1 Coupled Shorted RMSA

The BW of the RMSA has been increased by feeding one patch and gap-coupling other patches along the radiating or the nonradiating edges as described in Chapter 3. The problem is that the size of the antenna becomes too large. Therefore, if compact RMSAs are coupled, their overall size will still be small, but BW will increase.

6.8.1.1 Radiating Edge Gap-Coupled Shorted RMSA

Two shorted RMSAs that are gap-coupled along one of their radiating edges are shown in Figure 6.22(a). Both the patches are identical having L = 2.3 cm and W = 4.6 cm. A shorting post of diameter 0.1 cm is placed at the center of the extreme edges along the width of the two patches as shown in Figure 6.22(a). Only one patch is fed at x = 0.65 cm, and the other patch is parasitically coupled with a gap of s = 0.1 cm. The antenna is fabricated on a low-cost glass-epoxy substrate having ϵ_r = 4.3, h = 0.159 cm, and tan δ = 0.02 [23]. The measured input impedance and VSWR plots are shown in Figure 6.22(b, c). The loop is within the VSWR = 2 circle and

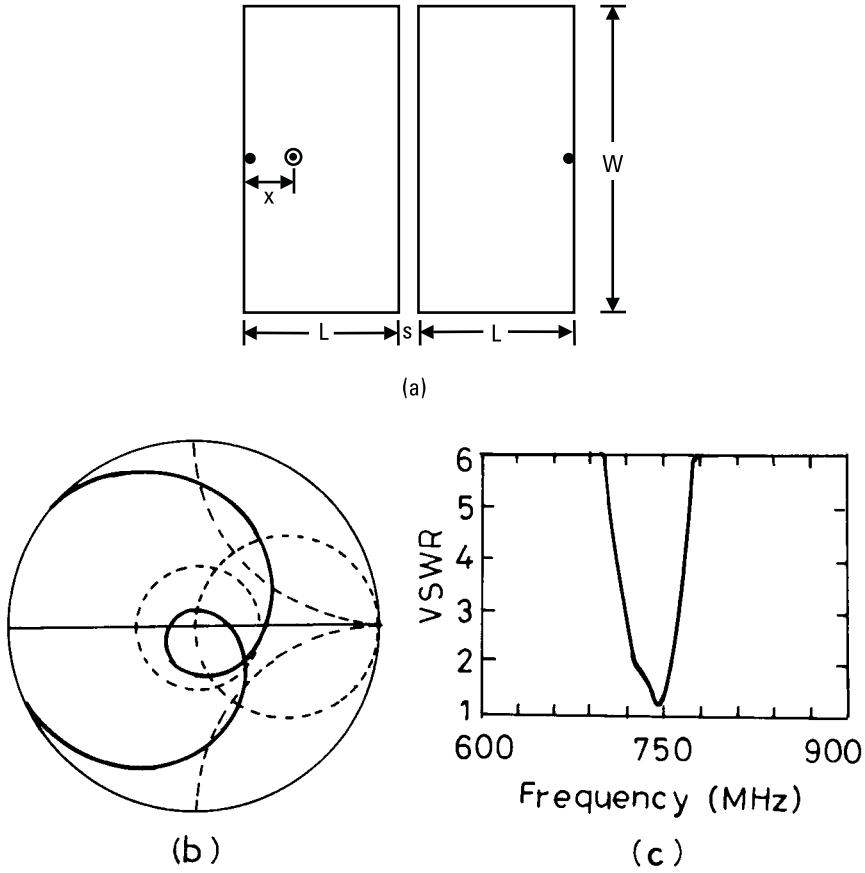

Figure 6.22 (a) Radiating edge gap-coupled shorted RMSA and its measured (b) input impedance and (c) VSWR plots.

the BW is 30 MHz (4%). This BW is 2.5 times of the corresponding shorted RMSA. The radiation pattern remains in the broadside direction with higher cross-polarization than the RMSA.

6.8.1.2 Nonradiating Edge Hybrid-Coupled Shorted RMSA

Two shorted RMSAs are coupled along the nonradiating edges as shown in Figure 6.23. The two RMSAs are identical having L = 4.6 cm and W = 2.3 cm. Only one patch is fed at y = 0.35 cm. When the patches are only gap-coupled with s = 0.1 cm, no loop is formed in the impedance plot, because of reduced coupling between the nonradiating edges. To enhance the coupling, either gap can be reduced or a shorting strip can be used.

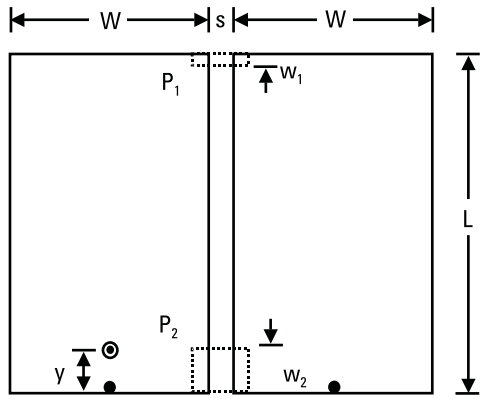

Figure 6.23 Nonradiating edge hybrid-coupled shorted RMSA.

Since the field is not uniform along the nonradiating edges, the coupling depends upon the location of the shorting strip and its width. When the shorting strip is placed at P_1, a broad BW of 36 MHz (4.9%) is obtained for the shorting strip width w_1 = 0.2 cm. A thicker shorting strip w_2 is required at P_2 because the field is smaller at this location. For w_2 = 0.8 cm a BW of 30 MHz is obtained [23].

6.8.2 Broadband Gap-Coupled Shorted 90°-Sectoral MSA

Two gap-coupled shorted 90°-sectoral MSAs of radius a = 3 cm with a gap s = 0.15 cm are shown in Figure 6.24(a). The antenna is fabricated on a glass-epoxy substrate. The shorting is done with closely spaced posts having a diameter of 0.04 cm. For y = 0.75 cm, the measured input impedance and VSWR plots are shown in Figure 6.24(b, c). The BW is 69 MHz at 1.358 GHz. The loop in the input impedance plot can be brought near the center of the Smith chart by reducing the parasitic patch dimensions slightly. For comparison, the response of a CMSA of radius a = 3 cm with a feed point at 1.1 cm from the center, is also given in Figure 6.24. The BW of the CMSA is 28 MHz at 1.375 GHz. Therefore, the BW of the gap-coupled configuration is almost 2.5 times of that of the CMSA, and its area is nearly half of that of the CMSA.

The measured radiation pattern in the E- and H-planes of the gap-coupled shorted 90°-sectoral MSA at the center frequency is compared with that of the CMSA in Figure 6.25. The copolar radiation pattern of the two antennas is similar. However, the cross-polar level of the gap-coupled antenna is higher than that of the CMSA [24].

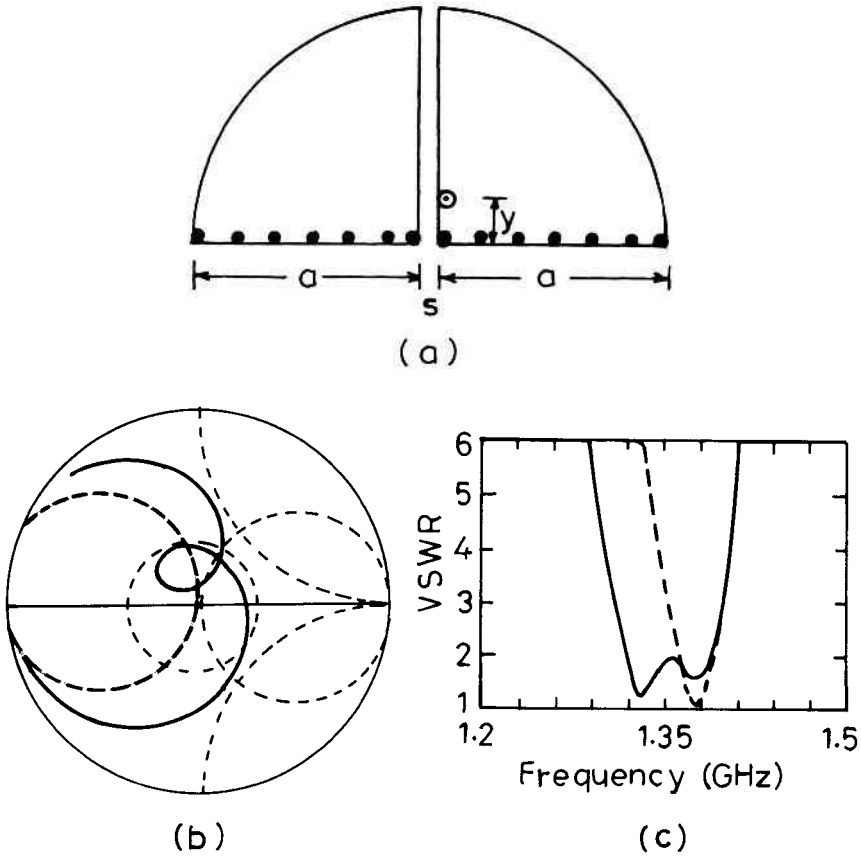

Figure 6.24 (a) Broadband gap-coupled shorted 90°-sectoral MSA and its measured (b) input impedance and (c) VSWR plots: (——) gap-coupled shorted 90°-sector and (- - -) CMSA.

Section 6.1 explained that the resonance frequency of the shorted 90°-sectoral antenna decreases with a decrease in the number of shorting posts and that it is at a minimum when a single shorting post is used in the middle of the uncoupled straight edge. When two sectoral MSAs with a single short are coupled with a gap of 0.15 cm, a BW of 41 MHz is obtained at 784 MHz, thereby realizing a compact configuration with a BW of 5.2% [24, 25].

6.8.3 C-Shaped MSA Coupled with a Shorted RMSA

Instead of using two identical compact patches, different compact patches could be coupled to increase the BW and retain the overall compactness of

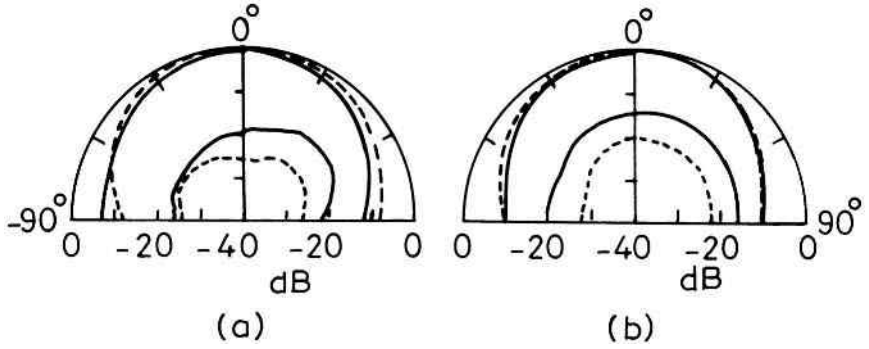

Figure 6.25 Measured radiation pattern in the (a) E- and (b) H-planes: (——) gap-coupled shorted 90°-sectoral MSA and (- - -) CMSA.

the antenna. A C-shaped MSA is gap-coupled to the shorted RMSA as shown in Figure 6.26(a). The antenna is fabricated on a low-cost glass-epoxy substrate. Only the shorted RMSA is fed, and the C-shaped MSA is parasitically coupled. To excite the fundamental mode of the C-shaped MSA, a shorting strip is used. To obtain broad BW, various parameters to be optimized are patch dimensions, the number of shorting posts, the gap between the patches, the width and location of the shorting strip, and the feed-point location. For the optimized dimensions given in Figure 6.26(a), the measured input impedance and VSWR plots are shown in Figure 6.26(b, c). A BW of 34 MHz (5%) is obtained. The radiation pattern is in the broadside direction with a higher cross-polarization.

The area of this gap-coupled configuration is 27 cm^2. On the other hand, with same area, an RMSA of $L = 6$ cm and $W = 4.5$ cm has a resonance frequency of 1.196 GHz and a BW of 22 MHz. Thus, the gap-coupled configuration gives a 43% reduction in the resonance frequency with more BW [26].

6.8.4 C-Shaped MSA with a Matching Network

Instead of placing a shorted RMSA within the slot of the C-shaped MSA, a LC resonant circuit also known as a matching network is connected as shown in Figure 6.27(a) [27]. The thin line represents the series inductance, whereas the thick line represents the shunt capacitance. The matching network is designed in such a way that it provides capacitive impedance below the resonance frequency of the unloaded patch, and inductive impedance above that frequency. As a result, the patch has two close resonance frequencies in the lower and upper sides of its unloaded resonance frequency giving

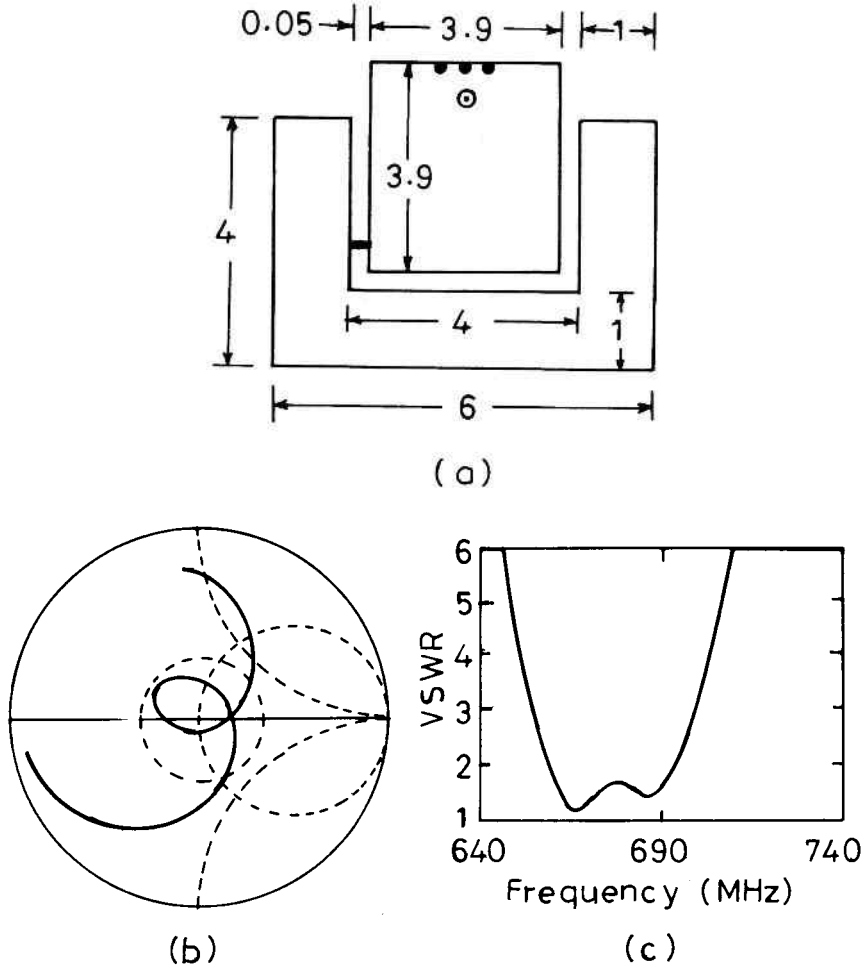

Figure 6.26 (a) C-shaped MSA gap-coupled to shorted RMSA and its measured (b) input impedance and (c) VSWR plots.

rise to broad BW. The transmission line model is used to analyze and design the antenna. The optimized dimensions in centimeters are shown in Figure 6.27(a). The substrate parameters are ϵ_r = 4.8 and h = 0.052 cm. The reflection coefficient Γ plots for the loaded and unloaded C-patch are shown in Figure 6.27(b). The loaded configuration yielded a BW of 75 MHz at the center frequency of 1.345 GHz as compared to 15 MHz for unloaded C-patch. The radiation is in the broadside direction and the cross-polarization levels are 17 dB below the copolar levels.

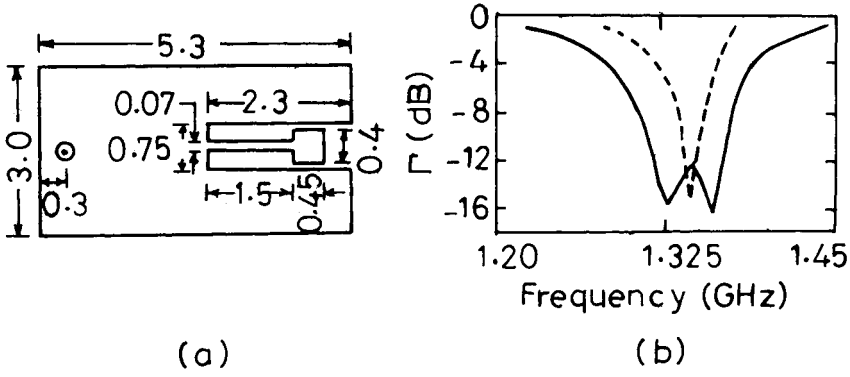

Figure 6.27 (a) C-shaped MSA with matching network and (b) reflection coefficient Γ plots for (——) loaded and (- - -) unloaded C-shaped MSA.

6.8.5 Circular Ring Containing a Shorted CMSA

The resonance frequency of a circular ring is much smaller than a CMSA as described in Chapter 2. However, the BW of a circular ring MSA is also small. To increase its BW without increasing its surface area, a shorted CMSA is placed inside the ring as shown in Figure 6.28(a). The CMSA is shorted so that its resonance frequency is close to that of the ring MSA. Only the shorted CMSA is fed using an SMA connector and the ring is gap-coupled. The optimized dimensions for ϵ_r = 1.13, h = 0.5 cm, and

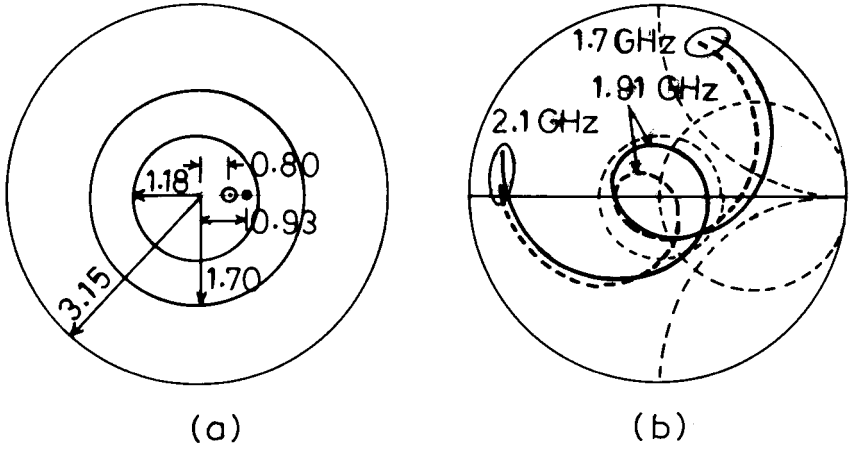

Figure 6.28 (a) Circular ring containing a shorted CMSA and (b) its input impedance plot: (——) theoretical and (- - -) measured.

tan δ = 0.001 are given in Figure 6.28(a). The radius of the shorting post is 0.033 cm. The measured and theoretical input impedance loci are shown in Figure 6.28(b). The theoretical results are obtained using the spectral domain electric field integral equation technique [28]. The measured BW is 6.8% at 1.9 GHz with a gain of 8.4 dB. This configuration is compact and gives wider BW as compared to the conventional CMSA.

6.8.6 Rectangular Ring Containing a Shorted RMSA

Similar to the gap-coupled circular ring MSA, a rectangular ring is gap-coupled to the shorted RMSA as shown in Figure 6.29(a) [29]. The optimized dimensions in centimeters for a glass-epoxy substrate are shown in Figure 6.29(a). The measured input impedance and VSWR plots are shown in Figure 6.29(b, c). The BW is 36 MHz centered at 842 MHz. This configuration gives a 30% reduction in the resonance frequency with twice the percentage BW as compared to the conventional RMSA.

6.8.7 Three Gap-Coupled Shorted C-Shaped MSA

Three compact shorted C-shaped patches are gap-coupled as shown in Figure 6.30(a) [30]. Only the central patch is fed; the other two patches are parasitically coupled. A large number of parameters are optimized to obtain broad BW. The most sensitive design parameters are the lengths of the fed and parasitic elements and the dimensions and the location of the apertures. The width of the partial short circuit and the location of the feed point have a strong effect on the input impedance of the antenna. The dimension of the ground plane has a significant effect on the performance of the antenna. Truncating the ground plane improves the isotropic characteristics of the radiation pattern, increases its sensitivity to horizontal and vertical polarized waves, and reduces the effect of human body on the antenna if mounted on a portable handset. The antenna is fabricated on a substrate with ϵ_r = 2.2 and h = 0.23 cm and the optimized dimensions are shown in Figure 6.30. The ground plane size is only 0.1 cm larger from all the sides of the gap-coupled patches.

The measured input impedance and return loss $|\Gamma|$ of the antenna are shown in Figure 6.30(b, c). The resonance frequency is around 900 MHz, and the BW is 40 MHz. Figure 6.31 shows the vertical and horizontal polarized radiation pattern at 900 MHz. The antenna is sensitive to both the polarizations, and the pattern is nearly isotropic. The variation of the pattern over the BW is very small. The total size of this antenna is much smaller than the conventional half-wavelength RMSA.

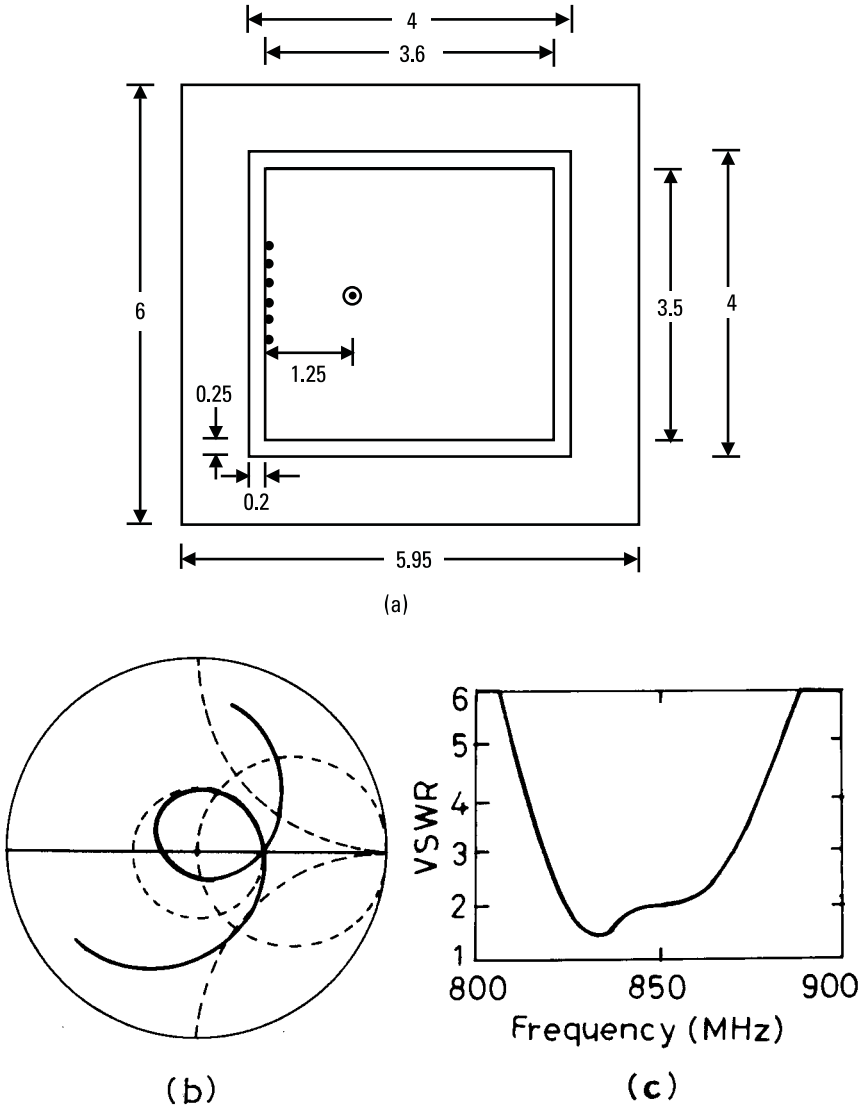

Figure 6.29 (a) Rectangular ring gap-coupled to a shorted RMSA and its measured (b) input impedance and (c) VSWR plots.

6.9 Broadband Stacked Compact MSAs

Instead of using compact MSAs in planar multiresonator configurations, the compact antennas can be stacked for BW enhancement. The stacked

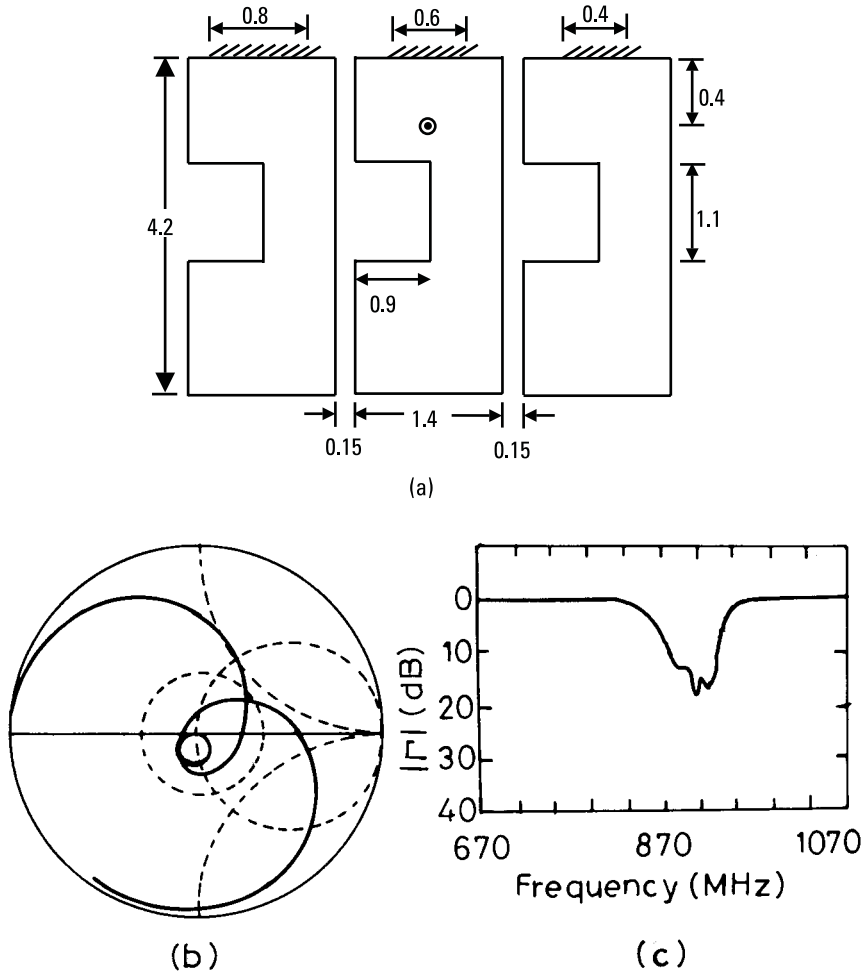

Figure 6.30 (a) Three gap-coupled shorted C-shaped MSA, and its (b) input impedance and (c) return loss $|\Gamma|$ plots.

configuration does not increase the planar area, but the thickness of the antenna increases.

The side and top views of a stacked shorted RMSA configuration are shown in Figure 6.32(a, b). The two patches are shorted using a single shorting post. The bottom patch is fed by a coaxial feed, which is extended and soldered to both the patches. Both these patches are fabricated on a thin RT Duroid 5880 substrate of thickness 0.0125 cm and supported by foam with $\epsilon_r = 1.07$. The shorting post radius is taken as 0.0325 cm. The

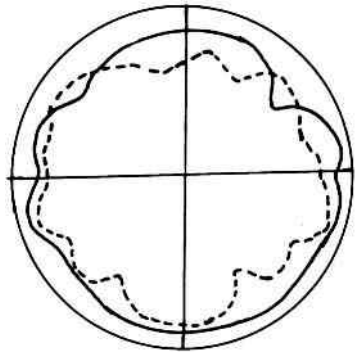

Figure 6.31 Radiation pattern of three gap-coupled shorted C-shaped MSA at 900 MHz: (——) vertical and (- - -) horizontal polarizations.

optimized dimensions of the configuration are given in Figure 6.32. The theoretical and measured input impedance loci are shown in Figure 6.32(c). The theoretical and measured BW is 32% and 34%, respectively. The measured radiation pattern in the E- and H-planes is shown in Figure 6.32(d), which is similar to that of the monopole antenna on a finite ground plane. The measured gain is more than 3.9 dB across the BW [31].

Similarly, other compact configurations using a single short or with a slot, such as rectangular ring and C-shaped patches, can be stacked to yield a broad BW [18].

6.10 Broadband MSAs with a U-Slot

It is observed in Section 6.6 that by cutting a slot inside or along the periphery of the RMSA, various compact configurations are realized with a reduced BW. If the resonance frequencies of the slot and the patch are close to each other, then broad BW could be obtained. However, care must be taken so that the polarization of the radiated field of the slot and the patch are similar, so that the pattern remains stable over the VSWR BW.

6.10.1 RMSAs with a U-Slot

A very promising configuration that yields broad BW is a RMSA with a U-shaped slot [32–36]. A resonant U-slot is cut symmetrically around the center of the patch. When a slot is cut inside the patch, the resonance frequency of the patch changes slightly in comparison with the resonance

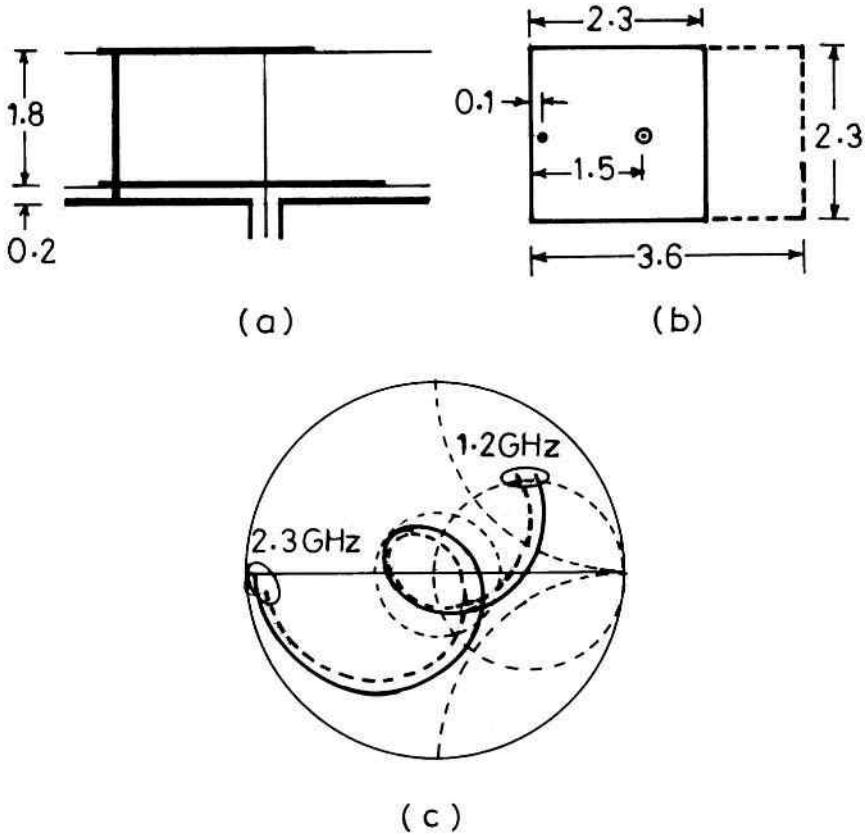

Figure 6.32 Stacked shorted RMSA: (a) side and (b) top views, (c) input impedance plots [(——) theoretical and (- - -) measured], and (d) measured radiation pattern [(——) E-plane and (- - -) H-plane.]

frequency of the slot. Accordingly, the dimensions of the slot are chosen such that its resonance frequency is close to that of the rectangular patch with a slot. A thick foam substrate of thickness $h = 2.7$ cm, which corresponds to 0.08λ at 0.9 GHz, is used to obtain a broad BW. All the dimensions, shown in Figure 6.33(a), are in centimeters. The measured input impedance and VSWR plots are shown in Figure 6.33(b, c). The measured BW is 47%. The wide BW is due to the appearance of two loops in the impedance plot representing the coupling between the rectangular patch and the U-slot. The resonance frequency of the RMSA with a U-slot is primarily determined by the length of the patch, and the position of the loop in the impedance plot primarily depends upon the total length of the U-slot. The loop in the lower

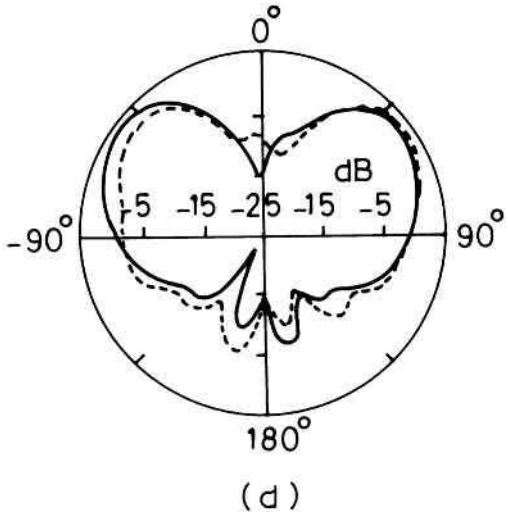

Figure 6.32 (Continued.)

frequency region is due to the resonance of the U-slot. The loop in the higher frequency region is due to the excitation of the second-order mode of the patch, when width W = 21.97 cm becomes equal to λ.

It may be noted from Figure 6.33(b) that there is no appreciable inductive component associated with the input impedance. On the other hand, for the RMSA without a U slot, there would be large inductive reactance in the input impedance of the patch, because the substrate is electrically thick and even if the feed point is shifted to the edge of the patch, it is not possible to achieve impedance matching. So, a U-slot adds a capacitive component in the input impedance that compensates for the inductive component of the coaxial probe.

The radiation pattern in the E- and H-planes at 0.9 GHz is shown in Figure 6.34. The H-plane pattern remains in the broadside direction at all the frequencies within the BW. In the E-plane, on the other hand, the maxima shifts from the broadside as the frequency increases within the BW, and the pattern becomes conical at the second loop corresponding to 1.2 GHz. Therefore, the useful BW from the pattern point of view is slightly less than the impedance BW. The HPBW in the H-plane is 59° at 0.812 GHz and 57° at 1.1 GHz. In the E-plane, it is 65° at 0.812 GHz and 70° at 1.1 GHz.

Since the second loop in the impedance plot corresponds to the width W becoming equal to λ, it can be shifted away by simply reducing W, which also reduces the size of antenna.

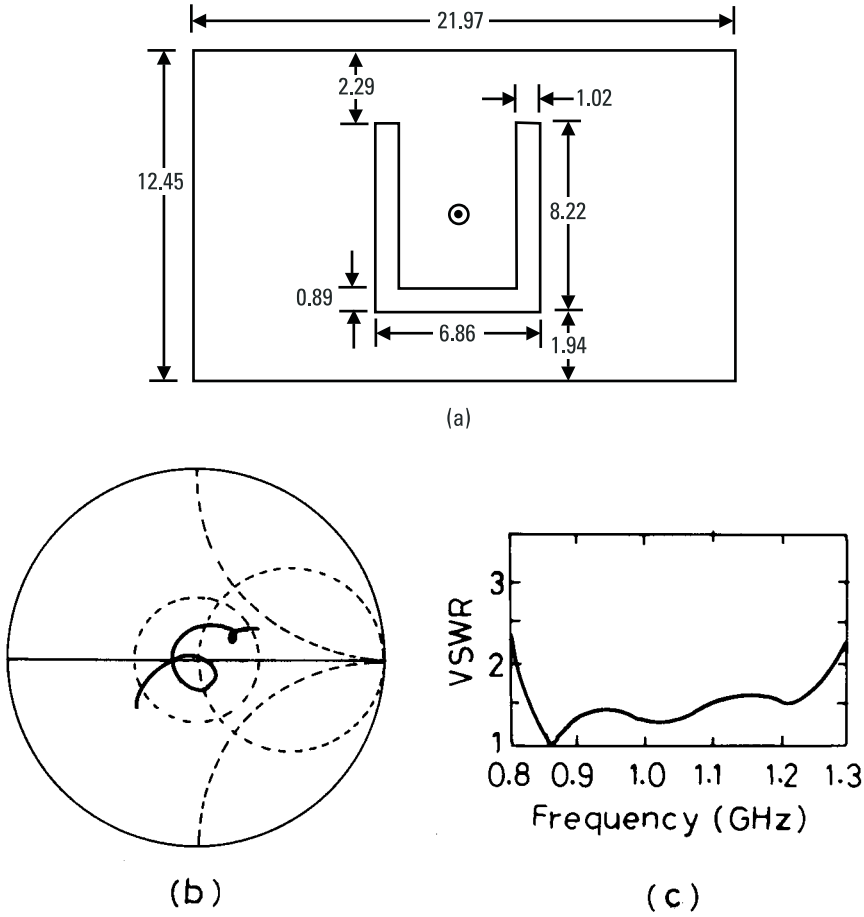

Figure 6.33 (a) RMSA with a U-slot and its measured (b) input impedance and (c) VSWR plots.

By using two U-slots in the RMSA as shown in Figure 6.35, and optimizing the slot dimensions, two loops appear in the Smith chart. These loops are due to the excitation of the inverted and noninverted slots. All the dimensions are given in Figure 6.35. The antenna is fabricated on a foam substrate with thickness h = 1.65 cm. The measured BW is 700 MHz (44%). The radiation pattern over the entire BW remains in the broadside direction [37]. Above configurations use coaxial feed. The coaxial feed can be replaced with an L-shaped probe, as described in Chapter 2, to further increase the BW [38].

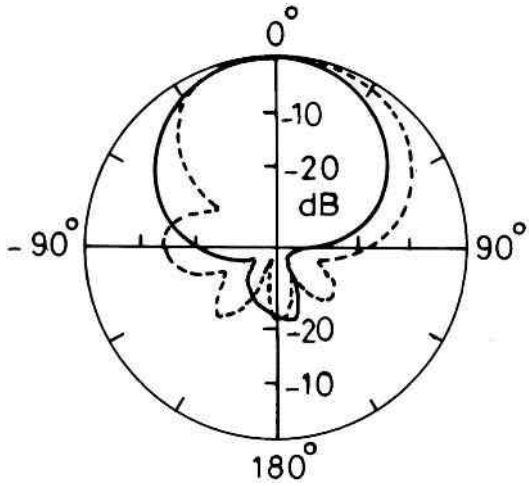

Figure 6.34 Radiation pattern of an RMSA with a U-slot at 0.9 GHz: (——) E-plane and (- - -) H-plane.

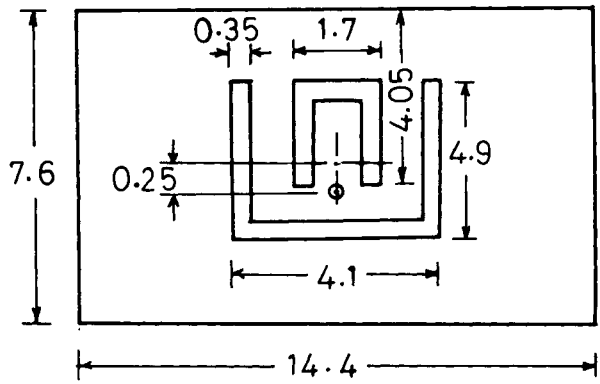

Figure 6.35 An RMSA with two U-slots.

6.10.2 CMSA with a U-Slot

Instead of cutting a U-shaped slot in the rectangular patch, it can be cut inside the circular patch as shown in Figure 6.36 [39]. The circular patch with a U-slot is fabricated on the low-cost *printed circuit board* (PCB) substrate in the inverted suspended configuration. As a result, the top layer acts as a protective superstrate layer. The inverted patch is supported by a foam substrate with h = 0.5 cm. An impedance BW for VSWR ≤ 2 is from

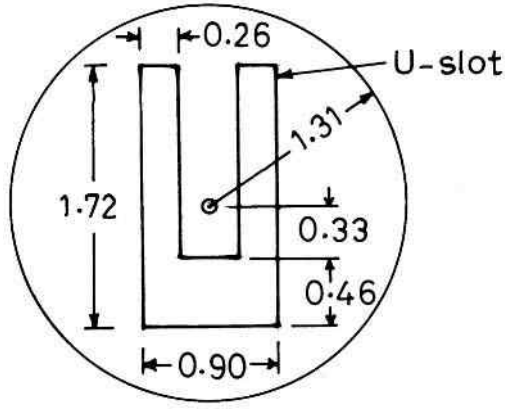

Figure 6.36 CMSA with a U-slot.

3.77 GHz to 4.78 GHz (24%). The gain is about 7 dB at a frequency of 4 GHz.

6.10.3 TMSA with a U-Slot

Similar to the RMSA and CMSA with a U-slot, an ETMSA with a U-slot as shown in Figure 6.37(a) also yields a broad BW [40]. A foam substrate of thickness 1.43 cm ($0.08\lambda_0$) is used. The measured return loss Γ plot is shown in Figure 6.37(b), and the measured BW is 18%. The resonance frequency for the fundamental mode of ETMSA without a slot is approximately 1.8 GHz. Due to the presence of the slot, its frequency reduces and two adjacent modes are excited at 1.563 GHz and 1.746 GHz. The higher resonance frequency is more sensitive to the variation in the horizontal length of the slot, and the lower resonance frequency strongly depends upon the total length of the U-shaped slot. The radiation pattern is in the broadside direction over the entire BW. However, higher cross-polarization radiation is observed in the H-plane.

Similar results are obtained when a U-slot is cut inside an ITMSA with flare angle α = 53.9°. The length of the horizontal slot and width of the parallel slot are reduced to adjust the occurrence of the two adjacent resonant modes for broadband operation. The measured BW is 304 MHz (17.8%) at the center frequency of 1,709 MHz. The radiation characteristics are similar to that of the ETMSA with a U-slot [40].

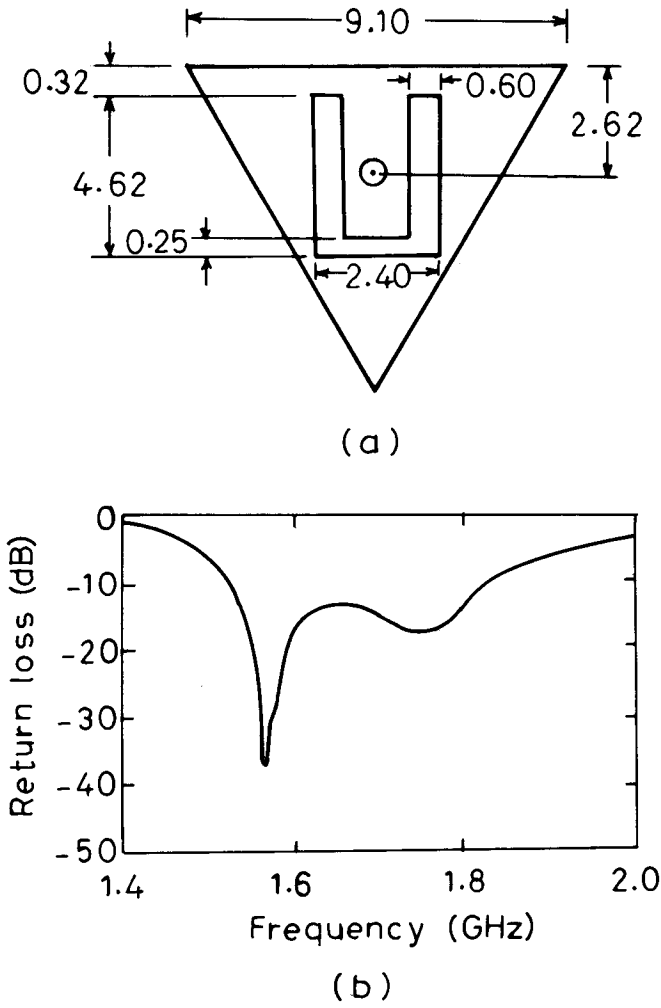

Figure 6.37 (a) TMSA with a U-slot and (b) its measured return loss plot.

6.11 Summary

Compact antennas are required for applications where limited antenna real estate is available. A compact MSA is realized by increasing the dielectric constant of the substrate, by using shorting posts, or by cutting a slot. Compact MSAs are realized by shorting along the zero potential line of the RMSA, CMSA, ETMSA, and 30°-60°-90° TMSA. The resonance frequency of the shorted RMSA decreases with a decrease in the shorting width and

is minimum for a single shorting post. Similarly, C- and H-shaped MSAs and RRMSAs are realized by cutting a slot in the RMSA. When both of these techniques (i.e., shorting and cutting slot) are combined, a very compact MSA is realized. Shorted C- and H-shaped MSAs fall in this category. However, the BW and gain of these antennas are significantly lower.

The BW of the compact MSAs is increased by using multiple resonators in planar configurations. Various shorted RMSAs, 90°-shorted sectors, and shorted C and ring antennas are gap- or hybrid-coupled to achieve a broad BW. The multiresonator concept is also used in a stacked configuration to obtain a broad BW.

By cutting a U-slot in the rectangular, circular, and triangular MSA on a thick, low dielectric substrate, a broad BW is obtained. This antenna is most attractive as it yields a large BW without increasing the surface area and with stable radiation characteristics over the entire BW.

References

[1] Hirasawa, K., and M. Haneishi, *Analysis, Design, and Measurement of Small and Low-Profile Antennas,* Norwood, MA: Artech House, 1992.

[2] James, J. R., and P. S. Hall, *Handbook of Microstrip Antennas,* Vol. 1, London: Peter Peregrinus, Ltd., 1989.

[3] IE3D 7.0, Zeland Software, Inc., Fremont, CA.

[4] Sanad, M., "Effect of the Shorting Posts on Short Circuit Microstrip Antennas," *IEEE AP-S Digest,* 1994, pp. 794–797.

[5] Satpathy, S., K. P. Ray, and G. Kumar, "Compact Microstrip Antennas Using a Single Shorting Post," *Proc. NSAML,* New Delhi, India, March 1998, pp. 69–72.

[6] Ray, K. P., et al., "Investigations on Shorted Rectangular Microstrip Antennas," *Proc. ELECTRO*-2000, BHU, Varanasi, India, January 2001, pp. 153–156.

[7] Satpathy, S., K. P. Ray, and G. Kumar, "Compact Shorted Variations of Circular Microstrip Antennas," *Electronics Letters,* Vol. 34, No. 2, 1998, pp. 137–138.

[8] Bahl, I. J., and P. Bhartia, *Microstrip Antennas,* Dedham, MA: Artech House, 1980.

[9] Waterhouse, R., "Small Microstrip Patch Antenna," *Electronics Letters,* Vol. 31, No. 8, 1995, pp. 604–605.

[10] Satpathy, S., G. Kumar, and K. P. Ray, "Compact Shorted Variations of Triangular Microstrip Antennas," *Electronics Letters,* Vol. 34, No. 8, 1998, pp. 709–711.

[11] Wong, K. L., and S. C. Pan, "Compact Triangular Microstrip Antenna," *Electronics Letters,* Vol. 33, March 1997, pp. 433–434.

[12] Wong, K. L., and Y. F. Lin, "Small Broadband Rectangular Microstrip with Chip Resistor Loading," *Electronics Letters,* Vol. 33, No. 19, 1997, pp. 1593–1594.

[13] Srinivasan, V., S. Malhotra, and G. Kumar, "Multiport Network Model for Chip-Resistor-Loaded Rectangular Microstrip Antennas," *Microwave Optical Technical Letters,* Vol. 24, No. 1, 2000, pp. 11–13.

[14] Kosiavas, G., et al., "The C-Patch: A Small Microstrip Element," *Electronics Letters,* Vol. 25, 1989, pp. 253–254.

[15] Sanad, M., "Double C-Patch Antennas Having Different Aperture Shapes," *IEEE AP-S Int. Symp. Digest,* 1995, pp. 2116–2119.

[16] Palaniswamy, V., and R. Garg, "Rectangular Ring and H Shape Microstrip Antenna—Alternative Approach to Rectangular Microstrip Antenna," *Electronics Letters,* Vol. 21, No. 19, 1985, pp. 874–876.

[17] George, J., et al., "New Compact Microstrip Antenna," *Electronics Letters,* Vol. 32, No. 6, 1996, pp. 508–509.

[18] Bafrooei P. M., and L. Shafai, "Characteristics of Single and Double Layer Microstrip Square Ring Antennas," *IEEE Trans. Antennas and Propagation,* Vol. AP-47, No.10, 1999, pp. 1633–1639.

[19] Srinivasan, V., "Multiport Network Model for Variations in Rectangular Microstrip Antennas," Ph.D. thesis, Indian Institute of Technology Bombay, India, 2000.

[20] Satpathy, S., et al., "Compact Microstrip Antennas for Personal Mobile Communication," *Proc. IEEE TENCON,* New Delhi, India, December 1998, pp. 245–247.

[21] Singh, D., P. Gardener, and P. S. Hall, "Miniaturized Microstrip Antenna for MMIC Application," *Electronics Letters,* Vol. 33, No. 22, 1997, pp. 1830–1831.

[22] Kumar, G., and K. C. Gupta, "Broadband Microstrip Antennas Using Additional Resonators Gap-Coupled to the Radiating Edges," *IEEE Trans. Antennas Propagation,* Vol. AP-32, 1984, pp. 1375–1379.

[23] Kapur, R., and G. Kumar, "Hybrid Coupled Shorted Rectangular Microstrip Antennas," *Electronics Letters,* Vol. 35, No. 18, 1999, pp. 1501–1502.

[24] Ray, K. P., and G. Kumar, "Compact Gap-Coupled Shorted 90° Sectoral Microstrip Antennas for Broadband and Dual-Band Operations," *Microwave Optical Tech. Letters,* Vol. 26, No. 3, 2000, pp. 143–145.

[25] Ray, K. P., "Broadband, Dual-Frequency and Compact Microstrip Antennas," Ph.D. thesis, Indian Institute of Technology, Bombay, India, 1999.

[26] Deshmukh, A., and G. Kumar, "Hybrid-Coupled Compact Variation of Rectangular Broadband Microstrip Antennas," *IEEE AP-S Int. Symp. Digest,* July 2000, pp. 1422–1425.

[27] Fayyaz, N., and S. S. Naeini, "Bandwidth Enhancement of a Rectangular Patch Antenna by Integrated Reactive Loading," *IEEE AP-S Int. Symp. Digest,* 1998, pp. 1100–1103.

[28] Kokotoff, D. M., R. B. Waterhouse, and J. T. Aberle, "An Annular Ring Coupled to Shorted Patch," *IEEE Trans. Antennas Propagation,* Vol. AP-45, No. 5, 1997, pp. 913–914.

[29] Deshmukh, A., and G. Kumar, "Shorted Compact Broadband Microstrip Antennas," *Proc. NCC-2000 Symp.,* Indian Institute of Technology, Delhi, India, 2000, pp. 49–52.

[30] Sanad, M., "A Wideband Microstrip Antenna for Portable Cordless Telephones," *IEEE AP-S Int. Symp. Digest,* 1995, pp. 1132–1135.

[31] Waterhouse R. B., "Broadband Stacked Shorted Patch," *Electronics Letters,* Vol. 35, No. 2, 1999, pp. 98–99.

[32] Huynh, T., and K. F. Lee, "Single Layer Single Patch Wideband Microstrip Antenna," *Electronics Letters,* Vol. 31, No. 16, August 1995, pp. 1310–1312.

[33] Lee, H. F., and W. Chen, *Advances in Microstrip and Printed Antennas,* New York: John Wiley & Sons, 1997.

[34] Lee, K. F., et al., "Experimental and Simulation Studies of the Coaxially Fed U-Slot Rectangular Patch Antenna," *IEE Proc. Microwaves, Antennas Propagation,* Pt-H, Vol. 144, No. 5, 1997, pp. 354–358.

[35] Clenet, M., and L. Shafai, "Multiple Resonances and Polarization of U-Slot Patch Antenna," *Electronics Letters,* Vol. 35, No. 2, 1999, pp. 101–103.

[36] Tong, K. F., et al., "A Broad-Band U-Slot Rectangular Patch Antenna on a Microwave Substrate," *IEEE Trans. Antennas Propagation,* Vol. AP-48, No. 6, 2000, pp. 954–960.

[37] Guo, Y. X., et al., "Double U-Slot Rectangular Microstrip Antenna," *Electronics Letters,* Vol. 34, No. 19, 1998, pp. 1805–1806.

[38] Luk, K. M., et al., "L-Probe Proximity Fed U-Slot Patch Antenna," *Electronics Letters,* Vol. 34, No. 19, 1998, pp. 1806–1807.

[39] Luk, K. M., K. F. Lee, and W. L. Tam, "Circular U-Slot Patch with Dielectric Superstrate," *Electronics Letters,* Vol. 33, No. 12, 1997, pp. 1001–1002.

[40] Wong, K. L., and W. H. Hsu, "Broadband Triangular Microstrip Antenna with U-Shaped Slot," *Electronics Letters,* Vol. 33, No. 25, 1997, pp. 2085–2087.

7

Tunable and Dual-Band MSAs

7.1 Introduction

Chapters 1–6 describe several broadband MSA configurations. In multichannel applications, a small instantaneous BW is required over a large frequency range. Accordingly, a tunable antenna provides an alternative to a broadband antenna in which an antenna with a small BW is tuned over a large frequency range. In some applications, the system must work within two frequency bands that are far apart. Here dual-band antennas rather than broadband antennas are used. Numerous applications such as satellite links, wireless local networks, cellular telephones, synthetic aperture radars, and radio frequency identification systems, require dual-frequency antennas. If the antenna operates only at two spot frequencies, then it is known as a dual-frequency antenna. When it operates over a finite BW at both of the frequencies, it is known as dual-band antenna. The requirements of tunable and dual-band antennas can be met using MSAs.

This chapter describes various tunable and dual-band MSA configurations. An MSA may be made tunable by connecting a variable reactive (inductive or capacitive) load to the patch. The variable reactance may be realized by changing the length of the small stub attached to the regular shaped MSA, or by changing the number or positions of the shorting posts. The tunabilty of the MSA is also achieved by integrating varactor or PIN diodes with the patch, and by varying their biasing conditions. The resonance frequency of the MSA can also be tuned by changing the air gap between the patch and the ground plane [1].

When two or more resonance frequencies of a MSA are close to each other, one gets broadband characteristics. When these are significantly separated, dual-band operation is obtained. In general, all the methods described in Chapters 3 and 4 for increasing the BW of the MSAs can be utilized to obtain dual-band operations.

Various single and multilayer MSA configurations for dual-band operations are possible. In the single-layer MSA, dual-band operation can be achieved by utilizing the multiresonance characteristics of a single patch, by reactively loading the patch with quarter-wavelength stubs, by using shorting posts, by cutting slots, and by adding lumped elements, among other techniques. Multiresonators in both planar and stacked configurations yield dual-band operations. Both electromagnetic as well as aperture coupling mechanisms are used in multilayer configurations.

7.2 Tunable MSAs

The resonance frequency of the MSA can be tuned by changing its resonant dimension. For the fixed dimensions of a patch, the same effect is achieved by reactively loading the patch. This section discusses these tuning methods.

7.2.1 Stub-Loaded Tunable MSAs

One of the techniques for obtaining tunability is to add a stub to an MSA. For a RMSA, the stub may be placed either along one of its radiating or nonradiating edges. When the length of the stub is small, it yields tunability, whereas when it is comparable to $\lambda/4$, it yields dual-frequency operation. The RMSA with a small stub for tuning the resonance frequency has been analyzed using MNM and IE3D [2–4]. Similarly, a CMSA with stubs also yields tunable and dual-band operation, which has been analyzed using an improved linear transmission line model [5–7].

7.2.1.1 Tunable RMSA with a Single Stub

An RMSA of length $L = 3$ cm and width $W = 4$ cm with a small stub of length l and width w is shown in Figure 7.1(a). The stub is placed at the center of one of the radiating edges of the RMSA. The substrate parameters are $\epsilon_r = 2.55$, $h = 0.159$ cm, and $\tan \delta = 0.001$. To account for the fringing fields from the stub-loaded RMSA, the periphery is extended outward as shown in Figure 7.1(b, c). The effect of the stub is to increase the overall effective resonant length of the RMSA from L_e to $L_e + \Delta l_1$. The value of

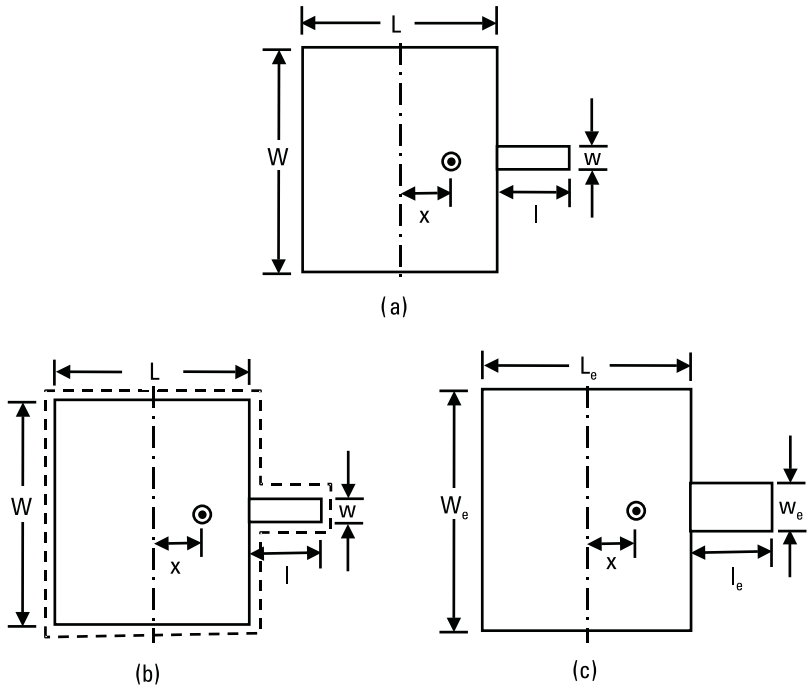

Figure 7.1 (a) RMSA with a single stub and its (b) edge extensions and (c) effective dimensions.

Δl_1 is obtained by equating the effective area of the stub ($= w_e \cdot l_e$) with that of the extension Δl_1 along the effective width of the RMSA as given below.

$$\Delta l_1 = w_e \cdot l_e / W_e \tag{7.1}$$

The values of w_e, l_e, and W_e are obtained from expressions given in Appendix B. The resonance frequency of the stub-loaded RMSA is approximately obtained by modifying (2.9) for the RMSA as

$$f_0 \approx \frac{c}{2(L_e + \Delta l_1)\sqrt{\epsilon_e}} \tag{7.2}$$

where L_e and ϵ_e are the effective length and effective dielectric constant corresponding to the rectangular patch.

The effect of the dimensions of the stub on the resonance frequency f_0 and BW for the feed point at $x = 0.7$ cm is given in Table 7.1. These

Table 7.1
Effect of Stub Dimensions on Resonance Frequency and BW of a Single Stub-Loaded RMSA (L = 3 cm, W = 4 cm, x = 0.7 cm, ϵ_r = 2.55, h = 0.159 cm, and tan δ = 0.001)

l (cm)	w (cm)	f_0 (GHz)	BW (MHz)
0.0	0.0	2.975	65
0.5	0.4	2.898	60
1.0	0.4	2.740	49
1.0	0.2	2.828	55
1.5	0.4	2.434, 3.377	23, 33

results are obtained using IE3D. As the length or the width of the stub increases, the resonance frequency decreases. For w = 0.4 cm, when the stub length l increases from 0 to 1.0 cm, the resonance frequency decreases from 2.975 GHz to 2.740 GHz, thereby giving a frequency tuning range of around 8%. Also, the corresponding BW decreases from 65 MHz to 49 MHz due to a decrease in the h/λ_0 ratio. With an increase in the stub length, the input impedance decreases slightly, because the effective center of the patch shifts toward the stub, and hence the distance between the center and the feed point decreases. When l is further increased to 1.5 cm, dual-band operation is obtained at 2.434 GHz and 3.377 GHz with a corresponding BW of 23 MHz and 33 MHz, respectively. The details of dual-band operation are described in the next section.

The decrease in the resonance frequency with an increase in stub length can also be explained in terms of an increase in the capacitance of the open-ended stub due to an increase in its length. Thus, the total capacitance of the equivalent patch increases and consequently the frequency decreases.

For l = 1 cm, when w decreases from 0.4 cm to 0.2 cm, its capacitance decreases and hence the resonance frequency increases from 2.740 GHz to 2.828 GHz. The value of frequency can also be calculated from (7.1) and (7.2).

The radiation pattern of a single stub-loaded RMSA is similar to that of the RMSA without a stub. However, the cross-polar levels increase with an increase in the stub length. This is due to the asymmetric loading of the patch. To reduce the cross-polar levels, the patch is symmetrically loaded with two equal stubs as described below.

7.2.1.2 Tunable RMSA with Two Stubs

An RMSA with two identical stubs placed at the center of its two radiating edges is shown in Figure 7.2. For w = 0.4 cm, the effect of the increase in

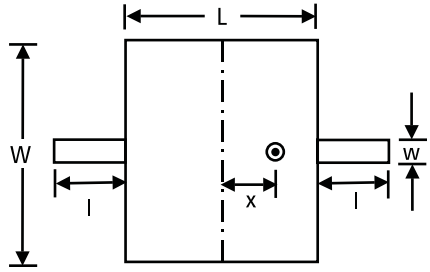

Figure 7.2 RMSA with two stubs.

the stub length l on the resonance frequency and BW of the antenna is given in Table 7.2. As in the case of single stub-loaded RMSA, with an increase in l, the resonance frequency decreases. In this case, the resonance frequency can be approximately calculated as:

$$f_0 \approx \frac{c}{2(L_e + 2\Delta l_1)\sqrt{\epsilon_e}} \tag{7.3}$$

It may be noted that Δl_1 is added on both the sides of the effective RMSA. With an increase in l from 0.0 to 1.5 cm, the resonance frequency decreases from 2.975 GHz to 2.243 GHz and the BW decreases from 65 MHz to 22 MHz. In this case, the radiation pattern is similar to that of the RMSA without a stub. The cross-polar levels are much smaller than those of the single stub-loaded RMSA. Dual-band operation is obtained for l = 1.5 cm at 2.243 GHz and 3.604 GHz.

Table 7.2
Effect of Stub Length on the Resonance Frequency and BW of a Dual Stub-Loaded RMSA (L = 3 cm, W = 4 cm, w = 0.4 cm, x = 0.7 cm, ϵ_r = 2.55, h = 0.159 cm, and tan δ = 0.001)

l (cm)	f_0 (GHz)	BW (MHz)
0.0	2.975	65
0.5	2.827	54
1.0	2.581	39
1.5	2.243, 3.604	22, 28

7.2.1.3 Tunable RMSA with a Stub Along a Nonradiating Edge

In the above two cases, the stub(s) are placed along the radiating edge(s) of the RMSA, where the field remains constant. As a result, the position of the stub along the radiating edge does not have a significant effect on the tuning characteristics of the RMSA. When the stub is placed along one of the nonradiating edges of the RMSA, the position of the stub influences the input impedance and tunability characteristics of the antenna because of the sinusoidal field variation along the edge. A RMSA with a single stub placed along one of its nonradiating edges is shown in Figure 7.3. The position of the stub x_s is varied from the center to the edge of the patch. For l = 1 cm, w = 0.4 cm, and x = 0.7 cm, the effect of x_s on the performance of the antenna is summarized in Table 7.3. As x_s increases from 0 to 1.3 cm, the resonance frequency decreases from 2.984 GHz to 2.793 GHz yielding a tuning range of 6.6%, while the input impedance Z_{in} decreases from 71Ω to 36Ω, which decreases the BW from 66 to 25 MHz. However, when x_s is moved from 0 to −1.3 cm, the resonance frequency variation is nearly same as before but the input impedance increases from 71Ω to 96Ω. Therefore, the input impedance of the antenna can be significantly controlled from 36Ω to 96Ω by moving the stub along the nonradiating edge from one extreme end to the other end.

7.2.1.4 Tunable CMSA with a Single Stub

A coaxially fed CMSA with a single stub placed along the feed axis is shown in Figure 7.4(a). The improved transmission line model is used to analyze the antenna [6–8]. The radius of the CMSA is a = 3 cm, ϵ_r = 2.33, h = 0.159 cm, and tan δ = 0.001. For x = 0.95 cm, w = 0.4 cm, and different

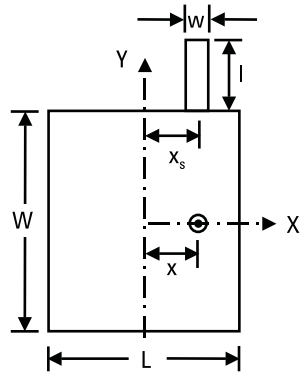

Figure 7.3 RMSA with a stub along the nonradiating edge.

Table 7.3
Effect of the Position x_s of Stub Along the Nonradiating Edge of an RMSA (L = 3 cm, W = 4 cm, l = 1 cm, w = 0.4 cm, x = 0.7 cm, ϵ_r = 2.55, h = 0.159 cm, and tan δ = 0.001)

x_s (cm)	f_0 (GHz)	Z_{in} (Ω)	BW (MHz)
0.0	2.984	71	66
0.5	2.940	53	58
1.0	2.853	37	39
1.3	2.793	36	25
−0.5	2.945	87	53
−1.0	2.858	95	34
−1.3	2.800	96	29

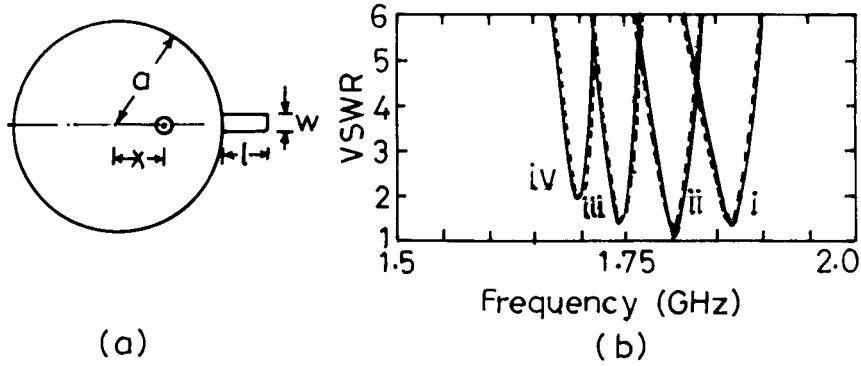

Figure 7.4 (a) CMSA with a single stub. (b) VSWR plots for various stub lengths l (i) 0, (ii) 1.2, (iii) 1.85, and (iv) 2.2 cm: (- - -) theoretical and (——) measured.

stub lengths l (0 to 2.2 cm), the results are given in Table 7.4. The theoretical and measured VSWR curves for four different stub lengths are shown in Figure 7.4(b).

As l increases from 0.0 to 2.2 cm, the measured resonance frequency f_0 decreases from 1.868 GHz to 1.693 GHz, which yields a tuning range of nearly 9%. The increase in l increases the effective area of the CMSA, which decreases its resonance frequency. With an increase in the stub length, the effective center of the antenna shifts toward the feed point from the physical center. Therefore, the real part of the measured input impedance Z_{in} decreases from 53.4Ω to 30.0Ω, and hence the BW decreases from 29 MHz to 9 MHz. The decrease in the BW is also due to the decrease of

Table 7.4
Theoretical and Experimental Results of a CMSA with a Single Stub for Various Values of Stub Length l (a = 3 cm, w = 0.4 cm, x = 0.95 cm, ϵ_r = 2.33, h = 0.159 cm, and tan δ = 0.001)

l (cm)	f_0 (GHz)		Z_{in} (Ω)		BW (MHz)	
	Theoretical	Experimental	Theoretical	Experimental	Theoretical	Experimental
0.00	1.866	1.868	$52.5 + j0.6$	$53.4 + j2.3$	28	29
0.80	1.832	1.829	$47.3 + j1.8$	$50.4 + j0.9$	25	25
0.95	1.825	1.823	$45.5 + j0.1$	$49.1 + j0.3$	24	25
1.20	1.810	1.808	$42.3 - j1.9$	$45.5 - j0.4$	23	23
1.40	1.795	1.788	$40.5 - j0.1$	$44.0 - j0.3$	21	22
1.60	1.777	1.768	$39.0 + j0.1$	$41.3 - j0.2$	18	19
1.85	1.746	1.741	$35.5 + j0.5$	$39.0 + j0.5$	16	17
2.00	1.733	1.723	$30.7 - j0.7$	$34.0 - j0.8$	13	15
2.10	1.717	1.711	$28.9 + j0.1$	$30.5 + j0.6$	10	11
2.20	1.695	1.693	$28.0 + j0.1$	$30.0 + j1.0$	8	9

the resonance frequency, which effectively reduces h/λ_0. For a larger stub length, the feed point needs to be shifted away from the center for impedance matching, which will also improve the BW.

7.2.1.5 Tunable CMSA with Double Stubs

The CMSA with a single stub gives tunability, but the main disadvantage is that the same feed point does not give impedance matching for a larger stub length. The feed point needs to be moved away from the center to get a good match for longer stub. A CMSA with two stubs, shown in Figure 7.5(a) overcomes this problem [9]. When the two stubs are equal, then the configuration is symmetrical, and the effective center remains close to the physical center of the configuration. So, even for longer stub lengths, the feed point remains unchanged for a 50-Ω match. The theoretical and experimental resonance frequencies, input impedance and BW for VSWR ≤ 2 for different stub lengths l_1 and l_2 are given in Table 7.5. The theoretical and experimental VSWR plots for four different combinations of stub lengths are given in Figure 7.5(b). As the stub lengths (l_1 and l_2) increase from (0, 0) to (1.45, 1.70) cm, the measured resonance frequency decreases from 1.868 GHz to 1.696 GHz, leading to a tuning range of about 9%, whereas the real part of the input impedance decreases slightly from 53.4Ω to 50.0Ω. Also, the BW decreases from 29 MHz to 19 MHz, because the resonance frequency decreases, which decreases h/λ_0. When the difference between the two stub lengths increases, the change in the impedance is more.

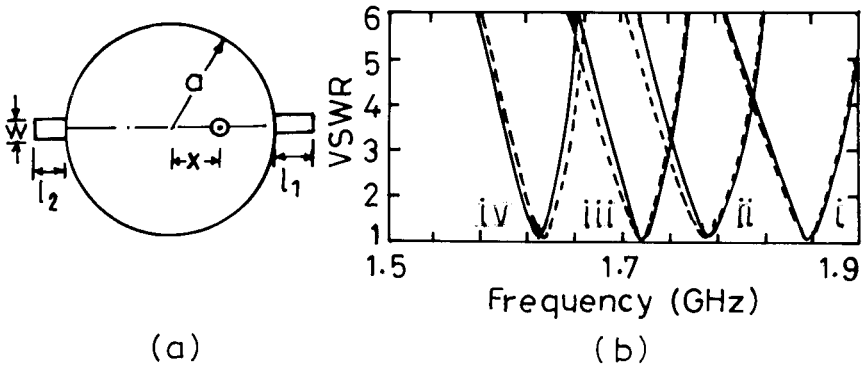

Figure 7.5 (a) Double stub-loaded CMSA and (b) VSWR plots for various stub lengths (l_1, l_2) in centimeters [(i) (0, 0), (ii) (0.45, 0.95), (iii) (1.25, 0.95), and (iv) (1.45, 1.7)]: (- - -) theoretical and (——) measured.

Table 7.5
Theoretical and Experimental Results of the Double Stub-Loaded CMSA for Different Stub Lengths l_1 and l_2 (a = 3 cm, x = 0.95 cm, ϵ_r = 2.33, h = 0.159 cm, and tan δ = 0.001)

Stub Lengths (cm)		f_0 (GHz)		Z_{in} (Ω)		BW (MHz)	
l_1	l_2	Theoretical	Experimental	Theoretical	Experimental	Theoretical	Experimental
0.00	0.00	1.866	1.868	$52.5 + j0.6$	$53.4 + j0.3$	28	29
0.45	0.40	1.826	1.832	$53.0 + j1.8$	$53.6 - j0.3$	27	27
0.45	0.95	1.800	1.804	$58.2 + j0.8$	$55.1 - j0.1$	26	24
1.25	0.95	1.760	1.763	$50.7 + j0.9$	$48.1 + j0.9$	22	21
1.25	1.45	1.725	1.732	$57.6 + j0.3$	$53.0 + j0.4$	21	19
1.45	1.45	1.710	1.721	$54.7 + j1.5$	$50.0 + j0.4$	20	20
1.45	1.70	1.699	1.696	$51.5 - j0.7$	$50.0 - j0.5$	19	19

7.2.2 Tunable MSAs Using Shorting Posts

When a shorting post is placed between the patch and the ground plane, it changes the field distribution and provides inductive loading to the patch and hence changes its resonance frequency. The resonance frequency can be tuned by changing the position and the number of shorting posts in the patch. As discussed in Chapter 6, the conventional MSAs, such as the RMSA, CMSA, and ETMSA, are made compact by shorting the zero potential field lines and using part of the configuration. It is also described that by reducing the shorting width or number of shorting posts, the resonance frequency decreases, thereby achieving tuning.

An RMSA of length L = 1.2 cm and W = 1.2 cm with shorting posts placed along one of its radiating edges is shown in Figure 7.6(a) [10]. The feed point is at x = 0.155 cm, and the substrate parameters are ϵ_r = 2.55 and h = 0.12 cm. The variation of normalized frequency f/f_0 with respect to the shorting ratio w_s/W (ratio of width of the shorted portion to the width of the patch) is shown in Figure 7.6(b). As the shorting ratio decreases from 1.0 to 0.1, the normalized resonance frequency decreases from 1.0 to 0.65, which is similar to that described in Section 6.2.

Another configuration for tuning the resonance frequency of the RMSA by using two shorting posts inside the patch is shown in Figure 7.7(a) [10, 11]. The dimensions of the RMSA are L = 6.2 cm and W = 9.0 cm, and the substrate parameters are ϵ_r = 2.55 and h = 0.16 cm. For the feed at x = 1.6 cm along the nonradiating edge, the variation of the frequency with s'/L

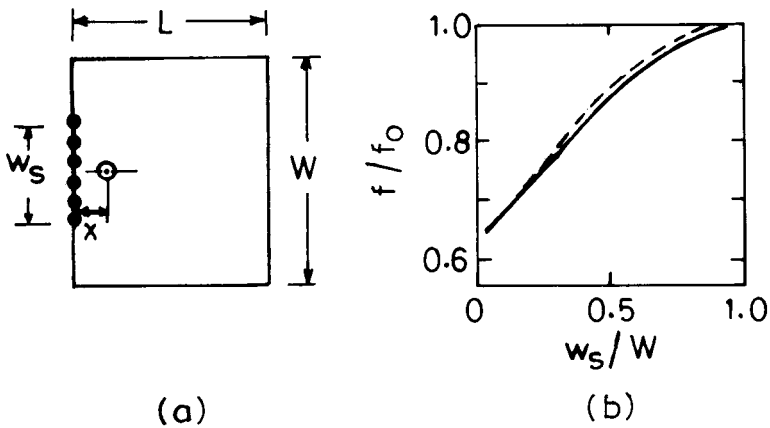

Figure 7.6 (a) RMSA with shorting posts placed along one of its radiating edges and (b) its normalized frequency f/f_0 variation with the shorting width ratio w_s/W: (- - -) theoretical and (——) measured.

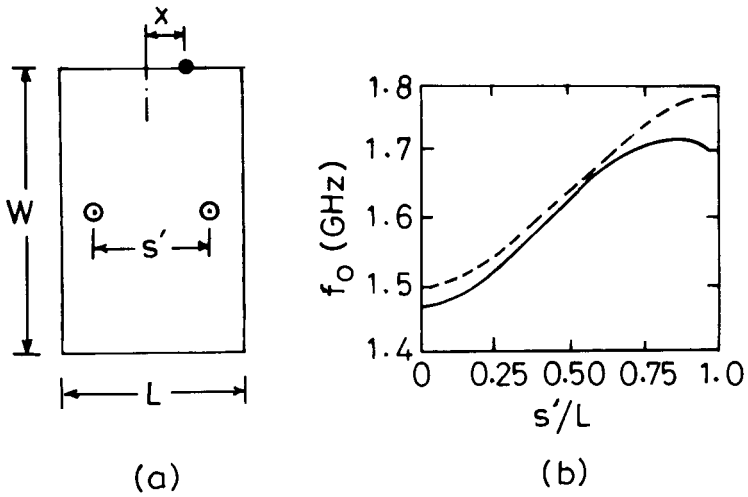

Figure 7.7 (a) RMSA with two shorting posts and (b) its frequency variation with s'/L: (- - -) theoretical and (——) measured.

ratio (separation of the two shorting posts to the length of the patch) is shown in Figure 7.7(b). As s'/L increases (i.e., the two shorting posts are shifted away from the center to the edge of the patch), the measured resonance frequency increases and then decreases slightly, and a tuning range of approximately 18% is obtained. The radiation pattern remains in the broadside direction.

7.2.3 Tunable MSAs Using Varactor Diodes

Instead of using two shorting posts, which provide inductive loading to the patch for tuning its resonance frequency, two varactor diodes are connected at the two radiating edges of the patch to the ground plane, as shown in Figure 7.8(a). The dimensions of the patch are L = 4.65 cm and W = 3.0 cm and the feed point is located at x = 1.7 cm. Frequency tuning is achieved by varying the reverse-bias voltage applied to the varactor diodes. The plot of measured resonance frequency versus reverse-bias voltage (V) is shown in Figure 7.8(b). With an increase in the reverse-bias voltage, the diode capacitance decreases, which decreases the overall capacitance of the patch; hence the resonance frequency of the antenna increases. Due to the nonlinear behavior of the varactor capacitance with bias voltage, frequency variation is not linear with bias voltage. As the bias voltage is increased from 0 to 30V, the frequency increases from 1.40 GHz to 1.81 GHz, giving a tuning range of about 30% [12].

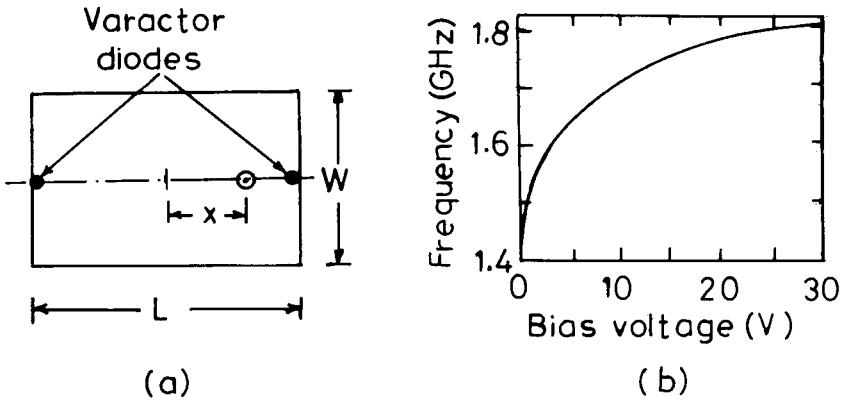

Figure 7.8 (a) RMSA with two varactor diodes and (b) plot of measured resonance frequency versus reverse-bias voltage.

7.2.4 Optically Tuned MSA

Another configuration for tuning the resonance frequency of the MSA uses an optically controlled PIN diode as depicted in Figure 7.9. A stub is connected or disconnected to the patch by means of an optically controlled PIN diode depending upon whether the diode is forward-biased or reverse-biased, respectively. When the diode is reverse-biased, its impedance is high; it acts as an open circuit; and the resonance frequency of the antenna corresponds to the patch frequency. When the diode is forward-biased, its impedance is low, and the resonance frequency corresponds to the combination of the patch and the stub [13].

7.2.5 Tunable MSAs Using an Air Gap

The above planar methods provide a frequency tuning range of 5–30%, but one has to add external components, such as stubs, shorting posts, varactor

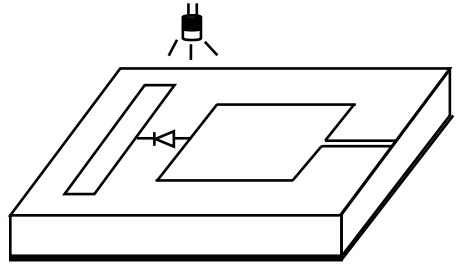

Figure 7.9 RMSA with an optically controlled PIN diode.

diodes, an optically controlled PIN diode, and their associated biasing circuits [1]. Another method for tuning the resonance frequency of the MSA, which avoids the placement of the external components, is to change the effective dielectric constant ϵ_e of the antenna by introducing an adjustable air gap between the substrate and the ground plane as shown in Figure 7.10. By varying the air gap Δ, the resonance frequency of the MSA is tuned. A similar configuration is discussed in Chapter 2 for a broad BW for fixed air gap. As Δ increases, ϵ_{eq} decreases as given by (2.25), which increases the resonance frequency. Also, the BW of the antenna increases due to an increase in the total height $H = h + \Delta$ and a decrease in ϵ_{eq}.

A circular patch of radius $a = 5$ cm is fabricated on a substrate with $\epsilon_r = 2.32$ and $h = 0.159$ cm. Spacers are used between the substrate and the ground plane to maintain an air gap as shown in Figure 7.10. The patch is fed at $x = 4.75$ cm. For $\Delta = 0$, 0.05 and 0.1 cm, the measured resonance frequencies for the fundamental mode are 1.128, 1.286, and 1.350 GHz, respectively. This gives a frequency tuning range of about 20%. The BW of the antenna increases from 0.89% to 2.07% due to an increase in the total height of the antenna and a decrease in ϵ_e. There is no significant effect of the air gap on the radiation pattern of the antenna. Similar results are also observed for higher order modes of the CMSA [14, 15].

Instead of a CMSA, when an ARMSA with an outer radius of 7.0 cm and an inner radius of 3.5 cm is used, its resonance frequency for the fundamental TM_{11} mode is 626, 720, and 778 MHz for $\Delta = 0.0$, 0.05, and 0.1 cm, respectively [16]. BWs at these frequencies are 0.6%, 0.7%, and 0.8%, respectively. For the TM_{12} mode, the corresponding resonance frequencies are 2.757, 3.040, and 3.240 GHz, with respective BWs of 4.0%, 8.0%, and 8.6%.

A simple formula for calculating the resonance frequency f_{gap} of a patch with small air gap spacing Δ is as follows:

$$f_{\text{gap}} = \frac{f_0\sqrt{\epsilon_r}}{\sqrt{\epsilon_{eq}}} \tag{7.4}$$

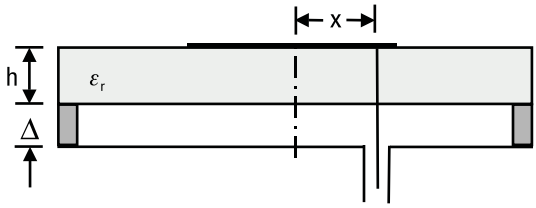

Figure 7.10 Tunable MSA with an air gap between the substrate and the ground plane.

where f_0 is the resonance frequency of the patch without any air gap and ϵ_{eq} is the effective dielectric constant of the two layers given by (2.25). The above equation is valid for small values of Δ and any patch shape.

7.2.6 Tunable MSAs Using a Ferrite Substrate

A ferrite substrate has a large permeability μ_r and high dielectric constant ϵ_r. When an RMSA is fabricated on a ferrite substrate, its resonance frequency is given by

$$f_0 = \frac{c}{2L_e\sqrt{\mu_e \epsilon_e}} \tag{7.5}$$

where μ_e is the effective permeability.

Because of its large value in the lower UHF band, the size of the patch on a ferrite substrate reduces drastically for a given frequency. A fully shorted quarter-wave RMSA with L = 4 cm, W = 1.12 cm, and a feed point at x = 1.12 cm from the open end is fabricated on a ferrite substrate, whose parameters are h = 0.2 cm, μ_r = 14.74, ϵ_r = 15, dielectric loss tangent factor = 0.0476, and magnetic loss tangent factor = 0.0476. The measured BW of the antenna is 7 MHz (3.2%) at 219 MHz for VSWR ≤ 1.5 [17]. When a CMSA of radius a = 1 cm and x = 0.5 cm is fabricated on the above ferrite substrate, it has a resonance frequency of 661 MHz. The antenna yielded wider BW of 12.4% for VSWR ≤ 1.5 because of increase in h/λ_0 [18].

When a ferrite substrate experiences a varying magnetic field, its permeability changes, which yields frequency tuning. An RMSA of L = 1.4 cm and W = 1.8 cm is fabricated on a ferrite substrate with h = 0.127 cm, ϵ_r = 15 and $4\pi M_s$ = 1,720 Gauss [19]. The RMSA is fed at the middle of one of the radiating edges for the TM_{10} mode. The tuning of the resonance frequency is achieved by varying the dc magnetic bias field, which is realized by placing a permanent magnet behind the ground plane of the MSA. The strength of the magnetic field is changed by adjustable spacers. The tuning range of 40% is achieved at 4.6 GHz for VSWR ≤ 2. The radiation pattern remains in the broadside direction with cross-polar level less than −10 dB in the complete tuning range.

The continuous tuning of the resonance frequency of the MSA over the large frequency range is also possible by changing the biasing current of the electromagnet placed below its ground plane as shown in Figure 7.11 [20]. The electromagnet is biased by setting the current through the fixed

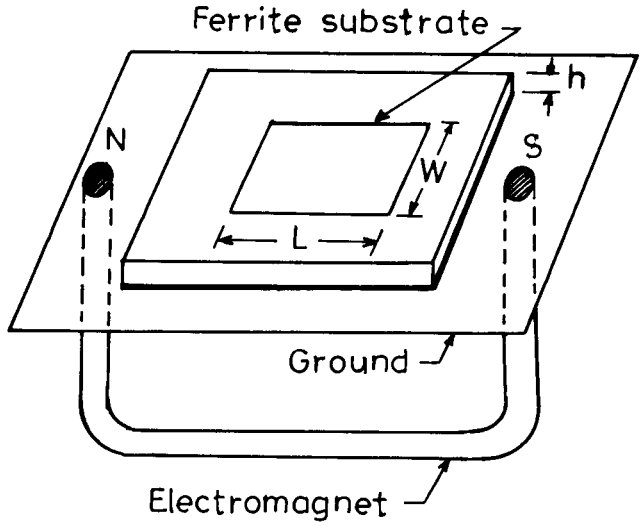

Figure 7.11 An MSA on a ferrite substrate with an electromagnet.

turns of wire wound over it, which changes the effective permeability of the ferrite substrate. A rectangular patch of $L = 4$ cm and $W = 1.12$ cm on a ferrite substrate with $h = 0.2$ cm and $\epsilon_r = 14.78$ operated over the frequency range 200–500 MHz with a change in the biasing current of the electromagnet. However, there are disadvantages connected with these configurations, including very poor efficiency, which reduces the gain. In addition, the requirement of additional magnets makes the overall size of the antenna very large.

7.3 Dual-Band MSAs

There is a considerable amount of interest in the development of a dual-band MSA because of its usefulness in various applications [21]. These dual-band operations can be at fixed frequencies, or tunable at both or one of the frequencies. Figure 7.12 depicts the VSWR plots for the fixed and tunable categories. The solid lines show two fixed frequencies, and the dotted lines show the tunability. Either both or one of the frequencies of dual-band operation could be tunable based on the application. Several MSA configurations for obtaining dual-band characteristics are discussed in this section.

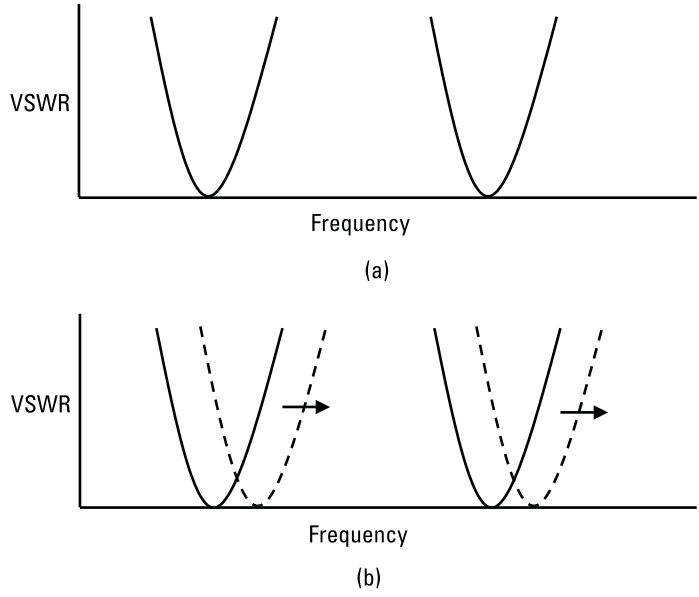

Figure 7.12 VSWR plots of two categories of dual-band operation: (a) fixed and (b) tunable.

7.3.1 Higher Order or Orthogonal Mode Dual-Band MSAs

An MSA operates at many frequencies corresponding to its various resonant modes, which makes it a natural choice for dual-frequency operation. However, characteristics such as the radiation pattern, polarization, and input impedance are not the same for the different modes. Therefore, all these modes are not useful for a given application. Also, for a given MSA geometry, all the modes are at a fixed resonance frequency. A single element can produce dual-band operation either with a single or dual feed as described below.

7.3.1.1 Single Feed Dual-Band MSA

An RMSA operating in the TM_{10} and TM_{30} modes has radiation patterns in the broadside direction with the same polarization at both the frequencies as described in Chapter 2. The resonance frequency of the TM_{30} mode is nearly three times of that of the fundamental TM_{10} mode of the RMSA. Consequently, these modes may be used for dual-band operation.

Similar to the RMSA, the dual-frequency operation may be achieved by using higher order modes of the CMSA and TMSA as discussed in Chapter 2. For the CMSA, the resonance frequencies corresponding to higher order modes are spaced at an interval given by the roots of the derivative of the Bessel function of order n. For ETMSA, the TM_{10}, TM_{20}, and TM_{21}

modes yield broadside radiation with similar polarization. A single feed point yields good impedance matching for all these three modes. Thus, it is possible to utilize the ETMSA for dual- or even triple-frequency operation.

The above configurations give dual-frequency operation with the same polarization. However, many applications require orthogonal polarization at the two frequencies. An RMSA may be used to operate at TM_{10} and TM_{01} modes. The two frequencies correspond to the length and the width of the RMSA. The ratio of resonance frequency of these two modes is approximately equal to the L/W ratio of the RMSA. Accordingly, for a desired frequency ratio, the length and the width can be appropriately chosen.

For an RMSA, both the orthogonal modes may be excited with good impedance matching at both the frequencies using a single feed as shown in Figure 7.13(a). The coaxial feed is displaced from the two principal axes of the patch to excite both the orthogonal modes [22]. The antenna is analyzed using IE3D for $L = 3$ cm and different values of W with $\epsilon_r = 2.55$, $h = 0.159$ cm, and $\tan \delta = 0.001$. For $W = 4$ cm, the input impedance and VSWR plots for the feed at $x = 0.7$ cm and $y = 0.5$ cm are shown in Figure 7.13(b, c). For three values of W (3.5, 4.0, and 4.5 cm), the results are summarized in Table 7.6. As W increases from 3.5 cm to 4.5 cm, the higher resonance frequency f_2 decreases slightly due to an increase in ϵ_e, but the lower resonance frequency f_1 decreases from 2.594 GHz to 2.044 GHz. The ratio of the two frequencies for all these cases is approximately the same as that of the ratio of effective length and the effective width of the RMSA. The BW at the two frequencies is almost the same as that of the BW of the corresponding RMSA when only a single mode is excited.

As W increases from 3.5 cm to 4.5 cm, the BW at the lower resonance decreases from 37 MHz to 19 MHz, because f_1 decreases, which in turn decreases h/λ_0. Also at this mode, length L of the patch acts as width, so L/λ_0 decreases with an increase in f_1; therefore, radiation resistance increases leading to larger resistance variation and hence a decrease in BW. However, BW at the higher resonance increases from 60 MHz to 69 MHz with an increase in W. This is because at this mode, f_2 remains nearly constant as L is constant, but W/λ_0 increases, resulting in increase in BW.

Instead of using a single coaxial feed for the dual-band RMSA, similar results are obtained by using an aperture coupled RMSA, in which an inclined slot is cut in the ground plane with respect to the microstrip feed line as shown in Figure 7.14 to give proper matching at both the frequencies [23].

A single feed elliptical MSA, shown in Figure 7.15(a), also yields dual-frequency operation with orthogonal polarization. The coaxial feed is placed at approximately 45° from the major axis. Its location is optimized to excite

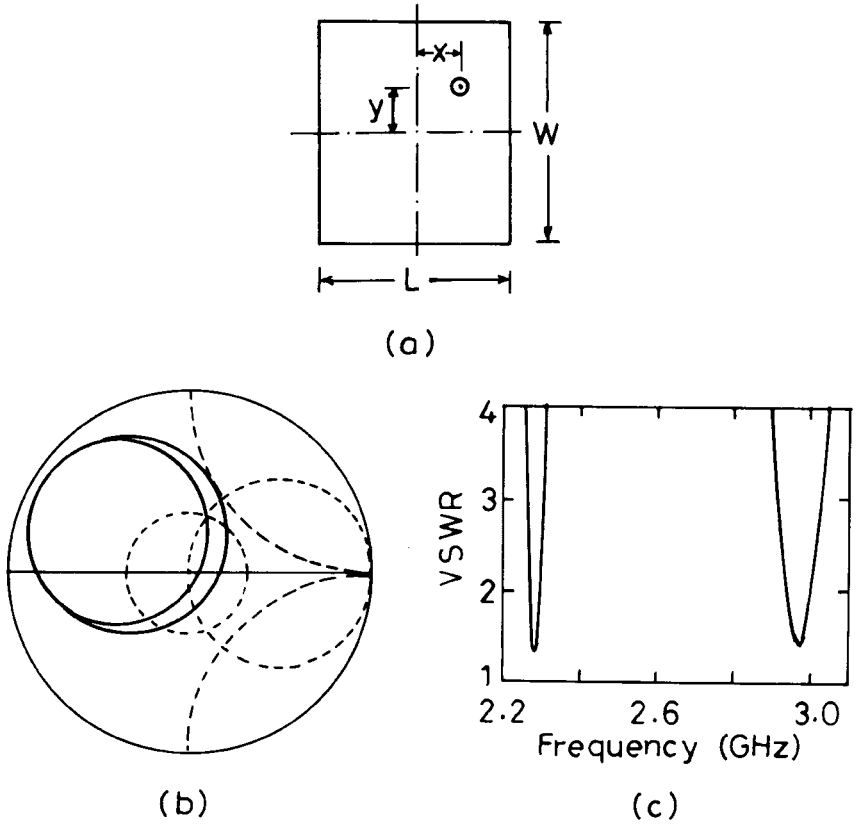

Figure 7.13 (a) RMSA with a single feed for orthogonal dual-band operation and its (b) input impedance and (c) VSWR plots.

Table 7.6
Dual-Band Response of RMSA with Single Feed for Different Values of W
(L = 3.0 cm, ϵ_r = 2.55, h = 0.159 cm, and tan δ = 0.001)

W (cm)	x, y (cm, cm)	Lower Resonance f_1 (GHz)	Lower Resonance BW (MHz)	Higher Resonance f_2 (GHz)	Higher Resonance BW (MHz)	f_2/f_1
3.5	0.6, 0.5	2.594	37	2.978	60	1.15
4.0	0.7, 0.5	2.285	26	2.973	64	1.30
4.5	0.8, 0.5	2.044	19	2.968	69	1.45

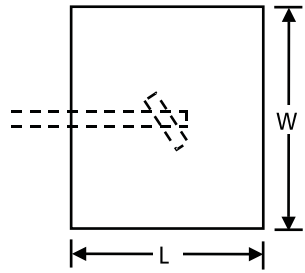

Figure 7.14 Aperture coupled RMSA with an inclined slot.

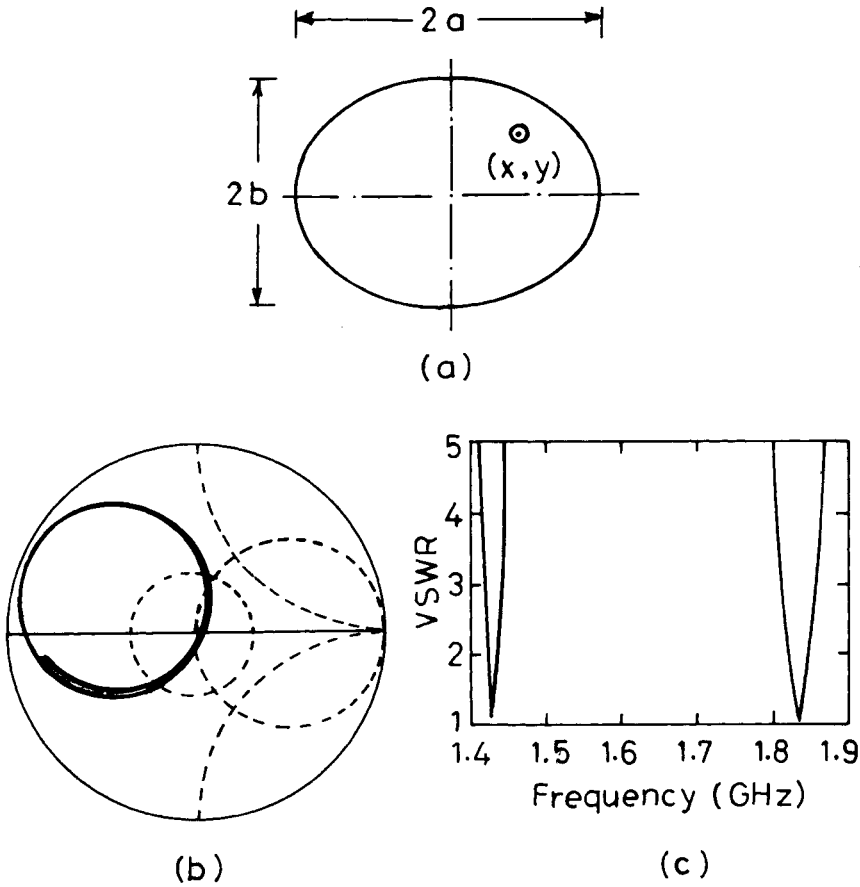

Figure 7.15 (a) Elliptical MSA with a single feed for dual-band operation and its (b) input impedance and (c) VSWR plots.

both the orthogonal modes with proper impedance matching. For a = 4 cm, b = 3 cm, ϵ_r = 2.33, h = 0.159 cm, and tan δ = 0.002, the input impedance and VSWR plots for the feed at x = 1.0 cm and y = 1.05 cm are shown in Figure 7.15(b, c). The lower and higher resonance frequencies are 1.430 GHz and 1.835 GHz with BWs of 13 MHz and 27 MHz, respectively. The ratio of the two resonance frequencies is approximately the same as that of the ratio of the effective radii in the two orthogonal planes.

7.3.1.2 Dual Feed Dual-Band MSAs

For a single feed dual-band MSA, if one frequency is used for transmission and the other is used for reception, a circulator or diplexer is required to isolate the receiver from the transmitter. The use of a circulator or diplexer may be avoided by feeding the RMSA at two orthogonal points as shown in Figure 7.16(a) [24]. Since these feed points are at null locations of the respective orthogonal modes, the loading of one feed point does not affect the input impedance at the other feed point. For the RMSA with W = 4 cm and other dimensions given in Table 7.6, the input impedance plots corresponding to the two ports and the magnitude of S-parameters (S_{11}, S_{22}, and S_{21}) are shown in Figure 7.16(b, c). For the feed at x = 0.7 cm, the resonance frequency is 2.980 GHz, and for the feed at y = 0.5 cm, the resonance frequency is 2.287 GHz. The isolation between the two modes using orthogonal feeds is nearly 30 dB and 40 dB at the lower and higher resonance frequencies, respectively. These results are similar to those described in Section 2.2.3.

Similar results are obtained for an ellipse with two orthogonal feed points. The dimensions of the ellipse are the same as in Section 7.3.1.1. The two orthogonal feed points are at x = 1 cm and at y = 1.05 cm as shown in Figure 7.17(a). The isolation between the two frequencies is nearly 30 dB. Instead of using two coaxial feeds, orthogonal polarization could be excited using electromagnetic or aperture coupling. A variation in the ellipse is obtained by using only the intersecting portion of the two circles of same radius as shown in Figure 7.17(b). This configuration is fed with two orthogonal electromagnetically coupled microstrip lines [25]. As before, the frequency ratio of dual-band operation is approximately equal to the ratio of the orthogonal dimensions in the two planes. The isolation between the two ports is 27 dB. Another variation using a circular patch is shown in Figure 7.17(c). It is excited by two orthogonal microstrip lines through the two orthogonal slots cut in the ground plane. By changing the slot dimensions, the two orthogonal resonance frequencies can be changed [26].

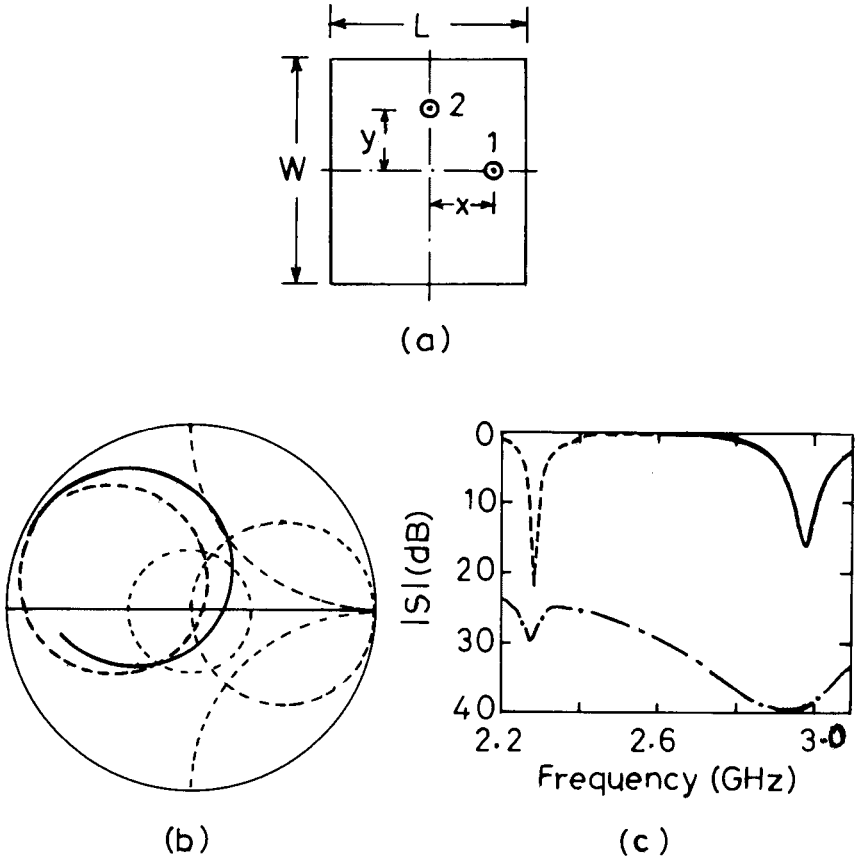

Figure 7.16 (a) RMSA with two orthogonal feeds for dual-band operation and its (b) input impedance plots at two ports: (——) port 1 and (- - -) port 2, and (c) S-parameter plots: (——) S_{11}, (- - -) S_{22}, and (– · –) S_{21}.

A dual-band operation is also obtained by loading the MSA with a reactive load. The reactive load modifies the field configuration of the patch and gives a dual resonant behavior. The reactance could be in the form of a single stub or double stubs, a lumped capacitor, shorting posts, or a slot in the patch, among others. In the reactive loaded MSA, both the resonance frequencies of the dual-band operation can be tuned by changing the value of the reactance. These configurations are discussed one by one in the following subsections.

7.3.2 Stub-Loaded Dual-Band MSAs

For dual-band response, the concept of loading an RMSA with a short-circuited coaxial line stub as shown in Figure 7.18(a) was first demonstrated

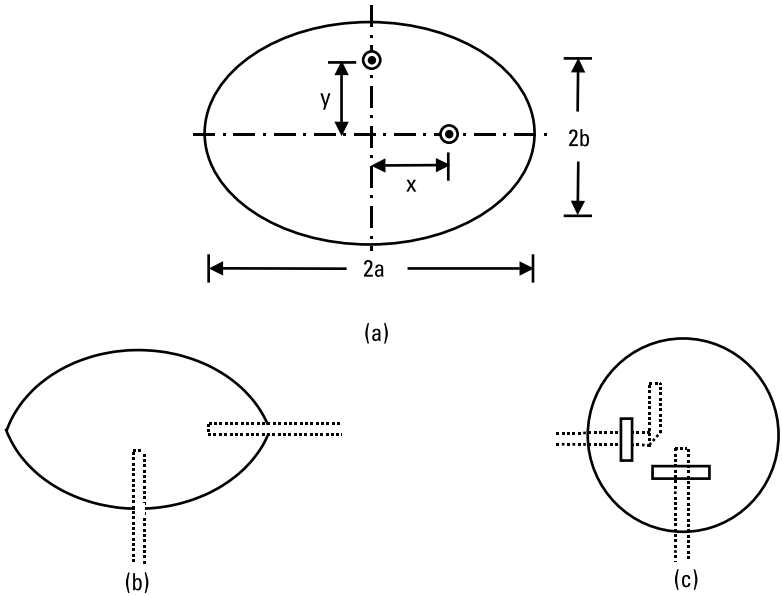

Figure 7.17 Various dual-band MSA configurations: (a) elliptical MSA with two orthogonal feeds (b) common portion of two intersecting circles, and (c) CMSA with two orthogonal slots.

experimentally [27]. The tuning of the two frequencies was obtained by changing the length of the short-circuited coaxial line. Instead of short-circuited coaxial line, a $\lambda/2$ short-circuited microstrip line is used as shown in Figure 7.18(b), which can be etched on the same substrate along with the patch [28]. The separation between the two resonance frequencies is varied by either changing the short-circuited length of the microstrip line or by introducing an inset in the patch, as shown in Figure 7.18(c). A compact version is obtained by using an open-circuited $\lambda/4$ stub (which is equivalent to a short-circuited $\lambda/2$ stub) as shown in Figure 7.18(d). For frequency tuning, the length of the stub is varied slightly. A single or double open-circuited $\lambda/4$ stub is connected to the RMSA or CMSA to obtain the dual-band operation as described below [5, 29].

7.3.2.1 Single Stub-Loaded RMSA

The tuning of the resonance frequency of the antenna with a small open-ended stub is discussed in Section 7.2. When the length of the stub is comparable to $\lambda/4$, a dual-frequency operation is obtained. At the lower frequency, the open stub presents a capacitive load, whereas at the higher frequency, it presents an inductive load.

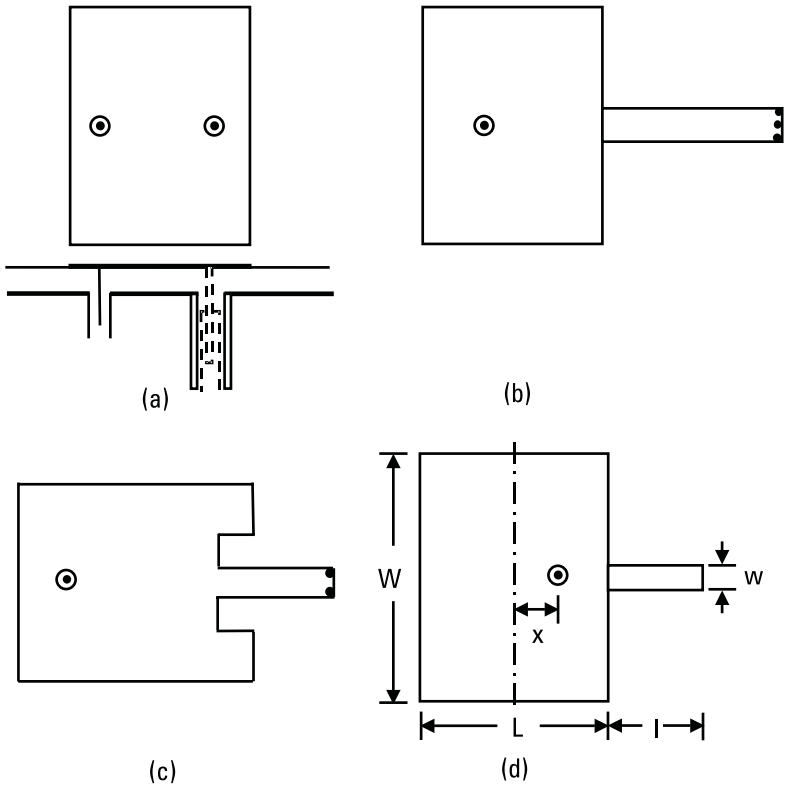

Figure 7.18 Various dual-band stub-loaded RMSA configurations: (a) short-circuited coaxial line, (b) short-circuited $\lambda/2$ stub, (c) short-circuited $\lambda/2$ stub with inset, and (d) open-circuited $\lambda/4$ stub.

For the single stub-loaded RMSA shown in Figure 7.18(d), the dimensions of the patch are taken as L = 3 cm and W = 4 cm, and the substrate parameters are ϵ_r = 2.55, h = 0.159 cm, and tan δ = 0.001. For the feed at x = 0.8 cm and the stub dimensions l = 1.5 cm and w = 0.4 cm, the theoretical input impedance and VSWR plots are shown in Figure 7.19. A dual-frequency response is obtained at f_1 = 2.434 GHz and f_2 = 3.377 GHz with the corresponding BWs of 26 MHz and 35 MHz, respectively. The radiation pattern remains in the broadside direction at both f_1 and f_2 with cross-polar levels less than 24 dB and 14 dB, respectively. The stub length is varied for tuning both the frequencies, and the results are summarized in Table 7.7. As the length of the stub is increased from 1.4 cm to 2.0 cm, both the resonance frequencies decrease, and the ratio f_2/f_1 changes from 1.37 to 1.54.

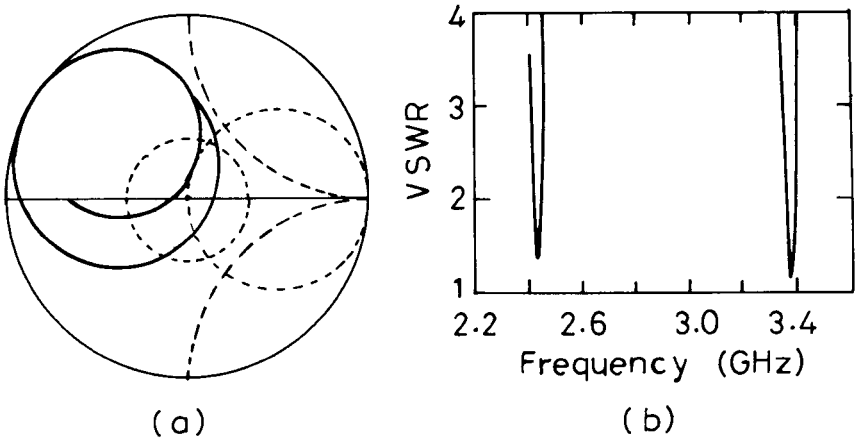

Figure 7.19 (a) Input impedance and (b) VSWR plots of single stub-loaded RMSA for dual-band operation.

Table 7.7
Resonance Frequencies of Single Stub-Loaded RMSA for Various Values of Stub Length l
(L = 3 cm, W = 4 cm, x = 0.8 cm, ϵ_r = 2.55, h = 0.159 cm, and tan δ = 0.001)

Stub Length l (cm)	**f_1 (GHz)**	**f_2 (GHz)**	**f_2/f_1**
1.4	2.508	3.443	1.37
1.5	2.434	3.377	1.39
1.6	2.361	3.324	1.41
1.8	2.214	3.245	1.47
2.0	2.074	3.188	1.54

7.3.2.2 Double Stub-Loaded RMSA

An RMSA with a single stub has slightly higher cross-polar level because it is asymmetrical configuration. To make the configuration symmetrical, a $\lambda/4$ open-circuited stub is placed along both the radiating edges of the rectangular patch as shown in Figure 7.2(a). For l = 1.5 cm and x = 0.6 cm, the input impedance and VSWR plots are shown in Figure 7.20. Dual-frequency operation is obtained at 2.243 GHz and 3.603 GHz with BWs of 23 MHz and 26 MHz, respectively. The radiation pattern is in the broadside direction at both frequencies. The ratio of the two resonance frequencies is 1.6, which can be varied by changing the length of the stubs.

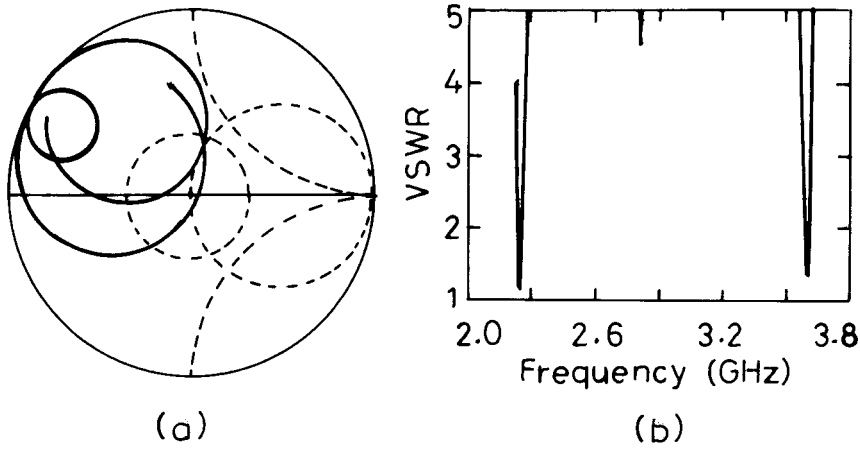

Figure 7.20 (a) Input impedance and (b) VSWR plots of double stub-loaded RMSA for dual-band operation.

A small loop may be noted at 2.813 GHz, but the radiation pattern at this frequency is conical. By using unequal stub lengths, the size of the smaller loop can be increased to yield triple-frequency response [29].

7.3.2.3 Single Stub-Loaded CMSA

A CMSA with a single stub is shown in Figure 7.21(a). When the stub length is small, its resonance frequency is tunable as described in Section 7.2.1.4. However, when the stub length is comparable to $\lambda/4$, dual-band operation is achieved [5]. For a = 3 cm, ϵ_r = 2.33, h = 0.159 cm, and tan δ = 0.001, the theoretical and the measured input impedance and VSWR plots for stub length l = 1.85 cm and width w = 0.4 cm are shown in Figure 7.21(b, c). The theoretical (obtained using the linear transmission line model) and the experimental dual-band resonance frequencies for different stub lengths are given in Table 7.8. The agreement between the theoretical and the experimental resonance frequencies are within 1% at the lower frequency f_1 and within 4% at the higher frequency f_2. The measured f_2/f_1 ratio increases from 1.350 to 1.527 as l decreases from 3.40 cm to 1.60 cm.

The measured radiation pattern of the antenna in the E- and H-planes remains in the broadside direction at f_1. However, at f_2 for some cases, a dip in the broadside direction in the E-plane is noted as given in Table 7.8. It is observed that as f_2/f_1 approaches near the ratio of 1.6588 (the ratio of the first two roots of the derivative of the Bessel function or 3.054/1.84118), the dip in the broadside in the E-plane becomes more pronounced.

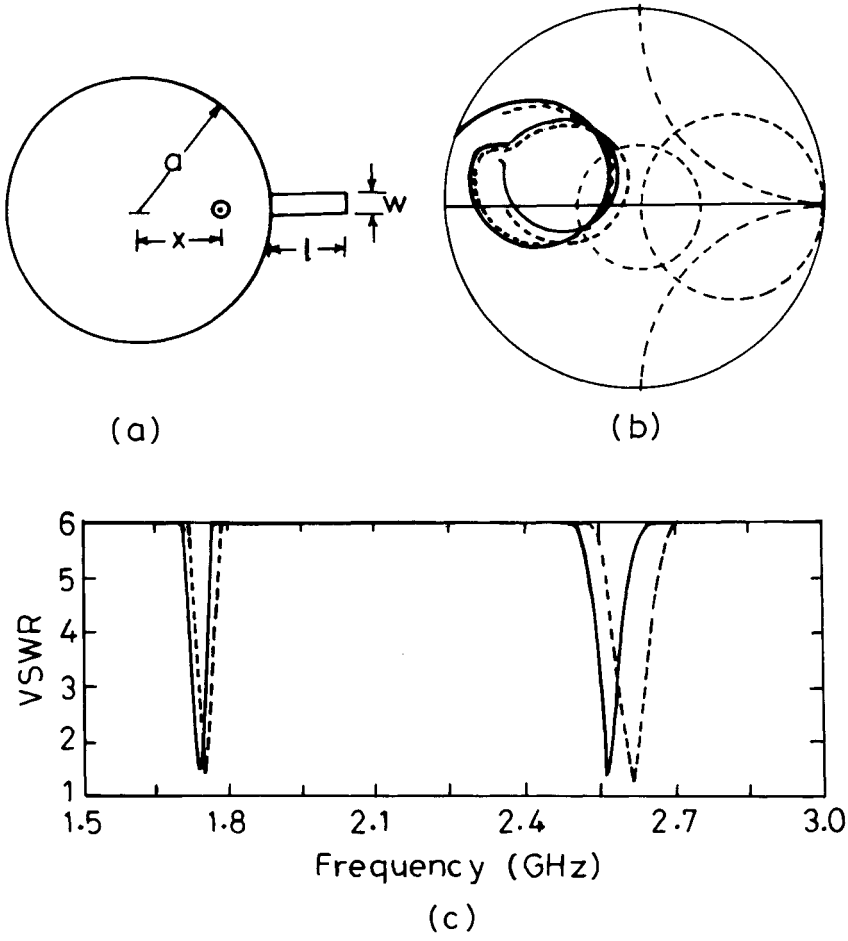

Figure 7.21 (a) Single stub-loaded CMSA and its (b) input impedance and (c) VSWR plots: (- - -) theoretical and (——) measured.

This is due to the fact that higher resonance corresponds to the next higher order mode TM_{21}, which has a conical pattern. As the frequency ratio deviates away from 1.6588, the dip reduces and finally disappears, yielding a broadside radiation pattern.

7.3.2.4 Double Stub-Loaded CMSA

A CMSA loaded by two stubs along the feed axis is shown in Figure 7.22(a). When either of the two stubs is comparable to $\lambda/4$, dual-band operation is achieved. The two frequencies are varied by altering the individual stub

Table 7.8
Theoretical and Experimental Results of Single Stub-Loaded CMSA for Various Values of Stub Length l
(a = 3 cm, x = 0.95 cm, ϵ_r = 2.33, h = 0.159 cm, and tan δ = 0.001)

Stub Length l (cm)	f_1 (GHz)		f_2 (GHz)			Measured Dip in Broadside at f_2 (dB)
	Theoretical	Experimental	Theoretical	Experimental	Measured f_2/f_1	
3.40	1.515	1.507	2.105	2.034	1.350	0.0
2.75	1.595	1.593	2.190	2.162	1.357	1.5
2.50	1.640	1.635	2.275	2.242	1.371	2.0
2.30	1.680	1.679	2.385	2.330	1.388	2.5
2.20	1.700	1.695	2.450	2.385	1.407	3.1
2.00	1.732	1.720	2.600	2.503	1.455	4.4
1.85	1.750	1.744	2.635	2.565	1.471	5.6
1.60	1.777	1.769	2.765	2.701	1.527	9.1

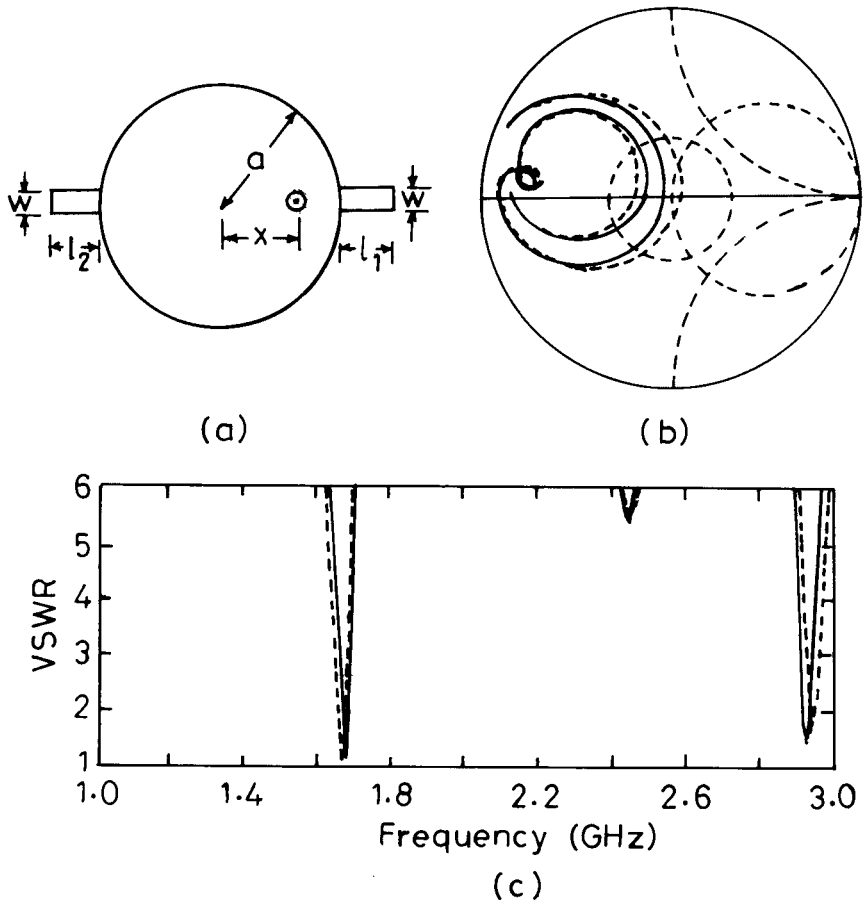

Figure 7.22 (a) Double stub–loaded CMSA and its (b) input impedance and (c) VSWR plots: (- - -) theoretical and (——) experimental.

length. The theoretical and experimental input impedance and VSWR plots for stub lengths l_1 = 1.75 cm and l_2 = 2.0 cm are shown in Figure 7.22(b, c). The comparison between the theoretical and experimental dual-band resonance frequencies for various combinations of stub lengths l_1 and l_2 is given in Table 7.9. When the stub lengths are varied, the change in f_1 is less as compared to that in the f_2. As the stub length is increased, the BW at both the resonance frequencies decreases because of the decrease in the resonance frequency, which decreases h/λ_0.

For a double stub-loaded CMSA, the radiation fields are in the broadside direction at f_1, whereas there is a dip in the broadside direction in the

Table 7.9
Theoretical and Experimental Results of Double Stub-Loaded CMSA for Various Stub Lengths
(a = 3 cm, x = 0.95 cm, ϵ_r = 2.33, h = 0.159 cm, and tan δ = 0.001)

Stub Lengths (cm)		f_1 (GHz)		f_2 (GHz)			Measured Dip in
l_1	l_2	Theoretical	Experimental	Theoretical	Experimental	Measured f_2/f_1	Broadside at f_2 (dB)
2.55	1.50	1.590	1.582	2.190	2.142	1.354	0.0
2.55	1.20	1.600	1.590	2.210	2.168	1.363	0.0
2.25	1.00	1.660	1.647	2.385	2.294	1.393	1.8
2.00	1.00	1.695	1.685	2.465	2.431	1.443	6.0
2.00	0.50	1.715	1.705	2.565	2.468	1.448	7.0
2.25	2.25	1.585	1.598	2.591	2.583	1.616	13.5
1.75	2.00	1.660	1.679	2.950	2.935	1.748	11.0
1.65	1.75	1.678	1.685	2.982	2.973	1.764	5.0

E-plane at f_2. The variation of dip in the broadside in the E-plane at f_2 is also given in Table 7.9. As the ratio f_2/f_1 approaches 1.6588, the dip in the E-plane is more pronounced, indicating that higher resonance corresponds to the higher order TM_{21} mode of the CMSA. When the length of the two stubs are nearly equal, the ratio f_2/f_1 is close to 1.6588, and hence there is a larger dip in the broadside at f_2. As f_2/f_1 deviates from 1.6588, the amount of the dip reduces and finally disappears.

7.3.3 Notch-Loaded MSAs

Reactive loading to the patch could also be provided by cutting a notch or spur line in one of the edges of the MSA to obtain dual-band operation. It creates the same effect as the stub loading, with the advantage of reduced size [30–34].

A square MSA with a rectangular notch of depth w along its nonradiating edge is shown in Figure 7.23(a). The antenna is similar to that of a C-shaped MSA, but it is fed along the diagonal, which excites orthogonal polarization at the first and second resonance frequencies. The antenna parameters are as follows: side length of the square patch L = 2.5 cm, notch length l = 1.0 cm, ϵ_r = 1.79, h = 0.08 cm, and tan $\delta = 3.2 \times 10^{-4}$. The antenna is fed along the diagonal by a 50-Ω coaxial line at $x = -y = 0.523$ cm. For the square patch without the notch (w = 0), the resonance frequency is 4.3 GHz. The variation of the resonance frequencies f_1 and f_2 as a function

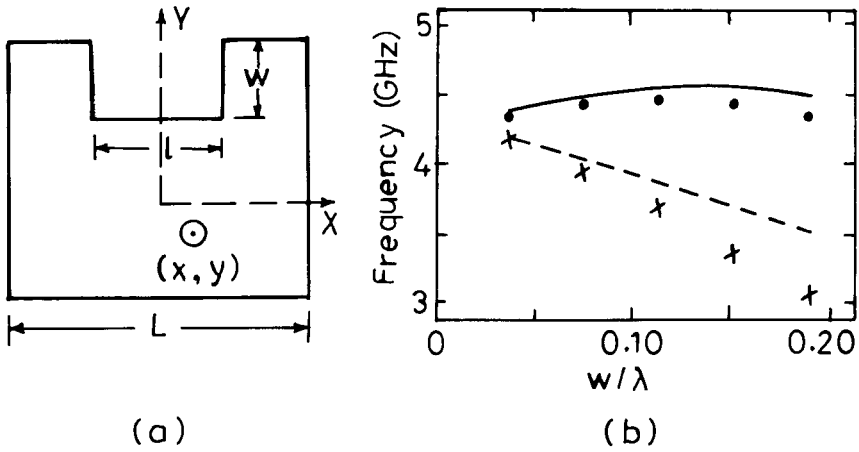

Figure 7.23 (a) Square MSA with a notch and (b) variation of resonance frequencies with w: (——) f_2 theoretical and (· · ·) f_2 experimental, and (- - -) f_1 theoretical and (x x x) f_1 experimental.

of the normalized notch width w/λ is shown in Figure 7.23(b). With an increase in w, the variation of f_2 is small as compared to that of f_1, so the difference between the two resonance frequencies with orthogonal polarization increases.

7.3.4 MSAs Using Shorting Posts

In the previous two methods of reactively loaded MSAs, the frequency ratio f_2/f_1 of dual-band operation is less than 2. For obtaining higher values of f_2/f_1, various shorting configurations may be used. The shorting post is used in such a way that it selectively modifies the current distribution of one of the modes of the patch, thereby changing the resonance frequency of only that mode, whereas the other mode does not get perturbed significantly.

7.3.4.1 Dual-Band RMSA by Using Shorting Posts

An RMSA operating in the TM_{10} and TM_{30} modes has a broadside radiation pattern with the same polarization at the two frequencies. The ratio of their resonance frequencies is approximately three. A shorting post placed at the null position of the TM_{30} mode will not change its corresponding resonance frequency but will have a strong effect on the TM_{10} mode frequency [35].

An RMSA with six shorting posts is shown in Figure 7.24. The patch is fabricated on a h = 0.3175 cm copper-cladded Rexolite 2200 substrate. The feed is chosen at the middle of the edge. A small open-circuited (capacitive) stub is attached at the feed point for neutralizing the reactance, especially

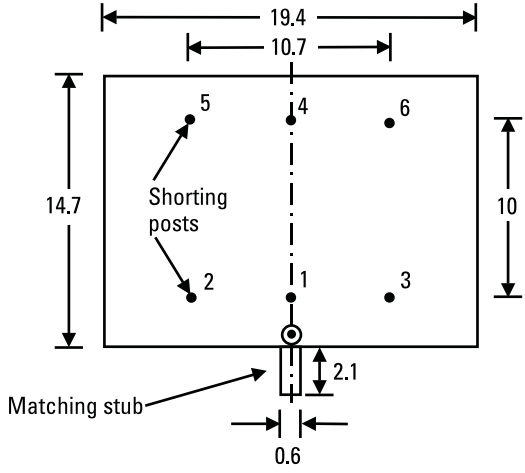

Figure 7.24 An RMSA with shorting posts for dual-band operation.

at higher frequencies to improve the matching. The effects of successively adding more posts (each approximately 0.05 cm in diameter) at the positions indicated in Figure 7.24 are shown in Table 7.10. Since all these posts are located at the nulls of the TM_{30} mode, f_2 remains constant at around 1,865 MHz, while f_1 varies from 613 MHz to 891 MHz. The ratio f_2/f_1 varies from 3.0 to 2.1, which could be lowered by using more shorting posts.

The radiation pattern remains in the broadside direction at both the frequencies with the same polarization. However, a sidelobe at f_2 appears in the E-plane pattern, which is due to the large spacing (normalized with respect to the free-space wavelength) between the two radiating edges of the patch. It can be easily reduced or even removed by using substrate with higher ϵ_r.

7.3.4.2 Dual-Band RMSA Using a Single Short

A compact dual-frequency RMSA using a single shorting post is shown in Figure 7.25(a). The patch dimensions are L = 3.73 cm and W = 2.487 cm, and the feed point is kept within a few millimeters from the shorting post. The substrate parameters are ϵ_r = 4.4 and h = 0.0762 cm. The diameter of the shorting post is 0.064 cm, and the feed diameter is 0.126 cm. When the location d_s of the shorting post is changed, the two resonance frequencies vary as shown in Figure 7.25(b). The lower resonance frequency f_1 varies in the range of 722–950 MHz and the higher resonance frequency f_2 varies in the range of 1,900–2,310 MHz. This yields a frequency-tuning range of 2.0–3.2. When the shorting post is near the edge of the patch, it gives a maximum separation of frequencies. The antenna has a broadside radiation pattern at both the frequencies [36, 37].

Table 7.10
Variation of Resonance Frequencies with a Number of Shorting Posts of Multiple Shorted RMSA

Number of Posts	Post Position	f_1 (MHz)	f_2 (MHz)	f_2/f_1
0	—	613	1861	3.0
1	1	664	1874	2.8
2	1-2	706	1865	2.6
3	1-3	792	1865	2.4
4	1-3, 5	813	1865	2.3
5	1-3, 5-6	846	1865	2.2
6	1-6	891	1865	2.1

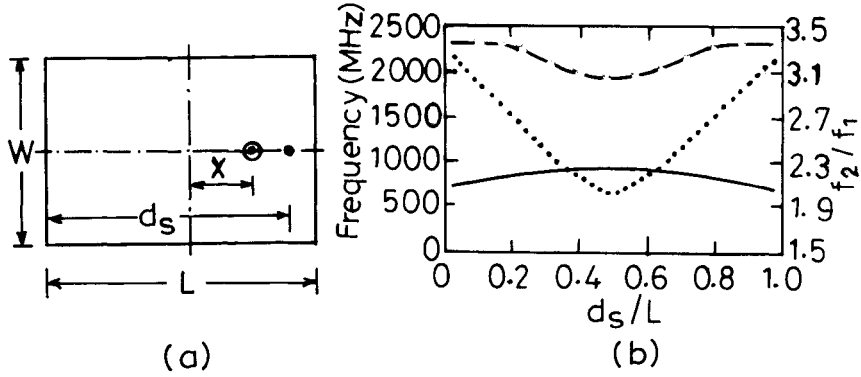

Figure 7.25 (a) An RMSA with a single shorting post for dual-band operation and (b) variation of the resonance frequency with the location of the shorting post: (——) f_1, (- - -) f_2, and (· · ·) f_2/f_1.

7.3.4.3 Dual-Band CMSA Using a Single Short

A CMSA with a single short is shown in Figure 7.26(a) [38]. For a = 2.186 cm, ϵ_r = 4.4 and h = 0.159 cm, the fundamental resonance frequency (without a shorting post) is 1.9 GHz. The radius of the shorting post is 0.032 cm, and its location d_s is varied from the center to the periphery of the CMSA. The feed position is kept at 0.3 cm away from the shorting

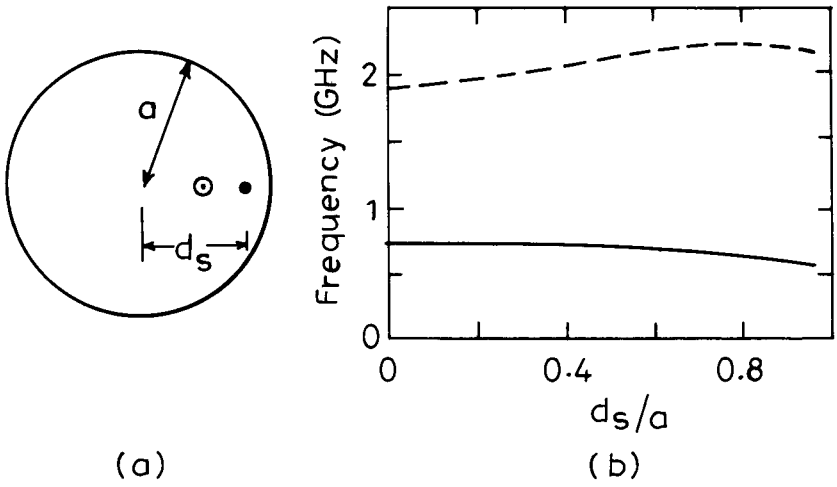

Figure 7.26 (a) CMSA with a single shorting post for dual-band operation and (b) variation of resonance frequencies with the location of the shorting post: (——) f_1 and (- - -) f_2.

post. The variation of the two resonance frequencies f_1 and f_2 with d_s/a is shown in Figure 7.26(b). By increasing the normalized position of the shorting post from 0 to 1, f_1 decreases and f_2 increases, so the ratio of the two frequencies f_2/f_1 varies from 2.6 to 3.8. The radiation pattern is in the broadside direction at both the resonance frequencies.

7.3.4.4 Dual-Band TMSA Using a Single Short

A coaxial probe-fed ETMSA with a single short is shown in Figure 7.27(a) [39]. The ETMSA of side length S = 5 cm is fabricated on the substrate having ϵ_r = 4.4 and h = 0.16 cm. The resonance frequency of the ETMSA for the fundamental TM_{10} mode without any shorting post is 1.90 GHz. The position d_s of the single shorting post of radius = 0.032 cm is varied along the line from the vertex to the base of the patch. The optimal feed position for the impedance matching is within a few millimeters of the shorting post. The variation of f_1, f_2, and f_2/f_1 with d_s/H is shown in Figure 7.27(b). When d_s/H is increased from 0 to 1, the ratio f_2/f_1 varies between 2.5 and 4.9. The frequency ratio is maximum when the shorting post is close to the tip of the triangle and is minimum when the short is at d_s/H = 0.33, which corresponds to the null position for the fundamental TM_{10} mode of the ETMSA.

A general design guideline can be drawn from the above MSA configurations with a single shorting post. When an f_2/f_1 ratio of 2 to 3.2 is required, then an RMSA with a single shorting post may be used. For a slightly larger ratio of 2.6 to 3.8, a CMSA with a single short is desirable. Finally, for a

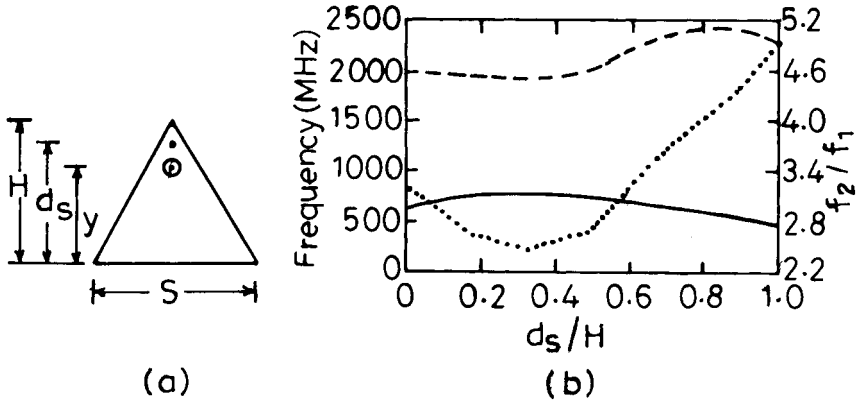

Figure 7.27 (a) ETMSA with a single shorting post for dual-band operation and (b) variation of resonance frequencies with the location of the shorting post d_s/H: (——) f_1, (- - -) f_2, and (· · ·) f_2/f_1.

larger f_2/f_1 of 2.5 to 4.9, an ETMSA with a single shorting post may be designed.

7.3.4.5 Dual-Band Shorted Planar Inverted F-Antenna

Two modified dual-band inverted F-antenna configurations to cover the GSM and DCS 1800 systems are shown in Figure 7.28 [40]. The two frequencies are around 0.9 GHz and 1.8 GHz. The antenna may be excited either using dual or single coaxial feed as shown in Figure 7.28. The configuration with two feeds has a shorted rectangular element for the 1.8-GHz and a shorted L-shaped element for the 0.9-GHz operation. The dimensions of the antenna are shown in centimeters, and the substrate parameters are $\epsilon_r = 1$ and $h = 0.9$ cm. The shorting posts are placed near the gap between the two patches to reduce mutual coupling (less than −17 dB). The antenna is fed by two 50-Ω coaxial cables, which are located very close to the shorting posts with reasonably good match. The dual-frequency response is achieved at 0.9 GHz and 1.76 GHz with respective BWs of 63 MHz and 110 MHz. The radiation pattern is almost omni-directional at both the resonance frequencies.

Dual-band operation is also achieved with a single feed as shown in Figure 7.28(b). The substrate parameters are $\epsilon_r = 2.2$ and $h = 0.1143$ cm. The ratio between the two dual frequencies of 1.8 is achieved with return loss better than −17 dB at both the frequencies [40].

A patch could be loaded with a chip resistor instead of a short to yield dual-frequency operation [41]. With an increase in the resistor value from 0 to 2Ω, the loss in the chip resistor increases, which increases the BW but significantly decreases the efficiency.

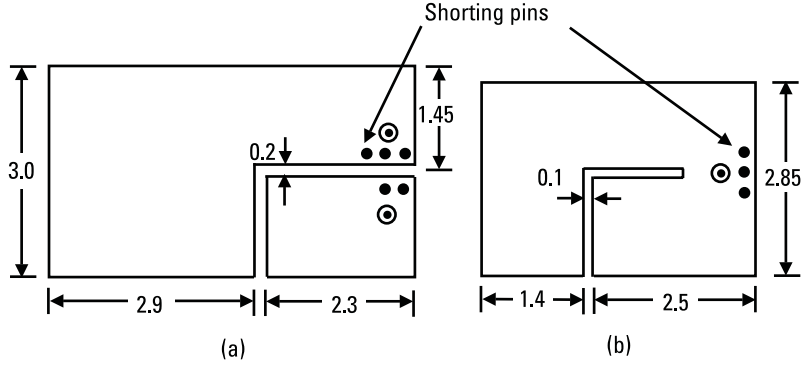

Figure 7.28 Modified inverted F-antenna for dual-band operation using (a) dual feed and (b) single feed.

7.3.5 Dual-Band MSA Using Lumped Element Loading

Instead of using shorting posts, two lumped capacitors may be used to obtain dual-band operation. The capacitor can be realized using varactor diodes with reverse-bias voltage. An RMSA with two varactor diodes is shown in Figure 7.29(a). It is fed at the edge by a microstrip line and double-stub impedance-matching network to improve the impedance characteristics. The microstrip patch length L is designed for the resonance frequency f_2 of 2.1 GHz for ϵ_r = 2.17 and h = 0.079 cm. The varactor diodes are placed symmetrically at the positions $0.3L$ and $0.7L$ to reduce the effects of cross-polarization. Because of the loading of the patch with varactor diodes, a lower resonance frequency f_1 is obtained; this is tuned with the bias voltage of the varactor diodes as shown in Figure 7.29(b). A tuning range of 375–650 MHz is obtained for f_1 as the reverse-bias voltage increases from 2.5V to 16V. The measured BW at both frequencies is 1–2% [42].

7.3.6 Dual-Band MSAs Using Slots

Reactive loading can also be introduced by etching slots inside the patch to yield dual-band operation. A combination of slot and shorting posts is also used for tuning the dual-band operation.

7.3.6.1 Dual-Band RMSAs with Slots for Orthogonal Polarization

An RMSA with a square slot at the center is shown in Figure 7.30(a) [43]. The slot in the center lengthens the excited surface current path for both

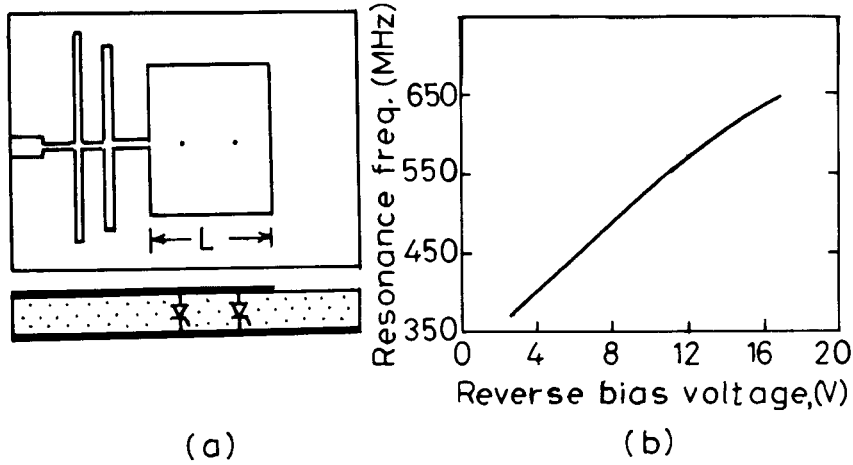

Figure 7.29 (a) An RMSA with two varactor diodes for dual-band operation and (b) variation of lower resonance frequency with the reverse-bias voltage.

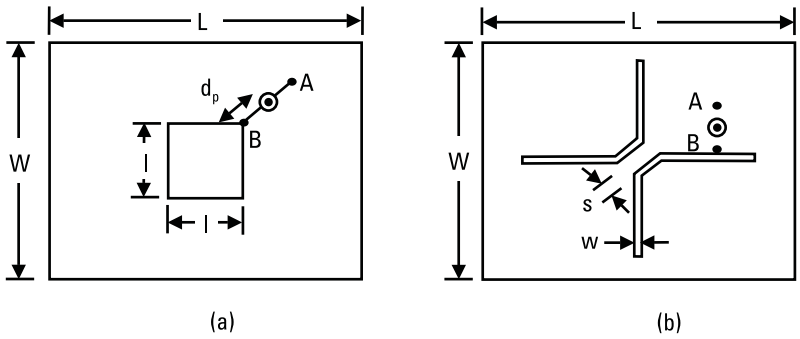

Figure 7.30 RMSA with (a) a square slot at the center and (b) a pair of bent slots.

the TM_{01} and TM_{10} modes and hence reduces the corresponding resonance frequency. A feed point along the diagonal generates a dual band with orthogonal polarization. The length and the width of the RMSA are 3.32 cm and 2.55 cm, respectively, with $\epsilon_r = 4.4$ and $h = 0.16$ cm. The variation of the two frequencies with slot length l is given in Table 7.11. The feed point location d_p is optimized for different slot lengths, and it varies between points A and B. Point B is at the corner of the slot. With an increase in l from 0.0 to 0.9 cm, both the resonance frequencies decrease by about 9%. The frequency ratio f_2/f_1 remains nearly the same because the two dimensions increase with the same proportion because of the square slot. The resonance frequencies decrease further with an increase in the slot length, but the input impedance is too large even for the feed point at the corner of the slot.

A square slot is replaced by a pair of bent slots in the center of the RMSA as shown in Figure 7.30(b) [44]. The configuration with $L = 3.77$ cm, $W = 2.84$ cm, $s = 0.14$ cm, and $w = 0.1$ cm is fabricated on the substrate having $\epsilon_r = 4.4$ and $h = 0.16$ cm. Tunable dual-frequency operation with

Table 7.11
Variation of Resonance Frequencies of RMSA with a Square Slot with Slot Length l ($L = 3.32$ cm, $W = 2.55$ cm, $\epsilon_r = 4.4$, and $h = 0.16$ cm)

l (cm)	d_p (cm)	f_1 (GHz)	f_2 (GHz)	f_2/f_1
0.0	0.6	2.115	2.698	1.27
0.25	0.5	2.094	2.675	1.27
0.75	0.2	2.034	2.587	1.27
0.90	0.0	1.932	2.475	1.28

orthogonal polarization is obtained by varying the length of the bent slots. When the length of the bent slot is increased from 0 to 2.6 cm, both the resonance frequencies decrease, thereby realizing a compact MSA. The percentage decrease in the lower frequency is slightly more than the second frequency and hence the frequency ratio increases slightly from 1.29 to 1.38. This configuration has the advantage that even for a large slot length, impedance matching is obtained at both the frequencies by varying the feed point between the points A and B. The radiation pattern for both the above configurations is in the broadside direction with orthogonal polarization at the two frequencies, and the cross-polar levels remain below 15–20 dB.

The orthogonal polarization at the two frequencies is not acceptable for applications requiring the same polarization. The following subsections describe various configurations to yield dual-frequency operation with the same polarization.

7.3.6.2 RMSAs with Slots Near the Nonradiating Edge for the Same Polarization

A dual-band RMSA with a pair of step slots embedded close to its nonradiating edges is shown in Figure 7.31(a). The dimensions given in Figure 7.31 are in centimeters, and the substrate parameters are $\epsilon_r = 4.4$ and $h = 0.16$ cm. Two slots are chosen to be identical for symmetry, but different widths are selected in one-half of the length to obtain impedance matching at the two frequencies using a single feed as shown in Figure 7.31(a). These slots are resonant at one frequency, and the rectangular patch is resonant at the other frequency. Since the polarization of the slots and the patch is same, this antenna yields dual-frequency operation with the same polarization. By increasing the larger width w of the slot, tunable dual-band operation is obtained as shown in Table 7.12. The optimum feed-point location x and the BWs at the two frequencies are also given in Table 7.12. As w increases from 0.2 cm to 1.0 cm, the effective length of the slot increases, and hence its resonance frequency f_1 decreases from 1.878 GHz to 1.480 GHz. With an increase in w, the resonance frequency f_2 corresponding to the patch decreases initially because of the increase in the path length, but later, the effect of the decrease in ϵ_e becomes dominant, which increases f_2. Therefore, f_2/f_1 increases from 1.23 to 1.63 as w increases from 0.2 cm to 1.0 cm [45].

Instead of using step slots, angular bent slots can be used as shown in Figure 7.31(b) [46]. The effect of an increase in the bent angle is similar to that of increasing the step width discussed above. The tuning of both the frequencies is obtained by changing the angle of the bent slot, which

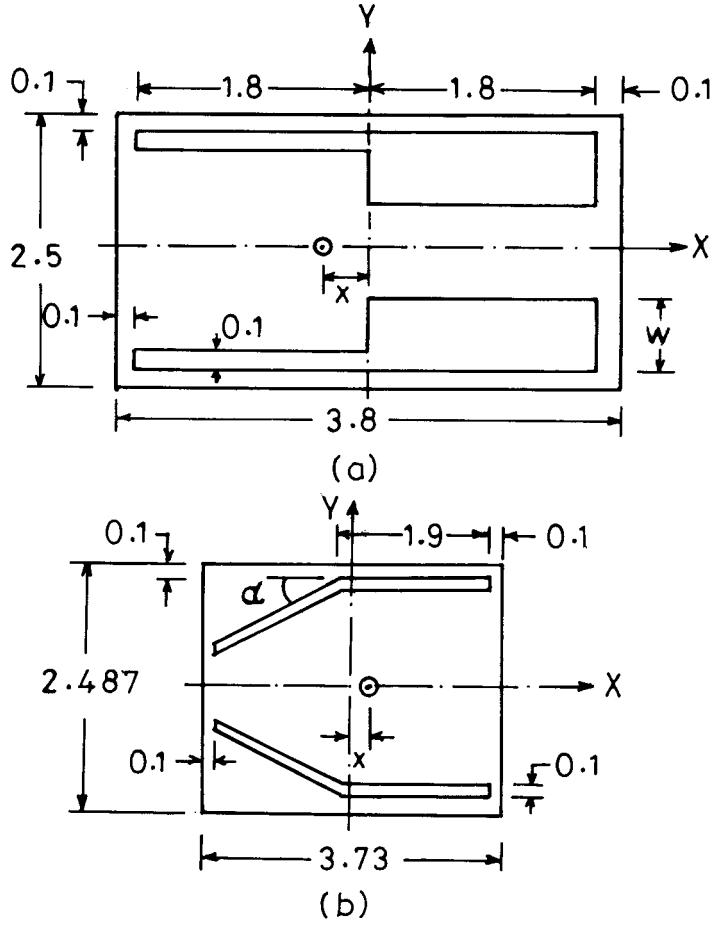

Figure 7.31 RMSA with a pair of (a) step slots and (b) angular bent slots.

Table 7.12
Effect of the Slot Width *w* on the Performance of RMSA with a Pair of Step Slots

w (cm)	*x* (cm)	Lower Resonance f_1 (GHz)	BW %	Higher Resonance f_2 (GHz)	BW %	f_2/f_1
0.2	0.65	1.878	1.76	2.320	1.42	1.23
0.4	0.42	1.834	1.53	2.278	1.19	1.24
0.6	0.35	1.750	1.49	2.272	1.50	1.30
0.8	0.31	1.644	1.70	2.334	1.41	1.42
1.0	0.22	1.480	1.35	2.414	1.33	1.63

increases the total slot length and hence decreases its resonance frequency. As the slant angle increases from 15° to 30°, the f_2/f_1 ratio increases from 1.29 to 1.60. The feed-point location has to be moved toward the center when the slant angle is increased. The radiation pattern is in the broadside direction with the same polarization at the two frequencies for these two configurations.

In the above cases, dual-band operation is due to the resonance of the slot and the patch. In the following subsection, the nonresonant slot is used to change the effective current path length for the TM_{10} and TM_{30} modes of an RMSA for which the radiation is in the broadside direction with the same polarization. The parameters and locations of the slots are chosen in such a way that they change the current path lengths for the two modes in a different ratio to obtain the desired frequency ratio of dual-band operation.

7.3.6.3 Slotted RMSA for Higher Order Modes

An RMSA with two narrow slots etched inside the patch, which are close to and parallel to the radiating edges is shown in Figure 7.32(a) [47, 48]. The dual-band operation of the slotted RMSA can be explained as arising from the perturbation of the two modes (i.e., the TM_{10} and TM_{30} modes of the RMSA), as shown in Figure 7.32(b, c). These narrow slots are placed close to the radiating edges, where the current is nearly minimum for the TM_{10} mode. Consequently, the current distribution for this mode is only slightly perturbed. Hence, its resonance frequency is only slightly different from that of the RMSA without a slot. For the TM_{30} mode, slots are located where the current of the unperturbed TM_{30} mode is significant, leading to the strong modification of the current distribution. As a result, the resonance frequency decreases due to the increase in the current path length introduced by the slot. For ϵ_r = 2.2 and h = 0.08 cm, dual-frequency operation is obtained at 2.22 and 3.48 GHz corresponding to the modified TM_{10} and TM_{30} modes of the RMSA. The frequency ratio is 1.57, which is much smaller than the ratio of 3 for the RMSA without slots. The ratio of two frequencies can be changed by varying the dimensions and location of the slots. The radiation pattern remains in the broadside direction at both the frequencies.

The size of the antenna can be reduced by short-circuiting along the vertical central axis, which corresponds to the zero-potential plane for the TM_{10} and TM_{30} modes, and by using only one-half of the antenna [49]. The two resonance frequencies corresponding to the modified TM_{10} and TM_{30} modes are further reduced by decreasing the shorting width. This leads to a large reduction in the antenna size as compared to the regular slot-

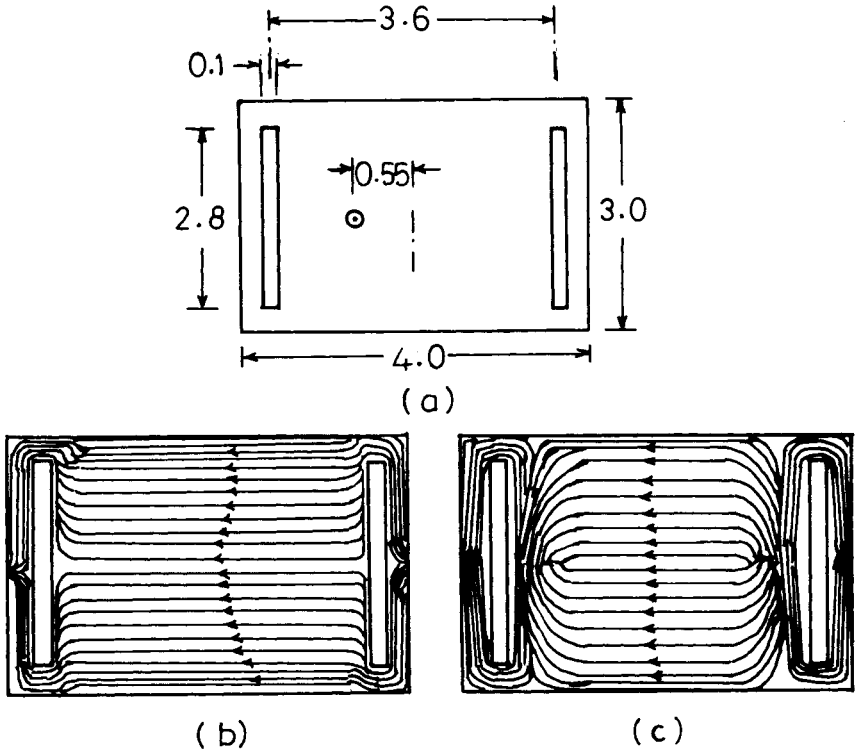

Figure 7.32 (a) RMSA with two slots near the radiating edge and current distributions for the (b) TM_{10} and (c) TM_{30} modes.

loaded RMSA. This configuration, along with its dimension in centimeters, is shown in Figure 7.33(a). The antenna is fabricated on a foam substrate of $h = 0.3$ cm. The input impedance matching is obtained for both the modes with a single feed point. The return loss plot for various shorting width ratios w_s/W is shown in Figure 7.33(b). As w_s/W increases from 0.1 to 1, the f_2/f_1 ratio decreases from 2.2 to 1.6. For $w_s/W = 0.1$, the lower resonance frequency is 1.535 GHz, which is 0.29 times the resonance frequency of 5.35 GHz for a conventional RMSA of the same size.

Section 7.3.1 explained that by feeding the RMSA or square MSA at two orthogonal feed points, orthogonal polarization is obtained. This concept is extended to two pairs of orthogonal slots cut in a square MSA to yield a dual-band (corresponding to the modified TM_{10} and TM_{30} modes), dual-polarized response using two coaxial feeds as shown in Figure 7.34(a). The slotted square patch antenna exhibits a smaller range of frequency ratio than

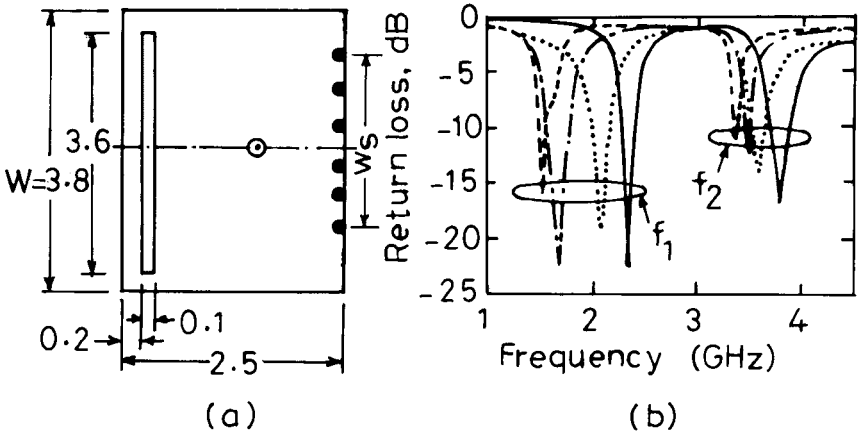

Figure 7.33 (a) Partially shorted RMSA with a slot near its radiating edge and (b) its return loss plot for various values of w_s/W: (——) 1.0, (· · ·) 0.5, (– · –) 0.25, and (- - -) 0.1.

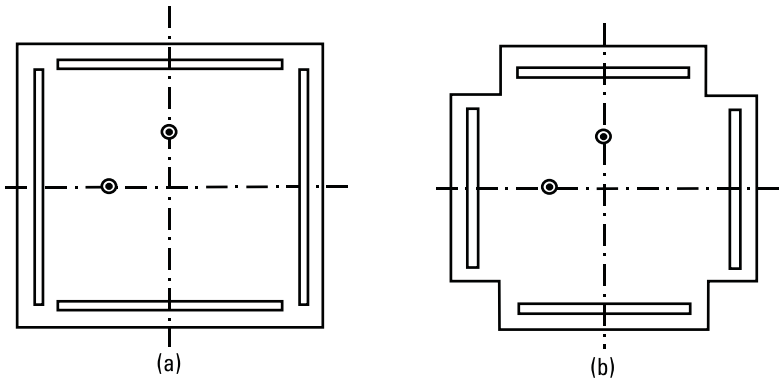

Figure 7.34 Dual-feed (a) square MSA and (b) cross MSA with two pairs of orthogonal slots.

the unslotted patch. At the lower and upper frequencies, an isolation of 35 dB and 40 dB is obtained between the two ports, respectively [21].

In the above configuration, when all the four corners of the square are removed, it becomes a slotted cross patch antenna as shown in Figure 7.34(b). By chopping off the four corners, the isolation between the two orthogonal ports at the lower frequency is improved by 5–6 dB [21]. Also, it occupies less space and has reduced cross-polar components.

A compact dual-band antenna is realized when multiple slits are cut along the length of the slot loaded RMSA [50]. The geometry looks like a

meandered structure as shown in Figure 7.35. With the slits on the nonradiating edges, the surface current path for the two modes TM_{10} and TM_{30} increases, leading to a reduction in the resonance frequency. For the dimensions shown in Figure 7.35 in centimeters, the variation of resonance frequencies with slit length l is given in Table 7.13.

As l increases from 0 to 1.3 cm, the lower resonance frequency f_1 decreases from 1.915 GHz to 1.096 GHz, and the higher resonance frequency f_2 reduces from 3.620 GHz to 2.590 GHz, thereby giving variation of f_2/f_1 ratio from 1.89 to 2.36. The feed point is shifted toward the center to obtain impedance matching, because with an increase in l, resonance frequency decreases, which increases the radiation resistance. The radiation pattern is in the broadside direction at both the frequencies. At the lower frequency, the cross-polarization is less than 20 dB, whereas at a higher frequency, it increases slightly.

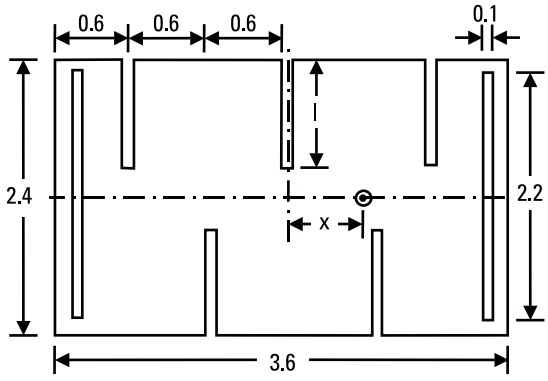

Figure 7.35 RMSA with multiple slits for dual-band operation.

Table 7.13
Variation of Two Frequencies of RMSA with Multiple Slits for Different Slit Length t

l (cm)	x (cm)	Lower Resonance f_1 (GHz)	BW %	Upper Resonance f_2 (GHz)	BW %	f_2/f_1
0.0	0.67	1.915	1.78	3.620	1.19	1.89
0.4	0.63	1.811	1.60	3.620	1.16	2.00
0.6	0.59	1.698	1.53	3.531	1.13	2.08
0.8	0.50	1.553	1.48	3.318	1.12	2.14
1.0	0.50	1.390	1.37	3.062	1.08	2.21
1.2	0.50	1.196	1.34	2.730	1.17	2.28
1.3	0.50	1.096	1.46	2.590	1.24	2.36

7.3.7 Multiresonator Planar MSAs for Dual-Frequency Operation

Dual-frequency operation can also be obtained by using multiresonators, similar to that of the broadband MSA configurations described in Chapters 3 and 4. These resonators could be either coplanar or stacked in two or more layers. If the individual resonators are compact, then the composite dual-band configuration is also compact.

7.3.7.1 Dual-Band Gap-Coupled RMSA

When two rectangular patches are gap-coupled, a broad BW is obtained as described in Section 3.3. A two gap-coupled RMSA configuration is shown in Figure 7.36(a). The dimensions of the antenna are $L = 3$ cm, $W = 4$ cm, $L_1 = 2.9$ cm, $x = 1.1$ cm, $\epsilon_r = 2.55$, $h = 0.159$ cm, and $\tan \delta = 0.001$. For three values of the gap s, the input impedance and VSWR plots are shown in Figure 7.36(b, c). As the gap decreases from 0.1 cm to 0.01 cm, the coupling increases and hence the loop size increases. Accordingly, the broadband operation becomes dual-band operation, and the separation between the two resonance frequencies increases. The upper resonance frequency corresponds to the parasitic patch, and it increases slightly because with a decrease in the gap, the extension along the coupled side decreases, which reduces its effective length. The lower resonance frequency corresponds to the fed patch, and it decreases with a decrease in the gap because of the increase in the value of the series gap capacitance. Thus, for given fed and parasitic patch dimensions, the tunable dual-frequency operation is obtained by simply varying the gap between the two patches. The radiation is in the broadside direction at the lower frequency only, and it is shifted away from the broadside at a higher frequency, because of the phase delay experienced by the parasitic patch as described in Section 3.3.

Instead of using $\lambda/2$ RMSA in a two gap-coupled configuration, if a compact RMSA with a single short (described in Section 6.2.2) is used, a compact dual-band MSA is realized. The tunability of the two frequencies can be obtained either by reducing the air gap or by changing the width of the shorting strip across the gap between the two patches as described below.

7.3.7.2 Hybrid-Coupled Compact Shorted RMSA

A radiating edge hybrid-coupled shorted RMSA is shown in Figure 7.37(a). Both the patches have a single shorting post at the center of the extreme radiating edges. The dimensions of the antenna are $L = 2.3$ cm, $W = 4.6$ cm, $s = 0.1$ cm, $x = 0.65$ cm, $\epsilon_r = 4.3$, $h = 0.16$ cm, and $\tan \delta = 0.02$. For gap coupling between the fed and the parasitic patches, the loop size is within the VSWR = 2 circle leading to the broadband response. To increase the

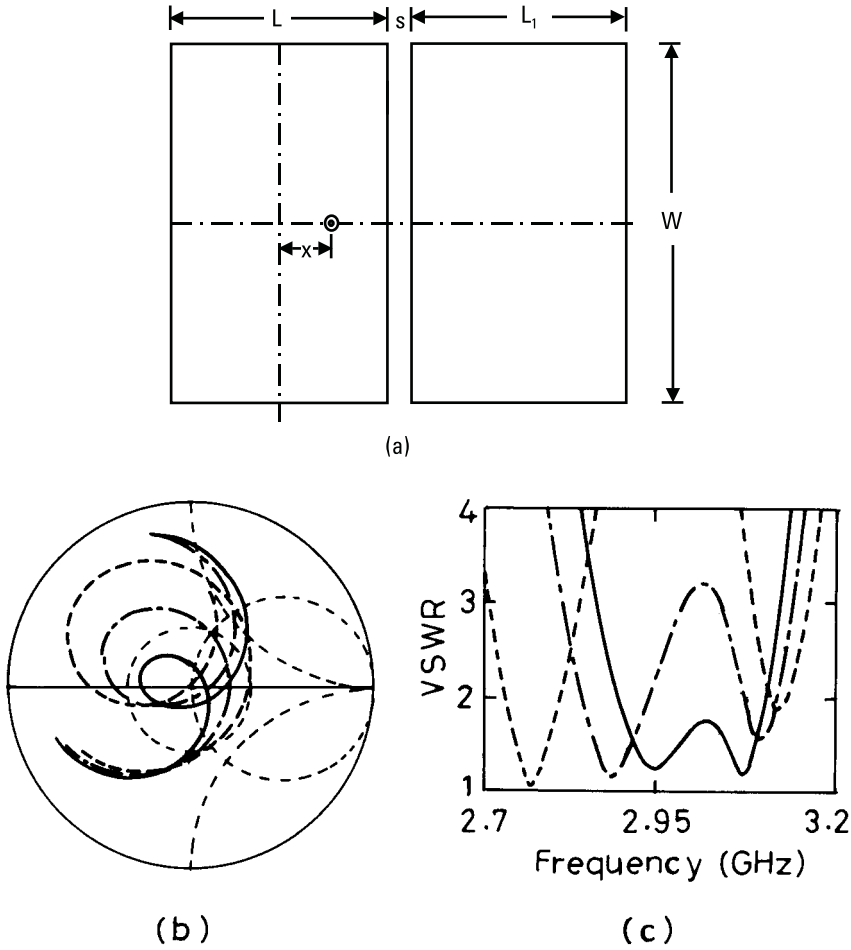

Figure 7.36 (a) Dual-band gap-coupled RMSA and its (b) input impedance and (c) VSWR plots for three values of gap s: (——) 0.1 cm, (– · –) 0.05 cm, and (- - -) 0.01 cm.

coupling, a copper strip is placed across the gap as shown in Figure 7.37(a). Because of the hybrid (gap and direct) coupling, the loop size increases, and it does not completely remain inside the VSWR = 2 circle, thereby yielding a dual-band response [51]. The measured results for different shorting strip widths w are summarized in Table 7.14. With an increase in w from 0.1 cm to 1.0 cm, the lower frequency f_1 decreases from 716 MHz to 621 MHz, while the upper frequency f_2 remains between 752 MHz and

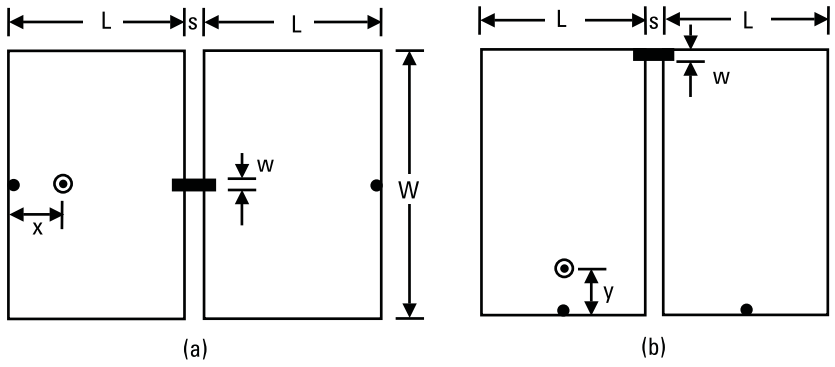

Figure 7.37 Hybrid-coupled shorted RMSA coupled along one of its (a) radiating edges and (b) nonradiating edges.

Table 7.14
Measured Results of Radiating Edge Hybrid-Coupled Shorted RMSA for Different *w*

w	Lower Resonance		Upper Resonance		
(cm)	f_1 (MHz)	VSWR	f_2 (GHz)	VSWR	f_2/f_1
1.0	621	1.39	753	1.74	1.21
0.8	642	1.38	753	1.75	1.17
0.5	660	1.82	753	1.69	1.14
0.3	690	1.74	752	1.61	1.09
0.1	716	1.89	752	1.47	1.05

753 MHz, resulting in an increase in the f_2/f_1 ratio from 1.05 to 1.21. For all these cases, the VSWR remains less than 2 at both the frequencies.

A nonradiating edge hybrid-coupled shorted RMSA is shown in Figure 7.37(b). Along the nonradiating edge, the field variation is sinusoidal. Therefore, the width as well as the position of the copper strip determines the coupling between the fed and the parasitic patches [51]. The coupling is maximum when the strip is placed at the farthest point from the short, as shown in Figure 7.37, where the field is maximum. For L = 2.3 cm, W = 4.6 cm, s = 0.1 cm, y = 0.5 cm, ϵ_r = 4.3, h = 0.16 cm, and tan δ = 0.02, the results for various coupling strip widths w are given in Table 7.15. When w is reduced from 1.0 cm to 0.2 cm, f_2 stays around 637 MHz, while f_1 increases from 560 MHz to 617 MHz, resulting in a variation of the f_2/f_1 ratio from 1.14 to 1.03.

Table 7.15
Measured Results of Nonradiating Edge Hybrid-Coupled Shorted RMSA for Different *w*

w (cm)	Lower Resonance f_1 (MHz)	VSWR	Upper Resonance f_2 (GHz)	VSWR	f_2/f_1
1.0	560	1.40	636	1.22	1.14
0.8	573	1.37	637	1.18	1.11
0.6	585	1.32	637	1.17	1.09
0.4	601	1.25	637	1.21	1.06
0.2	617	1.30	637	1.32	1.03

Similarly, SCMSAs, shorted 90°-sectoral MSAs, and other compact configurations described in Chapter 6 can be gap- or hybrid-coupled to realize a tunable dual-band MSA [52, 53].

7.3.7.3 Dual-Frequency MSA at the S- and X-Bands

Many radar and communication systems often require a large separation between the two frequencies, so the multiresonator configuration requires patches of very different resonant lengths. A simple example of this concept is shown in Figure 7.38 [54]. It consists of a cross-shaped patch at the S-band and a subarray of four patches at the X-band. The dimensions of the patches and the separation between them are shown in Figure 7.38,

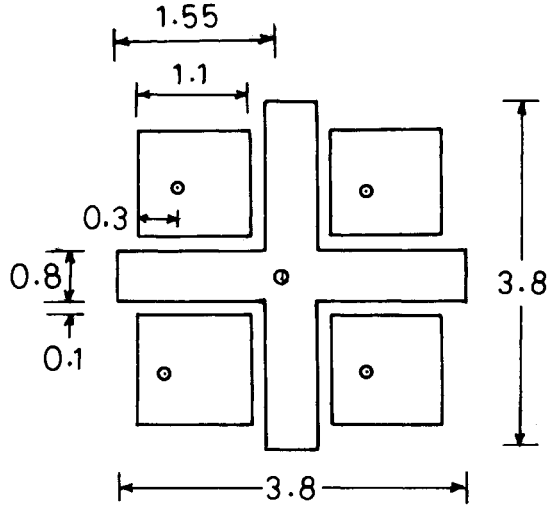

Figure 7.38 Dual frequency MSA at the S- and X-bands.

and the substrate parameters are ϵ_r = 2.2 and h = 0.08 cm. The layout is suitable for use in dual-frequency arrays. The cross-shaped patch resonates at 2.85 GHz, and four square patches operate as a subarray at 8.65 GHz. The resonance frequency of the cross-patch is only slightly perturbed by the addition of four square patches, since the radiating edges of the cross patch are away from the four square patches. However, the resonance frequency of the square patches is affected by the presence of the cross patch, which causes a reactive loading to the square patch. Therefore, the upper resonance frequency corresponding to the four square patches is slightly lower than that of the isolated square patches. The decrease of this upper frequency is noticeable when the spacing is less than the substrate thickness because of increased gap coupling. In designing the antenna, one should carefully choose the distance between the square patches, which should be less than $0.7\lambda_0$ to avoid scan blindness at the upper frequency.

7.3.8 Stacked MSAs for Dual-Frequency Operation

The stacked ECMSA and ACMSA configurations are discussed in Chapter 4 for broadband operations. These configurations also yield dual-band operation by optimizing the dimensions of the patches and the coupling between them. The ECMSA and ACMSA geometries for dual-band operation are discussed separately in the following subsections.

7.3.8.1 Dual-Band Circular ECMSAs

A dual-frequency stacked CMSA is shown in Figure 7.39 [55]. Air gaps Δ_1 and Δ_2 are introduced between the ground plane and the lower patch and between the two patches for tuning the resonance frequency. The coaxial

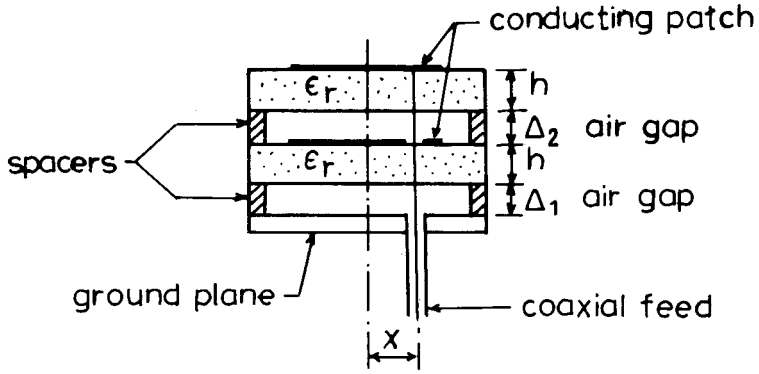

Figure 7.39 Tunable dual-frequency circular ECMSA.

feed is directly connected to the top patch and the bottom patch is electromagnetically coupled. Two circular discs with an equal diameter of 7.0 cm are fabricated on a substrate with ϵ_r = 2.32 and h = 0.159 cm. For Δ_1 = 0, when Δ_2 is varied from 0 to 0.1 cm, the higher resonance frequency f_2 increases from 825 MHz to 910 MHz, whereas the lower resonance frequency f_1 remains fixed around 775 MHz. This yields f_2/f_1 variation from 1.06 to 1.17. When Δ_2 = 0 and Δ_1 is varied, then both the resonance frequencies change. Hence, the convenient way to tune f_2/f_1 is to fix the values of Δ_1 and patch dimensions for given f_1 and then vary Δ_2 to realize f_2.

Similar results of dual-band operation can be obtained by stacking rectangular, annular ring, and triangular patches [56–61]. Instead of using regularly shaped patches, various compact antennas described in Chapter 6 may also be stacked to realize compact dual-band antennas [62, 63].

7.3.8.2 Dual-Band ACMSAs

Instead of using a coaxial feed for the stacked patches, these can also be excited using an aperture-coupling technique to yield a dual-band response. Similarly, compact configurations described in Chapter 6 and other coaxial-fed dual-band configurations covered in this chapter can be aperture-coupled [64, 65]. To give an example, an RMSA with two slots described in Section 7.3.6 could be fed by a microstrip line through an aperture in the ground plane as shown in Figure 7.40. A rectangular aperture is cut in the ground plane and a microstrip line feed is used on the other side of the ground plane. The dimensions of the antenna are shown in Figure 7.40. The upper substrate where the square patch is located has ϵ_{r1} = 2.2 and h_1 = 0.16 cm. The feed transmission line on the lower substrate with ϵ_r = 2.55 and h = 0.08 cm has a width of 0.22 cm and extends by length l_s = 2.06 cm beyond the slot as shown in Figure 7.40(b). The two equal slots with lengths l are equidistant from the center and are at distance d_s from the respective edges. This configuration is analyzed using the cavity model and the input impedance is calculated using the theorem of energy conversion [65].

The position and length of the slots primarily change the third-order resonance frequency f_2 and to a lesser extent the fundamental TM_{10} resonance frequency f_1. For l = 4.6 cm and d_s = 0.15 cm, the theoretical resonance frequencies are 1.810 GHz and 2.610 GHz, against the respective measured frequencies of 1.835 GHz and 2.590 GHz. The variation of the f_2/f_1 ratio with the slot length l and distance d_s are shown in Figure 7.40(c, d). As l increases from 2.5 to 4.5 cm, the f_2/f_1 ratio decreases from 2.1 to 1.4. As the separation between slots increases (i.e., d_s decreases from 0.4 cm to

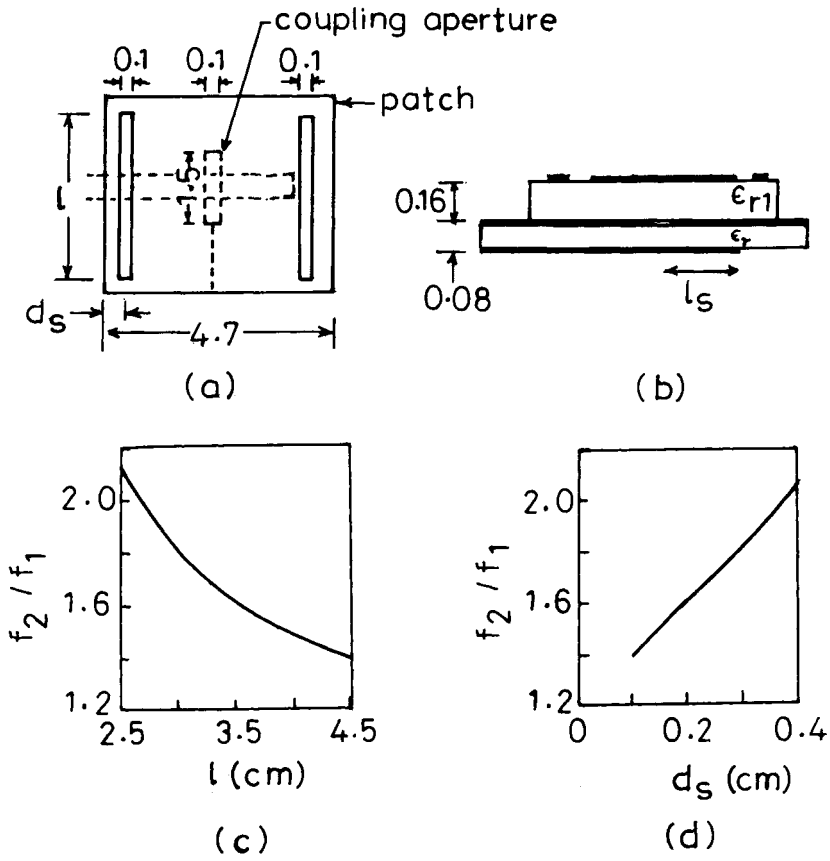

Figure 7.40 An aperture-coupled RMSA with two slots: (a) top and (b) side views. Variation of f_2/f_1 with (c) slot length l and (d) slot position d_s.

0.1 cm), the f_2/f_1 ratio decreases from approximately 2.0 to 1.4. Consequently, a low value of the f_2/f_1 ratio requires longer slots located closer to the two edges.

7.3.8.3 Aperture-Coupled Coplanar Parallel Dipoles for Multifrequency Operation

Coplanar parallel dipoles fed by aperture coupling could be used to obtain multifrequency operation. The dipoles of different lengths are fed by a microstrip line through a rectangular slot cut in the ground plane. In general, this antenna consists of $2N$ dipoles of N different lengths, which are symmetrically excited through the aperture at N frequencies [66]. Either the longest identical pair of dipoles could be placed in the center of the slot and smallest

identical pair close to the edges of the slot, or the smallest dipoles could be placed in the center and the longest at the edge. For the latter case, six symmetrical dipoles are shown in Figure 7.41. Starting from the edge dipole, the lengths are l_1, l_2, and l_3, and the widths are w_1, w_2, and w_3, and the distance between the two identical pairs of the dipoles are d_1, d_2, and d_3. The various dimensions of dipoles are: l_1 = 2.05 cm, l_2 = 1.775 cm, l_3 = 1.55 cm, w_1 = 0.1 cm, w_2 = 0.075 cm, w_3 = 0.05 cm, d_1 = 0.65 cm, d_2 = 0.425 cm, and d_3 = 0.1 cm. The parameters of the foam where the dipoles are located are ϵ_{r1} = 1.07, h_1 = 0.52 cm and tan δ_1 = 0.00042. The radiating elements are covered with a radome whose parameters are ϵ_{r2} = 2.33, h_2 = 0.0762 cm and tan δ_2 = 0.0012. The bottom layer feed substrate parameters are ϵ_r = 2.2, h = 0.0762 cm, and tan δ = 0.0009. The length and width of the feed transmission line are 0.36 cm and 0.232 cm, respectively. The aperture (slot) has a length of 1.4 cm and a width of 0.08 cm.

Since there are three pairs of dipoles, there will be three resonance frequencies. The theoretical (obtained using the SDT) and the measured resonance frequencies and their corresponding BWs are given in Table 7.16 [66].

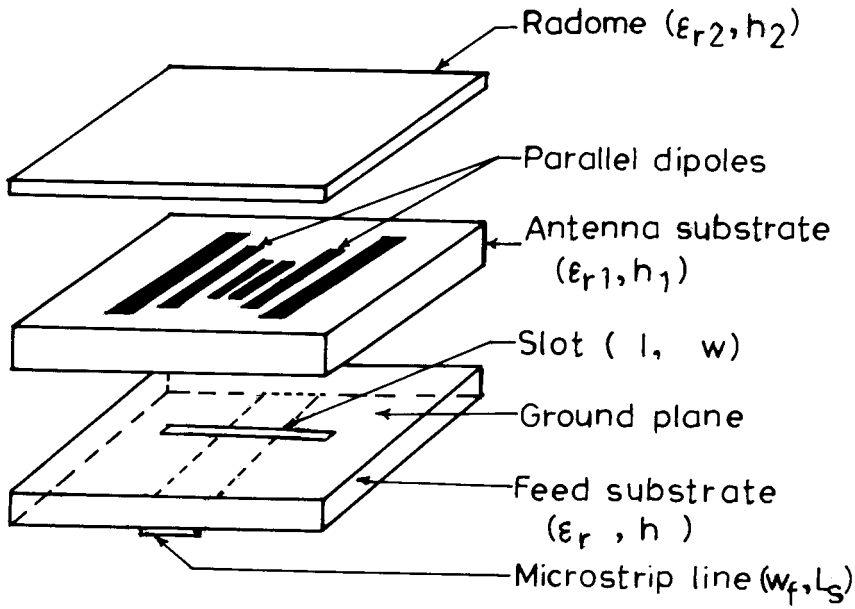

Figure 7.41 ACMSA with six coplanar parallel dipoles.

Table 7.16
Theoretical and Measured Resonance Frequencies of Aperture-Coupled Coplanar Parallel Dipoles

Resonance Frequency (GHz)		BW (%)	
Theoretical	**Measured**	**Theoretical**	**Measured**
5.12	5.17	7.6	7.2
6.36	6.25	2.4	1.9
7.30	7.16	1.5	1.1

This configuration yielded low BWs at the second and third frequencies, because proper matching is achieved only at the first frequency and the matching is not very good at higher frequencies. The theoretical and measured ratios of extreme frequencies are 1.426:1 and 1.385:1, respectively. Similarly, the configuration with three pairs of dipoles arranged with longest pair near the center and the smallest pair at the edge also yields triple-frequency operation. The radiation pattern is in the broadside direction at all the three frequencies, and the antenna is attractive for its simplicity.

7.4 Summary

In multichannel applications, the antenna is required to operate over a broad BW to cover all the channels. However, at any given time, it requires a small BW to cover a single channel. In this case, a tunable MSA is required. If the antenna is designed to operate at two far-away frequencies, then a dual-band MSA could be used.

Various techniques have been described to tune the resonance frequency of the MSA. The tuning of the resonance frequency around the 20% range is achieved by loading the MSA with external reactive components such as stubs, shorting posts, and varactor and PIN diodes. The frequency is also tuned by varying the thickness of the air gap between the patch substrate and the ground plane. This tunable configuration is useful if the increased thickness of the antenna is acceptable.

Dual-frequency operation with the same or orthogonal polarizations at two frequencies is described. Different methods such as higher order modes, stub loading with lengths comparable to $\lambda/4$, loading the patch with lumped components, shorting posts, and slots are discussed. By using shoring posts, two modes of the rectangular patch TM_{10} and TM_{30} are excited at

which the radiation pattern is in the broadside direction. The separation between the two resonance frequencies is controlled by changing the position of the single shorting post. When a lower dual-frequency ratio is required, then RMSA or CMSA with a single short can be used, whereas a single short TMSA yields a higher dual-frequency ratio. The separation between the two frequencies can be reduced significantly by using slots inside the patch.

Dual-frequency operation is also achieved by coplanar or stacked multiresonator configurations, when the separation of the two frequencies is in the range of 10–20%. A stacked geometry offers the advantages of operating in the same mode and the flexibility of tuning the separation by means of an air gap. Aperture-coupled coplanar parallel dipoles yield multifrequency operation. This configuration has the advantage that individual resonance frequencies can be easily tuned by changing the length of the dipoles.

References

[1] James, J. R., and P. S. Hall, *Handbook of Microstrip Antennas,* Vol. 1, London: Peter Peregrinus, Ltd., 1989.

[2] Plessis, M. Du., and J. H. Cloete, "Tuning Stub for Microstrip Patch Antenna," *IEEE AP-S Int. Symp. Digest,* June 1993, pp. 964–967.

[3] Srinivasan, V., "Multiport Network Model for Variations in Rectangular Microstrip Antennas," Ph.D. thesis, Indian Institute of Technology, Bombay, India, 2000.

[4] IE3D 7.0, Zeland Software, Inc., Fremont, CA, 2000.

[5] Ray, K. P., and G. Kumar, "Tunable and Dual Band Circular Microstrip Antenna with Stubs," *IEEE Trans. Antennas Propagation,* Vol. AP-48, July 2000, pp. 1036–1039.

[6] Babu, S., and G. Kumar, "Parametric Study and Temperature Sensitivity of Microstrip Antennas Using an Improved Linear Transmission Line Model," *IEEE Trans. Antennas Propagation,* Vol. AP-47, 1999, pp. 221–226.

[7] Ray, K. P., "Broadband, Dual-Frequency and Compact Microstrip Antennas," Ph.D. thesis, Indian Institute of Technology, Bombay, India, 1999.

[8] Ray, K. P., and G. Kumar, "Stub Loaded Circular Microstrip Antennas," *Proc. APSYM-98,* Kochi, India, December 1998, pp. 84–87.

[9] Ray, K. P., and G. Kumar, "Circular Microstrip Antenna with Double Stubs," *Proc. ISRAMT-99,* Malaga, Spain, December 1999, pp. 381–384.

[10] Daniel, A. E., and G. Kumar, "Multiport Network Model for Tunable Rectangular Microstrip Antennas," *Proc. NSMAL,* New Delhi, India, December 1995, pp. 572–577.

[11] Schaubert, D. H., et al., "Microstrip Antennas with Frequency Agility and Polarization Diversity," *IEEE Trans. Antennas Propagation,* Vol. AP-29, 1981, pp. 118–123.

[12] Bhartia, P., and I. J. Bahl, "A Frequency Agile Microstrip Antenna," *IEEE AP-S Int. Symp. Digest,* 1982, pp. 304–307.

[13] Daryoush, A. S., K. Bontzos, and P. R. Hercsfeld, "Optically Tuned Patch Antenna for Phased Array Applications," *IEEE AP-S Int. Symp. Digest,* 1986, pp. 361–364.

[14] Lee, K. F., K. Y. Ho, and J. S. Dahele, "Circular-Disc Microstrip Antenna with an Air Gap," *IEEE Trans. Antennas Propagation,* Vol. AP-32, 1984, pp. 880–884.

[15] Dahele, J. S., and K. F. Lee, "Theory and Experiment on Microstrip Antennas with Air Gap," *IEE Proc. Microwaves, Antennas Propagation,* Pt. H, Vol. 132, 1985, pp. 455–460.

[16] Lee, K. F., and J. S. Dahele, "The Two Layered Annular Ring Microstrip Antenna," *Int. J. Electronics,* Vol. 61, 1986, pp. 207–217.

[17] Das, N., and S. K. Chowdhury, "Rectangular Microstrip Antenna on a Ferrite Substrate," *IEEE Trans. Antennas Propagation,* Vol. AP-30, No. 3, 1982, pp. 499–502.

[18] Das, N., S. K. Chowdhury, and J. S. Chaterjee, "Circular Microstrip Antenna on a Ferrite Substrate," *IEEE Trans. Antennas Propagation,* Vol. AP-31, No. 1, 1983, pp. 188–190.

[19] Pozar, D. M., and V. Sanchez, "Magnetic Tuning of a Microstrip Antenna on a Ferrimagnetic Substrate," *Electronics Letters,* Vol. 24, June 1988, pp. 729–731.

[20] Mishra, R. K., S. S. Patnaik, and N. Das, "Tuning of Microstrip Antenna on Ferrite Substrate," *IEEE Trans. Antennas Propagation,* Vol. AP-41, No. 2, 1993, pp. 230–233.

[21] Maci, S., and G. B. Gentilli, "Dual Frequency Patch Antenna," *IEEE AP Magazine,* Vol. 39, December 1997, pp. 13–17.

[22] Chen, J. S., and K. L. Wong, "A Single-Layer Dual-Frequency Rectangular Microstrip Patch Using a Single Probe Feed," *Microwave Optical Tech. Letters,* Vol. 11, No. 2, 1996, pp. 83–84.

[23] Antar, Y. M. M., A. I. Ittipiliboon, and A. Bhattacharya, "A Dual-Frequency Antenna Using a Single Patch and an Inclined Slot," *Microwave Optical Tech. Letters,* Vol. 8, No. 6, 1995, pp. 309–310.

[24] Srinivasan, V., K. P. Ray, and G. Kumar, "Orthogonal Polarized Microstrip Antennas," *Proc. NSAML-2000,* Delhi, India, March 2000, pp. 43–46.

[25] Deepukumar, M., et al., "Broadband Dual Frequency Microstrip Antennas," *Electronics Letters,* Vol. 32, August 1996, pp. 1531–1532.

[26] Murakami, Y., et al., "Dual Slot Coupled Microstrip Antenna for Dual Frequency Operation," *Electronics Letters,* Vol. 29, October 1993, pp. 1906–1907.

[27] Richards, W. F., S. E. Davidson, and S. A. Long, "Dual Band Reactively Loaded Microstrip Antenna," *IEEE Trans. Antennas Propagation,* Vol. AP-33, May 1985, pp. 556–561.

[28] Davidson, S. E., S. A. Long, and W. F. Richards, "Dual Band Microstrip Antennas with Monolithic Reactive Loading," *Electronics Letters,* Vol. 21, September 1985, pp. 936–937.

[29] Daniel, A. E., and G. Kumar, "Tunable Dual and Triple Frequency Stub Loaded Rectangular Microstrip Patch Antenna," *IEEE AP-S Int. Symp. Digest,* 1995, pp. 2140–2143.

[30] Nakano, H., and K. Vichien, "Dual Frequency Square Patch Antenna with Rectangular Notch," *Electronics Letters,* Vol. 25, August 1989, pp. 1067–1068.

[31] Palit, S. K., A. Hamadi, and D. Tan, "Design of a Wideband Dual-Frequency Notched Microstrip Antenna," *IEEE AP-S Int. Symp. Digest,* 1998, pp. 2351–2354.

[32] Hernandez, D. S., and I. D. Robertson, "Analysis and Design of a Dual Band Circularly Polarized Microstrip Patch Antenna," *IEEE Trans. Antennas Propagation,* Vol. AP-43, February 1995, pp. 201–205.

[33] Hernandez, D. S., and I. D. Robertson, "Triple Band Microstrip Patch Antenna Using a Spur-Line Filter and a Perturbation Segment Technique," *Electronics Letters,* Vol. 29, August 1993, pp. 1565–1566.

[34] Vaello, A. S., and D. S. Hernandez, "Printed Antenna for Dual Band GSM/DCS 1800 Mobile Handsets," *Electronics Letters,* Vol. 34, January 1998, pp. 140–141.

[35] Zhong, S. S., and Y. T. Lo, "Single Element Rectangular Microstrip Antenna for Dual Frequency Operation," *Electronics Letters,* Vol. 19, No. 8, 1983, pp. 298–300.

[36] Pan, S. C., and K. L. Wong, "Design of Dual-Frequency Microstrip Antennas Using a Shorting-Pin Loading," *IEEE AP-S Int. Symp. Digest,* 1998, pp. 312–314.

[37] Srinivasan, V., R. Kapur, and G. Kumar, "MNM for Compact Dual Frequency Rectangular Microstrip Antenna," *Proc. APSYM-98,* Kochi, India, December 1998, pp. 88–91.

[38] Tang, C. T., H. T. Chen, and K. L. Wong, "Small Circular Microstrip Antenna with Dual-Frequency Operation," *Electronics Letters,* Vol. 33, June 1997, pp. 1112–1113.

[39] Pan, S. C., and K. L. Wong, "Dual-Frequency Triangular Microstrip Antenna with Shorting Pin," *IEEE Trans. Antennas Propagation,* Vol. AP-45, December 1997, pp. 1889–1891.

[40] Liu, Z. D., P. S. Hall, and D. Wake, "Dual-Frequency Planar Inverted-F Antenna," *IEEE Trans. Antennas Propagation,* Vol. AP-45, October 1997, pp. 1451–1458.

[41] Srinivasan, V., S. Malhotra, and G. Kumar, "Multiport Network Model for Chip-Resistor-Loaded Rectangular Microstrip Antenna," *Microwave Optical Tech. Letters,* Vol. 24, No. 1, 2000, pp. 11–13.

[42] Waterhouse, R. B., and N. V. Shuley, "Dual Frequency Microstrip Rectangular Patch," *Electronics Letters,* Vol. 28, September 1992, pp. 606–607.

[43] Chen, W. S, "Single Feed Dual Frequency Rectangular Microstrip Antenna with Square Slot," *Electronics Letters,* Vol. 34, February 1998, pp. 231–232.

[44] Wong, K. L., and K. P. Yang, "Compact Dual Frequency Microstrip Antenna with a Pair of Bent Slots," *Electronics Letters,* Vol. 34, February 1998, pp. 225–226.

[45] Lu, J. H., "Single-Feed Dual-Frequency Rectangular Microstrip Antenna with Pair of Step-Slots," *Electronics Letters,* Vol. 35, March 1999, pp. 354–355.

[46] Wong, K. L., and J. Y. Sze, "Dual Frequency Slotted Rectangular Microstrip Antenna," *Electronics Letters,* Vol. 34, July 1998, pp. 1368–1370.

[47] Maci, S., G. B. Gentilli, and G. Avitabile, "Single Layer Dual Frequency Patch Antenna," *Electronics Letters,* Vol. 29, August 1993, pp. 1441–1443.

[48] Maci, S., et al., "Dual Band Slot Loaded Patch Antenna," *IEE Proc. Microwaves, Antennas Propagation,* Pt. H, Vol. 142, June 1995, pp. 225–232.

[49] Guo, Y. X., K. M. Luk, and K. F. Lee, "Dual-Band Slot-Loaded Short Circuited Patch Antenna," *Electronics Letters,* Vol. 36, February 2000, pp. 289–291.

[50] Lu, J. H., and K. L. Wong, "Slot Loaded, Meandered Rectangular Microstrip Antenna with Compact Dual Frequency Operation," *Electronics Letters,* Vol. 34, May 1998, pp. 1048–1049.

[51] Kapur, R., and G. Kumar, "Hybrid Coupled Shorted Rectangular Microstrip Antennas," *Electronics Letters,* Vol. 35, No. 18, 1999, pp. 1501–1502.

[52] Ray, K. P., and G. Kumar, "Hybrid Coupled Microstrip Antennas," *IETE Technical Review,* Vol. 16, No. 1, 1999, pp. 81–84.

[53] Ray, K. P., and G. Kumar, "Compact Gap-Coupled Shorted 90° Sectoral Microstrip Antennas for Broadband and Dual-Band Operations," *Microwave Optical Tech. Letters,* Vol. 26, No. 3, 2000, pp. 143–145.

[54] Salvador, C., et al., "A Dual Frequency Planar Microstrip Antenna at S and X Bands," *Electronics Letters,* Vol. 31, No. 20, 1995, pp. 1706–1707.

[55] Long, S. A., and M. D. Walton, "Dual Frequency Stacked Circular Disc Antenna," *IEEE Trans. Antennas Propagation,* Vol. AP-27, No. 2, 1979, pp. 270–273.

[56] Dahele, J. S., and K. F. Lee, "A Dual Frequency Stacked Microstrip Antenna," *IEEE AP-S Int. Symp. Digest,* 1982, pp. 308–311.

[57] Bennegueouche, J., J. P. Damiano, and A. Papiernik, "Original Multilayer Microstrip Disc Antenna for Dual-Frequency Band Operation: Theory and Experiment," *IEE Proc. Microwaves, Antennas Propagation,* Pt. H, Vol. 140, December 1993, pp. 441–446.

[58] Dahele, J. S., K. F. Lee, and D. P. Wong, "Dual Frequency Stacked Annular Ring Microstrip Antenna," *IEEE Trans. Antennas Propagation,* Vol. AP-35, November 1987, pp. 1281–1285.

[59] Tagle, J. G., and C. G. Christodoulous, "Extended Cavity Model Analysis of Stacked Microstrip Ring Antennas," *IEEE Trans. Antennas Propagation,* Vol. AP-45, November 1997, pp. 1626–1635.

[60] Bhatnagar, P. S., et al., "Experimental Study on Stacked Triangular Microstrip Antennas," *Electronics Letters,* Vol. 22, 1986, pp. 864–865.

[61] Iwasaki, H., and Y. Suzuki, "Dual Frequency Multilayered Circular Patch Antenna with Self-Diplexing Function," *Electronics Letters,* Vol. 31, April 1995, pp. 599–601.

[62] Ollikainen, J., M. Fischer, and P. Vainikainen, "Thin Dual-Resonant Stacked Shorted Patch Antenna for Mobile Communications," *Electronics Letters,* Vol. 35, 1999, pp. 437–438.

[63] Zaid, L., et al., "Dual-Frequency and Broad-Band Antennas with Stacked Quarter Wavelength Elements," *IEEE Trans. Antennas Propagation,* Vol. AP-47, April 1999, pp. 654–660.

[64] Wang, J., et al., "Multifunctional Aperture Coupled Stacked Patch Antenna," *Electronics Letters,* Vol. 26, December 1990, pp. 2067–2068.

[65] Yazidi, M. E., M. Himdi, and J. P. Daniel, "Aperture Coupled Microstrip Antenna for Dual Frequency Operation," *Electronics Letters,* Vol. 29, August 1993, pp. 1506–1508.

[66] Croq, F., and D. M. Pozar, "Multifrequency Operation of Microstrip Antennas Using Aperture Coupled Parallel Resonators," *IEEE Trans. Antennas Propagation,* Vol. AP-40, November 1992, pp. 1367–1374.

8

Broadband Circularly Polarized MSAs

8.1 Introduction

The previous chapters emphasize broadband linearly polarized MSAs. However, there are many applications, where CP is required. In a communication system that uses circularly polarized radiation the rotational orientations of the transmitter and the receiver antennas are unimportant in relation to the received signal strength. With linearly polarized signals, on the other hand, there will be very weak reception if the transmitter and receiver antenna orientations are nearly orthogonal. Also in CP, after reflection from metallic objects, the sense of polarization reverses from *left-hand CP* (LHCP) to *right-hand CP* (RHCP) and vice versa to produce predominantly orthogonal polarization. The system then tends to discriminate the reception of such reflected signals from other signals arising from direct paths. Therefore, CP is useful for a number of applications, such as radar, communication, and navigational systems [1–3].

Before discussing various circularly polarized MSAs, different types of polarization are described briefly. The polarization of a wave is expressed in terms of the figure traced as a function of time by the extremity of the E-field vector at a fixed location in space, and the sense in which it is traced, as observed along the direction of propagation.

8.2 Linear, Circular, and Elliptical Polarizations

The polarization of an electromagnetic wave may be linear, circular, or elliptical [4]. The instantaneous field of a plane wave, traveling in the negative z-direction, is given by

$$E(z, t) = E_x(z, t)\hat{x} + E_y(z, t)\hat{y} \tag{8.1}$$

The instantaneous components are related to their complex counterparts by

$$E_x(z, t) = E_x \cos(\omega t + \beta z + \phi_x) \tag{8.2}$$

and

$$E_y(z, t) = E_y \cos(\omega t + \beta z + \phi_y) \tag{8.3}$$

where E_x and E_y are the maximum magnitudes and ϕ_x and ϕ_y are the phase angles of the x and y components, respectively, ω is the angular frequency, and β is the propagation constant.

For the wave to be linearly polarized, the phase difference between the two components must be

$$\Delta\phi = \phi_y - \phi_x = n\pi, \text{ where } n = 0, 1, 2, \ldots \tag{8.4}$$

The wave is circularly polarized when the magnitudes of the two components are equal (i.e., $E_x = E_y$) and the phase difference $\Delta\phi$ is an odd multiple of $\pi/2$; in other words,

$$\Delta\phi = \phi_y - \phi_x = \begin{cases} +(2n + 1/2)\pi & \textit{for RHCP} \\ \textit{or} & \\ -(2n + 1/2)\pi & \textit{for LHCP} \end{cases} \tag{8.5}$$

If $E_x \neq E_y$ or $\Delta\phi$ does not satisfy (8.4) and (8.5), then the resulting polarization is of elliptical shape as shown in Figure 8.1. The performance of a circularly polarized antenna is characterized by its AR. The AR is defined as the ratio of the major axis to the minor axis; in other words,

$$AR = \frac{\text{major axis}}{\text{minor axis}} = \frac{OA}{OB} \tag{8.6}$$

where

$$OA = \left[\frac{1}{2}\left\{E_x^2 + E_y^2 + \left[E_x^4 + E_y^4 + 2E_x^2E_y^2\cos(2\Delta\phi)\right]^{1/2}\right\}\right]^{1/2} \tag{8.7}$$

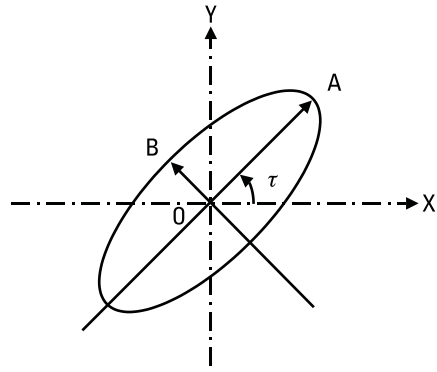

Figure 8.1 Elliptically polarized wave.

and

$$\mathrm{OB} = \left[\frac{1}{2}\left\{\mathrm{E}_x^2 + \mathrm{E}_y^2 - \left[\mathrm{E}_x^4 + \mathrm{E}_y^4 + 2\mathrm{E}_x^2\mathrm{E}_y^2\cos\left(2\Delta\phi\right)\right]^{1/2}\right\}\right]^{1/2} \tag{8.8}$$

The tilt angle τ of the ellipse is given by

$$\tau = \frac{\pi}{2} - \frac{1}{2}\tan^{-1}\left[\frac{2\mathrm{E}_x\mathrm{E}_y}{\mathrm{E}_x^2 - \mathrm{E}_y^2}\cos\left(\Delta\phi\right)\right] \tag{8.9}$$

For CP, OA = OB (i.e., AR = 1), whereas for linear polarization, AR $\rightarrow \infty$. The deviation of AR from unity puts a limit on the operating frequency range of the circularly polarized antennas. Generally, AR = 3–6 dB (numerical value 1.414 to 2) is acceptable for most of the practical applications.

8.3 Dual-Feed Circularly Polarized MSAs

A circularly polarized MSA can be realized by exciting two orthogonal modes with equal magnitudes, which are in phase quadrature. The sign of the relative phase determines the sense of polarization (LHCP or RHCP) [1, 3]. The simplest way to obtain CP is to use two feeds at orthogonal positions that are fed by $1\angle 0°$ and $1\angle 90°$ as shown in Figure 8.2. For a

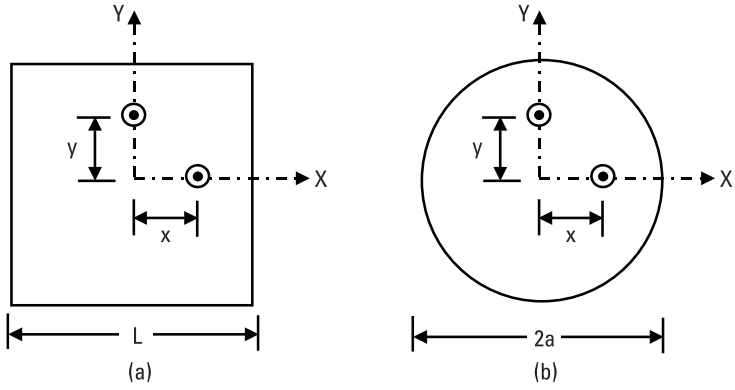

Figure 8.2 Dual-feed (a) square MSA and (b) CMSA.

square or circular patch operating in the fundamental mode, when the two feeds are placed orthogonal to each other, the input impedance and resonance frequency of the antenna remain unaffected as the two feeds are at the null location of the orthogonal mode. An isolation of more than 30 dB is obtained between the two feeds as described in Sections 2.2.3 and 2.3.8. Equal power with 90° phase difference to the feeds can be obtained either by using an external two-way 0° and 90° power divider or it can be integrated along with the antenna itself as described below.

8.3.1 Square MSA with Two Feeds

A linearly polarized square MSA with L = 3 cm, ϵ_r = 2.55, h = 0.159 cm, and tan δ = 0.001 is described in Section 2.2.3. When this square is fed at the two orthogonal points at x = 0.5 cm and at y = 0.5 cm with $1\angle 0°$ and $1\angle 90°$, respectively, as shown in Figure 8.2(a), LHCP is obtained. The configuration is analyzed using IE3D [5]. The left- and right-hand circularly polarized field components (E_L and E_R) in the ϕ = 0° and 90° planes at f_0 = 3.0 GHz are shown in Figure 8.3. The RHCP level is more than 30 dB below the LHCP level in the broadside direction.

The VSWR and AR variation with frequency are shown in Figure 8.4. The AR remains below 0.25 dB within the BW of 54 MHz for VSWR ≤ 2. In this case, the BW of the antenna is limited by its VSWR and not by its AR. If the two feed points are interchanged or if the phase of the feed at y is changed to −90°, then RHCP is obtained with the similar performance.

For the square MSA with L = 3 cm, the BW of the antenna increases when the substrate thickness is doubled (i.e., h is made 0.318 cm). For the feeds at x = y = 0.6 cm, the BW increases to 112 MHz at center frequency

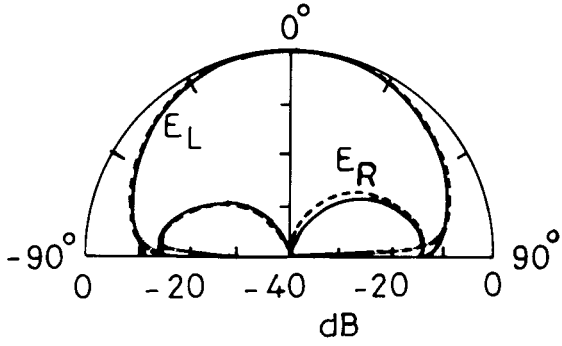

Figure 8.3 LHCP and RHCP field components (E_L and E_R) of dual-feed square MSA at 3.0 GHz: (——) $\phi = 0°$ and (- - -) $\phi = 90°$ planes.

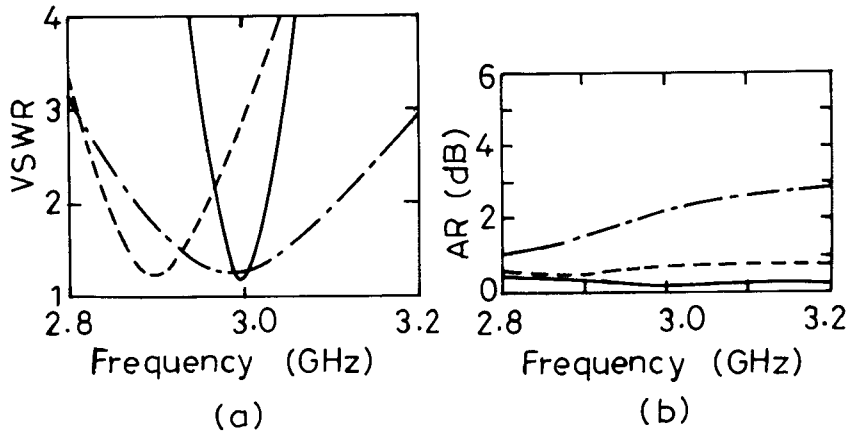

Figure 8.4 Variation of (a) VSWR and (b) AR with frequency of dual-feed square MSA for different values of ϵ_r and h: (——) $\epsilon_r = 2.55$ and $h = 0.159$ cm, (- - -) $\epsilon_r = 2.55$ and $h = 0.318$ cm, and (– · –) $\epsilon_r = 1$ and $h = 0.5$ cm.

$f_0 = 2.904$ GHz. However, the AR increases slightly within the VSWR BW as shown in Figure 8.4(b). When a thick substrate with a low dielectric constant is used, the VSWR BW of the antenna further increases. For a square MSA with $L = 4.5$ cm, $\epsilon_r = 1$, $h = 0.5$ cm, with two orthogonal feeds at $x = y = 1.4$ cm, the VSWR BW increases to 230 MHz (7.7%), but AR increases from nearly 1–3 dB as frequency increases as shown in Figure 8.4. The increase in AR is due to the increase in the undesired radiation from the increased probe length. The probe acts as a top loaded monopole antenna, which has only a E_θ component with maximum value in the

$\theta = 90°$ plane. With an increase in the substrate thickness, the probe length increases, so that the magnitude of the E_θ component increases, which vectorially gets added to the E_θ component of the patch. So, total E_θ is not equal to the E_ϕ component of the patch, thereby increasing AR. Thus, for a thick low dielectric substrate, the impedance BW increases at the expense of degradation in the AR.

The gain of the circularly polarized antenna can be defined in two ways. If the gain is measured using a linearly polarized spinning dipole, then the power received will be half of that received from a properly aligned linearly polarized MSA, transmitting in the same operating conditions. However, if the power is measured using a circularly polarized antenna, then power received will be 3 dB higher. The gain of the circularly polarized RMSA with $\epsilon_r = 1$ and $h = 0.5$ cm is 9.5 dB, if it is measured using a circularly polarized antenna.

8.3.2 Effect of Amplitude and Phase Imbalance

In practice, it is possible that the amplitude of the two outputs from the external two-way power divider may not be equal and that the phase difference between these may not be equal to 90°. For the square MSA with $L = 4.5$ cm, $\epsilon_r = 1$, $h = 0.5$ cm and two orthogonal feeds at $x = y = 1.4$ cm, the magnitude of the feed 2 is varied with fixed phase of 90°. The AR variation for four values of its amplitude (1.0, 0.9, 0.8, and 0.7) is shown in Figure 8.5(a). The excitation at feed 1 is kept constant at $1\angle 0°$. For an amplitude of 0.8, a flat AR of approximately 0.8 dB is obtained within the BW. This imbalance

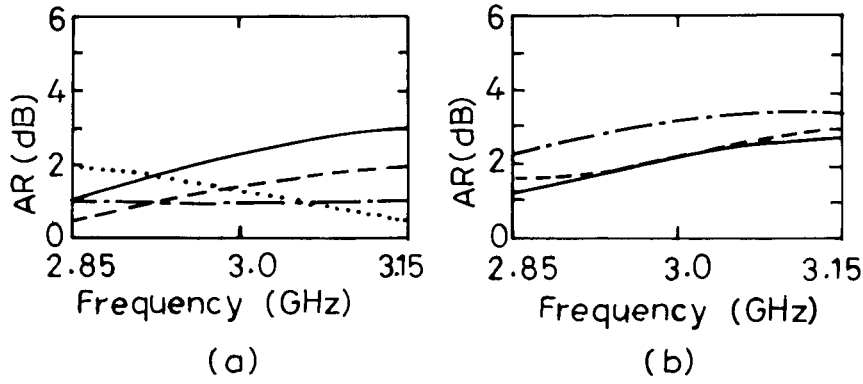

Figure 8.5 Variation of AR with frequency of a dual-feed square MSA for different values of (a) amplitude: (——) 1.0, (- - -) 0.9, (– · –) 0.8, and (· · ·) 0.7; and (b) phase: (- - -) 80°, (——) 90°, and (– · –) 100°.

in amplitude partly compensates the undesired radiation from the two orthogonal probes. For the fixed value of amplitude = 1.0 at the feed 2, the AR variation for three values of phase difference (80°, 90°, and 100°) is shown in Figure 8.5(b). When the phase changes from its ideal value of 90°, the AR increases.

8.3.3 Square MSA with Four Feeds

The AR of the square MSA having L = 4.5 cm, ϵ_r = 1, and h = 0.5 cm, with two orthogonal feeds at $x = y$ = 1.4 cm is significantly improved by using four feeds as shown in Figure 8.6(a). The four feeds are placed near the middle of the edges of the square MSA, and are fed at $1\angle 0°$, $1\angle 90°$, $1\angle 180°$, and $1\angle 270°$. The two opposite feeds are fed with equal amplitude having an 180° phase difference, which results in an excellent AR because

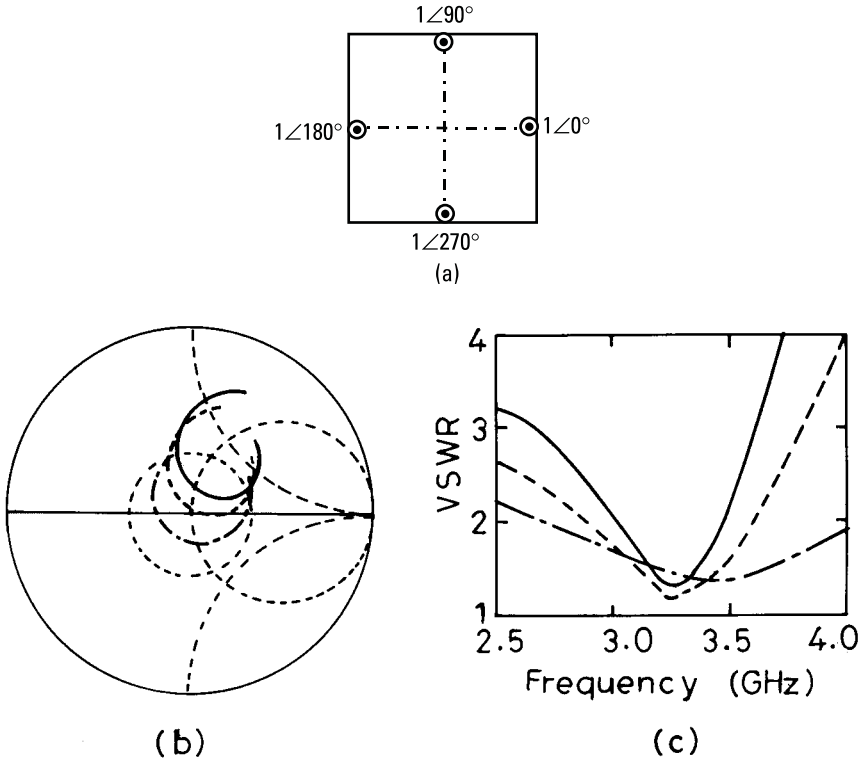

Figure 8.6 (a) Square MSA with four feeds and its (b) input impedance and (c) VSWR plots at one of the feed points for different probe diameters d: (——) 0.12, (- - -) 0.2, and (– · –) 0.4 cm.

of the cancellation of undesired radiation from the probe. The AR remains below 0.01 dB in the entire VSWR BW. However, since the two additional feed points are not at the null positions of the opposite feeds, impedance loading of 50Ω takes place. This impedance is in parallel with the impedance of the radiating edge, and hence the overall input impedance of the antenna at any feed-point is less than 50Ω. The input impedance and VSWR at all the four feed points are identical due to the symmetry of the configuration, and hence these plots are given for only one feed in Figure 8.6(b, c). The BW for VSWR ≤ 2 is 456 MHz (14%). It may be noted from the impedance plot that the input impedance is inductive due to large probe inductance and does not cross the real axis on the Smith chart. The probe inductance decreases with an increase in the probe diameter. Input impedance and VSWR plots for two larger probe diameter (d = 0.2 cm and 0.4 cm) are also shown in Figure 8.6(b, c). With an increase in the probe diameter, the impedance plot shifts downward on the Smith chart providing better matching. The BW of the antenna increases significantly to 1.3 GHz (38%) for d = 0.4 cm. The AR remains below 0.1 dB in the entire BW. This is theoretical BW, which assumes that the inputs at four feeds remain equal with 0°, 90°, 180°, and 270° phase difference over the entire BW, which is not practically feasible.

8.3.4 CMSA with Multiple Feeds

Instead of a square MSA, a CMSA with multiple feeds could be used to yield CP. A CMSA with two orthogonal feeds is shown in Figure 8.2(b). A CMSA of radius a = 3.1 cm, ϵ_r = 1, and h = 0.4 cm fed with $1\angle 0°$ and $1\angle 90°$ at $x = y$ = 1.3 cm, respectively, yields LHCP. The VSWR BW is from 2.521 GHz to 2.661 GHz, and the AR remains below 1.9 dB within the VSWR BW. As in the case of square MSA, when the CMSA is fed at four orthogonal feed points near the edges as shown in Figure 8.7, a wide VSWR BW of 481 MHz is obtained for a probe diameter of 0.12 cm with an AR less than 0.01 dB in the entire BW. The BW further increases to 1.267 GHz when a probe diameter of 0.4 cm is used, which gives better impedance matching.

8.3.5 Integrated MSA with Dual Feeds

Instead of using an external two-way 0° and 90° power divider, it can be integrated along with the MSA. Two different ways of realizing a power divider with a 90° phase difference for square MSAs are shown in Figure

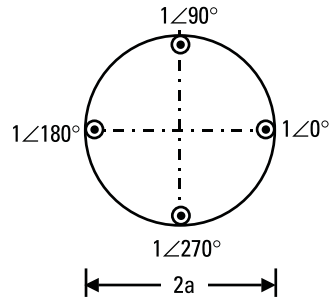

Figure 8.7 Circular MSA with four orthogonal feeds.

8.8. In Figure 8.8(a), the quadrature phase difference between the two orthogonal feeds is achieved by the difference in the line lengths. Quarter-wave transformers (line length = $\lambda/4$ having characteristic impedance Z_0) are used to transform the edge input impedance of the square MSA to 100Ω. The feed point is located on the 100-Ω line in such a way that one side length is longer than the other by $\lambda/4$ to provide a 90° phase difference at the two edges of the square MSA. This also ensures a match with the 50-Ω coaxial feed as two 100-Ω lines on each side of the feed point are in parallel.

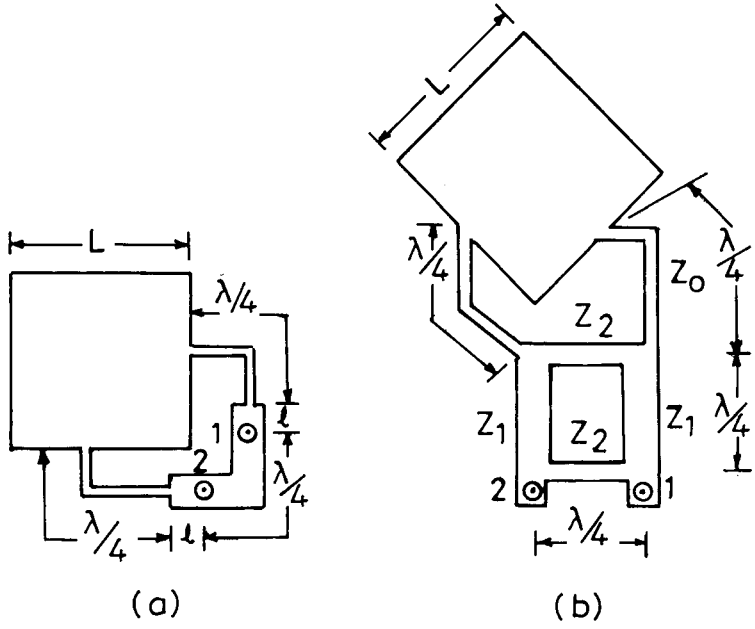

Figure 8.8 Square MSA with (a) an offset feed and (b) a 3-dB two-branch line coupler.

For the square MSA with L = 3 cm, ϵ_r = 2.55, h = 0.159 cm, and tan δ = 0.001, the edge impedance is 300Ω. A quarter-wave transformer of Z_0 = 173Ω is used to transform the impedance to 100Ω. If the feed point is placed at 1 or 2, then LHCP or RHCP is obtained, respectively. For the feed at 1, VSWR and AR variation with frequency are shown in Figure 8.9. The VSWR BW is 103 MHz (3.4%), but the AR BW is only 23 MHz (0.7%). The VSWR BW of the antenna is much larger in comparison with a square MSA having two orthogonal feeds, whose BW is 54 MHz as described in Section 8.3.1. This is because the reflected waves from the two edges of the patch are out of phase at the feed-point due to an additional $\lambda/4$ length in one side, and hence are cancelled. However, the reflected waves excite the opposite polarization, so AR BW decreases. Also, AR degrades due to the change in the phase of the feed line with frequency.

In Figure 8.8(b), a 3-dB two-branch line coupler with Z_1 = 35Ω and Z_2 = 50Ω is used to provide equal amplitude with a 90° phase difference at the center of the two adjacent edges of the square MSA. The coupler also provides isolation between the two feed points (i.e., the signal can be transmitted and received simultaneously without interference). For the square MSA with L = 3 cm, ϵ_r = 2.55, h = 0.159 cm, and tan δ = 0.001, the input impedance at the two adjacent edges is transformed to 50Ω by using quarter-wave transformers of Z_0 = 122.5Ω. These are then connected to the two outputs of the coupler. By locating the feed point at either 1 or 2, LHCP or RHCP is obtained, respectively. The VSWR and AR variations with frequency for the feed at port 1 are shown in Figure 8.9. In this case, the

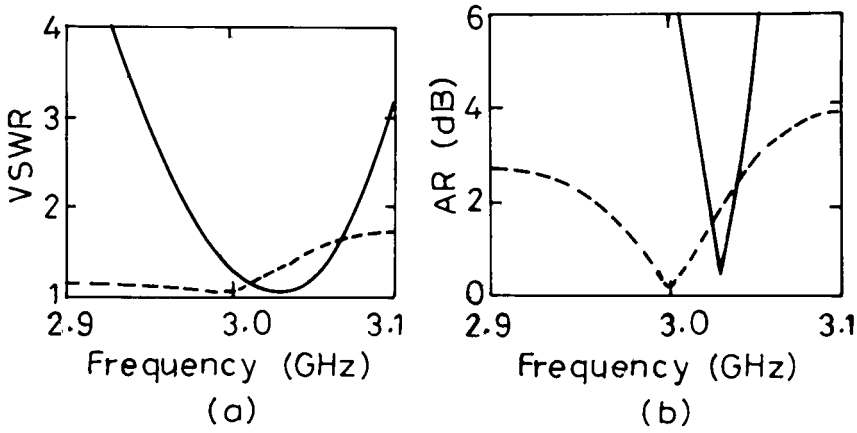

Figure 8.9 (a) VSWR and (b) AR variation with frequency for a square MSA fed by (——) an offset feed and (- - -) a 3-dB two-branch line coupler.

reflected power is absorbed in the matched load connected at the port 2 of the hybrid coupler. A BW of 155 MHz for AR ≤ 3 dB is obtained with VSWR ≤ 1.7. This configuration yields better AR and VSWR performance as compared to that of the offset feed at the expense of a decrease in the gain and an increase in the real estate.

Instead of placing the branch line coupler in the same plane, it can be fabricated on the bottom layer and the patch can be placed in the top layer to reduce the planar area. Alternatively, a coupler can be fabricated on a high dielectric constant substrate located on one side of the ground plane, and the antenna on a low dielectric constant substrate located on the other side to realize wideband CP MSA. The coupling between the patch and the coupler is accomplished by passing shorting posts through the ground plane [1].

8.4 Single-Feed Circularly Polarized MSAs

In the case of a dual-feed CP MSA, an external power divider with quadrature phase difference is required to generate the two orthogonal modes. Alternatively, an offset feed line or a 3-dB branch line coupler can be used, but it increases the overall size of the antenna. Instead of dual feed, various single-feed MSA configurations can be used to generate CP [6–14]. Some of the single-feed CP configurations that are obtained by modifying the square MSA are shown in Figure 8.10. These are diagonally fed nearly square, square with stubs and notches along the two opposite edges, corner-chopped squares, squares with a diagonal slot, among others. Similar single-feed CP MSA configurations are also obtained by modifying CMSAs and TMSAs. In all these configurations, the principle of obtaining the CP is same as described below.

The dimensions of the MSA are modified such that the resonance frequencies f_1 and f_2 of the two orthogonal modes are close to each other as shown in Figure 8.11(a). The antenna is excited at a frequency f_0 in between the resonance frequencies of these two modes, such that the magnitude of the two excited modes are equal. Also, the feed-point location is selected in such a way that it excites the two orthogonal modes with phase difference of $+45°$ and $-45°$ with respect to the feed point, which results in phase quadrature between the two modes. These two conditions are sufficient to yield CP. For a thicker substrate with a low dielectric constant, the BW of the MSA is large, and hence larger separation between f_1 and f_2 (slightly greater than the BW of the individual mode) should be taken as shown in

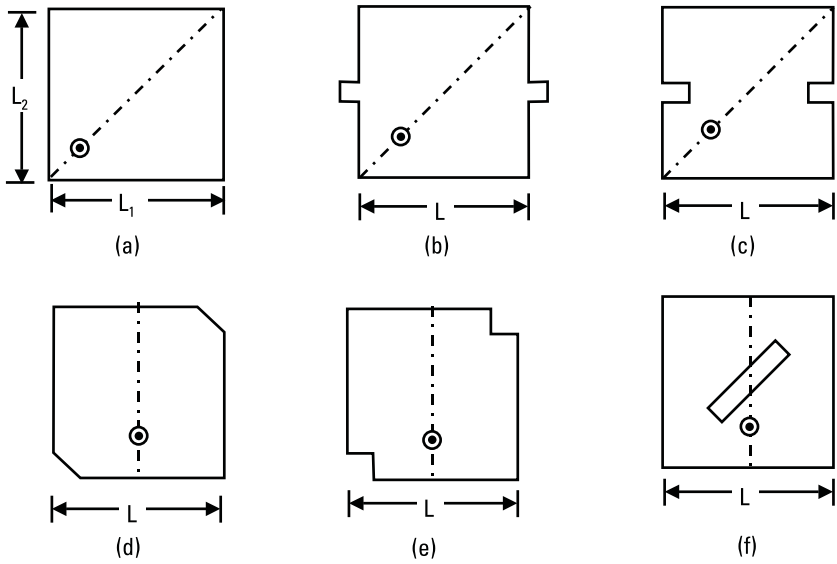

Figure 8.10 Various single-feed modified square MSA configurations: (a) diagonally fed nearly square and square with (b) two stubs, (c) two notches, (d) two corners chopped, (e) square notches at two corners, and (f) diagonal slot.

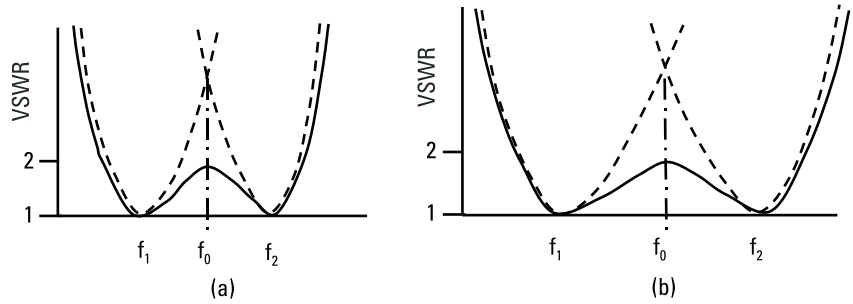

Figure 8.11 VSWR variation of two orthogonal modes of a single-feed MSA: (a) narrow band and (b) wideband [(- - -) individual mode and (——) overall response].

Figure 8.11(b). However, the magnitude of the two orthogonal modes is equal only at f_0, and hence the AR BW is generally limited for these single-feed MSAs, but the VSWR BW is large. The ratio f_2/f_1 is generally in the range of 1.01 to 1.10 depending upon the VSWR BW of the individual orthogonal mode of the MSA.

Another way to recognize whether the given dimensions are optimum for the best AR is to look at the impedance plot of the antenna. If there is

a kink (extremely small loop) in the impedance plot corresponding to the excitation of the two orthogonal modes, it will yield the best AR at the kink frequency. Instead of a kink, a small loop or the absence of the loop in the impedance plot yields poor AR.

8.4.1 Diagonally Fed Nearly Square MSA

A nearly square patch with a single feed along the diagonal as shown in Figure 8.12(a) is one of the simplest MSA configurations to generate CP. The ratio of the two orthogonal dimensions L_1/L_2 should be generally in the range of 1.01–1.10 depending upon the substrate parameters as described above. When the patch is fed along the diagonal, then the two resonance modes corresponding to lengths L_1 and L_2 are spatially orthogonal. The CP is obtained at a frequency, which lies between the resonance frequencies of these two modes, where the two orthogonal modes have equal magnitude and are in phase quadrature.

For a nearly square MSA with L_1 = 3 cm, ϵ_r = 2.55, h = 0.159 cm, tan δ = 0.001, and feed along the diagonal at $(-0.15L_1, -0.15L_2)$, the theoretical input impedance, VSWR and AR plots for three values of L_2 (2.90, 2.92, and 2.95 cm) are shown in Figure 8.12(b–d). As L_2 is increased from 2.90 cm to 2.92 cm, the loop in the impedance plot becomes a kink, and then it disappears as L_2 is further increased to 2.95 cm. The criticality of the dimension is to be noted. Even though a larger VSWR BW of 128 MHz is obtained for L_2 = 2.90 cm due to the loop in the impedance plot, the minimum AR is 2 dB at f_0 = 3.04 GHz. For L_2 = 2.92 cm, the VSWR BW is slightly reduced to 106 MHz, but the minimum AR at f_0 = 3.027 GHz is improved to 0.07 dB. In this case, the BW for AR ≤ 3 dB is 25 MHz (0.8%). The value of L_1/L_2 = 3.0/2.92 = 1.027 implies separation of 2.7% between the two resonant lengths, which is slightly greater than the VSWR BW (1.8%) of the square patch of length = 3 cm. For this feed, LHCP is obtained, and if the feed is shifted to the other diagonal, then RHCP is obtained.

In the above cases, even though the VSWR BW is larger than the AR BW, it is not useful for many applications. At the lower frequency, the radiation pattern is linearly polarized in the ϕ = 0° plane. As the frequency increases, it becomes elliptically polarized and then circularly polarized at the kink frequency followed by elliptical and linear polarization in the ϕ = 90° plane.

The AR and VSWR BWs are improved by doubling the substrate thickness to h = 0.318 cm. For L_1 = 3 cm, L_2 = 2.83 cm and feed along

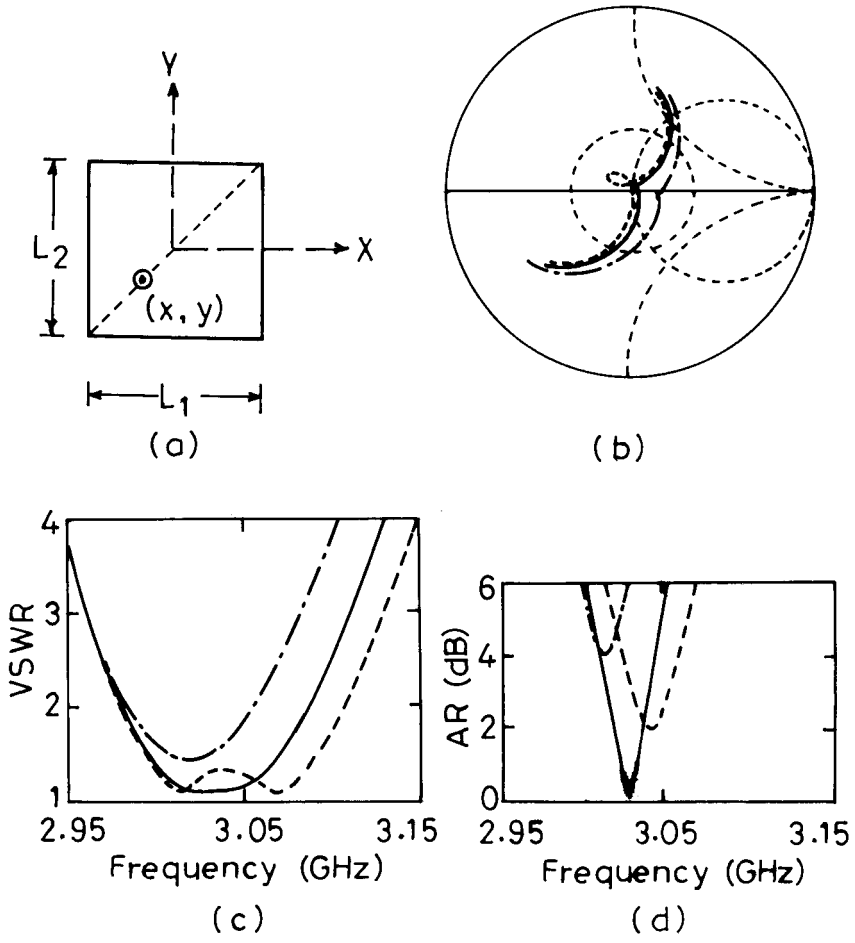

Figure 8.12 (a) Diagonally fed nearly square MSA and its (b) input impedance, (c) VSWR, and (d) AR plots for three values of L_2: (- - -) 2.9, (——) 2.92, and (– – –) 2.95 cm.

the diagonal at $(-0.16L_1, -0.16L_2)$, the input impedance and AR variations with frequency are given in Figure 8.13. A larger ratio of $L_1/L_2 = 1.06$ is taken in this case, because BW increases with an increase in the substrate thickness. For the SMA connector (probe diameter $d = 0.12$ cm), the kink in the input impedance plot is formed in the inductive region of the Smith chart, which is because of the larger probe inductance due to the increased substrate thickness. The probe inductance is reduced by increasing its diameter to 0.2 cm (BNC/TNC connector), which shifts the kink toward the

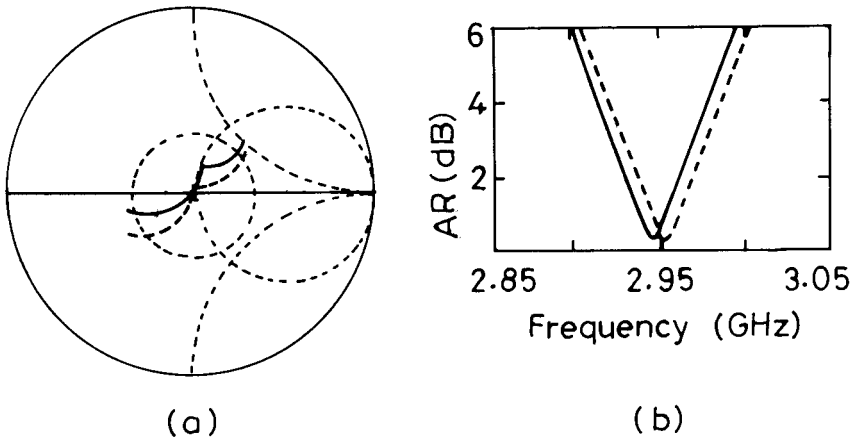

Figure 8.13 (a) Input impedance and (b) AR variation with frequency of single-feed nearly square MSA for h = 0.318 cm and two values of probe diameter d: (——) 0.12 cm and (- - -) 0.2 cm.

center of the Smith chart as shown in Figure 8.13, thereby improving the VSWR at the kink. The increase in the probe diameter increases the resonance frequency slightly because of a decrease in the probe inductance, which decreases the total inductance of the antenna. For the thicker probe, the BW for VSWR ≤ 2 is 220 MHz (7.4%) and the BW for AR ≤ 3 dB is 49 MHz (1.7%). The measured results are in agreement with these theoretical results [6, 7].

The AR BW is further improved when a thicker substrate with a low dielectric constant is used. A thicker probe diameter of 0.4 cm is taken to reduce the probe inductance, so that the kink in the impedance plot is within the VSWR = 2 circle. For L_1 = 4.5 cm, L_2 = 4.1 cm, ϵ_r = 1.0, h = 0.5 cm, and a feed along the diagonal at $(-0.16L_1, -0.16L_2)$, the VSWR and AR variations with frequency are given in Figure 8.14. The BWs for VSWR ≤ 2 and AR ≤ 3 dB are 425 MHz (14%) and 82 MHz (2.8%). The BW of the antenna is limited by its AR and not by its VSWR.

8.4.2 Square MSA with Modified Edges

Instead of using a nearly square MSA to generate CP, the edges of the square MSA can be modified by adding stubs or by cutting notches as shown in Figure 8.15. By adding only one stub or by cutting one notch, CP can also be obtained, but then the configuration is not symmetrical. However, as long as the total effective areas of these perturbations are of the same order,

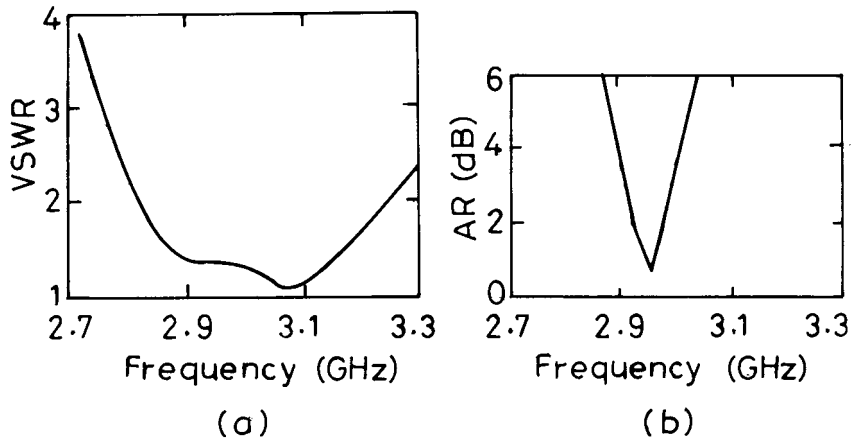

Figure 8.14 (a) VSWR and (b) AR variations with frequency of single-feed nearly square MSA for $\epsilon_r = 1.0$, $h = 0.5$ cm.

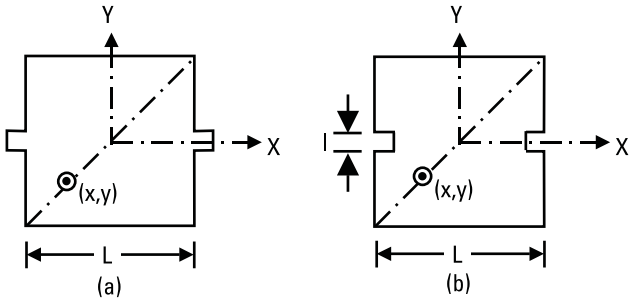

Figure 8.15 Diagonally fed square MSA with (a) two stubs and (b) two notches along its opposite edges.

the performance of one edge modified is similar to that of a two-edge-modified square MSA. The area of the stub or the notch is very critical to yield a lower AR value, just as in the case of a nearly square MSA, where L_1/L_2 ratio is very critical to yield CP.

A square MSA of length $L = 3$ cm and two square stubs of length $l = 0.25$ cm with $\epsilon_r = 2.55$, $h = 0.159$ cm, and $\tan \delta = 0.001$, yields LHCP when fed at $(x, y) = (-0.15L, -0.15L)$. The BW for AR ≤ 3 dB and VSWR ≤ 2 are 22 MHz and 95 MHz, respectively, at $f_0 = 2.970$ GHz. Similarly, when a square notch of length $l = 0.2$ cm is cut, then the RHCP is obtained when fed at $(x, y) = (-0.15L, -0.15L)$. The AR and VSWR BWs are 23 MHz and 95 MHz, respectively, at $f_0 = 2.975$ GHz. These values of AR

and VSWR BWs are similar to that of the nearly square MSA. The advantage of these configurations is that the fine-tuning can be easily done by trimming the dimensions of the stub or notch.

8.4.3 Square MSA with Modified Corners

CP can also be obtained by modifying corners of the square MSA. Small isosceles right angle triangular patches or small square patches are removed from the diagonally opposite corners of the square patch as shown in Figure 8.16(a, b). Chopping off two diagonally opposite corners makes the resonance frequency of the mode along this diagonal to be higher than that for the mode along the unchopped diagonal. The patch is fed along the central axis so that the orthogonal modes are generated. Instead of chopping the corners, small square patches could be added at the corners as shown in Figure 8.16(c) to obtain CP.

The length of the square patch is taken as L = 3 cm and substrate parameters are ϵ_r = 2.55, h = 0.159 cm, and tan δ = 0.001. When isosceles right angle triangular patches of side length l = 0.35 cm are removed from the two corners, LHCP is obtained for the feed at x = 0.65 cm. The BWs for AR ≤ 3 dB and VSWR ≤ 2 are 30 MHz and 93 MHz, respectively, centered at f_0 = 2.963 GHz.

Similarly, when a square patch of length l = 0.25 cm is removed from the two corners, LHCP is obtained for the feed at x = 0.65 cm. The AR and VSWR BWs are 25 MHz and 100 MHz, respectively, at f_0 = 3.02 GHz. When a small square of length l = 0.2 cm is added at the two corners of the square MSA as shown in Figure 8.16(c), RHCP is obtained for the feed at x = 0.7 cm. The AR and VSWR BWs are 24 MHz and 102 MHz, respectively, at f_0 = 2.95 GHz. In this case, the resonance frequency and

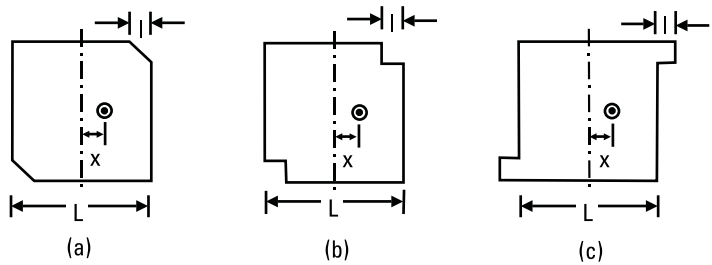

Figure 8.16 Square MSA with modified diagonally opposite corners: (a) small isosceles right angle triangles removed, (b) small squares removed, and (c) small squares added.

AR BW are slightly smaller than that of the corner-chopped cases because of its larger patch area.

8.4.4 Square MSA with a Diagonal Slot

A square MSA with a rectangular slot along its diagonal and the feed along its central axis is shown in Figure 8.17. The difference in the resonance frequencies of the orthogonal modes is caused by the rectangular slot, which makes the path lengths of the two diagonals unequal. In the ratio of length and width the slot governs the CP characteristics of the antenna for given patch and substrate specifications.

When a rectangular diagonal slot of length l = 0.75 cm and width w = 0.2 cm is cut at the center of the square MSA of L = 3 cm with a feed at y = 1.0 cm, RHCP is obtained. The AR and VSWR BWs are 23 MHz and 93 MHz, respectively, at f_0 = 2.963 GHz. These theoretical results follow the same trend as observed in the measured results [7].

In all the above cases, the ratio of the two orthogonal modes is very critical to yield CP with minimum AR at the resonance frequency. Due to the design limitations (e.g., software packages do have small error or sometimes approximations are made to reduce computation time) and fabrication error (tolerance in the patch dimensions and the substrate parameters), it is possible that the results may not be optimum and that fine-tuning of the dimensions is required. Whether to increase or decrease the dimensions can be determined by looking at the input impedance plot. If a loop is present in the plot, it implies that the separation between the two orthogonal modes is large, and hence it is to be reduced to obtain better AR. If there is only a slight bend in the impedance plot without any kink or loop, then the separation between the two modes is to be increased. In this regard, stub or notch configurations are more suitable as fine-tuning can be easily done to obtain lower AR with larger AR BW.

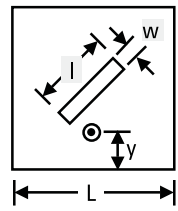

Figure 8.17 Square MSA with a diagonal slot.

8.4.5 Short or Chip Resistor-Loaded Square MSA

Instead of adding stubs or cutting slots or notches, in the square patch shorting posts or chip resistors could be used to obtain CP [15–17]. The resonance frequency of a square MSA changes when two shorting posts are placed symmetrically on either side of the center along the feed-axis as described in Section 7.2.3. When two shorting posts are placed closer to the center along the x-axis, the resonance frequency for the TM_{10} mode (oriented along the x-axis) changes slightly but it remains unaffected for the TM_{01} mode. When this configuration is fed diagonally as shown in Figure 8.18(a), it yields RHCP. When the feed is along the opposite diagonal, LHCP is obtained.

The measured resonance frequency of a square MSA of length L = 3 cm with ϵ_r = 4.4 and h = 0.16 cm is 2.355 GHz. Two shorts are placed at a distance s = 0.48 cm and the patch is fed along the diagonal at (x, y) = (−0.5, −0.5) cm to excite two orthogonal modes. The AR variation with frequency is shown in Figure 8.18(b). The BW for AR ≤ 3 dB is 22 MHz (0.9%) and the BW for VSWR ≤ 2 is 116 MHz (4.9%).

Both AR and VSWR BWs of the antenna increase when the shorting posts are replaced by chip resistors of value 4.7Ω, which is due to increase in the ohmic losses. The feed-point is shifted toward the corner to (−0.7, −0.7) cm and the separation between the resistors is increased to 0.78 cm. The BWs for AR ≤ 3 dB and VSWR ≤ 2 increase to 44 MHz and 164 MHz, respectively. However, the gain of the antenna decreases by 0.7 dB, when shorting posts are replaced by 4.7-Ω resistors. Therefore, the BW

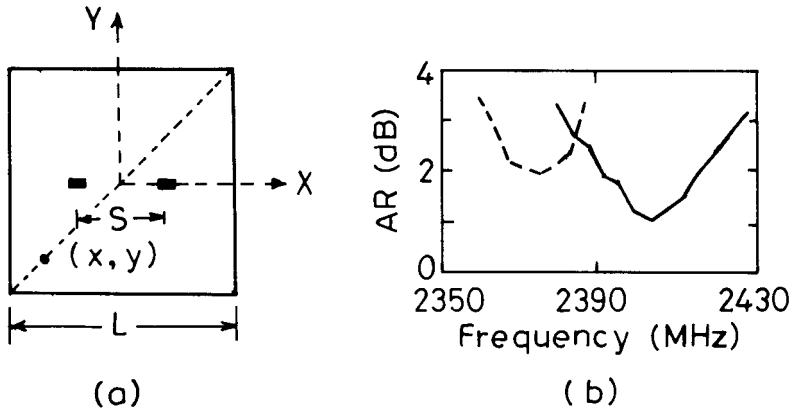

Figure 8.18 (a) Square MSA with two shorts (or resistors) and (b) variation of AR with frequency: (- - -) shorts and (——) resistors.

increases at the expense of a decrease in the antenna gain. Comparison of shorts and resistors loaded square MSA is given in Table 8.1.

In the above chip resistor-loaded configuration, the loading affects only the mode along the x-axis. If the chip resistors are placed orthogonally, as shown in Figure 8.19, both the modes along the x- and y-axes are modified. By adjusting the spacing d_x and d_y of the resistors from the center, larger BW is obtained. When $d_x > d_y$, RHCP is obtained and when $d_x < d_y$, LHCP is obtained. For d_x = 1.0 cm, d_y = 0.5 cm and the feed at (x, y) = (–0.65 cm, –0.65 cm), RHCP is obtained. The AR and VSWR BWs increase to 70 MHz and 237 MHz, respectively, and the center frequency also increases to 2.481 GHz. However, the gain of the antenna decreases from 4.35 dB to 2.45 dB as compared to the previous configuration.

8.4.6 Modified CMSAs and TMSAs

Similar to the modified square MSA, modified circular and triangular MSA configurations with a single feed also generate CP. Some of the modified circular patches are shown in Figure 8.20 [18–22]. A circular patch is modified to an elliptical patch as shown in Figure 8.20(a). CP is obtained

Table 8.1
Comparisons of Shorts or Resistors Loaded Square MSA

R (Ω)	s (cm)	(x, y) (cm)	f_0 (GHz)	VSWR BW (MHz)	VSWR BW (%)	AR BW (MHz)	AR BW (%)	Gain (dB)
0	0.48	–0.5, –0.5	2.375	116	4.9	22	0.9	5.05
4.7	0.78	–0.7, –0.7	2.404	164	6.8	44	1.8	4.35

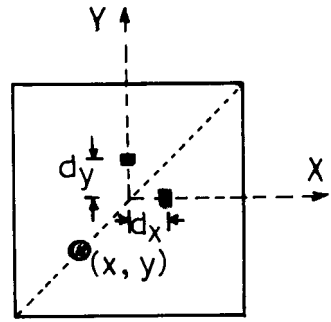

Figure 8.19 Square MSA with two orthogonal chip resistors.

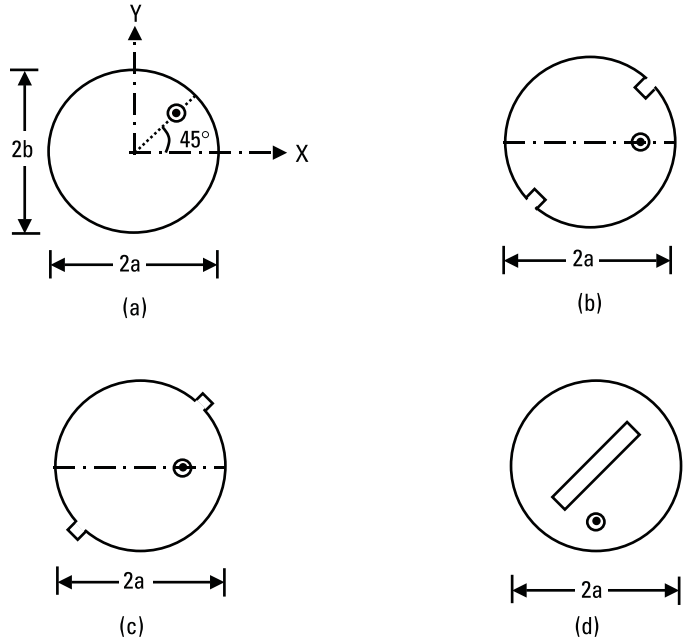

Figure 8.20 Single-feed modified CMSA: (a) elliptical MSA and CMSA with (b) two notches, (c) two stubs, and (d) a rectangular slot in the center.

when the ellipticity ratio (major axis to minor axis lengths) varies from 1.01 to 1.10 depending upon the substrate parameters. The feed is placed at an angle of 45° from the x-axis, which excites the two orthogonal modes with an equal amplitude and a 90° phase difference. In Figure 8.20(b), two notches are cut along the periphery of the circular patch at the diametrically opposite points. The feed is placed at an angle of 45° from the notch axis to excite the orthogonal modes in phase quadrature. Instead of cutting notches, two small stubs could be added as shown in Figure 8.20(c). Also, instead of cutting two notches or adding two stubs, only one notch or a stub could also be used. In Figure 8.20(d), a rectangular slot is cut at the center of the circular patch to yield CP. For all these antennas, the performance is similar to that of the modified square MSAs.

A modified ETMSA also generates CP [23–27]. Some of the modified ETMSA configurations are the nearly ETMSA (isosceles triangle with S_1/S_2 = 1.01 to 1.10), tip-truncated ETMSA, ETMSA with a rectangular slot, and ETMSA with a notch (also called slit) along the periphery, as shown in Figure 8.21. Depending upon the feed-point location and dimensions, LHCP or RHCP is obtained.

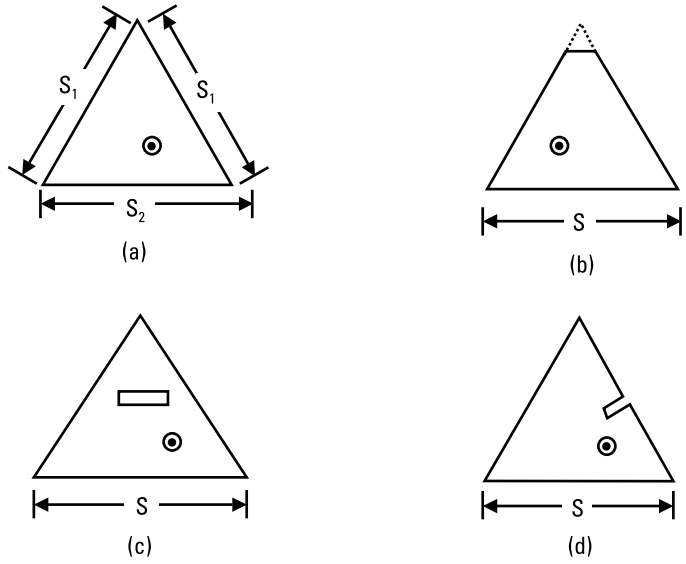

Figure 8.21 Single-feed modified ETMSA: (a) nearly ETMSA, (b) tip-truncated ETMSA, (c) ETMSA with a rectangular slot, and (d) ETMSA with a notch.

8.4.7 Sectoral- and Pentagon-Shaped MSAs

Sectoral MSA with a flare angle $\theta = 65°$ or $70°$ and pentagon-shaped MSA as shown in Figure 8.22, also yield CP [1, 28]. In both cases, AR BW is on the order of 1%.

In the previous subsections, the single-feed modified MSA elements are analyzed for CP. These configurations can be designed to yield CP at

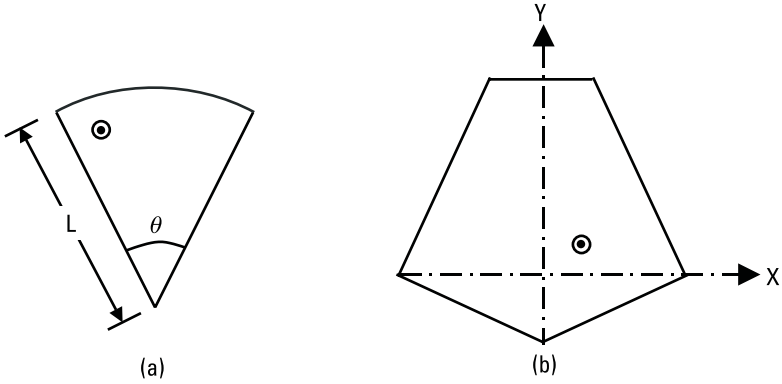

Figure 8.22 (a) Sectoral- and (b) pentagon-shaped MSA.

other frequencies by using frequency-scaling techniques described in Section 2.2.7. Alternatively, a single-feed modified MSA can be designed using the following procedures.

8.4.8 Design Procedure for Single-Feed Circularly Polarized MSAs

A square MSA with two corners chopped and a nearly square MSA are shown in Figure 8.23(a, b). To obtain CP with minimum AR, the dimensions of the perturbations are very critical as described earlier.

The approximate value of the total perturbation area $\Delta s = l^2$ for a two-corner-chopped square MSA can be obtained from the following relation [1, 29, 30]

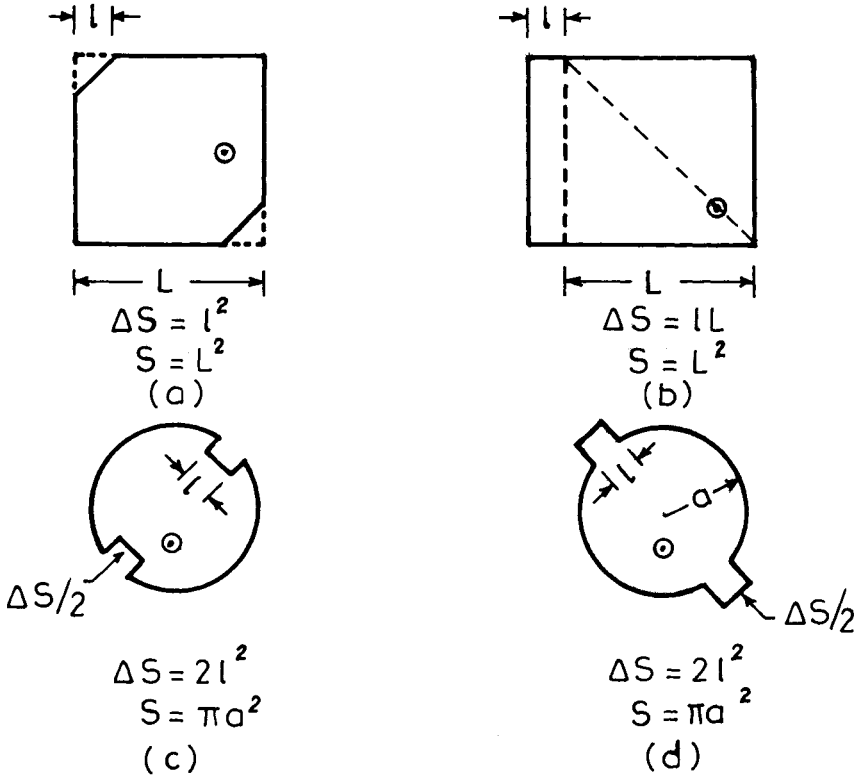

Figure 8.23 (a) Square MSA with two corners chopped, (b) nearly square MSA, and CMSA with (c) notches and (d) stubs.

$$\left(\frac{\Delta s}{S}\right) Q_0 \approx \frac{1}{2} \tag{8.10}$$

where S = area of the square patch without perturbation = L^2, and Q_0 = unloaded quality factor of the patch.

For the nearly square MSA, the perturbation area $\Delta s = l \cdot L$ is given by

$$\left(\frac{\Delta s}{S}\right) Q_0 \approx 1 \tag{8.11}$$

The value of Q_0 depends on the dimension of the patch and substrate parameters such as ϵ_r, h, and tan δ. The plot of Q_0 and efficiency η as a function of h/λ_0 for a square patch of $L = 0.914$ cm and $\epsilon_r = 2.55$ is given in Figure 8.24(a). The percentage variations of $\Delta s/S$ versus Q_0 for both the configurations are shown in Figure 8.24(b). These curves are for only one value of ϵ_r. For other values of ϵ_r, $Q_0(\epsilon_r)$ can be approximately calculated as

$$Q_0(\epsilon_r) = \frac{Q_0\sqrt{\epsilon_r}}{\sqrt{2.55}} \tag{8.12}$$

For the given substrate parameters, the value of Q_0 is obtained first. The value of the corresponding efficiency should be higher than 90%. Next,

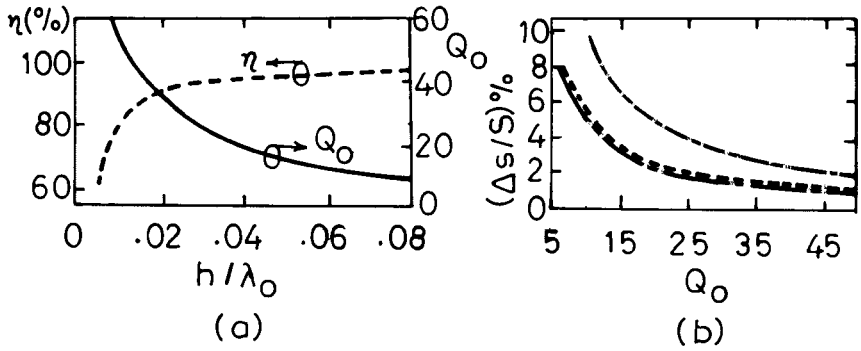

Figure 8.24 (a) Variation of Q_0 (——) and η (- - -) with h/λ_0 and (b) variation of Δ_s/S with Q_0: (——) corner-chopped square, (- - -) modified circular, and (– · –) nearly square.

the percentage of perturbation $\Delta s/S$ required for CP is calculated from (8.10) or (8.11), or read from the plots in Figure 8.24. Finally, the feed point is selected for the desired sense of CP polarization and input impedance matching.

Similarly, for the CMSA with two types of perturbation shown in Figure 8.23(c, d), the perturbation area $\Delta s = 2l^2$ can be obtained from [1, 29, 30]

$$\left(\frac{\Delta s}{S}\right) Q_0 \approx \frac{1}{K_{11}} \tag{8.13}$$

where $K_{11} = 1.84118$ = first derivative of the Bessel function of order 1. The variation of $\Delta s/S$ with Q_0 of CMSA is plotted in Figure 8.24. Once $\Delta s/S$ is obtained, the procedure to design a single-feed CMSA for CP radiation is the same as that of the square MSA with perturbation. A similar concept can be extended to other shapes of the single-feed CP MSA.

8.5 Compact Circularly Polarized MSAs

The size of the above CP MSA configurations is large in the UHF frequency range. By combining the techniques to realize compact MSAs covered in Chapter 6 and CP MSAs discussed in previous sections, several compact CP MSA configurations are possible. Some of these are described in the following sections.

8.5.1 Modified Square Ring MSA

A nearly square ring MSA is shown in Figure 8.25(a). The outer dimensions of the ring correspond to that of a nearly square MSA, and a square slot is cut in the center of the patch, which increases the path length of the surface current thereby reducing the resonance frequency. The patch is fed along the diagonal, and the feed point is very close to the slot [29, 31]. The MNM method has been used to analyze the antenna. A nearly square MSA of lengths $L_1 = 8.35$ cm and $L_2 = 8.2$ cm, having a square slot of length $l = 2.0$ cm cut in the center with $\epsilon_r = 2.5$ and $h = 0.159$ cm, yields LHCP. The BW for AR ≤ 6 dB is 1.5% at $f_0 = 1.043$ GHz. The antenna can be made more compact by increasing the slot dimensions, but then impedance matching is not possible for a 50-Ω coaxial feed point at any location on

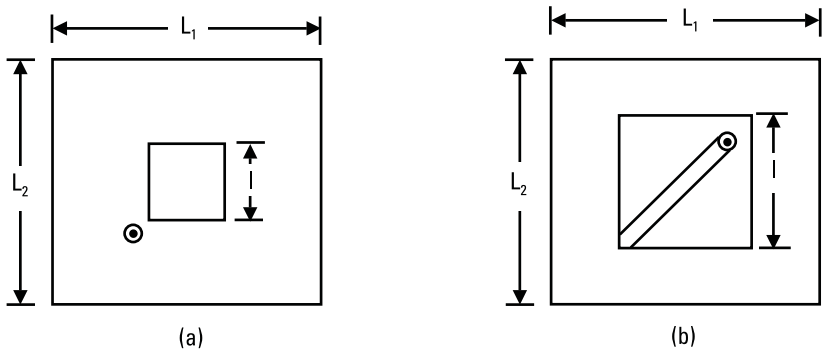

Figure 8.25 Nearly square ring MSA with (a) coaxial feed and (b) quarter-wave transformer.

the ring. However, a quarter-wave transformer can be placed inside the ring to obtain impedance matching as shown in Figure 8.25(b).

Many variations of the nearly square ring MSA with square slot are possible yielding similar performance. Three variations are shown in Figure 8.26. These are a square ring with a nearly square slot, a corner-chopped square ring with a square slot, and a square ring with a corner-chopped square slot [31–33]. In these configurations, either the external or the internal dimensions generate orthogonal modes for CP.

Instead of a single-feed nearly square ring MSA and its variations, a square ring is fed at two orthogonal feed points with an offset polarizer inside the ring to realize compact configuration as shown in Figure 8.27. A square ring MSA of outer length $L = 6$ cm and inner slot length $l = 4$ cm

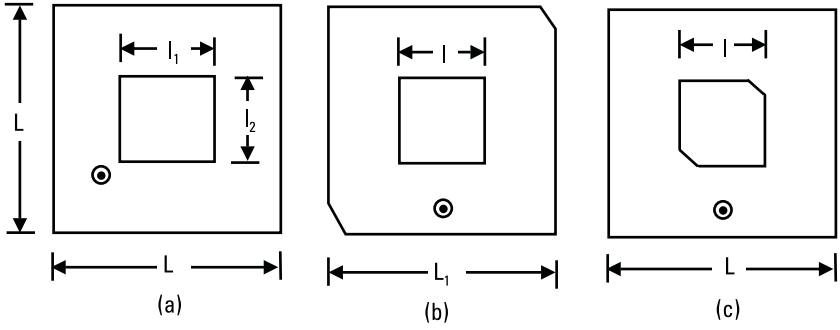

Figure 8.26 (a) Square ring MSA with a nearly square slot, (b) corner-chopped square ring MSA with a square slot, and (c) square ring MSA with a corner-chopped square slot.

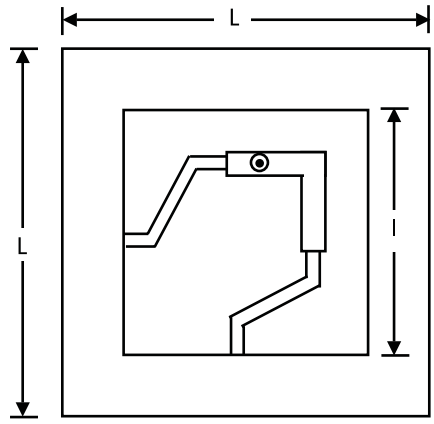

Figure 8.27 Square ring MSA with an inside offset polarizer.

is considered. The substrate parameters are $\epsilon_r = 4.3$, $h = 0.16$ cm, and tan $\delta = 0.02$. When a large slot is cut inside the square patch, the input impedance is large at the two orthogonal points inside the ring, so a quarter-wave transformer is used to transform this impedance to 100Ω. A 50-Ω coaxial feed point is located on the 100-Ω line, such that it provides equal amplitudes with a 90° phase difference to the two orthogonal points at the center of the two adjacent inner edges of the square ring patch. The measured and theoretical (obtained using IE3D) resonance frequencies are 830 MHz and 828 MHz, respectively. The BW for AR ≤ 3 dB is 8 MHz. This antenna has size reduction of 40% as compared to the square MSA for the same frequency of operation.

8.5.2 Modified Square MSA with Slits at the Edges

A compact CP MSA is also realized by cutting two pairs of slits of unequal lengths l_x and l_y of narrow width w ($w << l_x, l_y$), at the four edges of the square patch as shown in Figure 8.28(a). For the feed-point location shown in Figure 8.28, RHCP is obtained when $l_x > l_y$, and LHCP is obtained when $l_x < l_y$. With an increase in l_x and l_y, the resonance frequency of the antenna decreases with a corresponding decrease in the BW. For $L = 2.62$ cm, $l_x = 0.97$ cm, $l_y = 0.90$ cm, $w = 0.1$ cm, $\epsilon_r = 4.4$ and $h = 0.16$ cm, RHCP is obtained at 2.272 GHz. The BW for AR ≤ 3 dB is 32 MHz (1.4%).

The gain of this compact CP MSA can be increased by placing a $\lambda/4$ thick substrate of a high dielectric constant on top of the patch, which is

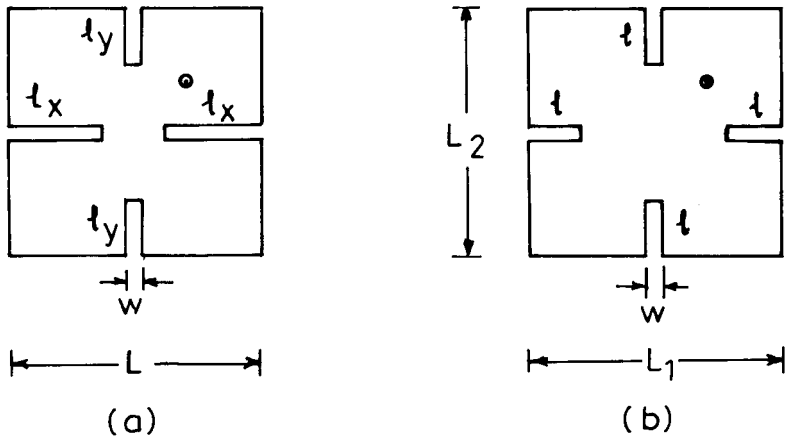

Figure 8.28 (a) Square MSA with two pairs of unequal slits at edges and (b) nearly square MSA with four equal slits at edges.

known as the superstrate [33]. The gain of the antenna increases by approximately 5 dB for a superstrate of $\epsilon_r = 79$ and $h = 0.392$ cm.

A compact CP configuration could be realized by cutting four equal slits of length l at the edges of nearly square MSA as shown in Figure 8.28(b). By varying the length l, the resonance frequency can be tuned. Instead of nearly square, any other single-feed CP MSA configuration could be used with similar performance.

8.5.3 Modified Square MSA with Four Bent Slots

A corner-chopped square MSA with bent slots is another compact CP antenna [34]. The four bent slots are of equal arm length l_1 and narrow width w as shown in Figure 8.29. For $L = 2.8$ cm and the feed at $y = 0.67$ cm, RHCP is obtained for various slot lengths l_1. The spacing s between the slots is 0.2 cm, and the substrate parameters are $\epsilon_r = 4.4$ and $h = 0.16$ cm. With an increase in l_1 from 0.8 to 1.2 cm, the measured resonance frequency of the antenna decreases from 2,153 MHz to 1,711 MHz, and the BW for AR $\leq$ 3 dB decreases slightly from 0.86% to 0.8%. For $l_1 = 1.2$ cm, the reduction in the size of the antenna is 52% as compared to the corner-chopped square MSA without slots. The corner-chopped square MSA could be replaced by any other single-feed CP configuration, or a square MSA could be taken with unequal bent slots to realize compact CP MSA.

The concept of cutting slots could be easily extended to square MSA with two orthogonal feeds, which are fed with $1\angle 0°$ and $1\angle 90°$ as described

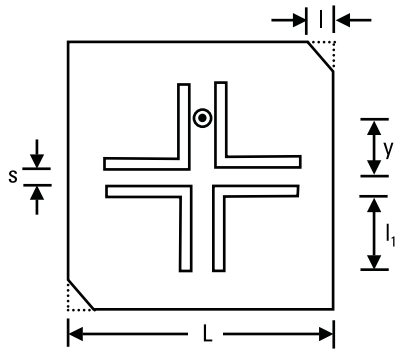

Figure 8.29 A square MSA with two corners chopped and four bent slots.

in Section 8.3 to realize a compact CP antenna. With an increase in the slot length, the resonance frequency decreases. Therefore, for a given frequency, a compact configuration can be realized.

8.5.4 Modified CMSAs and TMSAs

Several variations of CMSAs are possible to realize a compact CP antenna. Two variations are shown in Figure 8.30 [35, 36]. A CMSA with tuning stub along its periphery and cross-slots of equal lengths at its center is shown in Figure 8.30(a). With an increase in the slot length, the resonance frequency decreases and the tuning stub controls the excitation of the orthogonal modes. A quarter-wave transformer is used to obtain impedance matching with a 50-Ω microstrip line feed. Instead of rectangular cross-slots, four curved slots are cut along the periphery of the circular patch as shown in Figure 8.30(b). The orthogonal modes are excited by cutting another slot perpendicular to one of the curved slots. However, these compact CP configurations yield lesser AR BW and gain due to the smaller aperture area.

Several variations of circular ring MSAs are possible for generating CP, including an annular ring with an offset polarizer and a pair of narrow slits in the outer or inner circle of the annular ring, as shown in Figure 8.30(c–e). In general, either the outer circle or the inner circle should produce two orthogonal modes, which are excited equally, and in-phase quadrature by properly locating the feed.

Several variations of ETMSA are also possible to realize compact CP MSA. Two variations of ETMSA are shown in Figure 8.31. ETMSAs with unequal cross slots and bent slots are shown in Figure 8.31. The resonance

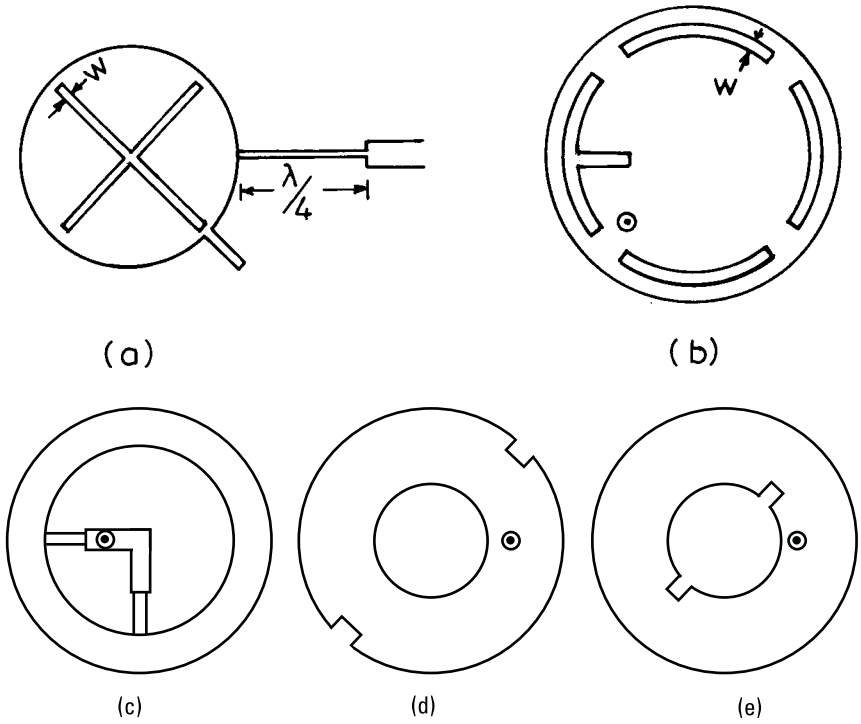

Figure 8.30 Compact CMSA with (a) cross slot with tuning stub and (b) curved slot with tuning stub. Annular ring MSA with (c) an internal offset polarizer and slits in the (d) outer and (e) inner circle.

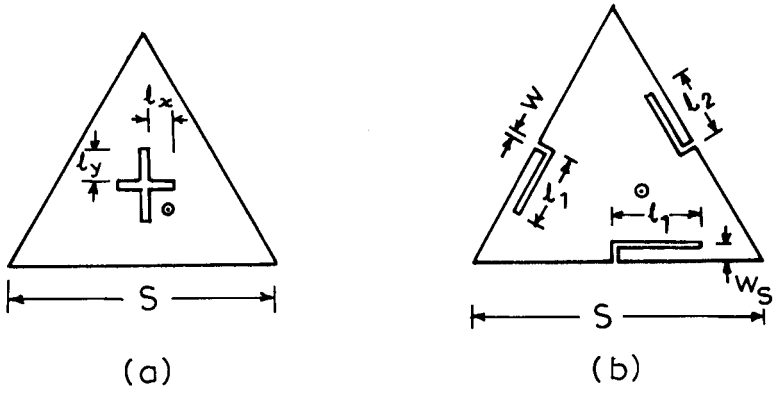

Figure 8.31 ETMSA with (a) unequal cross slot and (b) bent slots.

frequency of the antenna decreases with an increase in the length of the slots, thereby realizing compact configuration.

8.6 Broadband Circularly Polarized MSAs

It has been observed in the previous sections that the dual-feed MSA configurations yield a wider AR BW and narrower VSWR BW as compared to the single-feed MSA configurations. The single-feed configurations have narrow AR BW on the order of 1%. These small AR or VSWR BWs are not enough for many applications. This section describes several broadband CP configurations.

8.6.1 Dual-Feed Planar Multiresonator MSAs

Broadband CP is obtained by using planar multiresonator MSA configurations. The fed patch and the parasitic patches could be gap-coupled or directly coupled as described in the following sections.

8.6.1.1 Gap-Coupled Configurations

By combining the planar gap-coupled broadband techniques described in Chapter 3 and the CP techniques described in the previous sections, various broadband CP MSA configurations are realized. Three gap-coupled square patches are shown in Figure 8.32(a) [37, 38]. Only the central square patch

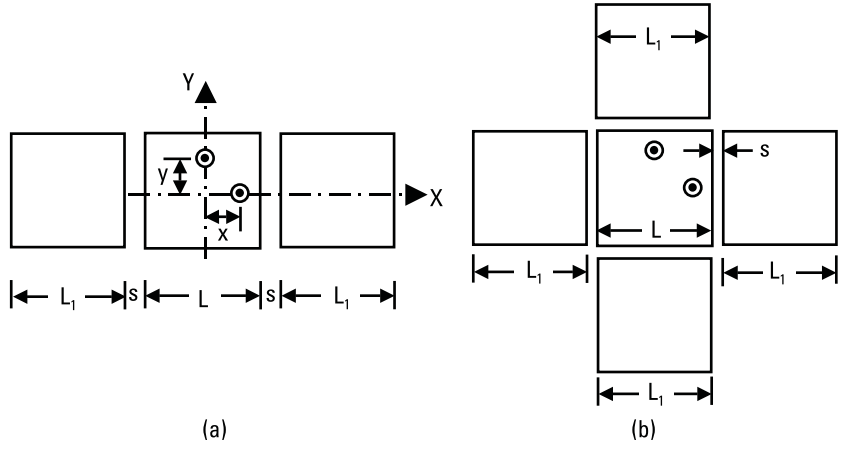

Figure 8.32 (a) Three gap-coupled and (b) five gap-coupled square patches with orthogonal feeds for CP.

is fed at two orthogonal points x and y with $1\angle 0°$ and $1\angle 90°$, respectively. The two identical parasitic square patches are gap-coupled to the central patch. For L = 4.5 cm, L_1 = 4.4 cm, s = 0.25 cm, feeds at $x = y$ = 1.4 cm, ϵ_r = 2.33, h = 0.159 cm, and tan δ = 0.001, BW for VSWR ≤ 2 is 70 MHz. The gain of the antenna is 8.4 dB at f_0 = 2.13 GHz. The AR remains less than 2 dB over the VSWR BW. In comparison, a single square MSA of length L = 4.5 cm has a VSWR BW of 30 MHz and gain = 6.1 dB, with AR remaining below 0.3 dB over the VSWR BW.

For three gap-coupled patches, AR degrades because for the feed along the x-axis, the parasitic patches are along the radiating edges of the fed patch. On the other hand, for the feed along the y-axis, the parasitic patches are along the nonradiating edges of the fed patch. Hence, the coupling to the parasitic patches due to the orthogonal feeds is not uniform, which results in amplitude imbalance.

The BW, gain, and AR improve when four identical parasitic square patches are placed around the fed patch as shown in Figure 8.32(b). For L = 4.5 cm, L_1 = 4.4 cm, s = 0.25 cm, and feeds at $x = y$ = 1.6 cm, the VSWR BW is 100 MHz and gain is 9.5 dB. The AR is better than 0.5 dB in the entire VSWR BW.

The BW increases further when ϵ_r is decreased to 1 and h is increased to 0.5 cm. The dimensions of the square patches are increased so that the antenna operates in the above frequency range. For the five gap-coupled configuration with L = 6.1 cm, L_1 = 5.2 cm, s = 0.6 cm, and feeds at $x = y$ = 2.8 cm, the BW is 400 MHz and gain is 9.5 dB. The AR is less than 2 dB in the lower frequency range but increases near the higher band-edge frequency. However, the overall BW for VSWR ≤ 2 and AR ≤ 3 dB is better than the earlier cases.

Similarly, five broadband gap-coupled CMSA configurations described in Section 3.5 yield broadband CP response, when the central patch is fed at two orthogonal feed-points with $1\angle 0°$ and $1\angle 90°$.

8.6.1.2 Direct-Coupled Configuration

Instead of gap coupling, direct coupling can be employed to obtain broadband CP [39]. Four square patches are directly coupled by thin resonant length transmission lines to the dual-fed central square patch as shown in Figure 8.33(a). The two orthogonal feed probes in the central patch are fed with equal amplitude that are in-phase quadrature. For L = 4.4 cm, microstrip transmission line length l = 3.96 cm and width w = 0.88 cm, ϵ_r = 1.01, and h = 0.25 cm, the BW for AR ≤ 3 dB is from 2.975 GHz to 3.22 GHz.

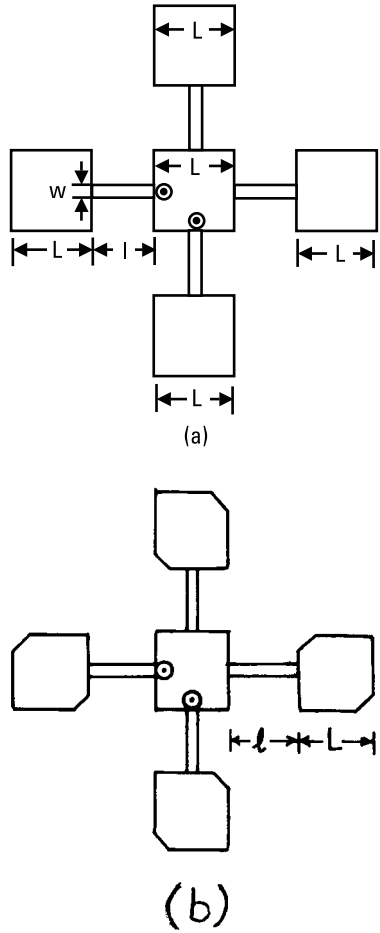

Figure 8.33 (a) Five directly coupled square MSA and (b) notches in the four square patches.

The AR BW is further improved by cutting square notches of 0.3 cm at the two diagonally opposite corners of the four coupled square patches and by rotating these patches by 90° with respect to each other as shown in Figure 8.33(b). By cutting these corners, the four patches yield CP and connecting them in sequential rotation yields AR BW of over 10% at f_0 = 3.1 GHz.

8.6.2 Stacked MSAs for CP

The BW of the MSA can be increased by stacking the patches on top of each other as described in Chapter 4. The top and side views of a square

patch stacked on a fed square patch are shown in Figure 8.34 [40]. The bottom patch is fed at two orthogonal points x and y with $1\angle 0°$ and $1\angle 90°$, respectively, and the top patch is electromagnetically coupled. For a single square patch of L = 4.5 cm, ϵ_r = 1, h = 0.5 cm, and dual-feed at $x = y$ = 1.4 cm, a BW of 230 MHz is obtained for VSWR ≤ 2 with an AR below 2 dB. When a square patch of length L_1 = 3.7 cm is stacked on top of the bottom patch with an air gap of h_1 = 0.4 cm between the two patches, a BW of 585 MHz (18%) is obtained for the feed points at $x = y$ = 1.8 cm. The AR is below 3 dB in the lower frequency range but increases to nearly 4 dB at the higher band-edge frequency.

Similarly, other stacked RMSA and CMSA configurations described in Chapters 4 and 5 yield broadband CP, when the bottom patch is fed at the two orthogonal feed-points with $1\angle 0°$ and $1\angle 90°$ [41, 42] The VSWR BW remains the same as those of the corresponding single-feed stacked CMSA configurations. The AR performance is similar to that of the stacked-square MSA.

8.6.3 Aperture Coupled Circularly Polarized MSAs

ACMSAs give wide impedance BW for linear polarization as described in Chapter 4. The ACMSA can be also designed for obtaining broadband CP by modifying the patch shape excited by a linear aperture or by modifying

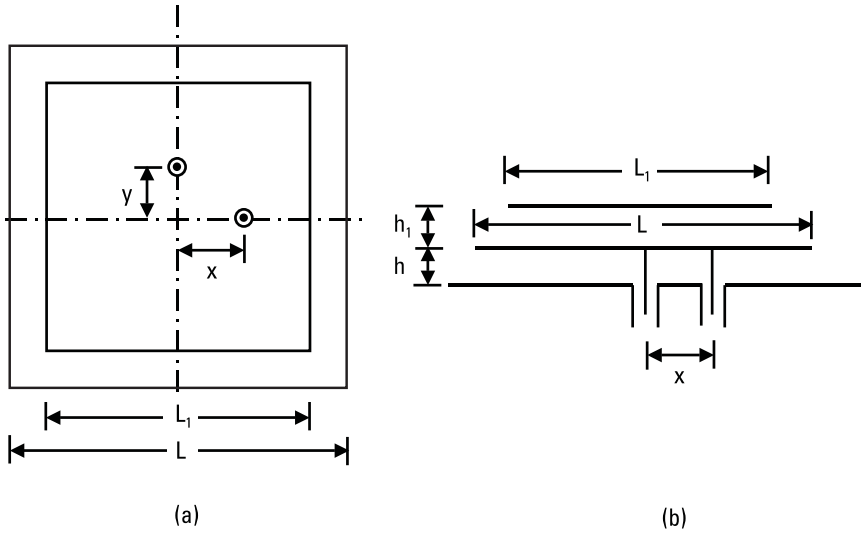

Figure 8.34 (a) Top and (b) side views of two stacked square patches.

the aperture itself. Several variations of apertures/slots, such as two orthogonal slots, single inclined slot, and inclined slot with V-slot loaded at both ends, can be used [43–48].

A square patch on the top layer with two orthogonal cross-slots of unequal lengths in the ground plane is shown in Figure 8.35(a). The cross-slots are centered below the square patch. A single microstrip feed line at 45° with respect to the arms of the cross aperture is used on the other side of the ground plane to generate CP. The feed substrate parameters are ϵ_{r1} and h_1 and the patch substrate parameters are ϵ_{r2} and h_2. The slot width W_{ap} is taken much smaller than the slot lengths L_{ap1} and L_{ap2}. The resonance frequency of the square patch reduces with an increase in the slot length.

Accordingly, by properly adjusting the slot length, the resonance frequency of the patch is made to split into two orthogonal resonant modes that are excited with nearly equal amplitudes and 90° phase difference. When $L_{ap1} > L_{ap2}$, RHCP is obtained and when $L_{ap1} < L_{ap2}$, LHCP is achieved, the tuning stub length l_s is optimized for impedance matching.

For a square patch of length L = 3 cm, $\epsilon_{r1} = \epsilon_{r2}$ = 4.4, h_1 = 0.08 cm, h_2 = 0.16 cm, W_f = 0.15 cm, l_s = 1.55 cm, W_{ap} = 0.1 cm, L_{ap1} = 1.42 cm, and L_{ap2} = 1.1 cm, RHCP is obtained. The measured input impedance plot is shown in Figure 8.35(b). The kink in the impedance plot is formed. The BWs for VSWR ≤ 2 and AR ≤ 3 dB are 135 MHz (5.9%) and 33 MHz (1.4%), respectively, at f_0 = 2.302 GHz. The gain of the antenna is 4 dB and the front-to-back ratio is 16.6 dB at the center frequency [43].

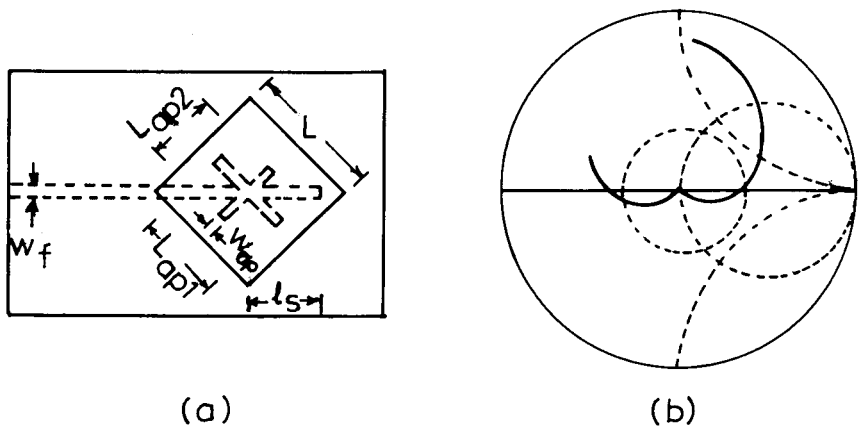

Figure 8.35 (a) Square patch with two orthogonal cross slots of unequal lengths and (b) its measured input impedance plot.

A circular patch could be used instead of a square patch with similar results. Alternatively, the single-feed CP MSA configurations, described in Section 8.4, could be used with equal slot lengths to realize CP ACMSA. A broader AR BW of 2.5% at 2.45 GHz is obtained by using the radiating patch in an inverted suspended configuration. The BW for VSWR ≤ 1.5 increases to 13.7% [44–46].

Instead of using two unequal cross slots, a single inclined slot at 45° can be used for a nearly square patch as shown in Figure 8.36(a) [47, 48]. For L = 3.08 cm, W = 3.0 cm, and slot length l = 1.4 cm with the other parameters the same as in the previous case, the measured BWs for VSWR ≤ 2 and AR ≤ 3 dB are 3.8% and 1.1% at f_0 = 2.34 GHz [48].

Both VSWR and AR BWs improve, when the inclined slot is loaded at each end by two perpendicular V-slots as shown in Figure 8.36(b) [48]. The arm length l_{arm} of the perpendicular slots is taken equal. The length of the patch, slot length, and l_{arm} are optimized to obtain broadband CP. The configuration gives RHCP or LHCP when $L > W$ or $L < W$, respectively. For L = 3.35 cm, W = 3.0 cm, l = 0.5 cm, and l_{arm} = 0.62 cm, the VSWR and AR BWs increase to 7.7% and 2.2%, respectively, at f_0 = 2.232 GHz. The BW of the antenna increases due to the orthogonal loading of the slot. The center frequency reduces from 2.340 GHz to 2.232 GHz due to an increase in the patch length. The BW of the antenna can be further increased by using a thick substrate having a low dielectric constant for the radiating patch.

8.6.4 Sequentially Rotated MSAs

The AR BW of the single-feed MSAs can be significantly increased by using them in sequentially rotated array configuration [1, 30, 49]. The elements could be circularly or linearly polarized as described below.

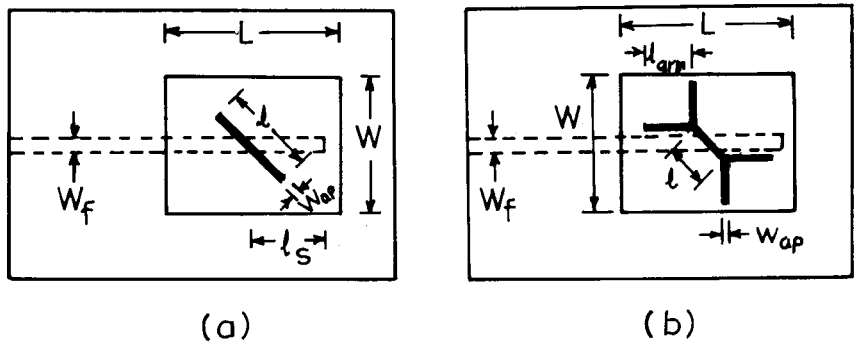

Figure 8.36 Nearly square patch with (a) a single inclined slot at 45° and (b) an inclined slot loaded with two perpendicular V-slots.

8.6.4.1 Sequentially Rotated Array using Circularly Polarized Elements

An array of two circularly polarized circular patches with two opposite notches is shown in Figure 8.37(a) [1]. With reference to the patch 1, patch 2 is rotated by 90° and is fed by an equal magnitude through a power divider, with a 90° phase difference due to an additional line length.

This array configuration gives a wider AR BW as compared to the single CP element. For one of the patch, at the lower frequency within the BW, the major axis of the elliptical polarization is aligned along the $\varphi = 0°$ plane, whereas at the higher frequency, it is aligned along the $\varphi = 90°$ plane. For the other patch, the two axes will be rotated by 90°. The elliptically polarized pattern of the two patches near the center frequency is shown in Figure 8.37(b). The superposition of the two patterns yields CP over a wide BW as shown in Figure 8.37(b). Instead of using circular patch with notches, any other single-feed circularly polarized MSA configurations described in Section 8.4 could be used with similar results.

The concept of using an array of two CP elements is extended to four CP elements in a sequential rotation configuration to enhance the AR BW as shown in Figure 8.38 [49]. In Figure 8.38(a), a 0° and 90° rotation is provided between the two pairs of CP elements, whereas in Figure 8.38(b), 0°, 90°, 180°, and 270° rotation as well as the same amount of phase difference is provided to each successive element. The second configuration gives wider AR and VSWR BWs in comparison with the first configuration because of cancellation of reflections from each element.

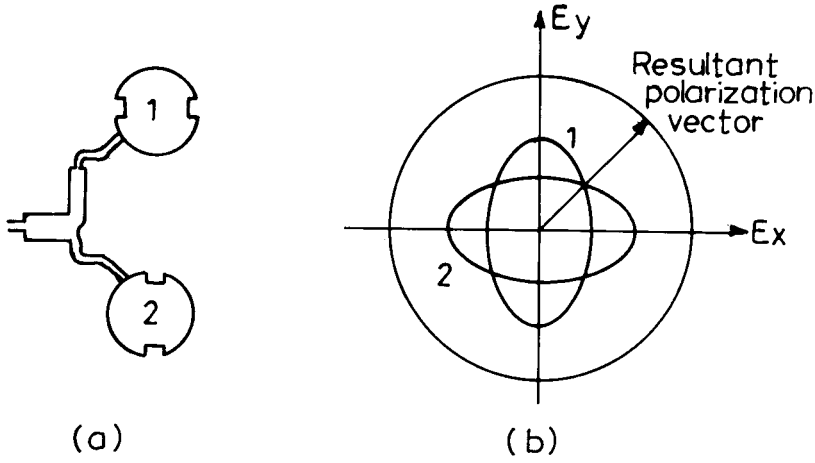

Figure 8.37 (a) Sequentially rotated array of two circularly polarized circular elements and the (b) superimposed CP response of the two elements.

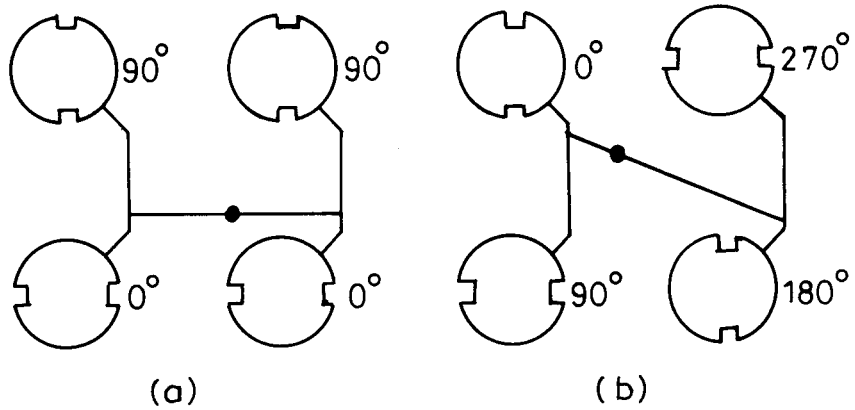

Figure 8.38 Sequential array of four CP elements with a rotation of (a) 0° and 90° and (b) 0°, 90°, 180°, and 270°.

The concept of a sequentially rotated array can be extended to larger arrays. An example of 2×4 sequentially rotated array is shown in Figure 8.39. The elements are rotated and fed with equal amplitude but with a phase difference equal to that of the angle of rotation. The angle of rotation of each element is also shown in Figure 8.39(b). For comparison, a conventional array of 2×4 elements is shown in Figure 8.39(a). In the conventional array, there is no rotation of the CP elements and all elements are fed with equal amplitude and 0° phase difference. The measured AR and VSWR plots of these two arrays are compared in Figure 8.39(c, d). The BW for AR ≤ 3 dB of the sequentially rotated array is 14% at the center frequency of 2.3 GHz, which is 15 times of that of the conventional array. The BW for VSWR ≤ 1.5 of the sequentially rotated array is 13.7%, which is twice of that of the conventional array [50].

The BW of the sequentially rotated array can be increased further by using broadband CP elements instead of narrow band CP elements. Only stringent requirement for this wideband sequential rotation array is the requirement of a wideband phase shifter [51]. A sequentially rotated array could also be excited indirectly using electromagnetic or aperture coupling instead of direct feeds such as microstrip line or a coaxial line [52].

8.6.4.2 Sequentially Rotated Array Using Linearly Polarized Elements

Broadband CP is also obtained by using linearly polarized elements in a sequentially rotated array. Two single-feed linearly polarized rectangular patches that are orthogonal to each other and fed with a 90° phase shift as shown in Figure 8.40(a) yield CP [53]. Similarly, a 2×2 array configuration

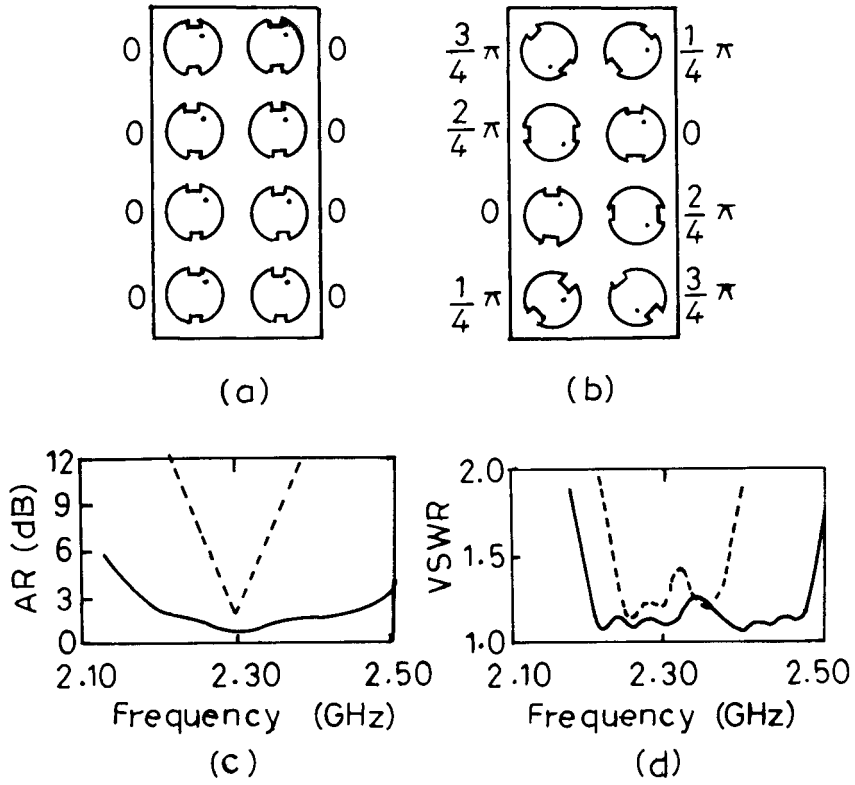

Figure 8.39 Circular patches with two notches are arranged in (a) conventional and (b) sequentially rotated 2×4 array configuration. Measured (c) AR and (d) VSWR plots [(- - -) conventional and (——) sequentially rotated.]

of single-feed rectangular elements with orthogonal orientation and phase difference of 90° between them yields broadband CP. The orientation and phase difference of the four elements could be arranged in 0°, 90°, 0°, and 90° or in 0°, 90°, 180°, and 270° manner. The latter configuration shown in Figure 8.40(b), gives better performance due to the cancellation of the undesired reflected and radiated fields from the 0° element with the 180° element, and from the 90° element with the 270° element, respectively.

The gain of the circularly polarized antenna array can be increased by using N linearly polarized elements arranged in a circular ring geometry as shown in Figure 8.41 [54]. The N elements are placed at an angle of $360/N$ degrees with respect to each other and are sequentially fed to generate CP response. The feed phase of each individual element is arranged in steps of $\varphi_n = 2\pi(n - 1)/N$, where $n = 1, 2, \ldots . N$. The initial phase α_0 could

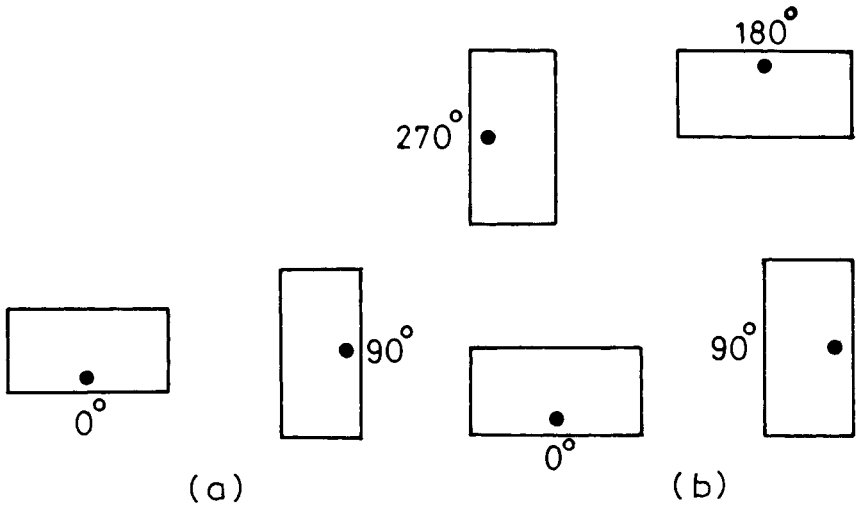

Figure 8.40 (a) Two linearly polarized rectangular patches with 90° rotation and phase difference. (b) A 2 × 2 array with rotation and phase difference of 0°, 90°, 180°, and 270°.

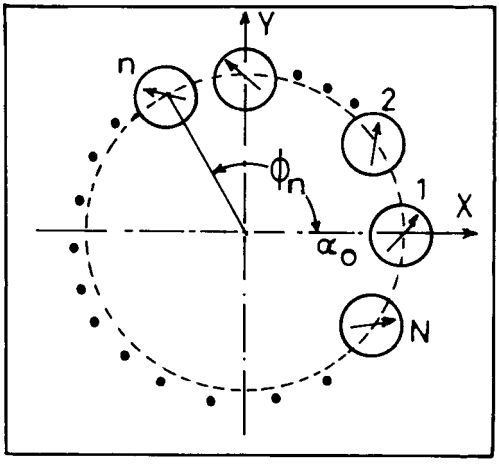

Figure 8.41 Array of *N* linearly polarized elements arranged in a circular ring geometry.

be given to the first element. For the single-ring configuration with four elements, the maximum gain is approximately 11.5 dB. The two-ring configuration with four elements in the inner ring and eight elements in the outer ring yielded a maximum measured gain of 15.4 dB. Similarly, a three-ring

configuration with four, eight, and sixteen elements yielded a maximum gain of 18.65 dB.

8.7 Traveling-Wave Circularly Polarized MSAs

Traveling-wave antennas are generally terminated in a resistor to dissipate the nonradiated power, so that it does not get reflected back from the open end and hence yield broad BW. The curved or linear microstrip transmission lines antennas can be designed to yield CP response and eliminate the use of complicated phase- and amplitude-controlled feed networks [1, 49, 55–59].

8.7.1 Curved MSAs

Two configurations of curved microstrip traveling-wave antennas, namely circular sector and spiral antennas, are shown in Figure 8.42. Both the antennas are fed at one end and terminated with a matched load at the other end.

The antennas are designed at 10 GHz for a substrate having $\epsilon_r = 2.32$ and $h = 0.159$ cm. For a circular sector of radius 0.345 cm and a sectoral angle of 285° and a spiral of pitch = 0.6 cm, the BW for AR ≤ 3 dB is 40% and VSWR remains below 1.3 over the BW. However, within the BW, gain varies from 0 to 6 dB and the beam squint is nearly 25%. Hence, these antennas are useful only if such variations in radiation pattern and gain are acceptable [55, 56].

8.7.2 Microstrip Line Arrays

A traveling-wave array consisting of microstrip transmission line that is bent periodically and arranged in different forms also yields CP. Some of the

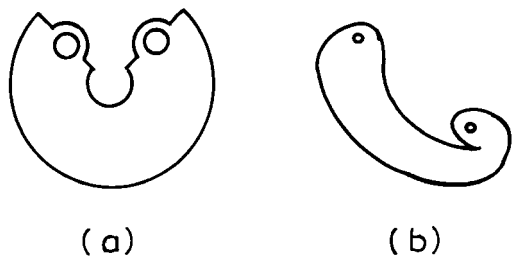

Figure 8.42 (a) Circular sector and (b) spiral MSAs.

examples are rampart line, chain antenna, square loop line, and crank line as shown in Figure 8.43. All the bends in the microstrip lines are chamfered to reduce the discontinuity susceptance [1, 49]. All these arrays are fed at one end and terminated in matched load at the other end, so that the reflected power does not degrade the CP response. When the antenna is fed from the left side, the field rotates in the counterclockwise direction yielding RHCP. Similarly, LHCP is obtained when the antenna is fed from the right side. For all these cases, the length of the unit cell, which is repeated periodically, is 2λ. In the unit cell, the polarity of the total radiated field rotates and completes one full cycle in the time period $T = 1/f_0$ to produce CP. The lengths of each section within the unit cell are adjusted such that the orthogonal field components have equal magnitude with a 90° phase difference.

All these traveling-wave CP configurations give wide AR and VSWR BWs, but the direction of the main beam is off broadside and the beam scan is frequency dependent. The problem of the beam scan with frequency is reduced by forming a line structure into the cross configuration [59].

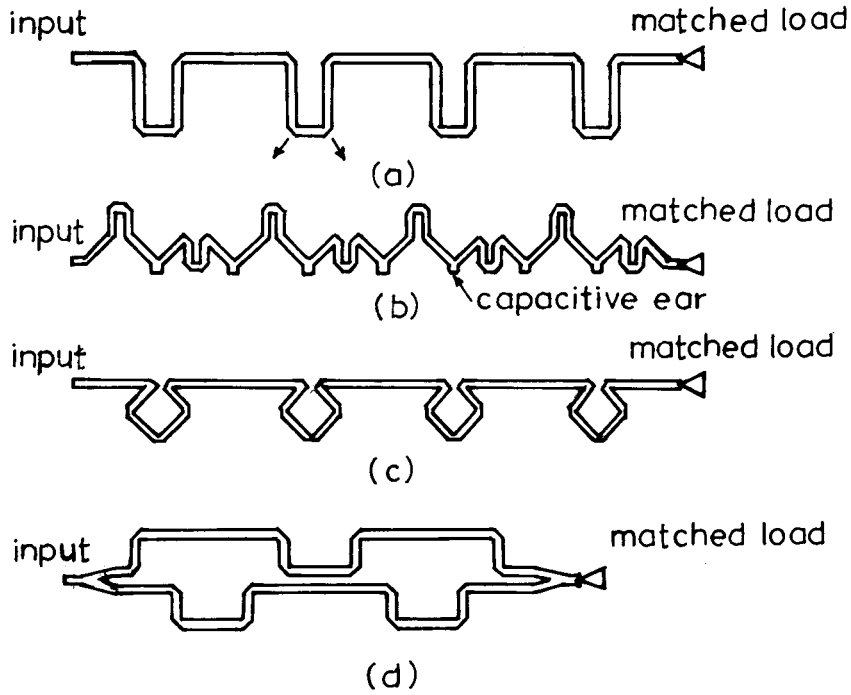

Figure 8.43 Microstrip line circularly polarized arrays: (a) rampart line, (b) chain antenna, (c) square loop line, and (d) crank line.

8.7.3 Cross Antenna

A one-turn eight-branch cross antenna is shown in Figure 8.44(a). The antenna is fed at one end and terminated at the other end by its characteristic impedance. To obtain CP, branch length and width are taken as $0.543\lambda_0$ and $0.136\lambda_0$, respectively and diameter of the cross is $1.42\lambda_0$. A thick foam substrate of $h = 0.1\lambda_0$ is taken to increase the BW. The variations of gain and AR with frequency are shown in Figure 8.44(b). The measured values are in good agreement with the computed values. The AR remains below 3 dB over a BW of 7% and gain is within 12.5 ± 1 dB over this BW. A transformer at the input provides a VSWR ≤ 2 over more than 15% BW

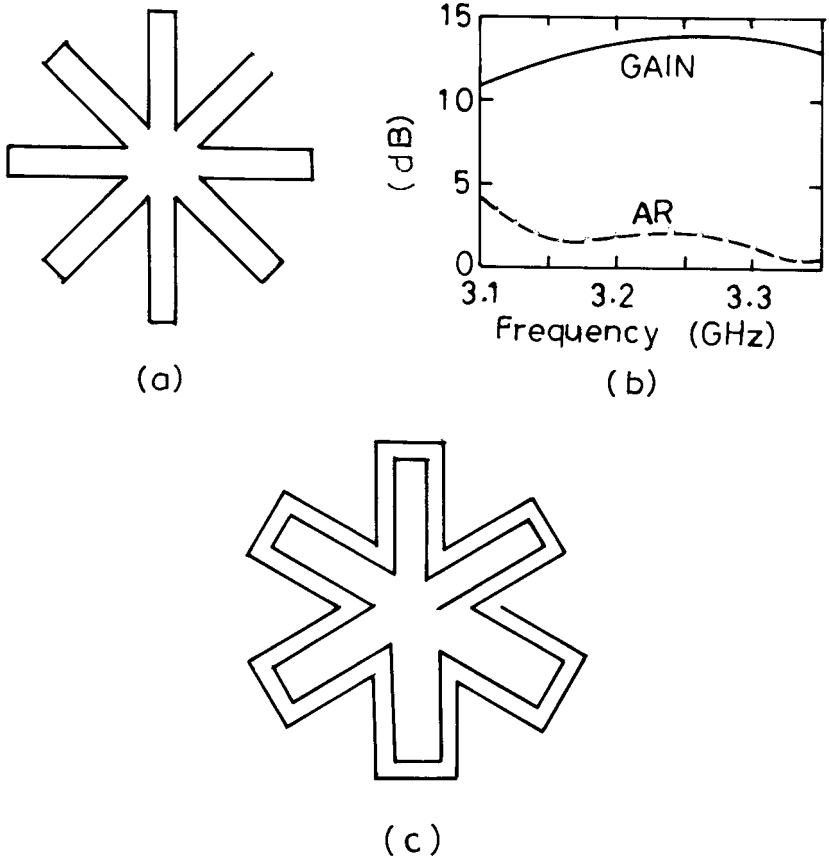

Figure 8.44 (a) Cross antenna with a single turn and eight branches and its (b) computed (——) gain and (- - -) AR variation with frequency and (c) cross antenna with two turns and six branches.

to the 50-Ω coaxial feed. The main limitation of the antenna is that its beam shape and peak directions vary with frequency.

The performance of the antenna is improved by using a two-turn six-branch cross as shown in Figure 8.44(c). The dimensions are scaled up to operate the antenna around 1.55 GHz. After matching with the transformer at the input, the BW for VSWR ≤ 2 is more than 15%. The measured gain of the antenna increases to 15 dB at 1.552 GHz. The AR remains below 1.5 dB over a 7% BW with stable radiation pattern [59].

8.8 Summary

CP is obtained when two orthogonal modes of an antenna are excited with an equal amplitude and a 90° phase difference. The CP response of an antenna is defined in terms of its AR. Several dual-feed and single-feed MSA configurations are described to yield CP. For a dual-fed patch, excited at two orthogonal feeds with an equal amplitude and a 90° phase difference, the BW is limited by its VSWR variation and not by its AR variation. When a thicker substrate is used to increase the VSWR BW, its AR degrades. A patch fed with four orthogonal feeds having an equal amplitude with a relative phase difference of 0°, 90°, 180°, and 270° yields an excellent AR response with a BW of more than 30% for VSWR ≤ 2.

Several single-feed modified square MSA configurations are discussed to obtain CP, including the diagonally fed nearly square, the corner-chopped square, the dual-stub loaded square, and the square with a diagonal slot. Similarly, CP is obtained using modified circular and equilateral triangular patches. These single-feed CP elements are limited by their AR variation and not by their VSWR variation. A typical AR BW is on the order of 1%, and hence these single-feed configurations are suitable for narrowband applications.

Compact CP configurations are realized by cutting slots inside the patch. Nearly square ring and square ring with the notches in the outer or the inner square are some examples. Similar compact configurations are realized using circular and triangular patches.

Broadband CP response is obtained by extending the conventional methods to increase the BW of linearly polarized MSAs. These are dual-feed gap-coupled patches, direct-coupled patches, stacked patches, aperture-coupled patches with cross-slots of equal or unequal arms, or inclined or V-loaded inclined slots. These configurations yield an AR BW of up to 15% and a VSWR BW of around 30%. The multiresonator planar configurations

give increased AR BW with higher gain. The AR BW of the single-feed CP configurations is increased significantly by forming their array in sequentially rotated manner. In the sequentially rotated array, each element or a group of elements are rotated and fed with a differential phase, which is same as the rotational angle with respect to each other. The elements of the array could be either circularly or linearly polarized. The gain of these configurations is higher than a single element since many elements are used in an array configuration.

Traveling-wave antennas arrays such as sectoral, spiral, and linear microstrip line arrays also yield CP. A maximum AR BW of up to 40% is obtained using these line geometries. However, the direction of the beam maximum varies with frequency. This problem is reduced by using cross antennas.

References

[1] James, J. R., and P. S. Hall, *Handbook of Microstrip Antennas,* Vol. 1, London: Peter Peregrinus, 1989.

[2] Sainati, R. A., *CAD of Microstrip Antennas for Wireless Applications,* Norwood, MA: Artech House, 1996.

[3] Lee, H. F., and W. Chen, *Advances in Microstrip and Printed Antennas,* New York: John Wiley & Sons, 1997.

[4] Balanis, C. A., *Antenna Theory, Analysis and Design,* New York: John Wiley & Sons, 1997.

[5] IE3D 7.0, Zeland Software, Inc., Fremont, CA, 2000.

[6] Sharma, P. C., "Desegmentation Method and Its Application to Circularly Polarized Microstrip Antennas," Ph.D. thesis, Indian Institute of Technology, Kanpur, India, 1983.

[7] Sharma, P. C., and K. C. Gupta, "Analysis and Optimized Design of Single Feed Circularly Polarized Microstrip Antennas," *IEEE Trans. Antennas Propagation,* Vol. AP-31, No. 6, 1983, pp. 949–955.

[8] Deshpande, M. D., and N. K. Das, "Rectangular Microstrip Antenna for Circular Polarization," *IEEE Trans. Antennas Propagation,* Vol. AP-34, No. 6, 1986, pp. 744–746.

[9] Haneishi, M., et al., "A Design of Back Feed Type Circularly Polarized Microstrip Disk Antennas Having Symmetrical Perturbation Element by One Point Feed," *Electron. Commu. Japan,* Vol. 64B, No. 7, 1981, pp. 52–60.

[10] Shen, L. C., "The Elliptical Microstrip Antenna with Circular Polarization," *IEEE Trans. Antennas Propagation,* Vol. AP-29, 1981, pp. 90–94.

[11] Long, S. A., et al., "An Experimental Study of the Circular Polarized Elliptical Printed Circuit Antenna," *IEEE Trans. Antennas Propagation,* Vol. AP-29, 1981, pp. 95–98.

[12] Lu, J. H., "Single Feed Circularly Polarized Triangular Microstrip Antennas," *IEEE AP-S Int. Symp. Digest,* 1999, pp. 264–267.

[13] Suzuki, Y., N. Miyano, and T. Chiba, "Circularly Polarized Radiation from Single Fed Equilateral Microstrip Antenna," *IEE Proc. Microwaves, Antennas Propagation,* Pt. H, Vol. 134, 1987, pp. 194–198.

[14] Wong, K. L., and J. Y. Wu, "Single Feed Small Circular Polarized Square Microstrip Antenna," *Electronics Letters,* Vol. 33, No. 22, 1997, pp. 1833–1834.

[15] Wong, K. L., and Y. F. Lin, "Small Broadband Rectangular Microstrip Antenna with Chip Resistor Loading," *Electronics Letters,* Vol. 33, No. 19, 1997, pp. 1593–1594.

[16] Wong, K. L., and J. Y. Wu, "Bandwidth Enhancement of Circularly Polarized Microstrip Antenna Using Chip Resistor Loading," *Electronics Letters,* Vol. 33, No. 21, 1997, pp. 1749–1751.

[17] Huang, C. Y., J. Y. Wu, and K. L. Wong, "Broadband Circularly Polarized Square Microstrip Antenna Using Chip-Resistor Loading," *IEE Proc. Microwaves, Antennas Propagation,* Pt. H, Vol. 146, No. 1, 1999, pp. 94–96.

[18] Wong, K. L., and Y. F. Lin, "Circularly Polarized Microstrip Antenna with a Tuning Stub," *Electronics Letters,* Vol. 34, No. 9, 1998, pp. 831–832.

[19] Bhattacharya, A. K., and L. Shafai, "Theoretical and Experimental Investigation of the Elliptical Annual Ring Antenna," *IEEE Trans. Antennas Propagation,* Vol. AP-36, No. 11, 1988, pp. 1526–1530.

[20] Chen, H. M., and K. L. Wong, "On the Circular Polarization of Angular-Ring Microstrip Antennas," *IEEE Trans. Antennas Propagation,* Vol. AP-47, No. 8, 1999, pp. 1289–1292.

[21] Chen, W. S., C. K. Wu, and K. L. Wong, "Compact Circularly Polarized Microstrip Antenna with Cross-Slot and Peripheral Cuts," *Electronics Letters,* Vol. 34, No. 11, 1998, pp. 1040–1041.

[22] Yang, K. P., and K. L. Wong, "Inclined Slot Coupled Compact Dual Frequency Microstrip Antenna with Cross Slot," *Electronics Letters,* Vol. 34, February 1998, pp. 321–322.

[23] Lu, J. H., C. L. Tang, and K. L. Wong, "Circular Polarization Design of a Single-Feed Equilateral-Triangular Microstrip Antenna," *Electronics Letters,* Vol. 34, No. 4, 1998, pp. 319–321.

[24] Tang, C. L, J. H. Lu, and K. L. Wong, "Circularly Polarized Equilateral-Triangular Microstrip Antenna with Truncated Tip," *Electronics Letters,* Vol. 34, No. 13, 1998, pp. 1277–1278.

[25] Lu, K. L., H. C. Yu, and K. L. Wong, "Compact Circular Polarization Design for Equilateral Triangular Microstrip Antenna with Spur Lines," *Electronics Letters,* Vol. 34, No. 21, 1998, pp. 1989–1990.

[26] Lu, J. H., C. L. Tang, and K. L. Wong, "Single-Feed Slotted Equilateral-Triangular Microstrip Antenna for Circular Polarization," *IEEE Trans. Antennas Propagation,* Vol. AP-47, No. 7, 1999, pp. 1174–1178.

[27] Lu, J. H., and K. L. Wong, "Single Feed Dual Frequency Equilateral Triangular Microstrip Antenna with Pair of Spur Lines," *Electronics Letters,* Vol. 34, No. 12, 1998, pp. 1171–1173.

[28] Hsu, W. H., and K. L. Wong, "Circularly Polarized Disk-Sector Microstrip Antenna," *Electronics Letters,* Vol. 34, No. 23, 1998, pp. 2188–2190.

[29] Garg, R., et al., *Microstrip Antenna Design Handbook,* Norwood, MA: Artech House, 2001.

[30] Hirasawa, K., and M. Haneishi, *Analysis, Design, and Measurements of Small and Low-Profile Antennas,* Norwood, MA: Artech House, 1992.

[31] Palanisamy, V., and R. Garg, "Analysis of Circularly Polarized Square Ring and Crossed Strip Microstrip Antennas," *IEEE Trans. Antennas Propagation,* Vol. AP-34, No. 11, 1986, pp. 1340–1345.

[32] Chen, W. S., C. K. Wu, and K. L. Wong, "Single Feed Ring Microstrip Antenna with Truncated Corners for Compact Circular Polarization," *Electronic Letters,* Vol. 34, No. 11, 1998, pp. 1045–1047.

[33] Huang, C. Y., C. Y. Wu, and K. L. Wong, "High-Gain Compact Circularly Polarized Microstrip Antenna," *Electronic Letters,* Vol. 34, No. 8, 1998, pp. 712–713.

[34] Chen, W. S., C. K. Wu, and K. L. Wong, "Compact Circularly Polarized Microstrip Antenna with Bent Slots," *Electronics Letters,* Vol. 34, No. 13, 1998, pp. 1278–1279.

[35] Iwasaki, H., "A Circularly Polarized Small Size Microstrip Antenna with a Cross Slot," *IEEE Trans. Antennas Propagation,* Vol. AP-44, 1996, pp. 1399–1401.

[36] Wong, K. L., and M. H. Chen, "Small Slot-Coupled Circularly Polarized Microstrip Antenna with Modified Cross-Slot and Bent Tuning-Stub," *Electronics Letters,* Vol. 34, No. 16, 1998, pp. 1542–1543.

[37] Reddy, K. T. V., and G. Kumar, "Dual Feed Gap Coupled Square Microstrip Antennas for Broadband Circularly Polarization," *Microwave Optical Tech. Letters,* Vol. 26, No. 6, 2000, pp. 399–402.

[38] Reddy, K. T. V., and G. Kumar, "Gap Coupled Broadband Circularly Polarized Square Microstrip Antennas," *Proc. Int. Conf. on Computers, Communication and Devices,* ICCCD—2000, December 2000, pp. 365–368.

[39] Legay, H., and L. Shafai, "Analysis and Design of Circularly Polarized Series Fed Planar Subarray," *IEE Proc. Microwaves, Antennas Propagation,* Pt. H, Vol. 142, No. 2, 1995, pp. 173–177.

[40] Reddy, K. T. V., and G. Kumar, "Stacked Square Microstrip Antennas for Wideband Circular Polarization," *Proc. National Conf. on Communications, NCC—2001,* Indian Institute of Technology, Kanpur, January 2001, pp. 125–128.

[41] Reddy, K. T. V., and G. Kumar, "Stacked Microstrip Antennas for Broadband Circular Polarization," *IEEE AP-S Int. Symp. Digest,* Boston, MA, July 2001, pp. 420–423.

[42] Reddy, K. T. V., and G. Kumar, "Stacked Circular Microstrip Antennas for Wideband Circular Polarization," *Proc. Symp. Antenna Propagation,* Kochi, Japan, December 2000, pp. 47–50.

[43] Huang, C. Y., J. Y. Wu, and K. L. Wong, "Cross-Slot-Coupled Microstrip Antenna and Dielectric Resonator Antenna for Circular Polarization," *IEEE Trans. Antennas Propagation,* Vol. AP-47, No. 4, 1999, pp. 605–609.

[44] Vlasits, T., et al., "Performance of a Cross Aperture Coupled Single Feed Circularly Polarized Patch Antenna," *Electronic Letters,* Vol. 32, No. 7, 1996, pp. 612–613.

[45] Targonski, S. D., and D. M. Pozar, "Design of Wideband Circularly Polarized Aperture Coupled Microstrip Antennas," *IEEE Trans. Antennas Propagation,* Vol. 41, No. 2, 1993, pp. 214–220.

[46] Pozar, D. M., and S. M. Duffy, "A Dual-Band Circularly Polarized Aperture-Coupled Stacked Microstrip Antenna for Global Positioning Satellite," *IEEE Trans. Antennas Propagation,* Vol. 45, No. 11, 1997, pp. 1618–1625.

[47] Aksun, M. I., S. L. Chuang, and Y. T. Lo, "On Slot-Coupled Microstrip Antennas and Their Applications for Circular Polarization Operation," *IEEE Trans. Antennas Propagation,* Vol. AP-38, 1990, pp. 1224–1230.

[48] Huang, C. Y., C. Y. Wu, and K. L. Wong, "Slot-Coupled Microstrip Antenna for Broadband Circular Polarization," *Electronic Letters,* Vol. 34, No. 9, 1998, pp. 835–836.

[49] Pozar, D. M., and D. H Schaubert, *Microstrip Antennas: The Analysis and Design of Microstrip Antennas and Arrays,* New York: IEEE Press, 1995.

[50] Teshirogi, T., M. Tanaka, and W. Chujo, "Wideband Circularly Polarized Antenna with Sequential Rotations and Phase Shift of Elements," *Proc. ISAP,* 1985, pp. 117–120.

[51] Morrow, I., and J. R. James, "Sequentially Rotated Large Bandwidth Circularly Polarized Printed Antennas," *Electronics Letters,* Vol. 31, No. 24, 1995, pp. 2062–2064.

[52] Lo, W. K., C. H. Chan, and K. M. Luk, "Circularly Polarized Microstrip Antenna Array Using Proximity Coupled Feed," *Electronics Letters,* Vol. 34, No. 23, 1998, pp. 2190–2191.

[53] Huang, J., "A Technique for an Array to Generate Circular Polarization with Linear Polarized Elements," *IEEE Trans. Antennas Propagation,* Vol. AP-34, No. 9, 1986, pp. 1113–1123.

[54] Iwasaki, H., T. Nakajima, and Y. Suzuki, "Gain Improvement of Circularly Polarized Array Antenna Using Linearly Polarized Elements," *IEEE Trans. Antennas Propagation,* Vol. 43, No. 6, 1995, pp. 604–608.

[55] Gupta, K. C., and A. Benalla, *Microstrip Antenna Design,* Norwood, MA: Artech House, 1988.

[56] Wood, C., "Curved Microstrip Lines as Compact Wideband Circularly Polarized Antennas," *IEE Proc. Microwaves, Antennas Propagation,* Pt. H, Vol. 3, 1979, pp. 5–13.

[57] Ito, K., and H. Kogo, "Improved Design of Series Fed Circularly Polarized Printed Linear Antennas," *IEE Proc. Microwaves, Antennas Propagation,* Pt. H, Vol. 133, 1986, pp. 462–466.

[58] Nishimura, S., Y. Sugio, and T. Makimoto, "Crank Type Circularly Polarized Microstrip Antenna," *IEEE AP-S Int. Symp. Digest,* 1983, pp. 162–165.

[59] Roederer, A. G., "A Cross Antenna: A New Low Profile Circularly Polarized Radiator," *IEEE Trans. Antennas Propagation,* Vol. 38, No. 5, 1990, pp. 704–710.

9

Broadband Planar Monopole Antennas

9.1 Introduction

Chapters 1–8 have observed that the BW of the MSA increases with an increase in the substrate thickness and a decrease in the dielectric constant of the substrate. For a thick substrate with a low dielectric constant, a BW of 5% to 10% is obtained. Further increase in the substrate thickness decreases the efficiency of the MSA and increases cross-polar levels as described in Chapter 2. Also, a long coaxial probe is required to feed the radiating metallic patch suspended in air at a large height h as shown in Figure 9.1(a). The large h increases the probe inductance, and the input impedance becomes too inductive to obtain impedance matching. This large inductive input impedance can be taken care of by feeding the patch with a shorter probe of length p as shown in Figure 9.1(b). In this case, the patch is fed along the periphery and an additional perpendicular ground plane is required. If h is very large, the bottom ground plane would have a negligible effect and hence can be removed. This configuration becomes similar to that of a planar monopole antenna, as shown in Figure 9.1(c) [1–4].

The planar disc monopole antennas yield a very large-impedance BW, which can be explained in the following two ways:

1. A monopole antenna generally consists of a thin vertical wire mounted over the ground plane, whose BW increases with an

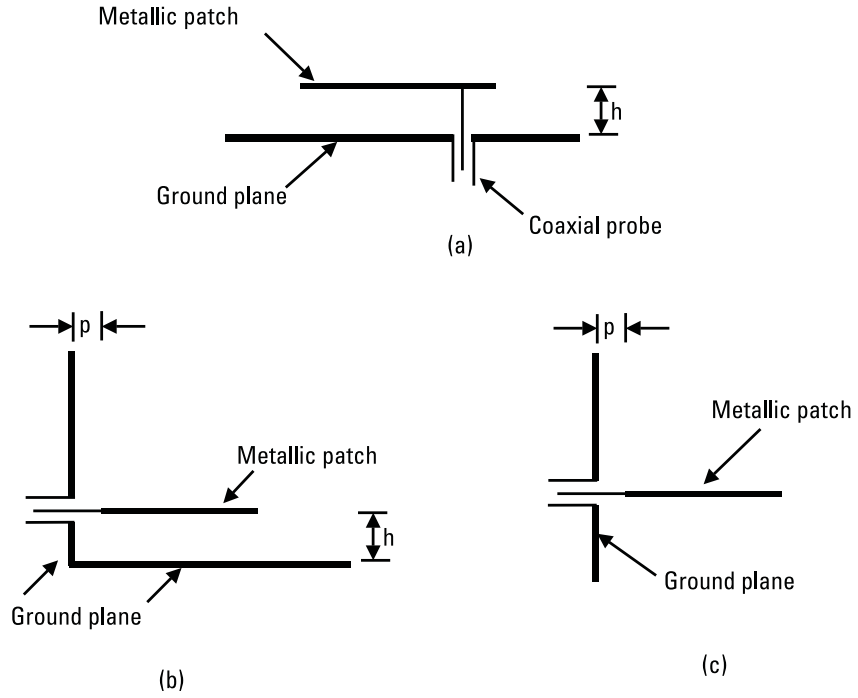

Figure 9.1 (a) MSA suspended in air, (b) modified MSA with side feed, and (c) planar monopole antenna.

increase in its diameter [5]. A planar monopole antenna can be equated to a cylindrical monopole antenna with a large effective diameter.

2. The planar monopole antenna can be viewed as a MSA on a very thick substrate with ϵ_r = 1, so a large BW is expected. In the radiating metallic patch, various higher order modes will get excited. Since all the modes will have a larger BW, these will undergo a smaller impedance variation. The shape and size of these planar antennas can be optimized to bring several modes within the VSWR = 2 circle in the Smith chart, leading to very large-impedance BW.

This chapter describes various planar monopole antennas, including square, rectangular, triangular, hexagonal, circular, and elliptical disc monopoles.

9.2 Planar Rectangular and Square Monopole Antennas

A planar rectangular monopole antenna can be thought of as a variation of the RMSA, in which the horizontal ground plane is considered to be located at infinity. The following discussions bring out this analogy.

9.2.1 RMSA Suspended in Air with Orthogonal Ground Plane

The side and the front views of a rectangular radiating patch with $L = W =$ 12 cm made of a copper plate of thickness 0.1 cm with two orthogonal ground planes are shown in Figure 9.2(a, b). The patch is fed with a 50-Ω SMA connector of probe length p through a fixed ground plane and the orthogonal ground plane is moveable. For the moveable ground plane spacing $h = 3$ cm from the radiating patch and the probe length $p = 0.4$ cm, the measured input impedance and VSWR plots are shown in Figure 9.2(c, d). Multiple loops occur due to the excitation of various higher order modes of RMSA. The impedance plot shows less inductive shift due to the smaller value of the feed probe length p, so the value of p is increased to 1 cm to shift the impedance plot in the clockwise direction. The results are summarized in Table 9.1. The measured BW for VSWR ≤ 2 is from 858 MHz to 988 MHz.

For analysis purpose, this structure can be thought of as an MSA on an air dielectric with an additional perpendicular ground plane. The analytical methods valid for MSAs could be applied to this configuration with suitable modifications.

The formula for RMSA is used to calculate the resonance frequency of this antenna. Since the dielectric medium for all the cases under consideration is air, the effective dielectric constant ϵ_e is equal to 1. The theoretical resonance frequency for the fundamental mode can be calculated using (2.9).

$$f_0 = c/(2L_e) \tag{9.1}$$

where:

L_e = effective resonant length;
c = velocity of light in free space.

For two orthogonal ground planes, $L_e \simeq L + \Delta L + p$, because the extension of length ΔL due to the fringing fields is applicable only for one side, and on the other side, it is restricted to p due to the orthogonal ground

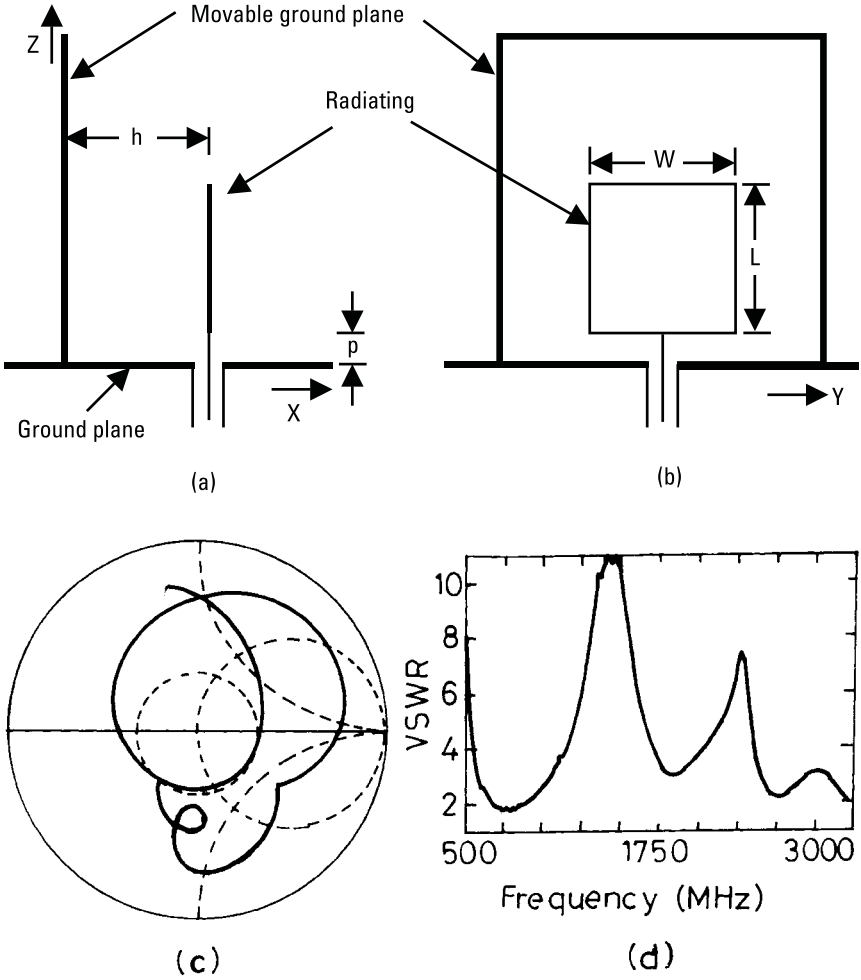

Figure 9.2 (a) Side and (b) front views of modified RMSA with orthogonal ground planes. Measured (c) input impedance and (d) VSWR plots.

plane. For a large width of the patch ($W/h > 10$) with $\epsilon_r = 1$, ΔL is approximately equal to h. The theoretical resonance frequency, calculated using (9.1) for $p = 1.0$ cm, is 937 MHz, which is close to the measured center frequency of 923 MHz.

Next, the effect of increasing h on BW of the antenna is considered. For different values of h with $p = 1.0$ cm, the measured lower and upper frequencies (f_L and f_H) corresponding to VSWR = 2 are given in Table 9.1. With an increase in h from 3 cm to infinity (∞), the percentage BW

Table 9.1
Resonance Frequency and Percentage BW of RMSA with $L = W = 12$ cm for Different Values of h

h (cm)	Measured Results for VSWR ≤ 2			Theoretical Frequency (MHz)
	f_L (MHz)	f_H (MHz)	% BW	
3	858	988	14.1	937[a]
6	752	934	17.7	789[a]
18	515	1,081	70.3	484[a], 483[b]
∞	501	1,154	81.2	0[a], 483[b]

[a]Calculated using (9.1).
[b]Calculated using (9.8).

of the antenna increases from 14.1% to 81.2%. As h increases, the measured lower resonance frequency decreases because of the increase in ΔL due to the large fringing fields. For smaller values of h, there is a reasonable agreement between the theoretical frequency obtained from (9.1) and the measured center frequency. As h increases, the theoretical frequency is close to the measured lower frequency corresponding to VSWR = 2.

For two different values of h [i.e., 18 cm (large) and ∞ (bottom ground plane removed)], the measured input impedance and VSWR plots are shown in Figure 9.3. As h increases from 18 cm to ∞ the measured lower frequency decreases slightly from 515 MHz to 501 MHz. For these two values of h,

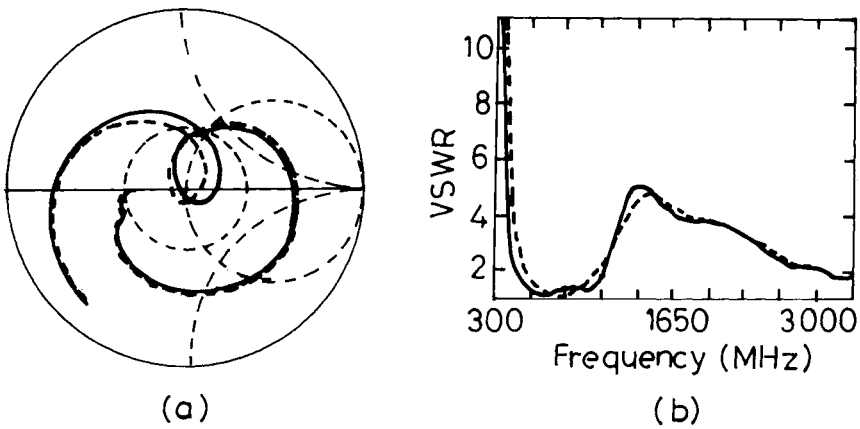

Figure 9.3 Measured (a) input impedance and (b) VSWR plots of RMSA for two values of h: (- - -) 18 cm and (——) ∞.

the input impedance and VSWR plots are nearly the same. Therefore, for a large h tending to infinity, the MSA configuration reduces to that of a planar monopole antenna. In this case, the approximate lower frequency corresponding to VSWR = 2 can be determined by using the monopole antenna concept described in Section 9.2.2.

9.2.2 Calculation of the Lower Frequency of the Planar Monopole Antennas

For a planar monopole antenna, the lower frequency corresponding to VSWR = 2 can be approximately calculated by equating its area (in this case, a rectangular disc monopole) to that of an equivalent cylindrical monopole antenna of same height L and equivalent radius r, as described below [3, 4]:

$$2\pi rL = WL \tag{9.2}$$

which gives

$$r = W/(2\pi) \tag{9.3}$$

The input impedance of a $\lambda/4$ monopole antenna is half of that of the $\lambda/2$ dipole antenna. Thus, the input impedance of an infinitesimally thin monopole antenna is $36.5 + j\,21.25\Omega$, which is inductive. The real input impedance is obtained when a slightly smaller length of the monopole is used as given by [5]:

$$L = 0.24\lambda F \tag{9.4}$$

where

$$F = (L/r)/(1 + L/r) = L/(L + r) \tag{9.5}$$

From (9.4) and (9.5), the wavelength λ is obtained as:

$$\lambda = (L + r)/0.24 \tag{9.6}$$

Therefore, the lower frequency f_L is given by:

$$f_L = c/\lambda = (30 \times 0.24)/(L + r) = 7.2/(L + r) \text{ GHz} \tag{9.7}$$

Equation (9.7) does not account for the effect of the probe length p, which increases the total length of the antenna thereby reducing the frequency. Accordingly, this equation is modified to

$$f_L = 7.2/(L + r + p) \text{ GHz} \tag{9.8}$$

where L, r, and p are in centimeters.

The theoretical frequency of 483 MHz for $h = \infty$ (monopole antenna) obtained using (9.8) is close to the measured f_L of 501 MHz. For h = 18 cm, the theoretical frequencies obtained using the MSA and monopole concepts are very close to each other.

Thus, an interesting transition in antenna characteristics (with respect to resonance frequency) is observed, as the ground plane spacing h is increased. For a smaller h, the measured resonance frequency is close to the theoretical frequency determined by the expressions applicable to the MSA and for a larger h, it is close to the frequency obtained using expressions for a monopole antenna.

9.2.3 Effect of Various Parameters of Planar Rectangular Monopole Antennas

The previous section observed that the planar *rectangular monopole* (RM) antenna yields a large impedance BW [3, 4]. The BW of these antennas depends mainly on the width W of the plate, the diameter d of the feeding probe, and the length of the probe p. The SMA connector is generally used above 1 GHz for feeding the antenna, and hence, d is kept fixed at 0.12 cm. When the height L of the monopole antenna increases (or decreases), the lower edge frequency decreases (or increases), which is quite obvious. Therefore, the effects of width W and probe length p on the performance of the antenna are described.

The RM and *square monopole* (SM) antennas are analyzed using IE3D software [6]. Initially, the effect of p is described by keeping $L = W$ = 4.5 cm. The input impedance and VSWR plots for two values of p are shown in Figure 9.4(a, b). As p is increased from 0.05 cm to 0.2 cm, the input impedance plot shifts up in the clockwise direction. This is because with an increase in p, the probe inductance increases and therefore the input impedance becomes more inductive. A broad BW of 1,335 MHz (68%) is obtained for p = 0.2 cm, compared to the BW of 668 MHz (40%) for p = 0.05 cm.

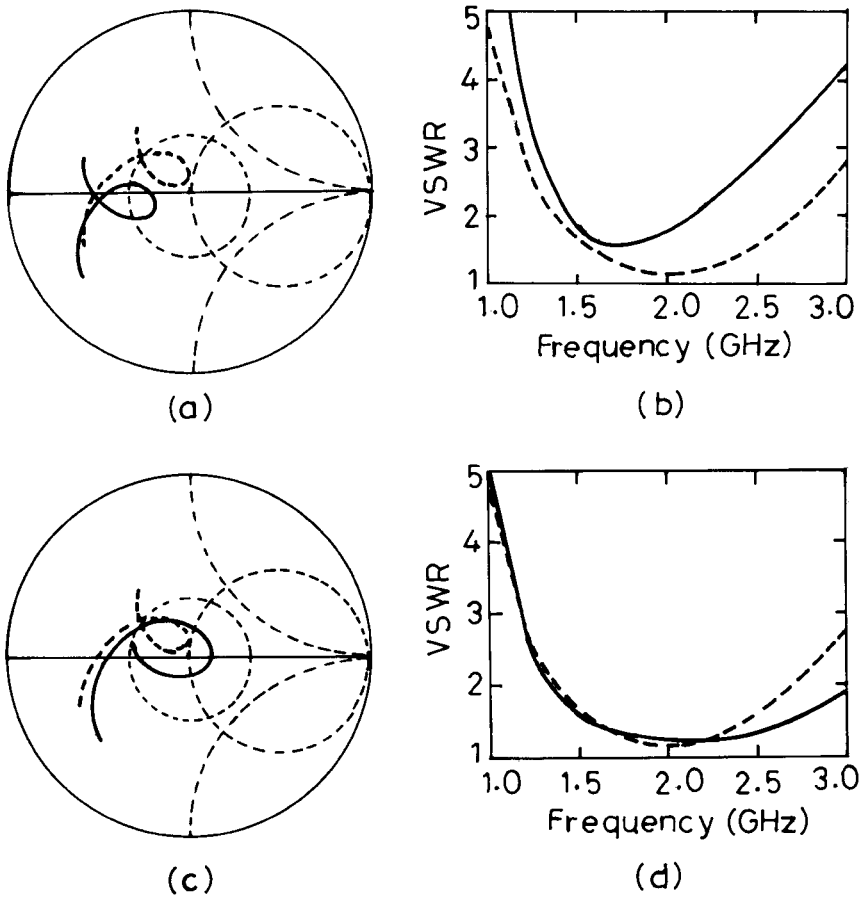

Figure 9.4 (a) Input impedance and (b) VSWR plots of RM antenna for two values of p [(——) 0.05 cm and (- - -) 0.2 cm]; (c) input impedance and (d) VSWR plots with L = 4.5 cm and p = 0.2 cm for two values of W [(- - -) 4.5 cm and (——) 3.5 cm].

Next, the effect of W is described by keeping other parameters fixed. The input impedance and VSWR plots for two values of W (4.5 cm and 3.5 cm) with L = 4.5 cm and p = 0.2 cm are shown in Figure 9.4(c, d). With a decrease in W, the size of the loop in the impedance plot increases and the plot shifts toward the right in the Smith chart. Since the lengths of these RMs are kept fixed at 4.5 cm, the lower band-edge frequency remains almost unchanged; this is predominantly determined by the length L of the planar monopole antenna. As W decreases from 4.5 cm to 3.5 cm, the BW increases from 1,335 MHz to 1,715 MHz due to an increase in loop size.

9.2.4 Radiation Pattern of RM Antennas

The theoretical radiation pattern of the square monopole antenna ($L = W =$ 4.5 cm) is obtained using IE3D for infinite ground plane [6]. For comparison, the radiation pattern of a thin (narrow width $W = 0.5$ cm) RM antenna with the same length $L = 4.5$ cm is also computed in the same frequency range. The E- and H-plane radiation patterns of both the antennas at 1.5 GHz and 2.5 GHz are shown in Figure 9.5. These two frequencies are

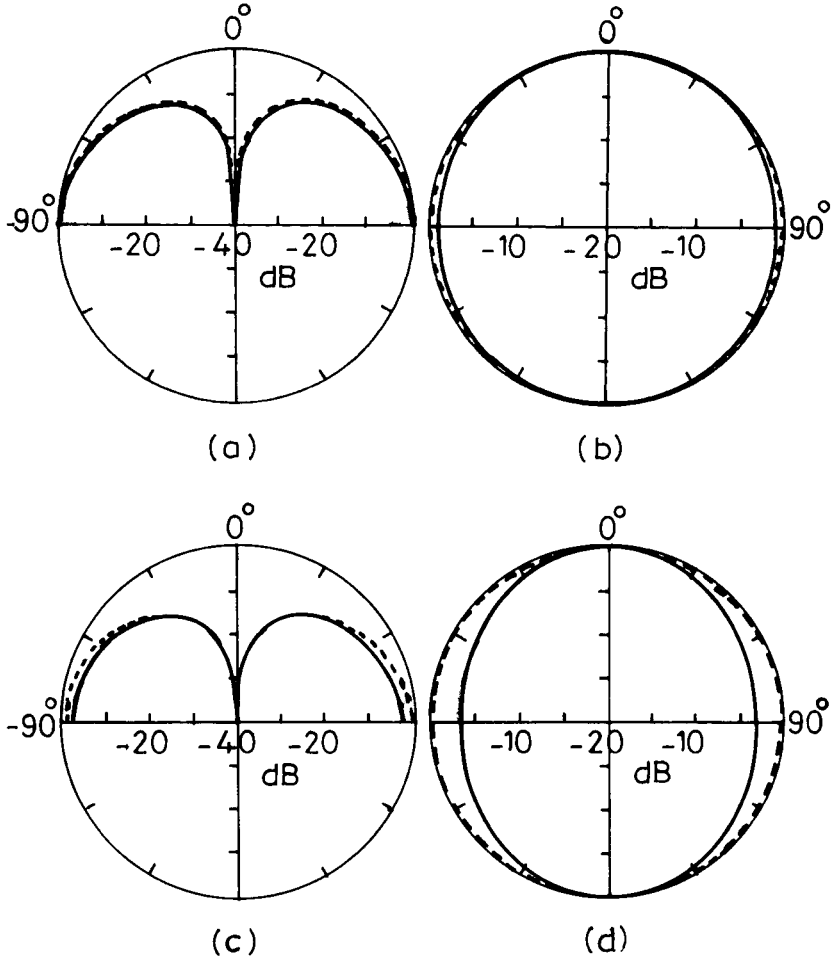

Figure 9.5 Radiation patterns of the two monopole antennas at 1.5 GHz (a) E-plane and (b) H-plane. Radiation patterns at 2.5 GHz and the (c) E-plane and (d) H-plane. [(- - -) Thin RM and (——) SM].

within the BW for VSWR = 2 of the SM antenna. In the E-plane, the radiation pattern of the SM is similar to that of the thin monopole antenna. With an increase in frequency from 1.5 GHz to 2.5 GHz, the variation in the azimuthal pattern (H-plane) increases from 1 dB to 3 dB for SM, because of the asymmetry in the X- and Y-planes of the structure as compared to the thin monopole antenna.

9.2.5 Various Planar RMs with Equal Areas

After observing the effects of various parameters on the BW of the monopole antenna, the dimensions L and W of RM are chosen such that their surface areas are equal, so that a comparison of performances of these planar monopole antennas may be made. For all the measurements, the size of the ground plane is chosen to be 30 cm × 30 cm with p = 0.1 cm. The SM is fed in the middle of the one side by a SMA connector as shown in Figure 9.6(a), whereas RM is fed in two different ways as shown in Figure 9.6(b, c). The RMs with feeds in the middle of the smaller and larger dimensions are coined RMAs and RMBs, respectively.

The dimensions and VSWR BW of these configurations are listed in Table 9.2. The theoretical lower frequency f_L for VSWR = 2 obtained using (9.8), is also tabulated. The percentage error is calculated using

$$\%\text{error} = \frac{f_L - f_m}{f_m} \times 100 \tag{9.9}$$

where f_m is the lower measured frequency. The theoretical frequencies predicted by (9.8) are within ±6.6% of the measured values. The f_L of RMB

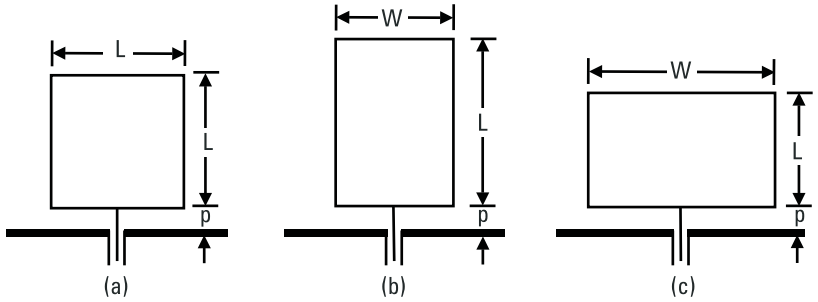

Figure 9.6 (a) Square monopole antenna. RM antennas with feed in the middle of (b) smaller W and (c) larger W.

Table 9.2
Comparison of Square, Rectangular, Triangular, and Hexagonal Monopole Antennas

Configuration	$L \times W$ (cm × cm)	Measured Frequency f_m Range for VSWR ≤ 2 (GHz)	f_L (GHz)	Measured BW Ratio	Percentage Error in Frequency
SM	4.5 × 4.5	1.27 to 2.81	1.354	1:2.2	+6.6
RMA	4.6 × 4.2	1.38 to 2.75	1.341	1:2.0	−2.8
RMB	4.2 × 4.6	1.40 to 2.02	1.431	1:1.4	+2.2
TMB	5.9 × 6.8	1.07 to 1.11	1.101	1:1.04	+2.9
HMA	4.8 × 5.6	1.37 to 2.68	1.282	1:1.9	−6.5
HMB	5.6 × 4.8	1.20 to 3.92	1.147	1:3.2	−4.4

is higher than that of the RMA, because the height of the RMB is smaller than that of the RMA.

The measured VSWR plots of SM, RMA, and RMB are given in Figure 9.7. The VSWR values fluctuate from as high as 8 to as low as 1.05 in the frequency range of 1–13 GHz. The measured BW ratios of SM, RMA, and RMB in the lower range of frequency are 1:2.2, 1:2.0, and 1:1.4, respectively. By adjusting the dimensions of the patches and length of the

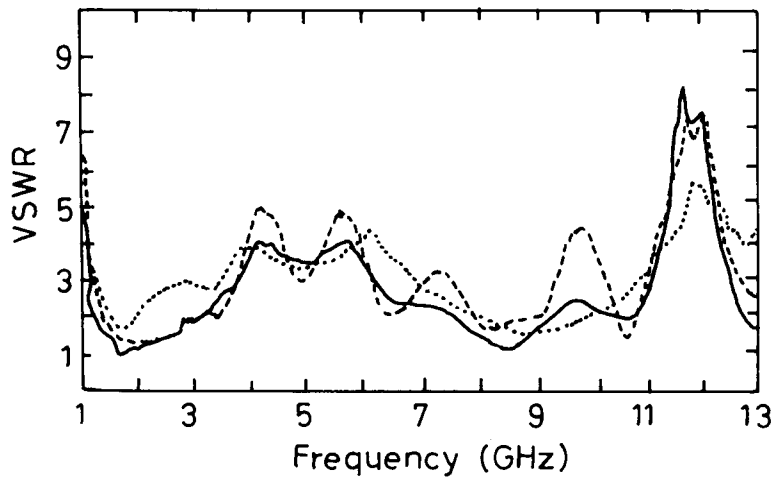

Figure 9.7 Measured VSWR plots for three monopole antennas: (——) SM, (- - -) RMA, and (· · ·) RMB.

probe, these configurations can be optimized to operate within selected frequency bands.

9.3 Planar Triangular and Hexagonal Monopole Antennas

Other polygon variations of planar monopole antennas, such as triangular and hexagonal monopole (TM and HM) antennas, are considered next. The surface area and other parameters of these monopoles are kept the same as those of the rectangular and square monopoles for comparison.

9.3.1 Planar Equilateral Triangular Monopole

The side length of the equilateral triangular patch is calculated to be 6.84 cm, so that its area is equal to that of the SM described in the previous section. Two feed configurations, TMA and TMB, are considered as shown in Figure 9.8(a, b). The TMA is fed at the middle of the side while the

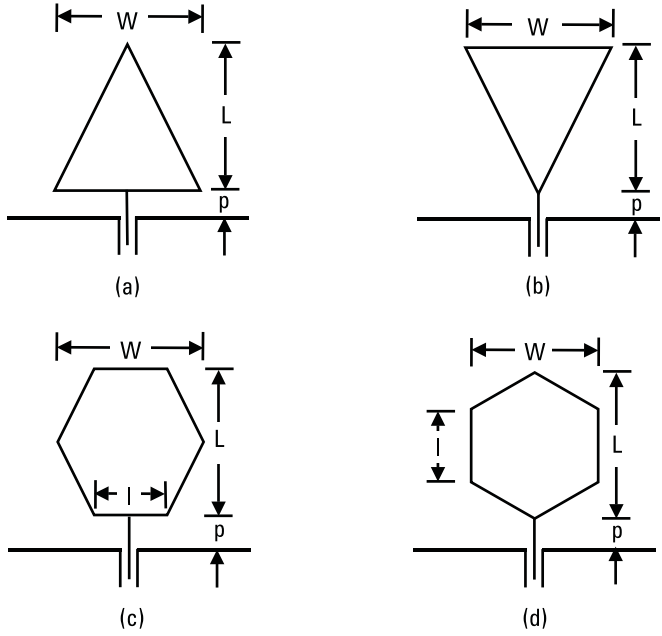

Figure 9.8 Triangular monopole antenna fed (a) in the middle of the side and (b) at the vertex. Hexagonal monopole antenna fed (c) in the middle of the side and (d) at the vertex.

TMB is fed at the vertex. The TMB configuration is equivalent to one-half of broadband bowtie dipole antenna [5].

For calculating f_L of the TMA and TMB antenna using (9.8), the values of L and r of the effective cylindrical monopole are determined as

$$L = \sqrt{3W/2} \tag{9.10}$$

$$r = W/(4\pi) \tag{9.11}$$

where W is equal to the side length of the equilateral triangle.

For TMA, the VSWR is always greater than 2, as there is no input impedance matching at any frequency. However, for TMB, which is like a half-bowtie dipole, matching is obtained at some frequencies. The results for the TMB are summarized in Table 9.2. The f_L of this antenna is the least amongst all the other configurations of the same area because it has the largest height. The measured BW is smaller as compared to the corresponding RM and SM antennas.

9.3.2 Planar Hexagonal Monopole

The side length l of the hexagon is obtained by equating its area with SM, and its value is calculated to be 2.8 cm. In this case also, two feed configurations, HMA and HMB, are used as shown in Figure 9.8(c, d). The HMA and HMB are fed in the middle of the side and at the vertex, respectively. The theoretical lower frequencies corresponding to VSWR = 2 are calculated separately for the HMA and HMB antennas as given below.

For the HMA, the L and r values of the equivalent cylindrical monopole antenna are obtained by equating their areas as follows:

$$L = \sqrt{3l} \tag{9.12}$$

$$r = 3l/(4\pi) \tag{9.13}$$

The parameters for the HMB are:

$$L = 2l \tag{9.14}$$

$$r = 3\sqrt{3}l/(8\pi) \tag{9.15}$$

For these values of L and r, the lower frequency f_L is computed from (9.8).

The VSWR plots for these two configurations are shown in Figure 9.9, and the results are summarized in Table 9.2. The f_L of HMB is lower than that of HMA because of its larger height L. The HMB has a larger BW than the HMA. This can be understood from the analogy that the HMB feed is similar to that of the TMB, which yields better matching than the TMA. The HMA feed is similar to the feed for the TMA and hence yields a smaller BW. The HMB provides a wider BW than the square and the RMs, as it is closer to the circular configuration, which has a very large BW as described in the next section.

9.4 Planar Circular Monopole Antennas

A planar *circular monopole* (CM) antenna yields very broad BW [1, 2]. A CM of radius a is shown as inset in Figure 9.10. The radius a is taken equal to 2.5 cm, so that its surface area is approximately equal to that of the other monopole antennas given in Table 9.2. As in the earlier cases, the size of the ground plane is kept same as 30 cm × 30 cm. For the CM, the values L and r of the equivalent cylindrical monopole antenna are given by:

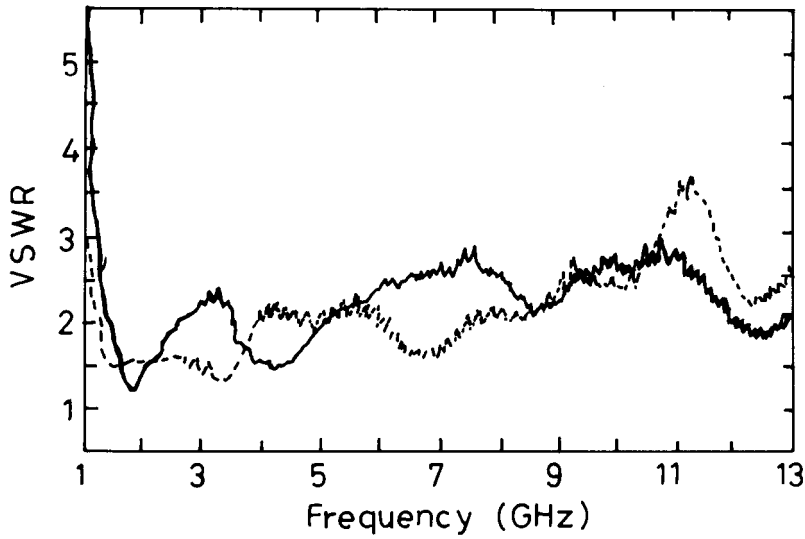

Figure 9.9 Measured VSWR plots of two-feed configurations of hexagonal monopole antennas: (——) HMA and (- - -) HMB.

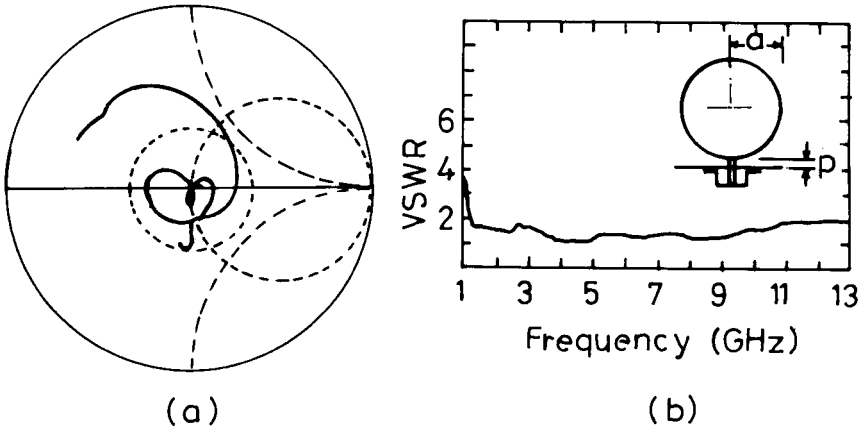

Figure 9.10 Measured (a) input impedance and (b) VSWR plots of CM antenna.

$$L = 2a \tag{9.16}$$

$$r = a/4 \tag{9.17}$$

For $p = 0.1$ cm, the measured input impedance and VSWR plots are shown in Figure 9.10. The BW for VSWR ≤ 2 is from 1.17 GHz to 12 GHz, which corresponds to a BW ratio of 1:10.2.

The BW of the CM is larger than all the monopole antennas described earlier. This could be interpreted in terms of various higher order modes of the circular patch. Unlike the various modes of rectangular resonator, modes of the circular resonator (characterized by the roots of the derivative of the Bessel function) are closely spaced as explained in Chapter 2. The BW associated with the various modes is very large because the disc is in the air; accordingly, the change in the input impedance from one mode to another mode is very small. This can also be noted from the impedance plot shown in Figure 9.10(a), which has multiple loops corresponding to the various modes. Since these loops are within the VSWR = 2 circle, a large BW is obtained.

9.5 Planar Elliptical Monopole Antennas

An *elliptical monopole* (EM) antenna is a generalized case of the circular monopole, wherein the major axis is not equal to the minor axis. The dimensions of EM (i.e., major axis length = $2a$ and minor axis length = $2b$)

are calculated, keeping its area equal to that of the CM. The ellipticity ratio is chosen as $a/b \simeq 1.1$, which is named as EM1. The EM is fed either along the minor axis (EMA) or the major axis (EMB) as shown in the insets of Figure 9.11.

For calculating f_L of the EM antenna, the L and r of the effective cylindrical monopole are determined by equating its area as:

$$2\pi rL = \pi ab \tag{9.18}$$

For EMA, $L = 2b$ and $r = a/4$, and for EMB, these parameters are $L = 2a$ and $r = b/4$. The f_L is calculated using (9.8).

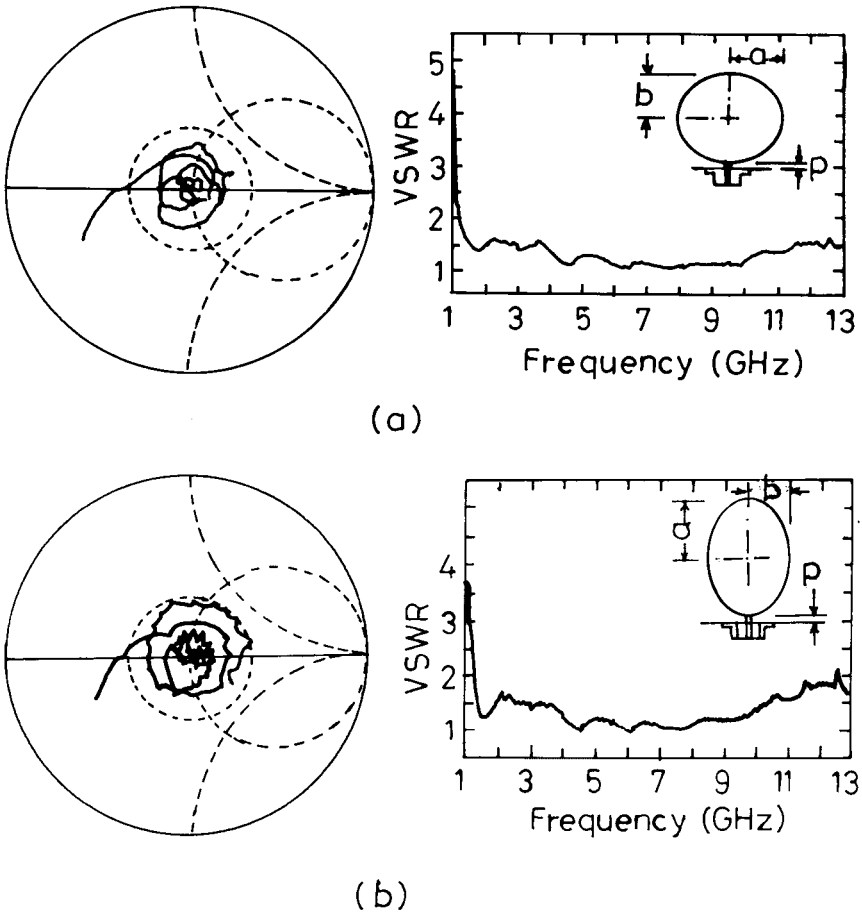

Figure 9.11 Measured input impedance and VSWR plots of (a) EM1A and (b) EM1B.

The measured input impedance and VSWR plots for EM1A and EM1B are shown in Figures 9.11. The performances of these configurations are compared with those of the CM in Table 9.3. Improved VSWR BWs are obtained for EM1A and EM1B as compared to CM. Therefore, the effect of varying the ellipticity ratio on the BW of the EM antenna is described in Section 9.5.1.

9.5.1 Effect of Ellipticity Ratio

Three elliptical disc monopoles with different ellipticity ratios are considered by keeping the area same as before. For these three monopoles, the values of a/b are chosen as 1.2 (EM2), 1.3 (EM3), and 1.4 (EM4) [3].

The measured VSWR plots of EM2, EM3, and EM4 in configurations "A" and "B" are compared in Figure 9.12. The dimensions and measured VSWR BWs for all these cases are summarized in Table 9.3. The f_L of EMBs is always smaller than that of the EMAs because of its larger height. As the ellipticity ratio a/b increases from 1.1 to 1.4, BW decreases. In comparison with the measured f_L, the theoretical f_L obtained using (9.18) and (9.8) is within ±7.5% for most of the cases as shown in Table 9.3.

9.5.2 Radiation Pattern of Circular and Elliptical Monopole Antennas

Among all these broadband monopole configurations, the CM and EM1A antennas provide a maximum BW. The measured radiation patterns of these

Table 9.3
Comparison of VSWR BW of CM and Various EMs [3]

Configuration	*a* (cm)	*b* (cm)	Measured Frequency Range (GHz)	Theoretical f_L (GHz)	Percentage Error in f_L
CM	2.5	2.5	1.17 to 12.0	1.258	+7.5
EM1A	2.6	2.4	1.21 to 13*	1.297	+7.2
EM1B	2.6	2.4	1.20 to 12.50	1.220	+1.7
EM2A	2.7	2.3	1.38 to 11.49	1.340	–2.9
EM2B	2.7	2.3	1.13 to 12.00	1.185	+4.9
EM3A	2.8	2.2	1.37 to 11.30	1.385	+1.1
EM3B	2.8	2.2	1.08 to 11.43	1.152	+6.7
EM4A	2.9	2.1	1.58 to 10.45	1.433	–9.3
EM4B	2.9	2.1	1.09 to 10.45	1.121	+2.8

*Gives VSWR < 2 above 13 GHz also.

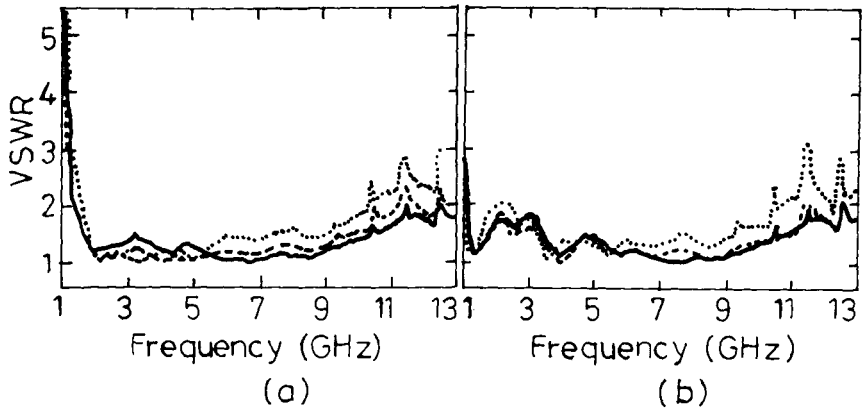

Figure 9.12 Measured VSWR plots of (a) EMA and (b) EMB for different a/b ratios: (——) 1.2, (- - -) 1.3, and (· · ·) 1.4.

two configurations at frequencies 2.5 GHz and 9 GHz are shown in Figure 9.13. The results are summarized as follows:

- At 2.5 GHz, the E-plane (elevation) pattern is conical, whereas the H-plane (azimuthal) pattern is nearly omni-directional with a maximum variation of 4 dB. The pattern is similar to that of a vertical 0.4λ linear monopole antenna (which is approximately the equivalent height of the antenna at this frequency) on a finite ground plane.
- At 9 GHz, the effective height of the disc monopole is $3\lambda/2$, the E-plane pattern resembles to that of a $3\lambda/2$ vertical linear monopole antenna. The maximum variation of 7 dB is observed in the azimuthal pattern.

These patterns are similar to those of the thick monopole antennas on a finite ground plane, which round off the nulls of the pattern of the infinitesimal thin (very small radius) monopole on infinite ground plane and enhance the radiation at higher angles from the zenith [7, 8]. Slight distortions might be attributed to the shape of the planar monopole, reflections from metallic surfaces, and edge diffraction.

9.6 Design Examples of Monopole Antennas

Based upon the above discussions regarding the analysis of various monopole antennas, two design examples are presented.

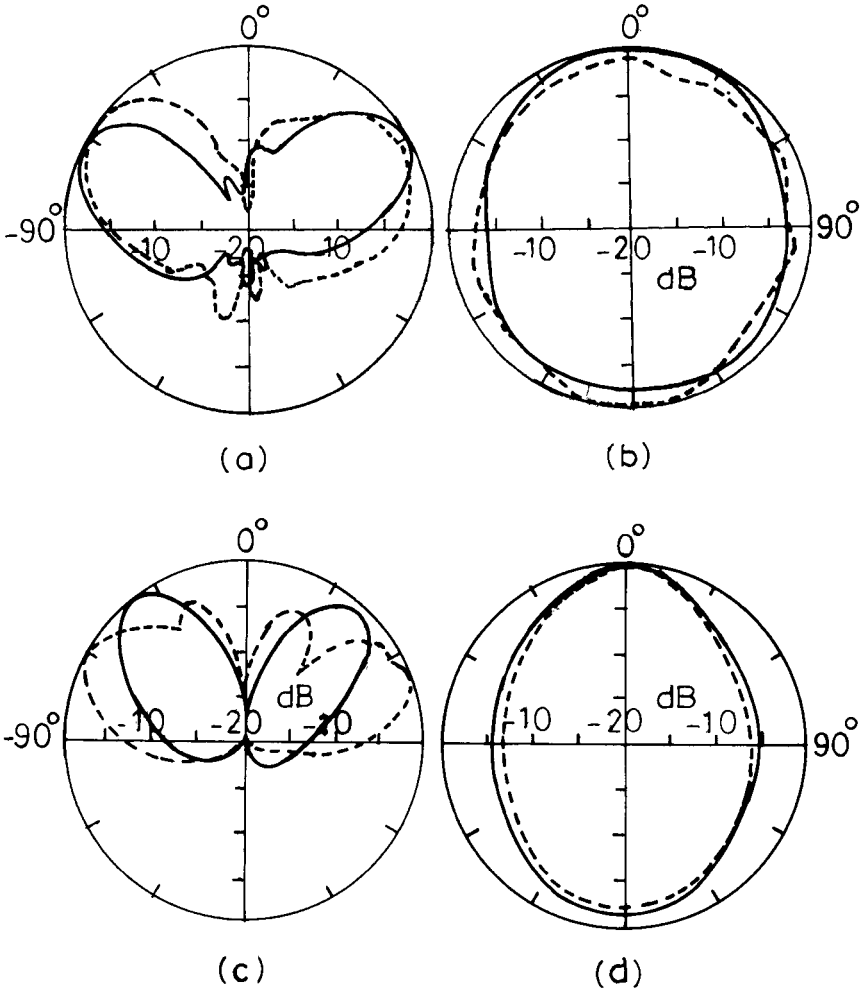

Figure 9.13 Radiation pattern of two monopole antennas at two frequencies: (a) E- and (b) H-planes at 2.5 GHz and (c) E- and (d) H-planes at 9.0 GHz. [(——) CM and (- - -) EM1A.]

9.6.1 Monopole Antenna for 225–400 MHz

To cover the frequency range of 225–400 MHz for defense applications, an inverted disk cone monopole antenna is typically used; this is structurally not very convenient. Consequently, there is a need for a simple planar monopole antenna that can be easily fabricated and installed. This BW can be achieved with the planar RM antenna described in Section 9.2.

Initially, the length L of the RM antenna is obtained as 27.6 cm for f_L = 0.225 GHz by using (9.3) and (9.7) by choosing $W = L$. It has been shown in Section 9.2.3 that a broader BW is obtained when W is smaller than L without significantly affecting the lower resonant frequency. To keep the margin in f_L, L is chosen as 28 cm and the width is chosen as 22 cm. These dimensions can be approximately obtained by using a frequency-scaling technique from the dimensions given in Section 9.2.3. Also, in this frequency range, an N-type connector is typically used instead of an SMA connector, which helps in supporting a large-size monopole antenna. Hence, the diameter of the probe is taken as 0.4 cm. For p = 0.7 cm, the theoretical input impedance and VSWR plots are shown in Figure 9.14. In the desired frequency range of 225–400 MHz, the VSWR is less than 2. The maximum variation of the pattern in the azimuthal direction is 2 dB at the higher frequency.

9.6.2 Monopole Antenna for 800–2,000 MHz

To cover the *wireless local loop* (WLL) and GSM communication frequency bands of 824–890 MHz and 890–960 MHz, respectively, and the proposed 1,710–1,880-MHz band, separate antennas are currently being used. A single planar monopole antenna can be designed to cover the entire frequency range. Since the BW is very large, a RM antenna will not meet the requirement, but a circular or elliptical monopole antenna can yield the BW as described in Sections 9.4 and 9.5, respectively.

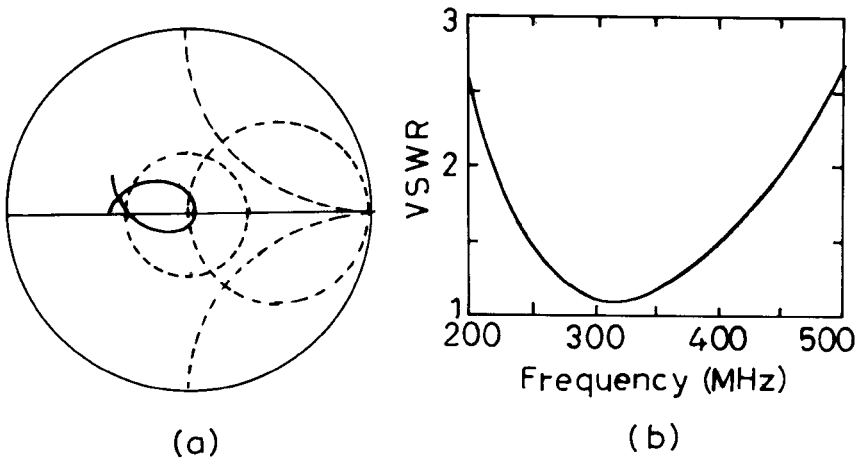

Figure 9.14 Theoretical (a) input impedance and (b) VSWR plots of RM with L = 28 cm, W = 22 cm, and p = 0.7 cm.

For simplicity, CM is considered. The radius of the CM is obtained as 4 cm corresponding to f_L = 800 MHz by using (9.16), (9.17), and (9.7). To keep the margin in f_L, the radius is chosen as 5 cm. For the SMA connector of diameter 0.12 cm, p = 0.3 cm and the circular ground plane of diameter 25 cm, the measured input impedance and VSWR plots are shown in Figure 9.15. A VSWR ≤ 2 has been obtained in the frequency range of 710 MHz to 3,000 MHz.

9.7 Summary

A suspended microstrip patch in air fed at its periphery through a perpendicular ground plane becomes a planar monopole antenna, when the bottom ground plane is removed. Differently shaped planar monopole antennas, such as, rectangular, square, triangular, hexagonal, circular, and elliptical disc monopoles are described for very large VSWR BWs. Simple equations are given to predict the lower frequency corresponding to VSWR = 2 for these antennas. The square, rectangular, triangular, and hexagonal monopole antennas yield a lower BW than the circular and elliptical monopoles, but these BWs are large enough for many applications. Moreover, these antennas are attractive due to their ease of fabrication. Circular and elliptical disc monopoles yield multi-octave BW, which is extremely useful for broadband applications. An elliptical disc with an ellipticity ratio of 1.1 provides a maximum BW of more than 1:11 for VSWR ≤ 2. The radiation pattern at

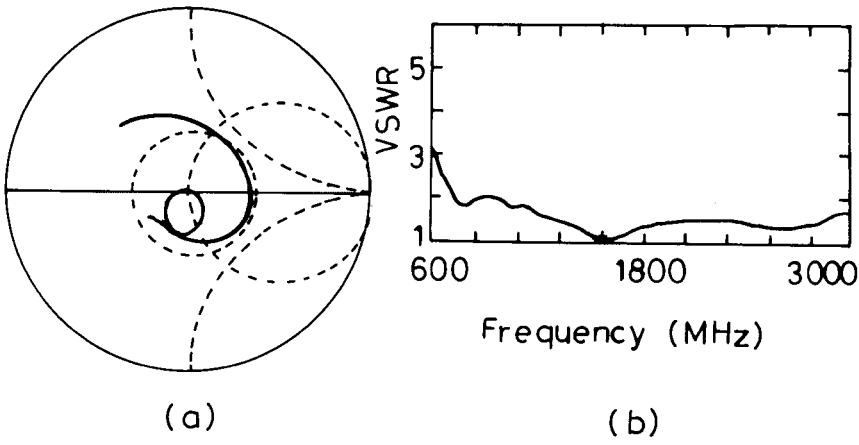

Figure 9.15 Measured (a) input impedance and (b) VSWR plots of CM antenna with radius a = 5 cm and p = 0.3 cm.

various frequencies in the E- and H-planes of these antennas is similar to that of a cylindrical monopole antenna of equivalent height on a finite ground plane. Design examples of planar RM and CM antennas are presented using simple design equations to cover the 225–400 MHz and 800–2,000 MHz frequency bands, respectively.

References

[1] Honda, S., et al., "A Disc Monopole Antenna with 1:8 Impedance BW and Omnidirectional Radiation Pattern," *Proc. ISAP,* Sapporo, Japan, 1992, pp. 1145–1148.

[2] Hammoud, M., P. Poey, and F. Colombel, "Matching the Input Impedance of a Broadband Disc Monopole," *Electronics Letters,* Vol. 29, February 1993, pp. 406–407.

[3] Agarwall, N. P., G. Kumar, and K. P. Ray, "Wide-Band Planar Monopole Antennas," *IEEE Trans. Antennas Propagation,* Vol. 46, No. 2, 1998, pp. 294–295.

[4] Ray, K. P., et al., "Broadband Planar Rectangular Monopole Antennas," *Microwave Optical Tech. Letters,* Vol. 28, No. 1, 2001, pp. 55–59.

[5] Balanis, C. A., *Antenna Theory Analysis and Design,* New York: John Wiley & Sons, 1997.

[6] IE3D 7.0, Zeland Software, Inc., Fremont, CA, 2000.

[7] Ballantine, S., "High Quality Radio Broadcast Transmission and Reception," *Proc. IRE,* Vol. 22, No. 5, 1935, pp. 564–629.

[8] Chang, D. C., C. W. Harrison, Jr., and E. A. Aroson, "Tubular Monopole of Arbitrary Dimensions: The Radiation Field," *IEEE Trans. Antennas Propagation,* Vol. 17, May 1969, pp. 534–540.

Appendix A: MSA Substrates

A dielectric substrate (also known as laminate) is a main constituent of the microstrip structure, whether it is a microstrip line, circuit, or an antenna. The comparison of the requirements for substrate parameters for microstrip circuits and MSAs are discussed in Chapter 1. For MSA applications, a thicker substrate with a low dielectric constant is preferred to enhance the fringing fields and hence the radiation. Another important substrate parameter is its loss tangent (tan δ). The tan δ indicates the dielectric loss, which increases with frequency. For a higher efficiency of the antenna, the substrate with a low tan δ should be used; this is costlier than the substrate with a high tan δ. Therefore, judicious selection of the substrate is required with consideration of the application and frequency of operation. Various substrates from the MSA point of view are described below [1–3].

Synthetic and composite materials are commonly used substrates for MSA applications. These have low ϵ_r and low tan δ and are available in various thicknesses. Generally, they are soft materials and can be bent to conform to the host surface. Some of the most common synthetic substrates are Teflon [popularly known as PTFE (polytetrafluoroethylene)], polypropylene, and polystyrene. The composite materials are made by adding suitable fiberglass, quartz, or ceramic in synthetic or organic materials.

Glass-epoxy substrate, commonly used in PCB, is referred to as FR4. It is one of the cheapest and most universally manufactured substrates. Its application is generally restricted to the low-frequency range of up to 1 GHz,

because of high dielectric loss. However, for testing new designs, the antennas are fabricated on this substrate at higher frequencies also to reduce cost.

To make the size of the antenna compact in the UHF range and for many other specific applications, substrates with a high ϵ_r are used. Some of the high ϵ_r substrate materials are ferromagnetic, ceramic, and semiconductor substances. Ferrite and YIG are the main ferromagnetic materials [3]. The magnetic permeability (μ_r) of these substrates can be changed by varying the biasing magnetic field, which is utilized to tune the resonance frequency of the MSA. Besides having high ϵ_r, these materials have high μ_r, leading to a further size reduction in MSAs. The most commonly used ceramic substrate is alumina, which has very low loss but which is brittle. The semiconductor materials are silicon and gallium arsenide (GaAs), which have a high ϵ_r. Table A.1 lists the primary parameters of all these substrates.

The substrates of synthetic and composite materials are suitable for designing MSAs, but the cost of these substrates is high. New varieties of substrates are available with reasonably low tan δ with prices as low as one-fourth of the prices of the synthetic and composite substrates, allowing for reductions in the cost of the MSA. Table A.2 details these low-cost substrates [3, 4].

To sum up, the choice of the substrate is the first important step in the successful design of an MSA. Besides electrical and mechanical parameters, there are many other physical and chemical properties of the substrate, including flexibility, power-handling capability, chemical resistance, ruggedness, strain relief, bondability, and nonporousness. These factors also influence the decision of the selection of the substrate.

Table A.1
Characteristics of Substrates at 10 GHz

Laminate/Substrate	Dielectric Constant	Loss Tangent	Relative Cost
Polymethacrylate foam, Rohacell 51	1.07	0.0009	Low
PTFE (Teflon)	2.1	0.0004	Medium
PTFE-glass, reinforced	2.17 to 2.35	0.0006	High
PTFE-glass, woven web	2.17 to 2.55	0.0009 to 0.0022	Medium
PTFE-glass, random fibre	2.17 to 2.35	0.0009 to 0.0015	Medium to high
Polypropylene	2.18 $\pm$ .005	0.0003	Medium
Irradiated polylefin	2.32	0.0005	Low
Irradiated polyolefin glass, reinforced	2.42	0.001	Medium
Teflon-ceramic, reinforced	2.47	0.0006	High
Teflon-quartz, reinforced	2.47	0.0006	High
Cross-linked polysterene	2.54	0.0005	Medium
Polypropylene oxide	2.55	0.0016	Medium
Teflon-glass, reinforced	2.55	0.0015	Medium
Cross-linked polystyrene-quartz	2.6	0.0005	Medium to high
Cross-linked polystyrene-glass, reinforced	2.62	0.001	Low
Cross-linked polystyrene-quartz, woven	2.65	0.0005	Medium to high
Cross-linked polystyrene-ceramic, powder filled	3 to 15	0.0005 to 0.0015	Medium to high
Silicon resin-ceramic	3 to 25	0.0005 to 0.004	Medium
Polystyrene-ceramic, powder filled	6	0.017	High
Polyester-ceramic powder filled glass, reinforced	6	0.017	Medium
Glass-bonded mica	7.5	0.002	Medium to high
Ferrite	9.0 to 16.0	0.001	Medium
Sapphire	9.4	0.0001	Very high
Alumina	9.8	0.0004	Medium to high
PTFE-ceramic, composite	10.2	0.002	High
Teflon-quartz, filled	10.3	0.002	Low
Silicon	11.9	0.0004	High
Semi-insulating GaAs	13	0.0006	Very high

Table A.2
Low-Cost Substrates

Material	Dielectric Constant (at 1 GHz)	Loss Tangent (at 1 GHz)	Manufacturer
R03003	3	0.0013	Rodgers Corp.
R03006	6.15	0.0013	Rodgers Corp.
R03010	10.2	0.0013	Rodgers Corp.
R04003	3.38	0.0022	Rodgers Corp.
TLC-32	3.2	0.003	Taconic Plastics
HT-2	4.3	0.0033	Hewlett Packard
Poly-guide	2.32	0.0005	Shawinigan Research
Glass-Epoxy	3.7–4.7	0.02	Worldwide

References

[1] Bahl, I. J., and P. Bhartia, *Microstrip Antennas,* Dedham, MA: Artech House, 1980.

[2] Zurcher, J. F., and F. E. Gardiol, *Broadband Patch Antennas,* Norwood, MA: Artech House, 1995.

[3] Garg, R., et al., *Microstrip Antenna Design Handbook,* Norwood, MA: Artech House, 2001.

[4] Sainati, R. A., *Microstrip Antennas for Wireless Applications,* Norwood, MA: Artech House, 1996.

Appendix B: Expressions for Various Parameters of RMSAs

Microstrip line or patch is an inhomogeneous configuration with a dielectric substrate between the ground and patch and air above the patch. As a result, the effective dielectric constant ϵ_e is less than ϵ_r. The fringing fields along the edge of the microstrip patch extend beyond the physical dimensions, thereby increasing the effective width W_e. The design equations for the rectangular patch antenna, which are also valid for planar transmission lines, are given below.

B.1 Effective Width and Effective Dielectric Constant

The effective width W_e is determined by using the following expression [1, 2],

$$W_e = 2\pi h / \ln\left[hF/W' + \sqrt{1 + (2h/W')^2}\right] \tag{B.1}$$

where

$$F = 6 + (2\pi - 6)\exp\left[(-4\pi^2/3)(h/W')^{3/4}\right] \tag{B.2}$$

and

$$W' = W + (t/\pi)\left[1 + \ln\left\{4/\sqrt{(t/h)^2 + (1/\pi)^2/(W/t + 1.1)^2}\right\}\right] \tag{B.3}$$

Here, W is width of the patch or microstrip line, ϵ_r is a dielectric constant of the substrate, h is the thickness of the substrate, and t is the thickness of the metallic patch conductor. The effective dielectric constant ϵ_e is given as

$$\epsilon_e = 0.5\,[\epsilon_r + 1 + (\epsilon_r - 1)\,G] \tag{B.4}$$

where

$$G = \left(1 + \frac{10h}{W}\right)^{AB} - \frac{\ln 4}{\pi}\,\frac{t}{\sqrt{Wh}} \tag{B.5}$$

$$A = 1 + \frac{1}{49}\ln\left[\frac{(W/h)^4 + \{W/(52h)\}^2}{(W/h)^4 + 0.432}\right] + \frac{1}{18.7}\ln\left[1 + \left(\frac{W}{18.1h}\right)^3\right] \tag{B.6}$$

$$B = 0.564\,\exp\,[-0.2/(\epsilon_r + 0.3)] \tag{B.7}$$

The above equations for obtaining ϵ_e have an accuracy of $\pm 0.2\%$ for $0.01 \leq W/h \leq 100$ and $\epsilon_r \leq 50$.

As the frequency of operation increases, the fields get more confined to the patch, thereby reducing the effective width. The frequency dependence of the parameters is taken into account by modifying expressions for ϵ_e and W_e. The frequency-dependent expressions for the effective dielectric constant $\epsilon_e(f)$ are given by

$$\epsilon_e(f) = \epsilon_r - (\epsilon_r - \epsilon_e)/(1 + P) \tag{B.8}$$

where

$$P = P_1 P_2\,[(0.1844 + P_3 P_4)\,f_n]^{1.5763} \tag{B.9}$$

$$P_1 = 0.27488 + [0.6315 + 0.525/(1 + 0.0157 f_n)^{20}]u - 0.65683\,\exp\,(-8.7513u) \tag{B.10}$$

$$P_2 = 0.33622\,[1 - \exp(-0.03442\epsilon_r)] \tag{B.11}$$

$$P_3 = 0.0363\,\exp(-4.6u)\,[1 - \exp\{-(f_n/38.7)^{4.97}\}] \tag{B.12}$$

$$P_4 = 1 + 2.751\,[1 - \exp\{-(\epsilon_r/15.916)^8\}] \tag{B.13}$$

$$f_n = f \cdot h \text{ (in GHz-mm)} = 47.713kh \tag{B.14}$$

$$u = [W + (W' - W)/\epsilon_r]/h \tag{B.15}$$

The frequency-dependent expression for the effective width $W_e(f)$ is given by

$$W_e(f) = W/3 + (R_w + P_w)^{1/3} - (R_w - P_w)^{1/3} \tag{B.16}$$

where

$$P_w = (W/3)^3 + (S_w/2)(W_e - W/3) \tag{B.17}$$

$$Q_w = (S_w/3) - (W/3)^2 \tag{B.18}$$

$$R_w = (P_w^2 + Q_w^2)^{1/2} \tag{B.19}$$

$$S_w = c^2/[4f^2\{\epsilon_e(f) - 1\}] \tag{B.20}$$

B.2 Characteristics Impedance $Z_0(f)$ of the Microstrip Transmission Line

The characteristic impedance Z_0 depends on W, ϵ_r and h, and its static value is given by [3]

$$Z_0(W/h,\ \epsilon_r) = \frac{Z_0(W/h,\ \epsilon_r = 1)}{\sqrt{\epsilon_e}} \tag{B.21}$$

where

$$Z_0(W/h,\ \epsilon_r = 1) = \frac{\eta_0}{2\pi} \ln\left\{\frac{F_1 h}{W} + \sqrt{1 + (2h/W)^2}\right\} \tag{B.22}$$

and

$$F_1 = 6 + (2\pi - 6)\exp\left[-(30.666h/W)^{0.7528}\right] \tag{B.23}$$

The frequency-dependent formula of the characteristic impedance of the microstrip line is given here [3].

$$Z_0(f) = Z_L(R_{13}/R_{14})^{R_{17}} \tag{B.24}$$

where

$$R_1 = 0.03891\epsilon_r^{1.4} \tag{B.25}$$

$$R_2 = 0.267(W/h)^{7.0} \tag{B.26}$$

$$R_3 = 4.766\exp\left[-3.228(W/h)^{0.641}\right] \tag{B.27}$$

$$R_4 = 0.016 + (0.0514\epsilon_r)^{4.524} \tag{B.28}$$

$$R_5 = (hf/28.843)^{12} \tag{B.29}$$

$$R_6 = 22.20(W/h)^{1.92} \tag{B.30}$$

$$R_7 = 1.206 - 0.3144\exp(-R_1)[1 - \exp(-R_2)] \tag{B.31}$$

$$R_8 = 1 + 1.275\left[1 - \exp\left\{-0.004625R_3\epsilon_r^{1.674}(hf/18.365)^{2.745}\right\}\right] \tag{B.32}$$

$$R_9 = 5.086R_4\frac{R_5}{0.3838 + 0.386R_4}\cdot\frac{\exp(-R_6)}{1 + 1.2992R_5}\cdot\frac{(\epsilon_r - 1)^6}{1 + 10(\epsilon_r - 1)^6} \tag{B.33}$$

$$R_{10} = 0.00044\epsilon_r^{2.136} + 0.0184 \tag{B.34}$$

$$R_{11} = \frac{(hf/19.47)^6}{1 + 0.0962(hf/19.47)^6} \tag{B.35}$$

$$R_{12} = 1/[1 + 0.00245(W/h)^2] \tag{B.36}$$

$$R_{13} = 0.9408\epsilon_e^{R_8} - 0.9603 \tag{B.37}$$

$$R_{14} = (0.9408 - R_9)\epsilon_e^{R_8} - 0.9603 \tag{B.38}$$

$$R_{15} = 0.707R_{10}(hf/12.3)^{1.097} \tag{B.39}$$

$$R_{16} = 1 + 0.0503\epsilon_r^2 R_{11}[1 - \exp\{-(W/h)/15\}^6] \tag{B.40}$$

$$R_{17} = R_7[1 - 1.1241(R_{12}/R_{16}) \exp\{-0.026(hf)^{1.15656} - R_{15}\}] \tag{B.41}$$

B.3 Extension Due to Fringing Field

The extension ΔL in the length of the patch dimension to account for the fringing fields is given by [1, 2]:

$$\Delta L = h\xi_1\xi_3\xi_5/\xi_4 \tag{B.42}$$

where

$$\xi_1 = 0.434907 \frac{\epsilon_e^{0.81} + 0.26}{\epsilon_e^{0.81} - 0.189} \frac{(W/h)^{0.8544} + 0.236}{(W/h)^{0.8544} + 0.87} \tag{B.43}$$

$$\xi_2 = 1 + \frac{(W/h)^{0.371}}{2.358\epsilon_r + 1} \tag{B.44}$$

$$\xi_3 = 1 + \frac{0.5274 \arctan[0.084(W/h)^{1.9413/\xi_2}]}{\epsilon_e^{0.9236}} \tag{B.45}$$

$$\xi_4 = 1 + 0.0377 \arctan[0.067(W/h)^{1.456}]\{6 - 5 \exp[0.036(1 - \epsilon_r)]\} \tag{B.46}$$

$$\xi_5 = 1 - 0.218 \exp(-7.5W/h) \tag{B.47}$$

The extension in the patch dimensions reduces with an increase in frequency. The dispersion effect of the fringing fields $\Delta L(f)$ is accounted by replacing ϵ_e by $\epsilon_e(f)$.

B.4 Attenuation Constant

The total attenuation constant α—to account for dielectric and conductor losses in a microstrip configuration—is given by [3]:

$$\alpha = \alpha_d + \alpha_{cs} + \alpha_{cg} \tag{B.48}$$

where

α_d = dielectric losses in the substrate
α_{cs} = conductor losses in the strip conductor
α_{cg} = conductor losses in the ground plane

Various attenuation constants are given by

$$\alpha_d = 0.5\beta \frac{\epsilon_r}{\epsilon_r - 1} \frac{\epsilon_e(f) - 1}{\epsilon_e(f)} \tan \delta \tag{B.49}$$

$$\alpha_{cs} = \alpha_n R_{ss} F_{\Delta s} F_s \tag{B.50}$$

$$\alpha_{cg} = \alpha_n R_{sg} F_{\Delta g} \tag{B.51}$$

$$R_{ss} = \sqrt{\pi f \mu_0 / \sigma_s} \tag{B.52}$$

$$R_{sg} = \sqrt{\pi f \mu_0 / \sigma_g} \tag{B.53}$$

$$\alpha_n = \frac{1}{4\pi h Z_0} \left(\frac{32 - (W'/h)^2}{32 + (W'/h)^2} \right) \qquad \text{for } W'/h < 1 \tag{B.54}$$

$$\alpha_n = \frac{\sqrt{\epsilon_e}}{2\eta_0 W_e} \left[(W'/h) + \frac{0.667 W'/h}{(W'/h) + 1.444} \right] \qquad \text{for } W'/h \geq 1 \tag{B.55}$$

$$F_{\Delta s} = 1 + (2/\pi) \arctan [1.4 (R_{ss} \Delta_s \sigma_s)^2] \tag{B.56}$$

$$F_{\Delta g} = 1 + (2/\pi) \arctan\left[1.4\left(R_{sg}\Delta_g \sigma_g\right)^2\right] \tag{B.57}$$

$$F_s = 1 + \frac{2h}{W'}\left(1 - \frac{1}{\pi} + \frac{W' - W}{t}\right) \tag{B.58}$$

where Δ_s and Δ_g are the rms surface error of the patch conductor and the ground plane, respectively. The α_s and α_g are the conductivity of patch conductor and ground plane, respectively. Copper is the most commonly used conductor in the substrate. Its conductivity $\alpha_s = \alpha_g = 5.6 \times 10^7$ mho/cm.

References

[1] James, J. R., and P. S. Hall, *Handbook of Microstrip Antennas,* Vol. 1, London: Peter Peregrinus, Ltd., 1989.

[2] Ray, K. P., and G. Kumar, "Determination of the Resonant Frequency of Microstrip Antennas," *Microwave Optical Tech. Letters,* Vol. 23, October 1999, pp. 114–117.

[3] Hoffmann, R. K., *Handbook of Microwave Integrated Circuits,* Norwood, MA: Artech House, 1987.

Appendix C: MNM for RMSAs

C.1 Introduction

In the MNM for analyzing MSAs, electromagnetic fields underneath the patch and outside the patch are modeled separately [1]. The fields underneath the patch are modeled using Green's function approach. The patch is analyzed as a two-dimensional planar network. The dimensions of the patch are extended outward to account for the fringing fields. Multiple numbers of ports are located along the extended periphery. The length of each port should be small so that the field over this length is uniform. The number of ports depends on the field distribution along the edge. A greater number of ports should be chosen when there is a larger variation in the field distribution. Green's function for the rectangle is given in Section C.2.

The fields outside the patch, namely the fringing fields along the edges and the radiation fields, are incorporated by adding *equivalent edge admittance networks* (EANs), as described in Section C.4. The impedance matrixes corresponding to the patch and the fringing fields are combined using the segmentation method to obtain the input impedance and voltage distribution around the periphery of the patch. The radiation pattern is obtained from the voltage distribution along the periphery of the antenna [1–4].

C.2 Green's Function for RMSAs

For a planar rectangular cavity having a perfect magnetic wall along its periphery, the mode vector Ψ is obtained from the solution of the wave equation:

$$\left(\nabla_T^2 + k^2\right)\Psi = 0 \tag{C.1}$$

The solution of Ψ is given by

$$\Psi = [A \sin(m\pi x/L) + B \cos(m\pi x/L)]\,[C \sin(n\pi y/W) + D \cos(n\pi y/W)] \tag{C.2}$$

where k is the propagation constant, also known as wave number, and is equal to $2\pi/\lambda$.

Here, L and W are the length and the width of the rectangular patch along the x and y directions as shown in Figure C.1, and m and n represent the modal indexes. The constants A, B, C, and D are obtained by applying the boundary condition: $\delta\Psi/\delta \boldsymbol{n} = 0$, where $\boldsymbol{n}$ represents the outward normal to the boundary.

The mode vector Ψ_{mn} for the mnth mode is given by

$$\Psi_{mn} = \cos(m\pi x/L)\,\cos(n\pi y/W) \tag{C.3}$$

The wave equation for a z-directed electric current source at a point (x_0, y_0) is given by

$$\left(\nabla_T^2 + k^2\right) G(x, y/x_0, y_0) = \delta(x - x_0, y - y_0) \tag{C.4}$$

where $G(x, y/x_0, y_0)$ is Green's function of the given geometry and δ is the delta function. Green's function of an RMSA is given by [1, 5]

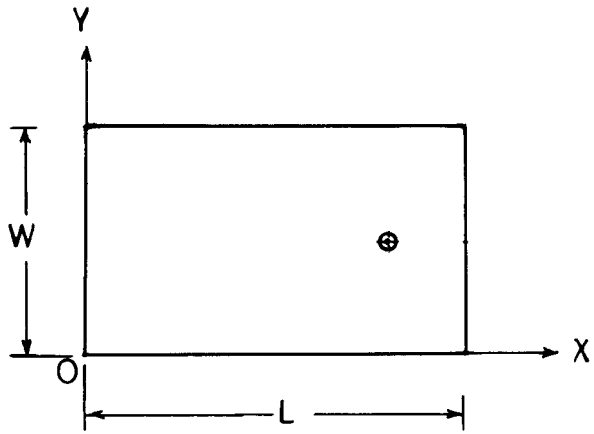

Figure C.1 RMSA.

$$G(x, y/x_0, y_0) = \frac{j\omega\mu h}{LW} \cdot \sum_{m=0}^{\infty} \sum_{n=0}^{\infty} \frac{\sigma_m \sigma_n \cos(k_x x) \cos(k_y y) \cos(k_x x_0) \cos(k_y y_0)}{k_x^2 + k_y^2 - k^2} \tag{C.5}$$

where $\omega = 2\pi f$ is the angular frequency and μ is the permeability, which is 1 for the nonmagnetic substrate, and

$$k_x = m\pi/L \text{ and } k_y = n\pi/W \tag{C.6}$$

$$\sigma_m = 1, \text{ if } m = 0 \text{ and}$$

$$\sigma_m = 2, \text{ otherwise}$$

$$\sigma_n = 1, \text{ if } n = 0 \text{ and}$$

$$\sigma_n = 2, \text{ otherwise}$$

$$k^2 = \omega^2 \mu_0 \epsilon_0 \epsilon_e (1 - j\delta_e) \tag{C.7}$$

$$\mu_0 = 4\pi \times 10^{-7} \text{ Henry/m}$$

$$\epsilon_0 = 8.854 \times 10^{-12} \text{ Farad/m}$$

where ϵ_e is the effective dielectric constant and δ_e includes the conductor and dielectric losses as described in Section C.3.

The electric field for the TM_{mn} modes for a thin substrate ($h << \lambda_0$) will be

$$E_z = j\omega\mu I_0 G(x, y/x_0, y_0) \tag{C.8}$$

where I_0 is the input current.

The voltage at any arbitrary point (x, y) will be

$$V(x, y) = -hE_z(x, y) \tag{C.9}$$

The element Z_{ij} of the Z–matrix, is the impedance between the ith and the jth port of the patch, and is given by

$$Z_{ij} = \frac{1}{W_i W_j} \int_{W_i} \int_{W_j} G(x_i, y_i/x_j, y_j)\, ds_i\, ds_j \tag{C.10}$$

where (x_i, y_i) and (x_j, y_j) denote the locations of the two ports of widths W_i and W_j, respectively.

The integral in (C.10) yields

$$Z_{ij} = \frac{j\omega\mu h}{LW} \sum_{m=0}^{\infty} \sum_{n=0}^{\infty} G(x_i, y_i/x_j, y_j) \sin c(k_x W_i/2) \sin c(k_y W_j/2) \tag{C.11}$$

Once the Z-matrix corresponding to all the ports is obtained, then the input impedance is calculated using segmentation method.

C.3 Effective Loss Tangent and Power Losses

The radiated power from the MSA is modeled by the EAN. The dielectric loss in the dielectric material of the substrate and the conductor losses in the patch and ground plane are taken into account by modifying the loss tangent tan δ of the substrate to the effective loss tangent tan δ_e. Consequently, tan δ_e is greater than tan δ as it accounts for both dielectric and conductor losses.

$$\tan \delta_e = \frac{P_d + P_c}{P_d} \tan \delta \tag{C.12}$$

where P_d is the power loss due to dissipation in the dielectric and P_c is the power loss in the conductor; they are given by [1, 6]:

$$P_d = h \int_S \sigma_d |\boldsymbol{E}|^2 \, ds \tag{C.13}$$

$$P_c = 2 \int_S R_s |\boldsymbol{H}|^2 \, ds \tag{C.14}$$

where $\boldsymbol{E}$ and $\boldsymbol{H}$ are the electric and magnetic fields, respectively. R_s is the skin-effect surface resistance of the conductor with conductivity σ_c and is given by

$$R_s = \sqrt{2\pi f \mu / \sigma_c} \tag{C.15}$$

and

$$\sigma_d = \omega\epsilon_0\epsilon_r \tan \delta \tag{C.16}$$

C.4 EAN

In MNM, the EAN represents the fields external to the patch, namely the fringing and radiated fields. If the physical dimensions of the patch are taken, then the EAN consists of parallel combinations of capacitance C and conductance G. The capacitance represents the energy stored in the fringing fields and the conductance G includes the radiation conductance corresponding to the radiated power, the surface wave conductance, and the mutual conductance.

Instead of loading with capacitance, edge extensions can be added to the physical dimensions of the patch, which accounts for the fringing fields. This approach of extending the edge is preferred because then EAN consists of only conductance G. The expressions for the edge extension, which takes into account the dispersion effect, are given in Appendix B.

The radiation conductance associated with an edge of the microstrip patch is defined as conductance, which will dissipate power equal to that radiated by the edge. If the edge is of width W and the power radiated for uniform voltage distribution is P_{rad}, then the radiation conductance per unit length of the edge is given by $G_r = 2P_{\text{rad}}/W$. The closed-form expression for radiation conductance G_r is given by [7]

$$G_r = \frac{w^2}{6\pi^2(60 + w^2)} \tag{C.17}$$

where

$$w = k_0 W_e$$

$$k_0 = 2\pi/\lambda_0$$

Here, $W_e = W + \Delta W$. The value of ΔW is obtained by using the edge extension formula given in Appendix B and λ_0 is the free-space wavelength. For n uniformly spaced ports along the edge, the radiation conductance connected to each port is chosen to be G_r/n.

The surface-wave conductance G_s is given by [1]:

$$G_s = k_0 h\,[20.493 + 65.167 k_0 h + 104.333 (k_0 h)^2]$$
$$10^{-4}\,[1 + 3.5(\epsilon_r - 2.45)(k_0 h)^3]/\lambda_0 \text{ mho/m} \qquad \text{(C.18)}$$

A schematic representation of the MNM is shown in Figure C.2.

The radiation from the RMSA can be taken into account by either using the two-slot or four-slot model [1, 2]. For the RMSA excited in the fundamental mode, the field distribution is constant along the radiating edges and varies sinusoidally along the nonradiating edges. In the two-slot model, only the radiating edges are loaded by the sum of the self-conductance and the mutual conductance between the radiating edges of the antenna. This loading scheme is similar to the T-line model, because the field varies only along one dimension. The model predicts the results with good accuracy for the linearly polarized fundamental mode.

When the field varies along both the dimensions—for example, the diagonally fed nearly square MSA—the two-slot model is not accurate. Therefore, all the edges of the RMSA should be loaded with their respective radiation conductance, which is known as the four-slot model. The four-slot model is a generalized model that yields an accuracy of ±1% against the accuracy of approximately ±5% for the two-slot model.

C.5 Segmentation Method

The segmented network for the four-slot model of RMSA is shown in Figure C.3. In Figure C.3, p stands for the feed port. The connected peripheral and external ports are represented by c and d, respectively. For a RMSA or any other regularly shaped patches, EAN represents the external network.

The Z-matrix of the patch and the EAN are combined using the segmentation method, which is given by

$$\begin{bmatrix} V_p \\ V_c \\ V_d \end{bmatrix} = \begin{bmatrix} Z_{pp} & Z_{pc} & Z_{pd} \\ Z_{cp} & Z_{cc} & Z_{cd} \\ Z_{dp} & Z_{dc} & Z_{dd} \end{bmatrix} \begin{bmatrix} I_p \\ I_c \\ I_d \end{bmatrix} \qquad \text{(C.19)}$$

where V_p, V_c, and V_d, and I_p, I_c, and I_d are the port voltages and currents, respectively. The number of c ports are the same as number of d ports, so the boundary conditions at these interconnections are $V_c = V_d$ and $I_c = -I_d$. The input impedance and the voltage distribution around the periphery of the patch are obtained by applying the segmentation method as:

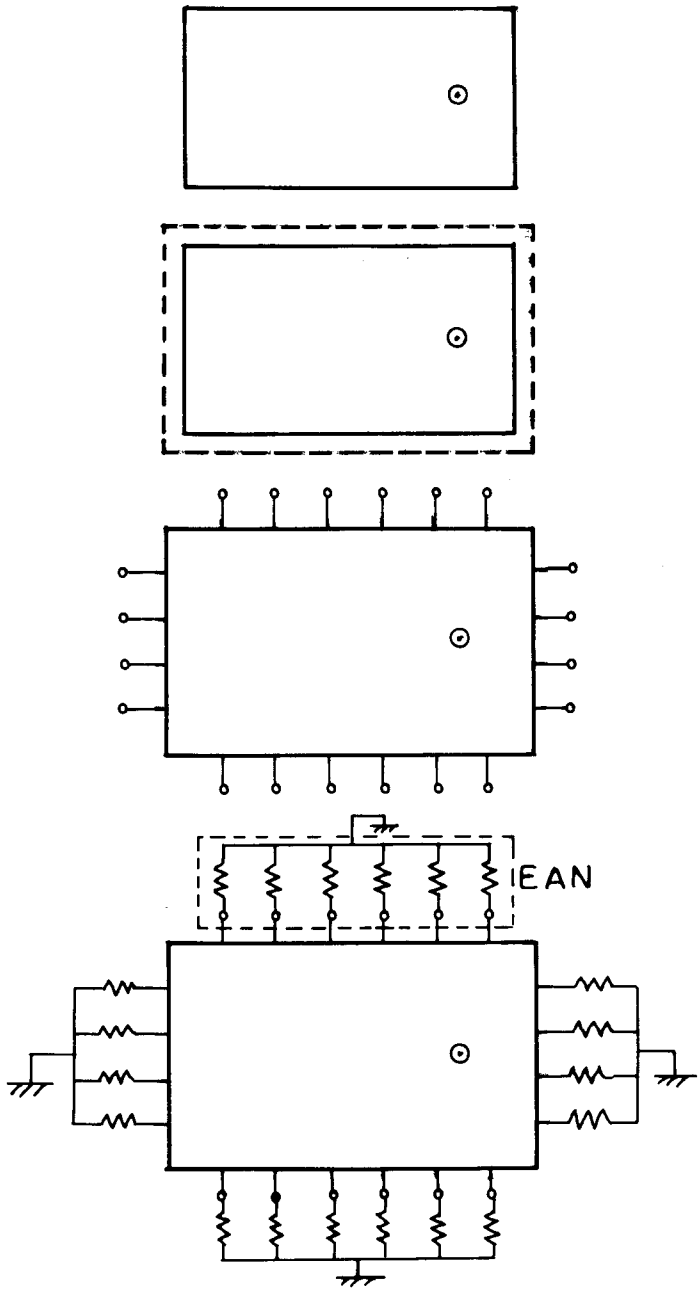

Figure C.2 Various steps for the MNM of the RMSA.

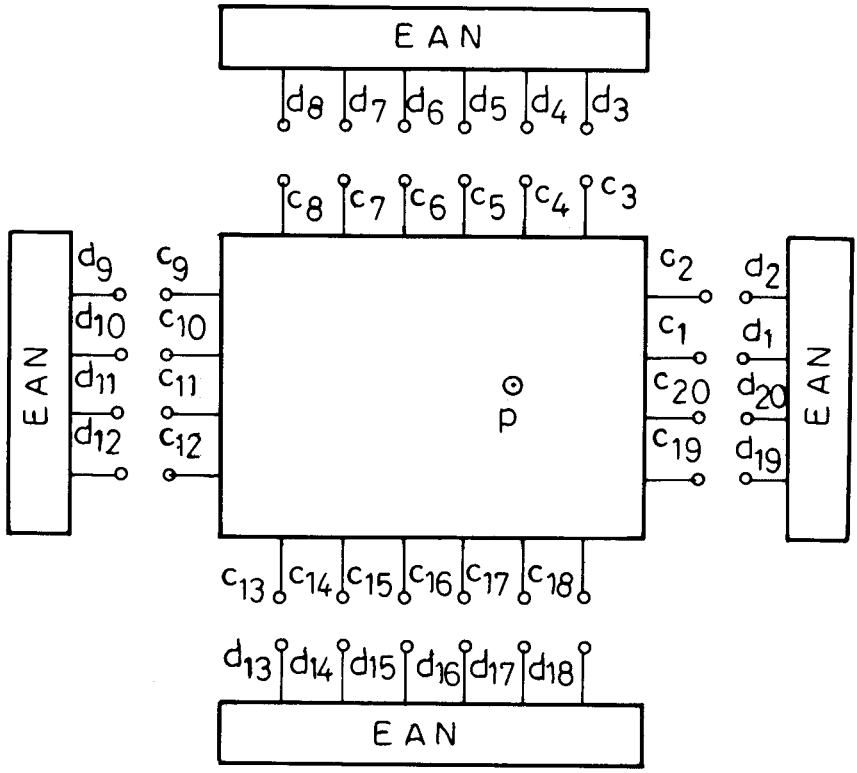

Figure C.3 Segmentation of an RMSA with its EAN.

$$Z_{\text{in}} = V_p / I_p = Z_{pp} + (Z_{pc} - Z_{pd}) Z_1^{-1} (Z_{dp} - Z_{cp}) \tag{C.20}$$

where

$$Z_1 = (Z_{cc} + Z_{dd} - Z_{cd} - Z_{dc}) \tag{C.21}$$

and

$$V_c = Z_{cp} + (Z_{cc} - Z_{cd}) Z_1^{-1} (Z_{dp} - Z_{cp}) I_p \tag{C.22}$$

The matrixes Z_{pp}, Z_{pc}, Z_{cp}, and Z_{cc} are obtained from the Z-matrix of the rectangular patch using Green's function. The Z_{pp} is an $N_p \times N_p$ matrix, where N_p is the number of external ports and for a single feed, $N_p = 1$. Z_{pc} and Z_{pd} are $N_p \times N_c$ matrixes, where N_c is the total number

of ports along the periphery of the patch. The Z_{cc} and Z_{cd} are $N_c \times N_c$ matrixes. For an RMSA, the impedance matrixes Z_{pd}, Z_{dp}, Z_{cd}, and Z_{dc} are zero. Z_{dd} is the loading matrix, which is obtained by taking the inverse of the EAN, described in the previous section. This matrix has only diagonal elements and its size is $N_c \times N_c$ [1, 4, 5].

MSAs of irregular shapes, which can be divided into regular shapes for which Green's functions are available, can be analyzed by using the segmentation method. For example, a C-shaped antenna, for which Green's function is not available, can be segmented into three rectangular patches as shown in Figure 6.17. The combined Z-matrix of these three patches using the segmentation method corresponds to that of the C-shaped patch. The complex configurations, which cannot be segmented into regular shapes, can be analyzed using the contour integral method [1].

C.6 Radiation Pattern of RMSA

The radiated power from the patch is obtained by using the concept of the magnetic wall along the periphery. At the magnetic wall, the induced magnetic current density is

$$\mathbf{K} = \mathbf{n} \times \mathbf{E} \tag{C.23}$$

where $\mathbf{n}$ is the unit normal to the magnetic wall [8, 9]. For a RMSA on the infinite ground plane, the above equation reduces to

$$K = -2\,(n \times E_z) \tag{C.24}$$

The factor 2 accounts for the effect of the ground plane. Assuming that $\mathbf{K}$ is constant along the port width, the far field electric potential is given by:

$$F_x = \frac{\epsilon_0}{4\pi r}\, e^{-jk_0 r} \sum_{i=1}^{m} K_{ix}(r') \int_{c_i} e^{jk_0 r' \cos\xi}\, dl(r') \tag{C.25a}$$

$$F_y = \frac{\epsilon_0}{4\pi r}\, e^{-jk_0 r} \sum_{i=1}^{n} K_{iy}(r') \int_{c_i} e^{jk_0 r' \cos\xi}\, dl(r') \tag{C.25b}$$

where K_{ix} and K_{iy} are the components of magnetic current vectors along the x- and y-directions, evaluated from (C.24), and ξ is the angle between the two vectors. Since **K** has no component in the z-direction, F_z is zero. Also,

$$\cos \xi = \cos \theta \cos \theta' + \sin \theta \sin \theta' \cos(\phi - \phi') \tag{C.26}$$

where r, θ, and ϕ correspond to the spherical coordinate system and ϕ' is shown in Figure 2.7. Since the magnetic current **K** has only x- and y-components, $\theta' = 90°$, so (C.26) reduces to

$$\cos \xi = \sin \theta \cos(\phi - \phi') \tag{C.27}$$

Using the rectangular-to-polar transformation,

$$F_\theta = (F_x \cos \phi \cos \theta + F_y \sin \phi \cos \theta) \tag{C.28}$$

and

$$F_\phi = (-F_x \sin \phi + F_y \cos \phi) \tag{C.29}$$

E_θ and E_ϕ are obtained from F_θ and F_ϕ as

$$E_\theta = \eta H_\phi = jk_0 F_\phi \tag{C.30a}$$

$$E_\phi = -\eta H_\theta = -jk_0 F_\theta \tag{C.30b}$$

The total radiated power P_r is obtained as:

$$P_r = \frac{1}{120\pi} \int_0^{2\pi} \int_0^{\pi/2} \left(|E_\theta|^2 + |E_\phi|^2\right) r^2 \sin \theta \, d\theta \, d\phi \tag{C.31}$$

The directivity of the antenna is given by

$$D = \frac{4\pi}{\iint P_n(\theta, \varphi) \, d\Omega} \tag{C.32}$$

Here $P_n(\theta, \phi)$ gives the normalized power in the (θ, ϕ) direction [8]. The efficiency η of the antenna is given by [1, 6]

$$\eta = \frac{P_r}{P_r + P_d + P_c} \tag{C.33}$$

where P_r is radiated power and P_d and P_c are the power loss in the dielectric substrate and conductor (patch and ground plane), respectively. The expressions for P_d and P_c are given in Section C.3.

For circularly polarized antennas, AR is obtained from E_θ and E_ϕ as described in [9].

References

[1] James, J. R., and P. S. Hall, *Handbook of Microstrip Antennas,* Vol. 1, London: Peter Peregrinus, Ltd., 1989.

[2] Srinivasan, V., "MNM for Variations in Rectangular Microstrip Antennas," Ph.D. thesis, Indian Institute of Technology, Bombay, India, 2000.

[3] Ray, K. P., "Broadband, Dual-Frequency and Compact Microstrip Antennas," Ph.D. thesis, Indian Institute of Technology, Bombay, India, 1999.

[4] Okoshi, T., and T. Miyushi, "The Planar Circuit—An Approach to Microwave Integrated Circuitry," *IEEE Trans. Microwave Theory Tech.,* Vol. 20, April 1972, pp. 245–252.

[5] Gupta, K. C., R. Chadha, and R. Garg, *Computer-Aided Design of Microwave Circuits,* Dedham, MA: Artech House, 1981.

[6] Bahl, I. J., and P. Bhartia, *Microstrip Antennas,* Dedham, MA: Artech House, 1980.

[7] Lier, E., and K. R. Jakobsen, "Rectangular Microstrip Patch Antenna with Infinite and Finite Ground Plane Dimensions," *IEEE Trans. Antennas Propagation,* Vol. 31, November 1983, pp. 968–974.

[8] Jordan, E. C. and K. C. Balmain, *Electromagnetic Waves and Radiating Systems,* Englewood Cliffs, NJ: Prentice Hall, 2000.

[9] Sharma, P. C., "Desegmentation Method and Its Application to Circularly Polarized Microstrip Antenna," Ph.D. thesis, Indian Institute of Technology, Kanpur, India, 1982.

Acronyms

ACMSA	aperture coupled microstrip antenna
ARMSA	annular ring microstrip antenna
ASP	aperture-stacked patch
AR	axial ratio
BW	bandwidth
CM	circular monopole
CMSA	circular microstrip antenna
CP	circular polarization
EAN	edge admittance network
ECMSA	electromagnetically coupled microstrip antenna
E-field	electrical field
EM	elliptical monopole
ETM	equilateral triangular monopole
ETMSA	equilateral triangular microstrip antenna
FDTD	finite-difference time-domain
FEM	finite element method
GCN	gap-coupled network
GSM	Global System for Mobile communication
GPS	Global Positioning System
HETMSA	half of equilateral triangular microstrip antenna (30°-60°-90° triangular microstrip antenna)
HM	hexagonal monopole
HPBW	half-power beamwidth
ITMSA	isosceles triangular microstrip antenna

LHCP	left-hand circular polarization
MIC	microwave-integrated circuit
MNM	multiport network model
MoM	method of moments
MSA	microstrip antenna
PCB	printed circuit board
RHCP	right-hand circular polarization
RM	rectangular monopole
RMSA	rectangular microstrip antenna
RRMSA	rectangular ring microstrip antenna
SCMSA	semicircular microstrip antenna
SM	square monopole
SSFIP	strip slot foam-inverted patch
TMSA	triangular microstrip antenna
UHF	ultra-high frequency
VSWR	voltage standing-wave ratio
WLL	wireless local loop

List of Symbols

a	radius of the circle, semicircle
a_e	Effective radius of the circle, semicircle
c	velocity of light
D	directivity
d	diameter of probe
d_s	distance of short from edge
E_θ, E_ϕ	electric fields in the two planes
f_0	resonance frequency
G_m	mutual conductance
$G_r(\ / \ )$	Green's function
G_r	radiation conductance
H	height of the triangular patch
h	height of the substrate
J_n	Bessel function of nth order
k	wave number in dielectric
k_0	free-space wave number
k_{nm}	mth root of the Bessel function
L	length of the rectangular patch
L_e	effective length of the rectangular patch
l	length of microstrip line, stub, or slot
l_e	effective stub length
l_s, L_s	length of stub in aperture coupled antennas
P_c	power lost in conductor
P_d	power lost in dielectric

P_r	radiated power
S	side length of the triangular patch
s	gap spacing
$\tan \delta$	loss tangent
t	conductor thickness
W	width of the rectangular patch
W_e	effective width of the rectangular patch
W_i, W_j	ith and jth port widths
w	width of the microstrip line, stub or slot
x	feed point
Z_{ij}	multiport impedance matrix
Z_{in}	input impedance
Z_0	characteristics impedance
$Z_0(f)$	frequency-dependent characteristic impedance
β	propagation constant
ΔL	edge extension in length
ΔW	edge extension in width
Δ	air gap
ϵ_o	free-space permitivity
ϵ_e	effective dielectric constant
$\epsilon_e(f)$	frequency-dependent effective dielectric constant
ϵ_{eq}	equivalent dielectric constant for two layers
ϵ_r	dielectric constant
η	efficiency
η_0	free-space impedance
λ	wavelength in dielectric
λ_0	free-space wave length
μ_0	free-space permeability
μ_r	permeability of the material
ϕ	azimuthal angle
θ	elevation angle
ω	angular frequency

About the Authors

Girish Kumar received a Ph.D. in electrical engineering from the Indian Institute of Technology (IIT) in Kanpur, India, in 1983. From 1983 to 1985, he was a research associate at the University of Manitoba in Winnipeg, Canada. From 1985 to 1991, he was an assistant professor in the electrical engineering department at the University of North Dakota in Grand Forks, North Dakota. Since 1991, he has been in the electrical engineering department at IIT in Bombay, India, where currently he is a professor. His research interests are in the areas of MSAs and arrays, broadband antennas, MICs, and EMI/EMC. He has successfully completed much research and sponsored projects in these fields. He has published more than 100 papers in journals and conference proceedings. Dr. Kumar is a senior member of the IEEE and a fellow of IETE, India.

K. P. Ray received an M. Tech. in microwave electronics from University of Delhi, South Campus, Delhi, India, in 1985. He joined SAMEER in Mumbai, India, in the same year and has been working on the design of different types of antenna elements and arrays, the high-power generation of RF and microwaves, and other microwave components and systems. He received a Ph.D. from the electrical engineering department of IIT in Bombay, India, in 1999; his thesis was in the field of MSAs. He has been a visiting faculty member at IIT in Bombay, and has been deputed to GTRI in Atlanta, Georgia, under the UNDP program. He has published more than 50 research papers in journals and conference proceedings. Currently, he is the head of the RF and microwave power system division in SAMEER. He is a member of the IEEE, a fellow of the IETE, and a life member of the Instrument Society of India.